Advanced Techniques for Surface Engineering

www.manaraa.com

EURO COURSES

A series devoted to the publication of courses and educational seminars organized by the Joint Research Centre Ispra, as part of its education and training program.
Published for the Commission of the European Communities, Directorate-General Telecommunications, Information Industries and Innovation, Scientific and Technical Communications Service.

The EUROCOURSES consist of the following subseries:

- Advanced Scientific Techniques
- Chemical and Environmental Science
- Energy Systems and Technology
- Environmental Impact Assessment
- Health Physics and Radiation Protection
- Computer and Information Science
- Mechanical and Materials Science
- Nuclear Science and Technology
- Reliability and Risk Analysis
- Remote Sensing
- Technological Innovation

MECHANICAL AND MATERIALS SCIENCE
Volume 1

The publisher will accept continuation orders for this series which may be cancelled at any time and which provide for automatic billing and shipping of each title in the series upon publication. Please write for details.

www.manaraa.com

Advanced Techniques for Surface Engineering

Edited by

W. Gissler
Institute for Advanced Materials,
Commission of the European Communities,
Joint Research Centre, Ispra, Italy

and

H. A. Jehn
Forschungsinstitut für Edelmetalle und Metallchemie,
Schwäbisch Gmünd, Germany

SPRINGER-SCIENCE+BUSINESS MEDIA, B.V.

www.manaraa.com

Based on the lectures given during the Eurocourse on
'Advanced Techniques for Surface Engineering'
held at the Joint Research Centre, Ispra, Italy,
November 10–13, 1992

ISBN 978-90-481-4214-9 ISBN 978-94-017-0631-5 (eBook)
DOI 10.1007/978-94-017-0631-5

Publication arrangements by
Commission of the European Communities
Directorate-General Telecommunications, Information Industries and Innovation,
Scientific and Technical Communication Unit, Luxembourg

EUR 14658
© 1992 Springer Science+Business Media Dordrecht
Originally published by Kluwer Academic Publishers in 1992

LEGAL NOTICE
Neither the Commission of the European Communities nor any person acting on behalf of the Commission is responsible for the use which might be made of the following information.

Printed on acid-free paper

All Rights Reserved
No part of the material protected by this copyright notice may be reproduced or utilized in any form or by any means, electronic or mechanical, including photocopying, recording or by any information storage and retrieval system, without written permission from the copyright owner.

www.manaraa.com

Table of Contents

Preface vii

Introductory Remarks

Hondros, E. D. / The Emergence of Interfacial Engineering 1

Part I: Fundamentals

Jehn, H. A. / Nucleation and Growth of Thin Films 5

Bull, S. J. / Interfaces and Adhesion 31

Part II: Techniques of Surface Engineering

Jacquot, P. / Nitriding, Boriding and Carburizing of Steels 69

Mazzoldi, P. / Ion Implantation for Surface Engineering 83

D'Agostino, R., Favia, P., Fracassi, F., Lamendola, R. / Plasma-Enhanced Chemical Vapor Deposition 105

Pauleau, Y. / Physical Vapor Deposition Techniques I: Evaporation and Sputtering 135

Moll, E. / Physical Vapor Deposition Techniques II: Ion Plating, Arc Deposition and Ion Beam Deposition 181

Brossa, F. and Lang, E. / Plasma Spraying - A Versatile Coating Technique 199

Frenk, A. and Kurz, W. / Laser Surface Treatments: Microstructural Aspects 235

Freller, H. and Lorenz, H. P. / Hybrid Processes 253

Part III: Characterization of Coatings and Surfaces

Taube, K. H. / Measurement of Mechanical Properties of Thin Solid Films I: Hardness, Elasticity and Stress 275

Matthews, A. and Holmberg, K. / Measurement of Mechanical Properties of Thin Solid Films II: Friction and Wear 295

Gissler, W. and Haupt, J. / Microstructural Characterization of Films and Surface Layers 313

www.manaraa.com

Part IV: Surface Engineering in the Industrial Practice

Stroosnijder, M. F., Bennett, M. J. and Mevrel, R. / Surface Engineering for High Temperature Corrosion Resistance 335

Jehn, H. A. / Decorative Coatings 359

Rossi, F. / Diamond and Diamond-Like Carbon Films 371

Subject Index 399

www.manaraa.com

PREFACE

Today's shortages of resources make the search for wear and corrosion resistant materials one of the most important tasks of the next century. Since the surface of a material is the location where any interaction occurs, it is that there the hardest requirements on the material are imposed: to be wear resistant for tools and bearings; to be corrosion resistant for turbine blades and tubes in the petrochemical industry; to be antireflecting for solar cells; to be decorative for architectural panels and to combine several of these properties in other applications. Surface engineering is the general term that incorporates all the techniques by which a surface modification can be accomplished. These techniques include both coating and modification of the surface by ion implantation and laser beam melting.

In recent years a continuously growing number of these techniques were developed to the extent that it became more and more difficult to maintain an overlook and to understand which of these highly differentiated techniques might be applied to resolve a given surface engineering problem. A similar development is also occuring for surface characterization techniques.

This volume contains contributions from renowned scientists and engineers to the Eurocourse the aim of which was to inform about the various techniques and to give a comprehensive survey of the latest development on this subject.

This book like the course is divided in four parts: Part I is devoted to fundamental aspects of coating and surface modification: nucleation and film growth, structural zone models, interfacial structures and adhesion. Part II deals with the techniques of surface engineering: nitriding, boriding and carburizing, ion implantation and chemical and plasma enhanced vapor deposition. Special emphasis is given to physical vapor deposition processes such as evaporation, sputtering, ion plating , arc evaporation and ion beam deposition. In addition plasma spraying, laser beam processing and hybrid processes are treated. In Part III techniques are presented to characterize morphology and structure and in particular mechanical properties such as hardness, elasticity and stress. Special importance is given to methods for testing the mechanical performance of films and surfaces. Part IV is devoted to some examples from the industrial practice of surface engineering: high temperature and corrosion resistant and decorative coatings. Also a review is given on recent developments of diamond and diamond-like coatings.

The editors wish to thank all the authors for having contributed to this volume and for their effort in preparing the texts. They are aware of the high personel commitment having been necessary to elaborate such excellent papers as presented at the Eurocourse and documented in this volume.

Thanks are also due to Dr. G. Pellegrini and his staff of the Eurocourses Ispra for the excellent organization of the course and to Kluwer Academic Publishers for printing, production and distribution of this book.

Ispra, November 1992

The editors

Wolfram Gissler and Hermann A. Jehn

www.manaraa.com

THE EMERGENCE OF INTERFACIAL ENGINEERING

OPENING REMARKS ON THE OCCASION OF THE EURO-COURSE: ADVANCED TECHNIQUES FOR SURFACE ENGINEERING

E.D. HONDROS
Director of the Institute for Advanced Materials
Joint Research Centre
Commission of the European Communities

From a conventional background in metallurgical treatments, such as case carburising, nitriding, galvanising and "shot peening", the technologies associated with the protection of surfaces, or the modification of the structural and chemical properties of the top atomic layers of materials surfaces have blossomed into a separate sub-discipline, now commonly referred to as "Surface Engineering".

The goal and motivation have not altered over the years - only the name and the truly astonishing range of highly sophisticated techniques, based largely on ion, laser and vacuum engineering. These are emerging from their former position as experimental laboratory techniques and are achieving commercially mature applications in engineering components. It is a remarkable, silent technological revolution - these often subtle techniques have been successfully scaled up and in many cases they have overcome the general conservatism in engineering practice and the reluctance to change from old established habits. This speaks well for the promise, efficacy and capability of these techniques.

Indeed, we are witnessing the emergence of a new landmark in the materials sciences and technologies which we refer to in the generic term, Interfacial Engineering. This embraces all interfaces in materials, including internal ones, such as grain boundaries and phase boundaries, the important two-dimensional junctions in polycrystalline matter where the constituent grains of the body are held together. They play a rôle during processing or in operation, where internal interfaces may provide short circuit pathways for mass migration and shape changes. We apply, by convention, the term Surface Engineering, the subject of this meeting, to the interface between the solid and its vapour. It is then in this respect a subset of the general subject of Interface Engineering.

Much can be said of the remarkable influence that interfaces - both internal as well as external surfaces - have on bulk properties, such as fatigue, corrosion, erosion, wear and other tribological properties. This reflects in practical terms the fundamental importance of interfaces as the theatre of action for phenomena based on kinetics, cohesion, and microstructure.

One of the main reasons for the apparent success of Surface Engineering techniques is that they can effect a demonstrable improvement in the life of many components used in engineering practice. Although cost is believed to be the main constraint in a more rapid market penetration of these methods, equipment manufacturers are continuing their

W. Gissler and H. A. Jehn (eds.), Advanced Techniques for Surface Engineering, 1–4.
© 1992 *ECSC, EEC, EAEC, Brussels and Luxembourg.*

www.manaraa.com

efforts in reducing the costs of the equipment and are seeking the introduction of greater automation for manufacturing efficiency.

In certain areas of application, remarkable life improvements have been demonstrated experimentally. This is indicated in the experimental data shown in TABLE 1 which have been culled from a variety of sources. The improvements cover many components, but in particular manufacturing tools. The materials scientist has done a good job and has demonstrated the potential of the technology: it is up to industrial firms, based on their evaluations on tecnico-commercial grounds to make the critical decision to embark on the capitalisation costs and to shift into the new technologies.

TABLE 1. Components by surface engineering.

Application	Method	Factor of Life Improvement
Drill	PVD	6 - 7
Milling Cutter	PVD	3 - 4
Abrasive Nozzle	PVD	6
Carbide End Mills	PVD	8
Punch	CVD	2
Form Tool	CVD	4 - 5
Cut Off Tool	CVD	6
Extrusion Punch	CVD	35
Slitters for Rubber	Ion Implantation	12
Injection Moulding Nozzle	Ion Implantation	5
High Speed Steel Tool	Ion Implantation	4
Die	Ion Implantation	3

Surface Engineering has thrown up many challenges in the materials sciences - such as the mechanisms of ion implantation, ion bombardment, ion beam mixing, of corrosion and erosion processes. However, the real measure of the emergence of Surface Engineering as a new technology is the potential for industrial exploitation. Here, we indicate some examples which contain the elements of industrial "pull" and contain opportunities for continuing R & D:

- in spite of efforts to develop ceramics to operate at very high temperatures, their intrinsic low ductility is still a fundamental problem. There is an underlying need to develop metallic materials for use at temperatures above 1250°C, such as the **refractory metals and alloys** of vanadium, tantalum, niobium and tungsten, provided that means are found to overcome their reactivity with the environment. Here some progress has been achieved for short-term applications in specialised areas such as space;
- **chromium** is a bizarre metal - however, it could be an interesting high temperature structural material if coatings could be developed to prevent its embrittlement by the ingress of oxygen and nitrogen;

www.manaraa.com

- **High Temperature Composite Materials,** being essentially metastable systems, can degrade through interdiffusion across the interface. This calls for the development of specific diffusion barriers at interfaces;
- the problem of **Adhesion of Coatings** is a general one and is related to that of the joining of dissimilar materials, such as metals and ceramics. There is much scope for the development of adhesion promoting layers at interfaces and to evaluate ion implantation techniques for this purpose;
- an important aspect of high temperature **Corrosion Resistant Coatings** is the self-healing capacity. Ceramic coatings would be the ideal protection layer, if only they were self-repairing. There are challenging materials science opportunities here;
- the presence of structural defects in deposited coatings could be a determinant of the useful life of the coating: how are these defects introduced in the course of processing and can **NDE techniques** be developed to study such defects?
- for good coating adhesion to a substrate, the **residual stress distribution** must be controlled through an appropriate combination of the different techniques and deposition parameters. NDE methods of measuring residual stresses must be developed;
- opportunities for the **perfection of coating processes** lie in the application of computer and sensor driven intelligent processing;
- protection with **diamond-like coatings** is becoming an exciting possibility. The mind boggles at the idea of a single crystal turbine blade coated with a diamond-like film;
- is it practicable to extend **ion implantation techniques** to improve the fatigue resistance of new structural ceramics, such as silicon nitride and syalons?
- ion implantation techniques should be explored further as a means of imparting protection and to change the electrical properties of **polymeric materials.**

In general, industrial manufacturing technologies are being penetrated by Surface Engineering procedures on a wide front. They offer solutions to diverse materials applications and for the improvement in life during operational conditions and, in addition, they offer innovative opportunities for new products. Applications range widely, for example, for optical and aesthetic reasons; corrosion resistance; improvements in high temperature performance. The economic potential of Surface Engineering is believed to be very high, as reflected in the market forecast in Europe and shown in TABLE 2.

TABLE 2. Market situation and forecast in europe for the period 1985-1995.

Function	1985 Million $	1995 Million $	Annual Growth % / Year
Optical	195	590	11
Tribological	196	292	6
Corrosion	15	240	28
Thermal Barriers	17	115	20
Decorative	2	3	6

www.manaraa.com

The rather optimistic, if not euphoric scenario represented in TABLE 2 which describes the functions which are expected to evolve rapidly, is, in turn, supported by the predicted rapid growth in the market for equipment as illustrated in TABLE 3.

TABLE 3. World-wide equipment market and expected growth rates.

	1985 Million ECUS	**Annual Growth 1985-1995 % / Year**
PVD	1500	15
CVD	400	25
Etching	430	28
Plasma CVD	22	40
Ion Implantation	350	28
Plasma Diffusion Processes	-	18
Thermal Spraying	65	14

Above I have presented a rather positive picture of Surface Engineering as a rapidly developing technology with considerable scientific and commercial potential. The subject of the present meeting concerns the techniques. Clearly, the momentum for the development of Surface Engineering as a technology can only be maintained as long as appropriate techniques continue to be developed, which have a focus on specific property improvements, on specific components and in which the cost of employing is not prohibitive. In addition, such equipment should be aimed not for the highly trained specialist, but for easy use and maintenance during manufacture.

In conclusion, I believe that it is timely to consider the developments in technical procedures in this burgeoning field in order to help ensure that Europe, which pioneered developments in this scene, will be in a position to reap the commercial benefits of Surface Engineering.

www.manaraa.com

NUCLEATION AND GROWTH OF THIN FILMS

H.A. JEHN
Research Institute for Precious Metals
and Metals Chemistry
Katharinenstr. 17
D-7070 Schwäbisch Gmünd
Germany

ABSTRACT. Nucleation and film growth determine the coating structure and the coating properties. In certain film/substrate systems an experimental study of the processes in the very initial stage of film formation is possible. They reflect the results of modeling using the kinetic nucleation theory or the thermodynamic approach. Tor practical systems, i.e. non-UHV conditions, alloy and compound deposition, the relation are much more complex, but the structures developed are very similar to those obtained for pure metal deposits. In the present paper the approaches of kinetic nucleation theory and of "thick" film growth modeling are outlined and the structures developed as a function of substrate temperature and particle energy are presented. In principal the theoretical investigations are very helpful even if they don't allow to draw quantitative conclusions for complex coating/substrate systems.

1. Introduction

With respect to thin films and coatings the discrepancy between the practical experience and the technological possibilities on one hand and the theoretical knowledge as well as the modeling of the processes on the other hand is particularly striking. This holds also for the nucleation and growth of thin films and coatings. There exist some models, which in part are proved experimentally. On the other hand quantitative relations can be taken in certain film-substrate systems. A number of prerequisites, however, have to be fulfilled like, e.g., ideal single-phase substrate surface, no alloy or compound formation of the deposited atoms with the elements of the substrate material or the deposition from evaporation sources under ultra high vacuum conditions. For practical conditions in technical coating deposition devieces at least the reactions of the substrate and film material with the gases of the residual

W. Gissler and H. A. Jehn (eds.), Advanced Techniques for Surface Engineering, 5–29.
© 1992 *ECSC, EEC, EAEC, Brussels and Luxembourg.*

www.manaraa.com

atmosphere have to be considered. In the case of the deposition of hard coatings, i.e. compound films like TiN, by CVD or reactive PVD processes, the reactive atmosphere has additionally to be regarded. Furthermore, the reactive gas as well as the inert plasma-assisting or sputter gas exhibits impurities which can lead to side reactions and contaminations. Finally, most of the process parameters affect the nucleation and film growth and the resulting film morphology. Such factors are the deposition process itself, the geometrical arrangement of vapour source and substrate, applied voltages, material and quality of the target and material and surface conditions of the substrate. The latter is influenced by mechanical and chemical pretretment processes. The often applied sputter cleaning also results in additional surface modifications. The substrate material normally is no single-phase single-crystalline material but most often an alloy or, as in the case of tool steels or hard metals for hard coatings, a complex multiphase material. As already mentioned, the substrate or (in a later stage) film surface is hit not only by the atoms to be deposited as well as the atoms or molecules of the inert, reactive or residual gas but also by ions (metal, gas) and possibly by electrons. With respect to these very complex conditions it is even more astonishing that the growing films can be fitted more or less sufficiently to a certain scheme.

The present paper describes the different effects on the nucleation and growth of thin films. A very detailed mathematical description is omitted on the favour of a more vivid presentation. The reader is referred to some original and review paper [1-7]. The major part of the fundamental investigations deals with the deposition of precious metals on single-crystalline surfaces of salt crystals (NaCl, and others) under UHV conditions. In these cases, clean surfaces are present and no side reactions take place. Detailed experiments are also reported for various metal-metal combinations. Inspite of almost no results on reactively deposited films (e.g. hard coatings), the results of the other films-substrate systemes form a good base also for the understanding of such systems.

2. Formation and Growth of Nuclei

The structure of all vapour-deposited films is predominantly controlled by the nucleation processes. This is stated in literature [8]: "Already a mean film thickness of 2 nm suffices to determine the film properties and the inherent growth of the films". The film formation, therefore, can only be understood on the base of the very initial stage of nucleation and growth.

www.manaraa.com

The theories of the formation and growth of nuclei are distinguished by their fundamental point of view: Phenomenological description on the base of the thermodynamic [9,10] and the kinetic nucleation theory with the microscopical atomistic treatment [5,11,12]. Because of the small number of atoms participating in the formation and growth of stable nuclei, the kinetic theory seems to describe the actual relations much better.

2.1. FUNDAMENTAL PROCESSES

The fundamental reactions occuring at the substrate surface are schematically shown in Fig. 1. From the gas phase atoms are impinging on the surface with the rate R, where they are adsorbed or directly reflected. On the surface they can diffuse a certain distance and desorb again (re-evaporation). The time of adsorption and, hence, the diffusion distance depend on the activation energies of desorption and diffusion. For very small impingement rates, an equilibrium between adsorption and desorption can be established, characterized by such a low coverage that no nucleation or film formation can take place. At high impingement rates metastable and stable clusters are formed which can grow by binding of diffusing atoms or by a direct impingement of atoms. At high supersatuations the critical nuclei are very small and can be formed by only two or three atoms. The nucleation rate term is defind as the rate of formation of

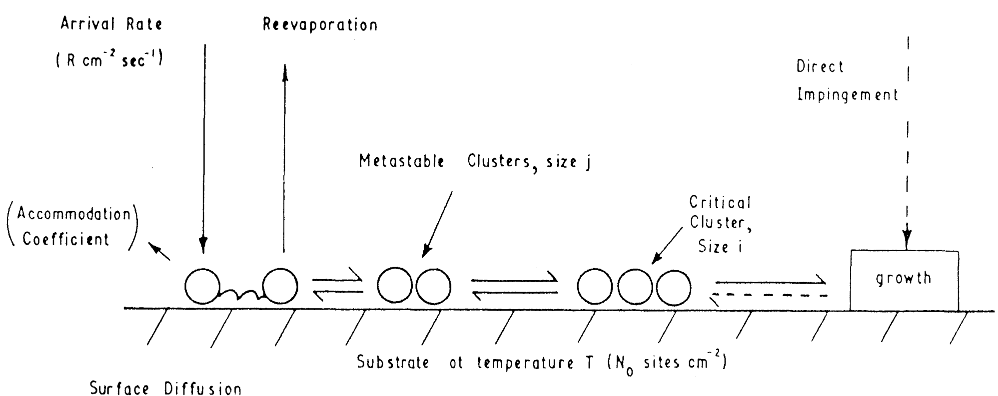

Fig. 1. Processes in the nucleation and growth of crystals on a substrate [2]

www.manaraa.com

stable nuclei. The continuous growth of the nuclei finally results in mutual contact of the nuclei, coalescence and a continous film. In part, also the migration of complete nuclei is observed. For the atomistic theory of nucleation [5] the activation evergies of diffusion and the binding energies between film-film and film-substrate atoms are of essential importance. Three types of binding energies have to be distinguished for the deposited atom, i.e. adsorption energy on the substrate (E_a), adsorption energy on top a layer of deposited atoms (E_a') and the binding energy between two adsorbed atoms (E_2). Figure 2 illustrates the different binding energies of adsorbed atoms on a substrate of triangular symmetry [2]. In this simgplified picture the following total energies are obtained: (a) isolated adatoms (E_a); (b) adatom in corner site ($E_a + 3\ E_2$); (c) adatom on film ($E_a' = 3\ E_2$); (d) adatom in corner site on film ($E_a' + 3\ E_2 = 6\ E_2$); (e) diffusing atom ($E_a - E_d$); (f) two-dimensional (2D) cluster ($4\ E_a + 5\ E_2$); and (g) 3D cluster ($3\ E_a + 6\ E_2$). Within the frame of this model the following types of nucleation and growth modi are obtained for the different deposition conditions.

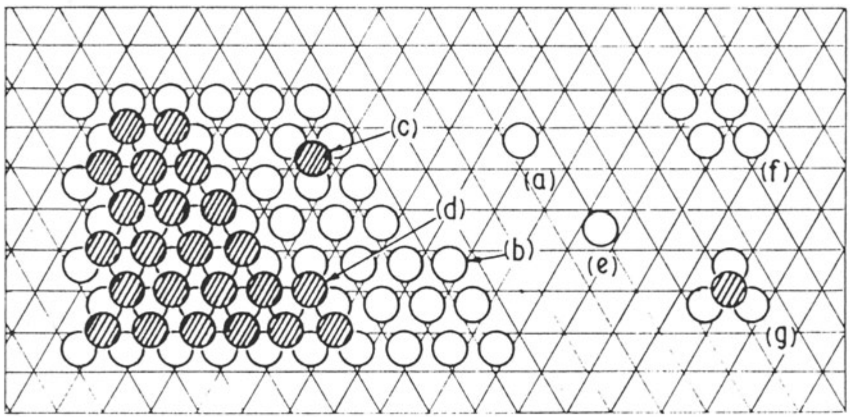

Fig. 2. Binding energies of atoms and clusters, on a nearest neighbour bond model of nucleation and growth on a triangular lattice [2]

For low substrate temperatures and high impingement rates ($R/N_o{}^2D \geq 1$) the impinging atoms pratically stick at their site of condensation, resulting in a relatively disordered film structure, Fig. 3a (R = impingement rate, N_o = number of sites on substrate surface, D = surface diffusion coefficient). In the case of strongly directed bonds between the deposited atoms, largely amorphous films are form-

المنارة للاستشارات
www.manaraa.com

ed (e.g. C, Si, SiO_2, ZrO_2). In the case of non-directed bonds very fine-grained polycrystalline films are obtained (e.g. metals).

For somewhat higher temperatures and low deposition rates ($R/N_o^2D \gg 1$) and a high adsorption energy on the substrate ($E_a > E_a'$) atomic layers are formed. The desorption of adatoms in the second layer is relatively easy (Fig. 3b). Furthermore, E_a' decreases with increasing layer number. This case of strong adatom-substrate bonding is characterized by the "layer growth" (Frank-van der Merwe mode).

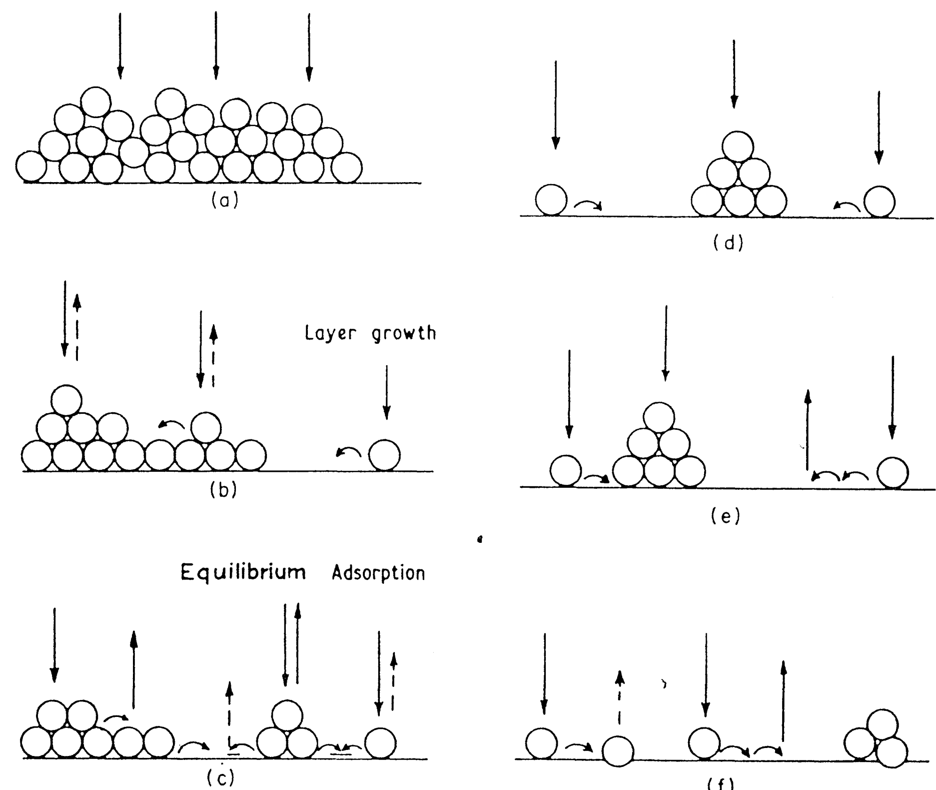

Fig. 3. Regimes of nucleation and growth [2]

In the case of a high mutual adatom bonding energy compared to the adsorption energy in higher film layers ($E_2 > E_a'$), islands are formed on top of the first layer (Stranski-Krastanow mode). At even higher deposition temperatures and low deposition rates, an equilibrium concentration of adsorbed atoms can be formed: Atoms desorb from the upper

المنارة للاستشارات
www.manaraa.com

layers at a sufficiently fast rate, thus the deposited film can only grow up to a certain thickness and no bulk crystals are formed. Such films show no stable microstructure (Fig. 3c).

If the bonding energy between the adatoms is higher than the adsorption energy on the substrate (3 $E_2 > E_a$), three-dimensional nuclei are predominently formed, even if the nucleus imitially is two-dimensional. For $E_2 > E_a$, the nucleus is three-dimensional from its initial formation. This film formation is characterized by a complete island growth (Volmer-Weber mode). This mode is mostly observed for metallic films on insulating substrate materials. Depending on the case whether single atoms desorb from the film surface or not, the process shows complete or incomplete condensation (Fig. 3d and e). The critical size of the nuclei is predominantly determined by the bonding energy E_2. As higher E_2 as smaller is the critical size, being one atom in its limiting case.

If E_a and E_2 are low compared to the thermal energy of the adatoms, no long-time adsorption and, hence, no nucleation takes place on a "perfect" surface. In that case, surface defects having higher adsorption energies act as nucleation centers (Fig. 3f).

In Fig. 4 the different growth modes are schematically illustrated in relation to the thermodynamic model. The relevant energies are surface and interface energy, respectively (σ_o, σ_i) and the elastic energy of the film (σ_{el}).

The effect of different substrate materials on the growth mode is schematically illustrated in Fig. 5, indicating the influence of the different energy values [13].

2.2 EFFECT OF DEPOSITION PARAMETERS

Nucleation processes can experimentally be studied in particular with relatively inert metals (e.g. Ag) on insulating substrate materials (e.g. alkaline halides), because side reactions are excluded. After an additional carbon deposition (by evaporation) the films can prepared for TEM studies by dissolution of the halide substrate crystal and nuclei in the size of 1 nm can be observed. This technique allows the relative easy investigation of the effect of various deposition conditions which can be altered within a wide range (e.g. evaporation in HV or UHV, sputter deposition). Also in-situ measurement in the TEM were successfully performed [16,17].

As an example for such an experimental series, the growth of Au nuclei on NaCl crystals depostted by evaporation under UHV conditous is shown in Fig. 6. Initially a random distribution of the nuclei can be observed. But also the clear decoration of a line-shaped lattice defect can already be noticed in an early state. By meaus of quantita-

www.manaraa.com

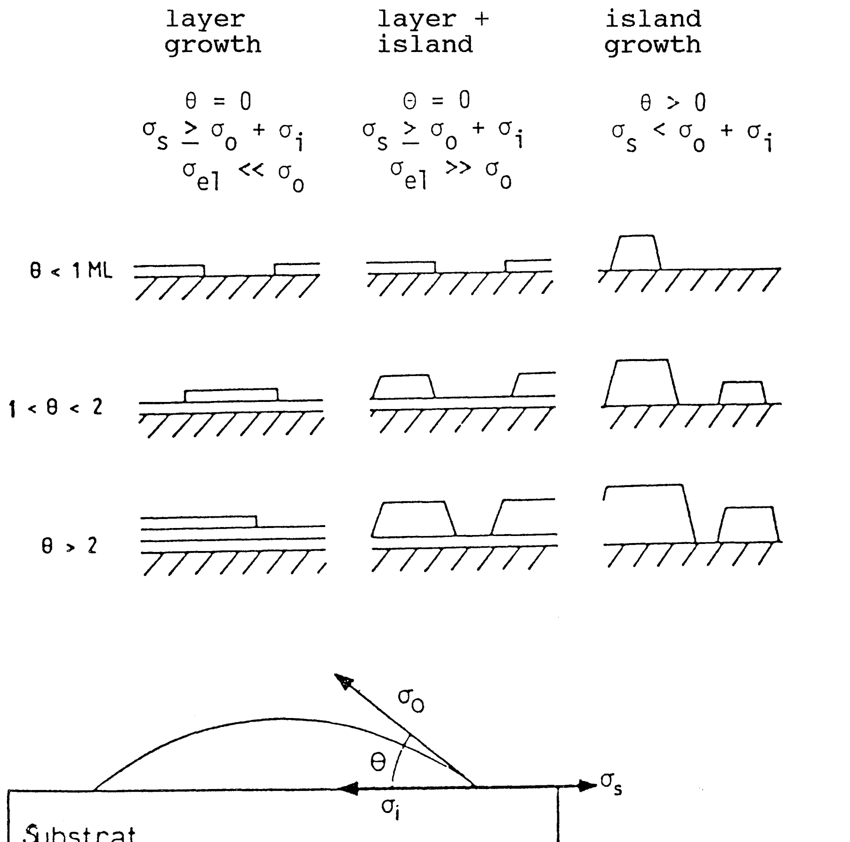

Fig. 4. Nucleation and growth in correlation with surface and interface energies ($\sigma_s = \sigma_i + \sigma_o \cos \Theta$)

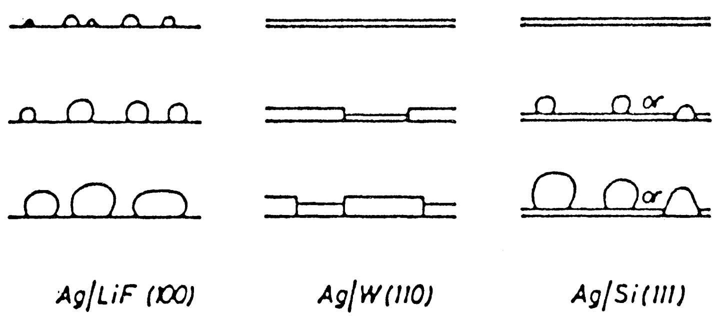

Fig. 5. Nucleation and growth of Ag films on various substrates [13]

www.manaraa.com

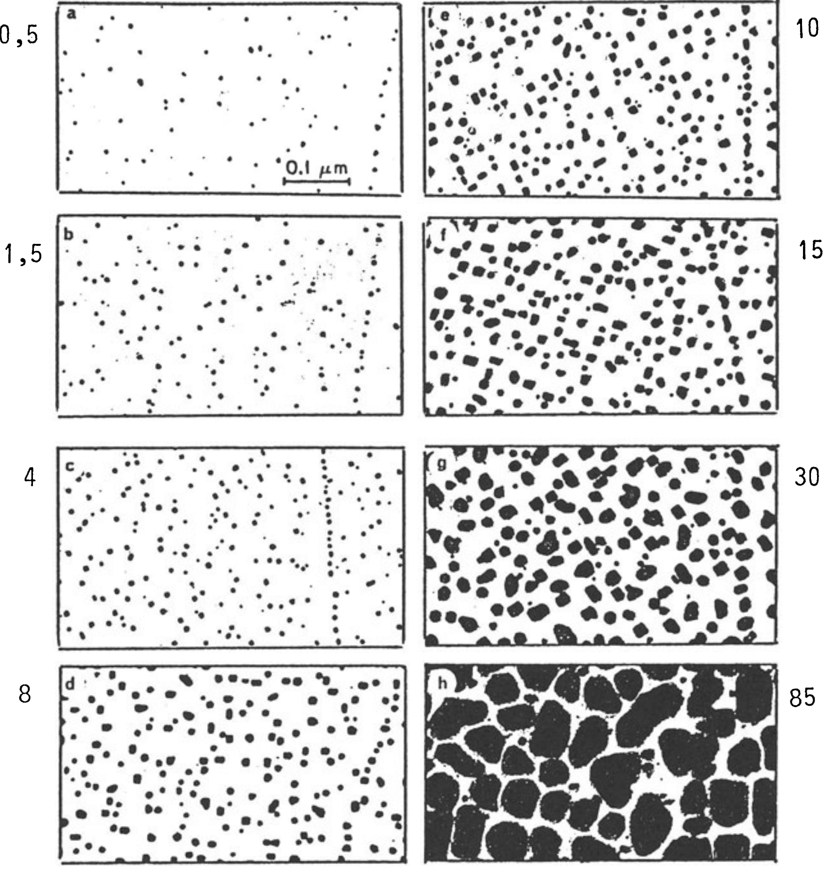

Fig. 6a. Electron micrographs of Au deposits on NaCl (10^{13} atoms$\cdot$cm^{-2}/s^{-1}, 250 °C, deposition time a: 0.5, b: 1.5, c:4, d: 8, e: 10, f: 15, g: 30, h: 85 s) [17]

tive image analyses the TEM photopraphs can be evaluated with respect to density, distance and size of the nuclei as well as to the fraction of the surface covered by nuclei. During the deposition, first the number of nuclei rises up to a mximum (saturation density), after which the number decreases again due to proceding coalescence (Fig. 6b). For a given system, nucleation rate and growth of the nuclei

www.manaraa.com

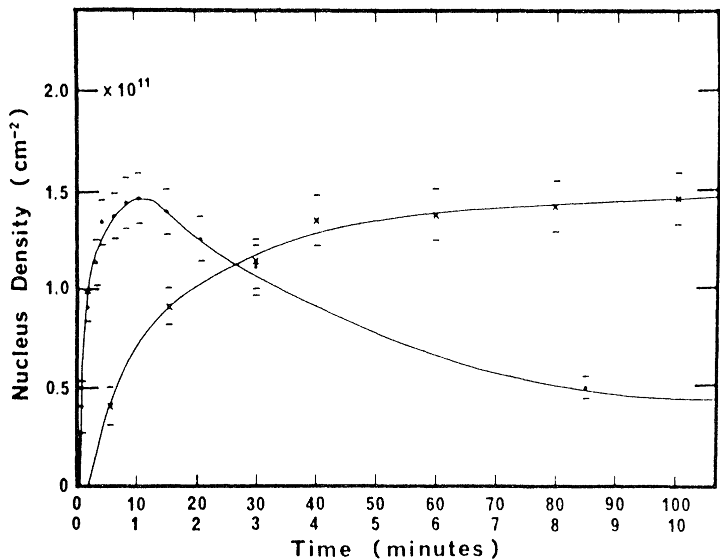

Fig. 6b. Density of nuclei as taken from Fig. 6a [13]

depend on the impingement rate and the substrate temperature, the latter determining the surface diffusion and re-evaporation.

The nucleation rate J of the deposition of Au and NaCl is proportional to the square of the impingement rate ($J \alpha R^2$). On the base of the kinetic nucleation theory it follows that already a two-atomic nucleus is stable. The temperature dependence shows a linear relationship between log J and 1/T, indicating a thermally activited process. The nucleation rate decreases with increasing temperature [6].

The saturation density N_S decreases with increasing impingement rate. Simultaneously, lower impingement rates yield a more pronounced size distribution of the nuclei, and high impingement rates result in a smaller size of the nuclei, as the investigations of Au on NaF have shown [14]. The saturation density decreases with increasing substrate temperature (Au on NaF or NaCl). Two ranges of different temperature dependencies are observed: a smaller slope of the log N_S - 1/T line at lower temperatures (below about 220 - 270 °C) and a higher slope at higher temperatures [14]. These dependencies can easily be explained qualitatively because the parameters impingement rate and temperature govern the ratio $R/N_o{}^2D$ which in turn determines the diffusion of adatoms towards the nucleus.

As mentioned above, the nucleation rate in precious metals-alkali halide systems was found to follow the dependency $J \alpha R^2$. In contrast, for strongly disordered sub-

www.manaraa.com

strate surfaces a defect-induced nucleation with J α R is observed. This is illustrated in Fig. 7 for the deposition of Au on Mica. Which exhibited an increased density of point defects by K pre-evaporation [19]. The relationship I α R hints to the assumption that already one atom trapped at the defect site forms a stable nucleus. In contrast to the nucleation, the growth of the nuclei does not depend on the defect density. The nuclei grow independently of their original formation.

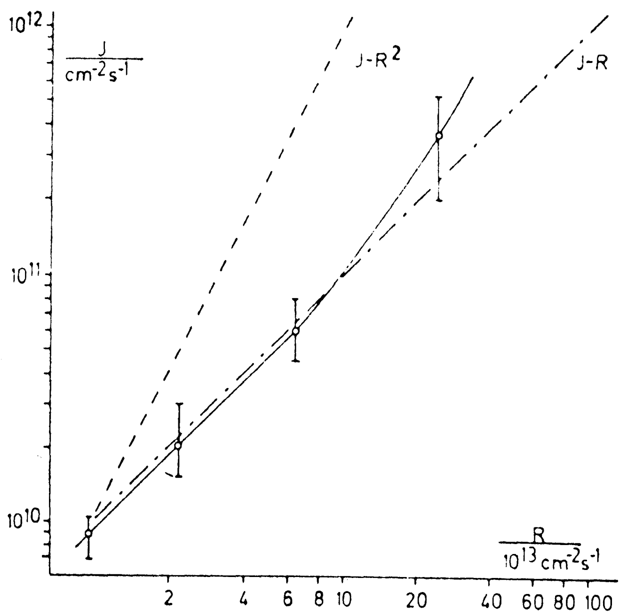

Fig. 7. Nucleation rate vs. deposition rate for normal and defect-induced nucleation (Au on mica, 475 K) [19]

2.3. PROCESSES DURING GROWTH OF NUCLEI

The stable nuclei randomly formed on the substrate surface grow by the diffusion and trapping of adatoms. This is especially the case for complete condensation of the impinging atoms. The second possibility is the direct impact of the atoms on the nuclei or clusters and the immediate sticking of the new atoms. This is the predomimant process in the case of incomplete condensation. Another possibility is a process - comparable to Ostwald ripening - in which single adatoms diffuse from smaller to larger nuclei. Finally, the complete migration of stable clusters was experimentally observed.

www.manaraa.com

Out of the three growth modes, the island growth (Volmer-Weber) can best be modeled. [e.g. 5,6]. In this model also the effect of surface defects [19], the deposition of binary alloys [20,21] and the initial stage of textured growth (epitaxy) [22] can unconstrainedly be described. The layer-by-layer growth (Frank-van der Merwe) can similarly be treated with respect to the first layer; the size of the stable nuclei, however, is markably larger. In modeling the further growth, the nucleation and growth processes have to be repeated in each layer. Concerning the Stanski-Krastanov mode, the initial stage corresponds to the layer growth. No modeling exists for the further growth. The mechanismus can, however, be studied by a number of experimental techniques, but their use and evaluation need a large effort, and in part a fundamental understanding is still missing [23].

Form the size distribution of the nuclei as a function of time conclusions can be drawn on the predominant growth mode. Figure 8 represents results for the deposition of Au on (100) NaCl crystals. The initially strong increase of the number of small nuclei is followed by a decrease of the number of nuclei and an increase of their size [24].

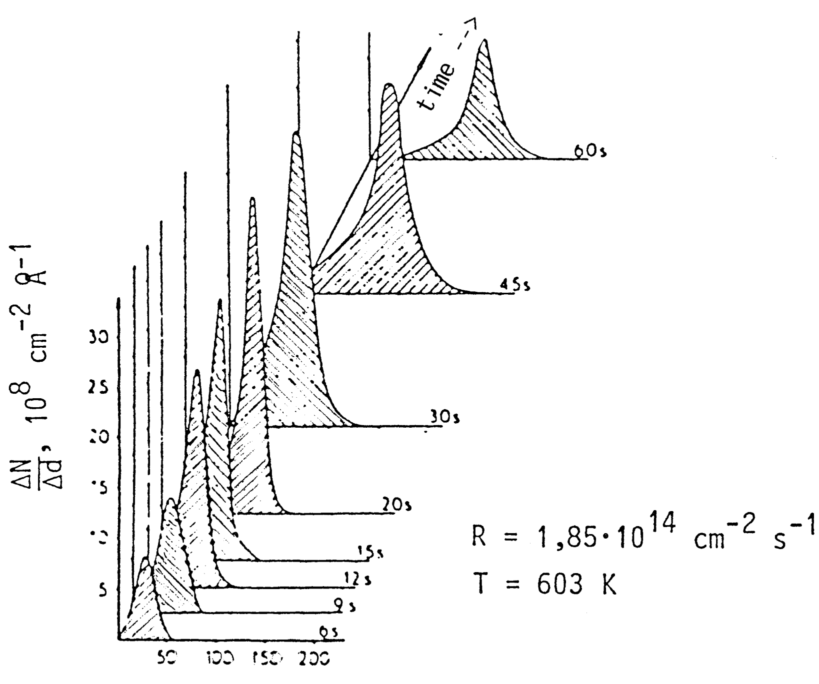

Fig. 8. Size distribution of Au nuclei on (100)NaCl [24]

www.manaraa.com

Typical size distributions for different processes are shown in Fig. 9 [25]. The predominant processes may differ for different temperatures and impingement rates even for the same film-substrate system. For Au/NaCl, e.g., the coalescence results from nucleus growth at 150 °C, while at 300 °C it is caused by nucleus mobility. In both cases the impingement rate was kept constant at 1×10^{13} atoms$\cdot$cm$^{-2}\cdot$s^{-1} [18].

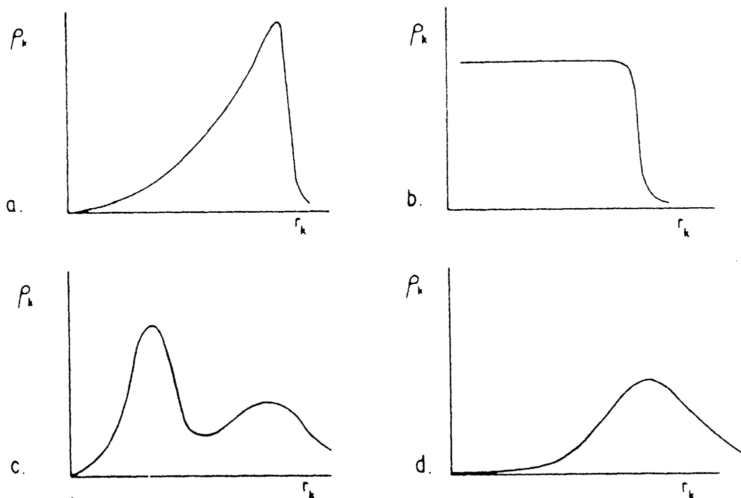

Fig. 9. Schematic size distribution when various processes are dominant. a: diffusion, no coalescence; b: direct impingement, no coalescence, c: coalescence by growth, d: coalescence by cluster mobility [25]

2.4 SPUTTER DEPOSITION AND ION PLATING

The discussion above has already shown the complexity of the nucleation and growth processes. They become even more complex if the films are dposited by sputtering or ion plating. In principal, the same processes occur at the substrate surface, but differences exist due to the presence of the working gas and the much higher energy of the impinging particles. In the case of sputtering, the sputtered atoms have energies in the range of 1 - 10 eV compared to 0.2 - 1 eV for evaporated atoms [26]. In the ion plating process the energy of the ions can easily be increased by the application of a substrate bias or by a high-energy ion source. The high-energetic particles can create defects on the substrate surface which act as trapping sites increasing the adsorption probability and resulting mono-atomic

المنارة للاستشارات
www.manaraa.com

stable nuclei. Hence, sputtered films exhibit a higher nucleation rate and, correspondingly, a higher nucleus density. The growth is comparable to the deposition from evaporation sources; no inert gas effect is noticed. For Au on NaCl with He sputter gas, the various dependencies can be evaluated from the experimental results using the kinetic nucleation theory [27]. Analogously, the ion plating processes cause a strongly increased nucleus density and decreased nucleus sizes (e.g. Au on (001)NaCl [28]).

2.5 REACTIVE DEPOSITION PROCESSES

During the reactive deposition of compounds like oxides, carbides or nitrides in principal the same processes take place as in the case of non-reactive deposition. The surface diffusivity of the adatoms, however, is reduced by the adsorbed gas atoms (N, O, C) as well as other surface contaminations of the substrate surface. Thus, formation and growth of the nuclei should be analogous to the non-reactive processes at lower temperatures. On the other hand, the heat of reaction deliberated during the compound formation can increase the effective substrate temperature. In the case of a plasma-assisted reactive deposition, the impingement and interaction of high-energetic particles (gases, metal-ions) has also to be considered, when a substrate bias is applied.

2.6 FILM DEPOSITION BY CVD

For chemical vapour deposition (CVD) the relatious are more complex because different gaseous species are adsorbed on the substrate surface and react with each other. In principal, these reactions can also take place in the gas atmosphere but with a much lower reaction probability. In detail the following partical reactions occur [30]:

$$\begin{array}{llcllcl}
\text{Gas phase:} & H_2(g) & + & 2\,AX(g) & \rightleftharpoons & 2\,A(g) & + & 2\,HX(g) \\
 & \uparrow\downarrow & & \uparrow\downarrow & & \uparrow\downarrow & & \uparrow\downarrow \\
\text{Adsorption:} & H_2(ad) & + & 2\,AX(ad) & \rightleftharpoons & 2\,A/Ad & + & 2\,HX(ad) \\
 & & & & & \uparrow\downarrow & & \\
\text{Nucleus:} & & & & & A(s) & &
\end{array}$$

The adsorbed atoms and molecules can desorb (re-evaporation), diffuse and form metastable and stable nuclei which grow and coalesce, then forming the continuous film. The partial steps correspond to those of the PVD nucleation and film formation, but the theoretical treatment is rather complex because almost nothing is known about the adsorbed radicals and intermediate products [31]. During the CVD deposition, a high degree of supersaturation of the species

المنارة للاستشارات
www.manaraa.com

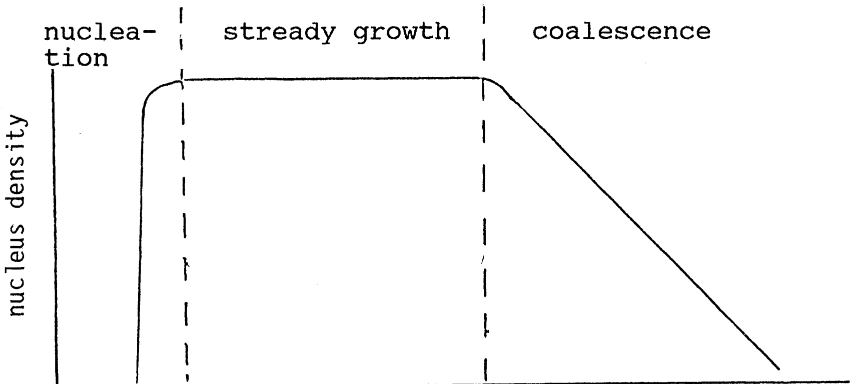

Fig. 10. Nucleus density for CVD (schematically) [30]

to be deposited exists. This means that quickly a high nucleus density at small nucleus sizes is reached. Figure 10 shows the nucleus density as a function of the deposition time. After reaching the maximum density, it remains constant for a certain time (steady growth), i.e. no new nuclei are formed, but the newly deposited atoms move to the existing nuclei and are trapped there. For longer deposition periods coalescence processes start and the number of nuclei decreases [30]. In the case of Al_2O_3 deposition on hard metal a growth of the nuclei in height and width is observed. The nuclei reach each other not directly on the surface but in a certain distance (Fig. 11). The film-substrate area is increased by a higher nucleus density, which in turn needs a high supersaturation of the relevant molecules in the gas phase [31].

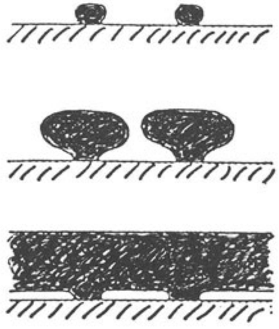

Fig. 11. Nucleation and growth of CVD-Al_2O_3 on hard metal [31]

المنارة للاستشارات
www.manaraa.com

2.7 EXPERIMENTAL INVESTIGATIONS

The experimental investigation of nucleation and growth processes needs a heavy effort, thoroughful sample preparation and advanced evaluation of the measured values. Most information can be obtained from evaporated films because the experiments can be performed under UHV conditions and no contaminations by the working or reactive gas occur. Within the frame of the present paper only the most often used techniques and their resulting conclussions shall shortly be mentioned. For experimental details the reader is referred to the original literature.

Transmission electron microscopy (TEM). TEM conbined with quantitative image analysis offers the most suitable technique for the investigation of formation and growth of the nuclei, expecially because of its high lateral resolution. The measurements yield information on nucleus density, saturations density, size distribution and degree of coverage. The deposition of precious metals on freshly cut alkali halide crystals can very successfully be studied after carbon deposition and film removal [14]. In-situ measurements are rather difficult because a UHV-TEM and thinned substrated are needed and the electron bombardment can cause defects and substrate heating both altering the nucleation process. In-situ observation yields information on diffusion and migration processes.

Auger electron spectroscopy (AES). AES is suited especially for the investigation of the growth modes. The intensity of the film and substrate elements depend characteristically on the time for all three growth modes [3]. A specific advantage of AES is its high sensitivity, being able to analyse coverages far below one monolayer.

Other surface analysis techniques. The other methods of surface analyses all suffer from a more or less pronounced limitation in their application. The electron spectroscopy for chemical analysis (ESCA - XPS, UPS) as well as low and reflected high energy electron diffraction (LEED, RHEED) need a relatively large surface area and, hence, are not applicable for investigations in the nm range. ESCA and AES show calibration problems. In special cases the scanning electron microscope (SEM) is also used nut shows also limited resolution and the problem of electron bombardment of the sample under investigation. Field electron and ion microscopy (FEM, FIM) are able to detect single atoms and clusters but need high experimental experience.

www.manaraa.com

3. Growth of "Thick" Films

In the following, in contrast to the initial states of film formation treated above, where only single nuclei and few atomic layers are considered, "thick" films shall be defined as sufficiently thick to define selection processes determing the coating structure. Structure zone models were developed for the coatings formed by vapour deposition, which correlate the observed structures with the predominant processes and the deposition parameters.

3.1 FUNDAMENTAL PROCESSES

As in the initial stage of nucleation, the partial steps condensation, surface diffusion and desorption are of importance also for the further growth of the film. At higher temperature the bulk diffusion in the crystals of the coatings plays an additional role. The coating structure, therefore, is determined by the impingement rate and substrate temperature. Figure 12 illustrates the structure development of vapour deposited films (evaporation source) for various conditions [32]. Generally, the growth of "thick" films starts at discrete nuclei. For a parallel flow of perpendicular direction and a low substrate temperature with almost no surface diffusion, single free-standing crystallites are formed. The crystal planes of high condensation probabilities grow preferentially. The coating structure is open and shows a rough surface topography (Fig. 12a). In the case of a slightly varying direction of the impinging atoms and a complete condensation, the initially spherical nuclei grow, coalesce and a dense colemmar caoting structure is developed having a relatively smooth surface topography. The orientation of the crystallites is determined by the orientation of the initial nuclei (Fig. 12b). At higher substrate temperatures differences in the condensation coefficients can easily be balanced; all crystal planes grow with the same rate. Dense structures with a relative smooth but facetted surface are formed (Fig. 12c). If repeated nucleation occurs, a structure corresponding to Fig. 12d is observed.

At low substrate temperatures, i.e. vanishing surface diffusion, shadowing effects are observed which result in a porous coating structure composed of single, free-standing crystallites. The shadowing is caused by an increased condensation rate at exposed sites of the substrate (shape of the nuclei, surface roughness) compared to lower, more hidden areas.

This phenomenological description of the structures developing in evaporation or sputter deposition results in different structure zone models (see below).

www.manaraa.com

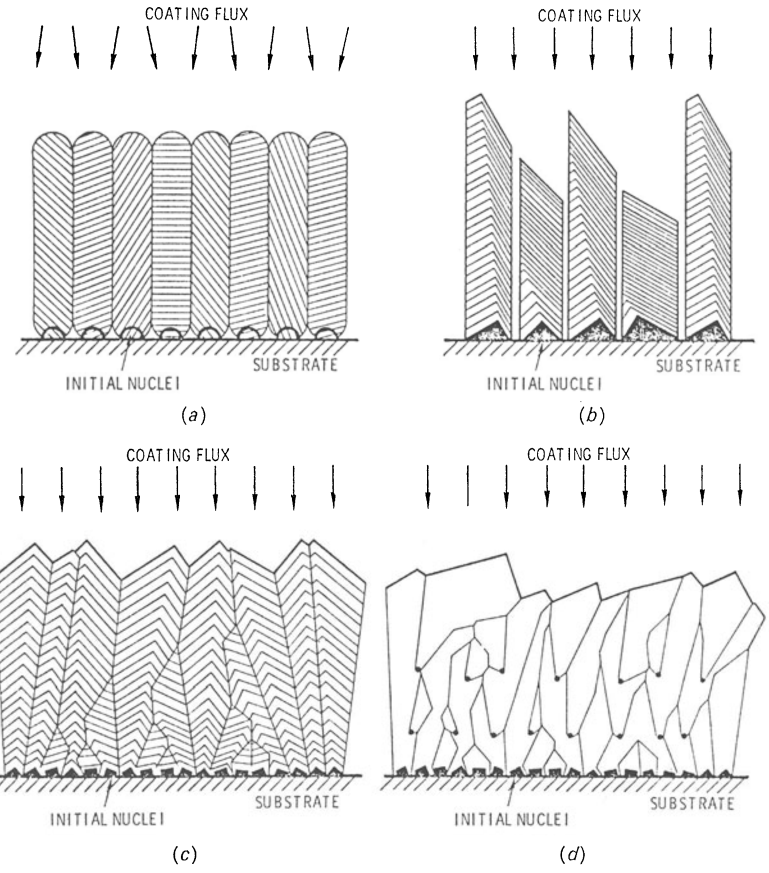

Fig. 12. Structure development under various conditions [32]

3.2 MODELING OF FILM GROWTH

As mentioned above, columnar crystallites are formed in vapour-deposited films. Very offen they also exhibit a preferential orientation (texture) because of the preferred growth in certain lattice directions. A detailed discussion at the principles of the selection criteria is given by v.d.Drift [33]. The films are textured even if the nuclei are randomly oriented. It is assumed that the vertical growth rate is as more pronounced as steeper the orientation of the crystallite is (Fig. 13). As higher the vertical growth rate, as easier a crystallite with a more fa-

www.manaraa.com

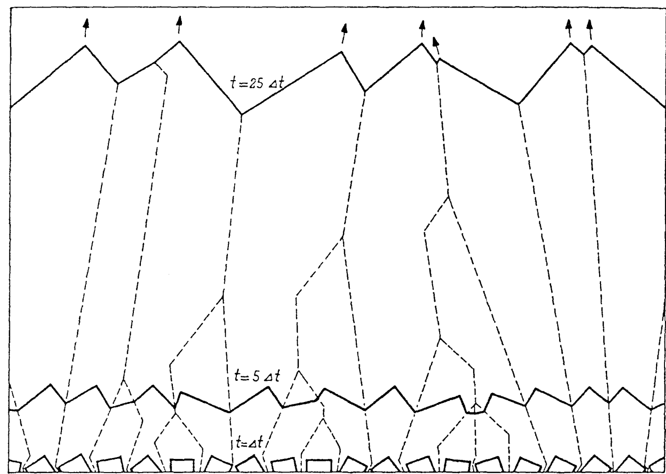

Fig. 13. Modeling of film growth for randomly oriented cubic nuclei [33]

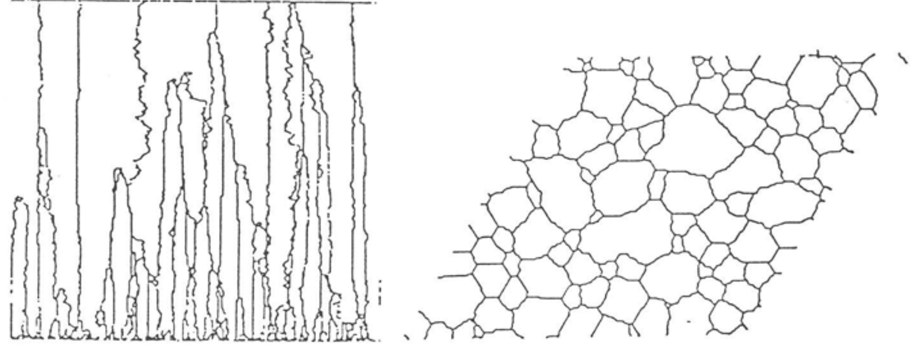

Fig. 14. Monte-Carlo modeling of film growth [34]

vourable orientation can grow compared to less favorably oriented neighbouring crystallites. Real system exhibit a somewhat more complex situation, but the same principles of film growth are followed. The structure development is characterized by the condensation probability of the impinging atoms on the different crystal planes and by the surface diffusion. The condensation probability can also depend on the angle of incidence.

www.manaraa.com

The development of the structure of vapour deposited films was calculated by a Monte-Carlo modeling, taking into consideration also the atoms diffusion on the film surface and the processes resulting in grain bondary migration. This means that recrystallization processes are also regarded. Figure 14 shows an example of the structure in longitudinal and cross section.

3.3 STRUCTURE ZONE MODELS

On the basis of the film structures observed with PVD films, structure zone models were established and modified. The phenomenological description correlates the physical processes (condensation, surface diffusion, bulk diffusion, recrystallization) with the structure as a function of substrate temperature and other deposition parameters.

First, Movchan and Demchisin [35] defined three structure zones in evaporated films (0,3 - 2 mm thick) depending on the homologous temperature (T_S/T_m; T_S = substrate temperature, T_m = melting temperature), see Fig. 15. Zone 1 is characterized by a porous structure of free-standing columnar crystals with rounded tips. The internal structure is poorly defined and exhibits a high dislocation density. The diameter of the crystellites increases with rising temperature. Such a structure is caused by the above-mentioned shadowing effects when the surface diffusion is negligible. At higher temperatures, diffusing atoms can fill the voids and a dense structure consisting of colummar grains is formed (zone 2). The film surface is rather smooth. The grain size again increases with rising substrate temperature. At very high temperatures, recrystallization pro-

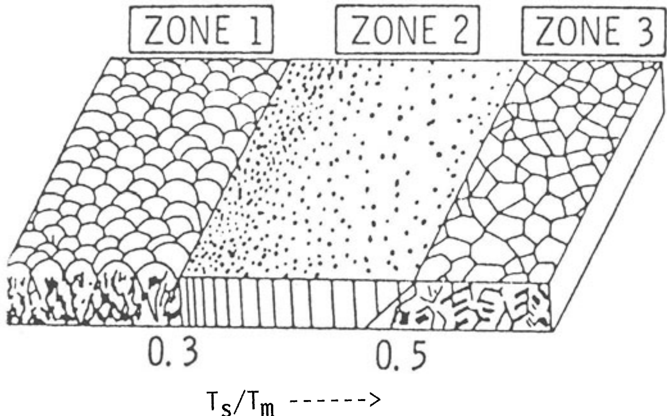

Fig. 15. Structure zones after Movchan and Demchisin [35]

المنارة للاستشارات
www.manaraa.com

cesses can occur already during the film deposition and a dense coarse-grained structure is observed (zone 3). The temperature ranges are found to be $T_S/T_m < 0.3$ (zone 1), $T_S/T_m = 0.3 - 0.45$ (zone 2) and $T_S/T_m > 0.45$ (zone 3) of metals are deposited. For oxide films analogous structures were observed with a somewhat smaller temperature range of zone 2 ($T_S/T_m < 0.26$).

A similar structure zone classification was given by Sanders [36]. The zones 1 and 2 are, however, shifted to lower temperatures, i.e. $T_S/T_m < 0.1$ and $T_S/T_m = 0.1 - 0.3$, respectively.

The Movchan-Demchisin model was modified by Thornton [37] considering the sputtering atmosphere as additional parameter (Fig. 16). The structure zones are shifted to higher temperatures with increasing inert gas pressure. In detail, the zones are charaterized as follows: zone 1: porous, tapered crystallites seperated by voides; zone T: (newly introduced): densely packed fibrous grains; zone 2: columnar grains, and zone 3: recrystallized grain structure. The effect of the inert sputtering atmosphere is not known in detail. The adsorption of impurities (from the sputtering atmosphere) seems to reduce strongly the surface mobility of adatoms. This relation would also reflect the fact that the inert gas pressure does not affect the structure at higher temperatures because the gas adsorption does

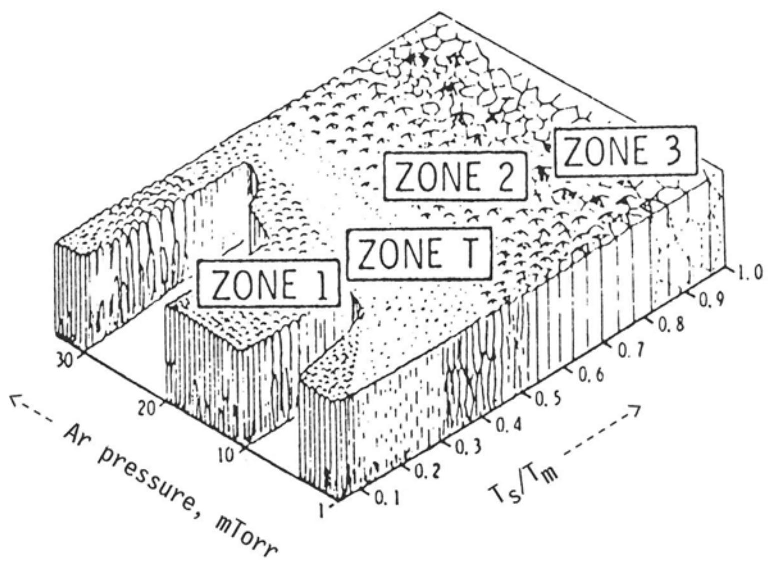

Fig. 16. Structure zones after Thornton [32]

www.manaraa.com

not play a role any longer. Intense ion bombarding during the deposition (bias sputtering, ion plating) the development of the open structure of zone 1 is strongly reduced. It is attributed to the formation of nucleation centers or the smoothening of the surface roughness [38] as well as a sputter-induced redistribution of film material [39]. On the basis of these finding, Thornton's model was modified by Messier et al. [15] in order to show the influence of the energy of the incident ions. As can be seen from Fig. 17, the transition zone T is widened to lower temperatures at the expense of zone 1. This is caused by an ion bombardment-induceds mobility of the surface atoms. The revised structure zone model shows the equivalence of thermal and ion beam-induced mobility.

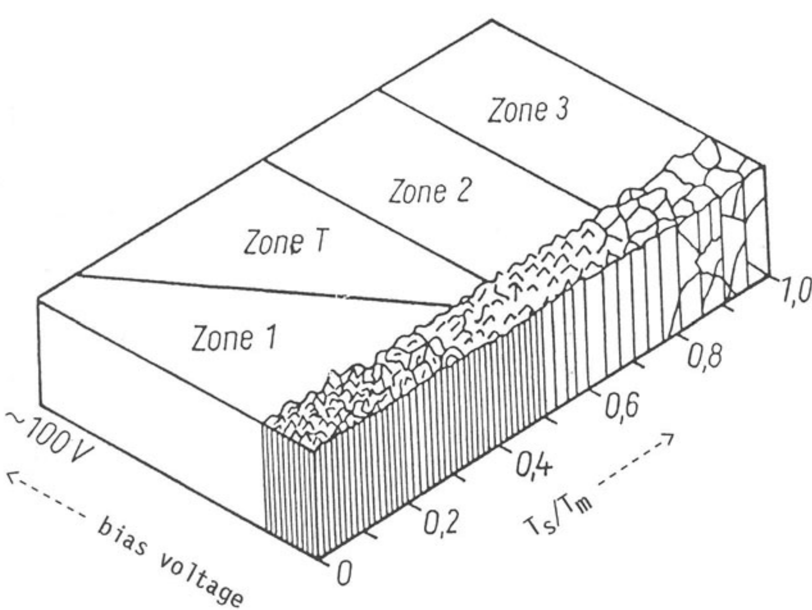

Fig. 17. Structure zone modification by ion-assisted vapour deposition after Messier [15]

All the structure zone models reflect the effect of substrate temperature, impinging rate, gas pressure and substrate bias on the film structure. In addition, the position of the substrate in relation to the source, i.e. the angle of incidence, affects the structure as well as substrate pretreatment (mechanical, chemical cleaning). Finally, high energy ion bombardment during the deposition results in lattic defects in the crystallites.

المنارة للاستشارات
www.manaraa.com

All models discussed above describe the growth and structure of elemental coatings like metal films. For evaporated or sputtered compound film or reactively formed coatings, however, a quantitative relation to the existing structure zone models is difficult because no information is available on the melting temperature to be used and on the surface diffusion of the different kinds of atoms. Principally, the same structure zones are observed for multicomponent films as for elemental ones. This, e.g. has been proved in many investigations on the structure of hard coatings. In the case of (TiAl)N on HSS steel coatings the experimental results showed a structure correlated with a higher substrate temperature than actually applied. This could be caused in part by the heat of reaction. On the other hand, no information exists on the diffusion behaviour of the nitride molecules compared to the case of metal deposition.

4. Conclusions

The inital stages of formation and growth of nuclei can be model+ed by the kinetic nucleation theory regarding atomic bonding and diffusion as well as the phenomenological thermodynamic description. Experiments in model systems verify the theories and yield quantitative data for the system regarded. The most important parameters are rate of impingement and substrate temperature.

The film growth depends on the same parameters. Structure zone models were established considering the deposition parameters. Theoretical calculations can explain the experimental findings.

All models hold only for deposition under UHV conditions. Contamination of the surface is not regarded as is a multiphase substrate. The structure zone, however, are also found with compound films and for reactive deposition.

Thus, the theoretical models help to understand the processes, but only to a limited extend to select quantitatively the deposition parameters. In practical the conditions of the deposition process and the surfache properties of the substrate material are too complex.

References

[1] Venables, J.A. and Spiller, G.D.T. (1981), in Th. Binle (ed.), Surface Mobilities on Solid Surfaces, Plenum Press, New York, NATO-ASI pp. 339-402

[2] Venables, J.A. and Price, G.L. (1975), 'Nucleation of thin films', in J.W. Matthews (ed.), Epitaxial Growth, Pt. B, Academic Press., New York, pp. 381-436

www.manaraa.com

[3] Kern, R., Melay, G. and Metois, J.J. (1979), in E. Naldis (ed.), Current Topics in Material Science, Vol. 3, North Holland, Amsterdam, Chapt. 3

[4] Vook, R.W. (1982) 'Structure and growth of thin film', Int. Met. Rev. 27, 209-245

[5] Zinsmeister, G. (1966), in Niedermayer und H. Mayer (eds.), Vandenhoek and Ruprecht, Göttingen, pp. 19

[6] Schmeisser, H. and Harstdorff, M. (1970) 'Studies on the nucleation of gold on NaCl single crystal planes in UHV', Z. Naturforsch. 25 a, 1896-1901

[7] Reichelt, K. (1986) 'Nucleation growth of films', in Dünne Schichten und Schichtsysteme (Lecture Notes, 17th IFF Ferienkurs), KFA Jülich,

[8] Adam, R.W. (1968) 'Investigations on the epitaxy of thin vapour-deposited gold films on alkaline halides in ultra high vacuum', Z. Naturforsch. 23a, 1526-1536

[9] Becker, R. and Döring, W. (1935), Am.Phys. 24, 719

[10] Hirth, J.P. and Pound, G.M. (1963) 'Condensation and evaporation', Pergamon, London

[11] Zinsmeister, G. (1968) 'Theory of thin film condensation, Pt.B: Solution of the simplified condensation equation', Thin Solid Film 2, 497

[12] Harsdorff, M. (1968) 'Oriented deposition of material on single crystalline surface', Z. Naturforsch. 23a, 1253-1258

[13] Bauer, E. and Poppa, H. (1972) 'Recent advances in epitaxy', Thin Solid Films 12, 167-175

[14] Robinson, V.N.E. and Robins, J.L. (1970) 'Nucleation kinetics of gold deposition onto UHV-cleaved surfaces of KCl and NaF', Thin Solid Films 5, 313-327

[15] Messier, R., Giri, A.P. and Roy, R.A. (1984), J. Vac. Sci.Technol. A2, 500

[16] Honjo, G. and Yagi, K. (1980), in E. Kaldis (ed.), Current Topics in Matierals Science, Vol. 6, North Holland, Amsterdam, Chapt. 3, p. 195

[17] Takayanagi, K., Yagi, K., Kobayashi, K. and Honja, G. (1978), 'Techniques for routine UHV in-situ electron microscopy of growth processes of epitaxial thin films', J. Phys. E 11, 441

[18] Donohoe, J.A. and Robins, J.L. (1972) 'Mobility and coalescence of nuclei in metal vapour deposition on alkali halide substrates', J. Cryst. Growth 17, 70

[19] Cardoso, J. and Harsdroff, M. (1978) 'The influence of surface defects on the heterogeous nucleations and growth of thin films', Z. Naturforsch. 33 a, 442

[20] Anton R., and Harsdorff, M. (1977) 'Extension of the kinetic nucleation model to binary alloys', Thin Solid Films 44, 341-350

[21] Anton, R., and Harsdorff, M. and Martens, Th. (1979) 'Nucleation and growth of binary alloys on single crystalline substrates', Thin Solid Film 57, 233-239

www.manaraa.com

[22] Puskeppel, A. and Harsdorff, M. (1976) 'Epitaxial nucleation of gold on potassium bromide (100) surfaces', Thin Solid Films, 35, 99
[23] Venables, J.A. (1983) 'Nucleation and growth of thin films: recent progress', Vacuum 33, 701
[24] Schmeisser, H. (1974) 'Growth and mobiliy effects of gold clusters on rock salt (100) surfaces studied with the method of quantitative image analysis. I. - Cluster size distributions', Thin Solid Films 22, 83-97; 'II. - Spatial distribution of clusters', Thin Solid Films 22, 88.119
[25] Venables, J.A. (1976) 'Capability and limits of nucleation theories', Thin Solid Films 32, 135-141
[26] Stuart, R.V., Welmer, G.K. (1964) 'Energy distribution of sputtered Cu atoms', J. Appl. Phys. 35, 1819-1824
[27] Harsdorff, M. and Jark W. (1985) 'Nucleation and growth kinetics of gold films deposited onto rock salt single crystal (100) surfaces by R.F. sputtering with helium', Thin Solid Films 128, 79-92
[28] Kashiwagi, K. and Murayama, Y. (1984) 'Effects of ionized particles on the growth processes of films formed by ion plating', J. Metal Finsh. Soc. Jap. 35, 32
[29] Robin, J.L. (1979) 'Problems and progress in describing quantitatively the development of thin film deposits', Surface Sci. 86, 1-13
[30] Venable, J.A. (1973) 'Rate equation approaches to thin-film nucleation kinetics', Phil. Mag. 27, 698
[31] Johannesson, T.R. and Lindstrom, J.N. (1975) 'Factors affecting the initial nucleation of alumina on cennented carbide substrates in the CVD process', J. Vac. Sci. Technol. 12, 854-857
[32] Thornton, J.A. (1977) 'High rate thick films', Rev. Mater. Sci. 7, 239-260
[33] v.d.Drift, A. (1967) 'Evolutionary selection, a principle governing growth orientation in vapour deposited layers', Philips Res. Repts. 22, 267-288
[34] Srolovitz, D.J. (1986) 'Grain growth phenomen a in films: A Monte-Carlo approack', J. Vac. Sci. Technol. A4, 2925-2931
[35] Movchan, B.A. and Demchisin, A.V. (1969) 'Study of the structure and properties of vacuum condensates of Ni, Ti, W, Al_2O_3 and ZrO_2', Phys. Metals Metallogr. 28, no. 4, 83
[36] Sanders, J.V. (1971), in J.R. Anderson (ed.), Chemisorption and Reaction of Metallic Films, Academic Press, London, pp.1
[37] Bland, R.O., Kominiak, G.J. and Mattox, D.M. (1974) 'Effect of ion bombardment during deposition of thick metal and ceramic deposits', J. Vac. Sci. Technol. 11, 671

www.manaraa.com

[38] Thornton, J.A. (1977) 'The influence of bias sputter parameters on thick copper coatings deposited using a hollow cathode', Thin Solid Films 40, 335

[39] Jehn, H.A., Kopacz, U. and Hofmann, S. (1986) 'Effect of substrate temperature and sputtering atmosphere on the properties of magnetron-sputtered nitride coatings', Proc. PVD '86 (2nd Intern. Meeting, Darmstadt 1986), TH Darmstadt, pp. 131-143

[40] Jehn, H.A. Hofmann, S. Rückborn, V.E. and Münz, W.-D. (1986) 'Morphology and properties of magnetron-sputtered (Ti, Al)N layers on HSS substrates as a function of depostion temperature and sputtering atmosphere', J. Vac. Sci. Technol. A4, 2701-2705

المنارة للاستشارات

www.manaraa.com

INTERFACES AND ADHESION

S.J. Bull
Surface Science and Technology Department
AEA Industrial Technology
Harwell Laboratory
Oxfordshire, OX11 0RA, U.K.

ABSTRACT. In most applications the minimum criterion for adequate coating performance is that it remains attached to the substrate over the lifetime of the component. Control of the factors affecting adhesion is thus essential and this equates to careful control of the structure and composition of the interfacial layers if the best performance of the coating is to be achieved. Practical adhesion is a macroscopic property which depends on chemical and mechanical bonding at the interface, residual stress and the presence of any stresses imposed by the application and the mechanism of interfacial failure which depends on the coating and substrate materials and the working environment. In this paper the mechanisms of adhesion and how these relate to interfacial structure are discussed in detail. In addition techniques for assessing and improving adhesion are also reviewed.

1. Introduction

The use of coatings to modify the surface properties of engineering materials independent of their bulk properties is now well established. It is extremely important that such coatings should be adherent without degrading the performance of the substrate and this has led to the development of a range of techniques to improve adhesion and monitor these improvements. However, to fully understand the effects of these treatments and the results of any adhesion test it is necessary to determine the structure and composition of the interfacial region and how this affects failure within it. In the following sections the factors influencing adhesion and the adhesion tests used for a range of coatings will be discussed in terms of the interfacial structure.

W. Gissler and H. A. Jehn (eds.), Advanced Techniques for Surface Engineering, 31–68.
© 1992 *ECSC, EEC, EAEC, Brussels and Luxembourg.*

www.manaraa.com

2. Practical versus Basic Adhesion

The fundamental property of adhesion is defined by the American Society for Testing and Materials (ASTM) [1] as " the state in which two surfaces are held together by interfacial forces which may consist of valence forces or interlocking forces or both." The nature of these forces may be van der Waals, electrostatic and/or chemical bonding forces which are active across the coating/substrate interface. The approximate ranges of binding energies have been considered by a number of workers [e.g. 2] and typical values are shown in Figure 1. In addition to the types of bonding listed in the Figure it is also possible to achieve adhesion by mechanical interlocking of coating and subatrate which produces bond strengths comparable to that of electrostatic or metallic bonding but which cannot strictly be expressed in terms of an energy per bond. It is clear from Figure 1 that covalent or ionic bonding leads to much greater levels of adhesion than electrostatic bonding or mechanical interlocking. The Basic Adhesion (BA) of a coating/substrate system is thus a maximum possible attainable value and can differ substantially from the measured Practical Adhesion (PA) which may be referred to as the bond or adhesion strength [3]. The relationship between BA and PA is given by [4]

$$PA=f(BA, \text{other factors}). \qquad (1)$$

PA«BA owing to the influence of difficulties with the in-service conditions or measuring technique and other factors such as interfacial flaws and residual stress. Pulker et al [4] further define the relationship between experimentally observed and basic adhesion as

$$PA=BA-IS\pm MSM, \qquad (2)$$

where IS is the internal stress factor and MSM is a method-specific error in measurement. Both of these factors increase the discrepancy between basic and measured adhesion and it is soon apparent that most measurement techniques can never give a true measure of adhesion because of the inherent measurement errors. This is further complicated by the existence of interfacial structure, rather than atomically sharp interfaces, and the mechanisms of failure induced in most adhesion tests. These are discussed in more detail in later sections.

3. Interfacial Structures

There are a number of possible interfacial structures the most common of which are shown schematically in Figure 2. The type of interface formed

www.manaraa.com

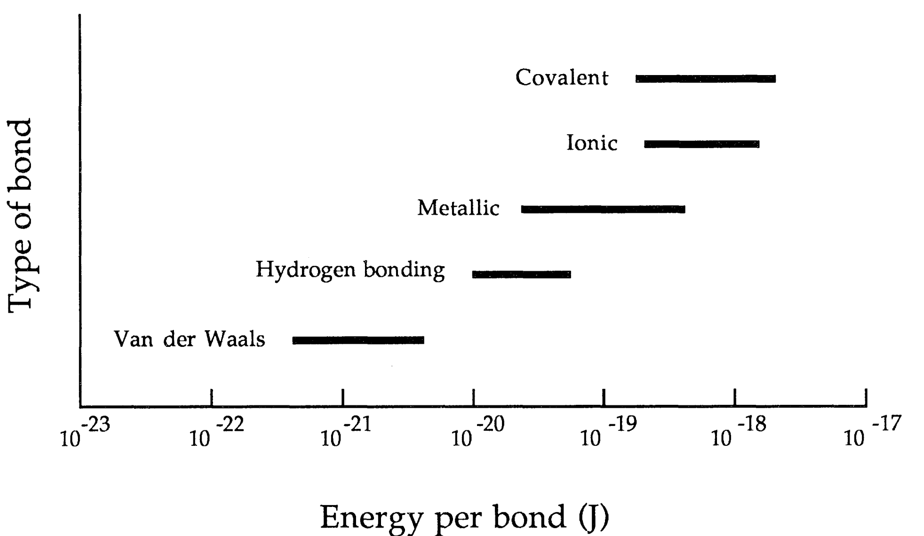

Figure 1: Relative bond strengths for a range of potential interfacial binding forces.

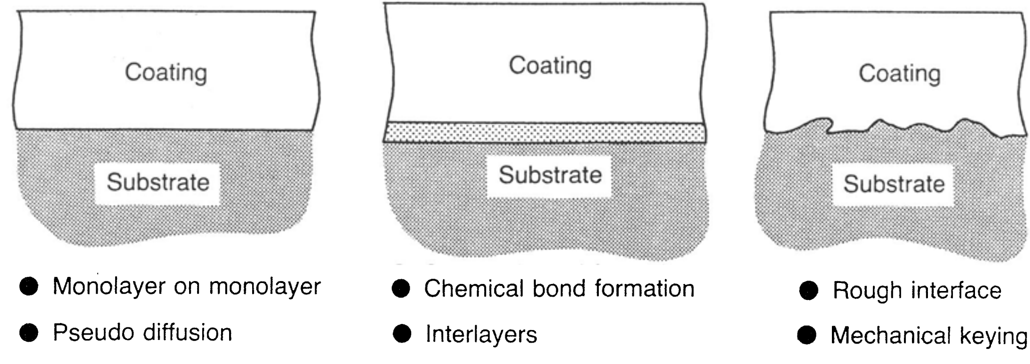

Figure 2: Types of interface formed between coating and substrate.

المنارة للاستشارات
www.manaraa.com

during deposition depends on the substrate surface morphology, contamination, chemical interactions, the energy and flux of arriving particles and the nucleation behaviour of depositing atoms.

When atoms impinge on a surface they do not immediately become bound to it but lose energy to the surface and move about until they are captured at a suitable site. In the early stages of film growth adatoms will condense into stable nuclei and the spacing and size of these nuclei will determine the interfacial structure of the coating. A strong substrate/coating atom interaction will result in low adatom mobility and a high density of nuclei whereas a weak interaction will result in more widely spaced nuclei. These nuclei will then grow to form a continuous film, during which the rate at which lateral spreading of the nuclei occurs will influence the effective porosity at the interface as well as the nucleation density. The nucleation density and the size of individual nuclei will determine the effective contact area between coating and substrate which can be directly related to adhesion. In general an increase in nucleation density is desirable if the adhesion of a film is to be improved. This is particularly important in the case of diamond thin films and hence substrate preparation techniques have been developed to increase the nucleation density and hence coating density and adhesion [e.g. 5]. In this case it is difficult to grow continuous films unless steps are taken to increase the nucleation density by, for instance, abrading a silicon substrate with diamond grit. The nucleation density can be increased by ion bombardment (and hence reducing the gas pressure in sputtering systems) [6, 7], substrate defects [5] and special deposition techniques [8]. The presence of surface impurities [9] and contamination [10] has a tendency to reduce nucleation densities.

Mechanical keying of the surface can be produced by roughening the surface of the substrate prior to coating. This technique is often used for thick plasma sprayed coatings [11]. There is a tendency to increase the effective area of contact between coating and substrate by such an approach which leads to improvements in adhesion in a similar manner to the increases in nucleation density described previously. Significant interlocking of coating and substrate is rarely produced so such interfaces cannot be regarded as entirely mechanical and some bonding between coating and substrate is necessary. This is promoted by the damage caused by the roughening process since it has been observed that the improvement in adhesion of plasma sprayed coatings produced by grit blasting is much greater than the change in interfacial area produced by the treatment [12].

In low temperature deposition processes and in the absence of any ion bombardment it is possible to achieve a monolayer to monolayer interface between coating and substrate. In such cases the change from coating to substrate material occurs over a distance of the order of the separation of atoms (2-5Å). For this to occur there needs to be little or no diffusion or

www.manaraa.com

chemical reaction between the coating and the substrate. This may be due to a lack of solubility between the two materials, the availability of little or no reaction energy or the presence of contaminant layers. In this type of interface defects and stresses are confined to a very narrow region and adhesion is often poor.

If reaction between coating and substrate can occur a compound interfacial layer can be formed which may appear as a discrete layer. Such layers can be beneficial but if a brittle layer is produced this can be detrimental to adhesion. Often during the formation of such compound layers there are segregations of impurities at the phase boundaries and stresses generated due to lattice mismatch or differences in thermal expansion [13]. As the deposition or service temperature increases the potential for the formation of interfacial phases is also increased. It is clear that long term assessments of interfacial phase formation are necessary if coatings are to be used at high temperatures successfully. The interactions between coating and substrate may need to be prevented by the use of a diffusion barrier if any deleterious interfacial reactions occur.

High temperature deposition or service may not necessarily lead to compound formation but it is possible to achieve significant interdiffusion between coating and substrate. In such interfaces there is a gradual change in composition, residual, and applied stress across the interfacial region and this usually leads to very good adhesion. If there is a marked difference in the diffusion rates of coating and substrate atoms Kirkendall porosity may be formed in the interfacial region [14]. This is often very detrimental to adhesion.

Under conditions of energetic deposition involving plasmas or ion bombardment a pseudo-diffusion type of interface may be formed by materials which are normally insoluble. Ion bombardment may increase the substrate solubility of coating atoms by direct implantation or by the introduction of point defects [15] and stress gradients [16] which promote diffusion.

4. Interfacial bonding, structure and adhesion

A simplistic picture of the adhesion of a coating to a substrate might be gained by taking the sum of the strengths of the individual chemical bonds across the interface. The interfacial energy should then be the summation of all the interfacial bond energies minus any interfacial strain and defect energies. In such cases the adhesion strength would increase as the bond strength increases and from the data in Figure 1 it might be expected that the best adhesion would be obtained for covalent or ionic bonded interfaces. Indeed in cases where there is little tendency for the coating to react with the substrate

www.manaraa.com

the adhesion is normally poor reflecting the fact that the bonding is dominated by Van der Waals forces.

Electrostatic bonding may be regarded as a special case of physisorption and also leads to relatively poor adhesion [17]. When two materials of very different electron affinities are brought together an electrical double layer forms which contributes to the adhesion (as has been suggested is the case for evaporated metal coatings on polymers [18]). Adhesion can be improved by increasing the strength of the electrostatic bonding; increasing the number of charged defects in ceramics would lead to an effective increase in the adhesion of a metal coating due to the formation of oppositely charged image charges in the metal [19]. However, such effects will only be important in cases where there is little or no chemical bonding between coating and substrate. When the coating is deposited under conditions where ion bombardment can promote some ionic or covalent chemical bonding at the interface considerable increases in adhesion have been reported; this is the basis of some of the adhesion improvements reported in ion beam assisted deposition [20].

However, in practice the simple model of the coating/substrate system with coating and substrate separated by a flat planar interface almost never occurs as described in the previous section. Adhesion is generally much better in cases where there is a more gradual change from coating to substrate as produced by interdiffusion or mixing by ion bombardment. In such layers a complex mixture of chemical bonding can occur and the interfacial layer can minimise interfacial stress gradients and the mismatch in properties between coating and substrate. It is often difficult to identify the position of the interface in such cases; failure is nucleated at some weak point in the interfacial region which may be associated with contamination which is different to the highly localised failure initiation events when a well-defined interface is present. In addition, the type of failure is important; in cases where covalent and ionic bonds dominate in the interface, brittle fracture can occur, whereas the failure is often more ductile for metallic bonding. Thus, despite the higher bond energies of the ionic and covalent bonds, metallic bonded interfacial layers tend to show higher levels of practical adhesion [21].

Another important factor in interfacial bonding is chemical reaction at the interface to produce new phases during coating. This is often a very deposition temperature-dependent process and will also depend on the substrate and coating materials and any interfacial contamination. For instance the use of a titanium interlayer has been found to improve the adhesion between titanium nitride coatings and an M50 tool steel substrate [22]. Cross sectional transmission electron microscopical analysis shows that this occurs because the titanium interlayer has transformed to titanium carbide as a result of carbon diffusing from the substrate during coating.

المنارة للاستشارات
www.manaraa.com

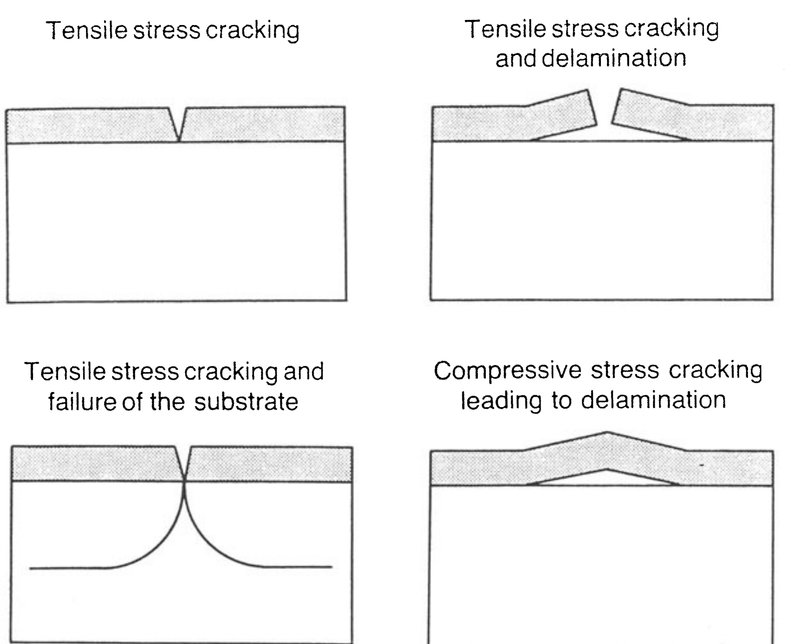

Figure 3: Schematic diagram of the surface cracking which can lead to coating detachment under compressive or tensile stresses.

5. Mechanisms of Interfacial Failure

Depending on the brittle/ductile properties of the coating and substrate a number of possible failure modes can occur in any application [23]. The major failure modes are shown schematically in Figure 3. Although the failure may start at the interface it can propagate in to the substrate. Alternatively, through-thickness cracking can lead to failure at the coating/substrate interface. Both tensile and compressive applied stresses can generate failure and the location of the failures will depend on the brittleness of the substrate and coating (see Tables 1 and 2). In the simplest case such applied stresses may be the internal stresses within the coating which are introduced during coating, or the thermal expansion mismatch stresses which arise on cooling to room temperature from the deposition temperature. Such stresses often limit the maximum thickness to which a coating can be deposited before spallation occurs spontaneously.

Interfacial failure leading to loss of the coating is mainly dependent on fracture. For most systems two distinct fracture properties are important, namely the stress required to initiate fracture and the stress required for propagation. The initiation stress is a function of the distribution of flaws in the interfacial region which will depend on surface contamination and

المنارة للاستشارات
www.manaraa.com

Table 1: Tensile failure modes for thin films

Film	Substrate	Interface bonding	Decohesion mechanism(s)
Brittle	Ductile	Good Poor	Film cracking - no decohesion Film cracking - interface decohesion
Ductile	Brittle	Good Poor	Edge decohesion in substrate Edge decohesion at interface
Ductile	Ductile	Good Poor	Film/substrate splitting - substrate decohesion Edge decohesion at interface
Brittle	Brittle	Poor	Edge decohesion at interface (higher film toughness) Film cracking - interface decohesion

Table 2: Compressive failure modes for thin films

Film	Substrate	Interface bonding	Decohesion mechanism(s)
Brittle	Ductile	Good Poor	Buckle propagation in film Buckle propagation at interface
Ductile/ Brittle	Brittle	Good Poor	Substrate splitting Buckle propagation at interface
Ductile	Ductile	Good Poor	No decohesion Buckle propagation at interface

المنارة للاستشارات
www.manaraa.com

coating processing as well as on the choice of substrate and coating. The crack propagation stress is influenced to a much greater extent by interfacial structure and composition. In a ductile material the stress at the tip of the crack is relaxed by plastic deformation of the surrounding material and thus a larger amount of energy is necessary to propagate the crack than for a brittle material where this does not occur. For this reason the area of interfacial cracking is much less for a ductile material than a brittle material under similar loading conditions and the adhesion of coatings onto substrates where failure occurs in a ductile fashion is apparently much better than for brittle substrates [24]. Control over the initiation of failure can often be achieved by improving the cleanliness of the coating system whereas control of the crack propagation behaviour requires a much more detailed understanding of interfacial composition. For this reason it is important to characterise the failure modes associated with any application and tailor the interfacial region so that ductile failure occurs in a region of high strength.

6. Factors affecting Adhesion

Clearly, from the previous sections it can be seen that adhesion is a complex phenomenon and there are a number of factors which can influence it. For adequate in-service performance of many coating/substrate combinations it is necessary to control as many of the factors affecting adhesion as possible and this involves careful selection of coating material and substrate as well as control of component manufacture and coating processes. The following factors are important:

1) Coating and substrate material dependent:

> 1) Interfacial bonding (ionic, covalent, metallic, Van der Waals etc.);
> 2) Interfacial phases (native oxides, reactions during deposition);
> 3) Surface Roughness (area of contact, coating uniformity etc.);
> 4) Substrate preparation (white layers, grinding burn, reaction layers etc.).

2) Coating process dependent:

> 1) Choice of deposition technology;
> 2) Contamination;
> 3) Deposition temperature;
> 4) Ion bombardment;
> 5) Interlayers;
> 6) Residual stress.

المنارة للاستشارات

www.manaraa.com

3) Service dependent:

1) Applied stress;
2) Operating environment (temperature, atmosphere, etc.);
3) Long term coating/substrate reactions.

For most applications the requirements of coating and substrate and the in-service conditions are well-defined and the coating process has to be adjusted to maximise the adhesion of the coating to the substrate. A number of techniques have been developed to achieve this and some of these are discussed in more detail in the next section.

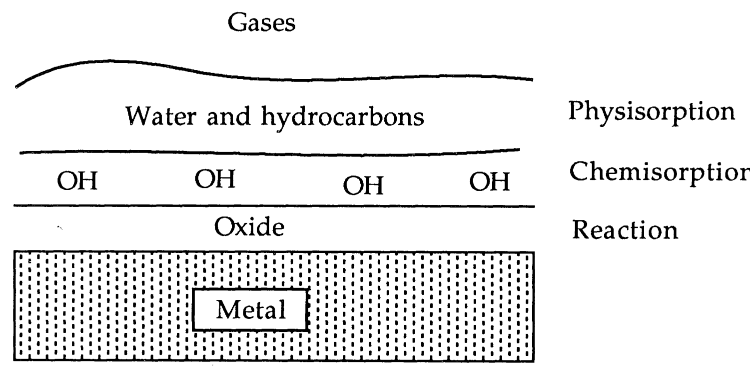

Figure 4: Surface contamination layers on a typical metal surface.

7. Techniques for Improving Adhesion

In order to improve the adhesion of a coating to its substrates a number of techniques have been developed which can be divided into three categories:-
1) Pretreatments - cleaning and degreasing of components prior to loading coating system,
2) In situ treatments - such as heating, plasma treatment, sputter cleaning,
3) Bonding layers - to form strong interfacial phases, minimise interfacial stresses and getter (i.e. dissolve) contaminants.

المنارة للاستشارات

www.manaraa.com

Most coating processes will use several different treatments prior to deposition of the coating material and thus cleaning is a multi-stage process for which there are many possible variations.

The development of techniques for improving coating/substrate adhesion has been based on a knowledge of the types of surface structures which are present on substrate materials and how this influences the coating process. A typical metal surface is shown schematically in Figure 4. Most metal surfaces are covered by an oxide layer which can be up to a few tens of nanometres thick depending on the material. Strongly bound chemisorbed layers are attached to the outer surfaces of this with much weaker physisorbed layers on top of them. Such layers consist predominantly of water but there will be an increasing amount of hydrocarbon contamination towards the surface of the contamination layer. In order to promote adhesion between coating and substrate it is necessary to remove or at least neutralise the effects of these contamination layers.

The cleaning and pretreatment techniques which can be used are critically dependent on the choice of deposition technology. For instance in air plasma spraying the surface of components is degreased and then grit blasted to improve adhesion prior to coating, whereas in vacuum plasma spraying some heating and transferred-arc sputter cleaning may also be used. In general the cleaning pretreatments are more important as the deposition temperature is reduced. In the plasma spraying process molten droplets of coating material impinge on the substrate surface with a reasonable velocity. It has been shown that this leads to some melting of the substrate and fusion of substrate and coating material at the interface which promotes good adhesion [25]. Even so, in air plasma spraying, there are oxides and gases trapped at the interface as an inherent feature of the deposition process, which lead to a reduced area of contact between the splat and the substrate. In vacuum plasma spraying, the molten droplets move at higher velocities and have a lower probability of atmospheric reactions and gas entrapment. For this reason the adhesion of vacuum plasma sprayed coatings is often much better than that of air plasma sprayed materials. Under such conditions the presence of small amounts of surface contamination has a minor effect on adhesion. However, in the case of vacuum evaporated metal coatings the energy of the condensing atoms is very low (~0.1eV) and this means that there is little chance that such atoms can sputter anything but the most weakly bound contaminants and there is little energy available to drive chemical bonding reactions. Thus surfaces need to be very much cleaner than in the plasma sprayed case if good adhesion is to be achieved. The ability to sputter etch and the possibility of ion bombardment during deposition (as in ion plating or ion beam assisted deposition) can improve adhesion by promoting chemical and metallurgical bonding and sputtering of contamination.

المنارة للاستشارات

www.manaraa.com

Components and test pieces for coating will pick up a wide range of contaminants which can affect coating/substrate adhesion. For instance metal components are often shipped in transit oils and can pick up dust and grease during storage. Similarly corrosion products can form if the component encounters a damaging environment. For this reason it is necessary to adequately clean any component prior to coating. The majority of the contamination can be removed by heating to high temperatures under ultra-high vacuum conditions and sputter cleaning can help to reduce the concentration of contamination under these conditions but in most cases both experimental and commercial coating systems can not even hope to remove all contamination. For instance at a pressure of $\sim 10^{-5}$ mbar, a monolayer of contamination will be deposited on any surface in the coating chamber every second. Any cleaning process will need to desorb this contamination at a faster rate.

To remove gross contamination prior to coating a range of cleaning and degreasing treatments have been developed, generally based on the use of solvents [26]. Transit oils and heavy contamination can be removed by scrubbing the component with a detergent solution and heavy chemical contamination is generally removed by use of acids etches. The combination of a solvent and high shear forces is particularly effective at removing more tenacious contamination. This is the reason for the effectiveness of wipe cleaning in which a solvent-soaked tissue is wiped across the surface, dragging the contaminants to the edge. Ultrasonic cleaning followed by vapour degreasing can improve matters further. A typical cleaning process for metal components might consist of several stages as follows:-

1) Ultrasonic clean in solvent for greases;
2) Vapour degrease in same solvent;
3) Ultrasonic clean in detergent;
4) Rinse in pure water;
5) Ultrasonic clean in solvent containing water absorber;
6) Vapour degrease in same solvent;
7) Load into coating system taking care not to recontaminate the component.

The cleaning and degreasing media will become contaminated with the material removed from the components and will need to be continually filtered and refreshed. It is especially important to avoid particulate contamination from the coating system and for this reason a clean dust-free location for the equipment is usual and the operators should avoid allowing dust and debris to fall on the cleaned components. Finger grease and dust from the operators (skin, hair) can also be problematic and care is necessary in order that such contamination is minimised.

المنارة للاستشارات

www.manaraa.com

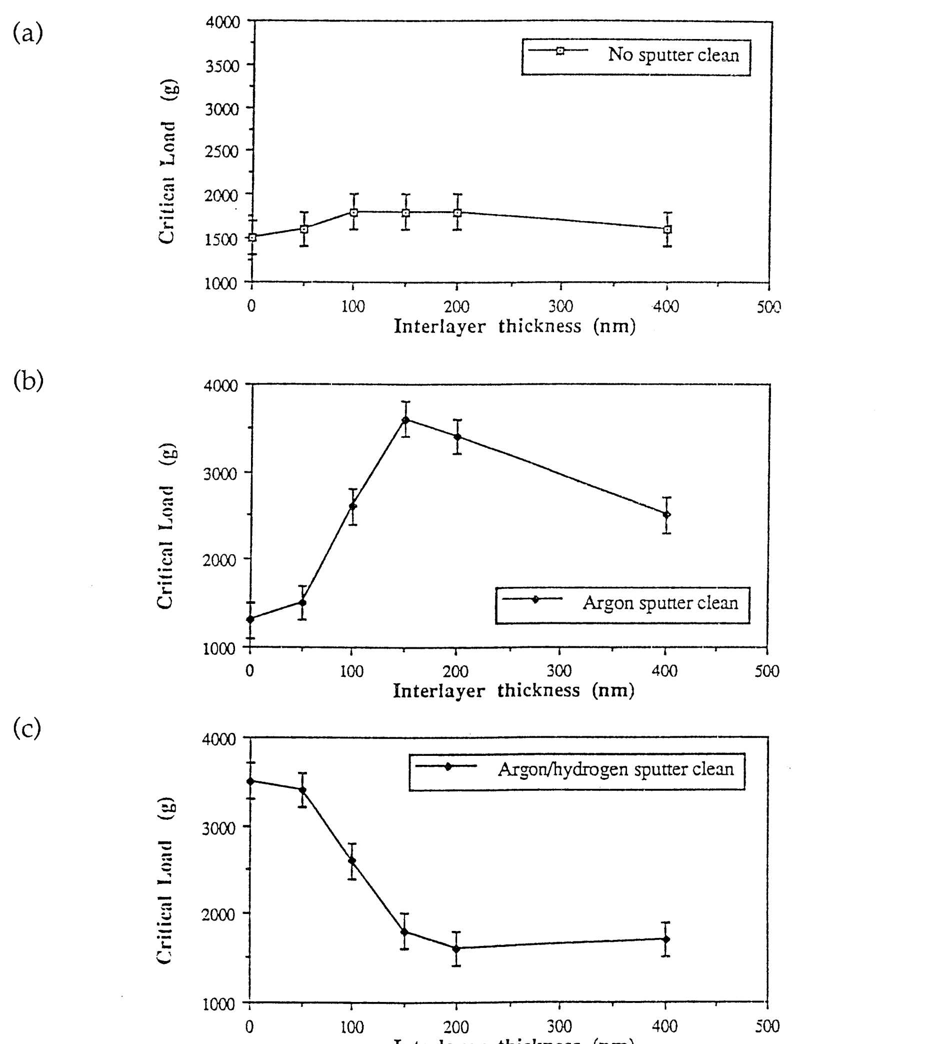

Figure 5: Variation of critical load for coating detachment (a measure of adhesion) as a function of titanium interlayer thickness for titanium nitride coatings on stainless steel, (a) no sputter etch, (b) argon sputter etch, and (c) argon/hydrogen sputter etch. Sputter etching leads to an increase in adhesion as it allows the titanium interlayer to dissolve the oxide on the steel. Hydrogen in the sputter gas removes a greater proportion of the oxide.

المنارة للاستشارات
www.manaraa.com

Most substrate materials can be further cleaned by heating under vacuum. This removes friable hydrocarbon contaminants and some water. However, depending on the substrate material and heat treatment there is a limit to the temperature which can be used. For most metals, heating to 150°C to 250°C is sufficient as higher temperatures can allow some of the contaminants to react with the substrate or diffuse into it.

Sputter etching is a very effective method of improving adhesion (Figure 5) and this is often attributed to the removal of surface contaminants and oxides by the process. In fact bombardment of the surface of the sample with energetic ions can lead to some material removal but it is more effective at breaking up oxides rather than removing them [27]. The process can often be improved by the introduction of reactive gases into the sputtering discharge which can lead to increases in etch rate. For instance the introduction of some hydrogen into an argon discharge can more rapidly remove the oxide layer on stainless steel than a pure argon discharge (Figure 5).

The temperature at which the coating is deposited can be a very strong factor in determining coating/substrate adhesion. In general, as the deposition temperature increases then so does the adhesion (Figure 6). This is due to the increase in surface mobility, inter-diffusion and the formation of chemical bonds at higher temperatures. The temperature rise caused by ion or electron bombardment during deposition can thus be harnessed to improve adhesion and for the best results it is often sensible to coat the substrate at the highest temperature it can stand without changes in microstructure or mechanical properties. However, this can lead to problems with residual stress.

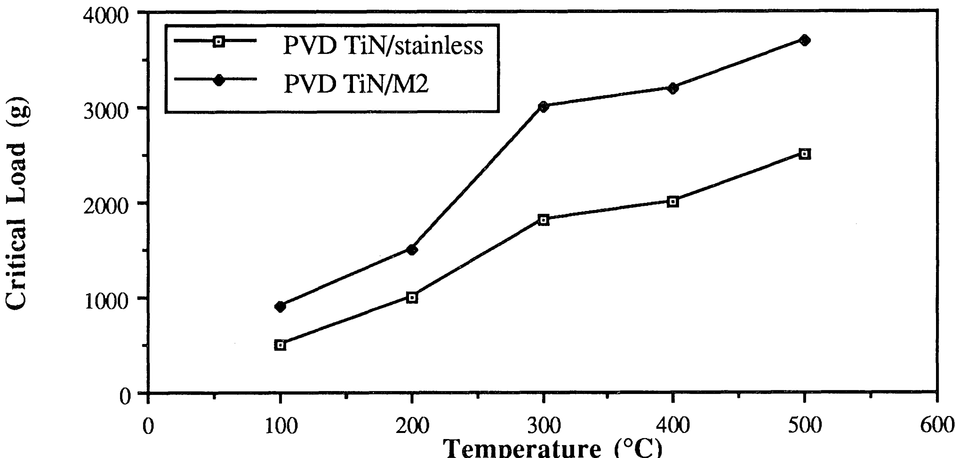

Figure 6: Variation of critical load for coating detachment with deposition temperature.

www.manaraa.com

Ion bombardment during the early stages of deposition can also be useful since it leads to some mixing of the atoms at the coating/substrate interface [28] and can also promote chemical bonding [29]. For this reason the adhesion of coatings deposited by ion-beam assisted deposition is very good at much lower deposition temperatures than need to be used by other coating processes [30].

Adhesion may also be improved by the deposition of an interlayer between coating and substrate. Chromium metal is often deposited as a flash layer prior to the evaporation of gold onto glass in order to improve adhesion [31]. In this case the chromium oxidises easily to form a strong bond with the glass, and alloys well with gold to form a diffusion layer. In the case of titanium nitride films on a range of substrates, the use of a thin titanium interlayer to improve adhesion is commonplace [e.g. 32-36]. The success of this interlayer has been attributed to two main effects:-

1) Chemical gettering. The interlayer dissolves interfacial contaminants and surface oxides.
2) Mechanical compliance. The interlayer acts as a soft compliant layer reducing interfacial stress gradients.

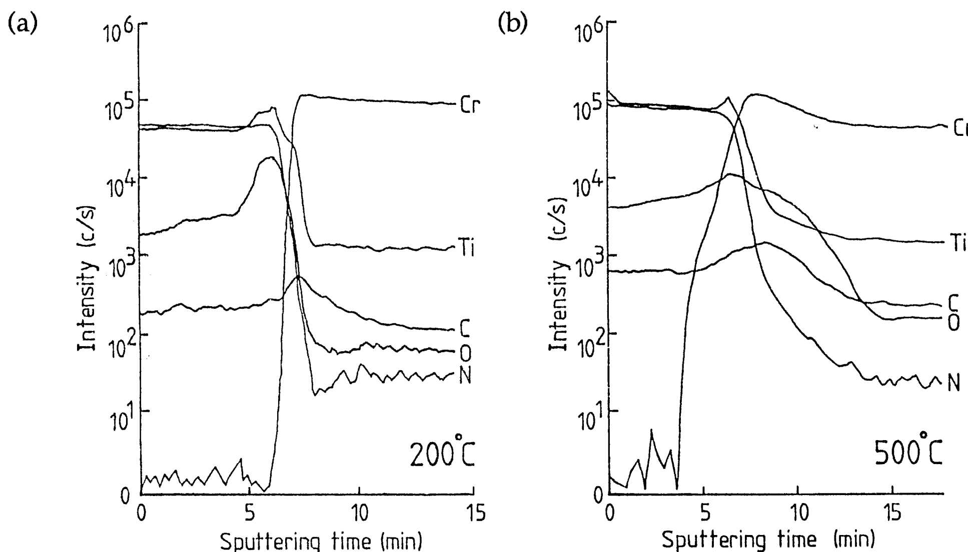

Figure 7: Secondary ion mass spectrometry (SIMS) depth profiles for titanium nitride coatings deposited onto a stainless steel substrate by sputter ion plating at (a) low deposition temperature (200°C) and (b) normal deposition temperature (500°C).

www.manaraa.com

The fact that there is an optimum interlayer thickness, which varies as a function of substrate material, deposition temperature, and the nature of the sputter clean, leads to the conclusion that the chemical effect is dominant in this case [36]. Figure 7 shows Secondary Ion Mass Spectrometry (SIMS) depth profiles for titanium nitride coatings on a stainless steel substrate deposited at low and high temperature. In both cases a 100nm titanium interlayer was used to promote adhesion. In the case of the low temperature deposited film there is a narrow region of high oxygen and carbon concentration at the interface which becomes much broader as the deposition temperature increases. The interfacial contamination dissolves in the interlayer material and its effect on adhesion is consequently reduced; this process is thermally activated and must depend on the diffusion of contaminants in the interfacial layer. The optimum interlayer thickness occurs when the layer can just dissolve all the interfacial contaminants at the deposition temperature used. There is some evidence that nitrogen migrates from the titanium nitride layer into the titanium layer leading to a graded interface, where the properties of the coating change smoothly through the interlayer and there is not such an abrupt change at the substrate [37]. This acts to reduce the residual stress gradient across the interface but it should be realised that a layer a few hundred nanometres in thickness does not have any effect on the total stress levels in coating and substrate. The mechanical compliance effect is much more important for the thick bond coats used in plasma spraying [38].

Post-deposition heat treatment can also be used to improve adhesion of coatings onto high temperature substrates but it is often observed that significant inter-diffusion leads spallation during thermal cycling. This behaviour may be due to interfacial oxidation or the formation of brittle interfacial phases [39]. In cases where such a deleterious reaction occurs between coating and substrate (or with an impurity which can diffuse to and react at the interface) a bonding layer can be deposited as a diffusion barrier to improve performance.

8. Measurement of Adhesion

8.1 REQUIREMENTS OF AN IDEAL ADHESION TEST

Though there are a large number of possible adhesion tests available at present, none can really be considered ideal. For an ideal test the following criteria need to be met:

1) Non-destructive;
2) Easily adaptable to routine testing of complex shapes;
3) Simple to perform and interpret;
4) Amenable to standardisation and automation;

www.manaraa.com

5) Reproducible;
6) Quantitative;
7) Directly related to coating reliability in specific applications.

No test currently has all these attributes and nearly all commonly used tests are destructive in nature. Indeed it is difficult to see how a non-destructive test can be developed given the current level of theoretical understanding and it is thus necessary to make the best use of the available tests recognising their weaknesses.

8.2 ADHESION TEST METHODS

Adhesion test methods fall broadly into three categories namely nucleation methods, mechanical methods and miscellaneous methods [3]. Table 3 shows some of the methods developed to measure the adhesion of thin films that have occurred in the literature.

Table 3: Methods that can be used to determine coating/substrate adhesion

Qualitative	Quantitative
Mechanical Methods	
Scotch tape test [40] Abrasion Test [41] Bend and scratch test [42]	Direct pull-off method [43-45] Laser spallation test [60-62] Indentation test [54-57] Ultracentrifuge test [3] Scratch test [64-73, 75-79] Bend test [50, 51] Double cantilever beam test [52]
Non-Mechanical Methods	
X-ray diffraction [46]	Thermal method [47] Nucleation test [40] Capacity test [3, 48]

www.manaraa.com

At the atomic level, the nucleation methods probe adhesion via the breaking of individual coating-substrate atomic bonds, generating lamellar defects. The macroscopic experimental adhesion is simply a summation of the individual atomic forces, which it should in principle be possible to relate to the energy of adsorption of single adatoms onto the atomically clean substrate. In concept the nucleation methods are very simple however evaluation of the adsorption energy on real component surfaces is impractical.

In mechanical methods, adhesion is determined by applying a force to the coating substrate system. The force is either applied directly, normal or parallel to the coating/substrate interface as in, respectively, the pull and shearing stress tests. Alternatively the force may be introduced indirectly by some stimulus as in the indentation and laser spallation tests. These methods of adhesion evaluation are now considered in more detail.

8.2.1 *Pull-off methods*. The simplest and probably most widely used of the practical adhesion tests is the tape test. This method requires the minimum of test equipment. A pressure sensitive tape is applied to the coating surface and then pulled off to determine the coating detachment stress. The maximum adhesion that can be tested is less than strength of the tape bonding material and consequently the test can only be applied to rather weakly adhering coatings; the upper limit being about 20 MNm^{-2} [40]. Alternatively rods can be bonded to the coating and substrate using commercially available adhesives, usually an epoxy resin, and then a force applied normal to the coating-substrate interface to determine the force for detachment as shown in Figure 8. This method can be used to estimate coating adhesion in the range 65 to 90 MNm^{-2} but like the tape test suffers from the following difficulties: (i) simple tensile tests frequently involve a mixture of tensile and shear forces which make interpretation difficult; (ii) alignment must be perfect to ensure uniform loading across the interface; and (iii) there is the possibility the the adhesive or solvent may penetrate the coating and affect the film-substrate interface.

Another form of the pull-off method is the tangential shear or lap shear technique in which the load for detachment is applied parallel to the coating-substrate interface, in which case the measured shear stress is the tangential force per unit area required to break the bond between the film and substrate. The advantages that the lap shear test have over the tensile test [49] are: (i) that it avoids severe deformation of the substrate; (ii) the film is gripped over a relatively large area and thus the stress is less concentrated; and (iii) it approximates to a nominally pure stress measurement.

www.manaraa.com

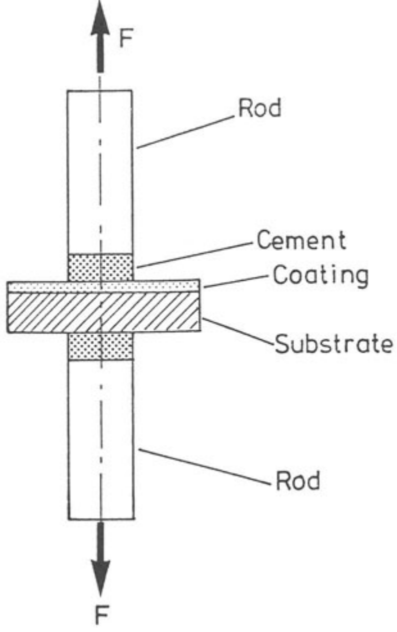

Figure 8: Pull-off adhesion test.

8.2.2 *Tensile and bend testing*. The simple pull off test is a special case of a number of tests which aim to produce coating detachment by tensile testing or bending. In the simplest test the coating/substrate composite is pulled in a tensile testing machine until the coating spalls, the whole sample cracks or the coating cracks perpendicular to the loading direction. The precise mode of failure depends on the relative properties of coating and substrate and is often dominated by yield effects in the substrate. However, for brittle coatings on ductile substrates (including some very thinmetal layers on polymers) the test can give useful comparative information about adhesion. In this test cracks initially form perpendicular to the loading direction; once fracture has occurred slip can occur at the coating substrate interface and the tensile stress in the coating is reduced either side of the crack. This effectively controls the minimum crack spacing. Further tensile loading can lead to some spallation of the coating between the cracks due to the Poisson's ratio contraction of the substrate placing the cracked strips in compression. Clearly the load at which such failures occur depends on both the substrate and coating properties but it can be used as a method for monitoring adhesion-promoting treatments (Figure 9).

المنارة للاستشارات
www.manaraa.com

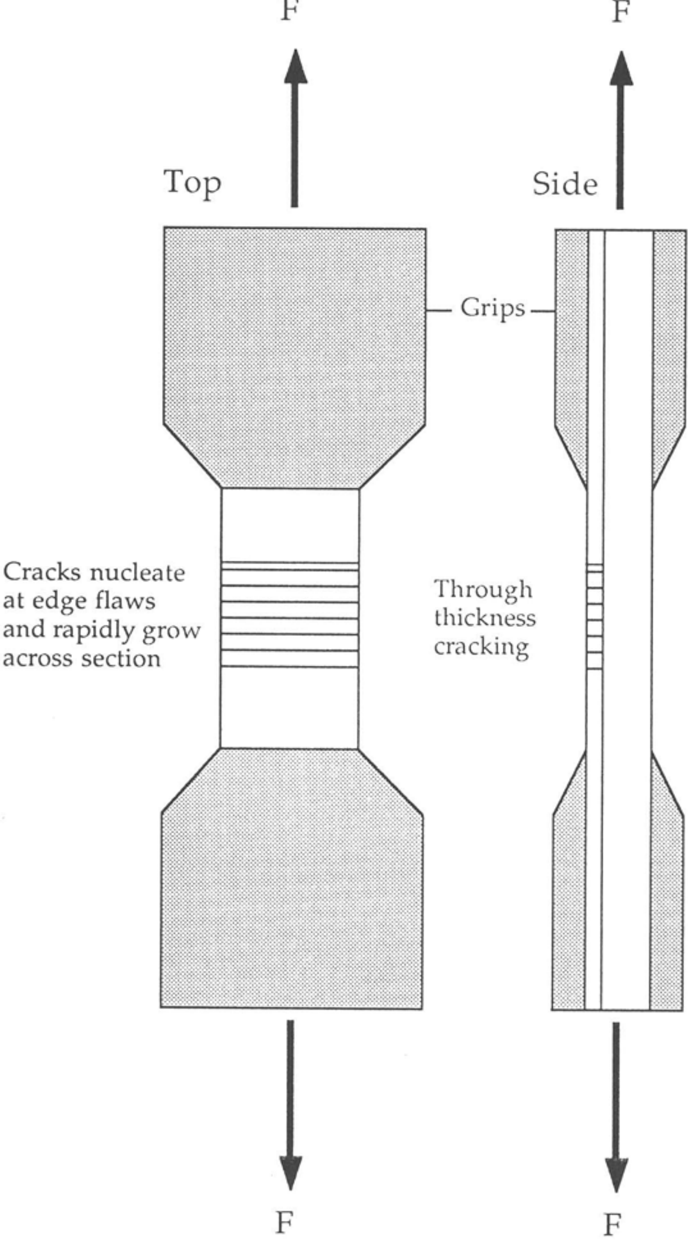

Figure 9: Schematic of the cracking observed in the tensile testing of metal samples coated with brittle materials. The interfacial flaw distribution and yielding in the substrate limits the crack spacing observed.

المنارة للاستشارات
www.manaraa.com

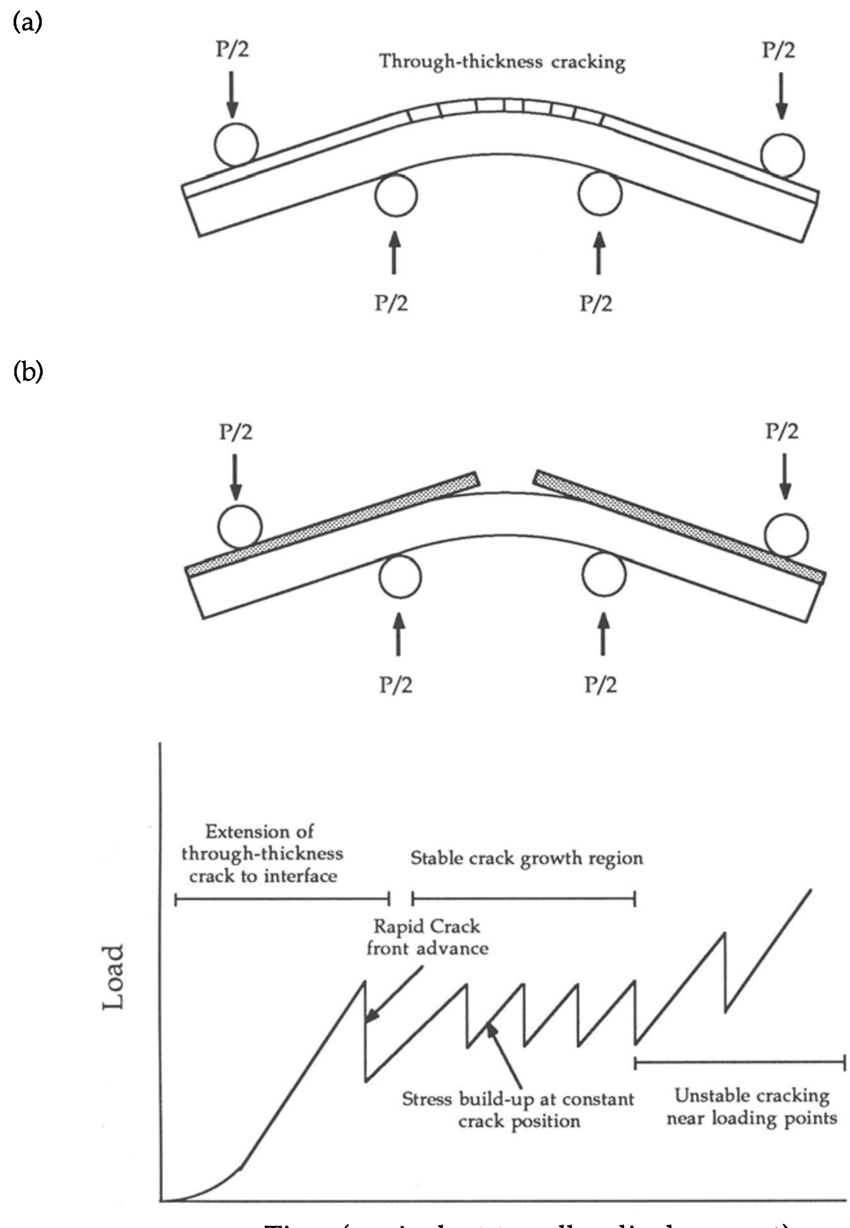

Figure 10: Schematic of the four point bend tests used for (a) thin coatings and (b) thick coatings.

www.manaraa.com

The spacing of tensile cracks in a bend test (Figure 10a) has been used to estimate the interfacial shear strength by using a computer simulation approach [50]. In this work the coating fracture strength, Weibull modulus, and interfacial shear strength are used to predict the crack distribution, and these parameters are adjusted to give the best fit to experimental data. An interfacial shear strength of 2GPa was determined for TiN on an M2 tool steel substrate by this method.

For thicker deposits such as plasma sprayed coatings it is often possible to induce stable crack growth at the coating/substrate interface by careful control of the bending process. For instance in the bend test of Clyne and co-workers [51] (Figure 10b) a four point bending sample is prepared with the coating on the tensile side. A saw cut through the coating is carefully introduced to allow the formation of interfacial cracks once bending commences. As the bending stress is increased the crack starts to propagate and will run until the crack driving force becomes insufficient. The distance which a crack propagates as a function of the bending stress can thus be used to determine the critical crack driving force.

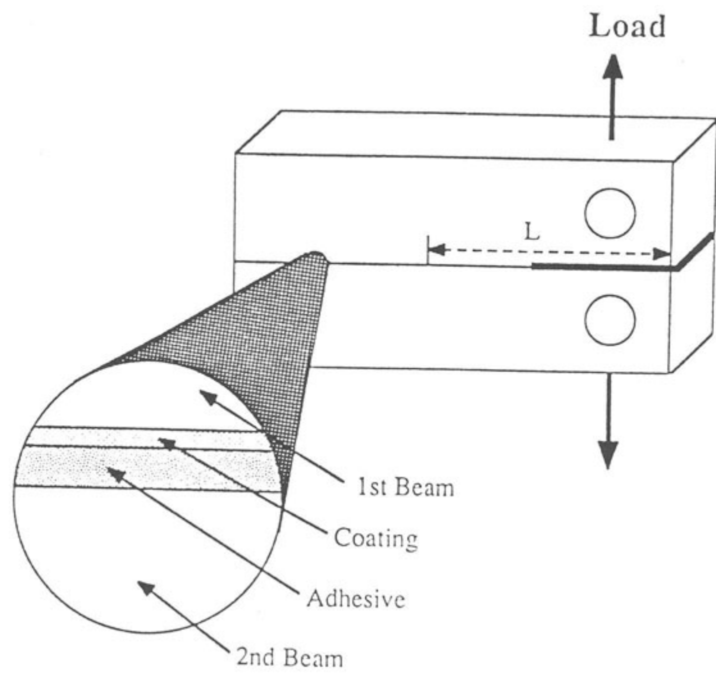

Figure 11: Schematic of the DCB test arrangement for the measurement of the adhesion of plasma sprayed coatings.

www.manaraa.com

A similar principal is used in the Double Cantilever Beam (DCB) test [52] which is similar to the test used for fracture toughness testing of bulk materials (Figure 11). This method requires a sample which consists of a steel beam which has been coated along one edge which and glued to a second beam. A pre-crack is introduced (by a saw cut) which extends approximately 20mm past the loading points which reduces the load necessary for crack extension. The crack can stop once it propagates, before total failure of the sample occurs, allowing several measurement cycles per sample. The interfacial critical strain energy release rate G_{ic} was determined using a linear elastic fracture mechanics approach [52], where G_{ic} is given by

$$G_{ic} = \frac{P_c^2}{2W} \frac{dc}{dl} \tag{3}$$

where P_c is the critical load for crack propagation, W is the specimen width and c is the sample compliance at the load points for a crack of length l. The determination of crack length during the test by a direct measurement is difficult; this problem can be solved by obtaining a compliance versus crack length curve by testing uncoated samples with known crack lengths and recording the observed sample compliance. For vacuum plasma sprayed alumina coatings on steel, low strain energy release rates have been measured by this method – 5.8-11.95 Jm^{-2} [53] as opposed to values around 21Jm^{-2} for air plasma sprayed material [52]. The difference can be attributed to the higher residual stress in the vacuum plasma sprayed coatings.

8.2.3 *Indentation methods*. The indentation adhesion test involves introducing a mechanically stable crack into the coating/substrate interface, by the use of conventional indentation procedures, using either Brale or Vickers indenters [54, 55]. A measure of adhesion is obtained using the resistance to crack propagation along the coating/substrate interface which may be characterised by both a fracture resistance parameter and a strength parameter. The bonding across the interface is uniquely related to the fracture resistance parameter and is a more fundamental measure of adhesion. The strength parameter is determined by the combined influences of the fracture resistance, the strength controlling defects and residual stresses within the film. The test assumes that the interface within the vicinity of the plastic zone created during indentation has a lower toughness than either the film or substrate material and consequently will be a site of preferential lateral crack formation. If fracture occurs in the film or substrate rather than at the interface it may be concluded that the interface toughness is at least as large as that of the weaker component.

المنارة للاستشارات
www.manaraa.com

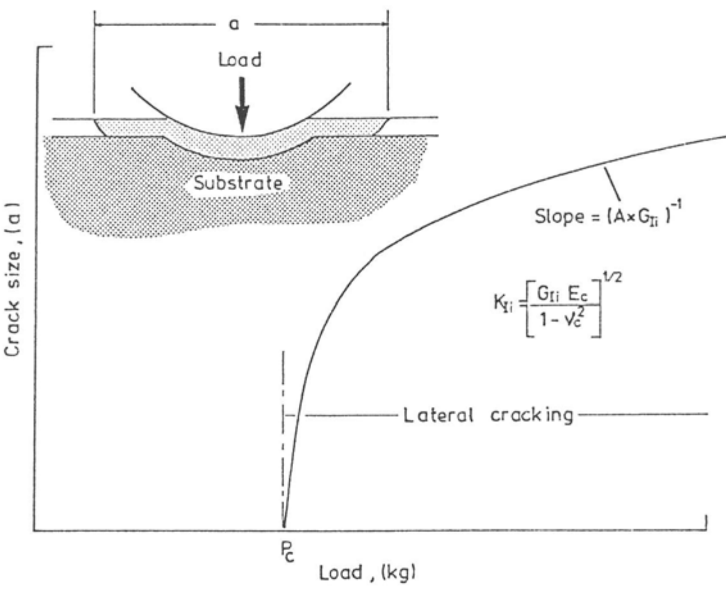

Figure 12: Indentation adhesion test; after Jindal et al [55].

A schematic representation of the indentation test used by Jindal et al [55] is shown in Figure 12 and shows the results of a series of indents made at different loads. The average change in lateral cracking is monitored as a function of load, and the interfacial fracture toughness K_{Ii} is derived from the linear portion of the indentation load versus lateral crack length plot according to

$$K_{Ii} = \left[\frac{G_{Ii}\,E_c}{1-\nu^2}\right]^{1/2} \tag{4}$$

where in Figure 12, A is a constant and E_c and ν_c are the Young's modulus and Poisson's ratio of the coating. An advantage of this technique is that the indentation adhesion parameters P_c and K_{Ii} are relatively insensitive to the substrate hardness which is a problem of with the scratch adhesion test. To further illustrate the differences between these two test methods, Figure 13 shows indentation test results for carbide inserts, CVD coated with TiC/Al_2O_3 layers, differentiated in terms of the η-phase occurrence at the coating/substrate interface. On the basis of the slope of the load/lateral crack diameter function the coatings which are deposited onto a continuous layer

المنارة للاستشارات
www.manaraa.com

of the brittle η-phase have poorer adhesion (toughness) compared with similar coatings which are formed with a discontinuous η-phase layer, but in both cases the scratch adhesion test indicated essentially identical L_C values for adhesion failure at the coating/substrate interface [55].

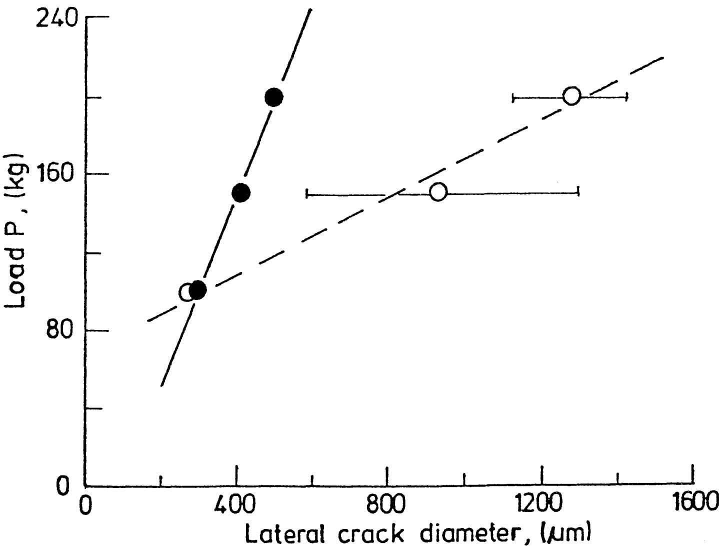

Figure 13: Indentation load vs. lateral crack diameter for multilayer TiC/Al_2O_3-coated samples with thin discontinuous η-phase (●) and thick continuous η-phase (o).

The approach of Evans and co-workers [54, 56, 57] is based on the observation that in the absence of buckling, and for planar interfaces, there is no driving force for growth of a delamination which exists at the coating substrate interface. This initial delamination may arise due to interfacial contamination or by void formation and coalescence. Consequently, for such interfaces, buckling becomes a pre-requisite for fracture propagation and eventual spalling. The critical stress for buckling of a circular delamination being given by [58]

$$\sigma_c = \left(\frac{K E_c}{12(1-\nu_c^2)}\right)\left(\frac{t}{a}\right)^2 \tag{5}$$

www.manaraa.com

where t is the coating thickness, a is the delamination radius, and $K \approx 14.7$. Once buckling occurs, a crack driving force (G) develops given by [59]

$$G = (1-\nu_c)(1-a)t\,(\sigma^2-\sigma_c^2)/E_c \tag{6}$$

where σ is the net compressive stress in the coating and $a = 0.38$. Further growth of the delamination occurs if $G > G_c$ either for the interface or for the coating and the delamination radius for coating spallation, a_s, is given by [60].

$$a_s/t \approx 1.9\,(E_c/\sigma)^{1/2} \tag{7}$$

For indentation-induced spalling [54, 56, 57]

$$\sigma = \sigma_R + \frac{E_c V}{2\pi(1-\nu_c)ta^2} \tag{8}$$

where σ_R is the initial residual stress and V the indentation volume. With

$$V = 0.24\,(P/H)^3 \cot\psi \quad \text{and} \quad a = \lambda P^{3/4} \tag{9}$$

where P is the indentation load, ψ is the indenter half-angle, H is the hardness, and λ is an experimentally determined coefficient. The critical indentation load for spalling, P_s, is given by

$$P_s^{3/2} = 3.7\,t^2 E_c\,[\lambda^2 \sigma_R + 0.24\,E_c \cot\psi/2\pi\,(1-\nu_c)t\,H^{3/2}]^{-1} \tag{10}$$

Figure 14 shows some results obtained from indentation testing of ZrO_2-Y_2O_3 coatings [56]; the data exhibits the expected trend from equation (9) in that $a \approx \lambda P^{3/4}$ and the fracture toughness G_c along the delamination path was found to be approximately 40 Jm^{-2} comparable to literature values for cubic zirconia. Similar results to those presented in Figure 14 were obtained for indentation spalling tests on a series of ZnO/Si samples and excellent agreement was obtained between theoretical values of P_s (equation (10)) and experimental measurements, indicating that the methods outlined above have some merit when it comes to assessing the adhesion of thin films. However, further work is needed before the indentation method can be recommended as a technique for determining interfacial adhesion.

المنارة للاستشارات

www.manaraa.com

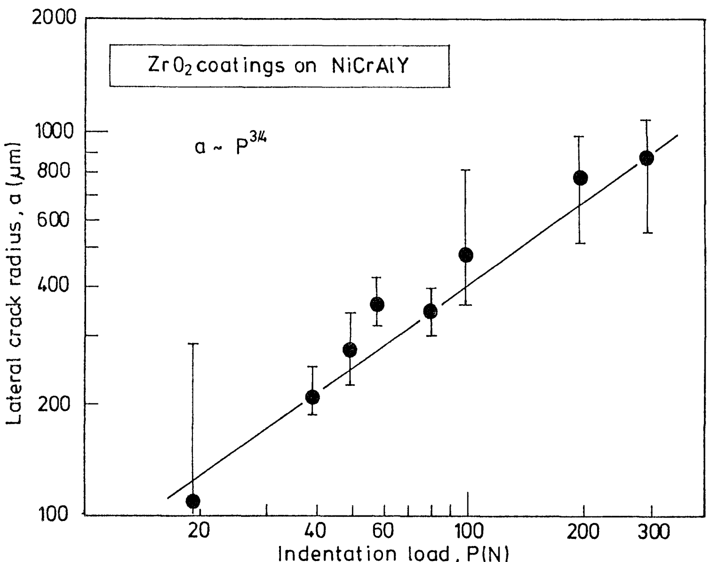

Figure 14: Plot of trend in delamination radius with indentation load for ZrO_2-Y_2O_3 coatings on NiCrAlY superalloy.

8.2.4 *Shockwave methods*. Mechanical stimuli can be introduced into the coating-substrate system in order to produce delamination by shockwave loading methods [60-63]. These techniques involve the absorption of energy either from the impact of erosive particles [63] or from an impinging laser beam [60-62]. In the laser method the absorbed energy may induce a stress wave, and the acoustic waveform from the rear side of the substrate can be monitored whilst the laser probes the coating surface as shown in Figure 15. If the incident probe is pulsed it is also possible to image the propagation of thermal waves within the coating and can be used to detect the presence of cracks or debonded regions. The technique has the advantage that it simulates the spall problems which occur during thermal cycling and impact damage in addition to being relatively non-destructive and applicable to complex components.

Loh et al [60] have examined the quasi-heating due to laser impingement onto a coating system. This had the effect of introducing localised compression which, in conjunction with the existing residual stresses, was sufficient to cause spallation. By varying the power and duration of laser pulses, the spall resistance of brittle coatings could be effectively measured. However, the calculation of critical crack driving force values for the data cannot be achieved directly and simulation methods are being developed to allow such analyses [62].

المنارة للاستشارات
www.manaraa.com

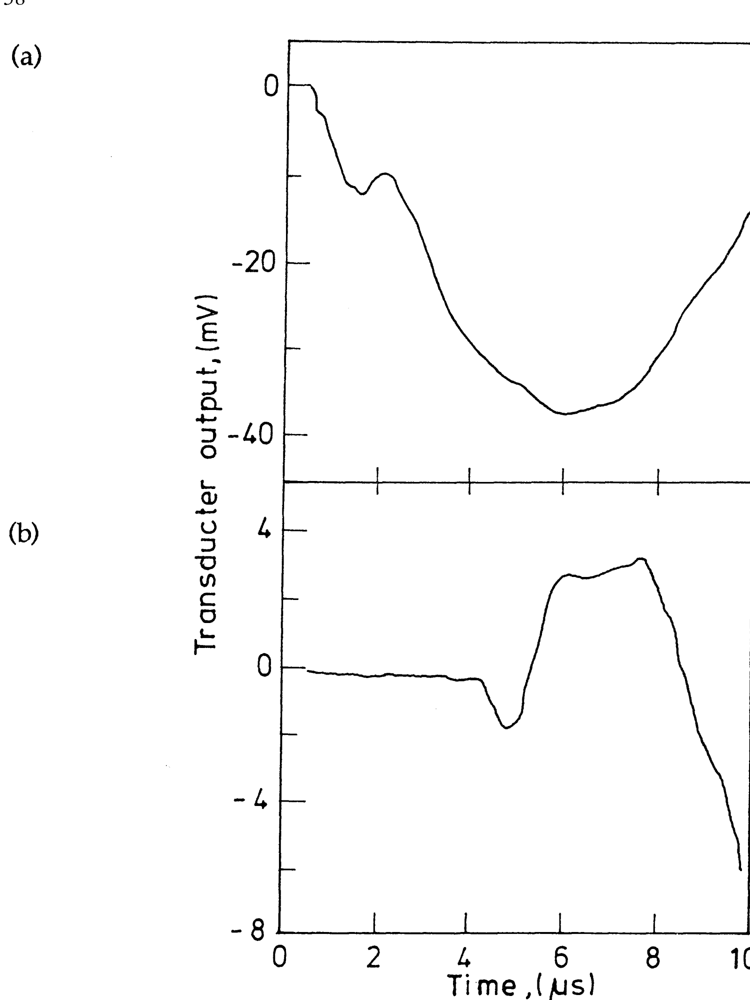

Figure 15: Transducer outputs for plasma sprayed coatings investigated using the laser acoustic adhesion test. The upper curve (a) is for a coating with good adhesion and the lower curve (b) for a coating with poor adhesion. The main difference between the two curves is the signal propagation time which is shorter when adhesion is good.

www.manaraa.com

8.2.5 *The scratch adhesion test method.* In the scratch adhesion test a stylus is drawn over the coating surface and a stepwise or continuously increasing normal force until the coating detaches [64]. In practice complete removal of the coating within the channel behind the stylus seldom occurs and therefore a critical load at which the coating is removed in a regular way along the whole channel length [65] is defined. Coating detachment can either be monitored using optical or scanning electron microscopy, acoustic emission [66] or frictional force measurement [67, 68]. The two latter procedures (acoustic emission and frictional force measurement) provide traceable signals which can be used to compare results from different samples and may avoid some of the subjectivity of measurements made by eye. The sensitivity of the frictional measurement procedure is particularly enhanced when the scratch test is applied to hard coatings of less than one micron in thickness.

There are a large number of failure modes associated with the scratch test – through-thickness cracking, interfacial and cohesive failure among others [24, 69]. The main interfacial failure modes are based on spallation and buckling which arise as a function of the type of loading induced by the scratch test and the nature of the interface (i.e. brittle or ductile behaviour [24]). In any attempt to use the scratch test to measure adhesion it is important to use a failure mode which is dependent of coating/substrate adhesion. In most cases these will be spallation or buckling failures; spallation and buckling occur ahead of the scratch stylus if the origin of the failures is the compressive stresses induced by stylus/coating friction, whereas spallation behind the stylus can occur due to the combined effects of through-thickness cracking and elastic recovery.

Benjamin and Weaver [70] performed the first analysis of the mechanics of the scratch test using the theories developed for fully plastic indentation, giving an expression for the critical shearing force for coating removal in terms of the scratch geometry, the substrate properties and the frictional force on the stylus.

$$F = \frac{k\,A\,H}{(R^2 - A^2)^{1/2}} \qquad (11)$$

where $A = (w/pH)^{1/2}$, w is the critical load, R is the indenter tip radius, F is the shearing force strength of the coating per unit area, A is the radius of the circle of contact, H is the indentation hardness of the substrate material and k is a constant varying between 0.2 and 1.0 [70, 71]. It is inappropriate to assume fully plastic deformation in many cases and further attempts to modify this expression have given some account of elastic-plastic indentation behaviour [71].

More recently, Laugier [72, 73] has suggested that the adhesion behaviour can be modelled in terms of the strain energy released during removal of the

www.manaraa.com

coating. Using a Griffith energy balance approach [74], the elastic strain energy released provides the surface energy for a crack to form at the coating substrate interface. By balancing the released elastic energy with the surface energy of the crack, it is possible to relate the local stress σ responsible for coating detachment to the work of adhesion, W, by [72, 73]

$$W = \frac{\sigma^2 t}{2E_c} \tag{12}$$

where t is the coating thickness. Attempts have been made to calculate σ expressed as a combination of the applied stresses due to the sliding indenter and the internal stresses within the coating. For example, in the analysis of Laugier [72, 73] the applied stresses were calculated from the elastic equations of Hamilton and Goodman [75]. Clearly this is insufficient to describe the stresses for materials where some plasticity has occurred. Burnett and Rickerby [76] have identified three contributions to the stresses responsible for coating detachment: (i) an elastic-plastic indentation stress; (ii) internal stress; and (iii) a tangential frictional stress. This analysis has been extended by Bull et al [77-79] where each of these contributions is expressed in terms of their effects on the measured coefficient of friction as shown in Figure 16. The advantage of expressing all the stress contributions in these terms is clear when experimental measurements of the tangential force can be made during scratching [67].

The total frictional force is given by [80]

$$F = A_1 p + A_2 \tau \tag{13}$$

where p is the ploughing flow stress, τ the interfacial shear stress (or the shear stress of the softer material and A_1 and A_2 are the cross sectional area of the track and the contact area respectively (see Figure 16). Since $A_2 \gg A_1$ in most cases the shear stress is small compared to p and this dominates the stress responsible for coating removal. Assuming that for a moving stylus the load is supported on the front half of the contact, the critical load, L_c, can be given by

$$L_c = \frac{\pi d_c^2 p}{8} \tag{14}$$

where d_c is the track width at L_c. By combining equations (12) and (14) and setting $p=\sigma$ an expression for the work of adhesion in terms of L_c is produced

المنارة للاستشارات

www.manaraa.com

$$L_c = \frac{\pi d_c^2}{8}\left[\frac{2EW}{t}\right]^{1/2} \tag{15}$$

This equation has been used to determine values for the work of adhesion of titanium nitride coatings on a range of steel substrates which are in the range 1-150Jm^{-2} [81]. These are somewhat smaller than those determined in fracture toughness studies on steels (10kJm^{-2})[82], but are larger than the surface energies of either substrate or coating material (typically in the range 1-10Jm^{-2}). This illustrates the importance of some plastic deformation at the crack tip in the coating removal process.

In addition to the extrinsic factors that influence the scratch test, a number of intrinsic parameters also have an important bearing of the derived value of critical load and some of these are listed in Table 4 [83]. The scratch adhesion test appears to be the only available practical method to study the adhesion of hard tribological coatings in many situations. However, care is needed in both the performance of the test and in the interpretation of the results if reliable conclusions are to be drawn about coating substrate adhesion owing to the influence of these extrinsic and intrinsic parameters.

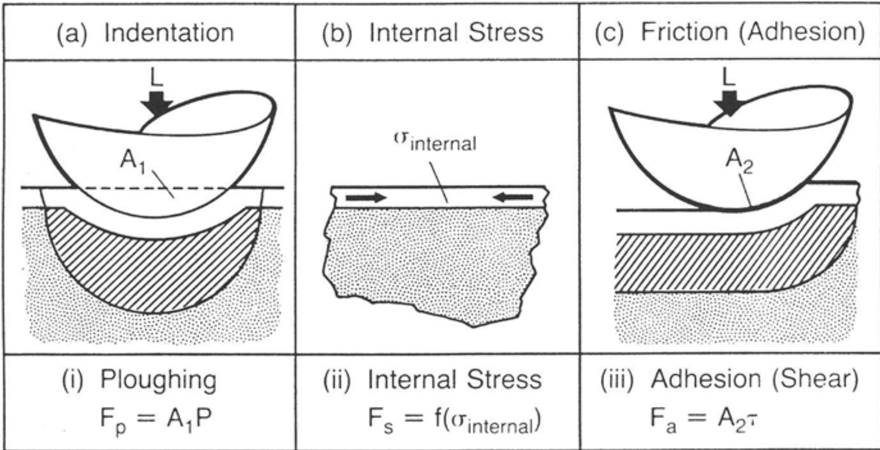

Figure 16: The scratch adhesion test represented as the sum of three contributions; an indentation term, an internal stress term and a frictional term. These may be represented as three frictional contributions; a ploughing component, an internal stress component and an adhesive component.

المنارة للاستشارات
www.manaraa.com

Table 4: Factors affecting the critical load for coating detachment in the scratch test method.

Intrinsic Parameters	Extrinsic parameters
Loading rate [67, 81, 83] Scratching speed [67, 81, 83] Indenter tip radius [67, 81, 87] Indenter wear [83] Machine factors [77]	Substrate properties [83, 88] - Hardness - Modulus - Thermal expansion coefficient Coating properties [83, 89] - Hardness - Modulus - Stress and interfacial properties - Thickness Friction force and friction coefficient [67, 76, 83] - Surface condition and testing environment.

Commercial scratch testers are basically of two types. In the automatic scratch test the normal load is continuously increased along the length of the scratch track by a spring loading mechanism. This test is very quick and simple to perform but has the disadvantage that catastrophic failure occurs at the first sufficiently large flaw and thus the critical load may be an underestimate of the practical adhesion in any application. Also the critical load has been found to be a sensitive function of the machine loading geometry and this makes comparison between laboratories with various types of machine quite difficult [67, 81, 83]. The alternative manual scratch tester uses dead weight loading and hence requires the performing of many scratches to assess the critical load, a much more time consuming process. However, it has the advantage that the interfacial flaw distribution can also be assessed by counting the number of failures that occur at each load [79]. The number of failures is found to saturate at a certain load (usually just before it becomes impossible to distinguish individual failures in the track) as observed by both reflected light microscopy or acoustic emission detection where each failure generates a small burst of acoustic emission. Thus a cumulative failure probability P(L) can be defined as

$$P(L) = N(L)/(N_{sat} - N_O) \qquad (16)$$

www.manaraa.com

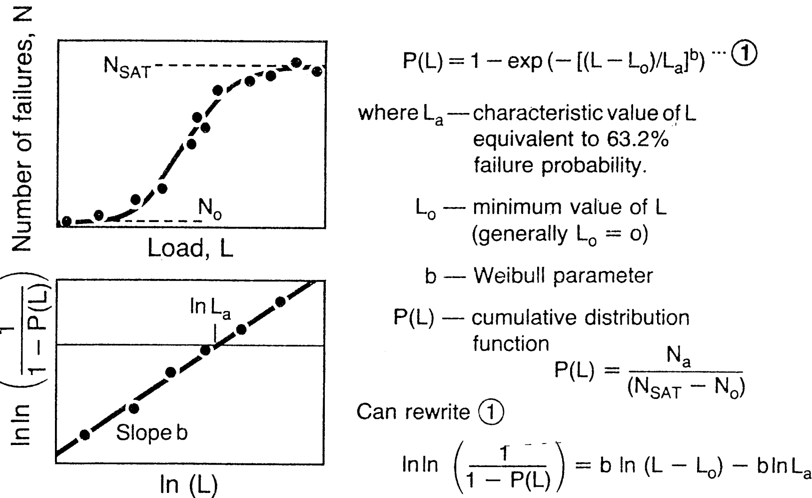

Figure 17: Weibull statistical analysis of the scratch test.

where N(L) is the number of failures at load L, N_o is the number of failures on low loads (usually N_o = 0) and N_{sat} is the saturation failure number. P(L) can be given by the Weibull distribution

$$P(L) = 1 - \exp [-(L - L_o)/L_a]^b \qquad (17])$$

where L_o is the load at which the probability of failure is zero (generally L_o= 0), L_a is a constant equal to the load at which there is a 63.2% cumulative failure probability (which can be used as a critical load criterion related to the flaw distribution) and b is the Weibull parameter. As b increases the distribution becomes narrower and the critical load becomes a better measure of coating adhesion. Details of the analysis are shown in Figure 17. The advantage of this method is that it offers the possibility of providing a completely automated way of determining the critical load for coatings which produce well defined pulses of acoustic emission associated with coating detachment failure events. The acoustic emission trace at each load can be recorded and examined by computer, the number of failures counted and stored and the variation with load determined. From this a value of L_a can be calculated which involves no subjective decisions by the operator and hence is a much more reliable adhesion criterion. However, much more

المنارة للاستشارات
www.manaraa.com

work is needed to determine the viability of such an approach in a wide range of coating/substrate systems.

The scratch test has also been used to determine both interfacial and cohesive failure strengths for thick films in a modified form suggested by Beltzung et al [84, 85]. In this case the material to be tested is in the form of a polished cross section and the scratches are performed across the coating starting from the substrate using stepwise increasing loads. A cone of damage is produced as the scratch diamond exits from the face of the coating, the size of which can be used to determine the cohesive strength of the coating [86]. However, in a smaller number of cases a crack is also produced at the coating/substrate interface once a critical load has been reached, and this can be used to rank coating/substrate adhesion in these situations.

8.3 SELECTION OF ADHESION TESTS

From the previous section it can clearly be seen that there is no ideal adhesion test and the tests available cannot be used to assess all coating/substrate systems. For instance, the pull-off test is limited to coatings with relatively poor adhesion (due to the strengths of available glues), whereas the indentation spallation technique is only really useful where the interfacial failure mode is brittle. There are no hard and fast rules about the selection of the appropriate adhesion test for any coating/substrate combination, as each test critically depends on the type of failures which occur within it. The scratch test is perhaps the most widely applicable test for the routine monitoring of adhesion but it is not really suitable for very soft substrate materials.

Due to all these problems the best approach for the initial selection of an adhesion test is to pick the test which most closely approximates the in-service conditions of the coated component. For tribological applications this could be the scratch test, whereas the laser spallation test may be more relevant to thermal barrier applications. However, once a test has been selected it may be difficult to generate meaningful results for a given coating/substrate system and the user should assess several tests in such applications.

9. Conclusions

Practical adhesion is not a simple fundamental property but depends on a number of factors in the coating/substrate system and the method by which it is measured. There are no ideal adhesion tests so it is necessary to make use of a test which gives some information about in-service performance in the intended application, if useful results are to be determined. Two quantifiable

www.manaraa.com

measures of adhesion are important in any application, namely the adhesion strength which is controlled by the interfacial flaw distribution as well as by interfacial bonding) and the crack driving force (which is much more related to bonding across the interface). In general, the adhesion is better when the modes of failure are ductile and the crack driving force is high. The interfacial structure is thus critically important in determining coating substrate adhesion. It is also necessary to know what phases and interfacial contamination are present on the substrate prior to coating and how these are affected by the coating process if the adhesion of the coating is to be optimised. Only if all the factors which affect adhesion are controlled can the performance of the coated component be optimised for its intended application.

References

[1] ASTM Definition of Term Relating to Adhesion D907-70, ASTM, Philadelphia, PA, 1970.
[2] R.J. Good, J. Adhes., 8 (1976) 1.
[3] K.L. Mittal, Electrocomp. Sci. Technol., 3 (1976) 21.
[4] H.K. Pulker, A.J. Perry and R. Berger, Surf. Technol., 14 (1981) 25.
[5] A. Badzian and T. Badzian, Surf. Coat. Technol., 36 (1988) 283.
[6] M.L. Tarng, and G.K. Werner, J. Appl. Phys, 43 (1972) 2268.
[7] G.G. Paulson, and A.C. Friedberg, Thin Solid Films, 5 (1970) 47.
[8] W.D. Westwood, Prog. Surf. Sci. 7 (1976) 71.
[9] R.C. Sunahl, J.Vac. Sci. Technol., 9 (1972) 181.
[10] A.G. Elliot, Surf. Sci., 51 (1975) 489.
[11] R.L. Apps, J. Vac. Sci. Technol., 11 (1974) 741.
[12] M.G. Nicholas and K.T. Scott, Surf. J., 12 (1982) 2.
[13] M.P. Seah, Surf. Sci., 53 (1975) 168.
[14] D. A. Porter and K.E. Easterling, "Phase Transformations in Metals and Alloys," Van Nostrand Reinhold (UK) Ltd, Wokingham, 1981, p88.
[15] E.V. Kornelson, Rad. Eff. 13 (1972) 227.
[16] G. Dearnaley, Appl. Phys. Lett., 28 (1976) 244.
[17] H. Harrach and B. Chapman, Thin Solid Films, 22 (1974) 305.
[18] K.L. Mittal, J. Vac. Sci. Technol., 13 (1976) 19.
[19] A.M. Soneham and P.W. Tasker, J. Phys. C: Sol. Stat. Phys., 18 (1985) L543.
[20] R.A. Kant and B.D. Sartwell, Mat. Sci. Eng., 90 (1987) 357.
[21] H. Holleck, Proc. Conf. Surface Engineering and Heat Treatment, Ed. P.H. Morton, Institute of Metals, London, 1991, p312.

المنارة للاستشارات
www.manaraa.com

[22] C.C. Cheng, A. Erdemir, and G.R. Fenske, Surf. Coat. Technol., 39/40 (1989) 365.
[23] M.D. Thouless, Thin Solid Films, 181 (1989) 397.
[24] S.J. Bull, Surf. Coat. Technol., 50 (1991) 25.
[25] H.-D. Steffens, B. Wielage and J. Drozak, Surf. Coat. Technol., 45 (1991) 299.
[26] H.K. Pulker, "Coatings on Glass", Elsevier, Amsterdam, 1984.
[27] S.J. Bull, Vacuum, in press (1992).
[28] D.K. Sood, P.D. Bond, and S.P.S. Badwal, Mat. Res. Soc. Symp. Proc. 27 (1984) 565.
[29] A.A. Galuska, J. Vac. Sci., Technol., A10 (1992) 381.
[30] G. Dearnaley, Proc. Conf. Surface Engineering and Heat Treatment, Ed. P.H. Morton, Institute of Metals, London, 1991, p285.
[31] G.J. Zydzig, T.G. Uitert, S. Singh and T.R. Kyle, Appl. Phys. Lett., 31 (1977) 697.
[32] J.E.E. Baglin, Mat. Sci. Eng., B1 (1988) 1.
[33] M.Y. Al Jaroudi, H.T.G. Hentzell, S.E Hornstrom and A. Bengston, Thin Solid Films, 182 (1989) 153.
[34] V. Helmersson, B.O. Johansson, J.-E. Sundgren, H.T.G. Hentzel and P. Billgren, J. Vac. Sci. Technol., A3 (1985) 308.
[35] S.J. Bull, P.R. Chalker, C.F. Ayres and D.S. Rickerby, Mat. Sci. Eng., A139 (1991) 71.
[36] S.J. Bull and P.R. Chalker, Proc 5th Int. Conf. Surface Modification Technologies, Birmingham, September 2-4, 1991, in press.
[37] A. Erdemir and C.C. Cheng, Ultramicroscopy, 37 (1991) 286.
[38] B. Rhouta and B. Pieraggi, J. Mat. Sci. Lett, 11 (1992) 278.
[39] D.J. Wortman, E.C. Duderstadt and W.A. Nelson, J. Eng. Gas Turbines and Power, 112 (1990) 527.
[40] D.S. Campbell in L.I.Maissel and R.Glang (eds) "Handbook of Thin Film Technology", MacGraw Hill, New York, (1970) Chapter 12.3.
[41] E.M. Ruggiero, Proc. 14th Ann. Microelectronics Symp., St. Louis Section IEEE, May 24-26, 1965, IEEE, New York, 6B-1.
[42] D. Davies and B. Whittaker, Metall. Rev., 12 (1976) 15.
[43] R. Jacobsson, Thin Solid Films, 34 (1976) 191.
[44] G. Katz, Thin Solid Films, 33 (1976) 99.
[45] P. Bodo and J.-E. Sundgren, J. Appl. Phys., 60 (1986) 1161.
[46] K.L. Chopra, "Thin Film Phenomena", McGraw-Hill, New York, 1969, p313.
[47] B.N. Chapman, J. Vac. Sci. Technol., 11 (1974) 106.
[48] T.R. Bullet and J.L. Prosser, Prog. Org. Coat., 1 (1972) 45.
[49] D.S.Lin J. Phys. D, 4 (1971) 1977.
[50] P.M. Ramsey, H.W. Chandler and T.F. Page, Thin Solid Films, 201 (1991) 81.

www.manaraa.com

[51] S.J. Howard and T.W. Clyne, Surf. Coat. Technol., 45 (1991) 333.
[52] C.C. Bernt and R. McPherson, Materials Science Research, 14 (1981) 619.
[53] R. Kingswell, PhD Thesis, Brunel University, 1992.
[54] S.S. Chiang, D.B. Marshall and A.G. Evans, in J. Pask and A.G.Evans (eds) "Surfaces and Interfaces in Ceramic-metal systems" Plenum, New York 1981, p603.
[55] P.C. Jindal, D.T.Quinto and G.J. Wolfe, Thin Solid Films, 154 (1987) 361.
[56] D.B. Marshall and A.G.Evans, J. Appl. Phys., 56 (1984) 2632.
[57] C. Rossington, D.B.Marshall, A.G.Evans. and B.T.Khuri-Yakub, J. Appl. Phys., 56 (1984) 2639.
[58] S. Timoshenko and J.M.Gere, "Theory of Elastic Stability", McGraw-Hill, New York, 1961, p390.
[59] A.G. Evans and J.W.Hutchinson, Int. J. Solid. Struct., 20 (1984) 455.
[60] R.L.Loh, C. Rossington and A.G.Evans, J. Am. Ceram. Soc., 69 (1989) 139
[61] J.L.Vossen in K.L.Mittal (ed) "Adhesion Measurement of thin films, thick films and bulk coatings", Special Tech. Publ. 640, ASTM, Philadelphia, 1978, 122.
[62] V. Gupta, A.S. Argon, J.A. Cornie and D.M. Parks, Mat. Sci. Eng., A126, (1990) 105.
[63] W.E. Snowden and I.A. Aksay in J.Pask and A.G.Evans (eds) "Surfaces and Interfaces in Ceramic and Ceramic-metal systems", Plenum, New York, 1981, p651.
[64] A.J. Perry, Surface Eng, 3 (1986) 183.
[65] A.J. Perry, Thin Solid Films, 107 (1983) 167.
[66] A.J. Perry, Thin Solid Films, 81 (1981) 357.
[67] J. Valli, J. Vac. Sci. Technol., A4 (1986) 3007.
[68] S. Jacobson, B. Jonsson and B. Sundquist, Thin Solid Films, 107 (1983) 89.
[69] P. Hedenqvist, M. Olsson, S. Jacobson, and S. Soderberg, Surf. Coat. Technol., 41 (1990) 31.
[70] P.Benjamin and C. Weaver, Proc. Roy. Soc. Lond. Ser. A 254 (1960) 177.
[71] C.Weaver, J.Vac. Sci. Technol., 12 (1975) 18.
[72] M.J. Laugier, Thin Solid Films, 117 (1984) 243.
[73] M.J. Laugier, J. Mater. Sci., 21 (1986) 2269.
[74] A.A.Griffith, Phil. Trans. Roy. Soc. Lond. Ser. A 221 (1920) 163.
[75] G.M. Hamilton and L.E. Goodman, J. Appl. Mech., 33 (1966) 371.
[76] P.J. Burnett and D.S.Rickerby, Thin solid Films, 154 (1987) 403.
[77] S.J. Bull, D.S. Rickerby, A. Matthews, A. Leyland, A.R. Pace and J.Valli, Surf. Coat. Technol., 36 (1988) 503.

المنارة للاستشارات
www.manaraa.com

[78] S.J.Bull and D.S.Rickerby, Brit. Ceram. Trans. J., 88 (1989) 177.
[79] S.J.Bull and D.S.Rickerby, Surf. Coat. Technol. , 42 (1990) 149.
[80] F.P.Bowden and D.Tabor, "The Friction and Lubrication of Solids", Clarenden Press, Oxford, 1954.
[81] S.J.Bull, D.S.Rickerby, A.Matthews, A.R.Pace and A.Leyland, Proc. Inst. Conf. Plasma Surface Engineering, Garmisch-Partenkirken, September 19-23, 1988, DGM Informationsgesellschaft, 1989, p1227.
[82] O.H. Wyatt and D. Dew-Hughes, "Metals, Ceramics and Polymers", Cambridge University Press, Cambridge, 1974, p411.
[83] P.A. Steinmann, Y. Tardy and H.E. Hintermann, Thin Solid Films, 154 (1987) 333.
[84] E. Lopez, F. Beltzung and G. Zambelli, J. Mat. Sci. Lett., 8 (1989) 346.
[85] F. Beltzung, G. Zambelli , E. Lopez and A.R. Nicoll, Thin Solid Films, 181 (1989) 407.
[86] R. Kingswell, D.S. Rickerby, S.J. Bull, and K.T. Scott, Thin Solid Films, 198 (1991) 139.
[87] J. Hamersky, Thin Solid Films, 3 (1969) 263.
[88] B. Hammer and A.J. Perry, Thin Solid Films, 96 (1982) 45.
[89] P.J. Burnett and D.S. Rickerby, Thin Solid Films, 157 (1988) 233.

المنارة للاستشارات

www.manaraa.com

NITRIDING , BORIDING AND CARBURIZING OF STEELS

PATRICK JACQUOT
INNOVATIQUE SA
25 rue des frères Lumière
69680 Chassieu
France

ABSTRACT . This paper describes three surface hardening processes of steels and mainly the basic principles , technical advantages and limitations, industrial applications of these diffusion methods of carbon, nitrogen and boron . Thermo-chemical treatments like : carburizing, boriding and nitriding are described. Specificities of each treaments are reviewed .

1 . INTRODUCTION

Surface engineering or surface hardening are processes which include a wide variety of techniques used to improve the wear, friction and fatigue resistances of parts without affecting the more soft, tough, core of the part .This combination of hard surface, high strengh of the case, and the relative ductility of the core of components is useful in parts such as gear or cam that must have a hard surface to resist wear , and a tough interior to resist again impact, strain produced by shocks, alternating stresses, that occurs during operation .
This paper focuses exclusively on three methods for surface hardening, which are diffusion methods, such as : carburizing, nitriding and boriding . Diffusion methods modify substantially the chemical composition of the surface with introduction of interstitial elements or hardening species like : carbon, nitrogen or boron, by diffusion mechanism . Diffusion treatments are divided into two main categories : those operating at high temperatures (800-950 °C) with the steel in an austenitic condition , like : carburizing and boriding , and those operating at lower temperature with the steel in a ferritic condition (below 600 °C), like nitriding .
Selective or localized hardening methods, such as carburizing and boriding generally involve transformation hardening (from heating and quenching), but some hardening methods (nitriding) are based only on compositional modification with chemical interactions of the substrat, without heat treatment cycle .

2 . CARBURIZING OF STEELS

2.1 DEFINITION

Carburizing is a case-hardening process in which carbon is diffused in the surface layers of a low carbon steel part at a temperature sufficient to transform the steel austenitic, followed by quenching and tempering to form a hard martensitic

W. Gissler and H. A. Jehn (eds.), Advanced Techniques for Surface Engineering, 69–82.
© 1992 *ECSC, EEC, EAEC, Brussels and Luxembourg.*

www.manaraa.com

microstructure.
The gradient in carbon content obtained below the surface of the component causes a gradient in hardness, creating a strong , wear-resistant surface layer on a ferrous material, usually low-carbon steel (figures 1 and 2) .

2 .2 PROCESS PRINCIPLE

The most important thermochemical treatment is the carburizing process (also called case hardening). Low-carbon steel parts exposed to carbon-rich atmosphere will carburize at temperatures of 800 ° C and above . The carbon source must be not to rich , if not the solubility limit of carbon in austenite can be reach at the surface of the steel and some carbides may form at the surface (3) .
The carbon gradient produced by maintaining saturated austenite at the surface of the steel is referred to as the normal carbon gradient (1)(2) .
Carbon is diffused into the steel surface from either a solid, liquid or gaseous carbonaceous media (CO-CO2, C3H8 . .) at a temperature in the range of 800 to 1000 °C. The steel is then quenched and tempered to produce a hard, tough case with a depth of up to several millimeters (0,3 to 2 mm).
The maximum rate at which carbon can be added to steel is limited by the rate of diffusion of carbon in austenite .This diffusion rate increases greatly with increasing temperature . The highest hardness in a hardened steel is obtained when the carbon content of the steel is high (figure 4) .
The most useful carburizing process is gas carburizing.
It consists of a case hardening treatment where a finished part is exposed to a carburizing atmosphere in a batch or continuous furnace , at a high temperature.
It is important to achieve high surface hardness in a carburized part, and that is usually accomplished by controlling surface carbon content with process atmosphere control (in-situ oxygen probe and CO-CO2 infrared analysis).
Many factors, especially those that control surface carbon concentration, such as time and temperature during the various stages of a carburizing process, affect case depth (figure 3). Frequently, the first stage of carburizing inroduces a high surface carbon content, on the order of 1,1 to 1,2 wt %, depending on the maximum solubility of carbon in austenite at the temperature of that stage. Such carbon contents would produce undesirable quenched microstructures. Therefore to produce optimum surface carbon concentrations of 0,8 to 0,9 %, the second stage of carburizing is performed with lower carburizing atmosphere carbon potentials.Carbon already introduced in the first stage then ajusts to the lower surface potential and also diffuses deeper into the core. This two-stage approach is commonly referred to as the boost-diffuse method of carburizing .
If the superficial carbon content in the case depth is too high, austenite that have not transformed during quenching , is referred to as retained austenite and is present because of the high stability of high - carbon austenite. Increasing carbon content significantly lowers the " Martensite Start " (Ms) and decreases the temperature range for martensitic transformation to below room temperature . Consequently there are always significant amounts of retained austenite in the cases of carburized steels quenched to room temperature. Reduction of retained austenite content can be achieve by reheating cycles below Acm or by cryogenic treatment .

2.3 CARBURIZING PROCEDURE

The main steps to carburize mechanical parts are summarized as follows (figure5).
When machining of the parts is completed, they are placed in a basket or moun-

www.manaraa.com

ted on some type of fixture (figure 6) . Then, the basket is charged into a furnace, which normally has a temperature of about 880-950 °C for gas carburizing and 800-850 °C for carbonitriding (diffusion of carbon and nitrogen) (figure 7).
Conveyor-belt furnaces, shaker-hearth furnaces or rotary-retort furnaces are used for small parts, such as screws .
The furnaces that are used vary widely in size and appearance . For the automotive industry, which uses mass production lines , pusher-type furnaces are very common .
There is a carburizing gas atmosphere in all furnaces. When the load has reached the carburizing temperature, the effective transfer of carbon from gas to steel surface begins. Carburizing cycle is proceeded until the desired depth of carbon penetration is reached .The charge is then moved from the furnace chamber to a cooling chamber, which normally has an oil tank .The load is lowered quickly into the oil tank . After complete cooling, the charge is washed and tempered . The last step include generally a phase of dimension-adjusting grinding to completely-finish the parts .

2.4 CARBURIZING ATMOSPHERE

The primary function of the furnace atmosphere is to supply the needed carbon and provide the right surface carbon content in carburized parts . The atmosphere must have a composition that corresponds to these needs . To control the surface carbon content, it must be possible to control the composition of the gas . This is normally done with a separate enriching gas, a hydrocarbon, usually : propane or methane. A ferrous base alloy held at a temperature sufficient to provide complete austenitization is brought into contact with a carbonaceous environment that consists of an endothermic carrier gas enriched with either a hydrocarbon gas or a vaporized hydrocarbon liquid. The carrier gas is usually composed of nitrogen (N_2), carbon monoxide (CO), and hydrogen (H_2). Methane (CH_4) or propane (C_3H_8) are the principal hydrocarbon enriching gases employed. Frequently, vaporized methanol is used as the hydrocarbon source. At the temperatures typically employed during gas carburizing (850-950 °C), the gaseous hydrocarbons break down into CO,CO_2,CH_4, and H_2O (g), and of these gases, CH_4 is the primary source of carbon with CO serving as the transport medium for the carbon. The N_2 and H_2 gases only serve to dilute the atmoshere. A sufficient carbon potentiel must be maintened throughout the process to promote absorption of carbon at the steel - atmosphere interface. The carbon potentiel is controlled by the proper chemical balances between CO and CO_2 and H_2 and H_2O , by the carburizing temperature, and by the solubility of carbon in the austenite .As carbon is absorbed by the steel, a carbon concentration gradient is established between the surface and the interior of the steel and carbon atoms diffuse , by way of an interstitial mechanism, down this composition gradient according to Fick's second law for diffusion in one dimension. As the carbon atoms diffuse down the established carbon gradient, a carburized case is developed. The depth of this case is a function of temperature, time and steel grade . Carbon absorption at the steel-atmosphere interface is a critical process . A number of factors can exert a significant influence on the carbon absorption process during gas carburizing.
The main constituents present in the furnace atmosphere are CO,N_2,H_2,CO_2,H_2O and CH_4 gases. Carbon monoxide gas is the most active of these six atmosphere constituents, and is directly responsible for the transfer of carbon from the atmosphere to the austenite at the steel-atmosphere interface.The transfer of carbon

www.manaraa.com

can occur as a direct result of the interaction of CO with iron or as a result of the interaction of CO and H2 at the interface. These reactions are described by the following reversible reactions :

$$2\,CO\,(g) \rightleftharpoons C + CO_2\,(g)$$

$$CO\,(g) + H_2\,(g) \rightleftharpoons C + H_2O\,(g)$$

" C " is carbon in solid solution in the austenite .
If these reactions are correctly balanced so that the reactions proceed to the right, then carburization will occur . However, both CO_2 and H_2O are strong decarburizers, and excessive amounts of these two phases will cause these reactions to proceed to the left .
Typical carburizing atmosphere are endothermic gas (blend of : CO,H_2,N_2 and with smaller amounts : CO_2,H_2O,CH_4) produced in a generator , and endogas formed from a nitrogen-methanol blend . More recently , vacuum carburizing process used only a partial pressure of a pure hydrocarbon gas, such as : propan , that is dissocied at low pressure (4).

2.5 MECHANICAL APPLICATIONS

The typical carburized component is equivalent to a "composite material", with a high hardness in the case on a lower carbon base, that is lower in hardness but higher in toughness.
The carbon-rich case, useful for its wear resistance, also interacts with the low carbon core during quenching to generate favorable compressive residual stress which enhance the load carrying ability of the "composite".
The microstructural gradient and the residual stress profile define the fatigue and fracture properties of carburized components. Maximum performance in a carburized part is achieved when the as-quenched microstructure in the case comprises only martensite and retained austenite, and the microstructure in the core comprises only martensite and / or bainite.
It is know that martensitic structures (and / or bainite in the core) are required for optimal performance of gears. To resist gear fatigue failure due to cyclic bending stresses at the root fillet, the optimum case structure must be a mixture of high carbon martensite and austenite with enough martensite to assure a hardness of at least 57 Rockwell C .
A major benefit of carburizing is the introduction of compressive residual stresses into the surfaces of carburized parts. These stresses counteract applied tensile stresses and therefore improve bending fatigue performance.
Generally, the compressive stresses reach a maximum at some distance from the surface, and gradually decrease.
Carburizing is used for a wide range of mechanical components : transmission parts, car engine components, roller and ball bearings , gears , wear parts, fatigue stressed parts such as shafts .

3 . PLASMA NITRIDING OF STEELS

3. 1. HISTORIC

The origins of the plasma thermochemical process lie in the patents filed by the Swiss engineer Bernard Berghaus in the 1930s . However the development of

www.manaraa.com

plant for general commercial use was extremely slow . In europe , over the period 1957 to 1967 , the technology is introduce in several companies for industrial exploitation . Actually , we can count between more than 1300 - 1600 ion nitriding equipments worldwide .

3.2. DEFINITION

Plasma nitriding is a method of surface hardening using glow discharge technology to create firstly atomic nitrogen by direct ionic dissociation of molecular nitrogen and secondly to introduce atomic nitrogen , by diffusion mechanism , to the surface of a heated metal parts (5) .

3.3. PROCESS PRINCIPLE

The components to be nitrided are introduced in a vacuum chamber and these parts are made the cathode of an electrical circuit and subjected to a glow discharge generated by applying a critical voltage at a pressure of 1 - 10 mbar in an atmosphere of hydrogen and nitrogen. Some exemples of glow discharges applied on mechanical parts are shown in figures : 11 , 12 .
The applied electric field ionises the gas mixture causing nitrogen ions to bombard the component surfaces so generating heat flux and the active nitrogen diffuses into the steel surface . The temperature of the parts can be controlled by adjustments to the applied voltage and gas pressure or by using auxiliary radiant heating system. While the gas composition can be adjusted by mass flowmeter to control precisely the nitriding potentiel in order to obtain the desired nitriding configuration (compound layer types , diffusion layer).

3.4.METALLURGICAL ASPECTS

In this process , only nitrogen (plasma nitriding) or both nitrogen and carbon (plasma nitrocarburising) are introduced into the surface of steel , by diffusion mechanism , at temperatures in the range 500 - 570 °C from the plasma applied on the components. High surface hardness are achieved after gas cooling (figure 9) .
The process is carried out at a temperature below the eutectoid temperature (ferritic domain) and involves the formation of hard , wear resistant iron-alloy nitrogen compounds , therefore the steels do not require quenching to achieve full hardness .
The majority of the steels which are nitrided contain combinations of aluminium, chromium , molybdenum and vanadium .
An exemple of such steel contains : 0.4 % C, 1.8 % Cr , 1 % Al , 0.25 % Mo (Afnor : 40CAD6.12). We can obtain with this steel a very high surface hardness level : about 1100 HV. For another types of steels the hardness is 300-500 HV for carbon steels (XC10-XC45), 500 - 900 HV for alloy steels (42CD4 - 30NCD8), 300-600 HV for cast iron , 900-1100 HV for nitrided steels (30CD12 - 40CAD6.12) cold and hot working steels (Z40CDV5 - Z160CDV12) , 1000-1100 HV for tool steels, 900-1200 HV for stainless steels (Z20C13-Z6CN18.9-Z35CD17) .
These nitrided steels must be austenitised, quenched and tempered at a high temperature, usually 900-950 °C, to produce a fully stabilised tempered martensitic structure , prior to nidriding cycle .
Nitriding involves the formation of alloy nitrides at the surface of the steel. Any steel with nitride-forming elements like chromium or aluminium can be nitrided but the response differs according to the composition of the steel .
Generally, the case hardness increases as the alloying element content increases, though the case depth becomes more shallow and there is an abrupt transition to

www.manaraa.com

the substrate . For instance, Chromium- rich stainless steels can be most effectively plasma nitrided . But it must be remenbered that nitriding a stainless steel can greatly impair its corrosion resistance . The case structure of a nitrided steel may include a nitrogen diffusion zone with or without a compound layer (Fig. 10) depending on the type and concentration of alloying elements , temperature, and nitrogen potentiel .The diffusion zone of a nitrided case is composed of the original core microstructure (martensite) with some solid solution and fine precipitation strengthening .Hard metallic nitride precipitates are formed with alloying elements in the base material (Cr ,Va , Al, Si, Mo). The depth of the diffusion zone depends on the nitrogen concentration gradient , time - temperature and steel type.The compound layer can be composed of one or two iron nitrides : Fe4N (gamma prime nitride) or Fe2-3N (epsilon nitride). Because carbon in the material aids epsilon formation , methane is added to the treatment gas when an epsilon layer is desired . Because the nitriding potentiel can be very precisely controlled by the regulation of the nitrogen content in the gas mixture , it should be possible to select a monophase layer of Fe4N or Fe2-3N , or to prevent the white layer formation in order to favour only the diffusion layer formation .The epsilon layer is generally used for wear, friction and fatigue applications without shock, excessive load or localized stresses . The diffusion zone holds the nitrided case in compression and then increases the surface harness and the endurance limit of the part (figure 9) .

3.5. EQUIPMENT

A plasma nitriding system is shown in Figure13. The parts to treated are cleaned by vapor degreasing , loaded into the vacuum chamber .The pressure is reduced to a level of 0,01 to 0,1 mbar . The load is heated by the glow discharge itself or by a combination of plasma and auxiliary heating to reach the nitriding temperature, which is usually in the range 400 to 570 °C . Auxiliary radiant heating can be used as a convective heating to increase the heating speed , and is able to heat large workloads, including different size. Since the load is heated to desired temperature , gas mixture is admitted in the vessel and pressure is regulated in the 1 to 8 mbar range. After these steps, a high negative potentiel is applied on the parts by using a high-frequency pulsed plasma power supply . The unit is fully computer controlled for the full floor-to-floor process cycle . After the ionic treatment, the load is cooled by nitrogen circulation or use of an heat exchanger to extract faster the heat .

3.6.INDUSTRIAL APPLICATIONS

Plasma nitriding is a technique that has been used for the surface hardening of both ferrous and non-ferrous components on an industrial mass-production basis for over twenty years . Used primarily to enhance surface wear- resistance, ion nitriding can be used as a direct replacement for conventional gas and salt-bath nitriding treatments .
A large variety of production tooling such as stamping and forming dies hot forging dies, aluminium extrusion dies, ejectors for plastic molds , screws for plastic extrusion, are routinely plasma nitrided to produce wear resistant case layers that help increase the performance and life time of the tool . An increasing number of engineered components including : gears, valves, crankshafts, hydraulic parts , camshafts, sintered parts, are also now being plasma nitrided on a large volume production level (see: Figures 12, 13).
In summary, the overall application range of plasma nitriding is very wide and

www.manaraa.com

concerns all the parts submitted to wear, friction, adhesion, abrasion, to prevent galling, metal pick-up and to improve wear and fatigue strength .

3.7. ADVANTAGES

Plasma nitriding offers many advantages over other nitriding processes and is a technique producing uniform surface hardening of a variety of components . The main advantages are :

- improved control of case thickness
- ability to select the compound layer type or to prevent white layer formation
- no environmental hazard compared to conventional process
- ability to automate the system
- shorter cycle time
- reduced energy consumption
- ability to use mechanical masking
- flexibility and reliability
- posibility to nitride stainless steels , titanium alloys (2), stellite
- possibility to use lower nitriding temperature and to limit distortion . (finished machined components can be processed without the risk of distortion)

4. BORIDING OF STEELS

4.1. DEFINITION

Boriding , is a thermochemical surface treatment , whereby boron is diffused into, and combines with , the substrate material forming a single or double phase metal boride layer at the surface . Unlike many other surface treatments , hard boride layers can be developed on most alloys and metals by diffusion boron (6) .

4.2. PROCESS PRINCIPLE

All boriding treatments are carried out at 700-1000 ° C, usually for several hours, producing hard layers about 30-180 microns thick .
Unlike carburizing treatment on ferrous materials , where there is a gradual decrease in composition from the carbon-rich surface to the substrate, the boriding of ferrous materials results in the formation of either a single-phase or double-phase layer of borides with definite composition (figure 8) .
The phase equilibrium diagram of the binary system iron-boron according to Hansen, shows the existence of two iron borides : Fe2B with 8,83 wt % boron and FeB with 16,23 wt % boron . The formation of either a single or double phase depends onthe availability of boron . The formation of a single Fe2B phase, with a sawtooth morphology due to preferred diffusion direction , is more desirable than a double-phase layer with FeB. The boron-rich FeB phase is considered undesirable , because FeB is more brittle than Fe2B . Therefore , the FeB phase should be avoided or minimized in the boride layer .
The boriding process consists of two types of reaction . The first reaction takes place between the boronizing agents and the part surface .The nucleation rate of the particles at the surface is a function of the boriding time and temperature .This produces a thin , compact boride layer .The second reaction is diffusion controlled. The total thickness of the boride layer growth at a given temperature can be calculated by the formula : *d= k square root of t* , where d is the boride layer thickness in cm , k is a constant, depending on the temperature , and t is the time in sec at a given temperature .

www.manaraa.com

Industrial boriding can be carried out on most ferrous materials such as case-hardened, tempered, tool and stainless steels , cast steels, gray and ductile cast irons , sintered steel . As the alloying element and / or carbon content of the substrate steel is increased, the formation of a sawtooth configuration in the interface is suppressed , and for high-alloy steels a smooth interface is formed . The sawtooth configuration of the boride is dominant with unalloyed low-carbon steels, and low-alloy steels . Alloying elements retard the boride layer growth caused by formation of a diffusion barrier . During boriding , carbon is diffused away from the boride layer to the matrix and can form boro-cementite .Like carbon, silicon and aluminium are not soluble in the boride layer and are unfavourable for boriding . Chromium steels improve the formation of boron-rich layer , decrease the boride depth and give a smooth coating / interface .
Borided parts can be quench hardened in air, surpressed gas, oil and salt bath . Heating to the hardening temperature should be carried out in an oxygen-free protective atmosphere .

4.4 BORIDING TECHNIQUES

There are different boriding techniques : solid phase boriding like pack boriding and paste boriding , liquid phase boriding , gaseous phase boriding , plasma phase boriding .
4.4.1. *Pack boriding* .The technique involves packing the parts in a boriding powder mixture contained in a heat-resistant steel box . Powders contain boron carbide (B_4C) , the main source of boron, together with SiC or Al_2O_3 which act as inert diluents , and an activator compound such as KBF_4 .
4.4.2 .*Paste boriding* .This process is used when pack boriding is difficult or more expensive . A paste of 45% B_4C and 55% cryolite or conventionnal boronizing powder mixture in a binding agent is brushed or sprayed over the parts to form a coating of 1 to 2 mm thick . Subsequently , the steel parts are heated at 900 °C to 1000 °C inductively, resistively or in a conventional furnace in a protective atmosphere (N_2, NH_3, Ar). This process is very useful in the case of large parts or for those requiring localized boriding .
4.4.3 . *Liquid boriding* . Liquid boriding is grouped into electroless and electrolytic salt bath processes . Electroless method is carried out in a borax-based melt at 900-950 °C to which about 30 % B_4C is added. Another salt bath composition can be used . In electrolytic salt bath boriding, the metallic part acting as the cathode and a graphite anode are immersed in the electrolytic molten borax at 950°C. The fused salt bath decomposes into boric acid (B_2O_3) , and sodium ions react with boric acid to liberate boron . These processes have several disadvantages: difficulties to remove the excess salt, quality of the salt, environment .
4.4.4 . *Plasma boriding*. Mixtures of B_2H_6-H_2 or BCl_3-H_2-Ar may be used in plasma boriding. The control of composition and depth of the borided layer is possible , but the use of a very toxic gas and the difficulties to obtain good layer uniformity limit the diffusion of this technology .

4. 5 . INDUSTRIAL APPLICATIONS

Borided parts have been used in a wide variety of industrial applications . The high hardness of borided materials makes them suited to resisting wear, particularly to that caused by abrasive particles. The wear resistance performances are obtained when contact stresses are minimized. The hardness of boride layers on iron materials is about 1800 to 2100 HV and higher for alloyed alloys .

www.manaraa.com

Parts used in sliding wear situations have had their service life increased. Industrial applications include: extrusion screws, cylinders, textile nozzles, punching dies, stamping dies, molds for plastic and ceramic, die-casting molds, pressing rollers, mandrels, hot forming dies . . . Borided steel parts have been used for molten nonferrous metals (Al, Zn,Sn). Boriding can increase the resistance of low-alloy steel to acids. Borided austenitic steels are resistant to HCl acid. Large scale boriding was applied, on small drive gears for oil pump in a Volkswagen diesel engine, to increase resistance to adhesive wear.

5. CONCLUSION

Surface hardening processes such as carburizing, nitriding and boriding are used in a wide variety of industrial applications to mainly improve the wear resistance of steel parts. In most cases, the three different thermochemical methods described in this paper, can resolve et satisfy the mechanical engineering demands. Depending of the application type of the mechanical part and its environmental factors, adequate materials and surface treatments should be selected. The wide range of available surface hardening methods and their performances can provide mechanical, tribological and environment-compatible surfaces for a given application.

REFERENCES

(1) Krauss, G. (1990) ' Steels, heat treatment and processing principles 'ASM International.

(2) Krauss, G. (1978) ' 'The microstructure and fracture of a carburized steel ', Metall. Trans. A, Vol 9A, p. 1527-1535.

(3) Jacquot, P et al. (1992), ' Plasma overcarburizing of chromium steels for hot working and wear applications ' , Materials Science Forum, Vols. 102-104, p.155-168, Trans Tech Publications Ltd ,CH, Proceedings of the first ASM heat treatment and surface engineering Conf., Amsterdam, may 22nd-24 th 1991.

(4) Jacquot ,P et al., (1992), ' Vacuum carburizing of steel parts in an industrial oil quenching vacuum furnace', 8 th Int. Congress on heat treatment of materials ,Kyoto, Japan.

(5) Jacquot, P et al. (1992), ' Surface engineering using plasma technology. Industrial applications of plasma nitriding and PVD coating ', European seminar on Electro-technologies for industry, proceeding, Bilbao, Spain, may 20th-22nd.

(6) Vermesan, G et al. (1986), ' Borurarea ', Polytechnique Institut of Cluj-Napoca, SID 47, p. 1-110, Romania.

www.manaraa.com

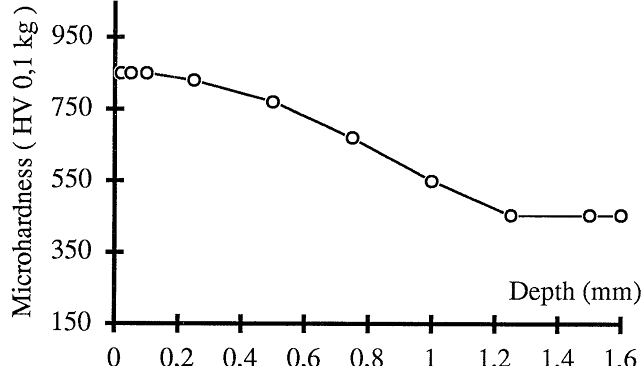

Figure **1** . Microhardness profile of a steel after carburizing .

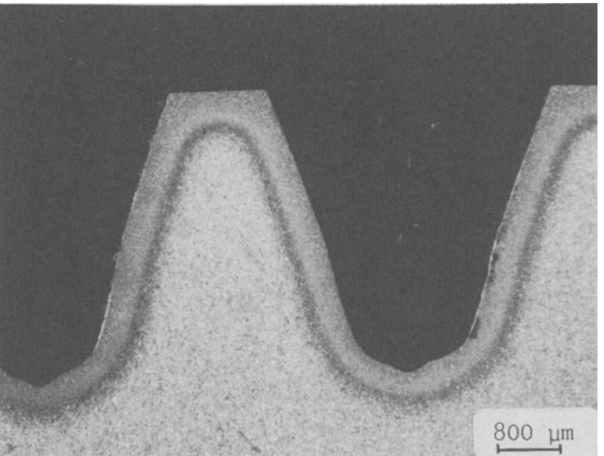

Figure **2** . Macrography of an helicoidal gear tooth made of 16NC6 steel, after carburizing .

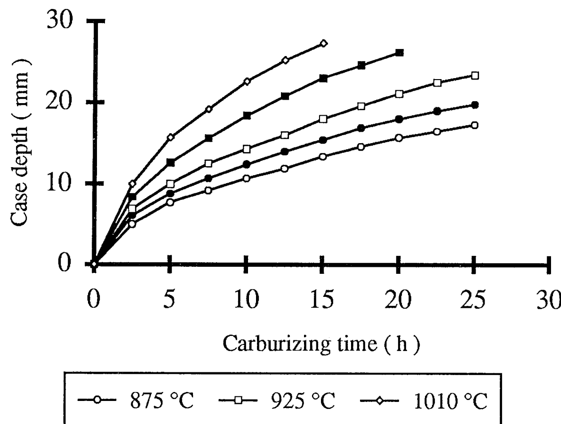

Figure **3** . Approximate relationship between temperature, time and carburizing depth .

المنارة للاستشارات
www.manaraa.com

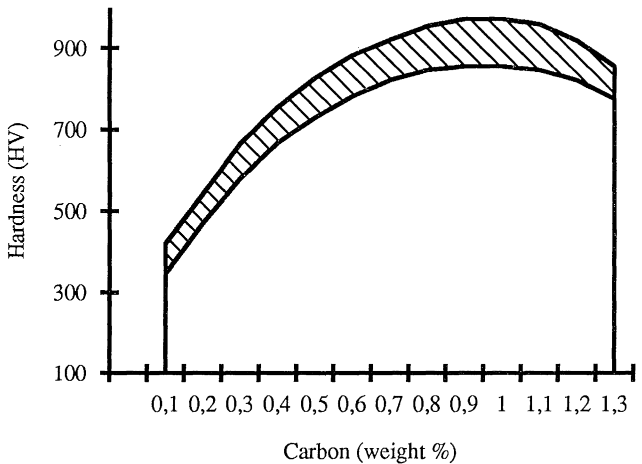

Figure **4** . Hardness as a function of carbon content in hardened steel. The hatched area shows the effect of retained austenite and alloy content of steel .

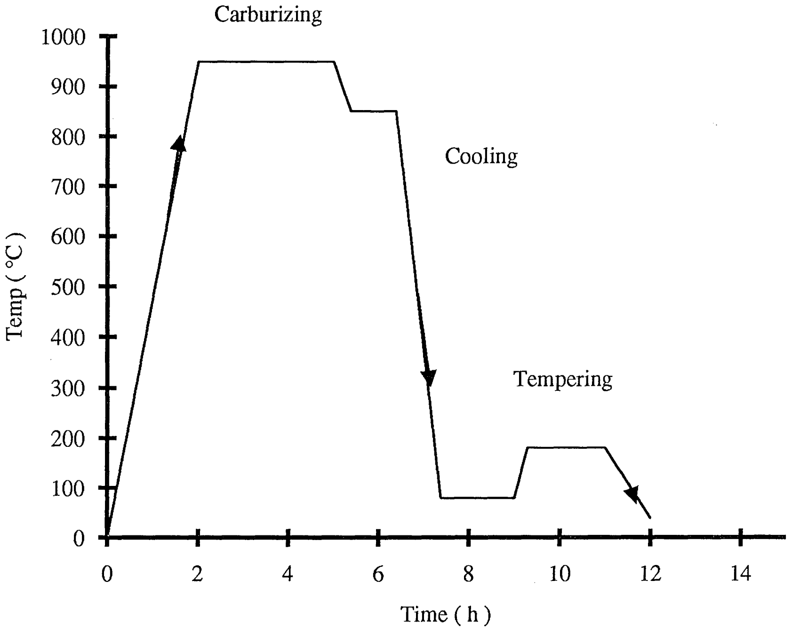

Figure **5** . Typical gas carburizing cycle. Temperature versus carburizing and tempering times .

للاستشارات المنارة
www.manaraa.com

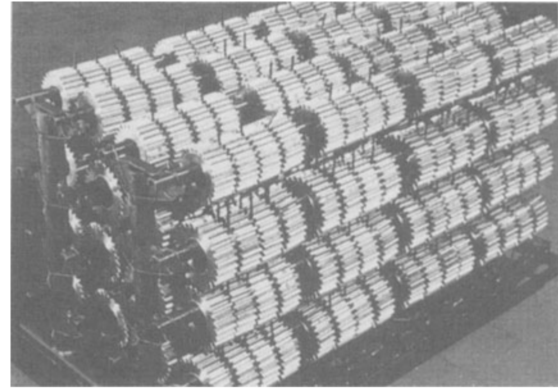

Figure **6** . View of a gear load on its fixture before introduction in the gas carburizing furnace .

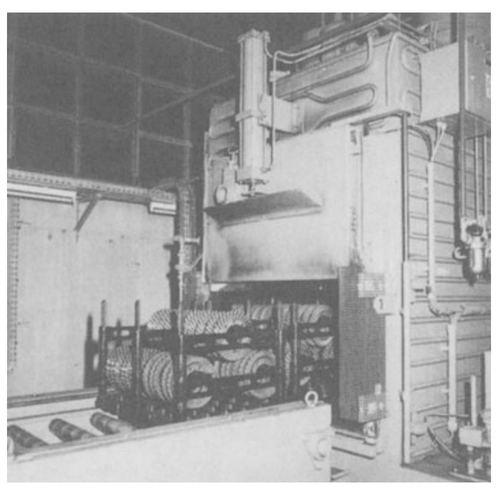

Figure **7** . View of a gas carburizing batch furnace and helicoidal gears load .

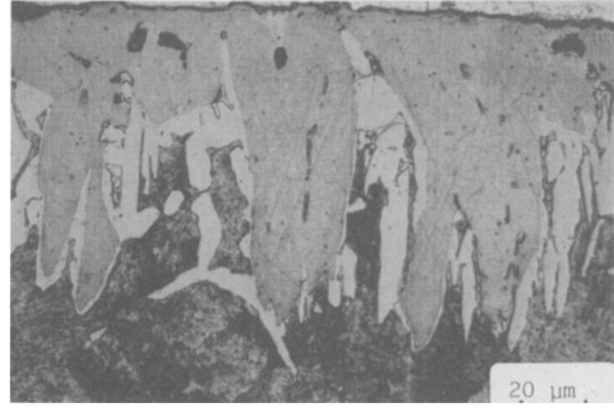

Figure **8** . Boride layer on a high carbon steel developed after pack boriding : exterior layer FeB, interior layer Fe2B .

المنارة للاستشارات
www.manaraa.com

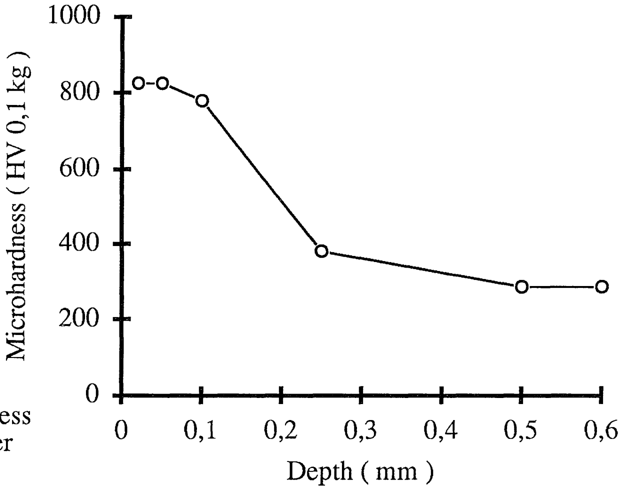

Figure **9** . Microhardness profile of a steel after plasma nitriding .

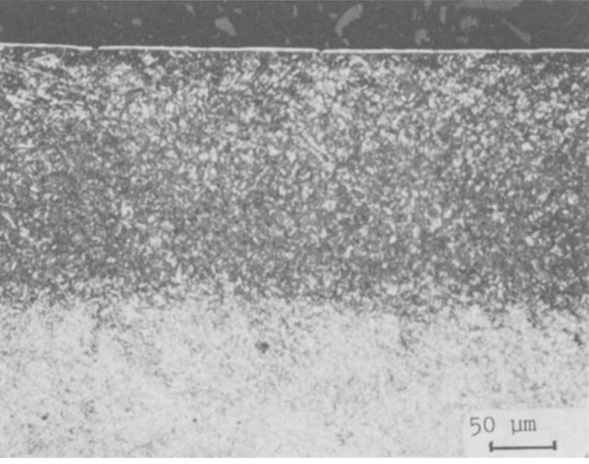

Figure **10**. Microstructure of 32 CDV 12 steel after plasma nitriding. View of a compound layer of Fe4N supported by a nitrogen diffused case .

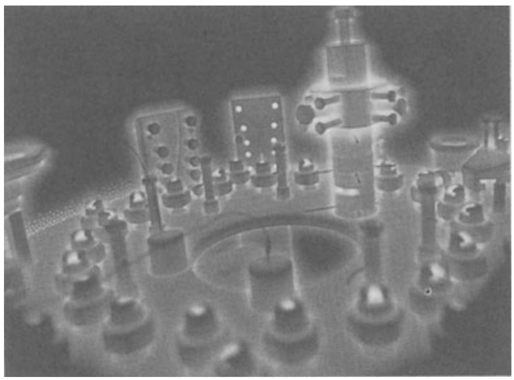

Figure **11** . Mechanical parts surrounded by an electrical glow discharge plasma of N2-H2 .

المنارة للاستشارات
www.manaraa.com

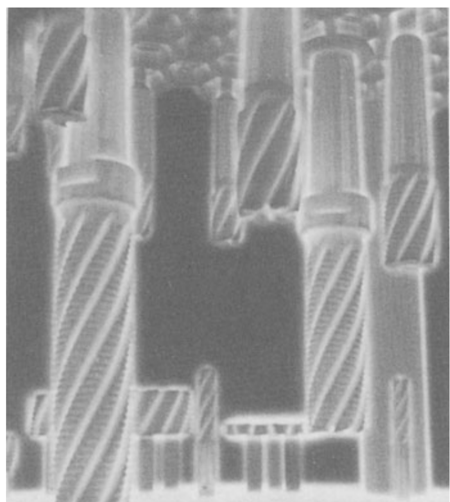

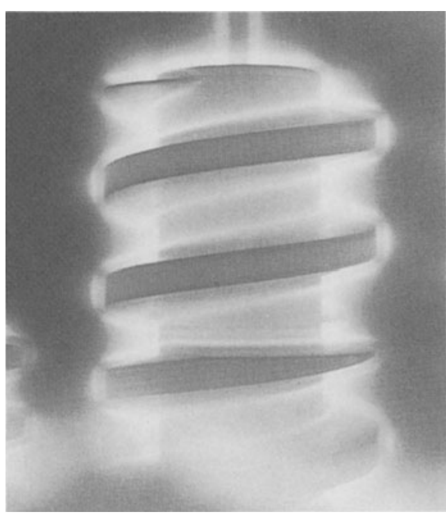

Figure **12**. View of cutting tools and screw for plastic injection machine during plasma nitriding cycle .

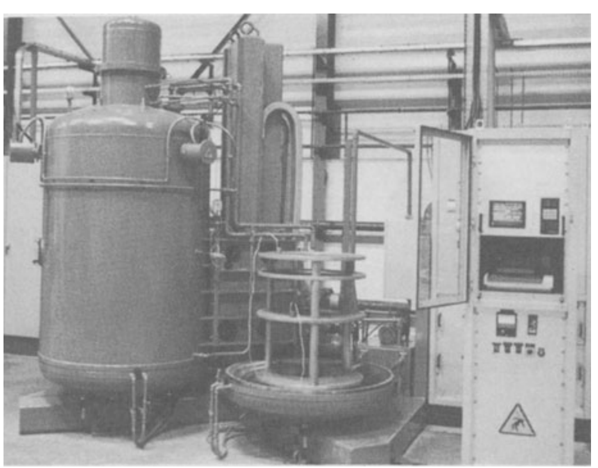

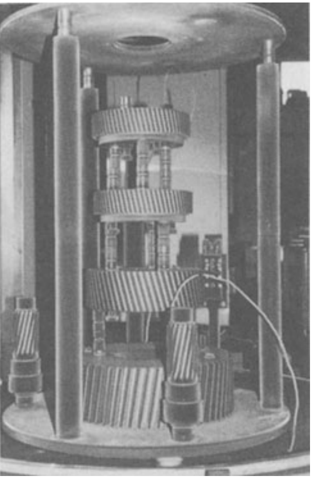

Figure **13**. Views of a pulsed plasma nitriding unit with auxillary heating system and double load-fixturing (on the left), load of gears plasma nitrided (on the right).

المنارة للاستشارات

www.manaraa.com

ION IMPLANTATION FOR SURFACE ENGINEERING

P.MAZZOLDI
Unita' Consorzio Interuniversitario
di Fisica della Materia (INFM)
Department of Physics
Via Marzolo 8 - 35131 Padova
Italy

ABSTRACT. Low energy accelerators are used widely for the modification of materials and in research on material properties. The ion implantation of semiconductors becomes an industrial application of major importance. The ion implantation technique has steadely been extended to the intire range of materials including metals, ceramics, glasses and polymers.. This paper considers a number of areas in which ion beams are now applied, such as microelectronics, metallurgy, corrosion science,optics.

1. Introduction

The ion implantation provides one method of introducing chosen atomic species into a material by direct ion bombardment. The incident ions come to stop in the bombarded material as a result of losing energy during collision with substrate atoms. The rsulting depth-concentration profile of implanted atoms can be calculated for most projectile-target combinations from well-established theoretical models.
During the slowing-down process, the incident ions transfer a significant amount of energy to the substrate resulting in the displacement of target atoms. As a consequence, there is a probability of atom ejection (sputtering) from the target surface and an equilibrium condition may be reached, where as many atoms are removed by sputtering as are replenished by implantation. In such conditions, the depth distribution of implanted atoms presents a maximum at the surface and falls off over a distance comparable to the initial range.
The important feature of ion implantation technique is that it allows the controlled introduction of almost any additive, albeit to a limited depth, without the necessity of elevated temperatures. The injection proceeds irrespective of the normal constraints of solid solubility or diffusivities.

An important attribute of ion implantation is that it is a violent process in which a considerable lattice disorder is introduced and the atoms of the bombarded material may

W. Gissler and H. A. Jehn (eds.), Advanced Techniques for Surface Engineering, 83–104.
© 1992 *ECSC, EEC, EAEC, Brussels and Luxembourg.*

www.manaraa.com

be displaced many times over. The implanted atoms will often associate with or segregate to the produced defects and these complexes influence the material properties.

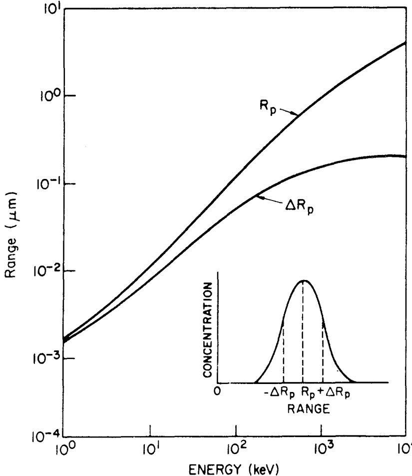

Figure 1. The projected range (R) and the range straggling (ΔR) as a function of implantation energy for nitrogen in iron.

Ion implantation has now been extended to the entire range of solid materials, for the modification and study of such different chemico-physical characteristics as corrosion, wear, catalytic properties, magnetic behaviour and optical properties.

Another approach has received much attention over recent years, and is generally described as ion beam mixing. If a thin (about 100 nm) coating is bombarded with energetic ions wich pass through into the substrate it is possible to bring about a progressive intermixing in which the atoms are transported either by rapid collisional effects or by various mechanisms of radiation enhanced diffusion. The end result is a non-equilibrium state wich resembles in many ways that produced by direct ion implantation. In many experimental situation ion-mixing technique ovrpass the concentration limits, observed in ion implantation process. At the initial stage of mixing process it is observed that there can be a considerable increase in thin coating adhesion and the particular physico-chemical effects that account for this are the subject of some interesting research.

Higher ion energies are used in material research in order to induce a controlled amount of near-surface radioactivity, in a process referred to as Thin Layer Activation (TLA). The purpose of this is so that subsequent erosion of surface, either by wear, sputtering or corrosion-erosion can be followed by monitoring the loss of radioactivity (or alternatively its appearance as debris elsewhere).

The present paper will attemp to give an overall perspective of these development in such different fields as microelectronics, metallurgical applications, medicine, corrosion science, catalysis, optics.....

www.manaraa.com

Necessary the review is superficial and for more details the reader is referred to the proceedings of several series of international conferences [1-4].
The advantages of ion implantation in comparison to other surface treatments, such as coatings, are :

a) controllable addition of impurity ions,
b) ion energy control of the ion range,
c) multi-energy implants offer a depth tailored profile,
d) small lateral spread of the implanted ions,
e) solid solubility limit can be exceeded,
f) no modifications are induced on bulk properties,
g) no significant dimensional changes are produced,
h) low temperature process,
i) no adhesion problems, since there is no a sharp interface,
l) clean vacuum process,
m) highly controllable and reproducible process
n) alloy preparation independent of diffusion coefficients,
o) allows fast screening of the changes in alloy composition, also if radiation effects may introduce modification in the alloy behaviour,
p) self alignement of the implant with surface masks and/or contacts,
q) implantation through existing layers or surface barrier oxide.

Limitations of the ion implantation technique are related to the application to samples having complicated reentrant surfaces, to the shallow implanted ion penetration, also if there are several situations involving both physical and chemical properties in which the effect of the implanted ions persists to depths far greater than the initial implantation range, and the relatively expensive equipment and processing cost.
Implanting ions into metals or semiconductors does not have the problems of substrate charging which occurs in insulating materials, i.e. wide band-gap materials. In the case of metals and semiconductors attaching ground to a substrate provides a route through which a charge to compensate the charge introduced by ion implantation can move into the implanted material. In presence of materials with wide band-gap and consequently resistivities > 10^{18} Ω·cm at room temperature, charging phenonemon frequently results in electrostatic discharges within the material. Another consequence is the growth of an electric field which repels subsequent charges. These effects may be reduced or eliminated if there are ions in the material with sufficient mobility to redistribute in the electric field produced by the added charges. If the material is in contact with an electron source, if the potential to injection is small and if the mobility of the injected charge is not too small then the charge added by irradiation may be compensated. It is possible to implant insulating materials, as glasses, mounting the samples on grounded metals supports. Thus the support provides a source of electrons to compensate the positive implanted charge.

المنارة للاستشارات
www.manaraa.com

2. Metallurgy

Ion implantation is a process by which nearly all elements can be incorporated in the near surface regions of materials without any metallurgical constraints. The concentration and the depth distribution can be well controlled, leading to a high degree of reproducibility in altering chemical and physical properties of the materials. Due to these unique capabilities for the modification of surface sensitive properties, the field of ion implantation into metals has expanded rapidly in the last decade. Numerous systematic studies have proved that mechanical, chemical, electrical and optical properties can be optimized for special applications. The improvement of mechanical properties such as friction, wear, hardness, adhesion and fatigue seems to have the greatest potential for commercial application. Thus, on the one hand systematic studies may provide a product which is of technological use, on the other hand, however, these studies provide insight in the relationship between materials properties and their microscopic structure.

Channelled Rutherford Backscattering provides information about the lattice location of implanted impurities heavier than the host. It was thus observed that normally insoluble additives would, as implanted into metal crystals, often occupy substitutional lattice sites. Thus molybdenum in copper can form a substitutional solid solution at concentrations of a few atomic per cent. One view is that the presence of bombardment-induced vacancies stabilizes the substitutional location of oversized impurities by accommodating additional lattice mismatch. This model relies upon the fact that interstitials are much more mobile than vacancies so that each ion trajectory will result in the production of a collision cascade with a vacancy-rich core. The constraint on differences in electronegativity, normally up to 15 per cent according to the Hume-Rothery rule, also proves to be relaxed under ion implantation conditions. Vacancies, though unchanged in a metal, effectively allow an excess of valence electrons to balance the influence of additives of low electronegativity, such as rare earth species. The detailed consideration must take into account the modified Fermi surface of the irradiated metal.

Beyond a critical composition the combination of lattice disorder and physico-chemical mismatch inevitably produces a breakdown in order and the metal becomes amorphous (by all available experimental criteria). This is a useful method of exploring 'glassy' metals, which otherwise need to be produced by a rapid quenching from the melt, for example as a ribbon 'splatcooled' on a rotating water-cooled cylinder. By analogy it has been argued that the energy deposited by ion implantation creates effective local temperatures well in excess of the melt temperature, but these "quench" in a time of less than 10^{-11} seconds, so that one has ultra-rapid cooling of each thermal "spike".

Once a non-equilibrium condition has been brought about by implantation, it is useful to observe how it relaxes, during for example a subsequent thermal annealing. For example, molybdenum in copper migrates, during annealing experiments, towards the surface. At the same time precipitation occurs and eventually small crystallities of molybdenum are visible (in the SEM) on the metal surface. It is obvious that, as the vacancies anneal out the oversized impurities will tend to segregate as a second phase, but it was evident that the impurities stabilize the presence of vacancies and the process required temperatures of

www.manaraa.com

700-800C, not far below the melting temperature. It is well established that there is a positive binding energy between oversized impurities and vacancies, and such complexes can migrate as an entity. The segregation process will thus take place to available sinks (for vacancies) such as the crystal surface. Once the vacancy is lost the impurity atom becomes immobilized, but it is easy to picture the action of precipitates as favourable sinks for further segregation.

Similar processes are observed during the irradiation of thin films of metals on a surface which they do not wet, and with which there is no chemical interaction. Thus tin and lead, deposited on aluminium and irradiated below the melting temperature undergo a remarkable degree of lateral transport to form islands and beads as a result of segregation.
Segregation of the constituents of homogeneous alloys under ion bombardment is an important area of research which is connected with the use of ion beams to simulate fast neutron irradiation effects in materials for nuclear reactor construction. Redistribution occurs througha variety of mechanisms as a result of the generation of point defects (vacancies and interstitials) within the alloy. Some constituents may bond preferentially to one of these defects and the complex so formed may diffuse at the temperature of exposure (generally this is above room temperature). Alternatively there may be a migration into the bombarded zone by a mechanism which is the inverse of the Kirkendall effect. If an impurity atom can exchange with a neighbouring vacancy more rapidly than the other nearby host atoms do so, then there will be a tendency for these impurities to drift into the region with the maximum vacancy concentration. Both types of mechanism have been observed in nickel alloys irradiated with nickel ions at 500C: manganese migrates towards the damaged zone by the inverse Kirkendall procss while silicon migrates away from this zone, probably in the form of a complex with nickel interstitials.
These segregation phenomena are connected with the process referred to as ion beam mixing. Relocation of atoms by single or multiple collisions bring about a progressive intermixing by a rapid non-thermal mechanism. At higher temperatures, when point defects are mobile, the various forms of enhanced diffusion can occur and this can augment the degree of mixing. These effects may be useful as an alternative to direct ion implantation, because mixing of a deposited coating can be induced by easily generated beams of gaseous species and this avoids the necessity for intense beams of metallic ions. Thus, ion beam mixed tin has proved to be just as effective as implanted tin in iron and steel for the improvement of wear resistance.
The accelerator requirements in the metallurgical field are significantly different from those in semiconductor device fabrication. Firstly, the variety of ion species is much wider and in general the ion currents are moderately large despite the fact that areas to be treated are relatively small. The simulation of radiation damage may call for very long exposures, particularly if dynamic properties such as creep are to be investigated.

3 Tribology

Tribology is the study of the processes of friction and wear of materials and its applications are aimed primarily at the reduction of wear in metals.

www.manaraa.com

The first investigations of the effect of ion implantation on friction and wear were commenced at Harwell about 1970. Success was quickly achieved following ion implantation of steel with nitrogen or carbon, chosen on the basis of the effectiveness of the diffusive treatments, nitriding or carburising. If some 10 to 30 atomic per cent of these additives are introduced, the wear resistance, as measured by pin-on-disc tests, is frequently reduced by factors of 100, dependent upon the pre-treatment of the steel. Microhardness measurements also show substantial increases as a result of the implantation treatment.
In Figure 2 we show the weight loss after a dry sliding wear test . The measurements were performed by Mettler balance with a sensitivity of 10^{-5} g.

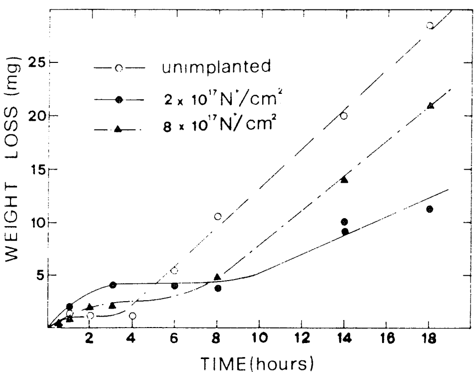

Figure 2. Weight loss of type 38NCD4 steel as a function of the dry sliding wear time, for high dose 30-keV nitrogen implantation and for unimplanted samples.

This process is believed to act by a combination of solid solution strengthening, in which implanted interstitial species pin dislocations, and dispersion hardening, in which a fine dispersion of hard nitrides (such as CrN in alloy steel) serve to harden the matrix. This corresponds well with the classical understanding of alloy hardening, but what is still debatable are the causes of the persistence of the effect, long after the initial layer of nitrogen-implanted metal has been worn away. One view is that interstitial atoms can migrate, in association with stress induced dislocations, and so be driven forward as wear proceeds. Others challenge the evidence on which this is based and consider that the implanted nitrogen may modify the initial mechanism of wear so that a mild, oxidative wear regime is initiated, which can persist.
Other species besides the light interstitial atoms also convey benefits in wear resistance: titanium, tin, yttrium and tantalum have been shown to improve the wear properties of steel. Implanted titanium reacts with carbon in the steel to produce a fine dispersion of TiC, while yttrium improves the retention of a protective oxide film. Tin may act by forming a hard oxide or by the production of iron-tin intermetallic particles.
The practical applications of ion implantation for wear resistance have been mainly in tools such as moulds, dies, punches, mill rolls and press tools. The advantages are that there is

www.manaraa.com

only a moderate temperature rise during treatment, and so no distortion.are not introduced The process brings about no dimensional changes and retains the full polish. Probably the most successful area of application has been to precision tools subjected to abrasive wear in the moulding of filled plastics. Often these are extended in life by a factor of ten. Nitrogen implantation has not been successful for cutting tools which operate at high temperatures (> 500 C) such as drills or cutting tool inserts. This may be because the nitrogen diffuses away, or the implanted layer is consumed by the growth of oxide. Implanted yttrium is, however, effective at 1000C .

Cobalt-cemented tungsten carbide is an important composite material used for long-life tools, and here again nitrogen implantation has sometimes given useful increases in life. The benefits are less reproducible than in steel, however, and it has been shown that a high temperature (300-400 C) during implantation leads to a greater hardness and wear resistance. This implies that the implanted atoms must be capable of migrating to associate with defects of some kind. Depending upon the grade of carbide there may be different degrees of improvement, and tentatively it appears that the greatest benefit occurs in the softer carbides. Successful practical applications have been made in punches, wire-drawing dies, knives and drills for printed circuit board manufacture.

Titanium alloys are light, have good tensile strength and are extremely resistant to corrosion. They are therefore favoured for a variety of advanced components, such as surgical prostheses (artificial joints). However, the wear resistance of titanium alloys is relatively poor by comparison with that of cast Co-Cr-Mo alloy. Ion implantation of nitrogen has proved to be a highly successful means of improving the wear resistance of titanium and its alloys, and the mechanism is almost certainly due to the production of a fine dispersion of hard titanium nitride within the metal. The surface retains its excellent corrosion resistance and yet, in tests against high molecular weight polyethylene, the wear rate is reduced by over 400 times.

The wear mechanism in this case is believed to be abrasive, as a result of particles of hard oxide debris which become embedded in the plastic. The useful life of artifical joints should be increased significantly because a known mode of degradation is the irritation and bacteriological infection which comes about as a consequence of wear debris in the joint.

This area of medical implants is advancing more quickly than some of the other applications, such as tooling. This is because ion implantation appears to be the only surface modification technique which can succssfully harden this alloy's surface without comprimising surface finish, dimensionality or cosmetic appearance. In addition there is not the concern of delamination that there would be for conventional coatings and the implanted nitrogen is accepted as being benign within the human body.

Ion accelerators are useful nowadays in quantifying wear rates by the technique of thin layer activation, which was applied to the prosthetic materials in the example above. The technique consists of bombarding the material with energetic charged particles chosen to induce a nuclear reaction in one of the alloy constituents. Preferably the nuclei produced by this activation give rise to a penetrating form of decay radiation, such as gamma rays: absorption within the test equipment is thereby minimised. Wear is determined either by

www.manaraa.com

the loss of radioactivity in the component or by the accumulation of active debris on a filter or within the lubricant. The thin layer activation method is being used on a growing scale for the evaluation of lubricants, or for the testing of surface treatments. It is not confined to metals since almost any material can be activated by a suitably chosen beam.

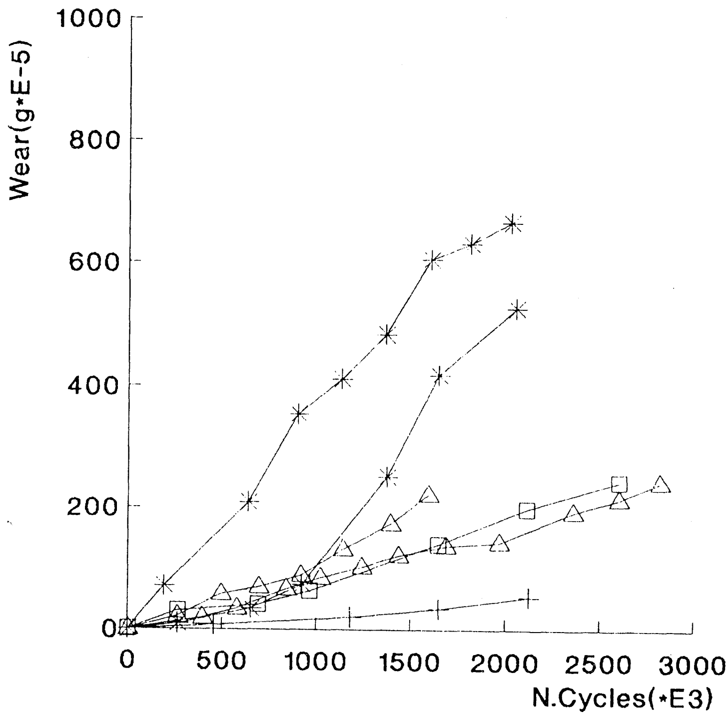

Figure 3. Wear diagrams of UHMWPE annuli sliding against 175 keV-nitrogen implanted Ti6Al4V discs. (+) dose $6 10^{17}$ ions/cm^2, 500C; (*) $6 10^{17}$ ions/cm^2, 200C.; ([]) $12 \cdot 10^{17}$ ions/cm^2, 500C; (Δ) $12 \cdot 10^{17}$ ions/cm^2, 200C

Diamond is, of course, the hardest known substance and its wear rate is very small. There is controversy about whether the mechanism of wear resembles that in metals or softer ceramics, involving the generation and entanglement of dislocations, or whether the erosion process is often more chemical in nature, involving the stripping of atoms from the surface. Undoubtedly, in contact with ferrous materials there is a physico-chemical interaction which destroys diamond rapidly. Ion implantation has been used successfully to improve the wear resistance of diamond tools of various kinds.Relatively light doses of nitrogen (< 10^{15} ions/cm^2) will extend the life of cutting tools used for machining acrylic resin, and of wire-drawing dies, used for copper wire manufacture. Diamond microtome knives, used extensively for the preparation of microscope specimens, are improved in life very significantly by the same treatment. It is not clearly

المنارة للاستشارات
www.manaraa.com

known how the implanted nitrogen acts, or indeed whether it could be said to harden the diamond. Instead, it could amount to some form of toughening. Nitrogen is believed to associate with carbon vacancies in diamond, and may interact with dislocations.

Other ceramics such as alumina have successfully been hardened by the ion implantation of additives such as chromium or zirconium which are known to be effective when added by other means. Even greater benefits are achieved at a comparable additive concentration if implantation is used, possibly because of the more uniform dispersion of the minor constituent. High fluence implantation into sapphire results in a decrease of hardness, correlated with the amorphization of the sample. At lower fluence, below the amorphization threshold, the substrate remains crystalline but the implantation damage induces high residual compressive stresses which improve resistance to crack propagation. Whatever the fluence, many parameters play a role in these modifications of mechanical properties in particular the temperature during the irradiation, the orientation of the lattice, the kind of incident ions. Titanium implants in silicon nitride increase the wear resistance of some order of magnitude.

4) Corrosion technology

In terms of cost to national budgets corrosion ranks with wear in representing a huge annual waste of materials and energy. It is a particularly dangerous form of degradation because it is less readily predictable and accounted than for the wear. It is also probably even more complex, being compounded with mechanical factors such as stress, wear and fatigue in practical situations.

The science of corrosion is divided according to whether the attack takes place in a gaseous environment or in a liquid (such as water) which allows an electrochemical circuit between different parts of the exposed surface (galvanic corrosion). During oxidation at high temperatures there is appreciable migration of cations and anions within the corrosion film, while loss of material from the surface occurs primarily in spalling or decohesion as a result of thermal mis-match. During aqueous corrosion there is likely to be a continual dissolution of the surface and stress effects occur in crevices or confined spaces.

Ion implantation provides a controllable and versatile means of altering surface composition and thereby examining the influence of different additives on corrosion. Since the material is introduced in a well-defined and shallow layer it is possible by subsequent analysis (often itself carried out using ion beams) to follow the movement or loss of additive. Unlike conventional alloying, implantation does not bring about variations in the grain size, but it is always necessary to recognise that it introduces a considerable amount of lattice damage. In metals this generally takes the form of a dislocation entanglement similar to that induced by cold working.

A systematic exploration of the effects of ion implantation on aqueous corrosion and electrochemical behaviour is reported.in literature . In general the results match closely those obtained with alloys containing an equivalent concentration of additive, e.g. chromium in iron, and the conclusions are that the ion bombardment itself has relatively minor consequences. Implanted molybdenum conveys the same resistance to pitting

www.manaraa.com

corrosion in stainless steel as it does when alloyed, and it was possible to show that this property of molybdenum also manifests itself following implantation into aluminium. However, one must recognize that ion implanted layers are extrelmely thin and may be bridged by even small second-phase inclusions in an alloy surface. During corrosion these may form pits and provide a source of galvanic attack. Where there is a catalytic effect of additives (such as platinum) the implanted material may be more active than its alloyed equivalent, perhaps as a consequence of the nonequilibrium state of the surface.

The practical application of ion implantation as a means of protection against aqueous corrosion is limited by the high cost of treating significant areas. It is being used, however, in cases of atmospheric corrosion. Ball bearings for naval aircraft often soffer from pitting corrosion in a marine atmosphere, and ion implantation of chromium has been shown to eliminate the problem. Other specialized applications in costly systems will probably be found.

The situation is more favourable in high temperature corrosion. There is no dissolution, nor galvanic processes, and the mechanisms of redistribution as the corrosion film grows can transport implanted material to greater depths. At first, exploratory surveys were carried out using many different ion species to compare their effects under given oxidation conditions. It was thus possible to show that titanium and zirconium, though metallurgically similar, have oxides which are sufficiently different that there is no correlation between additive effects. The protectiveness of ZrO_2 is governed primarily by stress, while oxygen transport dominates the oxidation of titanium. The trend has been to study the effect of a limited number of ion implanted additives in much greater detail, using sophisticated microscopic and analytical techniques. A good example has been the work on Ni-20%Cr. Implanted yttrium or cerium have dramatic effects on oxidation rate and oxide adherence in this, and other chromia-forming alloys. The implanted atoms are rapidly consumed in a Cr_20_3 film where they form minute second-phase oxide precipitates, uniformly distributed. They do not, as was earlier inferred, segregate at oxide grain boundaries and so hamper chromium out-diffusion. The oxide grain size is about four times smaller than in unimplanted alloy, and so the number of grain boundaries is increased. There is evidence that oxygen migration inwards dominates, and there are no voids at the metal-oxide interface. It is possible that the structure of the oxide grain boundaries has been modified. So far the value of ion implantation has been to allow tests which lead to a rejection of most explanations of the "rare earth effect".

5. Microelectronics

The success of ion implantation as a method of fabricating microelectronic devices has produced a very powerful driving-force in the development of sophisticated accelerators, wafer handling systems etc. The advantages of ion implantation over the previously used diffusion methods lie in its precision and reproducibility, combined with the versatility of an ion implanter, which can be applied to different processing steps required for device manufacture. It has for some years been possible to achieve an uniformity of implantation over 10 cm diameter wafers of approximately 1 per cent, and a reproducibility over many

www.manaraa.com

months which approaches this precision. As the chip size increases (though device size decreases) the requirements for high yield grow more demanding and the prospects for wafer scale integration involving very large chips make it essential to avoid non-uniformities arising from the beam sweeping (mechanical or electrical) system used. Research has been devoted to way of improving the mechanical manipulation of larger and larger wafers (20 cm diameter silicon is being produced in Japan) and to the problems of electrostatic sweeping of high intensity beams, in which space charge neutralisation between ions and electrons must be maintained. Ion source development is being spurred by the need for large currents of boron, the most widely used acceptor species.

High doses of oxygen (or in some cases nitrogen) ions are implanted into silicon wafers in order to produce a buried layer of silicon oxide (or nitride) dielectric for the isolation of devices. As CMOS circuits progressively shrink in size there is the risk of coupling between them and the so-called latch-up problem. Dielectric isolation is the most effective means of eliminating this, besides simplifying some CMOS processing steps. Bearing in mind that CMOS circuits are the key devices in major development initiatives it is clear that considerable effort is being directed at new fabrication methods. For economic reasons the ion beam intensities for oxygen implantation to doses of $2x10^{18}$ ions/cm^2 must be about 100 mA, at energies around 200 keV. The dissipation of this 20 kW of power is a difficult problem and ingenious methods of wafer cooling are explored. There is a very pressing commercial demand for accelerators which can meet the specification because it is conceivable that most future silicon CMOS circuits could be manufactured on implanted starting material.

Application of relatively high energy ions, at 2-5 MeV, is also now in progress in order to bury dopant ions much more deeply in certain silicon circuits, and this greater penetration is useful also in gallium arsenide and other compound semiconductors. By diffusion, of course, it is impossible to produce a buried concentration.

Because the implantation process is a violent one, heavily implanted silicon becomes amorphous. In the high dose implantation of oxygen (or nitrogen) the implantation is carried out at temperatures of about 500 C so that a continuous annealing takes place, and the silicon lying above the buried SiO_2 layer remains crystalline. Its crystallinity can best be verified by channelled RBS measurements, which are also used to demonstrate that the full oxide stoichiometry is achieved throughout an adequate thickness.

In most other cases of implantation into silicon the annealing to restore crystallinity and carrier mobility is carried out afterwards. Conventionally this has been done by furnace annealing at about 900°C, but increasingly rapid thermal annealing (RTA) is preferred because it can lead to less diffusive redistribution of implanted dopants. As the scale of devices shrinks this degree of control becomes more important. Laser annealing was for long time explored, but much simpler methods of heating by incoherent light (quartz halogen or xeron lamps).or by using high implantation currents (self-annealing) appear more convenient.

Modern microelectronic circuits are vulnerable to minute defects during the process of masking in photolithography. For this reason great pains are taken to minimise particulate contamination on the surface of the wafer during processing. This is especially important

www.manaraa.com

during ion implantation because even sub-micron particles can stop most incident ions. Much attention is therefore being given to the design of ion implanters so as to minimise moving parts or sliding surfaces at which debris can be generated. The breakage of wafers inside the accelerator must also be avoided.

The production of compound semiconductor devices presents more difficulties than in the case of silicon. High temperatures required to induce diffusion lead to dissociation of compounds such as GaAs, and for this reason ion implantation is preferred. However, the accompanying radiation damage must be annealed away, and this process demands high temperatures. Encapsulation by inert layers (such as silicon nitride) combined with rapid annealing of the material have proved to be the most successful methods.

6. Magnetic bubbles memory devices.

Certain ferromagnetic oxide materials based upon the yttrium-iron garnets are used increasingly as a basis for memory storage. Under applied magnetic fields ferromagnetic domains form and one class of domain can be caused to shrink to small circular regions a few microns in diameter. The material is transparent but the domains can be rendered visible by the Faraday effect in polarized light, and under such viewing conditions they resemble bubbles.

In the earlier devices these bubbles were caused to move along a superimposed pattern of magnetic elements produced, as a rule, by deposits of permalloy. In this manner a bubble could represent a bit of stored information, which could be manipulated magnetically and read by suitable output sensors.

It was found, however, that certain immobile or 'hard' bubbles would often exist and because these could not easily be collapsed would interfere with the action of the device. Ion bombardment could be used as a simple method of eliminating hard bubbles and he compressive stress induced in the crystal surface by bombardment would, in conjunction with the magnetostrictive properties of the material, create a shallow region of transverse magnetization at the surface of the film which effectively caps the bubble with a preferred distribution of magnetization.

More recently ion implantation through a masking film, for example of photoresist, has been used to induce a pattern of regions with an in-place magnetization (as in permalloy overlay films), and the bubbles are attracted to the discontinuity at the edge. The magnetic garnet is grown as an epitaxial film which may be only 1 micron thick, on a suitable latticematched substrate such as gadolinium gallium garnet (GGG).

The ions used for this application are generally light speeies, such as neon, oxygen etc. at doses of about 2.10^{14} cm^{-2} and energies of around 100 keV. The application has, however, stimulated continuing work on the physical mechanisms responsible for the magnetic behaviour, and it has been suspected for several years that the simple explanation above in terms of stress nduced anisotropy was insufficient. Thus, while the induced stress increases linearly with ion dose the intrinsic anisotropies are suppressed by a given dose irrespective of their initial value. Careful measurements have shown that the disorder of the crystal structure plays a part as well as the stress generation. The

www.manaraa.com

displacement of iron and oxygen atoms in the lattice is thus held to alter the intrinsic magnetic properties of the crystal. It is therefore possible that some anomalies observed when a range of different reactive and non-reactive ions are used to bombard garnet films can be due to the chemical interaction between constituent atoms, and the association between implanted atoms and point defects.

7. Image storage in PLZT ceramics.

The transparent ceramic lead lanthanum zirconate-titanate (PLZT) has a ferroelectric phase which can be used to store optical images by switching the material through a ferroelectric hysteresis loop while exposed to a UV image. The stored images, while non-volatile, can be erased or controlled electrically to provide contrast enhancement. The resolution is good (40 lines/mm).

The photosensitivity of this material is normally very poor by comparison with the photographic plate, but the photosensitivity has been improved by a factor up to 10^4 by the implantation of rare gas ions such as Ne or Ar The effect is believed to be due to a decrease in the dark conductivity in the near-surface region so that, under an applied elecric field, most of the potential is dropped across this region. Photogenerated carriers therefore have a high probability of being swept into the underlying ceramic to reorient ferroelectric domains (now in a reduced field).

Normally, PLZT is relatively insensitive to visible light, but an enhanced performance is reached by the ion implantation of chemically reactive species such as Al or Cr, and the best overall characteristics were achieved by 8×10^{14} Al ions/cm^2 at 500 keV together with 10^{15} Ne ions/cm^2, also at 500 keV energy.

8. Glasses

The effects of ion implantation in glasses have been extensively investigated, in particular for mechanical, optical and aqeous corrosion properties modifications [5-13]

The interaction of implanted ions with insulators results in the deposition of energy into electronic processes (ionization and excitation) and into atomic collisional events (Coulomb and hard-sphere interactions). The partitioning of energy into these two categories depends on the velocity of the ion relative to that of the target electrons. Although these interactions are common to all material classes, the utilization of electronic-energy deposition in physical property modification has been found to be significant only in insulators. This sensitivity is well known in the case of organic polymers.

A large number of microscopic processes are induced by ion implantation in glasses: preferential sputtering, radiation enhanced diffusion, internal electric field formation, electric field assisted diffusion and radiation induced segregation.

Chemical and physical transformations involved in ion implantation processes can be classified on the basis of two aspects: a) modifications only related to energy deposition and independent of the nature of the incident ion; b) modifications strongly dependent on the ions, because of the formation of chemical bonds between them and target atoms. In

www.manaraa.com

the former case modifications are due to radiation induced compositional changes occurring in the collisional cascade (radiation chemistry), while in the latter case processes equivalent to the so-called "hot atom" chemistry induced by recoil atoms produced in nuclear reactions or radioactive decay are involved.

The relative importance of each mechanism depends on the characteristic parameters of the implantation processes (ion, energy, target, temperature, current density) and glass composition and structure. Thus we expect different changes in mechanical and tribological properties, network dilatation, induced optical absorption and luminescence, compositional changes and modifications in chemical behaviour.

Heavy-ion implantation in alkali-silcate glasses first removes alkali ions, present in the glass composition, from the region of the implanted-ion distribution and for higher fluence levels removes alkali from the entire near-surface region to a depth well beyond the ion projected range, including the straggling contribution .

The alkali depletion has been analyzed in terms of a preferential removal of alkali ions during the implantation process, associated with a change in the alkali self-diffusion coefficient in the damaged region [5-6]. The evaluated alkali diffusion coefficient values are some order of magnitude higher than the thermal ones, indicating that the migration process is related to the damage produced by implantation .

8.1 Variation of etch rate

Chemical stability changes of silica are technologically important, considering that SiO_2 is used as a passivating layer in semiconductor devices and these modifications can be used to etch patterns onto a surface. Ion implantation technique may also be of use in the designing inner regions with different etching properties.

Vitreous silica is the most extensively studied material. Its etch rate with dilute HF is increased by a factor of about 5 under B and C, N, O, implantation at doses of 10^{12}-10^{16} ions/cm^2. The etch rate of the implanted layer has been found to be constant along the range of the ions and correlated to the electronic stopping power. Variation of chemical etch rate in HF are related to radiation damage and formation of compound. A systematic study of the etch rate changes in silica due to Ar, N, Si plus N implants has been performed. A general feature of the etch process is characterized by an initial high etch rate through the implant region and a subsequent decrease in the unimplanted one.[9]

For Ar implants the etch rate (0.25 nm/s) is of a factor 5 higher than the measured one in unimplanted silica (0.05 nm/s). Such an effect is due to radiation damage, which introduces new sites of different chemical reactivity.

In figure 4 the residual thickness as a function of etch time for 500 nm thick SiO_2 film/Si samples after 100keV-Ar implants, at different doses.

The etched thickness increases linearly with etching time till a depth at which the etching rate assumes the value observed for unimplanted samples.

www.manaraa.com

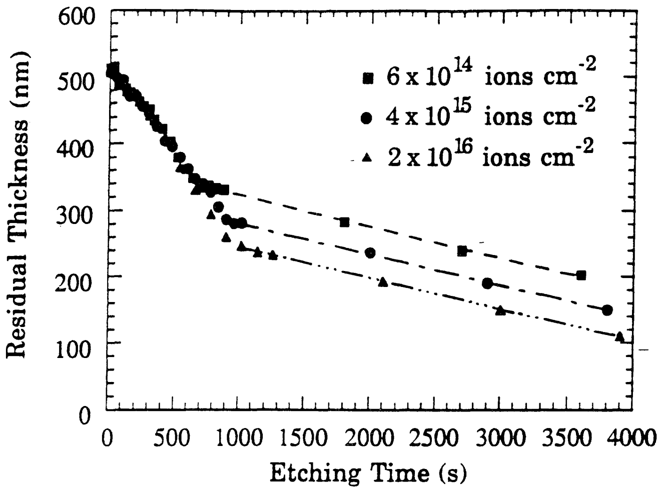

Figure 4 Etch curves in 0.5% HF solution for 100 keV Ar implanted silica glass at different doses.

If it is assumed that the depth at which the etching rate changes corresponds to the thickness of "damaged" region. Such a thickness is about a factor of 2 higher than the projected ranges, R_p, and range stragglings, ΔR_p, of the implanted ions, calculated by using the TRIM code. These results on extention of damaged region for high implantation fluences, by etching rate measurements, can be compared to those obtained from leaching and alkali depletion experiments.

Implants of nitrogen in silica determines the formation of SiO_xN_y compounds. The stoichiometry of SiO_xN_y compounds is limited by the redistribution of N during implantation, as shown in Figure 5.

Figure 5 reports the SIMS profiles of 50 keV-nitrogen implanted in silica at different doses. At doses higher than $5x10^{16}$ cm^{-2} the top of nitrogen profile begins to be flat. Further increasing the dose the nitrogen profile exhibits a long plateau which extends from the surface up to depths much greater than the range plus straggling. The total dose retained in the sample is reported in the inset as a function of nominal dose.

An increase of the N concentration is obtained for N implantation in Si-preimplanted silica. The presence of silicon oxynitride compounds is expected to lower the etch rate. Indeed in N or Si plus N implanted samples the etch rate is lower (0.15 nm/s) than the measured one for Ar implants. Moreover the etch rate value is still higher than for unimplanted samples due to the contribution of radiation damage,

After a annealing process (700C, 5 hours) Si plus N implanted samples present a very low etch rate value(0.03 nm/s), as a consequence of radiation damage annealing and the presence of a stable SiO_xN_y compound

www.manaraa.com

The compound formation and the evolution as function of a subsequent implant or annealing process has been studied by using X-Ray Electron Spectroscopy [3]

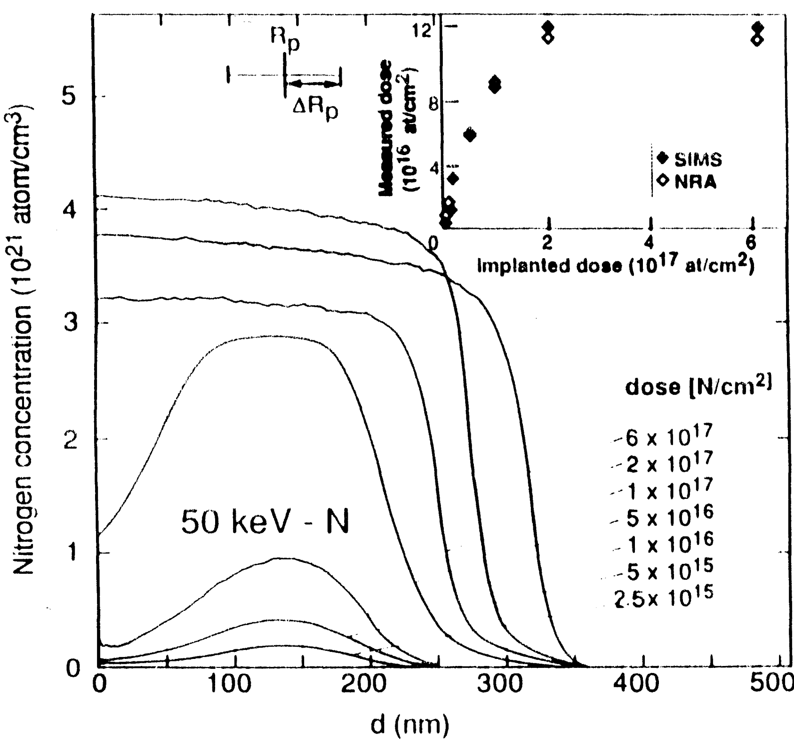

Figure 5. SIMS depth profiles of 50-keV nitrogen implanted in silica at different doses. The inset shows the retained nitrogen dose as a function of nominal dose.

8.2. Variation of hydration rate

The research activity in the field of ion bombardment effects on glass hydration has been determined from technological applications such as the durability of nuclear glasses and the potential of incorporated hydrogen as a means to decorate ion-induced defects. Ion-induced hydration of silica has been investigated with a wide variety of ions [12].

Figure.6 shows the hydrogen profiles in vitreous silica implanted with two doses of 207 keV Pb ions and leached in 100C water for increasing times. For the highest dose (10^{15}/cm^2) and long leach times the flat H profiles extend to a depth of about 1500 Å which has to be compared to the Pb projected range of 600 Å. The occurrence of a critical fluence which is one order of magnitude higher than that measured for matrix destruction is evident. This peculiarity was then reported for more complex silicate glasses .

www.manaraa.com

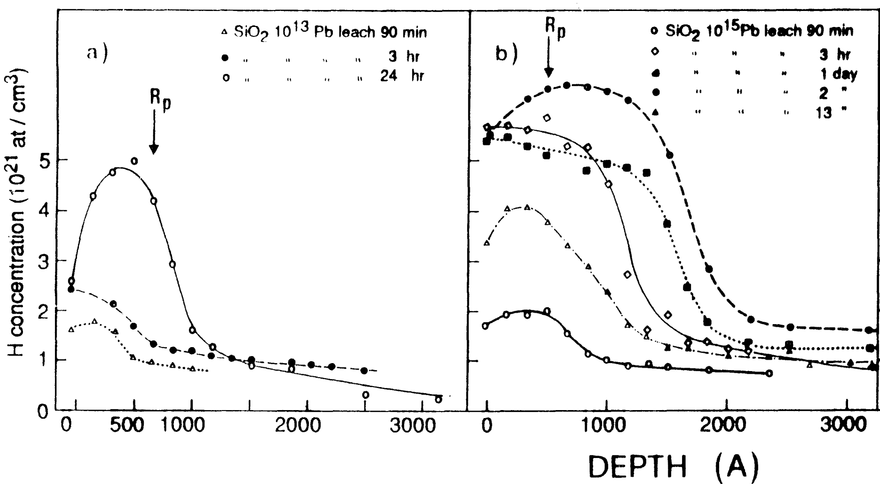

Figure 6. Hydrogen profiles, measured by using nuclear techniques, in vitreous silica after 207 keV-Pb implant at two doses and leaching in 100C water for increasing times.

Some hypotheses have been proposed for explaining this aspect: (i) the defects, produced locally, are mobile and propagate long distance; (ii) ion implantation induces a stress field penetrating further into the glass. The first mechanism has also been assumed to explain the Na-depletion in implanted soda-lime glasses. The thickness of the depleted layer is greater than the range of the implanted ions and is a function of the deposited energy. A redistribution of implanted gaseous elements, for high fluences, is also observed at depths greater than the projected range plus straggling values. At lower fluences the depth profiles follow the calculated distribution (using TRIM code).(see Figure 5).

The hydration process was interpreted as follows: hydrogen, in an unspecified form H^+, H_3O^+, H_2O, penetrates the material at an enhanced diffusion rate because of the heavily damaged structure and reacts with a chemically reactive defect, possibly a non-bridging oxygen, thus decorating the defect distribution. Such a model is supported by the results of post-leaching thermal annealing experiments.

8.3 Mechanical property modifications

Ion implantation induces volumetric changes, as a consequence of defect production, and concomitant surface stress, hardness and refractive index modifications [11].

For most simple silicate glasses, implantation results in compaction within the implanted region. This might be expected *a priori* on the basis of the large specific volume and open

www.manaraa.com

structure of the glassy state relative to that of its crystalline counterpart. On the contrary, crystalline materials generally expand due to lattice displacements.
The dilatation of the implanted surface also results in a lateral stress which can be tensile, due to compaction, or compressive, due to expansion in the implanted layer.
The compaction in simple silicate glasses is justifiable in terms of SiO_4 tetrahedra rotation into the adjacent voids, when bonds are broken.
When H-impregnated silica is irradiated, the hydrogen reacts with the broken bonds to form Si-OH and Si-H. The presence of H does not allow densification; instead, the network relaxes after bond-breaking and a net expansion results.
The addition of network modifiers, such as Na_2O, produces similar results.

8.4 Optical properties of glasses and insulator crystals.

Many effects determine a change in refractive index of ion irradiated insulators: phase change (e.g. quartz), microporosity (e.g. SiC, B_4C, Al_2O_3), introduction of colour centers (e.g. SiC, MgO), compaction (e.g. vitreous silica) or changes in composition (e.g. alkali silicate or heavy metal fluoride glasses) [7,8,10].
A systematic investigation of the optical behaviour of 40-100 keV Ar implanted soda-lime glasses has been performed.
Antireflective (AR) effects were obtained with low current irradiation densities (up to 2 $\mu A/cm^2$), whereas medium current densities and high implantation energies produced light diffusing surfaces.
For 50 keV Ar implantation, at doses lower than 10^{16} ions/cm^2 no significant changes were observed in the reflectance curves. For doses between 10^{16} and $5x10^{16}$ ions/cm^2 the specular reflectance curves showed an AR effect, which increased with the dose as shown in Fig7. The reflectance curves show an interferential minimum, which becomes deeper and shifts towards higher wavelengths as the dose increases. The thickness and average refractive index of the modified surface layers have been calculated from the position and height of the interferential minima in the reflectance curves.
The significant antireflectivity of the implanted glass has been associated with surface alkali (Na) depletion. The correlation between the Na depletion in the bombarded region, and the formation of an antireflective surface layer, was displayed by comparing the thicknesses of the Na-depleted layer, calculated from the Na profiles at 50% of the bulk value concentration and of the optically modified layer .
Fig.7 shows the specular reflectance curve for glass implanted with 50 keV Ar at a dose of $5x10^{16}$ ions/cm^2. The individual data points represent the calculated reflectance values. In the inset of the figure, the sodium profiles before and after the implantation obtained from $^{23}Na(p,\alpha)^{20}Ne$ nuclear reaction are shown.
For higher implantation energies, an increasing antireflective effect was observed while the interferential minima shifted toward higher wavelengths.

A number of crystalline insulators have proven to be useful as substrates for the formation of ion-implanted waveguides. Among these are crystalline quartz and the

www.manaraa.com

ferroelectrics $LiNbO_3$ and $KNbO_3$ these decrease in index for quartz is substantial (1.54-1.48) with collisional deposited energy.

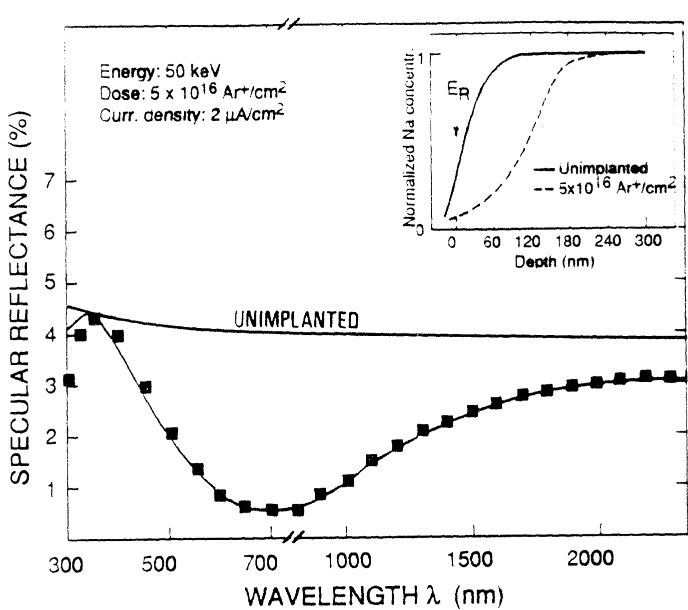

Figure 7. Experimental curve and calculated reflectance values (points) for soda-lime silicate glass implanted with 50keV-Ar. The corresponding sodium profile is reported in the inset.

For index-change saturation the material appears amorphous and the index is nearly the same as implanted compacted fused silica. Annealing removes point defects which causes light scattering without regrowth of the damaged region and the losses are reported to be <1dB/cm. MeV He implantations are used to form waveguides in quartz; this allows guided waves in the high region between the surface and the lowered -index region at the end of ion track. This barrier can allow leakage of higher-order modes but the barrier can be widened by multiple-energy implantations. By using this technique frequency-doubling in He-implanted guide has been achieved. The conversion was from 783 nm to 392 nm. This is an example of an optical nonlinearity and arise from the $\chi^{(2)}$ susceptibily term in the polarization induced by an external electric field, produced by laser light pumping.
$LiNbO_3$ has been the subject of many investigations into the production of waveguides because of its good electro-optical characteristica. Guides can be formed by proton exchange and by indiffusion of Ti and this latter method is that most often used. However this does not readily allow formation of guided regions in selected areas and the high-temperatures required precludes the prior application of electrodes. These drawback can

www.manaraa.com

be avoided by implantation. $KNbO_3$ is also interesting substrate for waveguide formation and electro-optical applications. It has so far not been possible to form guides by diffusion or ion exchange techniques. However a series of recent papers have demonstrated that 1-2 MeV He implantations at fluence as low as $5x10^{13}/cm^2$ can produce waveguides with tolerable losses.

The really exciting advance that has been made in the application of ion implantation to electro-optic technology is the fabrication of waveguide lasers. This has been achieved by forming waveguides by he implantation in $Nd:MgO:LiNbO_3$, Nd:YAG and Nd:GGG substrates. Following implants of Er in $LiNbO_3$ substrates(undoped) excitation of Er fluorescence spectra, which are almost identical to that from bulk $Er:MgO:LiNbO_3$ crystals has been obtained. Similar successes have been reported for Er implants in silica and phosphosilicate films as well as into Si_3N_4 films. These developments make it seem very probable that implantation doping of rare earth elements can be used to form lasers and amplifiers in selected portions of integrated electro-optical circuits.

One of the greatest challenges for optics in the development of a computer based on an all-optical photonic switch which would replace the switching done by electronic transistors. The optical switch would be competitive if ti could exhibit switching times less than 100 ps and have consumption less than 1 pJ. It has been suggested that the optical non-linearity of glass could be utilized for switching of this type. An all optical switch is one where switching can be accomplished through the changes in refractive index that are proportional to the ligh intensity. The third order susceptibility, $\chi^{(3)}$, is the non-linearity which provides this feature.

For glasses the non-linearity is generally quite small, however when light is confined to a waveguide region, the effect can be adequate for switching. The non-linear response can be enhanced by the introduction of microcrystallites of semiconductors (e.g. $CdS_x Se_{1-x}$) For the efficient design of optical circuits it would be desiderable to use a method in which the non-linearity could be confined to specific patterned regions. Ion implanted metals (Au, Ag, Pb) can form small radii collodal particles by suitable processing techniques.

These particles exhibit an electron plasmon resonance which depends on optical constants of the metal and refractive index of the glass host. The absorption can be handled in the Mie formalism and the radii of the particles can be determined from the measurement of the resonance wavelenght.

Figure 8 shows the absorption as a function of the wavelenght for silica implanted with silver and silver plus nitrogen. The Ag cluster sizes are of the order of 2-3 nm.

Modifications of the clusters configuration may be obtained, as observed for copper clusters, by subsequent implants. The control of size characteristics of metal colloids appears possible trough ion implantation technique.

Measurements of the non-linear optical properties of such colloids were performed and the optical Kerr susceptibility, $\chi(3)$, was found to be 2-3 orders of magnitude larger than that of Au and Ag. These results open the ways for advances in all-optical switching devices.

www.manaraa.com

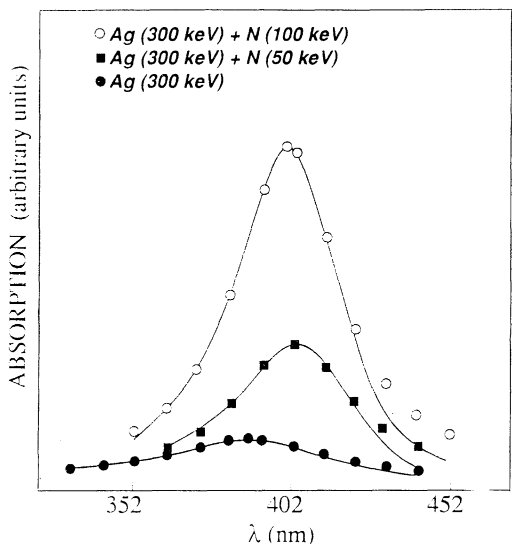

Figure 8 Optical absorption peak as a function of wavelenght for the Ag and Ag+N implanted silica glasses. Continous lines are experimental spectra; symbols correspond to results of calculations by using Mie teory.

9. References

[1] Proceedings of International Conferences "Ion Beam Modification of Materials" (IBMM)

[2] Proceedings of International Conferences "Surface Modifications of Metals by Ion Beams"

[3] Proceedings of International Conferences "Radiation Effects in Insulators"

[4] Proceedings of International Symposia organized by the Material Research Society, (MRS), annually at Boston and Strasbourg.

[5] P. Mazzoldi, in Nuclear Physics Application in Material Science (Ed. E. Recknagel and J. C. Soares) Kluwer Academic, Boston. 1988, pag. 313

[6] P. Mazzoldi, in: Materials Modification by High-Fluence Ion Beams, (Ed..R. Kelly and M. Fernanda da Silva) Kluwer Academic, Boston 1989 p. 339.

[7] Ion Beam Modification of Insulators, eds. P. Mazzoldi and G.W. Arnold (Elsevier, Amsterdam 1987)

[8] P. Mazzoldi, Journal Non-Cryst. Solids, 120, 223 (1990)

[9] P. Mazzoldi, F. Caccavale, E. Cattaruzza, A. Boscolo, R. Bertoncello, A. Glisenti, G. Battaglin, C. Gerardi, Nuclear Instrum. Methods, B65, 367 (1992)

G. W. Arnold, G. Battaglin, A. Boscolo, F. Caccavale, G. De Marchi, P. Mazzoldi, A. Miotello, Nuclear Instrum. Methods, B65, 387 (1992)

المنارة للاستشارات

www.manaraa.com

[10] P. Towsend, "Optical Effects of Ion Implantation" Rep. Prog. Physics 50, 501 (1987)
[11] G. Arnold, in Symposium on Chemical and Physical Modifications Induced by Irradiation in Glasses, Strasbourg (Ed. P. Mazzoldi, Elsevier Amsterdam 1992)
[12] J.C..Dran, in Reference 11.

المنارة للاستشارات
www.manaraa.com

PLASMA-ENHANCED CHEMICAL VAPOR DEPOSITION

R. d'AGOSTINO, P. FAVIA, F. FRACASSI, R. LAMENDOLA
Centro di Studio per la Chimica dei Plasmi, CNR
Department of Chemistry, University of Bari
4, Trav. Re David 200 - 70126 Bari, Italy

ABSTRACT. The basic principles of Plasma-Enhanced Chemical Vapor Deposition processes are examined along with reactor architectures. Emphasis is given to the chemistry of the discharge and to active species and deposition precursors with the aim of correlating film compositions with discharge internal parameters. The processes for the deposition of films of fluoropolymers, metal containing polymers, SiO_2-likes and silicone-likes are examined as case studies.

1. Introduction

It has been known for many decades that the introduction of a monomer into a glow discharge, independently of the presence of an inert gas carrier, produces various fragments which rearrange through many gas-phase and surface processes leading to the formation of a variety of addition compounds and of thin films on the inner surfaces of the reactor. For many years plasma thin films were considered an accidental occurrence in hydrocarbon discharges and undesirable by-products to be eliminated. Only after the 60's some researchers showed an interest in their advantageous characteristics [1]. If such films are obtained under controlled conditions, that is at the desired substrate temperature, gas pressure and electrical discharge parameters, they have unique characteristics allowing their classification as an entirely new class of materials with only small or negligible correlations with their counterparts obtained by conventional techniques.

Good quality plasma thin films have thickness ranging from few hundreds Å's to a few μ's, are pin-hole free, homogeneous, and show good adhesion to various substrates. The principal structural differences from conventional counterparts are variable stoichiometry (depending on the experimental conditions), higher cross-linking degree and variable chemical-physical properties, such as wettability, chemical inertness, dielectric parameters, barrier properties, hardness, etc.. A typical example is given by Plasma Polymerized Fluorinated Monomers (PPFM) which can be tailored either as teflon-like with an overall $(CF_{1.9})_n$ stoichiometry (non wettable and inert films), either as partially

W. Gissler and H. A. Jehn (eds.), Advanced Techniques for Surface Engineering, 105–133.
© 1992 *ECSC, EEC, EAEC, Brussels and Luxembourg.*

www.manaraa.com

fluorinated carbon films, *e.g.* $(CF_{0.2})_n$, (high cross-linking and wettability) [1,2], or as a diamond-like film, a-C:H,F [3] (hard, most carbon sp^3 hybridized)

In the remainder of this note some characteristics of deposition processes are given (sect. 2). Reactor geometries will be discussed in section 3. Then, as practical examples, in sections 4 through 6 fluoropolymer, metal-containing, and silicon-carbon containing films are examined.

2. Glow Discharge Deposition Processes

The reaction kinetics involved in glow discharge polymerization are extremely complex and the attempt of abstracting a general picture describing all possible situations would be sterile and misleading. The usual generalization used for conventional polymers can not be used with the same meaning, a particular example being the word "*monomer*" which indicates the unit molecule repeated in conventional polymeric chains; for instance, polytetrafluoroethylene denotes a polymer in which tetrafluoro-ethylene represents the monomer unit repeated n times in each chain. In glow discharge polymerization, in most cases, the structure of the feed gas is not retained because different radicals, ions, atoms, etc., can be formed in the discharge medium. Nevertheless, the word "monomer" is sometimes utilized in Glow Discharge Polymerization or Deposition simply to denote the feed gas.

Two general considerations on competing processes can, however, be made to describe discharge polymerization, *i.e. etching-deposition competition* and *gas phase-surface competition.*

2.1. ETCHING-DEPOSITION COMPETITION

It is well known that etching-deposition competition is a rather general phenomenon, some feeds can in fact be utilized in glow discharges both for deposition and etching processes [4]. A well known example is given by SiF_4- and $SiCl_4$-containing feeds, utilized for the deposition of amorphous silicon, a-Si:H,X (X=F or Cl), or for etching of many materials (*e.g.* Si, SiO_2, Al, GaAs, etc.). Usually atoms, particularly F- and O-atoms, are regarded as the active species for etching, while radicals are considered "*building blocks*" for the construction of organic and inorganic films. A glow discharge fed with reactive organic gases produces both types of species. The behavior of freon discharges can fairly well illustrate such competition: the discharge medium contains both classes of active species (F atoms and CF_x radicals), so their concentration ratio $[F]/[CF_x]$ in the plasma phase will characterize their ability as etchant or polymerizing discharges. However, if a gas is added to a freon feed able to reduce [F] in plasma phase, the radical concentration prevails and the plasma is switched into a polymerizing mode. In fact, if hydrogen is added, it reacts with F-atoms leading to unreactive HF. Similar conditions can be obtained either by adding to the freon feed an unsaturated, as for instance C_2H_2, C_2H_4, C_2F_4, etc., or by loading the reactor with large silicon surfaces (which react with F, leading to the etch products SiF_2 and SiF_4). On the other hand, if oxygen is now added to freon, it acts both as a polymer etchant and as a polymerization inhibitor: it reacts

www.manaraa.com

directly with polymer units leading to volatile compounds or it selectively reacts with CF_x radicals and subtract them from gas phase, inhibiting polymerization process. Figure 1 [4] illustrates the behavior of freon feeds in the presence of different additives.

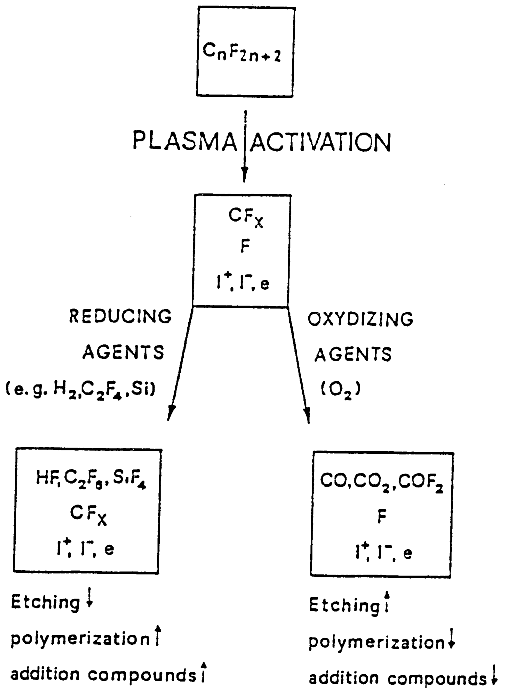

Figure 1. Effect of foreign gas additions to a freon on the etching/polymerizing capability of a glow discharge.

2.2. GAS PHASE-SURFACE COMPETITION

A quite general scheme representing the fate of a *"monomer molecule"*, A, entering a glow discharge is sketched as it follows:

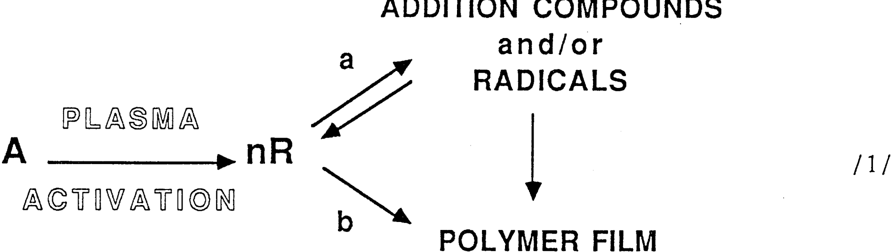

/1/

المنارة للاستشارات

www.manaraa.com

where R represents various radicals. In this scheme A is transformed by plasma activation into various fragments, including atoms, radicals, ions and other molecules.

Radicals (sometime also atoms) have a two-fold fate: they can, in fact, form addition compounds (branch a) through several reactions paths. These compounds can react in the gas phase with other radicals and unsaturates and form heavier radicals and/or intermediate polymeric chains. Radicals, on the other hand, can also contribute to the film growth directly by reacting with 'active' surface sites of the film (branch b).

The formation of heavier and heavier addition compounds in reaction 1 can be enhanced by increasing the production of radicals and decreasing their diffusion to the substrate, in other words at high powers and/or pressures. In this case, polymer formation can also occurs directly in the gas phase through the formation of polymer nuclea. If the radical production is decreased and also their diffusion is increased, route b is triggered and radicals can "stick" on polymer surface directly from gas-phase. Generally, the competition between gas-phase formation of intermediate compounds or gas-phase nuclea and surface reaction is frequently met and depends on discharge parameters and feed gases [2, 5-7].

3. Reactors

The most widely used reactor configurations for Plasma-Enhanced Chemical Vapor Deposition (PECVD) can be broadly divided into three classes:
a) electrodeless microwave (MW) or high frequency (HF) reactors,
b) external electrodes "tubular reactors",
c) internal electrodes "parallel plate reactors".

The choice of the experimental arrangement can greatly affect the deposition rate and deposit properties; consequently, it is important to use the experimental system which is appropriate to the specific applications.

3.1. ELECTRODELESS REACTORS

Microwave powered systems are characterized by the use of tubular quartz or pyrex reactors and a resonant cavity coupled with a power supply in the GHz (typically 2.45) region, as schematized in Figure 2. The plasma is generated in the cavity and the deposit is generally collected outside the glow [8-10].

Claude et al.[11-13] and Wertheimer et al.[14] have studied the difference between these discharges and RF ones. These authors have used systems connected to an electromagnetic Surface Wave (SW) generator in order to investigate the effect of frequency changes on the deposition processes (*e.g.* fluorocarbon deposition) keeping constant all other parameters. The ratio of deposition rate R to input power P *vs* the frequency is shown in Figure 3. It can be seen that R/P increases with frequency, reaching a plateu. The key parameter, however, is the ν/ω ratio, where ν is the effective average electron-neutral collision frequency for momentum transfer, and ω the wave angular frequency ($\omega = 2\pi f$). These experimental data are in agreement with the theoretical model of Ferreira and Louriero [15].

www.manaraa.com

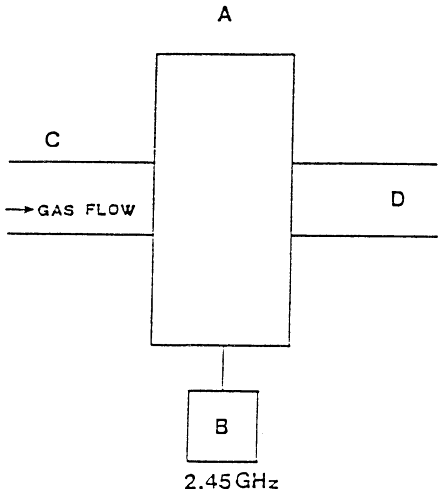

Figure 2. Schematic of a microwave powered tubular discharge: A) resonant cavity; B) generator; C) and D) usual sample position.

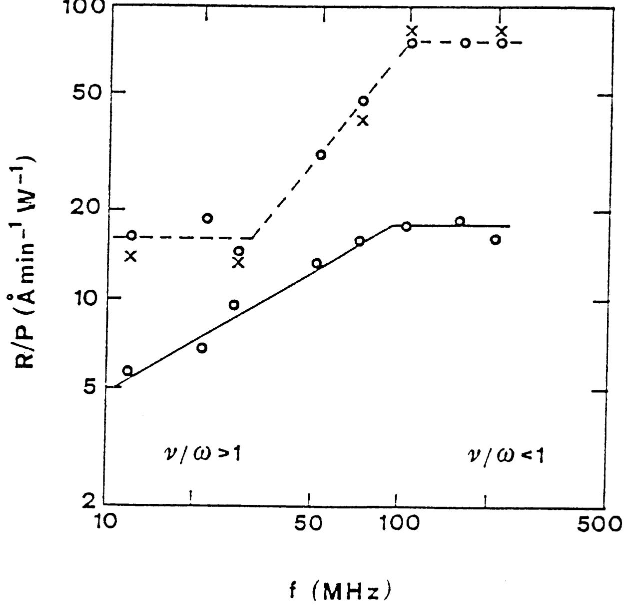

Figure 3. *Log log* plot of (R/P) *vs* excitation frequency. P is absorbed power and R deposition rate. Upper curve pertains to PP isobutylene, lower one to PP perfluorocyclobutane.

The differences between RF and MW discharges can be summarized as follows:

www.manaraa.com

1) the Electron Energy Distribution Function (EEDF) of the glows tends to become increasingly Maxwellian for MW discharges; at the same time the high-energy tail population increases with decreasing ν/ω (MW regime). This leads to a plasma composition with an enrichment of excited species having high excitation threshold energy;
2) the average electron energy slightly decreases with decreasing ν/ω;
3) MW plasmas are usually characterized by higher density of active species, electrons and ions for the same absorbed power.

Surfaces exposed to MW discharges are subjected to a non intense bombardment of either negative (mainly electrons) and positive (ions) particles, since the sheath potential drop (floating substrate) is quite small and the charged particles can not be accelerated during the applied cycle, which is too short.

Large differences are therefore expected between MW and RF generated thin films due to the different active species production and to the different role played by ions and electrons. Unfortunately, to these authors knowledge, a comprehensive study on this subject has never been performed. An attempt to study these phenomena is reported by Kammermaier *et al.* [8], but the different sample position with respect to the glow region in MW and RF discharges, makes the comparison of results rather difficult.

3.2. REACTORS WITH EXTERNAL ELECTRODES

External electrode reactors can be either capacitively or inductively coupled (Fig. 4a); insulating (glass, quartz, or alumina) tubular reactors are usually utilized. The power is transmitted from a power supply to the gas by a capacitor and a coil, respectively. Inductively coupled tubular reactors, when operating at low pressure ($P \ll 1$ Torr), are not uniformly coupled to the supply because coupling quality gradually increases with increasing working pressure [16]. These systems are generally used for experiments in which charged particles bombardment is not one of the major concerns.

When the discharge glows, after a short transient time, the gas reaches an average plasma potential V_p and any insulated surface, in contact with the plasma, reaches a floating potential V_f (always negative compared to V_p). Positive ions are accelerated and gain energy, electrons and negative ions are decelerated by (V_p-V_f) when they cross the sheath over a floating surface.

The evaluation of the positive-ions accelerating potential is not simple, because it depends on the experimental working conditions. However, by keeping constant the other parameters, the accelerating potential can be more easily varied in internal electrode configuration rather then in tubular reactors. As a consequence, charged particles bombardment is less effective in external electrode systems.

Many different experimental arrangements have been reported in the literature, which differ basically in power supplies, reactor geometry, and sample position. The working frequency of the most commonly used power generators ranges from 13.56 to 35 MHz, while tube geometry changes from author to author (see *e.g.* ref. 17-19) and sample position can vary, as it is schematically shown in Figure 4b [17, 18], in order to obtain films with different compositions and properties.

www.manaraa.com

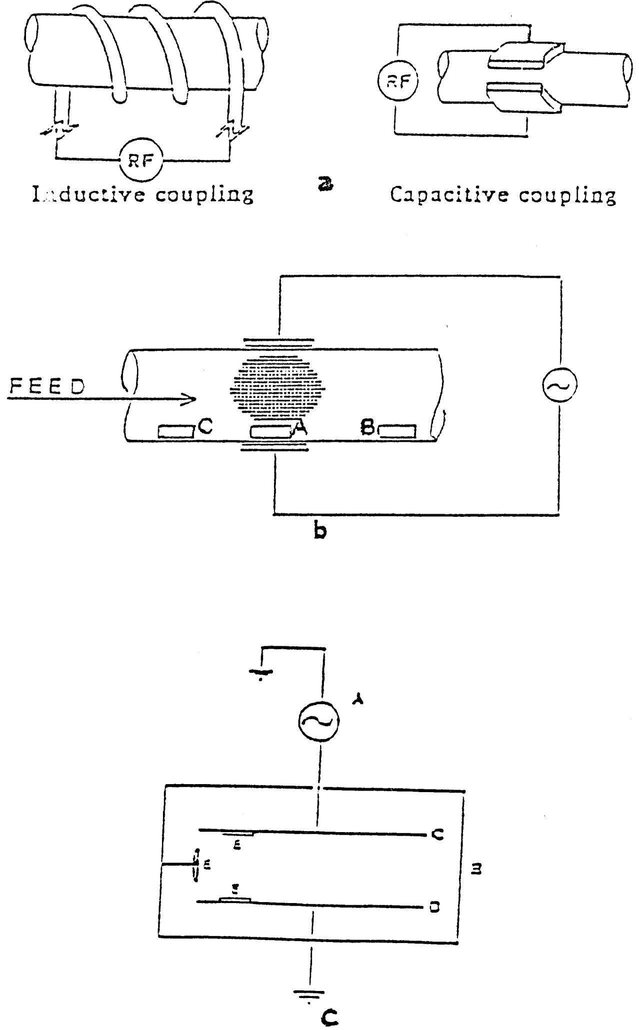

Figure 4. a) Schematics of capacitive or inductive external electrode reactors. b) Usual sample position. c) Internal electrode reactors.

3.3. REACTORS WITH INTERNAL ELECTRODES

Different type of reactors have been developed during the last years, as flat bed, parallel plate, planar, diode, etc. reactors; their main distinctive features are: power supply, coupling system, vacuum chamber, RF driven electrode, grounded electrode and eventually one or more substrate holders (Figure 4c). With these systems, attention must be paid to the appropriate working conditions and apparatus geometries, since they can deeply influence the extent of ion bombardment on the substrate (besides, of course, electron energy

المنارة للاستشارات
www.manaraa.com

distribution function and active species production). It is, in fact, reported by several authors [16, 20-22] that the A_t/A_d ratio, where A_d is the area of the driven electrode and A_t that of all other surfaces in contact with the plasma, as well as the coupling system, can affect both V_p-V_f and V_p-V_b, where V_b is the cathode dc self-bias potential (Figure 5A). As a consequence, A_t/A_d affects the energy of ions bombarding floating, grounded, and target surfaces. Increasing A_t/A_d ratio results in increasing the potential drop over the target and in decreasing the potential drop over a floating substrate [22]. An estimation of the average plasma potential V_p can be obtained by $V_p=(V_{pp}/2 + V_b)/2$ (see Figure 5A), where V_{pp} is the peak-to-peak voltage of the applied RF field [22].

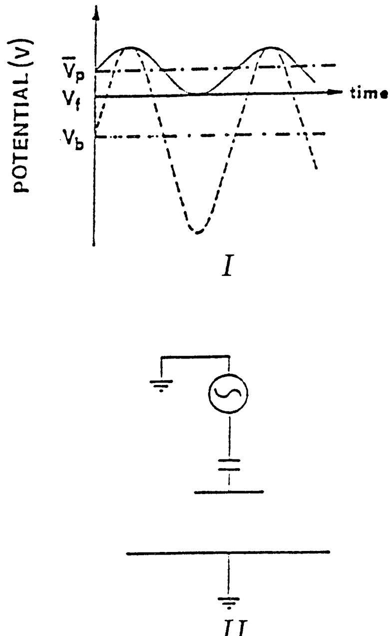

Figure 5A. I) Discharge potentials (p = plasma, f = floating, b = d.c. self bias) evolution. Dashed and continuous curve refer to instantaneous excitation and plasma potential values. II) Schematics of diode configuration maximizing d.c. self bias on target electrode.

Power supplies coupled to reactors with internal electrodes generally work in the KHz or MHz regions. The RF period influences the Ion Transit Frequency (ITF), defined as the frequency above which ions do not cross the sheath in less than half RF cycles. For frequencies below ITF, crossing ions are controlled by the instantaneous plasma potential, while for frequencies above ITF, ions cross the sheath slowly compared to plasma potential fluctuations, and this leads to an average plasma potential influencing the charged particles arrival to a surface

المنارة للاستشارات
www.manaraa.com

[23]. As a consequence, sharp distributions with a quite low maximum ion energy are expected at excitation frequencies over ITF.

Vacuum chambers can be made either of glass or conductive material, for a better shielding from external sources. In general, there are not particular design problems with the grounded electrode besides its area. On the contrary, the design and arrangement of the cathode require special care; a metallic shield surrounding the electrode highly improves the glow confinement inside the interelectrodic space, and the electrode material and area greatly affect the extent of sputtering on the target.

Asymmetric low-pressure systems (A_t/A_d>>1), coupled with high input power, can release large amounts of material by sputtering of the powered electrode. In order to avoid gas-phase and polymer contamination by non volatile material, it could be advisable to work with reactive targets that do not release contaminants. For fluorocarbon deposition, graphite, SiO_2 or teflon targets can be utilized [24, 25]; graphite produces fluorocarbon species and etch products:

$$C + xF \longrightarrow CF_x \qquad /2/$$

and acts as a fluorine atom scavenger leading to plasma conditions with low F/C ratio [25], a condition which is highly desirable in plasma polymerization. SiO_2 can produce SiF_4 and CO_2 according to:

$$SiO_2 + CF_4 \longrightarrow CO_2 + SiF_4 \qquad /3/$$

These species, however, do not appreciably change the C/F ratio, but they can change gas phase characteristics and can lead to some film contamination (Si, O). Teflon targets do not affect C/F ratio, but may require suitable arrangements due to their particular electrical properties.

Substrates are generally positioned on the ground electrode or on a third one (substrate electrode) which can be inserted into the glow. The three electrodes arrangement, called 'triode', is very useful for studying the effects of positive-ion bombardment on the deposition rate and on film properties. The substrate electrode can be negatively biased with RF voltage by means of a second RF generator [25], or by a capacitive power distribution between the driving and the substrate electrode [26, 27], as it is shown in Figure 5B. Since the substrate electrode can be made relatively small in comparison with the main RF-electrode, the arrangement allows to change significantly the substrate bias voltage with no appreciable change of total power input in the discharge [28, 29] and, consequently, its chemical composition. In any case a correct approach to the issue of controlling the effect of bias on the deposition is to verify, by means of some diagnostic techniques, the eventual changes induced by bias superposition in the plasma density and potential. Suitable techniques are, for example, Actinometric Optical Emission Spectroscopy (AOES) [30-33] and electrical probe analysis.

www.manaraa.com

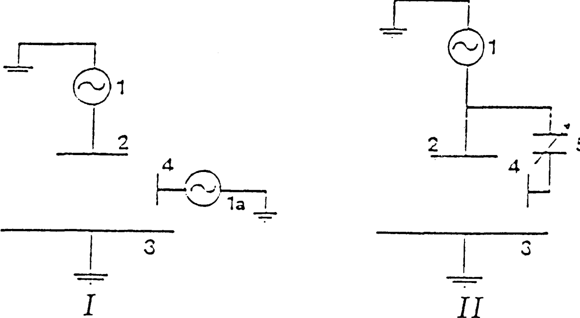

Figure 5B. Schematics of triode reactors utilized for thin film depositions. I) Target (2) and biased deposition electrode (4) are driven by separate RF generators (1,1a), 3 is the grounded surface. II) As for *I*, but driven by one RF generator with a capacitive power distribution device.

3.4 MAGNETRON REACTORS

Magnetron reactors constitute an important development in devices for plasma-assisted processing of materials. This kind of reactor includes all systems where an additional magnetic field is superimposed to the main electromagnetic field sustaining the discharge. In these systems the electrons, under the influence of the magnetic field, follow a spiral path which leads to a decrease of the effective mean free path and to an increase of electron and active species concentration; charged particles escape from the glow region is markedly decreased and a more intense and confined plasma is obtained. Usual problems met with magnetically-aided plasmas (also ECR systems fall in this category) are a higher inhomogeneity of both the growth rate and the chemical composition of the deposited material. The main advantages are a reduced working pressure (about one order of magnitude lower) and a reduced radiation damage of substrates. In fact, there are larger number densities of positive ions hitting the surfaces, but at lower accelerating potentials.

4. Fluoropolymers

The study of freon-fed discharges has been the object of intensive research in the last decade [4, 6, 7, 34-36], because of their relevance as: a) suitable plasmas to promote etching of a variety of substrates utilized in microelectronic technologies and, b) plasmas allowing the deposition of Plasma Polymerized Fluorinated Monomers (PPFM) films, also said Teflon-like films.

The reasons for the wide utilization of Teflon-like coatings are the good adhesion to many organic and inorganic substrates, the presence of low intermolecular forces, which give rise to relative inert surfaces with extremely

المنارة للاستشارات

www.manaraa.com

low free energy [7], the biocompatibility, the low friction coefficient [37,38], and the chemical composition and cross-linking degree, which can be changed in a broad range producing custom-tailored films for protection of a variety of plastics, fibers and metals [1,2,7].

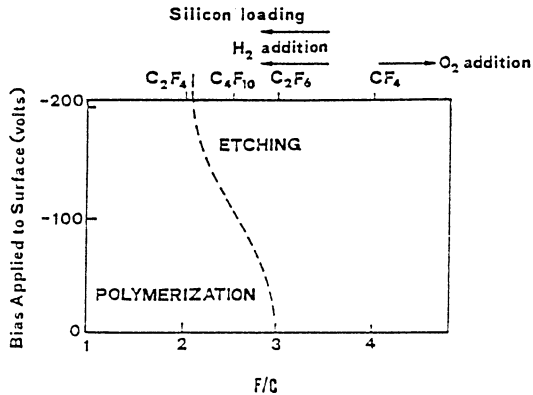

Figure 6. Polymerization and etching regimes as a function of feed F/C and of substrate bias.

The versatility of fluorocarbon plasmas essentially witnesses the ability to produce two kinds of long-lived active species in the discharge, *i.e.* F atoms and CF_x radicals. F atoms trigger the etching of many substrates and allow the fluorination of many organic surfaces, while the radicals form various deposits of Teflon-like films.

Coburn and Winters, and Kay *et al.* [36] have shown that, for discharges fed with fluorine-bearing gases, the fluorine-to-carbon ratio, F/C, of the feed monomer can be used as a simple parameter enabling to keep in perspective the polymerizing and etching nature of the glows. In fact, in figure 6 it is shown that a discharge can be operated in a polymerizing or etching mode depending on the monomer fluorine-to-carbon ratio, at a fixed bias voltage of the substrate.

The boundary region can be crossed by changing the monomer F/C ratio. This sort of "thumb rule" has been shown to be qualitatively valid because there is a direct quantitative correlation (even though non linear) between the monomer F/C and the plasma-phase concentration ratio $[F]/[CF_x]$, where F atoms and CF_x radicals are the active species for etching and polymerization, respectively [4]. The correlation between C/F and $[CF_x]/[F]$ can be appreciated from figure 7 [4], where the relative densities of CF, CF_2, and CF_3 radicals, of F atoms, and of fast electrons (> 11 eV) are reported for discharges fed with C_nF_{2n+2} (n=1-3) and CF_3Cl. Data for the tetrafluoroethylene are also included for comparison.

It can be seen from figure 7 that the density of radicals increases with increasing feed C/F, while the density of atoms decreases. The density of radicals, however, is not linear with C/F. The opposite trends shown by CF_x radicals and F atoms in fluorinated feeds is a direct consequence of the fast recombination process that these species undergo in the plasma, *i.e.* it is

www.manaraa.com

impossible to obtain both species in large concentration in the same medium. From the trends of Figure 7, one can classify the various fluorinated feeds on the basis of the expected polymerizing ability with the following order:

$$C_2F_4 > C_3F_8 > C_2F_6 > CF_4$$

obviously the opposite order has to be expected for the etching ability.

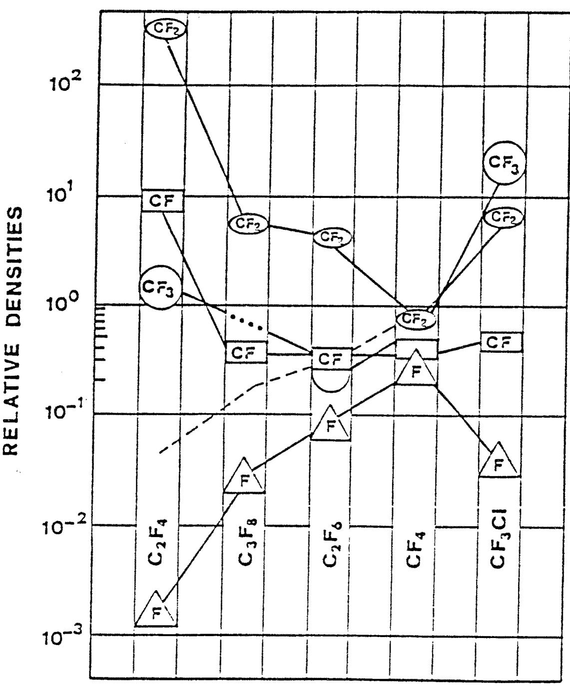

Figure 7. Histogram of the relative densities of radicals, F atoms and electrons (dashed curve), obtained by AOES (see text), for various fluorinated feeds.

For the aforesaid reasons, the detection and monitoring of active species, as well as the definition of discharge geometries, are important for justifying the deposition of teflon-like films, and allow a non-trivial classification of film properties, as it will be shown later.

Optical Emission Spectroscopy (OES), is generally the most utilized technique for low pressure discharges. In particular, however, Actinometric Optical Emission Spectroscopy (AOES) has been found to be one of the most powerful, non intrusive, diagnostic technique for monitoring CF_x radicals, F atoms and the trends of electrons at various energies. Since a discussion of AOES is out of the scope of this chapter, readers can make reference to Coburn *et al.* [39] and d'Agostino *et al.* [32,33,39-43]. Most of data shown in the remainder of this section have been obtained by means of AOES.

المنارة للاستشارات
www.manaraa.com

4.1. DEPOSITION MECHANISM OF TEFLON-LIKE FILMS

It has been shown [2,4,30-33,44] that a high $[CF_x]/[F]$ ratio in the discharge is not the only sufficient condition to obtain high polymerization rates; two additional conditions are required:
a) plasma media with relatively high density either of fast electrons (> 11 eV) for substrates under floating conditions, or of positive ions, for biased substrates. This can ensure, due to the bombardment of the surfaces by charged particles, a growth process which occurs through reactions of radicals with activated polymer sites;
b) rather low substrate temperatures. The adsorption-desorption equilibrium of CF_x radicals, which is exothermic, in fact regulates the overall kinetics of polymerization, leading to an apparent activation energy which becomes increasingly negative at higher substrate temperatures.

This behavior has been interpreted as a consequence of a film growth mechanism occurring through the reaction of radicals with polymer sites "activated" by charged particle bombardment. A simplified *Activated Growth Model* (AGM) has been suggested to give account of the experimental results. AGM implies that branch b of reaction /1/ in section 2.2 can be represented as:

$$CF_x \xrightarrow{(POL)^*_n} (POL)_{n+1} \qquad /4/$$

where CF_x radicals can stick efficiently only on activated polymer surface-sites, $(POL)_n$*, leading to an increase of one unit, $(POL)_{n+1}$. Obviously, activation by fast electrons and positive ions, and termination by neutrals M also occurs:

$$(I^+, e^-) + (POL)_n \longrightarrow (POL)^*_n \qquad /5/$$

$$(POL)^*_n + M \longrightarrow (POL)_n \qquad /6/$$

It can be shown [33], by the use of simple mathematics, that the kinetics equations /4/-/6/ lead to a polymerization rate, R_p, which can be expressed by:

$$R_p = K\,[CF_x]\,f(n_e) \qquad /7/$$

where $f(n_e)$ is a function of charged particles, either electrons or positive ions. Equation /7/ has been found to fit experimental data once trends of CF_x radicals and of electrons are obtained by AOES, whatever are feed composition, substrate position and discharge pressure (< 3 torr, otherwise step a of equation /1/ in section 2.2 becomes operative), provided substrate bias potential and input power are not so high to trigger the sputter-etching of the film, or the formation of nuclei in the gas phase, respectively.

www.manaraa.com

4.2. FEED COMPOSITION

The effect of feeding the glow with pure freons has been shortly discussed in section 4. It is important to realize, however, that discharge characteristics, particularly $[CF_x]/[F]$ ratio, can markedly be varied by adding to freon feeds variable amounts of different gases, which can act as scavengers of F atoms or of CF_x radicals.Oxygen is a typical CF_x scavenger and its introduction reduces the deposition performances while enhances the etching characteristics. Hydrogen, hydrocarbon and unsaturates, on the other hand, can all produce the opposite effects [30,33,40,45] according to an overall reaction scheme of the type:

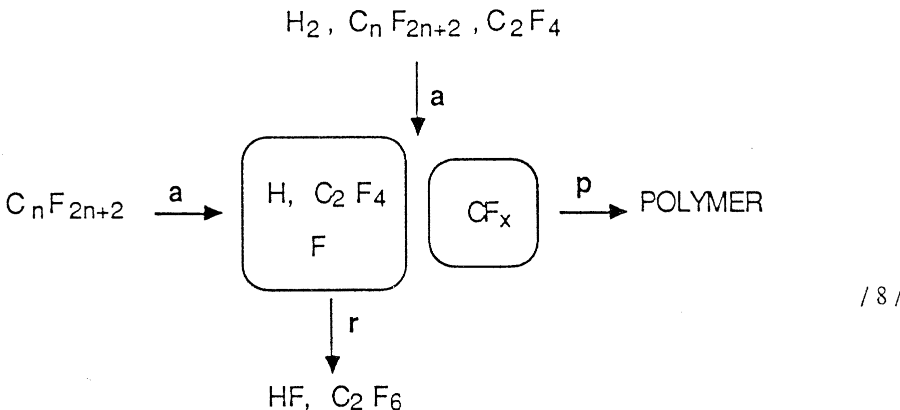

/8/

where steps a represent all the plasma activation channels in the presence or absence of plasma additives, step p accounts for polymer formation, and steps r are the recombinative routes, which are particularly important in the presence of additives).

As an example of the good fit to experimental data of AGM, one can examine figures 8 and 9, where trends of plasma active species and polymerization rates, both experimental and calculated according to equation /7/, respectively, are plotted as function of percent of hydrogen in a C_2F_6 feed.

When the substrates are placed on a negatively biased electrode [44], the charged particles activating polymer sites are likely positive ions, due to the negative self-bias of target electrodes. Figure 10 [25], obtained in CF_4-C_2F_4 discharges as a function of the substrate bias, shows another important effect of positive ions, *i.e.* by increasing the energy of ions impinging on the substrate, a competition of etching and sputtering processes occurs during polymerization. One can conclude that, in the presence of highly energetic ion bombardment, the rate expression for polymerization has to take into account the negative contributions of ion-assisted etching and sputtering:

$$R_p = K_p [CF_x] f(I^+) - K_e [F] g(I^+) - K_{sp} h(I^+) \qquad /9/$$

www.manaraa.com

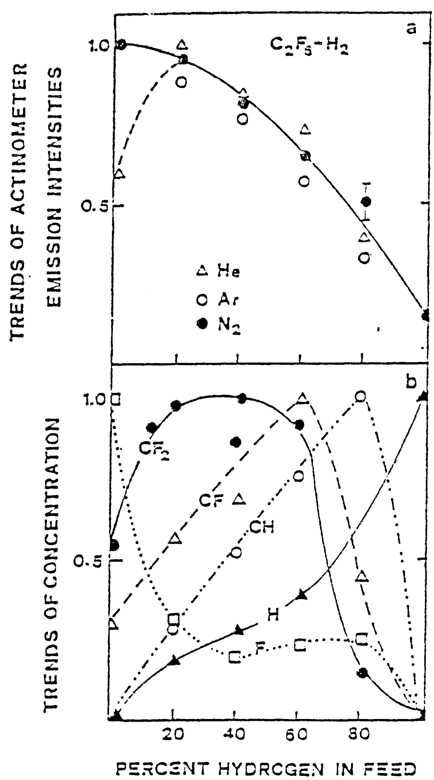

Figure 8. Trends of actinometer (He, Ar, N_2) emissions and of concentrations of radicals and atoms vs. H_2 % in C_2F_6.

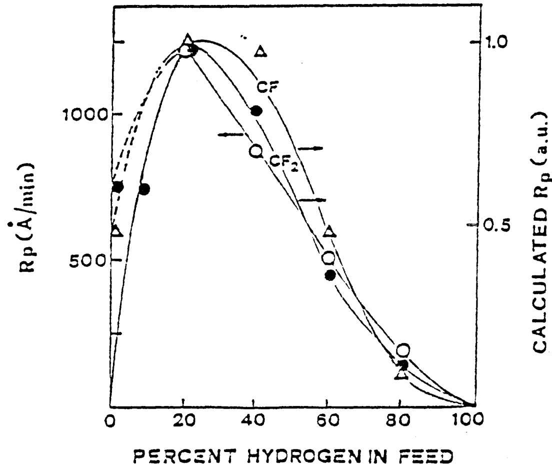

Figure 9. Comparison of experimental (open circles) and calculated (by means of AGM; black circles- curve obtained by using the experimental CF_2 trend; triangles- curve obtained by using CF trend) polymerization rates vs. H_2 % in C_2F_6.

www.manaraa.com

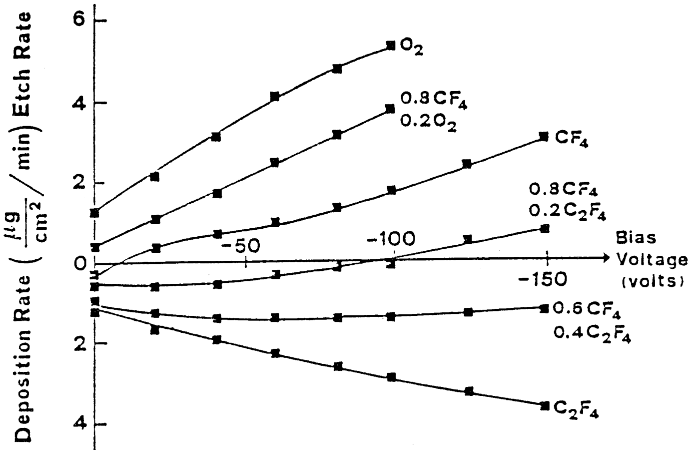

Figure 10. Deposition and etching rates *vs* bias voltage for different CF_4-C_2F_4 mixtures.

4.3. THE EFFECT OF SUBSTRATE TEMPERATURE

It has been shown [2] that, when polymerization occurs on a floating substrate immersed in the glow, the substrate temperature increases from room temperature up to 150°C, for discharges fed with C_2F_6-H_2 mixtures at 300 mtorr, 25 sccm total flow, and 45W. Under these conditions, it has been reported that instantaneous polymerization rates continuosly decrease and are characterized by two main features:

1) Rp's do not show an Arrhenius type behaviour because of the apparent negative activation energy;
2) at lower temperatures the apparent activation energy is close to zero.

A competition between two regimes, an adsorption-desorption equilibrium and a chemical surface reaction, can account for this behaviour:

$$CF_X(g) \rightleftharpoons CF_X(surf) \qquad /10/$$

$$CF_X\ (surf) + SS \longrightarrow POLYMER \qquad /11/$$

in which SS of equation /11/ are Surface Sites which can generate a polymer unit.

This formulation is not in contrast with AGM; it is, in fact, sufficient to consider branch b of equation /1/ or equation /4/ as overall processes made by the physical, /10/, and chemical, /11/, contributions.

المنارة للاستشارات
www.manaraa.com

4.4. THE CHEMICAL STRUCTURE OF TEFLON LIKES

The most attractive feature of plasma polymerized films and, in particular, of PPFM, or Teflon Like, coatings is the large range of compositions and structures and the possibility of controlling its variation by means of external plasma parameter, *e.g.* feed composition, bias superposition and power density, which effect CF_x radical distribution and charged particle bombardment. X-ray Photoelectron Spectroscopy (XPS or ESCA) is the most utlized technique to investigate the PPFM film chemical structure, because of the large differences in electronegativity between F and C. As a consequence, photoelectrons emitted by C1s display a broad overall spectrum which is the result of the superposition of several components with different binding energies (BE). Usually, decomposition procedures are available which allow an unambiguous deconvolution of the overall spectrum. Main features of these

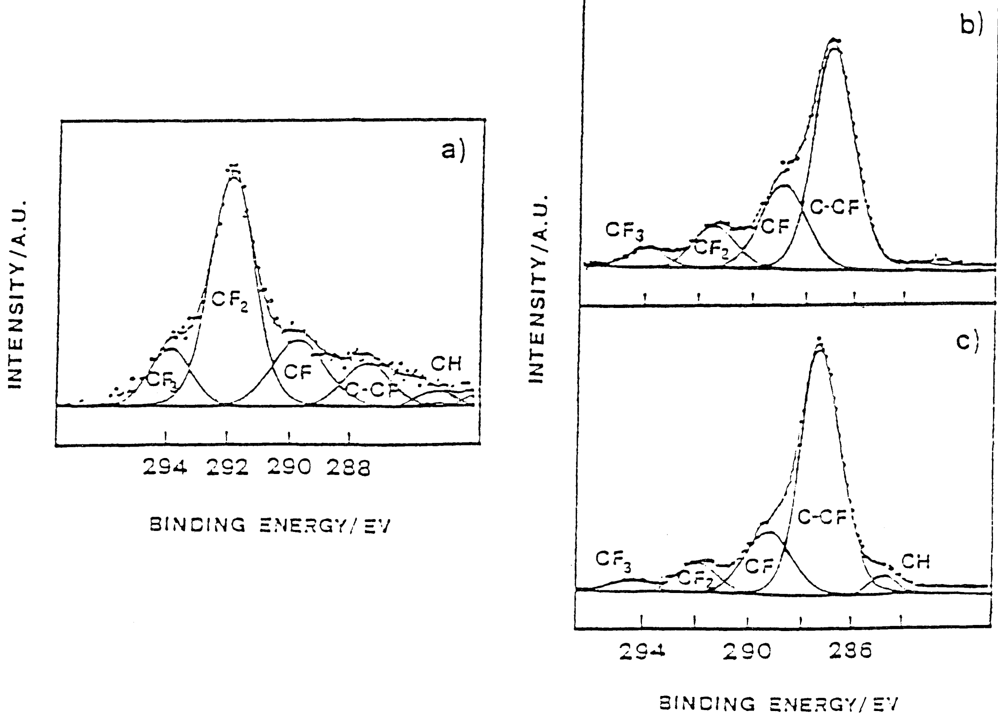

Figure 11. XPS C1s spectra of films deposited at various H_2 % in C_2F_6 : a) 20 %, b) 50 %, c) 70 %.

spectra are [2,46-48]:

> $-CF_3$ (BE = 294.0 eV), $-CF_2$ (BE = 292.1 eV), -CF (BE = 294.0 eV), -C-CF (BE = 287.3 eV), and -C- (BE = 285.0 eV)

www.manaraa.com

as shown in figure 11.

The peak centered at 285.0 eV can be due either to carbon not directly attached to fluorine, having no b-fluorine substituents, or to -CH groups. In some cases, the contribution of quaternary carbon is predominant. PPFM stoichiometry can easily be calculated either by the total integrated intensity of F1s and C1s or by the distribution of the integrated intensities of the various components of C1s spectrum. It is also important to notice that the integrated intensity of -C-CF and -C- components, with respect to the overall C1s, is a direct measurement of the degree of branching and cross-linking of the polymer films.

The continuous addition of hydrogen to a discharge fed by a perfluorinated freon, by keeping constant both pressure and total gas flow rate, causes a variation of film structure as it can be seen from figures 11 and 12.

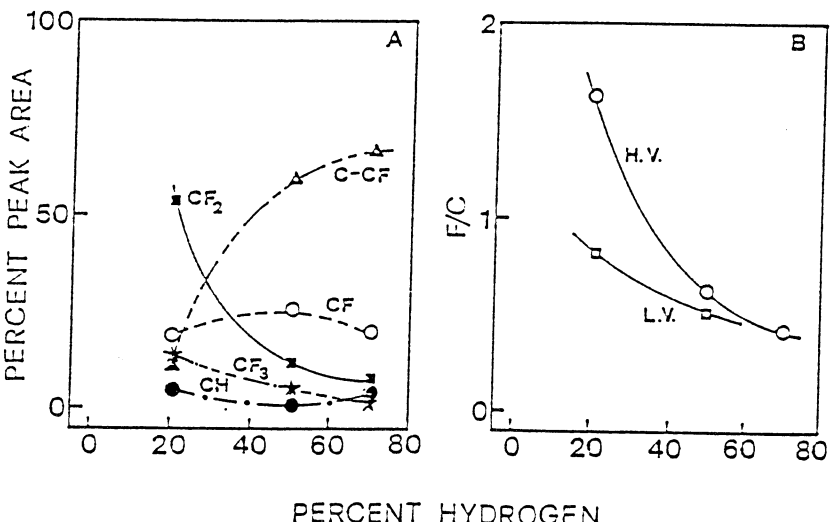

Figure 12. Relative abundance of carbon groups and overall F/C ratio of the films vs. H_2 % in C_2F_6.

Figure 12 shows that the hydrogen addition to inlet C_2F_6 changes the overall film stoichiometry and the component distribution by progressively favouring less fluorinated film compositions, film branching and cross-linking. These results should be compared with those of Figure 8 where the hydrogen effect on gas-phase radical distribution mirrors the effect on film components. In fact, also in the gas phase less fluorinated radicals are favoured. Obviously, the relative abundance of films components can not be a simple "fotography" of the gas-phase radical distribution because of ion and/or electron bombardment on the film. Such an effect is shown in figure 12 B where H.V. and L.V. traces refer to films obtained at high and low voltages, respectively, under the some power input. This means that trace marked with L.V. is obtained at higher current density, *i.e.* higher charged particle bombardment. It is evident that charged particle bombardment favours a reduction of F/C ratio and an increase of cross-linking in PPFM films. It can be shown that power input has a similar effect on PPFM chemical structure [6].

www.manaraa.com

5. Metal containing polymer films

Some of the unique characteristics of plasma deposited organic films, as for instance chemical inertness, hardness, and low friction, can be combined with the characteristics of metal deposited films, as electrical conductivity, by generating an entirely new class of materials: the plasma deposited metal-polymer composites. Recently some reviews appeared on this topic [49-52]. From the structural point of view, the principal difference of these composite films with plasma polymerized organometallics is that in metal-polymer composites one deals with a metallic dispersion in an organic matrix, while in organometallics metals are chemically bonded with carbon and/or other species (see § 6).

An interesting feature of plasma metal-polymer composites, from the point of view of the properties, is that, depending on the concentration of metal clusters, one has a dielectric behavior of the films when metal particles are well separated each other, a metallic behavior when there are interconnections, an intermediate behavior in the percolation region.

Both hydrocarbon and fluorocarbon originated polymer films are widely utilized for metal-polymer composites, and there are also interesting cases of amorphous carbon-metal composite films [51]; usual metals are Au, Al, Co, Pt. Our attention, however, will be here devoted mainly to Au-fluoropolymer films.

Two major systems have been mostly utilized for Au-PPFM films, *namely*, systems with simultaneous plasma polymerization and metal evaporation. In both cases, the most utilized configurations are diode reactors with substrates on grounded electrode. Usually for amorphous carbon films the substrates are placed over the cathode to enhance self-bias conditions. Recently, a triode configuration has also been utilized in order to allow sputtering of the metal target and to observe the effect of substrate bias [53].

The relative Au/C ratio for a fluoropolymer film obtained in a diode reactor with target sputtering depends on the relative gas-phase abundance of the active species for deposition, *i.e.* Au atoms and CF_x radicals. The gas-phase $[Au]/[CF_x]$ ratio is, in turn, affected by Au-sputtering, when the other parameters are kept constant. This can be accomplished either by increasing the self bias potential of the target or by feeding the discharge with Ar, besides fluorocarbons, in order to increase the sputter yield of target metal.

Monitoring of the ratio of the emission intensities of gold line (267.6 nm) and CF_2 band (265.0 nm) revealed to be an useful *in situ* measurement of the gas-phase $[Au]/[CF_2]$ ratio, linearly related to the actual Au/C film composition [54], as it can be seen in Figure 13.

www.manaraa.com

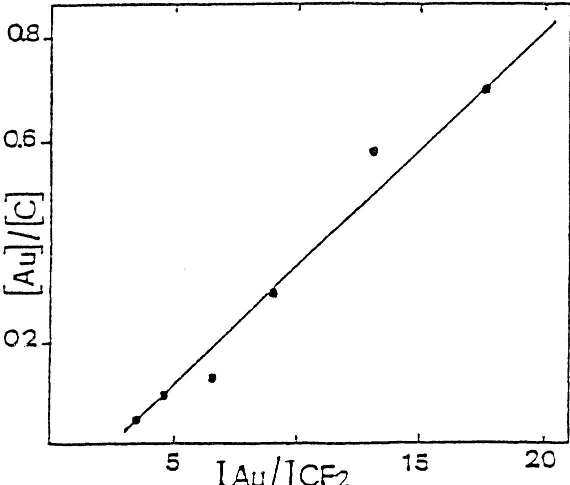

Figure 13. Atomic film composition *vs.* the ratio of Au and CF_2 emissions from discharge.

5.1. MECHANISM OF DEPOSITION

The microscopic mechanism of deposition is rather complex and involves several possible steps in the reaction route from the gaseous monomer unit and the metal to the formation of the metal-polymer composite. Both metal atoms and polymer building blocks are to be formed (independently) in the gas phase; they have then to diffuse to the deposition substrate, where the deposition can be differently affected by the bombardment with positive ion of different energies. A possible simplified reaction scheme is the following:

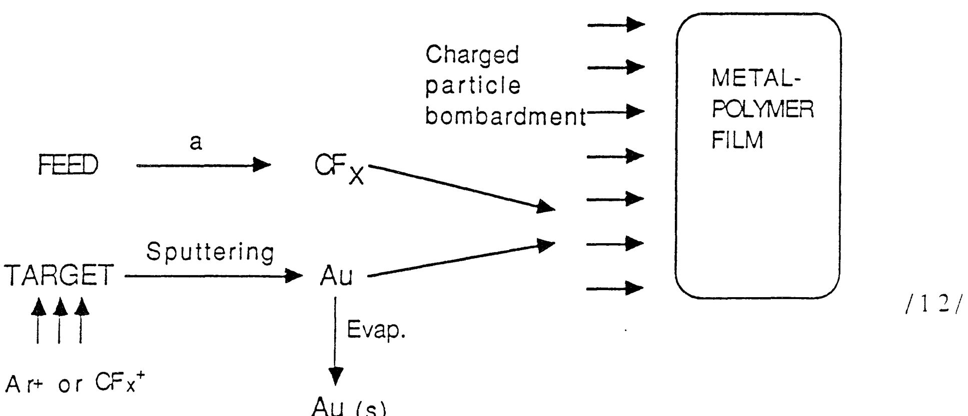

/12/

www.manaraa.com

where step a is the plasma activation. Martinu *et al*. [55] have shown, by utilizing probe measurements, that there is a considerable density of negative ions with Au target (with respect to Al target) which 'could affect' the deposition occurring on the ground electrode, since they claim that negative ions can be accelerated by a negative potential drop at the target when the electrodes face each other. On our opinion, however, such a chance seems remote in that both electrodes are *always negative with respect to the glow* potential, whatever is the discharge architecture.

On the other hand in ref. 53, where it was possible to bias the deposition electrode, it has been shown that positive ions do certainly affect the deposition process. In particular, when highly energetic ions are utilized the Au/C, Au/F, and C/F ratios of the film increase and also the chemical structure of the polymer matrix becomes more and more cross-linked.

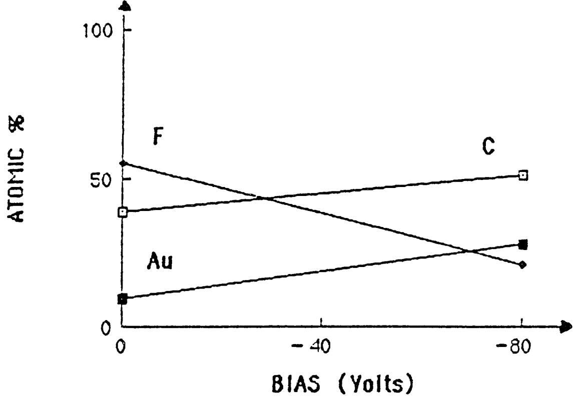

Figure 14. Atomic film composition *vs.* substrate bias (Ts = -13°C).

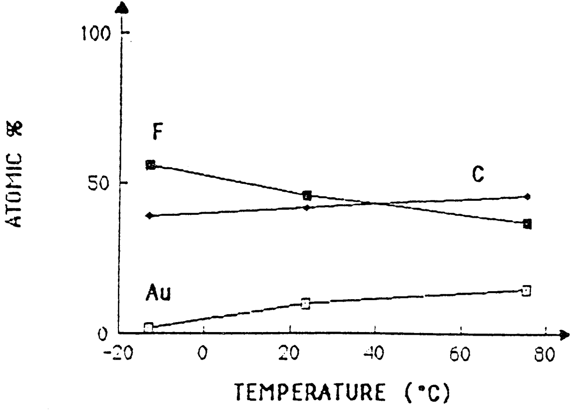

Figure 15. Atomic film composition *vs.* substrate temperature.

www.manaraa.com

This bias effect on the polymer composition can be seen in Figure 14 [53], where the growing film was kept at a constant nominal temperature of -13°C. It is interesting to notice that also the temperature of the substrate affects the chemical composition of the growing film in a similar way. In Figure 15 [53], it is shown that by increasing the nominal substrate temperature from -13°C to +75°C, Au/F and C/F ratios of the film increase, too. This effect can be due to the longer exposition of the film surface to the ion bombardment at the higher temperatures since the film growth is decelerated (see § 4.3) because of the exothermic adsorption-desorption equilibrium of CF_x radicals.

Finally, it should be mentioned that Kay *et al*. [56] have proposed that an oligomerization may occur by addition of CF_2 radicals. In this case, the route to polymerization in equation 12 should include $(CF_2)_n$ as intermediate to the polymerization, even though this route should be operative only at the higher pressures, as discussed in section 2.2.

5.2. STRUCTURE AND COMPOSITION OF Au-CONTAINING FILMS

Electron microscopy, ESCA and IR spectroscopy are the principal diagnostic tools which give an insight on film microstructure and composition.

The principal parameters which characterize metal-polymer composites are: the filling factor f, which is defined as the volume fraction of the metal contained in the unit volume of the film, the atomic composition (see figures 14 and 15), and the relative abundance of the various chemical components of the film.

Structural studies have shown that gold grains are randomly distributed in the polymer and their average diameters are in the range of 5-50 nm in the dielectric region ($f < 0.4$). At larger filling factors there is a dispersion of smaller grains among larger irregular particles. At still larger f (metallic region) there is a complex morphology of grainforms, which start to become more *wormlike* and interconnected.

Annealing seriously effects grains morphology because it increases the motion of gold particles in the relatively soft polymer matrix (particularly at temperature higher than the glass transition of PPFM, around 160°C); then one has a coalescence of particles coming into contact. This characteristic of Au containing PPFM films could seriously affect the utilization of this material due to aging effect. However, in ref. 53 it has been shown that crosslinking the polymer largely reduces this effect. This can be done by increasing the substrate bias and/or temperature during deposition. Going further in this direction, one can reach the conditions for amorphous carbon including metal particles, provided F abstraction is also ensured in the gas phase, either by using monomers with low F content or by adding hydrogen to the monomer feed [53].

المنارة للاستشارات
www.manaraa.com

5.3. FILM PROPERTIES AND APPLICATIONS

Plasma deposited metal-polymer films feature two important properties: an anomalous optical absorption in the visible and a conductivity response, both being a function of the filling factor.

The optical transmission of films obtained by Au and chlorotrifluoroethylene (CTFE) co-deposition, shown in Figure 16 [57], exhibits a typical minimum, due to optical resonance, the intensity and width of which

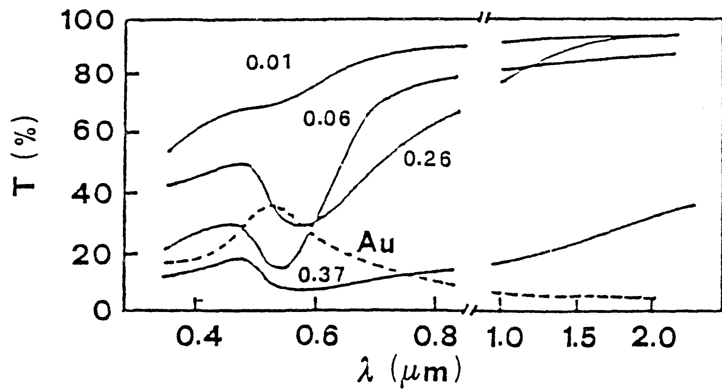

Figure 16. Optical transmission in the visible and near IR regions for gold-doped plasma deposited CTFE films with different metal volume fractions.

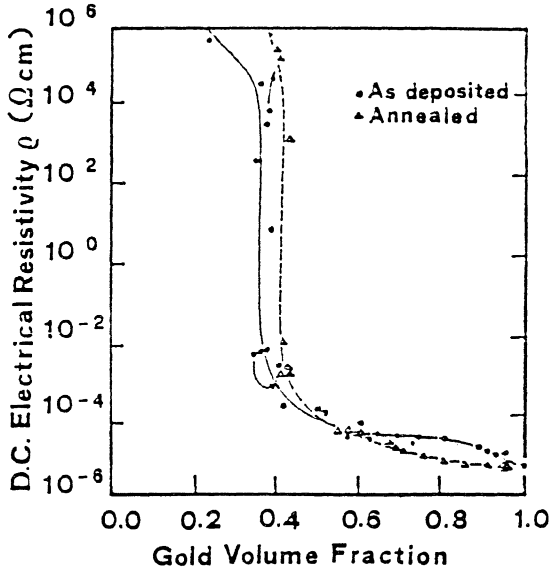

Figure 17. Resistivity variations (four point probe) *vs.* gold volume fraction for as-deposited and annealed plasma polymerized C_3F_8 films. Arrows indicate resistivities of films close to the percolation threshold upon annealing to 200°C.

المنارة للاستشارات
www.manaraa.com

are a function of gold volume fraction and grain distribution and morphology. It can be seen that the minimum at 0.55 μm intensifies and shifts with f. Therefore typical film color of gold-halocarbon films are pink (f = 0.02), red (f = 0.1), violet (f = 0.25), and blue (f = 0.4). Green is typical of sputtered gold films.

The electrical conductivity of Au-PPFM films is determined also by f and by metal grain distribution and shape. It can be seen from figure 17 [58] that the resistivity decreases with f, and shows a dramatic drop of about 8 orders of magnitude when f reaches 0.37 (which corresponds approximately to the percolation threshold [58,59]). It is also interesting to see that, after annealing at 200°C, the resistivity curve shifts toward higher f (the percolation threshold increases from about 0.40 to 0.42), as it should be expected on the basis of the discussed aging of metal composites due to the mobility and coalescence of metal grains. On the other hand, if the deposited organic matrix is amorphous carbon, one expects a more rigid behavior and less pronounced optical and electrical variations with both time and temperature. Such results can be obtained with gold-PPFM films deposited at higher substrate temperatures and/or bias voltages. A reduction of the aging effect is also observed if the film is post-annealed at T > 200°C.

For such films interesting applications have been suggested: as decorative coatings [60], optical filters [61] and humidity sensors [62]. Morita and Hattori [63] and Hori *et al.* [64] suggested the utilization of Au-plasma polymerized Styrene composites for a completely dry lithographic process. Kay suggested their utilization for optical recording [65].

6. Films from silicon-containing organic monomers

Silicon-containing organic compounds, called 'silorganic' monomers, are utilized in PE-CVD of Si-C alloys, silicone-like polymers, silicon oxide and nitride coatings. The composition of the coatings (*i.e.* O/Si ratio, nitrogen and/or carbon content), as well as their properties, depend on the choiche of the monomer and on the deposition parameters [66-71]. In order to deposit silicone- and silicon oxide-like films, widely used in optics, bio-medical applications, microelectronics and so on [66], the monomers are usually fed in variable percentages with oxygen or other oxidant gases (CO, N_2O, etc.), whose abundancy turns out to affect films deposition rate and chemical composition. In the remainder of this work Tetramethylsilane (TMS), Hesamethyldisilazane (HMDSN), and Tetraethoxysilane (TEOS) monomers will be compared, and it will be shown how the nature of the obtained films can be shifted from an 'organic' character (silicone-like structure) into a more 'inorganic' one (*i.e.* SiO_2) by increasing one or more of the following process parameters: oxygen per cent in the feed, substrate temperature, and substrate bias. Results regarding a fluorinated silorganic are also included.

6.1. THE EFFECT OF OXYGEN ADDITION TO THE FEED

When oxygen is added to the feed, the deposition rate and the composition of the coatings are influenced (figure 18), due to the reactivity of oxygen molecules and atoms in homogeneous and heterogeneous reactions [67,72]. Film

www.manaraa.com

chemical nature, as well as its growth rate, mirrors the precursor distribution in the plasma, which is affected by the oxygen content in the feed.

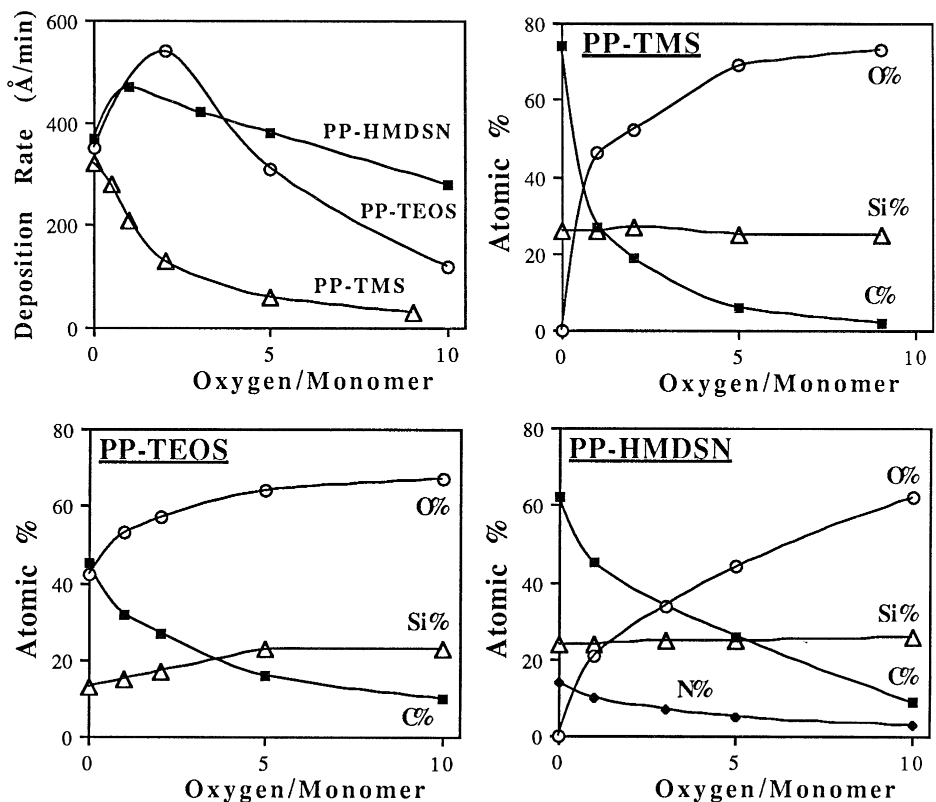

Figure 18. Deposition rates and XPS-measured compositions of coatings obtained by various monomers in mixture with oxygen. PP-TEOS films were analyzed after exposition to the atmosphere, and show an overextimated carbon content.

The overall deposition process can be schematized by assuming that two 'classes' of film precursors can be formed by plasma activation: the "inorganic" precursors, which contain silicon along with other elements (*e.g.* SiC_xH_y, $SiC_xH_yO_z$, etc.), and the "organic" precursors, which do not contain silicon. Even though this distinction can be only a matter of jargon, it can turn useful in order to rationalize the deposition mechanism as follows:

Step a- Monomer and oxygen fragmentation (electron impact), *i.e.* formation of organic and inorganic precursors, and of oxygen atoms and excited molecules.
Step b- Homogeneous reactions between oxygen species and precursors, which modify their distribution depending on the feed oxygen content. These

المنارة للاستشارات
www.manaraa.com

reactions result in scavenging organic precursors, and in decreasing the organic character of the inorganic ones. By products are non polymerizable species, such as CO, CO_2, H_2O. It is important to notice here that the increased feed oxygen-to-monomer ratio usually results in an increased electron density, as it can be revealed by means of AOES [6], which also could be responsible of modifications of the monomer fragmentation paths.
Step c- Polymerization of the adsorbed precursors on the substrate surface.
Step d- Heterogeneous surface oxidation of the growing film by oxygen atoms, and formation of $-SiO_x$ and $-CO_x$ functionalities [67-69,71].

The deposition rate of PP-TMS decreases by increasing the feed oxygen content, while those of PP-HMDSN and PP-TEOS are characterized by a trend with a maximum. These differences can be ascribed to the different importance of processes of steps a, b, and c, depending on the type and density of precursors, and/or on the structure and composition of the monomer (*i.e.* presence or absence of oxygen and nitrogen). On the other hand, the composition trends of PP-films as a function of the oxygen-to-monomer ratio are similar for the three monomers, and agree with reactions a-d.

XPS and FT-IR analyses have shown [67,69] that, when no oxygen is added to the feed, PP-films are characterized by stoichiometries close to those of monomers, but with different distribution of functional groups, and a lower carbon and hydrogen content. By increasing the oxygen per cent, the following modifications occur which, in effect, can be considered as general:
Carbon- Its abundancy decreses on the basis of reactions b, the decrease is steeper in PP-TMS. The detailed C1s XPS spectra show that the concentration of oxygenated functionalities increases.
Oxygen- Its concentration increases, the shape and position of XPS peak remains almost unchanged.
Silicon- Its content in the film is pratically unchanged; however, Si2p peak shifts to higher binding energies for the formation of silicone-like $(C_x\text{-}Si\text{-}O_y)_n$ structures. When a high O/Si ratio is obtained (ratios higher than 2 are due to Si-OH groups), the binding energy reaches its maximum (103,5 eV). It is interesting to notice that Si2p FWHM (mainly in PP-TMS, but also in PP-HMDSN) has a trend with a maximum, which mirrors a continuous composition change in the material with the increase of the feed oxygen content. Films with a "monomer-like" stoichiometry are deposited when no O_2 is added (Si-H, Si-C, eventually Si-N bonds in the film), while "silicone-like" (Si-O plus the aforesaid bonds), and "oxide-like" films (practically only Si-O bonds) are deposited at low and medium-high oxygen-to-monomer ratio, respectively.
Nitrogen- It is always present in PP-HMDSN films and the binding energy of N1s slightly increases with oxygen addition to the feed.

6.2. THE EFFECT OF SUBSTRATE TEMPERATURE AND BIAS

As for fluoropolymers, substrate temperature and bias influences plasma-surface interactions in PECVD from silorganics, by affecting the adsorption-desorption equilibrium of precursors and etchants (whatever they are),

www.manaraa.com

heterogeneous reactions, film pyrolysis, and by triggering ion-assisted etching or sputtering processes, depending on ion energy (see section 4 and ref. 66).

Figure 19 shows the effects of substrate temperature on the growth rate of PP-TMS and PP-TFC films, where TFC is a fluorinated silorganic, namely the trimethyil tri(trifluoro n-propyl) cyclo tri-siloxane [71]. The temperature enhancement decreases deposition rate also due to film pyrolysis, which plays a fundamental role in PECVD of organosilicons, as evidenced by *Wrobel et al.* [66]; the pyrolysis breaks Si-H, Si-CH_3 and C-H bonds, leading to crosslinked films. The overall effect on film composition, witnessed by ESCA and FT-IR analysis, are the increase of the Si per cent, and a dramatic decrease of C and H content, whatever is the monomer. In PP-TMS, film density increases from about 1.1 to about 2.0 mg/cm^3 for a temperature increase from 60 to 320 °C [70].

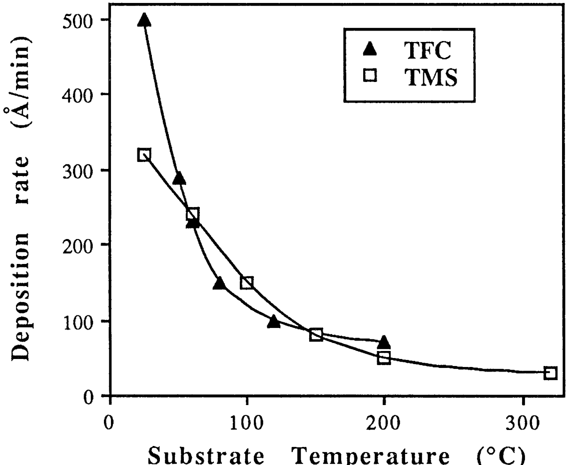

Figure 19. Deposition rate of PP-TMS and PP-TFC *vs* substrate temperature.

In figure 20 the deposition rate of PP-TFC and PP-TMS films (at 200 °C) are plotted as function of the substrate bias. Here both the activating and the disactivating effects of ion bombardment, discussed in the previous sections, are shown. Depending on film structure and ion energy, the ion-bombardment can enhance or depress the growth rate; this behavior can be attributed to the competition of two processes triggered at different energies:

a- Low-energy ions enhance film growth rate by creating surface "active sites" (dangling bonds, distortions), more reactive towards precursor radicals. This mechanism is described by the *Activated Growth Model* (see section 4).

b- High-energy ions assist film sputter-etching (at about -30 V the effect becomes evident for PP-TMS) with etchants, *e.g.* hydrogen or fluorine.

The bias effects, generally close to those of the temperature (more inorganic, cross-linked, hard, and dense coatings) can be exploited to design films with different structures. Low substrate temperature and bias lead to films with high monomer-structure retention, while the increase of ion bombardment and/or temperature drives the deposition toward "more inorganic" materials.

المنارة للاستشارات
www.manaraa.com

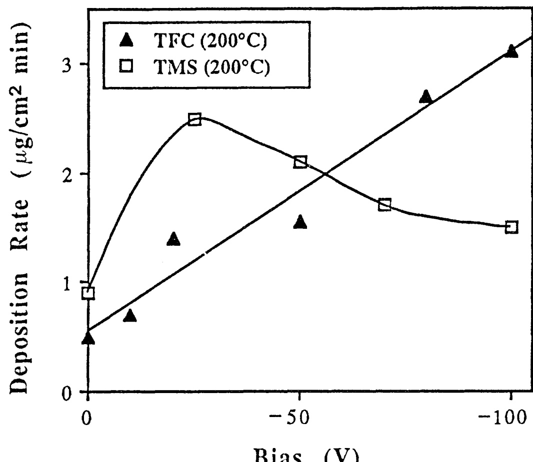

Figure 20. Deposition rate of PP-TMS and PP-TFC *vs* substrate bias (at 200 °C).

References

1) d' Agostino R., Cramarossa F., Fracassi F., Illuzzi F., Caporiccio G., European Patent Application no. 230993 (1987).
2) d' Agostino R., Cramarossa F., Fracassi F., De Simoni E., Sabbatini L., Zambonin P.G., Caporiccio G., Thin Solid Film, 143, 163, (1986).
3) Lamendola R., Favia P., d'Agostino R., submitted for publication.
4) d' Agostino R., Capezzuto P., Bruno G., Cramarossa F., Pure Appl. Chem., 57, 1287, (1985).
5) Yasuda H.K. in: "Thin Film Processes", Vossen J.L., Kern W. eds., Academic Press, (1978), and refs therein.
6) d'Agostino R., unpublished results.
7) Yasuda H.K.: "Plasma Polymerization", Academic Press (1985).
8) Kammermaier J., Rittmayer G., Schulte R., Proc. of the 6th Int. Symp. on Plasma Chemistry ISPC-6, Montreal, (1983).
9) Kammermaier J., Rittmayer G., Proc. of the 7th Int. Symp. on Plasma Chemistry ISPC-7, Eindhoven, (1985).
10) Carmi U., Inspector A., Avni R., Plasma Chem. Plasma Proc., 1, 233 (1981).
11) Claude R., Moisan M., Wertheimer M.R., Zakrzewski Z. in "Polymeric Materials Science and Engineering", Shen M., Bell A.T. eds., Proc. of the ACS Division of Polymeric Materials, 56, Denver, (1987).
12) Claude R., Moisan M., Wertheimer M.R., Zakrzewski Z., Appl. Phys. Lett., 50, 1797 (1987).
13) Claude R., Moisan M., Wertheimer M.R., Zakrzewski Z., Plasma Chem. Plasma Proc., 7, 451 (1987).
14) Wertheimer M.R., Moisan M., J. Vac. Sci. Technol., A3, 2643 (1985).
15) Ferreira C.M., J. Louriero, J. Phys. D., 17, 1175 (1984).
16) Vossen J.L., Electrochem. Soc., 126, 1308 (1978).
17) Yasuda H., Hsu T., Surface Science, 76, 232 (1978).
18) Rice D.W., O' Kane D.F., J. Electrochem. Soc., 123, 1308 (1976).
19) Ohki Y., Nakano T., Yahagi K., Proc. of the 7th Int. Symp. on Plasma Chemistry ISPC-7, Eindhoven, (1985).
20) Koenig H.R., Maissel L.I., IBN J. Res. Develop., 14, 168 (1970).
21) Coburn J.W., Kay E., J. Appl. Phys., 43, 4965 (1972).
22) Koler K., Coburn J.W., Horne D.E., Kay E., Keller J.H., J. Appl. Phys., 57, 59 (1985).
23) Bruce R.H., J. Appl. Phys., 52, 7064 (1981).
24) Coburn J.W., Winters H.F., J. Vac. Technol., 16, 391 (1979).
25) Fracassi F., Occhiello E., Coburn J.W., J. Appl. Phys., 62, 3980 (1987).
26) Christensen O., Jensen P., J. Phys. E, 5, 86 (1972).

www.manaraa.com

27) d' Agostino R., Cramarossa F., Fracassi F., Illuzzi F. in: "Plasma Deposition, Treatment and Etching of Polymer Films", R. d'Agostino ed., Academic Press (1990).
28) Fracassi F., Coburn J.W., J. Appl. Phys. 63 (5), 1 (1988).
29) d' Agostino R., Favia P., Fracassi F., J. Pol. Sci. A: Pol. Chem., 28, 3387, (1990).
30) d' Agostino R., Cramarossa F., De Benedictis S., Plasma Chem. Plasma Proc., 2, 213 (1982).
31) d' Agostino R., Cramarossa F., De Benedictis S., Fracassi F., Plasma Chem. Plasma Proc., 4, 163 (1984).
32) d' Agostino R., Cramarossa F., Fracassi F., Laska L., Masek K., Plasma Chem. Plasma Proc., 5, 239 (1985).
33) d'Agostino R., De Benedictis S., Cramarossa F., Plasma Chem. Plasma Proc., 4, 1 (1982).
34) d'Agostino R., Colaprico V., Cramarossa F., Plasma Chem. Plasma Proc., 1, 365 (1981).
35) Donnelly V.M., Flamm D.L., Doutremont-Smith W.C., Werder D.J., J. Appl. Phys. 55, 5974 (1984).
36) Coburn J.W., Winters H.F., J. Vac. Sci. Techn., 16, 391 (1979); Kay E., Coburn J.W., Dilks A., in: "Topics in Current Chemistry", Veprek S., Venugopalan M. eds., Plasma Chemistry III, 94, Springer-Verlag, Berlin, (1980).
37) Pittman A.G., in "Fluoropolymers" (L.A. Wall ed.), Wiley, New York, (1972).
38) Momose Y., Takada T., Okagaki S, in: "Polymeric Materials Science and Engineering", Shen M., Bell A.T. eds., Proc. of ACS Division of Polymeric Materials, 56, Denver, (1987).
39) Coburn J.W., Chen M.J. Appl. Phys., 51, 3134 (1980).
40) d'Agostino R., Cramarossa F., De Benedictis S., Ferraro G., J. Appl. Phys., 52, 1259 (1981).
41) d'Agostino R., Cramarossa F., De Benedictis S., Fracassi F., Plasma Chem. Plasma Proc., 4, 163 (1984).
42) d'Agostino R., Cramarossa F., Colaprico V., Plasma Chem. Plasma Proc., 1, 365 (1981).
43) d'Agostino R., Cramarossa F., De Benedictis S., Plasma Chem. Plasma Proc., 4, 21 (1984).
44) d' Agostino R., Cramarossa F., Illuzzi F., J. Appl. Phys., 61, 2754 (1987).
45) d'Agostino R., Proc. of XVI ICPIG, invited, Dusseldorf, (1983).
46) Dilks A. in: "XPS for Investigation of Polymeric Materials", Brundle C.R., Baker A.D. eds., Electron Spectroscopy 4, Acad. Press, London, (1981).
47) Clark D.T., in: "ESCA Applied to Organic and Polymeric Systems", Briggs D., ed., Handbook of X-ray and UV Photoelectron Spectroscopy, Heydem, London, (1978).
48) Dilks A., Kay E., Macromolecules, 14, 855 (1980).
49) Kay E., Z. Phys. D, 3, 251 (1986).
50) Biederman H., Vacuum, 37, 367 (1987).
51) Biederman H., Martinu L., Slavinska D., Chudacek I., Pure Appl. Chem. 60, 607 (1988).
52) Kay E., Dilks A., Hetzler U., Macromol. Chem. A, 12, 1393 (1978).
53) d'Agostino R., Martinu L., Pische V., Proc. of 9th Int. Symp. on Plasma Chemistry ISPC-9, Pugnochiuso, Italy, (1989).
54) Martinu L., Biederman H., Plasma Chem. Plasma Proc., 5, 81 (1985).
55) Martinu L., Spatenka P., Biederman H., Sicha M., Thin Solid Films, 141, L83 (1986).
56) Kay E., Coburn J., Dilks A., in: "Topics in Current Chemistry", 94, 1 (1981).
57) Martinu L., Biederman H., Vacuum, 36, 477 (1986).
58) Martinu L., Solar Energy Materials, 15, 135 (1987).
59) Perrin J., Despax B., Hanchett V., Kay E., J. Vac. Sci. Tech. A, 4, 46 (1986).
60) Beale H.A., Ind. Res. Develop., 23, 135 (1981).
61) Biederman H., Vacuum, 34, 405 (1984).
62) Mannini A., Bagnoli P., Diligenti A., Neri B., Pugliese S., J. Appl. Phys., 62, 2138 (1987).
63) Morita S., Hattori S., Pure Appl. Chem., 57, 1277 (1985).
64) Hori M., Yasuda T., Yamada H., Morita S., Hattori S., Plasma Chem. Plasma Proc., 7, 155 (1987).
65) Kay E., Proc. E-MRS Meeting, 15, 355, (1987).
66) A. M. Wrobel, M. R. Wertheimer in: "Plasma Deposition, Treatment, and Etching of Polymers", R. d'Agostino ed., Acad. Press (1990) and refs. therein.
67) Favia P., Colaprico V., Fracassi F., De Santis C., d'Agostino R., Proc. of the Meeting on Sintesi e Metodologie Speciali in Chimica Inorganica, Bressanone, Italy (1991).
68) Fracassi F., Favia P., d'Agostino, J. of Electrochem. Soc., in press.
69) Favia P., Fracassi F., d'Agostino R., J. Biomat. Sci.: Polym. Eds., in press.
70) Favia P., Lamendola R., d'Agostino R., Plasma Sour. Sci. Tech., 1, 59 (1992).
71) Favia P. Caporiccio G., d'Agostino R., work in preparation.
72) Favia P, Fracassi F, d'Agostino R, Proc. of 9th Symp on Elementary Processes and Chemical Reactions in Low Pressure Plasma, invited, Casta (Czekoslovakia), (1992).

www.manaraa.com

PHYSICAL VAPOR DEPOSITION TECHNIQUES I: EVAPORATION AND SPUTTERING

Y. PAULEAU
National Polytechnic Institute of Grenoble
ENSEEG, B.P. 75
38402, Saint Martin d'Hères
France.

ABSTRACT. Thin films of numerous materials can be deposited on various substrates at low temperatures via condensation of vapors generated by vacuum evaporation or cathode sputtering techniques. Thermodynamic and kinetics aspects together with other basic considerations involved in evaporative deposition techniques are discussed. Evaporation of compounds and alloys can be improved using activated reactive evaporation processes. The major experimental techniques employed in vacuum evaporation and sputtering processes of some elements or compounds are described. The principles and basic equipment of diode sputtering are briefly presented. The sputtering yield of materials can be determined from the Sigmund model. The yield value depends on various factors : ion energy, incidence angle of ions, crystallographic orientation of the target surface,... The characteristics of sputtered species are compared to those of evaporated species. Thorough investigations of experimental parameter effects on sputter-deposition processes are required for optimization of deposition rates and properties of films. Sputtering systems operating at low pressures and high frequency sputtering equipments for deposition of insulating films are also described.

1. Introduction

Thin films and coatings of material M can be deposited on various substrates via the condensation of M vapors on the substrate surface maintained at a temperature T_S nearly room temperature. The element or compound M is evaporated from a "source" either heated at high temperatures (evaporation process) or subjected to ion bombardment of sufficiently high energy (sputtering process). The energy required for production and transfer of vapor species from a condensed source material M to the substrate surface is provided by heat transfer in evaporation and by momentum transfer in sputtering. The deposition process involves essentially phase transformation and mass-transport phenomena. Therefore, evaporation ans sputtering are named physical vapor deposition (PVD) techniques in contrast to chemical vapor deposition (CVD) techniques where the formation of elements or compounds M takes place on the substrate surface via chemical reactions between gas precursors.

The first example of sputter deposition of thin films to be recognized as such was given by Grove [1] who studied fluorescent light tubes in the middle of the 19th century; he observed that a dark deposit formed on the inside wall of the glass tube and surmised that this material was transferred from the electrode to the wall. In fact, the technological

W. Gissler and H. A. Jehn (eds.), Advanced Techniques for Surface Engineering, 135–179.
© 1992 ECSC, EEC, EAEC, Brussels and Luxembourg.

www.manaraa.com

objective in the field of fluorescent tubes was to prevent the formation of these dark thin films on the glass tube. The sputter deposition technique was applied to produce reflective metal films in the latter years of the 19th century until about 1930. The vacuum evaporation technique can be comparatively simpler than sputter deposition; however, rigorous experimental conditions, particularly in terms of base pressure, must be adopted and respected to produce films of extreme purity with desired or pre-selected structure and properties. The development of diffusion pumps in the 1920's made possible to evacuate a deposition chamber to sufficiently low pressures (about 0.1 Pa) for deposition of mirror-like films by filament evaporation. In the next years, evaporation processes of different types were developed [2]. In the 1950's, the development of thin film applications as conductors and resistors in the electronics industry caused tremendous expansion of interest in sputter deposition techniques, in particular to produce thin films of refractory metals or compounds, such as Ta and Ta_2N, for hybrid circuits. By that time, vacuum evaporation techniques gave rise to difficulties for evaporation of refractory metals; as a result, sputtering deposition processes of refractory materials were developed for microelectronic applications. In the past decades, evaporative and sputter deposition techniques have become very widely used and accepted for deposition of thin films in a broad range of applications from architectural glass and food packaging to thin film microelectronics.

In this chapter, the techniques of evaporation and sputtering as a means of deposition of thin films are described. The growth mechanisms of evaporated and sputtered films as well as the process parameters are discussed and presented. The main purpose is to emphasize the advantages, benefits and limitations of these PVD techniques for a particular application.

2. Vacuum Evaporation

2.1. BASIC CONSIDERATIONS

The deposition process of thin films by evaporation consists of the following physical steps :

a) sublimation or vaporization of the solid or liquid material placed in the source
b) transfer of vapor species (atoms or molecules) from the evaporation source to the substrate
c) condensation of these particles on the substrate surface and film surface
d) rearrangement of atoms or modifications of chemical bonds on the surface.

Evaporative deposition processes are governed by thermodynamic and kinetic aspects essentially involved in steps a) to c).

2.1.1. Thermodynamics. For evaporation of a material, energy must be supplied to atoms or molecules of the condensed phase to overcome attractive interatomic or intermolecular forces and provide kinetic energy to vapor species leaving the surface of the material. Thermal energy which enhances the thermal motion of species at the surface of a material to be evaporated is supplied by heating the source material at sufficiently high temperatures to liberate large amounts of atoms or molecules from the condensed phase. In a closed and isothermal system, the pressure rises up to the saturation vapor pressure when the solid or liquid-vapor equilibrium is established. This type of equilibrium at constant temperature T and pressure P is governed by the Clapeyron equation :

www.manaraa.com

$$\frac{dP}{dT} = \frac{\Delta H_e}{T\,\Delta v} \quad (1)$$

with $\Delta v = v_{vapor} - v_{cond}$

in which dP and dT are infinitesimal changes of pressure and temperature promoting an infinitesimal transfer of matter between condensed phase and vapor phase such as the system reaches a new state of equilibrium at temperature (T + dT) and pressure (P + dP); ΔH_e is the molar heat of evaporation; v_{vapor} and v_{cond} are the molar volumes of vapor phase and condensed phase, respectively. Generally, the molar volume of a gas, v_{vapor}, is much larger than the molar volume of the condensed phase, v_{cond}, and the gas behaves ideally. Therefore, equ.(1) becomes :

$$\frac{1}{P}\frac{dP}{dT} = \frac{\Delta H_e}{R\,T^2} \quad (2)$$

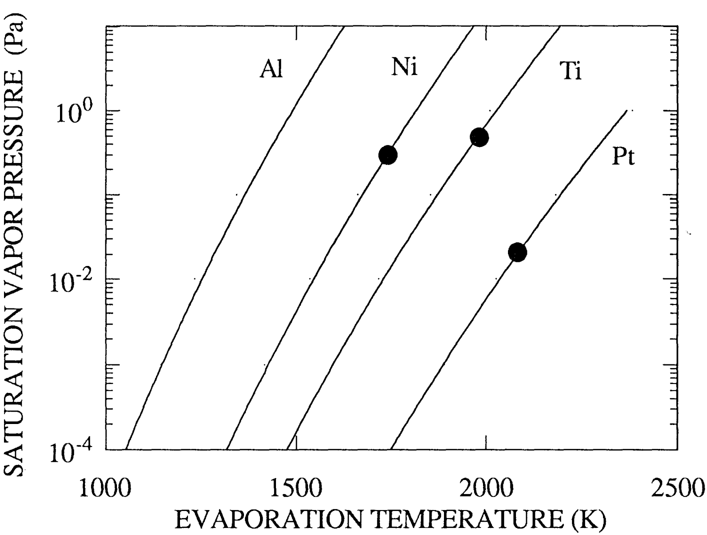

Figure 1 - Saturation vapor pressure of metals versus temperature; close symbols ● show the melting temperature of metals.

For many substances in a moderate temperature range, the molar heat of evaporation is substantially constant; equ.(2) can be integrated as follows :

$$\mathrm{Ln}P = -\frac{\Delta H_e}{R\,T} + \frac{\Delta S_e}{R} \quad (3)$$

with $\Delta G_e = \Delta H_e - T\,\Delta S_e$

www.manaraa.com

where ΔG_e and ΔS_e are the molar free energy and molar entropy of evaporation, respectively. Equ.(3) named the Clausius-Clapeyron equation can be used to predict vapor pressures of a liquid (or a solid) when the heat of vaporization (or sublimation) and one vapor pressure are known. The surface temperature required for evaporation of a material depends on its vapor pressure which is a strong fonction of temperature (Fig.1).

In the system at constant temperature T and pressure P, the number of collisions made by vapor species or particles (atoms or molecules) with the surface of the source material per unit area and per unit time at equilibrium or the collision frequency Z is equal to :

$$Z = \frac{1}{4} n \bar{v} = \frac{P}{\sqrt{2 \pi m k T}} = \frac{P N_{Av}}{\sqrt{2 \pi M R T}} \tag{4}$$

in which n and $\bar{v}$ are the density and average speed of particles, respectively; m and M are the mass of one molecule and molar mass of the gas, respectively; N_{Av} is the Avogadro number. Therefore, the number of particles N_e evaporated at a temperature T per unit area and per unit time at equilibrium is given by :

$$N_e = \frac{P_e N_{Av}}{\sqrt{2 \pi M R T}} \tag{5}$$

where P_e is the saturation vapor pressure or the vapor pressure at equilibrium at a temperature T. This flux of evaporated particles or the evaporation rate N_e can be expressed as the following practical formula :

$$N_e = 3.51 \times 10^{22} \frac{a_1 P_e}{\sqrt{M_e T_e}} \quad \left(\text{particles cm}^{-2} \text{s}^{-1}\right) \tag{6}$$

in which P_e(Torr) is the saturation vapor pressure at temperature T_e (K), M_e (g) is the molar mass of particles, and a_1 is an evaporation coefficient equal to unity for clean (non oxidized) evaporant surface.

2.1.2. Kinetics.

a) Path of evaporated particles

If some part in the previous system at temperature T_e and pressure P_e is cooled down to a temperature T_s, the system will not be longer at equilibrium, and vapor species will condense on surfaces at T_s. Thus, the conditions will be established for a transfer of material from evaporation source to the substrate surface at temperature T_s; the deposition of films by evaporation is a non equilibrium process.

The particles leave the surface of the source material with their thermal velocities v_{th} along a straight line in the gas phase until collision with another particle. The particle path between the source and substrate can remain a straight line when the concentration of particles in the gas phase and the pressure of residual gas are sufficiently low. Assuming that the evaporated particles are essentially scattered by collisions with atoms or molecules of residual gas, the number of particles scattered between the source and substrate at a distance d is given by :

$$N = N_0 \left[1 - \exp\left(\frac{d}{\lambda}\right)\right] \tag{7}$$

www.manaraa.com

where N_0 is the number of particles liberated from the surface of the source material (where d = 0) and λ is the mean free path of molecules in the residual gas; the mean free path can be expressed as follows :

$$\lambda = \frac{1}{\sqrt{2}}\,\frac{1}{\sigma n} = \frac{1}{\sqrt{2}}\,\frac{R\,T}{4\,\pi\,\rho_m^2\,P\,N_{Av}} \qquad (8)$$

with $\sigma = 4\,\pi\,\rho_m^2$

where ρ_m is the radius of a residual molecule considered as a rigid sphere; σ is the collision cross section; P and T are the pressure and temperature of the residual gas, respectively. The mean free path λ(cm) in air at room temperature is given as a function of the residual gas pressure P (Torr) by :

$$\lambda\ (\text{cm}) = \frac{5 \times 10^{-3}}{P\ (\text{Torr})} \qquad (9)$$

At 25°C with a pressure of residual gas in the range 10^{-4}-10^{-6} Torr, the mean free path lies between 50 cm and 50 m; therefore, to prevent a considerable dispersion of evaporated particles due to collisions with residual gas between the source and substrate, the residual gas pressure must be about 10^{-5} Torr with a source-substrat distance of the order of tens of centimeters.

b) Contamination of the surface of evaporated films by residual gas
The surface of substrates is bombarded not only by evaporated particles but also by molecules of residual gas (H_2O, CO_2, O_2, N_2, organic vapors, ...). These impurities can arise from outgassing from the chamber walls, decomposition of pump oils and desorption from elastomer rubber seals. The collision frequency of residual molecules, Z_g, striking unit area of the substrate or film surface is given as a function of the pressure by equ.(4). The number of molecules n_g adsorbed on the surface per unit area or the concentration of adatoms on the surface at equilibrium is a function of the collision frequency Z_g and average life time τ_g of an adatom before it re-evaporates from the surface :

$$n_g = Z_g\,\tau_g \qquad (10)$$

Since desorption of an atom or molecule from the substrate surface is an activated process, it is reasonable to expect that τ_g will be related to the absolute temperature T of the substrate by an equation of the form :

$$\tau_g = \frac{1}{\nu_0}\,\exp\left(\frac{E_a}{k\,T}\right) \qquad (11)$$

where E_a is the adsorption energy per particle and ν_0 is a constant. It is found experimentally that $1/\nu_0$ is typically of the order of 10^{-13} s at room temperature. When

www.manaraa.com

adsorption energy is given, an approximate value of $\tau_g(s)$ can be calculated from the practical formula :

$$\tau_g(s) = 10^{-13} \exp\left(\frac{1.16 \times 10^4 E_a(eV)}{T(K)}\right) \tag{12}$$

Combining equs.(4) and (12) with equ.(10), the concentration of gas particles (atoms or molecules) adsorbed on the substrate surface at equilibrium will be given by :

$$n_g(\text{part. cm}^{-2}) = 3.51 \times 10^9 \frac{P(\text{Torr})}{\sqrt{M(g)\,T(K)}} \exp\left(\frac{1.16 \times 10^4 E_a(eV)}{T(K)}\right) \tag{13}$$

Table I - densities of adatoms, n_g, at equilibrium on a substrate surface at 300 K and 600 K under various pressures of residual gas of molar mass M = 20.

Pressure	$E_a = 0.1$ eV		$E_a = 0.2$ eV		$E_a = 0.3$ eV	
(Torr)	300 K	600 K	300 K	600 K	300 K	600 K
10^{-5}	2.2×10^4	2.1×10^2	10^6	1.5×10^4	5×10^7	10^5
10^{-6}	2.2×10^3	2.1×10^1	10^5	1.5×10^3	5×10^6	10^4
10^{-8}	2.2×10^1	2.1×10^{-1}	10^3	1.5×10^1	5×10^4	10^2
10^{-10}	0.2	≈ 0	10^1	≈ 0.2	5×10^2	1

Values derived from equ.(13) given in Table I demonstrate interesting features of practical importance. In order to move from evaporation in the residual gas pressure range of 10^{-5}-10^{-7} Torr to that of 10^{-8}-10^{-10} Torr, the deposition chamber must be made of stainless steel instead of glass and must also have bake-out facilities and suitable cold traps. As a result, the capital cost is considerably increased and the experimental time can be greatly lengthened. Data given in Table I show that in every case, increasing the substrate temperature T_s from 300 to 600 K reduces residual gas contamination by about the same amount as does improving the base pressure by two orders of magnitude. Therefore, to minimize substrate and film contamination, an increase in substrate temperature is often sufficient and an ultra-high vacuum (UHV) evaporation equipment may not be necessary. In addition, the data demonstrate that with UHV systems, the residual gas contamination may be reduced to zero at relatively high substrate temperatures.

In practice, the nature of residual gas in a vacuum chamber as well as the adsorption energy, E_a, of atoms or molecules impinging on the film surface during condensation of vapor species are not well-known. The sticking coefficient and the average lifetime, τ_g, of residual gas species are rather difficult to be evaluated. Therefore, the major approach adopted to reduce the contamination of evaporated films by residual species is to reduce the ratio K :

$$K = \frac{\text{number of residual gas molecules impinging on 1 cm}^2\text{ of surface per second}}{\text{number of evaporated particles deposited on 1 cm}^2\text{ of surface per second}} \tag{14}$$

www.manaraa.com

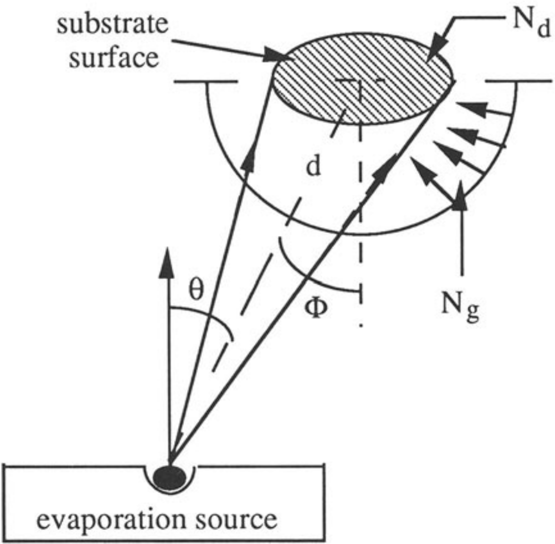

Figure 2 - Source-substrate arrangement.

For the ideal source-substrate arrangement (Fig.2), the number of vapor species condensed on the substrate surface area A, N_d, or the deposition rate of films is related to the evaporation rate N_e given by equ.(6) as follows :

$$N_d = \left(a_2 \, A \cos\Phi \, \frac{\cos\theta}{\pi \, d^2} \right) N_e \qquad \text{(particles s}^{-1}\text{)} \qquad (15)$$

in which θ is the angle between the normal to the surface of the source and the direction of the flux of particles emitted from the source; Φ is the angle between the normal to the surface of the substrate and the direction of the source; d is the source-substrate distance; a_2 is the sticking coefficient of vapor species.

The expression of the ratio K can be established in a particular case, e.g., for Si films deposited by evaporation at various deposition rates R and residual air pressures P_g. Assuming that the density of the Si films is equal to the bulk density (2.33 g cm^{-3}), the flux of Si atoms N_d (atoms cm^{-2} s^{-1}) can be expressed as a function of the deposition rate of Si films R (nm s^{-1}) :

$$N_d = 5 \times 10^{15} R \qquad (16)$$

The flux of residual air molecules on the film surface is given by the collision frequency (equ.(5)) with M = 29 g and T = 298 K. The flux of residual atoms N_g is twice the flux of air molecules, i.e., from equ.(6) :

www.manaraa.com

$$N_g = 2\,\frac{3.51 \times 10^{22}}{\sqrt{29 \times 298}}\,P_g \qquad (\text{atoms cm}^{-2}\,\text{s}^{-1}) \tag{17}$$

The ratio K is given by : $K = \frac{N_g}{N_d}$ or

$$K = 1.5 \times 10^{15}\,\frac{P_g(\text{Torr})}{R(\text{nm s}^{-1})} \approx 10^{15}\,\frac{P_g(\text{Torr})}{R(\text{nm s}^{-1})} \tag{18}$$

The ratio values reported in Table II were calculated with sticking coefficients of air molecules and Si atoms on the surface equal to unity. The situation is very unfavorable when $K >> 1$ since the number of residual gas species is much higher than the number of Si atoms condensed on the surface. In fact, the amount of residual gas incorporated in the film depends on the reactivity between residual gas and deposited material or on the adsorption energy E_a. The sticking coefficient of a residual gas depends on the deposition rate, temperature and structure of the substrate surface or deposited material. In fact, the value of K must be as low as possible, i.e., for a given base pressure in the deposition chamber, the deposition rate or the evaporation rate must be maximum. The values of key parameters such as pressure of residual gas, evaporation rate or deposition rate, substrate temperature and cleanliness of the substrate surface (or in situ surface treatment) must be carefully measured or controlled to produce thin films with suitable quality and to ensure excellent reproducibility of the evaporative deposition process.

Table II - Typical values of the ratio K calculated for evaporation of Si films in residual air ambient.

P_g (Torr)	R (nm/s)			
	0.1	1.0	10.0	100.0
10^{-9}	10^{-3}	10^{-4}	10^{-5}	10^{-6}
10^{-7}	10^{-1}	10^{-2}	10^{-3}	10^{-4}
10^{-5}	10	1	10^{-1}	10^{-2}
10^{-3}	10^{3}	10^{2}	10	1

c) Effect of the source-substrate arrangement

The flux of particles liberated per unit area, per unit time and per unit solid angle from a small hole in the wall of a vessel containing gas molecules or from a point-like evaporation source is given by :

$$\Phi_\omega = \frac{1}{4\pi}\,n\,\bar{v}\cos\theta \tag{19}$$

The number of particles emerging per unit solid angle is a maximum in the direction normal to the plane of the source and decreases to zero in the tangential direction. Therefore, the deposition rate of evaporated films depends on the source-substrate configuration. Equ.(15) gives the deposition rate, N_d, or the number of vapor species

www.manaraa.com

condensed on the surface area A per unit time. When the substrate surface is tangent to the circle of diameter h passing through the evaporation source (Fig.3a), the deposition rate is constant for all positions on the circle because for this geometry :

$$\cos\theta = \cos\Phi = \frac{d}{h} \tag{20}$$

and

$$N_d = \left(a_2 \frac{A}{\pi h^2}\right) N_e \tag{21}$$

N_d is a constant (independent of angles θ and Φ). However, the flux direction of particles condensed on the substrate surface is quite different for various positions on the circle, e.g., positions A, B and C. Usually, the deposited film exhibits a columnar structure with the axes of the columns making an angle γ with the flux direction Φ [3]. For instance, in Al films deposited at room temperature by vacuum evaporation, the angle γ increased from 0 to 35° as Φ increased from 0 to 60°; in addition, γ decreased with increasing substrate temperature. Generally, the substrates are mounted on a planetary motion holder and the angle Φ varies continuously during deposition. This planetary motion is associated with a rotatory motion of each substrate about its normal at a rate which is not a harmonic of the planetary motion.These various motions lead to continuous changes in flux arrival direction of vapor species on the substrate surface and ensure the same average flux on the substrates during deposition.

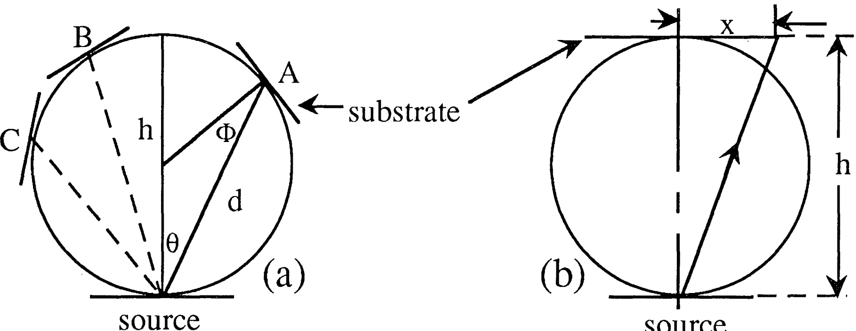

Figure 3 - Usual source-substrate configuration in evaporation systems; (a) substrates on spherical planetary with source and substrate tangent to the sphere of diameter h, (b) planar substrate parallel to the source at a fixed height h above the source.

The deposition rate N_d is constant only on the part of substrates tangent to the circle of diameter h; therefore, this diameter must be sufficiently large so that all points on a flat substrate have only a small deviation from the circle. The usual situation is schematically represented in Fig.3b. For a point-like source and a flat substrate with its center located on the normal to the source plane at a distance h, the thickness of films, t_0, obtained in the center of substrates is greater than the thickness, t, measured at a distance x from the center, according to the equation :

المنارة للاستشارات
www.manaraa.com

$$\frac{t}{t_0} = \frac{1}{\left[1 + \left(\frac{x}{h}\right)^2\right]^{3/2}} \tag{22}$$

With an evaporation source consisting of a small plate and a flat substrate having its surface parallel to the source, the thickness ratio is expressed as follows :

$$\frac{t}{t_0} = \frac{1}{\left[1 + \left(\frac{x}{h}\right)^2\right]^{2}} \tag{23}$$

In general, the source is not point-like, and the minimum distance h from the source of a flat substrate of 150 mm in diameter to obtain a thickness uniformity of evaporated films higher than 5 % can be calculated from equ.(23), e.g., in that case :

$$h = \frac{x}{\left(\sqrt{\frac{t_0}{t}} - 1\right)^{1/2}} = \frac{75}{\left(\sqrt{\frac{100}{95}} - 1\right)^{1/2}} \geq 46.5 \text{ cm} \tag{24}$$

Various configurations can be adopted and used so that flat substrates are located with their surface in a tangent plane to the circle of diameter h passing through the evaporation source.

2.2. EVAPORATION OF COMPOUNDS AND ALLOYS

Two types of evaporative deposition processes of compound films can be distinguished. It is possible to proceed to either (i) a direct evaporation of the compound or alloy to be deposited on the substrate, or (ii) a reactive evaporation where metal or compound of metal in a low valence state is evaporated in the presence of a reactive gas to form a compound on the substrate surface to be coated, e.g., pure Si or SiO (formed from a SiO_2-Si mixture) can be evaporated in oxygen to produce SiO_2 thin films.

2.2.1. Direct Evaporation Processes. A number of compounds such as B_2O_3, SiO, GeO, SnO, MgF_2, CaF_2 can be evaporated without dissociation. In this case, the compositions of the vapor phase and material condensed on the substrate are similar to that of the source material, and a coating having the stoichiometry of the source material can be directly deposited on the substrate.

In the general case, the compound to be evaporated decomposes into fragments at high temperatures in the evaporation source. Since the fragments have different saturation vapor pressures, the evaporation of each of them proceeds at different rates and the composition of the condensed film differs from that of the source compound. For instance, with a binary compound AB dissociated at high temperatures, a depletion of the more volatile element occurs in the source and the film is enriched in this higher vapor pressure element. Usually, the sticking coefficients of elements A and B are differents; they depend on the adsorption energy E_a on a given material. With a sufficiently high concentration of the compound AB in the gas phase, the best results can be obtained when the adsorption energy of the desired compound AB is higher than those of both elements A and B. In that

www.manaraa.com

case, the substrate temperature can be set so that the vapor species AB condense on the substrate surface but not the elemental species A and B. These conditions are necessary to deposit a compound AB in stoichiometric composition by evaporation of the source compound AB.

In fact, the stoichiometry of the deposited material depends on various factors including deposition rate, concentration ratios of the various fragments, flux of other gas molecules impinging on the substrate surface, surface mobility of fragments or atoms which depends on their kinetic energy and substrate temperature, lifetime of adatoms on the surface, recombinaison rate of fragments on the surface, and concentration of impurities. For instance, the direct evaporation of Al_2O_3 resulted in alumina films deficient in oxygen Al_2O_{3-x}. This oxygen depletion in the films could be eliminated by evaporating Al_2O_3 with a low partial pressure of oxygen in the evaporation chamber. The effect of decomposition of the source material AB may be compensated by depleting intentionally the evaporation source in the more volatile element. This solution was adopted to produce Ni-Fe permalloy films of nominal composition 80Ni-20Fe from an evaporation source of approximate composition 83Ni-17Fe. This approach is not valid when the vapor pressure of elements differs by several orders of magnitude at a given evaporation temperature.

Another possibility of direct evaporation consists in the use of a flash evaporation. In this method, powdery alloy AB with homogeneous grain size is dropped continuously into a hot boat and immediately vaporizes to form a condensed film on the substrate. With grain size suitably calibrated, one grain completely vaporized can form one monolayer of the desired alloy on the substrate surface, and the films are grown by regular sequences of stoichiometric monolayers condensed on the substrate. However, this ideal situation can be affected by variations in feed rate and deviations in grain size. In practice, the substrate temperature must be relatively high to ensure a correct homogeneity of constituents in the deposited films. A compound or alloy AB can also be deposited by evaporation from two separate sources containing elements A and B, respectively. The vapors A and B condense on the substrate surface maintained at a suitable temperature for formation of the compound AB. In this method, the control of three temperatures namely two evaporation temperatures and one substrate temperature is necessary to produce thin films with excellent reproducibility. This temperature control can be difficult in particular for evaporation of refractory metals to produce various compounds, e.g., WSi_2 thin films, and the manufacturability of this three-temperature system is rather poor.

2.2.2. Reactive Evaporation Processes.

a) Evaporation of compounds

The compound to be deposited (oxide, nitride, ...) is placed in the evaporation source and directly evaporated. With this direct evaporation process, the film condensed on the substrate can be deficient in the more volatile element (oxygen, nitrogen, ...). The stoichiometric composition of the film is restored when the compound is evaporated in the presence of a reactive gas (O_2, N_2, ...) at a pressure typically in the range 10^{-3} to 10^{-4} Torr. This improvement in stoichiometry can arise from reactive gas absorption by growing films, reactive collisions between gas molecules and vapor species emitted from the evaporation source, and surface reactions between gas molecules and condensed films. The relative complexity of interactions involved in this process can lead to difficulties to ensure exact and reproducible stoichiometry of films.

b) Evaporation of metals

The metal or element is directly evaporated from the source and the compound to be deposited forms by reactions between metal atoms and reactive gas introduced in the deposition chamber. The major drawbacks of this process are related to temperatures of

www.manaraa.com

evaporation source and substrates. The source must be at a sufficiently high temperature for a suitable evaporation of element so that the formation of the compound can take place directly in the source, and drifts or instabilities of the evaporation conditions can detrimentally affect the deposition process. In addition, high substrate temperatures and low condensation rates are needed to enhance reactive interactions between metal and gas. Chemical reactions between metal and gas to form a given compound are governed by thermodynamic and specially kinetic laws. From the thermodynamic point of view, metal-gas reaction is possible when the free energy of the reaction is negative; usually, this condition is easily fulfilled. In fact, the kinetic factors involved in the heterogeneous metal-gas reaction can play a dominant role. In reactive evaporation processes, the major rate-limiting steps can be the transfer of vapor species by gas phase diffusion from the source to the substrate surface, collision frequency between reactants, surface reaction between reactants and, diffusion of gas products from the surface. At low pressures, the growth kinetics of films is often limited by the surface reaction rate. Furthermore, the deposition rate of films depends on the arrival rate of metal atoms and gas atoms or molecules on the substrate surface. For instance, TiC films with C/Ti ratio of 1.0 could be formed by reactive evaporation of Ti atoms in presence of C_2H_2 and C_2H_4 molecules on substrates at a temperature ranging from 300° to 500°C with a deposition rate varying from 0.3 to 1.5 Å/s. At higher deposition rates, e.g., from 2 to 4 Å/s, a carbon depletion was observed in the films; the C/Ti ratio decreased from 1 to 0.2. The growth kinetics of TiC films was governed by the rate of surface reactions between Ti atoms and gas molecules [4]. To overcome the activation energy barrier between reactants and compounds, vapor species can be activated through the creation of a plasma in the deposition chamber. The presence of a plasma enhanced the deposition rate of TiC films [5]. This method was named activated reactive evaporation (ARE) process.

2.2.3. Activated Reactive Evaporation Processes.

a) Plasma effects

Excited species created in the plasma can participate in the surface reactions thereby the deposition rate of compound films can be enhanced. In addition, these changes in growth kinetics can modify various correlations between composition, morphology, structure and properties of films. Hence, properties of compound films deposited by ARE process differ from those of films produced by conventional evaporation process. By contrast, the plasma has little or no influence on the vaporation conditions of metal.

A variety of species are produced in the plasma from collisions of atoms and molecules with energetic electrons. These species can act as precursors in chemical reactions involved in the growth of films. The interactions in the plasma are dependent on the electronic density, electron energy and energy distribution function of electrons. As result, to obtain films with desired properties by ARE process, it is necessary to control not only the conventional deposition parameters (substrate and source temperature, base pressure, ...) but also the properties of the plasma affecting volume chemistry. During deposition, the surface of films is bombarded by energetic neutrals, ions and electrons coming from the plasma. The nature and energy of these particles depend on deposition parameters and position of substrates with respect to the plasma (substrate in or out of plasma). The bombardment of the substrate surface can lead to substrate heating (due to electronic bombardment), changes in surface reactions, gas incorporation in films, modifications of the film morphology, grain size, crystallographic orientation and defect density in the film. In addition, with a negative bias voltage applied to substrates, a fraction of the deposited material is removed or sputtered by energetic positive ions (bias sputtering). The composition and properties of films depend on the value of the bias voltage. The neutral

المنارة للاستشارات
www.manaraa.com

gas incorporation such as argon can be minimized in films deposited with the bias sputtering mode at a suitable bias voltage.

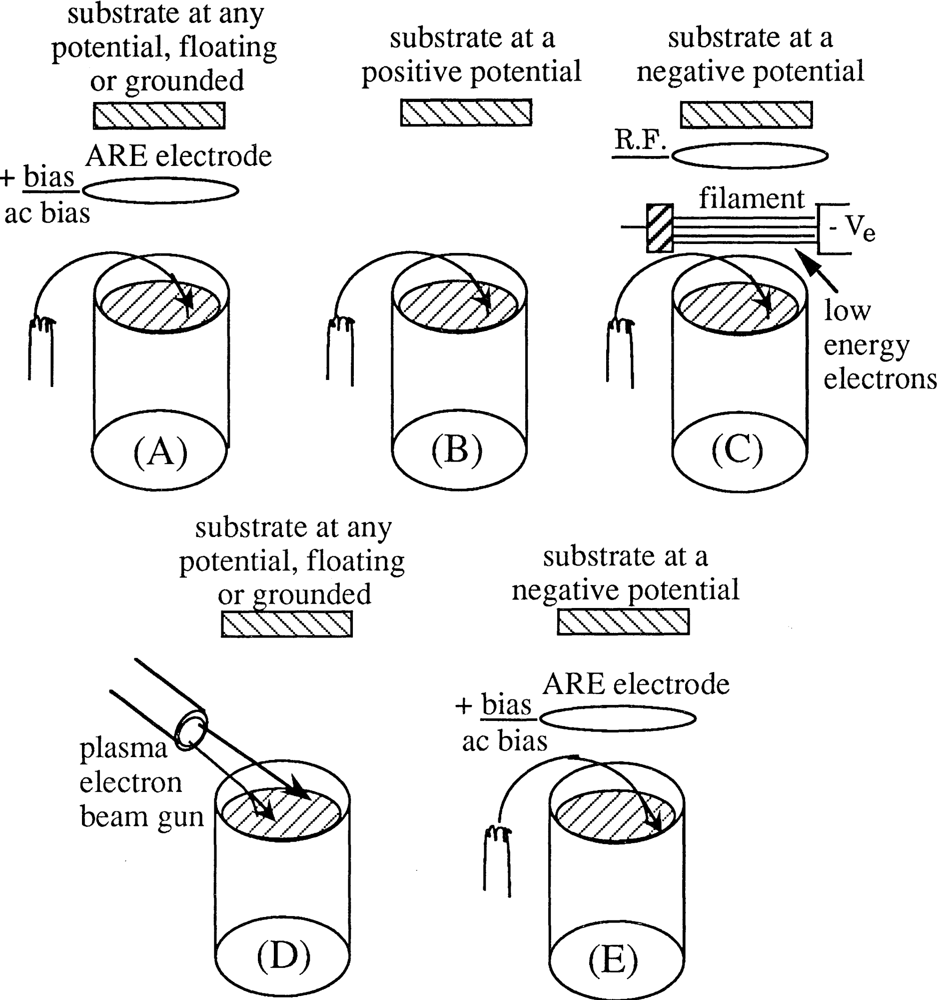

Figure 4 - (A) Basic ARE process, (B) low pressure plasma deposition process, (C) enhanced ARE process, (D) ARE process with hot hollow cathode electron beam gun or cold cathode discharge electron beam gun, (E) biased ARE or reactive ion plating process [6].

b) Implementation of the ARE processes

Various systems have been implemented for deposition of compounds by ARE processes. Basic and modified ARE processes are schematically represented in Fig.4. The basic ARE

المنارة للاستشارات
www.manaraa.com

system is equipped with electron beam evaporation source and metal atoms liberated from the source diffuse through the plasma generated by accelerating secondary electrons and thermoionically emitted electrons from the plasma sheath to an electrode connected to alternative current (a.c.) or positive direct current (d.c.) power supply (Fig.4A). The substrates and the films can be conductor or insulating materials and can be biased to any potential. This technique has been successfully used to produce carbides [5], nitrides [7], oxides [8,9], sulfides [10,11] and carbonitrides of titanium [12]. This basic system was slightly modified by substituting resistance heated evaporation source for electron beam source [13]. The plasma is created between a filament heated by Joule effect and a positively biased electrode (Fig.5). A magnetic field created by two magnetic coils is applied in the direction parallel to the filament-electrode axis. The electrons thermoionically emitted by the filament experience the magnetic field effect and travel in spiral paths thereby the probability of collisions and gas ionization are increased. Conductive coatings of indium oxide and indium tin oxide have been deposited by this technique [6].

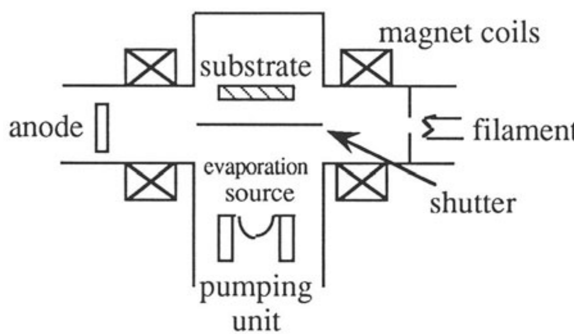

Figure 5 - Activated reactive evaporation system using a resistance heated evaporation source [6].

With conductive substrates and films, the plasma can be created directly between the electron beam evaporation source and the substrate holder positively-biased; the ARE electrode can be eliminated (Fig.4B). This technique is named low pressure plasma deposition (LPPD) process [14]. The major disadvantage is the impossibility to have the substrates grounded, left at the floating potential or biased negatively. The ARE processes with biased substrates are called (BARE) processes. Usually, the substrates are biased negatively to attract the positive ions generated in the plasma. This BARE process with substrates biased negatively (Fig.4E) was reported in 1978 and named reactive ion plating. Oxide and nitride films were produced in another BARE system (Fig.4C) equipped with an electron beam evaporation source and a coil of aluminum wire in the reaction zone to create an inductive radio frequency (R.F.) plasma at low reactive gas pressures [15]. The thermoionic electron source used to produce the electron beam in the evaporation source can be replaced by a plasma electron beam gun (Fig.4D). The major advantage provided by these guns is the abundant supply of low energy electrons; in addition, these systems are relatively rugged and long-lived. Hence, a wide variety of ARE systems and processes has been developed and implemented. These methods were reviewed and described in detail recently [6].

www.manaraa.com

2.3. EXPERIMENTAL TECHNIQUES

The experimental equipment to produce thin films by evaporation consists of an evaporation source, a substrate holder, a film thickness or deposition rate monitor mounted in the evaporation chamber evacuated by a pumping unit.

2.3.1. Pumping Units. The pumping techniques for evaporation were described previously [16,17]. A combinaison of oil diffusion pump backed with a mechanical pump fitted with an efficient liquid nitrogen trap is still used extensively. Base pressures of about 10^{-6} Torr in the evaporation chamber can be currently obtained with these systems. Ionic or sputter ion pumps and sublimation pumps are associated to obtain base pressures ranging from 10^{-8} to 10^{-10} Torr. Stable ultra-high vacuum (UHV) conditions in the evaporation chamber are attainable if all gases were desorbed from the walls of the chamber. The outgassing of chamber walls is achieved by backing treatment of the chamber for a long period (24 to 48 h) at temperatures in the range of 250° to 450°C. These high backing temperatures require the use of stable metal seals rather than rubber or elastomer seals mounted on systems equipped with diffusion oil pumps. The major drawback of sputter ion pumps is the large difference in pumping speed for different gases [16].

2.3.2. Evaporation Sources. Elements and compounds with relatively high saturation vapor pressures are usually evaporated from sources heated by Joule effect. Evaporation sources commonly used consist of tungsten spirals or tantalum boats in a wide variety of shapes and forms commercially available. The major problem is to avoid or minimize chemical reactions between the crucible and the material to be evaporated. These side reactions can be avoided using crucible-free techniques such as electron beam or laser beam evaporation sources (Fig.6). The source material is locally heated by a scanned electron or laser beam. The beam heats only the surface of the source material whereas the support holder is usually cooled.

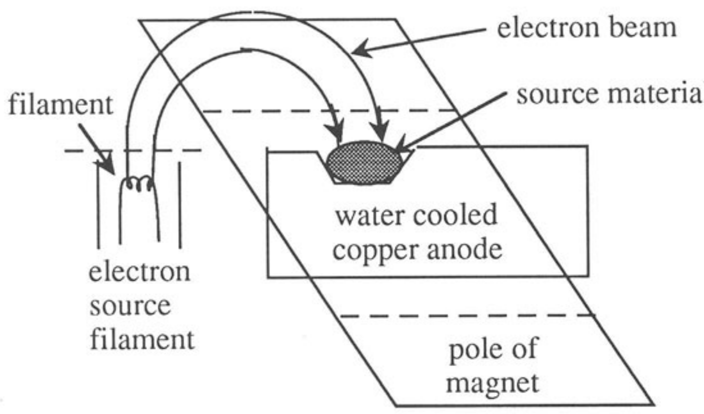

Figure 6 - Electron bombardment source for evaporation with electron gun magnetic focussing.

المنارة للاستشارات
www.manaraa.com

2.3.3. Substrate Holder. The plane substrates are mounted on a holder with its surface located on the circle passing through the evaporation source (Fig.3) to obtain films with uniform thickness. The substrate holder rotates about the vertical axis and substrates at different radial positions receive the same flux of vapor species but at different angles of incidence (Fig.7). With this system, a poor coverage of vertical steps can be obtained whereas with the planetary motion a conformal step coverage can be achieved.

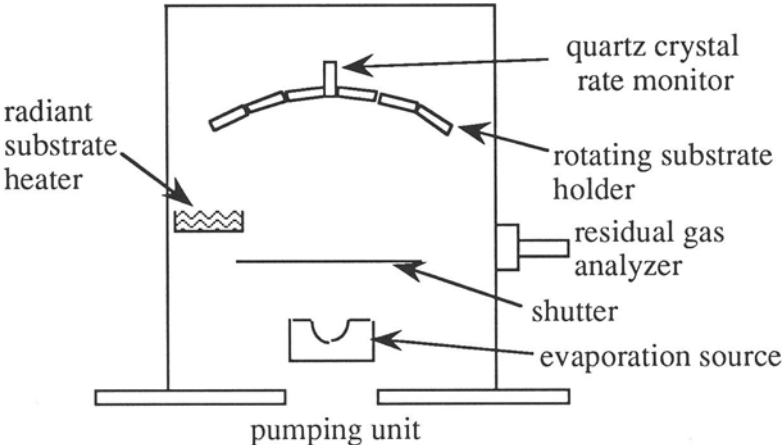

Figure 7 - Schematic representation of evaporation system.

2.3.4. Deposition Rate Monitor. Usually, the thickness of films must be obtained with accuracy since the properties of films such as electrical resistance, capacitance, reflectivity are strongly dependent on the film thickness. The deposition rate can be evaluated from equ.(15); however, the effect of the source-substrate configuration on the deposition rate is very important and an accurate deposition rate value cannot be determined directly by calculation. In addition, the calibration of the deposition rate for given deposition parameters must be avoided since the reproducibilities of evaporation temperature and evaporation rate are rather poor.

The deposition rate is currently monitored by a quartz crystal microbalance mounted on the same circle as the substrates (Fig.7). The resonant frequency of the quartz crystal decreases with an increase in the mass of films deposited on it [2]. The conversion from mass to thickness requires a knowledge of the density of films which is usually less than the bulk density of the deposited material. It is necessary to perform a calibration to obtain precise thickness values. The density value determined by the user is entered in the microprocessor controlled system to obtain the film thickness directly during the evaporation process. The quartz crystal must be replaced when the change of resonant frequency is about 5 %. With a conventional system, the evaporation chamber must be opened frequently to load substrates and to replace the evaporation charges. The quartz crystal can also be replaced easily during these operations when the evaporation chamber is opened. With UHV systems maintained under vacuum for long periods, ionization gauge rate monitors are preferable (Fig.8). In this case, a fraction of the evaporated flux is ionized by an electron beam and the ionization current is detected in the gauge. To avoid interferences caused by residual gas pressure in the system, the signal due to the ionized fraction of the evaporated beam is modulated by using a rotating shutter in front of the

www.manaraa.com

Table III - Evaporation of elements and compounds [17].

Material	Atomic mass	Density	Melting point (°C)	Evaporation temperature (°C)	Evaporation source
Ag	107.88	10.5	961	3	Mo, W, Ta
Al	26.98	2.7	660	3-4	W, Ta
Au	197.20	19.3	1063	4	W, Mo
Be	9.02	1.9	1284	4	Ta, W, Mo
Bi	209.00	9.78	271	2	W, AO, Mo, Ta
C	12.01	1.2	3700	6	C (arc)
Cr	52.01	6.8-7.1	1900	4	W
Cu	63.57	8.85-8.92	1084	4	W, Ta
Fe	55.84	7.9	1530	4	W, AO
Ge	72.60	5.35	958	4	W, AO, C, E
In	114.76	7.3	156	3	W, Mo
Ni	58.69	8.85	1453	4	W, C, E
Pt	195.20	21.5	1773	5	W, C, E
Pb	207.21	11.3	328	4	Fe,Ni,W,Mo,AO,E
Se	78.96	4.5	220	1	W, Mo
Si	28.06	2.4	1415	4	C, E
Sn	118.70	7.28	232	3-4	Mo, AO
Ti	47.90	4.5	1727	5	W, C, E
Zn	65.38	7.13	420	2	W, C, Ta, Mo, AO
Zr	91.22	6.53	1860	5-6	C, E
Ni-Cr	----	8.2	-----	4-5	W, Ta
SiO-Cr	----	----	-----	4-5	W
Al_2O_3	101.94	3.6	2046	6	E
CeO_2	172.12	6.9	2600	5-6	W
MgO	40.32	3.65	2640	6	E
SiO_2	60.09	2.1	1500	5-6	E
SiO	44.09	2.1	-----	4	Mo, W, Ta
ThO_2	264.10	9.69	3050	7	E
Ta_2O_5	441.76	8.7	1470	5	Ta, W, E
CdS	144.46	4.8	1750	3	W, Mo, Ta
ZnS	97.44	3.9	1900	3	Mo, E
CaF_2	78.08	3.2	1360	3	Ta, W
Na_3AlF_6	209.95	2.9	1000	3	Mo
LiF	25.94	2.6	870	3	Ta
MgF_2	62.32	2.9-3.2	1220	4	Ta, AO, W
NaF	41.99	2.8	990	4	Mo, Ta, W
PbTe	334.78	8.1	904	3	Mo, Ta, AO
CdTe	240.00	6.2	1041	3	Mo, Ta
NaCl	801	2.2	801	3	Ta, W, C

Evaporation temperature range (°C) : 1, 100 to 400; 2, 400 to 800; 3, 800 to 1200; 4, 1200 to 1600; 5, 1600 to 2100; 6, 2100 to 2800; 7, 2800 to 3500. Evaporation source : C, graphite; AO, alumina crucible; E, electron beam heated source.

www.manaraa.com

ionization gauge. If only the modulated component of the ion current is measured, variations in background pressure do not contribute to the reading and the system becomes much more sensitive to variations of film thickness.

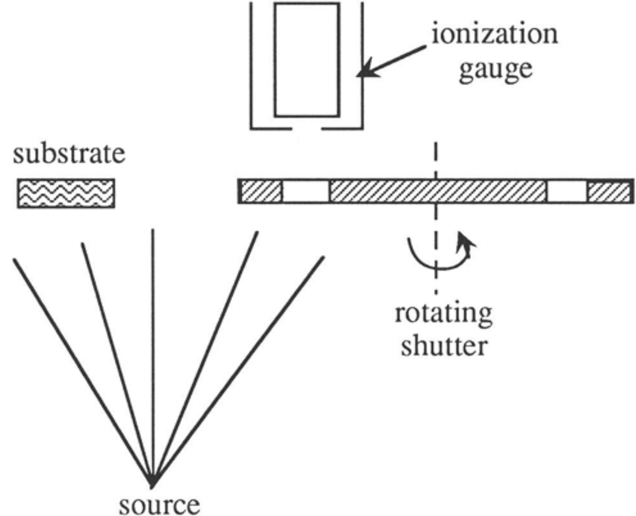

Figure 8 - Ionization gauge rate monitor system.

2.4. APPLICATIONS OF EVAPORATION PROCESSES

A large number of elements and compounds can be deposited on various substrates by vacuum evaporation process. The evaporation temperatures reported in Table III correspond to saturation vapor pressure values of 10^{-4} to 10^{-2} Torr. The evaporation crucible must be made from a material inert with respect to the material to be evaporated. The source material with a high purity is mostly used. To preserve the purity of the source material and deposited films, the residual gas pressure must be as low as possible. However, additional sources of contamination exist in the evaporation system at the beginning of the process. Impurities can arise from gas adsorbed in both evaporant and evaporation source. These impurities can be incorporated in the films. To prevent this type of contamination, the substrates are shielded by a shutter interposed between the evaporation source and the substrates for a given period at the beginning of the evaporation process.

3. Cathode Sputtering

Atoms can be ejected from the solid surface when this surface is bombarded by ions or atoms with sufficiently high energy (above about 30 eV). In this process, the solid material plays the role of a target sputtered by either an energetic particle (ion or molecule) beam or positive ions generated in a plasma and accelerated to the target biased at a negative voltage. This phenomenon was discovered about 150 years ago by Grove [1] who studied the forerunners of fluorescent light tubes and observed the formation of a dark deposit of the electrode material on the inside wall of the glass tube. The technological means

www.manaraa.com

available in the 19th century were not adequate to settle a correct use of this phenomenon in thin film deposition processes. The development of vacuum evaporation techniques invented some 50 years later was faster, and by this time, the sputtering process was confined to investigations of the physics of ion bombardment and ion-solid interactions. In fact, the sputtering process is of interest for deposition of refractory metals which are evaporated with difficulties using evaporation sources heated by Joule effect. The increasing interest in refractory metal films for microelectronics in the 1950's has caused a vigorous development of sputtering deposition techniques.

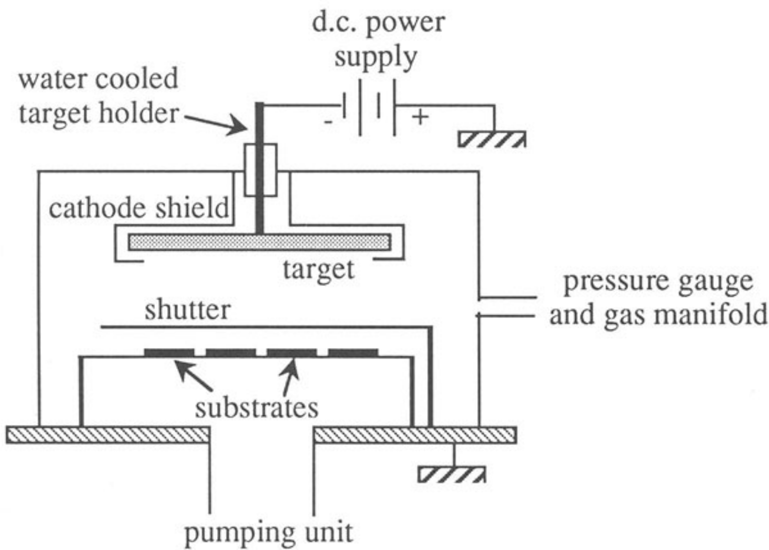

Figure 9 - Basic d.c. sputtering deposition system.

3.1. PRINCIPLE AND BASIC EQUIPMENT OF d.c. DIODE SPUTTERING

The basic system for cathode sputtering is composed of a bell jar backed up with a pumping unit to evacuate the deposition chamber and maintain the sputtering gas pressure at a value ranging from 0.1 to 0.01 Torr (Fig.9). The sputtering chamber is equipped with a target (or cathode) of the conductor material to be sputtered and deposited on substrates, and a substrate holder acting as the anode of the system. A glow discharge is established in an inert gas such as argon or xenon at low pressures (0.1 to 0.01 Torr) when a voltage of several kilovolts is applied between the target and the substrate holder which is usually grounded. The water cooled target holder is screened by a grounded cathode shield mounted at a low distance from the cathode (about 1 cm) to impede gas ionization and thereby to avoid sputtering of the target holder.

The current intensity between anode and cathode through an inert gas at low pressures (few Torr to some 10^{-3} Torr) is essentially zero for an interelectrode voltage below the breakdown voltage value (Fig.10). From about 500 V, the phenomena of gas ionization can occur and a glow discharge is established. The current varies strongly for a very small change in interelectrode voltage; the system runs at a constant voltage in this normal glow discharge regime. Above a certain voltage value, the current intensity through the gas

www.manaraa.com

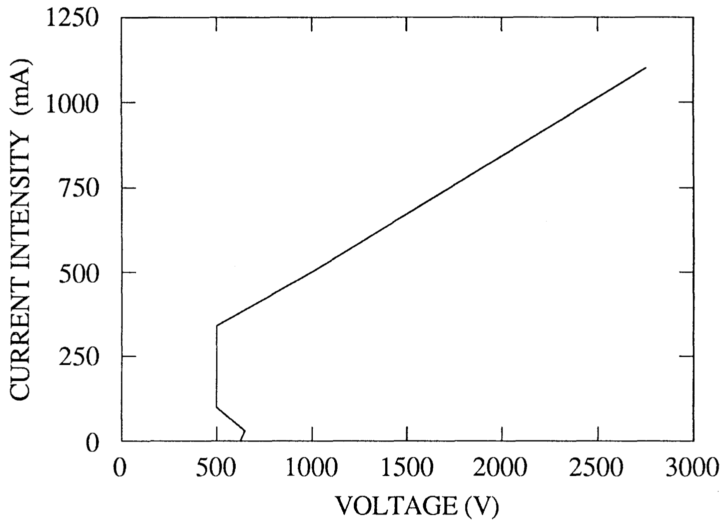

Figure 10 - Typical I(V) characteristics of a d.c. discharge through a gas at low pressures.

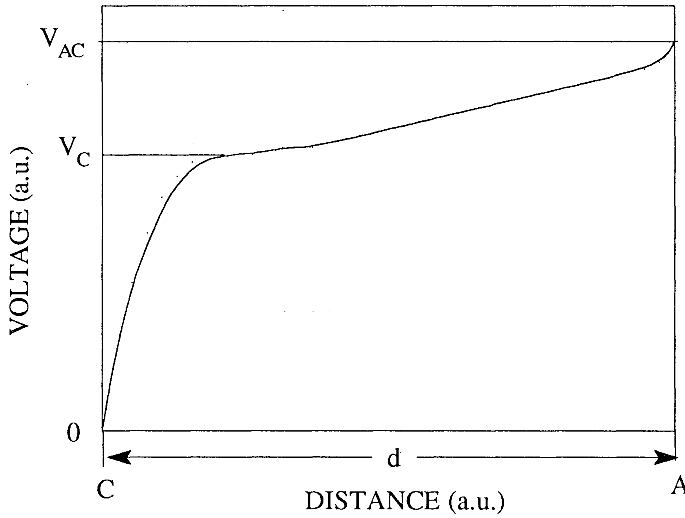

Figure 11 - Typical variation of interelectrode potential in a d.c. glow discharge between cathode C and anode A at a distance d; V_{AC} is the interelectrode voltage and V_C the cathode fall.

المنارة للاستشارات
www.manaraa.com

increases progressively as the interelectrode voltage increases; this regime used for sputter deposition of thin films is named abnormal glow discharge regime.

The potential between the electrodes does not vary evenly (Fig.11). The positive ions created by the discharge are accelerated towards the target biased to a negative voltage and strike the target surface with almost the same energy as that gained in the cathode fall region when the gas pressure is sufficiently low. The width of the cathode sheath depends on the sputtering gas pressure. The cathode fall depends on the nature of gas and cathode material; usually, its value is almost equal to the interelectrode voltage. The bombardment of the target by positive ions created in the plasma induces ejection of atoms at the target surface. The liberated atoms condense on surrounding areas and on the substrates placed on the substrate holder at few cm from the target.

3.2. SPUTTERING MECHANISMS

The target of material M to be sputtered and deposited on substrates is bombarded by energetic ions; during ion-solid interactions, sufficiently high energy can be transferred to atoms M and certain atoms are ejected from the target surface. This sputtering phenomenon is the result of momentum transfer from the incident particles to the target lattice.

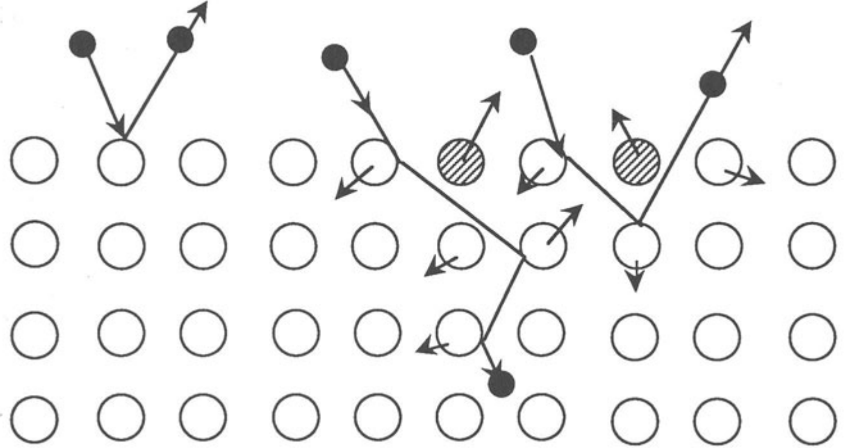

Figure 12 - Ion-solid interactions and sputtering mechanisms.

The ion-atom collision sequences occurring at the target surface are schematically represented in Fig.12. Some incident ions with low energies are scattered from the surface of the target in a binary or ternary collision sequences. The fraction of scattered ions depends on the ion energy, ion mass, M_i, and target atom mass, M_t; the fraction value increases from 0.01 to 0.25 as the ratio M_t/M_i increases from 1 to 10 [18]. For instance, the scattering coefficients of 500 eV Ar^+ ions on Ti and Au atoms are equal to 0.01 and 0.18, respectively. This phenomenon of ion elastic scattering on solid surfaces is currently used for surface analyses by low energy ion scattering spectroscopy [19]. In fact, most incident ions are neutralized on the target surface and are scattered as energetic neutral particles. Ions with relatively higher energies are also neutralized on the target surface but can penetrate in the solid. The incident particles cause displacement of atoms in the

www.manaraa.com

topmost layers of the target and provide a certain momentum to atoms M. These particles lose progressively their energy, are scattered by atoms M, and can either be emitted from the target surface or become implanted in the target. A fraction of atoms M displaced by incident particles can diffuse towards the target surface and are ejected or sputtered when their energy is sufficient high to overcome binding energy. More probably, a momentum transfer occurs from an atom to another in the target, and atoms M at the target surface receiving energy from internal atoms can be emitted from the target surface. The minimum energy of a primary ion for sputtering of atoms M or the threshold sputtering energy is about 20 to 30 eV, i.e., significantly higher than the energy needed to transfer one atom from the solid to the gas phase or sublimation energy which lies between 3 and 5 eV for most solid materials. The primary particles implanted in the target will later be ejected from the target surface since the target erodes progressively. This sputtering process using ion beams is utilized for depth profiling in surface analyses such as secondary ion mass spectroscopy and Auger electron spectroscopy. The ionic bombardment of the target also causes emission of secondary electrons with a yield of typically about 0.1 for metal targets [20]. Secondary electrons emitted from the target experience an acceleration passing through the cathode sheath and their energy becomes sufficiently high to ionize sputtering gas molecules during electron-molecule collisions. These ionization phenomena induced by secondary electrons sustain the glow discharge and are responsible for the strong increase in current intensity through the gas phase as the interelectrode voltage reaches the breakdown voltage value (Fig.10).

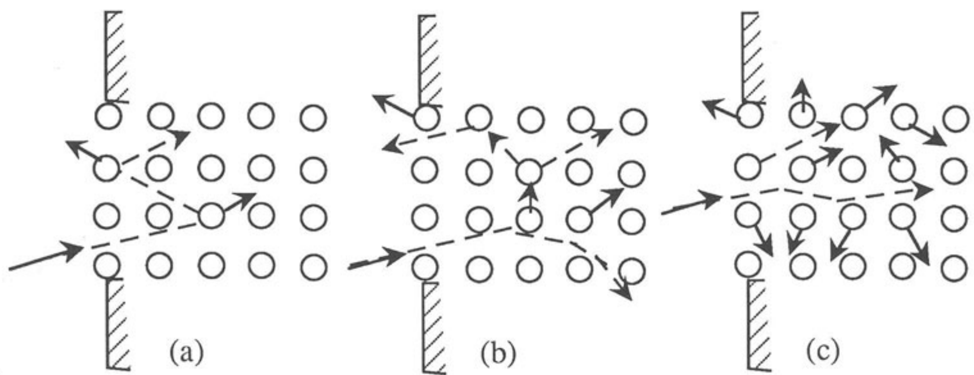

Figure 13 - Three regimes of sputtering by elastic collisions. (a) The single-knockon regime, (b) the linear cascade regime, and (c) the spike regime [21].

3.3. SPUTTERING YIELD

To realize a significant momentum transfer between incident ions and atoms M, the ion mass, M_i, must be comparable to the target atom mass, M_t. The sputtering yield value can be calculated as a function of sputtering parameters from equations established by Sigmund [21]. The Sigmund model involves three types of ion-atom collisions (Fig.13). In the single-knockon regime, the bombarding ion transfers energy to target atoms, and after having undergone a small number of further collisions, target atoms are emitted from the surface when their energy is sufficiently high to overcome binding forces. In other words, the energy provided to target atoms is sufficient to induce sputtering phenomena but too small to initiate cascade of collisions. This mechanism is preponderant in sputtering

www.manaraa.com

processes with light incident ions of low energies. In the two other regimes, recoil atoms are energetic enough to generate secondary and higher-generation recoils. Some of recoil atoms may approach the target surface and overcome the energy barrier. The linear cascade regime occurs in interactions between target atoms and incident ions of energy ranging from some keV to some MeV. In the spike regime, the spatial density of moving atoms is larger than that in the linear cascade regime. The spike case appears with heavy incident ions, i.e., diatomic molecular ion bombardment; these ions are slowed down rapidly and the energy transfer takes place in a relatively small volume of the target.

The theoretical calculations of the sputtering yield developed by Sigmund are adapted to the linear cascade regime; the two other regimes can be considered as limit cases and treated semi-quantitatively [21]. With an incident ion beam normal to the target surface, the sputtering yield, Y, expressed in atoms ejected per incident ion, is given by the following expression [22] :

$$Y = 3.56\ \alpha\ \frac{Z_i Z_t}{\left(Z_i^{2/3} + Z_t^{2/3}\right)^{1/2}} \frac{M_i}{M_i + M_t} \frac{s_n(\varepsilon)}{U} \tag{25}$$

where Z_i and Z_t are the atomic numbers of incident ions and target atoms, respectively; U (expressed in eV) is the binding energy of atoms at the target surface which is approximately equal to either the sublimation energy for a metal target or the covalent bond energy for a molecular material; α is a dimensionless parameter depending on the mass ratio, M_t/M_i (Fig.14).

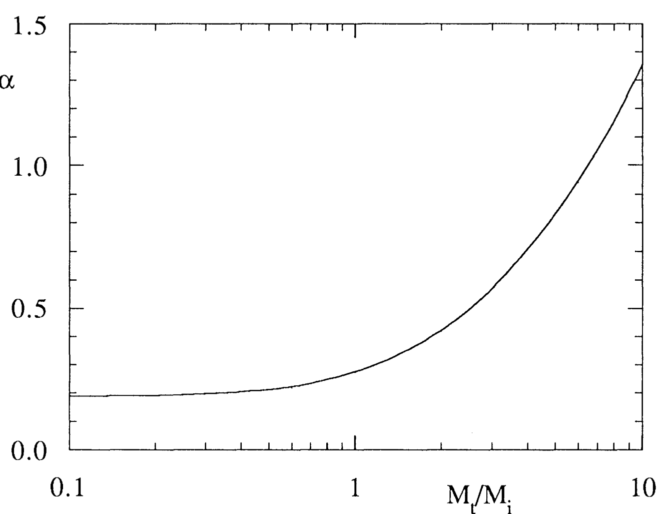

Figure 14 - Dependence of the factor α on the mass ratio M_t/M_i [21].

www.manaraa.com

The term $s_n(\varepsilon)$ is an universal function which depends on the energy variable ε defined by the following equation :

$$\varepsilon = \frac{M_t}{M_i + M_t} \frac{a}{Z_i Z_t e^2} E \tag{26}$$

with $a = \dfrac{0.855\, a_0}{\left(Z_i^{2/3} + Z_t^{2/3}\right)^{1/2}}$ and $a_0 = 0.529$ Å

where E (in eV) is the energy of incident ions, a (in cm) is the screening radius and e is the charge of electron in electrostatic units ($e = 4.8 \times 10^{-10}$ esu cgs). The universal function $s_n(\varepsilon)$ depends on the detailed form adopted for the screened Coulomb interaction. Several proposed forms are shown in Fig.15.

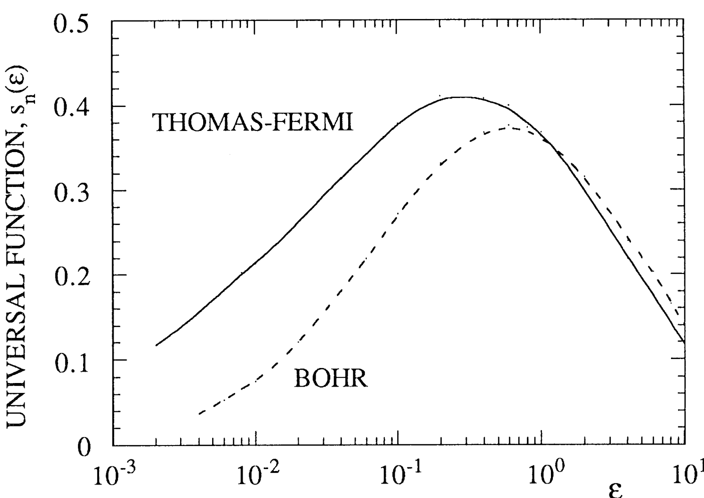

Figure 15 - Universal function, $s_n(\varepsilon)$, versus energy variable ε; the two curves refer to two different screening functions for the Coulomb interaction between two colliding atoms [21].

The sputtering yield can be determined experimentally from the mass loss of the target, ΔW, and ion current intensity, I, collected by the target for a given sputtering time, t :

$$Y\,(\text{atoms/ion}) = \frac{N_t}{N_i} = \mathcal{F} \frac{\Delta W}{I\, t\, M_t} \tag{27}$$

المنارة للاستشارات
www.manaraa.com

in which $\mathcal{F}$ = 1 Faraday = 96500 C; N_t and N_i are the numbers of sputtered atoms and incident ions, respectively. The sputtering yield increases with increasing ion energy (Table IV); generally, the yield values are given for incident ion beams normal to the target surface otherwise the incident angle value is mentioned.

Table IV - Sputtering yields for various materials bombarded by Ar^+ ions [23].

Target	Ion energy (keV)					
	0.2	0.6	1	2	5	10
Ag	1.6	3.4				8.8
Cu	1.1	2.3	3.2	4.3	5.5	6.6
Fe	0.5	1.3	1.4	2.0	2.5	
Ge	0.5	1.2	1.5	2.0	3.0	
Mo	0.4	0.9	1.1			2.2
Ni	0.7	1.5	2.1			
Si	0.2	0.5	0.6	0.9	1.4	
W	0.3	0.6				

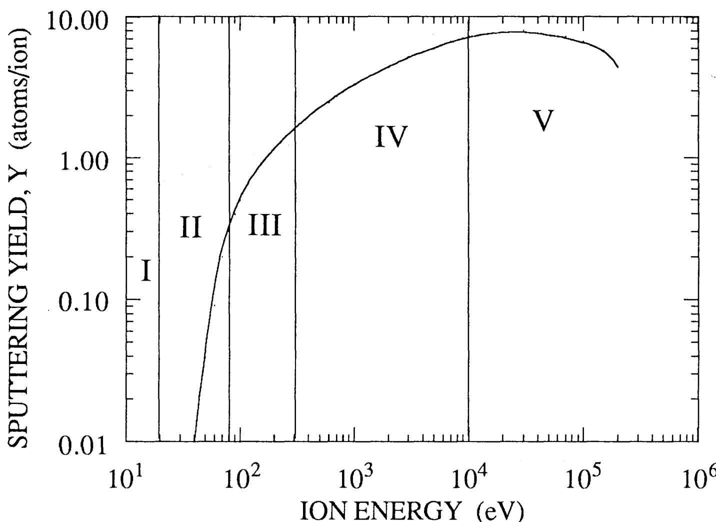

Figure 16 - Ion energy dependence of sputtering yield for copper bombarded by Ar^+ ions [24].

The experimental sputtering yield data for Cu targets reported in the literature are plotted versus Ar^+ ion energy in Fig.16. According to the ion energy, five parts can be

www.manaraa.com

distinguished in this diagram. In region I, the energy of ions below 20 eV is too low to induce copper sputtering detectable by the most sensitive methods available; the detection limit is about 10^{-4} at./ion. With an ion energy ranging from 20 to 80 eV (region II), the sputtering yield increases strongly with a small change in ion energy. The yield value is very difficult to measure; various techniques were developed, for example, resistance measurements of a thin film, use of microbalances, sputtering of radioactive species [23]. In region III, between 80 and 300 eV, the sputtering yield increases approximately linearly as the ion energy increases. Sputter deposition of metal thin films can be performed in this ion energy range. Between 300 eV and 10 keV in region IV, the sputtering yield continues to increase with increasing ion energy but less than linearly. The incident particles penetrate more deeply into the target with increasing ion energy and less atoms at the target surface can receive sufficiently high energy to escape as sputtered particles. This region IV is of interest for practical applications of sputtering in thin film deposition processes. For ion energies higher than 10 keV (region V), the sputtering yield reaches a maximum and is very insensitive to ion energy. the ion penetration depth becomes greater as the ion energy increases and a lower sputtering yield is observed. The maximum value is reached with few thousand eV H^+ or He^+ ions since these light ions penetrate easily in the metal target. For heavy ions (Xe, Hg), the maximum yield can be attained with ion energies of 50 keV or higher. In fact, the ion energy corresponding to maximum sputtering yield depends on the nature of the target material.

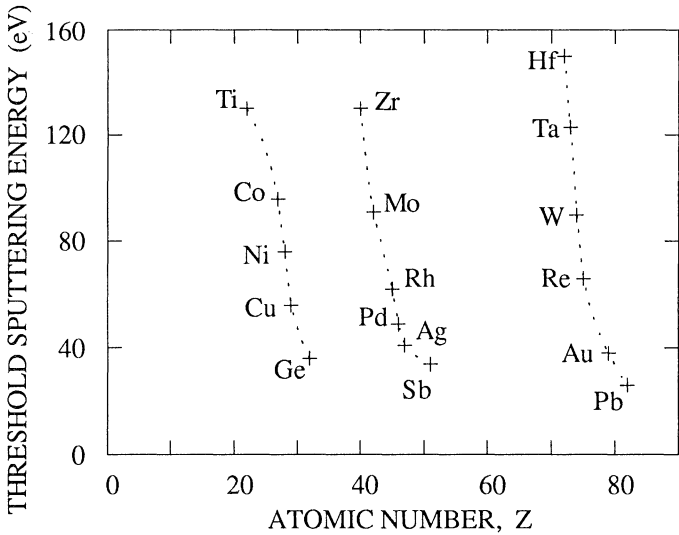

Figure 17 - Threshold sputtering energy versus atomic number of various elements bombarded by Hg^+ ions [17].

المنارة للاستشارات
www.manaraa.com

According to the nature of metal, the threshold sputtering energy (minimum energy to induce sputtering phenomenon) can vary from 40 to 130 eV for a given ion beam. For transition metals, the threshold energy decreases with increasing atomic number in each period of the table of elements (Fig.17).

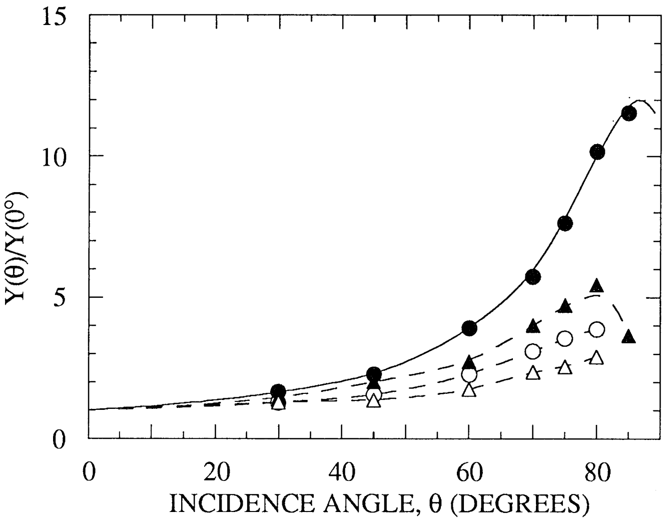

Figure 18 - Sputtering yields for Ni and Au versus incidence angle of light ions (θ is the angle between the ion beam and the normal to the target surface); ● 4 keV H^+/Ni, ❍ 4 keV H^+/Au, ▲ 1 keV D^+/Ni, Δ 1 keV D^+/Au; the solid line represents the computed results of Hoffmann et al. [25] for the 4 keV H^+/Ni system; experimental data are from Bay and Bohdansky [26].

A very rapid variation of the sputtering yield is observed with increasing incidence angle, θ, i.e., the angle between the ion beam and the normal to the target surface. The maximum yield is reached for angles higher than 80° (Fig.18). The maximum in the normalized yield, Y(θ)/Y(0°), was found to be higher as the projectiles are lighter, and to increase with increasing projectile energy as well as surface-binding energy of the target material. The sputtering yield also depends on the crystallographic orientation of a single crystal target and ion energy corresponding to the maximum yield depends on the crystallographic orientation of the crystal surface (Fig.19). The energy dependence of the yield for selected incidence directions and the angular dependence for different ion energies can be discussed in terms of the channeling model [28].

المنارة للاستشارات
www.manaraa.com

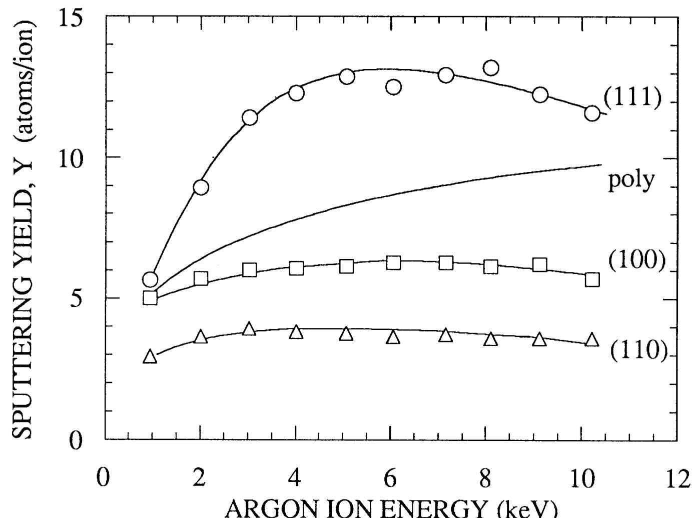

Figure 19 - Energy dependence of the sputtering yields of the (111), (100) and (110) planes of Ag [27] and energy dependence of the sputtering yield for polycrystalline Ag targets [28].

3.4. CHARACTERISTICS OF SPUTTERED SPECIES

3.4.1. Nature of Sputtered Particles. The particles ejected from the target surface are essentially emitted as neutral atoms (only about 1 % is charged). In general, the analyses by mass spectrometry show that a large number of different species exist in the flux of particles sputtered from the target. Polyatomic species such as SiO, CO, CH_3,... formed in the gas phase from residual impurities can also be detected; however, the abundance of these species is negligible compared to that of the target element or compound. The species emitted from a copper target bombarded by low energy Ar^+ ions were identified by mass spectrometry with a sensitivity of about 7 x 10^{-4} atom/ion [29]. Sputtered Cu atoms were detected down to an ion energy of 27 eV. Copper atoms were found to be ejected directly from the target as neutral species. The variation of the sputtering yield of copper as a function of the Ar^+ ion energy was similar to that represented by the typical curve given in Fig.16. Diatomic copper species were detected when the Ar^+ ion energy was higher than 50 eV; the concentration of these diatomic molecules in the flux of the sputtered material attained 5.5 % and decreased with decreasing ion energy. No other copper species with higher atomic mass such as Cu_3 were detected during sputtering of copper by Ar^+ ions under the experimental conditions investigated [29].

3.4.2. Energy of Sputtered Particles. The velocity of sputtered particles can be determined by measurements of the time of flight of the sputtered atoms [30]. Then, the energy of

www.manaraa.com

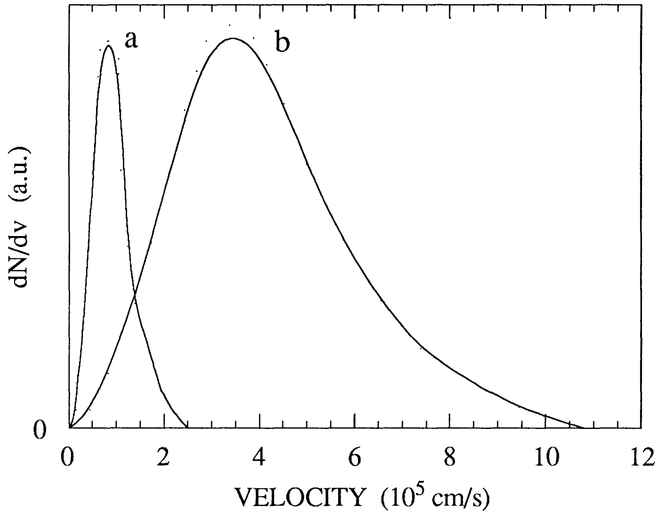

Figure 20 - Velocity distribution of evaporated (a) and sputtered (b) Cu particles [17].

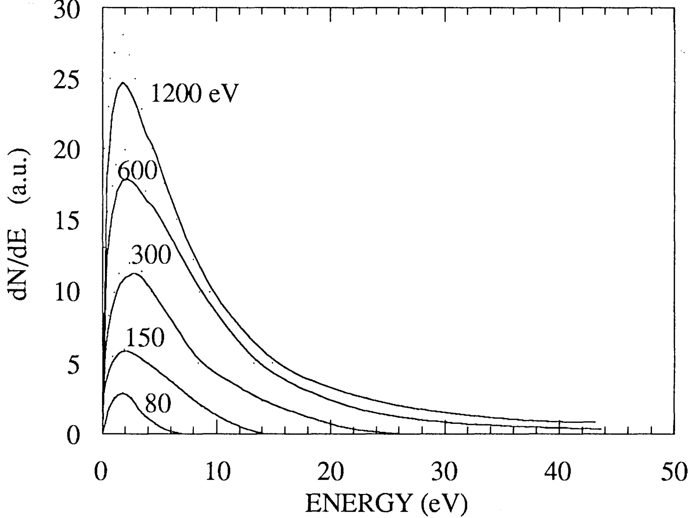

Figure 21 - Energy distribution of copper atoms ejected in the (110) direction normal to the single crystal surface for bombarding Kr^+ ion energies from 80 to 1200 eV [31].

المنارة للاستشارات
www.manaraa.com

these particles is deduced from their masses obtained by mass spectrometry measurements. To determine the time of flight of particles, the sputtered atoms are detected by optical absorption spectroscopy. A large current pulse is applied to the target and the interval of time between the pulse and the corresponding increase in intensity of the appropriate spectral line, i.e., the time of flight, is measured. The velocity distribution and energy distribution of sputtered particles can be deduced from these measurements.

The velocity distribution of evaporated and sputtered copper atoms are very different (Fig.20). The energy distribution of sputtered Cu atoms is broader than that of evaporated atoms. The mean energy of sputtered atoms is about 10 times higher than that of evaporated species. This result suggests (or confirms) that the mechanism of cathode sputtering is connected with momentum transfer and not with local heating of the target leading to evaporation of atoms from the target surface. The energy distribution of sputtered atoms depends on the energy of primary ions. For sputtering of a (110) oriented single crystal Cu target by Kr^+ ions, the kinetic energy of a number of Cu atoms ejected from the target can be higher than 20 eV when the energy of primary Kr^+ ions is above 600 eV (Fig.21). As a result, the sputtered atoms arriving at the surface of substrates will possess substantial energies compared to evaporated species. This high energy of sputtered particles can lead to better adhesion of films prepared by sputter-deposition processes.

3.4.3. Angular Distribution of Sputtered Particles. In the linear cascade regime, the flux of target atoms displaced by incident particles, i.e., the flux of recoil atoms is assumed to be isotropic. In other words, the probability of displacement of atoms in the target is independent of the direction considered in the crystal. From this assumption, the flux of atoms ejected from the target surface per unit area, per unit time and per unit solid angle is given by equ.(19). This law suffers from numerous exceptions; angular distributions depending on $\cos^2\theta$ can be found experimentally. With an oblique incidence bombardment, the deviation from the cosine law is all the larger as the energy of incident ions is low. Under these conditions, the mean direction of ejection becomes near the direction of the specular scattering as the energy of primary ions decreases [22].

3.5. SPUTTER-DEPOSITION OF THIN FILMS

3.5.1. Objectives. The properties of thin films are strongly dependent on purity, structure and morphology of the deposited material. These characteristics are significantly influenced by experimental deposition conditions, namely preparation or surface treatment of substrates, deposition parameters, post-deposition treatment of films. As a result, a deposition technique must meet various requirements or be able to respond positively to many of the challenges encountered in thin film processing. First of all, high deposition rates (up to few µm/min) are desired to produce films in reasonable deposition times in particular for implementation of the deposition process in a fabrication line. In general, films of high purity are required or sometimes films are deposited with a controlled incorporation of known impurities. Usually, substrates of complex shapes or geometries must be covered with uniform films, and the deposition technique must provide films with conformal step coverage. For obvious economic reasons in manufacturing, a high number of substrates processed by the system in a given time is desirable. The uniformity in film thickness and film quality is also an important challenge for a deposition technique. Since the target is progressively eroded, its life time is limited; for practical reasons, the target must retain the same properties throughout this life, in particular to achieve a correct process repeatability in a manufacturing environment.

www.manaraa.com

3.5.2. Optimization of Deposition Conditions. To prepare thin films with excellent quality in an industrial environment, the deposition conditions must be selected carefully in particular to produce thin films of high purity (or controlled composition) at high deposition rates. To illustrate these considerations, the deposition of films by d.c. diode sputtering can be examined in detail.

a) Optimization of the deposition rate

The deposition rate of films prepared by d.c. diode sputtering depends on the discharge gas pressure. As the pressure decreases, the current intensity through the sputtering gas and the number of ions striking the target per unit time decrease; as a result, to maintain the sputtering power at a given value, the interelectrode voltage must increase when the sputtering gas pressure decreases. The increase in interlectrode potential leads to higher energies of ions arriving at the target surface and higher sputtering yields. However, the effect of an increased sputtering yield on the deposition rate does not compensate totally the effect of a decrease in number of ions striking the target. This compensation is all the less achieved because the increase in sputtering yield due to higher ion energies is no so fast as the decrease in current intensity, in the ion energy range suitable for sputtering. From this point of view, relatively high sputtering gas pressures are of interest to produce thin films at high deposition rates.

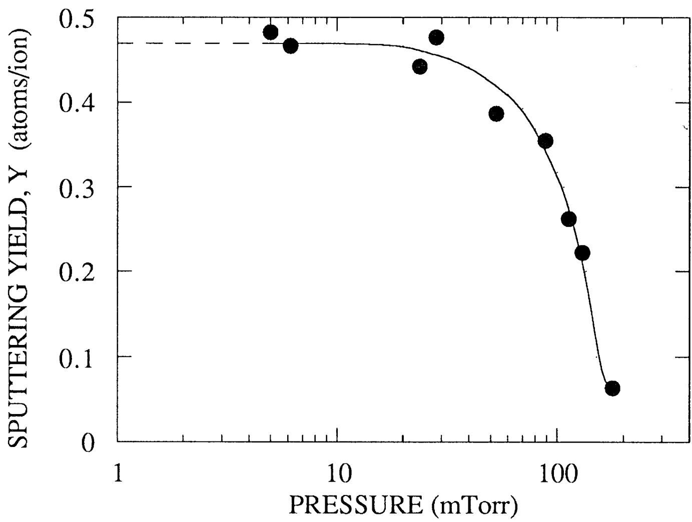

Figure 22 - Effect of the gas pressure on the sputtering yield of nickel bombarded by 150 eV Ar^+ ions [32].

Furthermore, as the pressure increases, the thickness or the width of the cathode sheath decreases, and the cathode fall occurs in a shorter distance (Fig.11); the electric field in the cathode sheath as well as energy of secondary electrons accelerated by this field increase. As a result, the ionization yield and the ion density increase. In the same time, the positive

المنارة للاستشارات
www.manaraa.com

ions arriving at the target surface with higher energies are more efficient to induce sputtering events. However, at very high pressures, this advantage is reduced or disappears because of collisions in the cathode sheath; most ions strike the target with energies considerably lower than that corresponding to the cathode fall, i.e., the ion energy has been reduced by the increased number of collisions. The real limiting factor to sputtering at high pressures is the higher probability that sputtered atoms return to the cathode by back diffusion. At a sputtering gas pressure of 0.1 Torr, only 10 % of atoms ejected from the target are able to get across the sheath and can diffuse beyond the sheath. Back diffusion phenomena play a dominant role in determining deposition of films when the sputtering gas pressure exceeds 100 mTorr; below of about 10 mTorr, the back diffusion becomes negligible. Actually, the sputtering yield depends on the sputtering gas pressure (Fig.22). Various factors affect the sputtering yield and act in opposing directions. The net balance of all these various opposing factors leads to an optimum pressure range for d.c. diode sputtering between 25 and 75 mTorr (Fig.22). Under these pressures, the width of the cathode sheath is of the order of 1 to 2 cm.

The deposition rate of films depends on the distance between the target and the substrate or cathode-anode spacing when substrates are placed on the anode. The sputtered particles diffuse through the ionized gas to reach the substrates. Some loss of material occurs during the mass transport from target to substrate. At first glance, to collect a maximum of sputtered material and eliminate or limit the loss of material, the substrates would be placed as close to the target as possible. However, when the electrode spacing becomes comparable to the sheath width or when the substrate penetrates within the sheath region, the impedance of the system rises rapidly, and the current intensity as well as the deposition rate decrease strongly. The best compromise was found experimentally when the cathode-substrate spacing is about twice the sheath width.

The deposition rate of films is also sensitive to the presence of impurities in the sputtering gas; in addition, these impurities can contaminate the deposited material. The deposition rate of metal films produced from metal targets sputtered by Ar^+ ions decreases as the concentration of hydrogen, helium or oxygen in argon increases. The sputtering yield of H^+ and He^+ ions is very low because of their light atomic mass. However, these gases have high ionic mobility in the discharge and the ionic current is essentially carried from the anode to the cathode by H^+ and He^+ ions. In other words, the contribution of these light ions to the discharge current is more elevated than that deduced from the gas composition, and these ions cause practically no sputtering events. The net result is a decrease in deposition rate of films. The effect of oxygen atoms on the deposition rate originates from other phenomena. In a d.c. glow discharge, the sputtering of a conductive material becomes efficient after elimination or etching of the native oxide (usually insulating) film from the target surface. In addition, the sputtering yield of a given oxide is significantly lower than that of the corresponding metal. If the native oxide layer and oxygen atoms adsorbed on the target surface are continuously replaced by oxygen atoms coming from the discharge gas, the deposition rate of films would be less than that obtained in sputter-deposition process from oxygen free sputtering gas. Oxygen atoms in the discharge gas can also originate from outgassing phenomena from sputtering chamber walls and elastomer seals.

The substrate temperature can affect both the properties and deposition rate of films. The effect of substrate temperature on the deposition rate was illustrated for sputter-deposition of SiO_2 films in R.F. sputtering system [33]; silica being an insulating material, the SiO_2 target is connected to an a.c. power supply. At relatively high substrate temperatures, a fraction of sputtered particles striking the substrate surface can be re-emitted and return to the vapor phase; in other words, the sticking coefficient of sputtered particles decreases with increasing substrate temperature (Fig.23). To eliminate this effect

www.manaraa.com

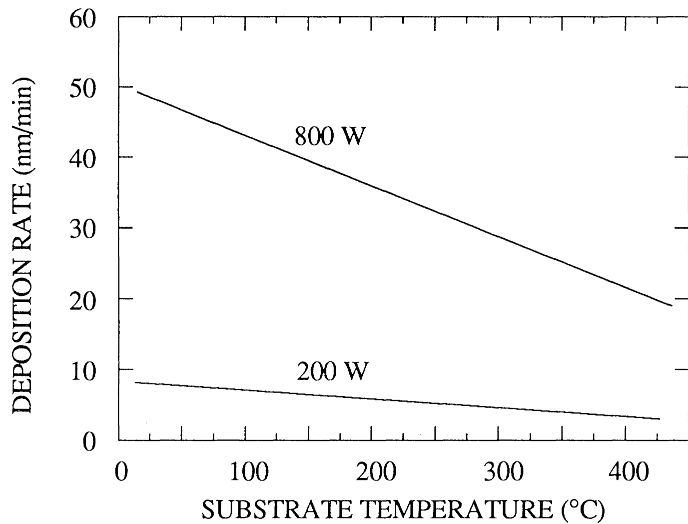

Figure 23 - Deposition rate of SiO_2 films deposited by r.f. sputtering from a SiO_2 target as a function of the substrate temperature for two sputtering powers [33].

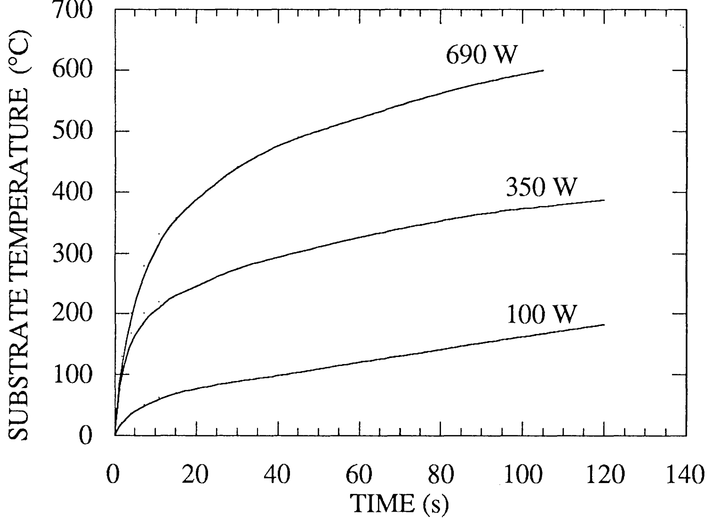

Figure 24 - Substrate temperature as a function of time for a substrate thermally isolated from its holder at various sputtering powers [33].

المنارة للاستشارات
www.manaraa.com

and produce thin film with uniform thickness, the temperature must be maintain uniform across the substrate during sputter-deposition. This temperature control is difficult since the substrate surface is constantly bombarded and heated by high energy electrons. A good thermal conductance between the substrate and the temperature controlled substrate holder is desirable and can be achieved by interposing a layer of liquid gallium (melting point : 37°C) between substrates and substrate holder. The substrate temperature can also be maintained at a constant value by allowing the substrates to float thermally during sputtering. In this case, a thermal equilibrium can be established between the heat loss due to radiation and heat gain caused by electron bombardment. According to the sputtering power, this equilibrium state can be attained more or less rapidly (Fig.24).

b) Control of contamination in sputtered films
Risks of incorporation of impurities in films are more important using sputtering process than an evaporation technique. Indeed, contaminant species are dissociated and ionized in the glow discharge, and are therefore more reactive. In addition, the chamber wall in contact with the ionized gas is subjected to bombardment by energetic particles so that impurities trapped on the chamber wall can be emitted and introduced into the sputtering gas.

To avoid sputtering of various systems such as the target holder and contamination of films, shields are mounted close to the target and walls to be protected from parasitic sputtering events (Fig.9). The cathode shield is grounded and acts as an anode. With a shield-cathode spacing below about 1 cm, secondary electrons emitted from the cathode cannot gain the energy required for ionization of gas molecules during the cathode-shield path, and the glow discharge is suppressed in the region encompassed with the shield.

Contamination in films can be reduced or eliminated using asymetric (a.c.) sputtering systems and bias sputtering techniques. With these techniques, the surface of films is bombarded by low energy ions during sputter-deposition. Under these conditions, a fraction of the deposited material on the substrates is re-sputtered and many impurities adsorbed on the surface are preferentially removed relatively to the film material it-self. These phenomena lead to significant improvements in film purity. In the asymetric a.c. sputtering system, a diode is mounted in reverse position in the external electric network. For one half-cycle, the electrical resistance is very high, the negative voltage applied to substrates is low, and the erosion of films is also low but sufficient for removing adsorbed gases and impurities. For the next half-cycle, the negative voltage applied to the target is high so that the target material can be sputtered and deposited on the substrates. With a d.c. sputtering system, the substrates can be biased to a negative voltage with respect to the anode voltage. By selecting bias voltages of - 100 to - 200 V, a small fraction of films is re-sputtered but elimination of impurities is suitable to improve the quality of films [33]; for example, the electrical resistivity of Ta films, and probably the oxygen concentration in the films are considerably reduced when the films are deposited on substrates with a bias voltage of - 150 V or below (Fig.25). Sputtering deposition on biased substrates leads to changes in crystal structure of deposited materials. For Ni-Cr alloy films, a substantial increase in the (111) preferred orientation is observed with increasing bias votage (Fig.26). Sometimes, the electrical resistivity of metal films depends on the crystallite orientation, e.g., electrical resistivity of Ta films. As a result, a bias sputtering process can improve the purity of Ta films; however, in the same time, the crystallographic orientation of Ta films is modified and the electrical resistivity is increased. The net effect of the bias voltage can be an increase in electrical resistivity of Ta films [33].

Sputtered films can also contain significant amounts of trapped sputtering gas. Intuitively, one can assume that the content of sputtering gas trapped in the deposited material would be lower in films produced at low pressures; in fact, the reverse situation is

www.manaraa.com

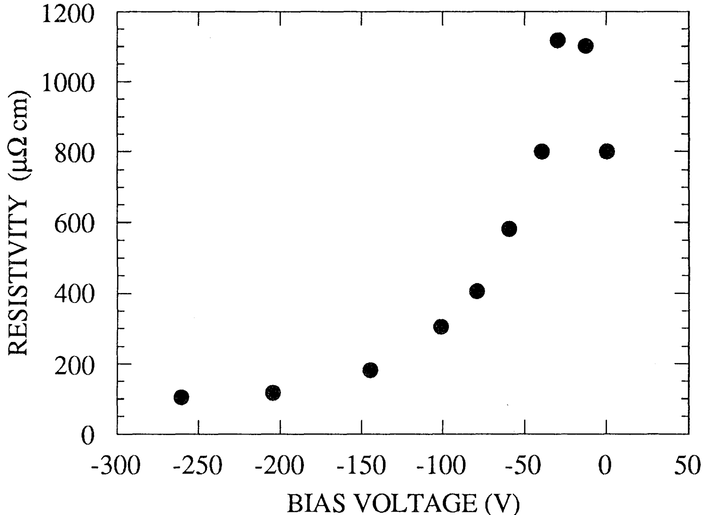

Figure 25 - Electrical resistivity of tantalum films as a function of bias voltage [34].

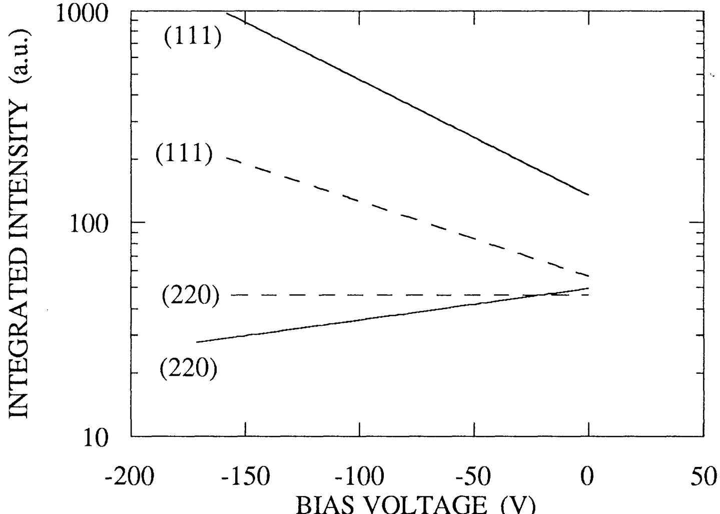

Figure 26 - Effect of the bias voltage on the crystallographic orientation of Ni-Cr films deposited by sputtering from argon with a residual oxygen pressure of : 2 x 10^{-7} Torr (solid lines) and 1 x 10^{-5} Torr (dashed lines) [35].

المنارة للاستشارات
www.manaraa.com

true (Fig.27). However, deposition on biased substrates can lead to a decrease in concentration of sputtering gas incorporated in the films. From various data described in previous sections, it would be concluded that films of high purity can be sputter-deposited at high deposition rates using high sputtering powers and relatively high sputtering gas pressures (resulting in high deposition rates and low trapping of sputtering gas), and also using negatively-biased substrate holders (for elimination of adsorbed gases and impurities).

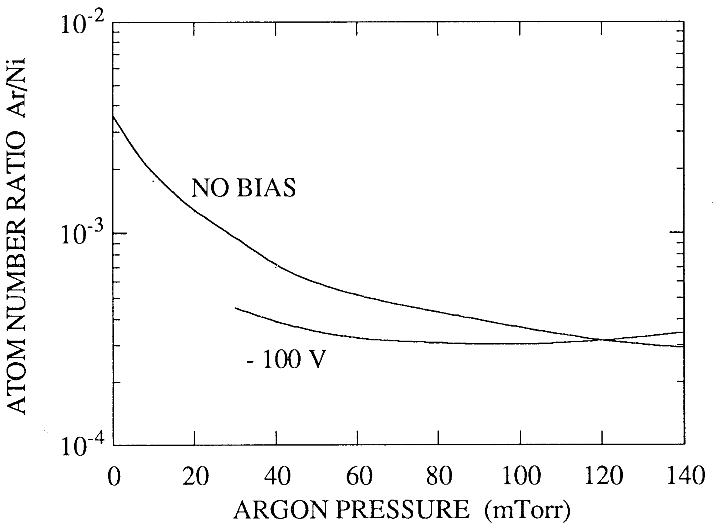

Figure 27 - Effect of the sputtering gas pressure on the concentration of argon atoms trapped in sputter-deposited Ni films [36].

c) Sputtering at very low pressures

For various reasons, it can be established that a relatively high pressure is suitable to deposit thin films by cathode sputtering. Nevertheless, sputtering process at low pressures (if possible) is intrisically interesting since an increased mean free path of sputtered particles leads to both a higher energy of ions striking the target surface and a higher number of sputtered particles susceptible to reach the substrate surface by diffusion in the sputtering gas. Consequently, the sputtering yield (proportional to ion energy) and deposition rate (adversely affected by back diffusion process) can be higher at low pressures; the effect of low pressure sputter-deposition on purity of films cannot be anticipated easily. Below about 20 mTorr, the discharge in a d.c. diode system cannot be self-sustained because of the rapid decrease in ion density with decreasing pressure. At low pressures, the mean free path of species increases and the number of collisions decreases; as a result, the mean energy of ions increases. However, the effect of an increased energy of ions on ionization processes is not sufficient to compensate the effect of a decrease in ion density. In fact, at low pressures, the flux of incident ions on the target is not sufficient to maintain the secondary electron emission required for ionization of

www.manaraa.com

sputtering gas and self-sustaining discharge. A significant increase in ion density is required for sputter-deposition of films at low pressures with reasonable deposition rates. This increase in ion density can be achieved by increasing both density of electrons having energy sufficiently high to ionize the sputtering gas and ionization yield of electrons available to induce ionization processes; an increased ionization yield can be obtained in the presence of a magnetic field.

3.6. SPUTTER-DEPOSITION PROCESSES AT LOW PRESSURES

Various techniques can be utilized to improve gas ionization phenomena and ion density as the sputtering gas pressure decreases.

3.6.1. d.c. Triode Sputtering System. In this system, an auxiliary source of electrons such as a heated tungsten filament emits electrons by thermoionic effect independently of gas pressure and plays the role of the requisite agent of ionization (Fig.28). The electrons generated by the filament heated by Joule effect are drawn by the anode; for a sufficiently high anode potential, these energetic electrons can ionize gas molecules during collisions at relatively low pressures (1 to 5 mTorr). The target material to be sputtered is inserted in this plasma and is negatively-biased to attract positive ions and repel electrons.

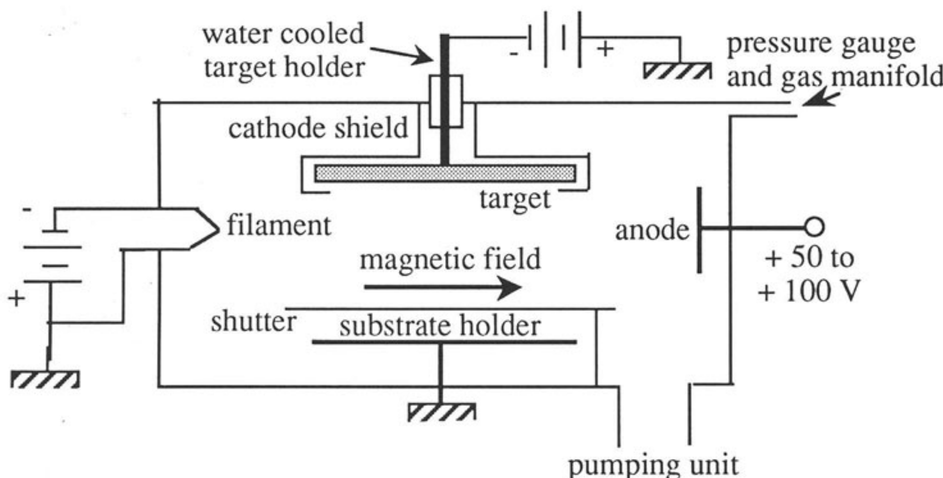

Figure 28 - d.c. triode sputtering deposition system.

Since the ion mobility is lower than that of electrons, a space charge is created in the immediate vicinity of the target surface and the potential fall between the target and the substrates is concentrated in this cathode sheath. In general, the substrate holder is biased to a negative voltage to avoid attraction of thermionically emitted electrons and distorsions in the uniformity of the plasma. The ionization yield is improved by application of a magnetic field of about 25 G (Fig.28). The electrons in motion in the magnetic field experience circular motion to the magnetic field direction. The magnetic field aids in the confinement of electrons, and increases the electron path lengths in the gas phase; thereby, the number of collisions and probability of gas ionization are enhanced at a certain distance from the filament. Typically, using the triode sputtering system, the deposition rate of

www.manaraa.com

metal films can reach 40 nm/min at a sputtering gas pressure of 1 mTorr. This type of discharge at low pressures is convenient to study the sputtering mechanisms. Indeed, in gas discharges operating at relatively high pressures, the energy of ions striking the target is not correctly defined because of collision effects in the cathode sheath. In this sputtering system, the ion current to the target can be varied without changing either the gas pressure or the target voltage; this is not the case for a d.c. diode sputtering system. As a result, the triode system allows a better control of the sputtering parameters than the diode system. However, the triode system can present some drawbacks. For example, using target of reasonable diameters (10 to 20 cm) with the configuration given in Fig.28, the sputtering rate is not uniform since the ion density is higher near the filament. To improve the sputtering uniformity, the target can be inclined relatively to the axis of the electron beam; this configuration can also provide higher sputtering yields than those obtained from a diode sputtering system since the sputtering yield increases with increasing incidence angle (Fig.18).

3.6.2. Sputtering in a High Frequency Induced Plasma. A glow discharge can be created and sustained in a gas at low pressures by interactions with a high frequency (H.F.) or radio frequence (R.F.) electromagnetic wave. At a frequency of some MHz, free electrons in the gas gain energy between two successive collisions, and the electron energy can become sufficiently high to induce gas ionization. The presence of electrodes in the chamber is not necessary for gas ionization and plasma generation (Fig.29); in fact, the plasma is excited in the left part of the quartz tube by an external R.F. coil. The species generated in the plasma can diffuse towards the target and substrates placed in the right part of the system. The target is negatively-biased with respect to an anode. Sputtering of materials can be performed at low pressures (about 2 mTorr). The major advantage of this sputtering system is the absence of electrodes or hot filament; as a result, reactive gases such as oxygen can be currently employed without detrimental effects on the system.

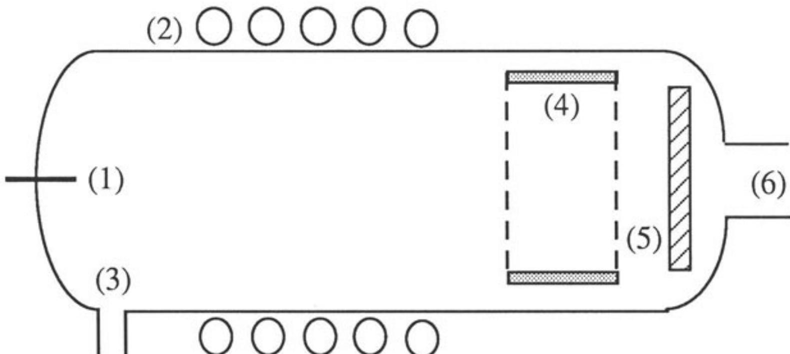

Figure 29 - Sputtering system with auxiliary high frequency glow discharge; (1) anode, (2) R.F. coil, (3) pressure gauge and gas manifold,(4) negatively-biased ring target, (5) substrate, and (6) pumping unit.

3.6.3. Magnetron Sputtering System. This sputtering system is similar to a diode system. However, the cathode is equipped with permanent magnets creating magnetic field with a direction parallel to the target surface; this arrangement is named magnetron target. In a d.c. diode system, the glow discharge is self-sustained by secondary electrons emitted

www.manaraa.com

from the target because of the ionic bombardment effect. These electrons attracted by the anode drive away from the cathode along paths essentially normal to the cathode surface (Fig.30). With the magnetron system, the magnetic field parallel to the target surface, i.e., perpendicular to the electric field, induces electron gyration along magnetic field lines; as a result, the probability of electron-molecule collisions and gas ionization as well as the ion density increase considerably at the vicinity of the target surface. The increased ion density near the target surface results in higher ion currents and higher sputtering rates than those obtained from a conventional diode system. The deposition rate of films can be multiplied by a factor of 50 as a magnetron sputtering system is used. Consequently, the target can be sputtered at relatively low pressures while the deposition rate values remain at a reasonable level; the d.c. magnetron sputtering system can currently operate at sputtering gas pressures as low as 1 mTorr. The typical magnetic field provided by permanent magnets of various materials (Al-Ni-Co alloy, rare earth (Co-Sm) alloy...) is between 200 and 500 G.

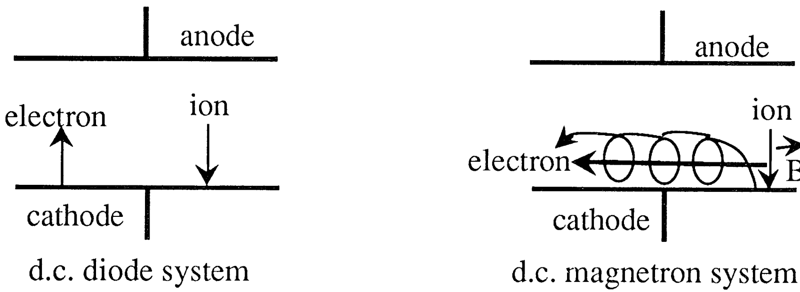

Figure 30 - Principle of the magnetron effect.

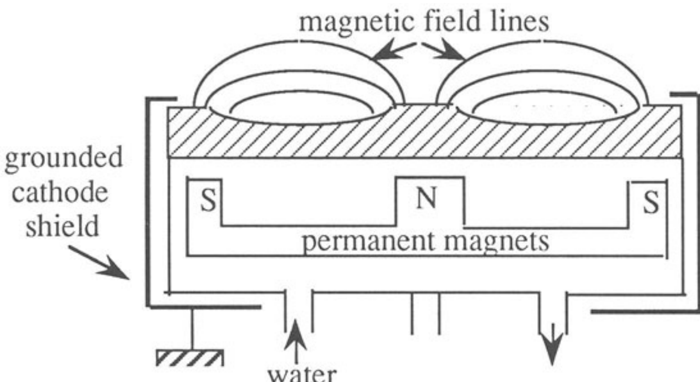

Figure 31 - Schematic of a planar magnetron target.

The geometrical arrangement of orthogonal electric and magnetic fields is required for electron confinement near the target surface. This required configuration can be achieved in many ways and magnetron systems have been developed in a wide range of geometries such as circular planar, rectangular planar, cylindrical post magnetron [37,38]. The major disadvantage of the magnetron target is related to a non uniform erosion of the target surface (Fig.31). The material erodes more rapidly in regions where the magnetic field lines are more tightened. For example, with a planar magnetron target, an erosion track

المنارة للاستشارات
www.manaraa.com

forms at the target surface leading to changes in distribution of magnetic field lines and variations in sputtering or deposition rates as the target wear increases.

3.6.4. Radio Frequency Sputtering System. With a d.c. power supply and a target of insulating material, nothing would happen when interelectrode voltage is applied, i.e., even if a plasma was created by some external means, positive ions striking the insulating target could not be neutralized and a positive charge would appear at the target surface preventing any further bombardment and sputtering by other ions. With an a.c. power supply, the current can flow between two electrodes of a diode system equipped with an insulating target. However, the electrical resistance of a plasma is much lower than that of the insulating electrode and the major part of the potential drops across the insulating material. Under these conditions and at low frequencies, ions generated in the plasma cannot gain the energy required for a significant sputtering by ion bombardment. At a frequency higher than 50 or 100 kHz, a new phenomenon appears; the electrons having a high mobility can follow easily the periodic changes in electric field. A high electron current can be collected by the target during a half-cycle. By contrast, heavy ions with lower mobilities cannot follow the periodic changes in electric field. These ions have less and less chance to reach the target surface for one cycle as the frequency increases.The electrons which cannot flow through the insulating target accumulate on the target surface since the ion current is not sufficient to neutralize these trapped electrons for one half-cycle at each cycle. The ions pile up in front of the target as they do in a d.c. system forming a space charge region. The target surface possesses rapidly a negative charge (a self-bias voltage) which repels most electrons (Fig.32).

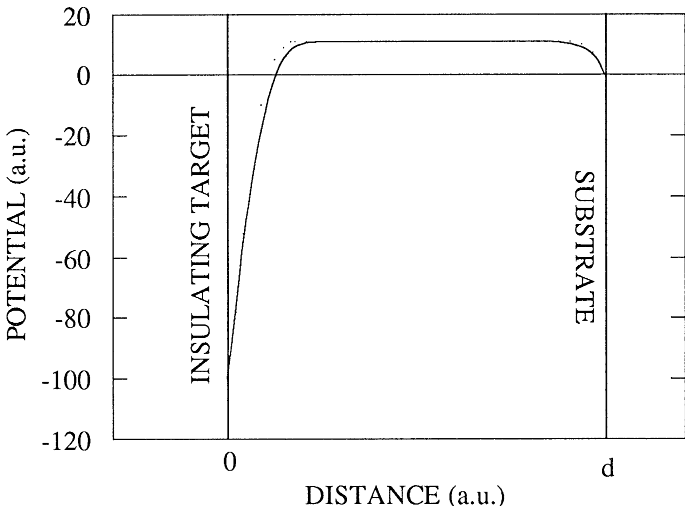

Figure 32 - Typical variation of interlectrode potential in a R.F. sputtering system with an insulating target.

Using frequencies higher than 100 kHz, energy can be supplied to both the plasma and ions to sustain the glow discharge and cause sputtering of the insulating target. In addition,

www.manaraa.com

at high frequencies, the discharge can be self-sustained at low pressures (up to about 1 mTorr). This R.F. discharge has an ionization yield higher than the d.c. discharge since the ionization phenomena are not only induced by secondary electrons emitted from the target. The electrons generated in the plasma can oscillate in the R.F. electric field, gain energy for each cycle without collisions at low pressures, and their energy can reach a level sufficiently high to induce ionization of molecules when collision events occur.

Since the R.F. system has an alternative configuration, the substrate can be sputtered at each cycle; however, the sputtering level of substrates is much less important than that of the target. The R.F. plasma potential is positive relatively to two electrodes and this potential is distributed essentially by capacitive coupling near the surfaces. The capacitance between the plasma and any grounded surface such as substrates is much higher than that between the plasma and the target; as a result, the major part of the potential fall takes place on the target side (Fig.32). Sputtering of substrates and other surfaces in contact with the plasma occurs during sputter-deposition; however, these surfaces are progressively covered with a layer of the target material and any contamination caused by this parasitic sputtering process is rapidly eliminated or negligible. The R.F. sputtering equipment is very similar to a d.c. diode sputtering system except the external electric network; the admission of power into the system must be done through a suitable impedance matching network [33,39].

Radio frequency magnetron targets can also be used to enhance the deposition rate of insulating films prepared by sputtering from an insulating target. However, the degree of enhancement is usually not so high for R.F. magnetron as it is for d.c. magnetron system; the fluctuations in electric field result in a less efficient confinement of electrons. In addition, thermal conductivity of insulating materials is relatively low, and the sputtering power must be limited in order to avoid degradation or fractures of the insulating target.

3.7. REACTIVE SPUTTER-DEPOSITION TECHNIQUE

The major objective of sputter-deposition techniques discussed in previous sections was to deposit thin films of a given material M from a target consisting of this material. In this case, an inert gas (Ar or Xe) of high purity is used as a sputtering gas. All sources of contamination such as residual gases or outgassing from chamber walls must be limited since energetic neutral or excited species are generated in the plasma from residual gases and the chemical activity of these atomic or molecular fragments can be relatively elevated. In reactive sputtering deposition techniques, the situation is reverse, i.e., chemical interactions between the depositing material and the gaseous environment are desired. This technique was initially used to deposit insulating compounds before the development of R.F. sputtering systems. For example, tantalum nitride layers were deposited by sputtering of a Ta target in N_2-Ar or NH_3-Ar mixtures. The reaction mechanisms involve in this deposition process can be rather complex. In the case of reactive sputter-deposition of TaN films, the material can form on the target surface, in the gas phase or on the substrate surface. When the reaction takes place on the target, the film formed on the target surface can block the sputtering process using a d.c. power supply or can lead to a decrease in deposition rate with an R.F. discharge. The homogeneous reaction in the gas phase between tantalum species and nitrogen can provide powdery materials. Usually, the formation of the depositing material on the substrate surface must be encouraged or favored by a suitable control of deposition parameters. To produce insulating thin films, a target of the insulating material can be sputtered in an inert gas; however, the composition of films can be different from that of the target. For example, R.F. sputtering of a Si_3N_4 target can provide thin films deficient in nitrogen since the molecular species ejected from the target may lose some of its nitrogen atoms. The stoichiometry of the deposited material

www.manaraa.com

can be improved by introducing nitrogen in the sputtering chamber and the composition corresponding to Si_3N_4 can be restored. Nevertheless, the non stoichiometric films may present superior properties to those having the bulk composition, i.e., this non stoichiometry is not necessarily a disadvantage. However, a close control of the process parameters is an important feature to produce thin films with a given composition.

3.8. CHARACTERISTICS OF SPUTTER-DEPOSITED THIN FILMS

3.8.1. Nucleation and Growth of Sputter-Deposited Films. Nucleation and growth phenomena of films produced by sputter-deposition are similar to those involved in growth of films deposited by evaporation except two specific features. The density of nuclei is larger and the distribution of nuclei is more uniform when films are produced by vacuum evaporation. The sputter-deposited films are continuous more rapidly, i.e., for lower amounts of materials deposited on the substrate or for lower thicknesses. This uniformity can contribute to better adhesion of films produced by sputtering. In addition, the relatively high energy of sputtered particles (Fig.20) arriving at the substrate surface can also contribute in the better adhesion of sputter-deposited thin films. The high nuclei density in sputter-deposition process leads to films with small grain size or with fine-grained structures. The sputter-deposited material can be amorphous when the substrate is maintained at low temperatures. The growth of sputter-deposited films is not isotropic. The surface roughness, shadow effects and nuclei distribution result in structures with preferred orientation in the direction normal to the substrate surface. This columnar structure depends essentially on sputtering gas pressure and substrate temperature (Fig.33).

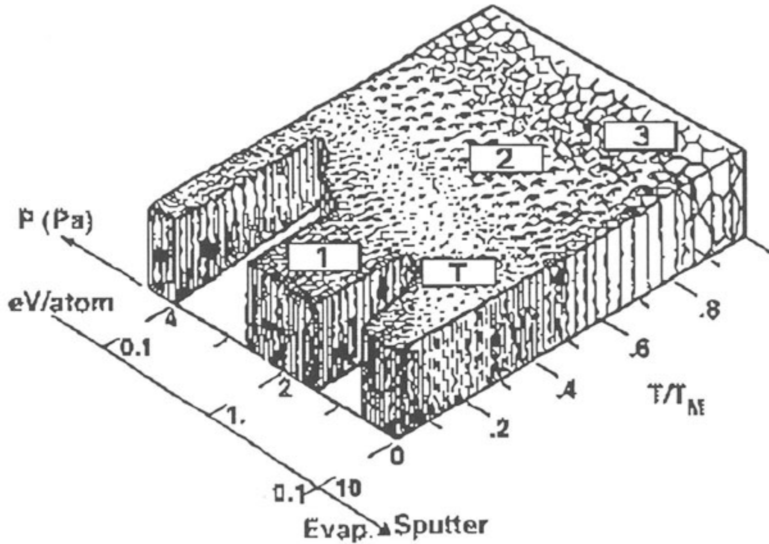

Figure 33 - Morphology and structure of films as functions of normalized temperature T/T_m and sputtering gas pressure or energy of deposited atom for both sputtering and evaporation; region 1 : porous structure, region T : transition zone, region 2 : columnar structure, region III : recrystallization of the deposited material; T (K) is the substrat temperature and T_m (K) the melting point of the material [40,41].

www.manaraa.com

3.8.2. Microstructure of Sputter-Deposited Films. The columns are large and close-packed when the deposition temperature is relatively high. By contrast, the films are less dense as the sputtering gas pressure is increased. According to this model [40,41], the films deposited at high pressures and low temperatures are porous (Fig.33). This porosity results from independent growths of various nuclei and the voids or cavities between adjacent columns cannot be reduced. At high temperatures, the surface mobility of atoms increases and the coalescence of nuclei can occur more easily. In addition, the cristallite sizes increase and the porosity decreases.

3.8.3. Purity of Sputter-Deposited Films. Contamination of films by residual and sputtering gases can be reduced when the films are deposited on substrates maintained at suitable temperatures. Another possibility consists in deposition on d.c. or R.F. biased substrates. The growing film is subjected to low energy ion bombardment and loosely bounded atoms can be removed easily from the surface. In addition to the desorption effect on impurities, this ion bombardment leads to significant improvement of surface step coverage caused by an increase in surface temperature and surface mobility of deposited species.

3.8.4. Adhesion of Sputter-Deposited Films. To ensure a correct adhesion of films, the substrate can receive a surface treatment to remove native oxide layer or other impurities. This surface cleaning treatment can be performed directly in the sputtering chamber prior to the sputter-deposition process via various means : vacuum heat treatment, ion etching,... Sometimes, the optimization of this in situ surface treatment is empirical.

4. Conclusion

Both vacuum evaporation and cathode sputtering have been extensively used to produce thin films for various applications. The properties of films prepared by these physical vapor deposition (PVD) techniques can be quite different since they depend strongly on the growth conditions of the films. Evaporative deposition processes are suitable for uniform coverage of planar substrates. Sputtering deposition processes are well suited to deposit refractory metals, alloys and compounds; in particular the composition of compounds can be closely controlled using reactive sputtering deposition processes. Enhanced deposition rates can be achieved using magnetron sputtering target arrangements. Insulating films are currently deposited by R.F. sputtering process from insulating targets. The choice of the appropriate deposition technique for a given film-substrate couple may depend upon numerous factors; for each particular case, the process parameters suitable for a given application must be carefully determined before implementation of the deposition process in manufacturing line.

REFERENCES

1. W.R. Grove, Philos. Trans. R. Soc. London, **A 142** (1852) 87.
2. R. Glang, "Handbook of Thin Film Technology", L.I. Maissel and R. Glang (eds.), Mc Graw-Hill, New York, Chap.1 (1970).
3. N.G. Nakhodkin and A.I. Shaldervan, Thin Solid Films, **10** (1972) 109.
4. T. Abe, K. Inagawa, K. Obara and Y. Murakami, Proceedings of the 12th Symposium on Fusion Technology, Zurich, Sept.13-17 (1982).
5. R.F. Bunshah and A.C. Raghuram, J. Vac. Sci. Technol., **9**(6), (1972) 1385.

www.manaraa.com

6. C.V. Deshpandey and R.F. Bunshah, "Handbook of Plasma Processing Technology", S.M. Rossnagel, J.J. Cuomo and W.D. Westwood (eds.), Noyes Publications, Park Ridge, NJ, (1990) pp.370.
7. A.K. Suri, R. Nimmagadda and R.F. Bunshah, Thin Solid Films, **72** (1980) 529.
8. R.F. Bunshah and R.J. Schramm, Thin Solid Films, **40** (1977) 211.
9. M. Colen and R.F. Bunshah, J. Vac. Sci. Technol., **13**(1), (1976) 536.
10. K.V. Chi, R.O. Dillon, R.F. Bunshah, S. Alterovitz and J.A. Woollam, Thin Solid Films, **54** (1978) 259.
11. H.S. Randhawa, D. Brock, R.F. Bunshah, B. Basol and O.M. Stafsudd, Sol. Ener. Mater., **6** (1982) 4456.
12. B.E. Jacobson, C.V. Deshpandey, H.J. Doerr, A.A. Karim and R.F. Bunshah, Thin Solid Films, **118** (1984) 293.
13. P. Nath and R.F. Bunshah, US Patent 4,336,277, June (1982).
14. K. Nakumara, K. Inagawa, K. Tsusuoka and K. Komiya, Thin Solid Films, **40** (1977) 155.
15. Y. Murayama, J. Vac. Sci. Technol., **12**(4), (1975) 818.
16. L.I. Maissel and M.H. Francombe, "An Introduction to Thin Films", Gordon and Breach Sciences Publishers, New York, Chap.2 (1973) pp.5.
17. L. Eckertova, "Physics of Thin Films", Plenum Press, New York, Chap.2 (1977) pp14.
18. F. Brown and J.A. Davies, Can. J. Phys., **41** (1963) 844.
19. T.M. Buck, "Methods of Surface Analysis", A.W. Czanderna (ed.), Elsevier Scientific Publishing Company, Amsterdam, The Netherlands, Chap.3 (1975) pp.75.
20. G.M. McCracken, Rep. Prog. Phys., **38** (1975) 241.
21. P. Sigmund, "Sputtering by Particle Bombardment I", R. Behrisch (ed.) Topics in Applied Physics, Springer-Verlag, Berlin, Germany, **Vol.47**, (1981) pp.9.
22. G. Gautherin, "Réactivité dans les plasmas", A.M. Pointu and A. Ricard (eds.), Editions de Physique, Les Ulis, France (1984) pp.243.
23. L.I. Maissel, "Physics of Thin Films", G. Hass and R.E. Thun (eds.), Academic Press, New York, **Vol.3** (1966) pp.61.
24. H.H. Andersen and H. Bay, Radiat. Eff., **13** (1972) 67.
25. T. Hoffmann, H.L. Dodds, M.T. Robinson and D.K. Holmes, Nucl. Sci. Eng., **68** (1978) 204.
26. H.L. Bay and J. Bohdansky, Appl. Phys., **19** (1979) 421.
27. G.D. Magnuson and C.E. Carlston, J. Appl. Phys., **34**(11), (1963) 3267.
28. H.E. Roosendaal, "Sputtering by Particle Bombardment I", R. Behrisch (ed.) Topics in Applied Physics, Springer-Verlag, Berlin, Germany, **Vol.47**, (1981) pp.219.
29. J.R. Woodyard, and C.B. Cooper, J. Appl. Phys., **35**(4), (1964) 1107.
30. R.V. Stuart, K. Brower and W. Mayer, Rev. Sci. Instr., **34** (1963) 425.
31. R.V. Stuart and G.K. Wehner, J. Appl. Phys., **35**(6), (1964) 1819.
32. N. Laegreid and G.K. Wehner, J. Appl. Phys., **32**(3), (1961) 365.
33. L.I. Maissel and M.H. Francombe, "An Introduction to Thin Films", Gordon and Breach Sciences Publishers, New York, Chap.3 (1973) pp.39.
34. L.I. Maissel and P.M. Schaible, J. Appl. Phys., **36**(1), (1965) 237.
35. E. Stern and T.B. Light, Appl. Phys. Lett., **13**(11), (1968) 381.
36. H.F. Winters and E. Kay, J. Appl. Phys., **38**(10), (1967) 3928.
37. W.D. Weswood, "Microelectronic Materials and Processes", R.A. Levy (ed.), NATO ASI Series, Series E : Applied Sciences, Kluwer Academic Publishers, Dordrecht, The Netherlands, **Vol.164**, Chap.4 (1989) pp.133.

www.manaraa.com

38. S.M. Rossnagel, "Handbook of Plasma Processing Technology", S.M. Rossnagel, J.J. Cuomo and W.D. Westwood (eds.), Noyes Publications, Park Ridge, NJ, (1990) pp.160.
39. J.S. Logan, "Handbook of Plasma Processing Technology", S.M. Rossnagel, J.J. Cuomo and W.D. Westwood (eds.), Noyes Publications, Park Ridge, NJ, (1990) pp.140.
40. J.A. Thornton, J. Vac. Sci. Technol., **11**(4), (1974) 666.
41. R. Messier, A.P. Giri and R.A. Roy, J. Vac. Sci. Technol. A, **2**(2), (1984) 500.

www.manaraa.com

PHYSICAL VAPOR DEPOSITION TECHNIQUES II: ION PLATING, ARC DEPOSITION AND ION BEAM DEPOSITION

E. MOLL
Dr. Eberhard Moll GmbH
Lübarser Str. 38
D-1000 Berlin 26
Germany

ABSTRACT. Ion plating, arc deposition and ion beam deposition are physical vapor deposition (PVD) processes for the production of nitride, carbide and oxide coatings. The application fields of these coatings are wear protection, decoration and optical interference coatings. Common features of these processes are the incorporation of reactive gas ions into the growing film and ion bombardment of the substrates before and during deposition. Ion impact facilitates process temperatures inferior to those in comparable chemical vapor deposition (CVD) processes, and ion bombarded coatings have higher adhesion strength, higher density and apparently higher elasticity than coatings prepared without ion bombardment.

1. DEPOSITION OF STOICHIOMETRIC COMPOUNDS

This lecture treats exclusively with films consisting of metal compounds like nitrides, carbides or oxides and their deposition by evaporation processes. Compared to sputtering, evaporation is a very gentle PVD process. Nevertheless, compounds are decomposed to a certain extent, i.e. the evaporation of oxides and nitrides also yields metal and oxygen or nitrogen atoms respectively. Most of them react with the growing film, but some atoms form oxygen or nitrogen molecules, which are pumped to a certain percentage by the vacuum pump of the coating system. This results in a substoichiometric film composition.

In reactive evaporation, these pumped gases are continuously replaced by means of a controlled gas inlet. But, due to the low reactivity of nitrogen molecules, only oxide films have been industrially produced by reactive evaporation. The pioneer of this technique has been Auwärter [1]. In industrial practice, oxides or sub-oxides are evaporated in a vacuum chamber in which the oxygen partial pressure is stabilized at about 0,01 Pa. The actual oxidation takes place to a great extent by chemisorption of oxygen molecules on the substrate surface [2]. Optical coatings produced by reactive evaporation are often still slightly substoichiometric and thus slightly absorbing. They have rough surfaces and a columnar or spongy

W. Gissler and H. A. Jehn (eds.), Advanced Techniques for Surface Engineering, 181–197.
© 1992 ECSC, EEC, EAEC, Brussels and Luxembourg.

www.manaraa.com

micro-structure with large void volume and great internal surface area. As a consequence of the low density, the refractive indices of these films are considerably lower than those for bulk oxides. Moreover, the refractive index and other physical properties change by the absorption of water vapor and other gases from the atmosphere. Their adhesion to the substrate is poor and their abrasion resistance and hardness are low. Most of these features can be improved by heating the substrates to about 300 °C. In fact, substrate heating has become a standard procedure in reactive evaporation. It has, however, the undesirable side-effect of producing coarser film micro-structures and higher surface roughness.

Even traces of non-oxidized metal atoms or metal suboxides in the film cause absorption [3]. Therefore, activation of oxygen [1,4] has been an important improvement in the production of films for highly sophisticated optical components such as laser mirrors with low absorption losses and high damage thresholds. Early oxygen activation methods use glow discharge ion sources, e.g. a cold hollow cathode inside a quartz tube [5]. In this context, activation means dissociation and/or excitation and/or ionization of the reactive gas. By activation, not only oxygen but also nitrogen and hydrocarbons can be made sufficiently reactive for the deposition of compound films by PVD.

A further increase of reactivity can be achieved if the activation is extended to all reactants, i.e. also to metal vapor. This is realized by using the evaporation source as the anode or cathode of a discharge. That is the way, which industrial PVD processes synthesize nitrides, carbides and borides for the production of hard coatings and of oxides for sophisticated optics.

Especially high ion densities are created by arc evaporators because the vapor itself is the preferred carrier of the arc discharge. Its high current of 100 to 300 A and even more is concentrated to the anodic or cathodic vapor source, where it ionizes practically all vapor atoms. Such an activated reactive deposition method was described by Berghaus as early as 1939 [6]. But Bunshah [7,8] was the real initiator of ARE in the field of metallurgical coatings.

A further increase of activation can be achieved when the reactive gas is introduced directly into this ion cloud [9]. In this kind of activated reactive evaporation (ARE) processes, activation is so powerful that it makes little difference whether the compound or the pure metal is used as an evaporation material.

2. CONDITIONING BY ION PLATING

The term ion plating was introduced by Mattox [10] for processes which include ion bombardment of the substrate and of the growing film. Historically, again Berghaus [11] was a pioneer of this technology. He proposed the exposure of a negatively biased substrate to a plasma in order to get "perfect structure and adhering strength".

A large number of process variants including triode and tetrode configurations have been developed. Not only evaporation sources are

www.manaraa.com

used for ion plating. Bias sputtering and some types of plasma CVD also come under the above mentioned definition. Instead of discussing the whole variety of ion plating processes, we will use the term ion plating according to Mattox's definition in which ion plating is exclusively related to effects produced on the substrate, the interface and the growing film. In fact, many effects of ion impact can easily be understood without taking the method used for ion production into consideration.

In sputter etching - the substrate preparation step preceding deposition - ion bombardment removes material from the substrate surface. However, it does not create a clean surface because the coating material previously deposited on the substrate holders is also sputtered off and redeposited on the new batch of substrates. Etching

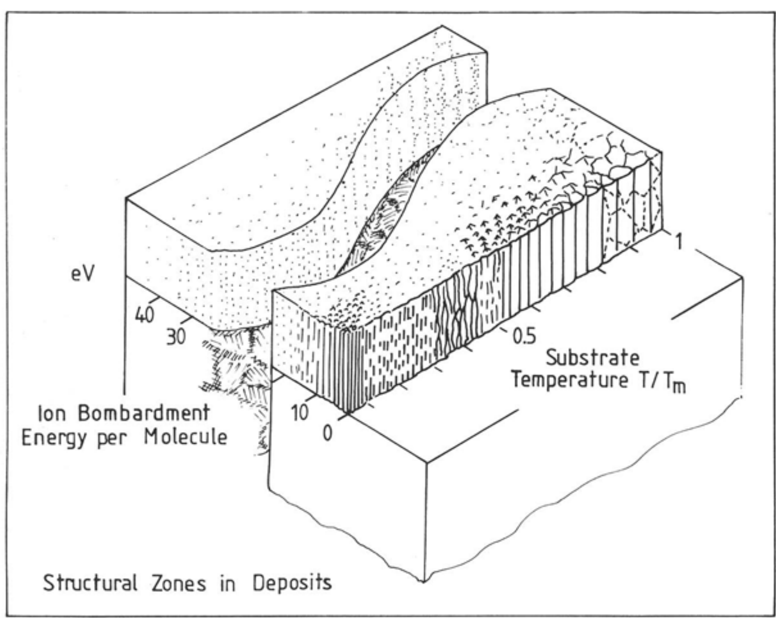

Figure 1. Structural zones in ion plated deposits. Without ion bombardment, breaking produces a crack along the interface between the film and the substrate. The edge of the film shows 3 zones: from the left to the right (1) no mobility at low temperatures (low compared to the melting point), i.e. the atoms stick at the place, where they arrived, (2) surface mobility creates columnar growth, typical for reactive evaporation, (3) surface and volume mobility create equiaxed crystallites. With ion bombardment, even at low temperatures dense and fine grained structures and a smooth surface can be achieved and the crack goes through the interface without any step. That is a simple but convincing proof for the adhesive strength to be higher than the strength of the substrate material.

www.manaraa.com

plus redeposition produce a very thin interface layer consisting of a mixture of substrate and film material. This pseudo-diffusion layer is supposed to improve film adhesion.

Ion impact during deposition causes cascades of atomic collisions in the growing film. The recoiled or displaced atoms cause a kind of continuous atomic mixing and also enhance surface migration. This results in the filling up of voids and in smoothed or graded grain boundaries. The famous structural zone diagram proposed by Movchan and Demchishin [12] and completed for sputter deposition by Thornton [13] can be modified for ion plating by adding an axis "ion bombardment energy per molecule" instead of the axis "argon pressure". In Fig. 1, such a diagram is shown [14]. The edge shows different zones, which are related to different atomic mobilities. With ion plating, even at low temperatures dense and fine grained structures and a smooth surface can be achieved, as needed for high quality optical coatings.

Another result of ion impact is the creation of point defects. These are frozen in under growth conditions that are comparable to rapid quenching. The macroscopic consequence of an increasing concentration of point defects is an increasing compressive intrinsic stress. Instead of the axis "ion bombardment energy" one could also use an axis "stress", because stress is a potential energy which is put in by ion bombardment. It would be interesting to study the relation between these two energies, which are microscopic and macroscopic descriptions of the same phenomenon. Perhaps one could find a formula for a more systematic use of residual stress in thin film engineering.

Unfortunately, there are only few attempts of a theoretical treatment of internal stresses at the interface between materials with different elastic behavior [15]. But we are aware of the fact, that the internal forces which result from all internal stresses compensate each other. Therefore, the interface, as well as the film material, and the substrate material near by the interface, are subjected to a high tensile stress with a direction normal to the film plane. This tensile stress increases with increasing film thickness, because the in-plane stresses caused by point defects and thermal expansion are independent from the film thickness, thus causing forces, which are proportional to the film thickness.

In practice, the normal tensile stress is seen by the burst off of small film particles. If good industrial wear resisting coatings are observed, one can usually find substrate material on these particles. This happens to films which are thicker than a certain critical film thickness, and it begins at sharp edges and other pointed places. The user of coated tools does not notice this phenomenon, because it happens in the coating plant during deposition or finally during the cooling down phase, if the thermal expansion coefficient of the film is inferior to that of the substrate.

The critical film thickness of ion plated titanium nitride (TiN) films on high speed steel (HSS) is on the order of 10 μm. One can show, that this limit is defined by the strength of the steel and not by the adhesive strength of the film. This can be demonstrated by bending: an ion plated film doesn't crack along the interface but, as shown in

www.manaraa.com

Fig. 1, without any step at the interface straight through film and substrate.

Often intrinsic stress is judged purely negatively, and methods are proposed to reduce it. As far as compressive intrinsic stress is concerned, there also exist very positive aspects. In my opinion, intrinsic stress is the most important reason for the surprising success of these brittle hard films, because without this stress, a hard coating on a softer substrate would break like a thin layer of ice on snow. The strain of such a prestressed film is relieved, when an external load is pressed on to the film. Obviously one should not tear the film. The usual tear off tests would yield very negative results. Fortunately, this kind of test is without any meaning.

An example: Three microns thick ion plated TiN coatings on HSS often have a total strain which is on the order of -0.5 %. This strain disappears when a ball with a diameter of 1 cm is used to make a spherical indentation with a depth of 0.43 mm. This example shows that it is impossible to deform such an ion plated TiN film up to the point where compressive stress changes to tensile stress without destroying the substrate through plastic deformation.

The total residual in-plane stress is caused not only by point defects, but also by crystal lattice mismatch between coating and substrate and by the difference between the thermal expansion coefficients of the film and the substrate. Unfortunately, only thermal stress can be calculated. For example, a TiN film on a HSS substrate deposited at 520 °C is compressed after cooling down to room temperature by a considerable 0,13 %. As a consequence, high working temperatures also reduce stress if the coating has a lower thermal expansion coefficient than the substrate. But even when the working temperature attains the deposition temperature, the prestressing by ion plating is left.

In summary, one can say that high quality coatings are both mechanically and thermally prestressed. As a consequence, they are relaxed when exposed to mechanical load and high operating temperatures.

Because of the unidirectional and temperature dependent prestressing, conclusions from mechanical tests to real mechanical applications are not easy at all. Furthermore, one should not forget, that in mechanical applications these films have only 2 purposes: (1) to continue to exist and (2) to be chemically inert.

Experience has shown that ion plating with predominantly film forming ions has many advantages over ion plating with inert gas ions. Therefore the combination of ion plating with those ARE processes in which the coating material is activated using anodic or cathodic evaporation sources results in a new type of process, which yields superior results. We call it "activated reactive ion plating" (ARIP). In the following sections of this paper exclusively ARIP processes are discussed.

www.manaraa.com

3. PROCESSES FOR WEAR RESISTING COATINGS

Chemical vapor deposition (CVD) has been the traditional method for the deposition of thin, wear resistant films. It is limited to cemented carbide tools, as only these substrates can withstand the high CVD process temperatures around 1000 °C.

In the late seventies, ARIP processes became an alternative industrial technology. As these are PVD methods, no thermal equilibrium has to be taken into consideration. Thus, wear resistant coatings can also be deposited on steel at temperatures below the annealing temperature, i.e. without soft-annealing the substrate. HSS is usually coated at about 500 °C.

Whereas CVD continues to be the most used coating technology for cemented carbide tools, there is a strong tendency to also use PVD for hard metal coating, because hard metal is not embrittled by decarbonization as it is in CVD. Therefore the cutting edges do not have to be rounded (e.g. $r = 50\ \mu m$) in order to reduce the danger of breaking. Even more than 10 times sharper PVD coated cemented carbide tools are successfully used with interrupted cutting, e.g. milling. Another advantage: steel tools with hard metal tips can be coated without destroying the brazed joint.

TiN is by far the most popular wear resistant coating. One of the reasons is the yellow color which facilitates controls of the film after deposition as well as during use. But this advantage was not the predominant argument when the development of TiN coatings on HSS tools was started. The more important reasons were the previous success of TiN coatings deposited by CVD on cemented carbide tools and, with respect to the steel substrate, the approximate correspondence of the Young's moduli and the thermal expansion coefficients. Of course, hardness and an almost vanishing chemical affinity to steel and other common materials were further important arguments. It does not seem to be easy to find a general purpose tool coating material better than TiN. In the future, perhaps Ti(C,N) will take on this job [16,17]. The color of Ti(C,N) is blue-grey and noticeably darker than that of steel.

Other coatings were developed for special tools or for tools to cut special materials. For example, (Ti,Al)N and (Ti,Al,V)N have improved high temperature resistance. Therefore, they are particularly suited to cut abrasive materials, or they are successfully used at high cutting speeds [18,19,20].

The following two sections give a short description of the predominant process technologies for the deposition of wear resisting coatings.

3.1. Thermionic Arc Ion Plating

Thermionic arc ion plating has been mainly applied to produce TiN films for wear protection as well as for decoration [21,22], but it is also appropriate to carbonitrides and to zirconium or chromium compounds. Some important details of the industrial coating sytem are shown in Fig. 2: The cathode of a non-self-sustaining arc discharge is a resistance heated filament situated in a separate chamber with raised

www.manaraa.com

argon pressure. The arc is transferred into the evaporation chamber to different anodes, depending on the process step. A small aperture mounted between the cathode chamber and the evaporation chamber confines and an axial magnetic field guides the arc plasma.

Heating is the first operation carried out inside the vacuum system. The thermionic arc, that will later be used for etching and evaporation, also serves as the heater. This is achieved by making the substrate holders and thus the substrates themselves the anode of the arc discharge (switch 6a closed). Sufficient uniformity can be achieved by magnetic dispersion [23].

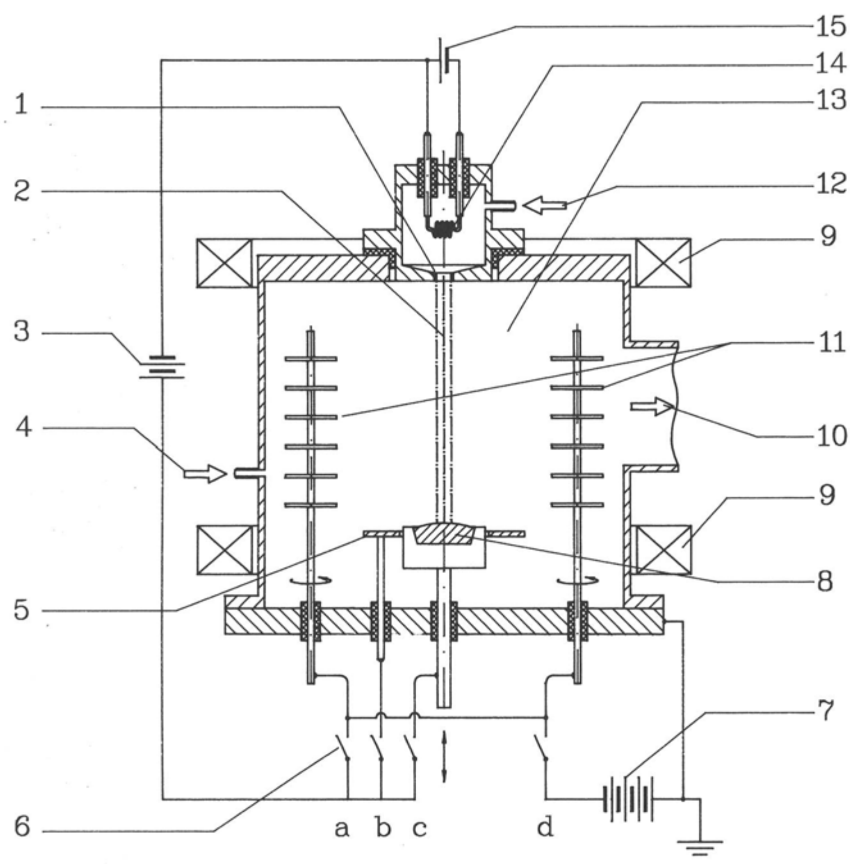

Figure 2. Thermionic arc ion plating. (1) aperture, (2) arc plasma, (3) arc supply, (4) reactive gas inlet, (5) etching anode, (6) anode switches, (7) bias supply, (8) crucible, (9) magnetic coils, (10) vacuum pump, (11) substrate holder, (12) argon inlet, (13) evaporation chamber, (14) cathode, (15) filament supply.

www.manaraa.com

Etching is performed using the thermionic arc in a triode arrangement. The substrates are immersed in the dense plasma of an arc discharge between the cathode and a metal electrode inside the evaporation chamber which acts as the anode in the etching step when switch 6b is closed. Argon ions drawn from this plasma by the bias voltage (when 6d is closed) bombard the substrates. The great advantage of this method is its high throwing power. The plasma boundaries perfectly follow the contours of geometrically complex substrates because the width of the dark space is less than 1 mm when the space charge limited ion current density is sufficiently high (e.g. > 1 mA/cm^2) and the bias voltage sufficiently low (e.g. < 200 V). In addition, the low argon pressure (e.g. 0,1 Pa) in this method ensures that the mean free paths are much longer (e.g. 5 cm) than the structural details of the substrates. Because a cathodic voltage drop needs about 10 mean free path length, the substrates are prevented from forming unwelcome hollow cathodes. Control is easy because the Langmuir characteristic facilitates the etching voltage to be adjusted independently to regulate the etching intensity.

After etching, a water cooled crucible is made the anode of the arc discharge (when 6c is closed). A magnetic field guides the arc plasma in a straight line to the anodic crucible. When the power

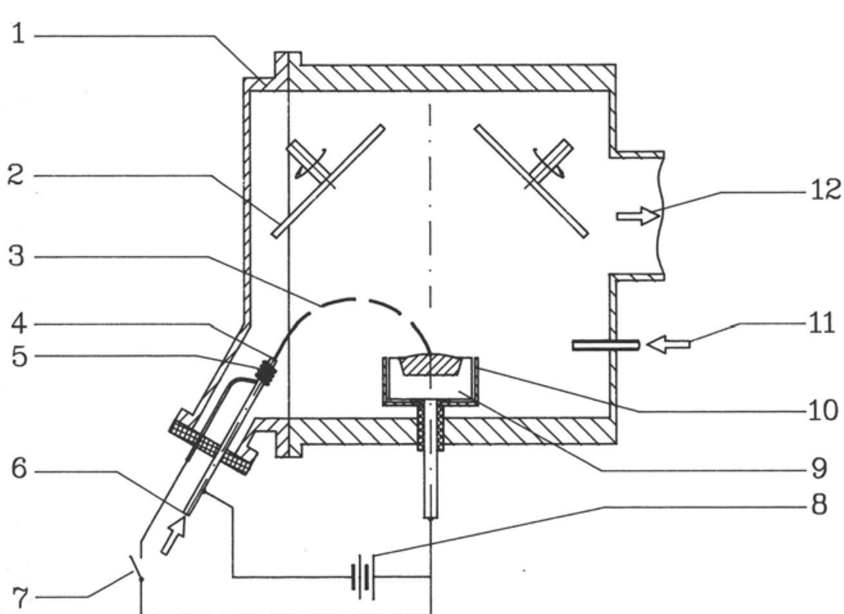

Figure 3. Hot hollow cathode discharge ion plating. (1) door, (2) substrate holder, (3) arc Plasma, (4) hollow cathode, (5) heating coil, (6) argon inlet, (7) heating switch, (8) arc supply, (9) crucible, (10) floating screen, (11) reactive gas inlet, (12) vacuum pump.

www.manaraa.com

density is high enough, certain materials such as Ti, Zr or Cr will be evaporated and then almost totally ionized. A negative dc-bias is applied to the substrates (when 6d is closed) to achieve the ion bombardment just described for etching. At high evaporation rates, the arc discharge takes place in the metal vapor instead of in the argon. This results in a concentration of the plasma beam, i.e. the formation of an anode spot.

An even more flexible system is obtained by combining an electron beam gun with a thermionic arc source [24]. This can be done by insulating the crucible of an electron beam evaporator and then using it as the anode of the arc discharge. Such systems are used in box coaters for the deposition of TiN coatings on big parts (e.g. moulds) or for the deposition of compounds which cannot be evaporated by thermionic arc evaporation alone. This dual beam evaporator also can produce extremely dense oxide coatings at low substrate temperatures as will be shown in section 4.1. in this paper.

Hot hollow cathode discharge (HCD) evaporation (Fig. 3) is closely related to thermionic arc evaporation because both processes use an arc discharge which is anchored anodically on the evaporating material. In contrast to the thermionic arc, the HCD arc is a self-sustaining discharge. The HCD evaporator for ion plating was invented by Morley in 1968 [25], and the use of an HCD device in a reactive process (chromium carbides and nitrides) was first reported by Komiya and Tsuruoka [26].

3.2. Cathodic Arc Deposition

Cathodic arcs have been used as early as 1962 to produce thin films [27]. Industrial use of cathodic arc deposition was started in the USSR where it has been called Bulat [28] or Pusk [29]. Bulat was a spin-off of the titanium getter pump development for nuclear fusion research at Charkow.

It would be more correct to use the term "cathode spot arc" in order to distinguish it from glow discharges with distributed cathodic glow as well as from anode spot arcs.

The cathode spot is the extremely small and hot cathodic root of a high-current low-voltage arc. It melts and evaporates the cathode material forming a kind of micro-crucible which has a diameter of about 1 to 20 μm and a live time of the order of 10 ns. When it extinguishes, a new micro-crucible is formed near by the former one. This way, the cathode spot moves with velocities of the order of 10 m/s on the cathode surface leaving irregular strings of small craters.

When the arc current is increased, a second, a third etc. arc splits off. This happens at characteristic current intensities, which strongly depend on the cathode material and possible contaminations or coatings. These individual arcs repulse each other, i.e. they adopt a balanced distribution on the cathode. The arc voltage is usually of the order of 20 V.

Ignition is normally realized by shorting the arc circuit either by using a mechanical contact at the cathode surface or by using a metallic coating on the insulating border of the cathode. This coating forms a conducting connection from the cathode to an ignition

www.manaraa.com

electrode, which can momentarily be shortened to the anode, e.g. by means of an electronic switch [30].

The arc moves in the direction of decreasing arc voltage. Therefore the anode should face the cathode in order to get a low voltage and stable conditions. A well suited anode is the vacuum chamber itself [28] or at least an electrode which surrounds the cathode. Also an anodic grid can be placed in front of the cathode.

On planar cathodes, the confinement of a random moving arc can be achieved by

(1) an insulated metal screen or
(2) grooves along the side edge [31] or
(3) a magnetic field (about 100 to 200 Oe) with vertical axis and acute angle (about 15° to 25°) at the side edge of the cathode [32,33,34] or
(4) a ring with high magnetic permeability [28,35] or
(5) a ring with high electrical conductivity [36] or
(6) a ring made of boron nitride [37].

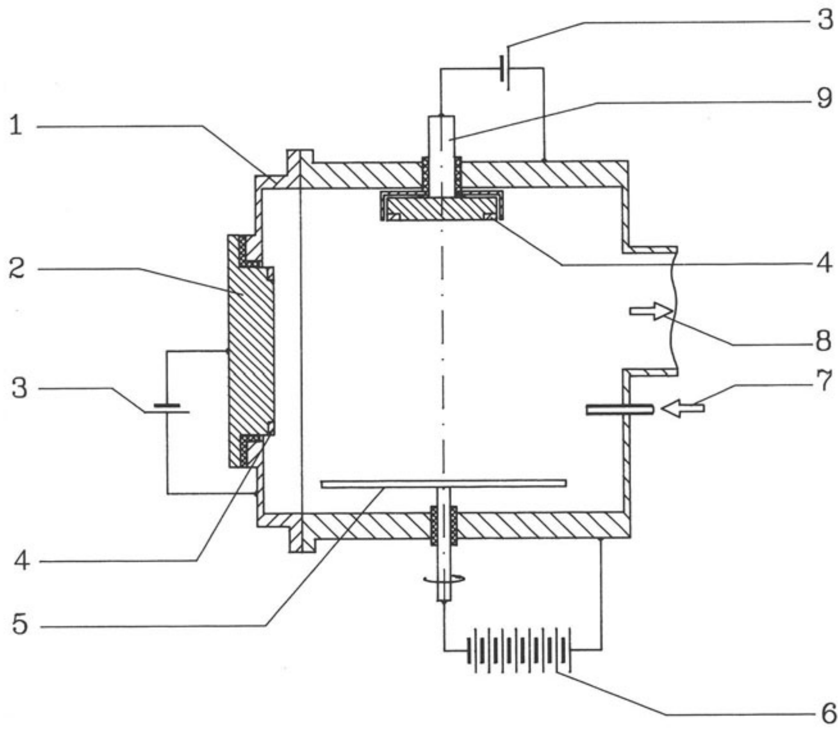

Figure 4. Cathodic arc deposition. (1) door, (2) cathode mounted from outside, (3) arc supply, (4) boron nitride insulator for arc confinement, (5) substrate holder, (6) bias supply, (7) reactive gas inlet, (8) vacuum pump, (9) cathode mounted from inside.

www.manaraa.com

In a planar magnetron field, arcs move along the race-track defined by a closed tunnel of magnetic field lines [38]. The explanation is the same as for point (3) of the preceding list: As a consequence of the Lorentz force, electrons are repelled from places where magnetic field lines come out of the cathode surface at acute angles. The ions follow the electrons by electrostatic attraction. Because ions move much slower than electrons, they are much less influenced by magnetic fields.

This type of cathodic arc is known as steered arc. In order to avoid a deep erosion groove (as known from sputter targets), the magnetic field is normally moved with respect to the cathode. An interesting curiosity is the fact, that the arc moves opposite to the direction which would be expected at first glance from the Lorentz force.

A rather new steering method is laser induced arc evaporation. Thereby, a pulsed arc voltage is applied and a locally defined laser pulse is directed to the arc cathode [39].

Besides the well-known planar cathodes, also rod shaped cathodes are in use [40]. Due to the magnetic field of its own current in the rod, the arc spot moves along the rod to its free end. There it extinguishes, and a new arc has to be ignited. One can make the spot run back and forth as well as around.

Fig. 4 shows a cathode spot arc set-up for tool coating by random arcs [41]. Unlike the processes with anodic crucibles, arc cathodes can be oriented in any direction. They can also be used to deposit alloys or hot-pressed mixtures of metal powders from a single source [19,20]. The composition of the coatings sometimes differs from that of the cathode, but corrections can be achieved by changing the bias voltage applied to the substrates [42].

In cathode spot arc processes, bombardment with cathode material ions is the most frequently used method to heat and etch the tools. These must be biased at a sufficiently high level to avoid cathode material deposition.

Other applications than tool coating seem to be prevented by the often discussed problem of micro-droplet deposition caused by splashing of the molten metal. These droplets have diameters up to about 3 μm. Their number and size decrease with increasing melting point and increasing vapor pressure at the melting point of the cathode material, increasing spot velocity and increasing surface nitridation [43]. The angular distribution of the total number of micro-droplets shows a maximum at an angle, which seems to be somewhere between 20° [31] and 60° [44] to the plane of the cathode depending on the experimental conditions.

In order to avoid micro droplets, the spot should be kept moving at high speeds. For instance, the above mentioned steering by a magnetic field can be used to speed up the motion. In fact, a decrease of micro droplet generation, but also a decrease of deposition rate compared to random arc deposition is observed at comparable test conditions (equal arc currents).

Also the positive effect of nitrogen contamination is probably due to the clearly recognizable increase in speed of the randomly moving

www.manaraa.com

spot. One should also keep in mind that most micro-droplets are already deposited during preparation by heating and etching, i.e. before the real deposition phase. Therefore, sometimes radiant heating and/or glow discharge etching is used to boost or to replace metal ion bombardment.

A rigorous method to get rid of micro droplets is the plasma-optical separator proposed by Aksenov and co-workers [45]. It guides electrons as well as positive ions on a curved trajectory through which droplets cannot pass. Thus only ions reach the substrate while droplets splash on to the chamber walls.

3.3. Ion Beam Assisted Deposition

In ion beam assisted deposition (IBAD), a beam of nitrogen, carbon, silicon or boron ions bombards the substrates. Broad high-current low-voltage ion beams can be generated by Kaufman ion sources [46]. These are multi aperture ion sources with magnetic field electron confinement and a hot filament electron source (Fig. 5). Beam diameters can be as large as 300 mm. Ion flux densities up to several mA/cm² are available at 500 to 1000 eV. Below 500 eV, flux densities decrease with decreasing ion energy.

Fig. 6 shows a system with a vapor source and suspended substrates, completed by an ion source in the bottom plate. Instead of

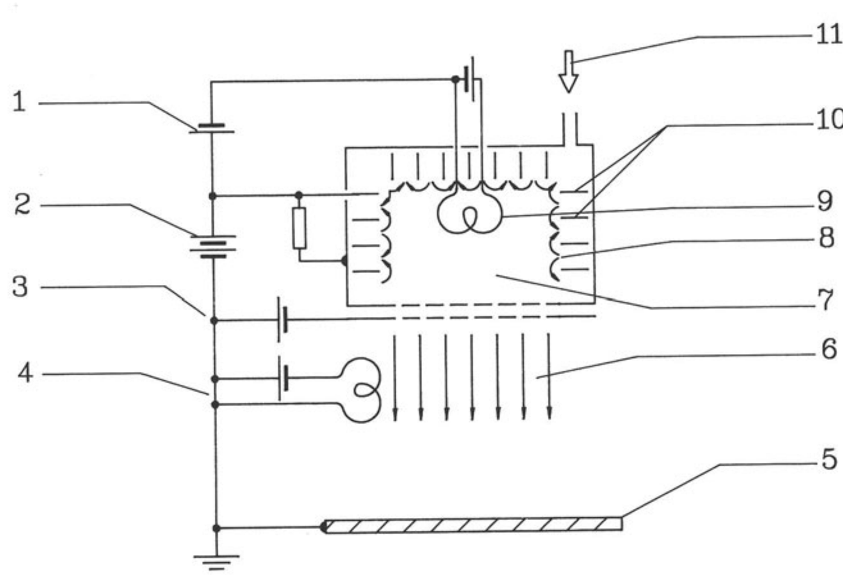

Figure 5. Kaufman ion source (according to Harper [47]). (1) discharge voltage, (2) anode potential, (3) extraction grid and acceleration voltage, (4) neutralizer filament with heating current supply, (5) target, (6) ion beam, (7) discharge plasma, (8) multiple magnetic field, (9) cathode (10) anodes, (11) gas inlet.

المنارة للاستشارات
www.manaraa.com

a normal evaporator, an ARE vapor source according to Bunshah is shown, as proposed by Shimizu and Doi [48]. The ion source is first used to clean the substrates with argon ions and in a second phase to bombard the growing film with reactive ions.

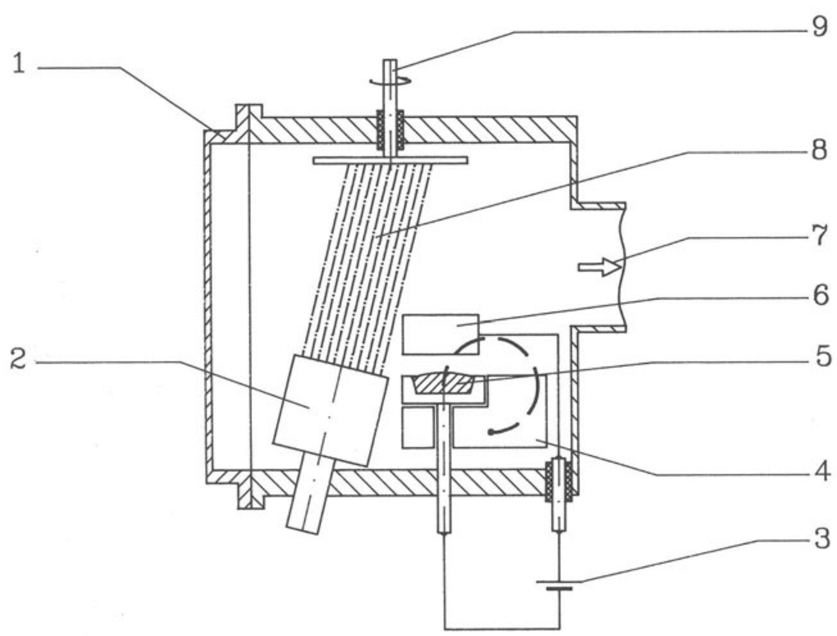

Figure 6. Ion beam assisted deposition. (1) door, (2) ion source, (3) arc supply, (4) electron gun, (5) crucible, arc cathode, (6) arc anode, (7) vacuum pump, (8) ion beam, (9) substrate holder.

IBAD is a very flexible tool for fundamental thin film research, because the ion energy has a narrow spread and can be controlled independently from the ion current as well as from the evaporation rate. IBAD can be used to synthesize new thin film materials and to tailor metastable phases [49].

4. PROCESSES FOR OPTICAL COATINGS

In optics, dielectric interference coatings are used as antireflex coatings on lenses, absorption free mirrors and filters etc. The mostly used optical film materials are fluorides and oxides. Whereas fluorides evaporate essentially without decomposition, oxides, nitrides and oxynitrides must be deposited by a reactive process in order to get low absorption.

المنارة للاستشارات

www.manaraa.com

4.1. Reactive Low Voltage Ion Plating

Optical parts are electrically insulating and cannot be biased like metal substrates. Instead, the negative charging of insulating surfaces in direct contact with a plasma can be used. Self-biasing is a well-known phenomenon with insulating substrates placed on rf-electrodes. But also in dc-plasmas, the big difference between the mean velocities of electrons and ions in the plasma causes a negative self-bias potential of about 20 to 30 V with respect to the plasma. This bias accelerates positive ions towards the substrate surface [6]. Their energies are usually not sufficient to cause sputtering, but they are higher than crystalline binding energies and can achieve all kinds of ion plating effects. The flux density can achieve the order of 1 mA/cm².

This kind of dc-self-biasing is used in reactive low-voltage ion plating (RLVIP) [6,50]. This is an ARIP process for the deposition of oxide and nitride coatings on to unheated insulating substrates such as glass. Fig. 7 shows a schematic diagram of an industrial RLVIP system [51]. The electron beam evaporator has a 270° electron gun and an insulated crucible, which can be used as the anode of a thermionic arc. In this way, two electron beams are directed to the evaporating material: the e-gun (e.g. 10 kV, 1A) and the arc (e.g. 50 V, 200 A). The e-gun is able to evaporate any material and the arc is able to

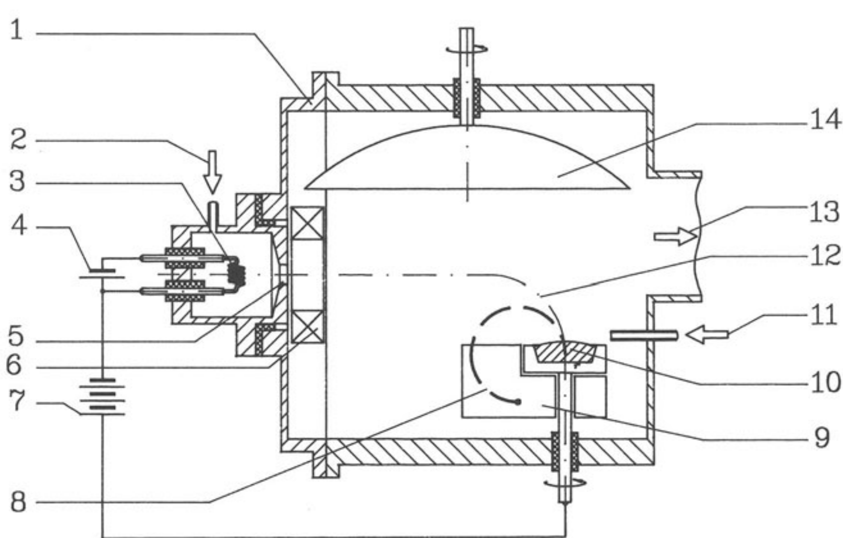

Figure 7. Reactive low voltage ion plating. (1) door, (2) argon inlet, (3) arc cathode, (4) cathode heating supply, (5) aperture, (6) coil, (7) arc supply, (8) electron beam, (9) electron gun, (10) insulated crucible, (11) reactive gas inlet, (12) arc plasma, (13) vacuum pump, (14) substrate holder.

www.manaraa.com

almost completely ionize this vapor. The substrate holder may be electrically insulated. An oscillating quartz crystal monitor or an optical thickness monitor can be used to control the deposition rate and film thickness. This system can also be used for conventional reactive evaporation, allowing alternating processes without requiring any modification of the system.

When used for RLVIP, the evaporation materials (metals or sub-oxides) form electrically conducting melts. Neither substrate heating nor any other special pretreatment is necessary. A typical gas composition is 0,05 Pa of argon plus 0,1 Pa of oxygen. Quarterwave films in the visible are deposited within two to three minutes. A film thickness uniformity of + 1 % across a 800 mm diameter substrate holder can be achieved when a static distribution shield is used.

Ion plated oxide films are fully oxidized. No absorption can be measured with simple photometric intensity methods. Measurements of the refractive indices give values close to those of the bulk materials. In all cases, the refractive indices are much higher than those of evaporated films.

The surface is very smooth compared to films deposited by conventional activated reactive evaporation. All films are very dense. That is an important feature because it hinders water absorption from a humid atmosphere and, as a consequence, it stabilizes the refractive index. RLVIP films are therefore especially suited as protective final layers.

Also the mechanical specifications of RLVIP films, especially their adherence on glass substrates and their abrasion resistance (eraser tests) are excellent.

4.2. Ion Beam Assisted Deposition

Oxygen ion beams can advantageously be generated by an ion source without hot filament, e.g. by multi-aperture rf (13 MHz) or microwave (2.7 GHz) ion sources.

As no current can flow in or on an insulating substrate, the ion bombardment of such substrates or films requires exactly the same number of positive and negative charges to impinge onto every point of the surface in order to achieve charge balance. Therefore electrons have to be added to the ion beam. This can be done by the vapor source or by a neutralizer filament (Fig. 5).

A similar deposition technique is dual ion beam sputtering, where the substrates are coated by ion beam sputtering and at the same time bombarded by a second ion beam, e.g. by oxygen ions [52]. Dual ion beam sputtering can be used for the production of multi-layer laser mirrors.

Comparing RLVIP with ion beam assisted evaporation and dual ion beam sputtering, the RLVIP film properties are similar. Nevertheless, the applications for RLVIP and the two ion beam processes probably will not overlap: Whereas ion beam processes are powerful tools for basic parameter investigations, for optimization studies or for the deposition of low-loss oxide films on a limited number of small to medium size substrates, the RLVIP process is fast and optimized for large scale production of high quality optical coatings.

www.manaraa.com

REFERENCES

1 M. Auwärter, US-Patent 2,920,002 (1952)
2 E. Ritter, J.Vac.Sci.Technol., 3 (1966) 225
3 H.K. Pulker, Coatings on Glass, Elsevier, Amsterdam 1984, 1985 and 1987, Chapter 6, p.262,
4 W. Heitmann, Appl.Optics, 10 (1971) 2414
5 J. Ebert, Proc. SPIE Vol.325 Optical Thin Films (1982) 29
6 B. Berghaus, German Patent 683 414 (1939)
7 R.F. Bunshah, US Patent 3,791,852 (1972)
8 R.F. Bunshah and A.C. Raghuram, J.Vac.Sci.Technol., 9(6) (1972) 1385
9 E. Moll, H.K. Pulker, W. Haag, US Patent 4,619,748 (1985)
10 D.M. Mattox, Electrochem.Technol., 2 (1964) 295
11 B. Berghaus, British Patent 510,933 (1937)
12 B.A. Movchan and A.V. Demchishin, Fiz.Metal.Metalloved 28 (1969) 83
13 J.A. Thornton, J.Vac.Sci.Technol., 11 (1974) 666
14 E. Moll, R. Buhl, H.K. Pulker and E. Bergmann, Surface and Coatings Technology 39/40 (1989) 475
15 H.S. Ahn and B.J. Roylance, Surface & Coatings Technol. 41 (1990) 1
16 E. Bergmann, H. Kaufmann, R. Schmid and J. Vogel, Surface & Coatings Technology 42 (1990) 237
17 J. Ebberink, Standzeitverbesserungen von Spiralbohrern mittels Oberflächenbehandlung bei der Bearbeitung von abrasiven metallischen Werkstoffen, PhD-Thesis, TH Aachen (1990)
18 H. Holleck, Surface & Coatings Technology 36 (1988) 151
19 O. Knotek, M. Atzor, H.-G. Preugel, Surface & Coatings Technology, 36 (1988) 265
20 H.-G. Prengel, PVD-Arc-Ion-Plating zur Herstellung von nitridischen Titan-Aluminium-Basis-Hartstoffschichten, VDI-Verlag Reihe 5 Nr. 205 (1990)
21 E. Moll, H. Daxinger, US Patent 4,197,175 (1977)
22 R. Buhl, H.K. Pulker, E. Moll, Thin Solid Films, 80 (1981) 265
23 E. Moll, US Patent 4,555,611 (1982)
24 R. Buhl, E. Moll, H. Daxinger, US Patent 4,448,802 (1981)
25 J.R. Morley, US Patent 3,562,141 (1968)
26 S. Komiya and K. Tsuruoka, J.Vac.Sci.Technol., 13(1) (1976) 520
27 M.S.P. Lucas, C.R. Vail, W.C. Stewart, H.A. Owen, American Vac.Soc.Trans., 2 (1962) 988
28 L.P. Sablev et al., US Patent 3,793,179 (1971)
29 A.I. Grigorov, A.M. Dorodnov, M.D. Kiselev, Tekhnol. automobilestr., 12 (1978) 10
30 Th.A. Howard, P.H. Nurkkala and G.E.Vergason, European Patent 0 211 413 (1985)
31 A.A. Plyutto, V.N. Ryzhkov, A.T. Kapin, Soviet Physics JETP 20 (1965) 328
32 H. Wroe, US Patent 2,972,695 (1958)
33 P. Sablew et al., US Patent 3,783,231 (1972)
34 A.A. Andreev and A.A. Romanov, US-Patent 4,512,867 (1981)

www.manaraa.com

35 C.F. Morrison Jr., US-Patent 4,448,659 (1983)
36 R. Buhl und Ch. Hasler, DE Patent 37 07 545 (1987)
37 W.M. Mularie, US Patents 4,559,121 and 4,559,125 (1983)
38 S. Ramalingam, C.B. Qi and K. Kim, US Patent 4,673,477 (1984)
39 D. Schulze et al., Patent DE 3901401 (1988); H.-J. Scheibe and P. Siemroth, Jahrbuch Oberflächentechnik 48 (1992) 339
40 E. Pinkhasov, DE-Patent 35 08 690 (1984)
41 H. Randhawa, Thin Solid Films 167 (1988) 175
42 H Freller, H Haessler, Surface & Coatings Technology, 36 (1988) 219
43 I.I. Aksenov, I.I. Konovalov, E.E. Kudryavtseva, V.V. Kunchenko, V.G. Padalka, V.M. Khoroshikh, Sov.Phys.Tech.Phys. 29 (1984) 893
44 A.W. Baouchi and A.J. Perry, Surface and Coatings Technology 49 (1991) 253
45 I.I. Aksenov, V.A. Belous, V.G. Padalka and V.M. Khoroshikh, Sov.J.Plasma Phys. 4 (1978) 425
46 H.R. Kaufman, J.J. Cuomo and J.M.E Harper, J.Vac.Sci.Technol. 21 (1982) 725
47 J.M.E. Harper, Solid State Technology, April 1987, 129
48 Y. Shimizu and A. Doi, US Patent 4,634,600 (1984)
49 B.G. Bovard, Thin Solid Films 206(1991)224
50 H.K. Pulker, W. Haag, M. Buehler, E. Moll, Proc.IPAT-85, Munich, CEP Consultants Ltd., Edinburgh, 1985, p.299
51 H.K. Pulker and M. Reinhold, Glastechnische Berichte 62 (1989) 100
52 C. Weissmantel, G. Reisse, H.-J. Erler, K. Bewilogua and U. Ebersbach, 3ème Colloque International sur la pulverisation cathodique et ses Applications, Nice 1979, supplement au vol. No. 196 (1979) du journal "le vide, les couches minces"

www.manaraa.com

PLASMA SPRAYING - A Versatile Coating Technique

F. Brossa(*), E. Lang(**)

CEC - Joint Research Centre
Institute for Advanced Materials
Ispra (I)(*) and Petten (NL)(**)

ABSTRACT. Plasma spray technology, with its great number of coating-substrate combinations, satisfies the demand of new materials needed to work in severe environments. After a general introduction on thermal spraying processes, the fundamentals specific to plasma spray are described. Depending on the pressure level, the chemical composition of the environment and the type of electrical arc, the plasma spray process is divided into the following types: atmosphere (APS), vacuum (VPS), inert gas (IPS), controlled atmosphere (CAPS), under water (UPS) and inductive coupled (ICPS) plasma spray. Their operating principles and their fields of application are reported. The components of the plasma torch, particularly their shapes influence, the shape at the produced arc and its capability to accelerate particles. The composition of the plasmogenic gases, their behaviour under discharge and the effects on melting and acceleration of powder particles are briefly discussed. The deposition parameters determine the microstructure of the coating: unmelted particles, poor adherence and coherence, cracks, open and closed porosity, are intrinsic to the coating procedure. Surface pretreatments, degreasing, sand blasting, sputter-cleaning and preheating, increase coating adherence. Post-coating treatments such as thermal annealing, sealing (e.g. liquid-metal, organic compound infiltration), hot isostatic pressing and electron beam or laser surface melting are used to increase the adhesion and reduce the porosity. Coating materials and coating evaluations are also considered. A broad list of industrial applications typical of plasma spray together with a potential list of further process and material developments are outlined.

W. Gissler and H. A. Jehn (eds.), Advanced Techniques for Surface Engineering, 199–234.
© 1992 *ECSC, EEC, EAEC, Brussels and Luxembourg.*

www.manaraa.com

1. INTRODUCTION

Plasma spraying belongs to the family of thermal spraying techniques which also includes traditional processes such as wire and powder flame spraying, arc spraying, transferred arc plasma spray welding, as well as high-tech methods like detonation gun coating and high-velocity flame spraying (HVOF). Plasma spraying has a particularly high potential for solving complex materials problems. It offers the possibility of coating parts made from all current base materials with almost any type of surfacing materials. Compared to other coating techniques, e.g. electron beam evaporation and sputtering, plasma spraying provides increased flexibility in the composition control of coatings, i.e. close agreement between the chemical composition of the starting powder and the deposited layer, together with reduced capital and operating costs. The technique is suitable for small parts as well as for large components. A high degree of automation can be easily accomplished, allowing the spray process to be integrated into fabrication sequences both for mass and individual part production [1].

In the past 20 years plasma spraying as a high-tech process has gained enormous importance. There is hardly any branch of industry today that does not make use of modern plasma spray coating processes, by which they can contribute substantially to improved performance of structural and machine components. Through an optimal pairing of the coating and substrate materials, properties are obtained which would not be possible with homogeneous materials.

The entire worldwide market for thermal spraying therefore amounts to several thousand million dollars annually. Of this the greatest part is represented by coatings provided by specialist firms for a variety of industries, while a significant part of the market volume is constituted by coating materials, marketed in the form of powder and wire and finally a substantial share consists of the equipment and facilities for producing coatings.

2. FUNDAMENTALS OF THE PROCESS

Thermal spraying processes have in common that they utilize a high energy heat source to melt (at least partially) and to accelerate fine particles onto a target surface. Upon impact these particles cool down and re-solidify instantaneously by heat transfer to the underlying base material and so form, by accumulation, a thick tenaciously bonded coating. While in flame spray processes the necessary energy is provided by combustion of gases, such as C_3H_8 and O_2, in plasma spraying a stream of gas is heated to a very high temperature by an electric arc. By this action the gas becomes electrically conductive due to ionization. Although the arc is already a plasma, the flow of gas heated up by the

www.manaraa.com

electrical arc is referred to as the actual plasma jet. The plasma generated by the arc consists of free electrons, ionized atoms, some neutral atoms and undissociated molecules if N_2 or H_2 are used.

The elements of a plasma spraying gun or torch are shown in Figure 1. It consists of two electrodes : a cone-shaped cathode, usually made of tungsten, inside a cylindrical copper anode which extends beyond the cathode to form a constricting nozzle. While the gas - usually argon or nitrogen or a mixture of these with hydrogen or helium - is flowing through the annular space between the electrodes, a high frequency discharge initiates an arc across the gap between the electrodes which is sustained by a steady direct current of many hundreds of amperes at a potential of ≈ 50 V. The stream of gas which flows between the electrodes stretches the arc, so that in its course from one electrode to the other, the arc loops out of the nozzle of the gun as a plasma flame [2,3].

The plasma of a plasma gun is about 1000 times denser than the low pressure plasma in a neon tube and by frequent collisions between electrons and positive ions a thermal equilibrium plasma of high enthalpy is established [3].

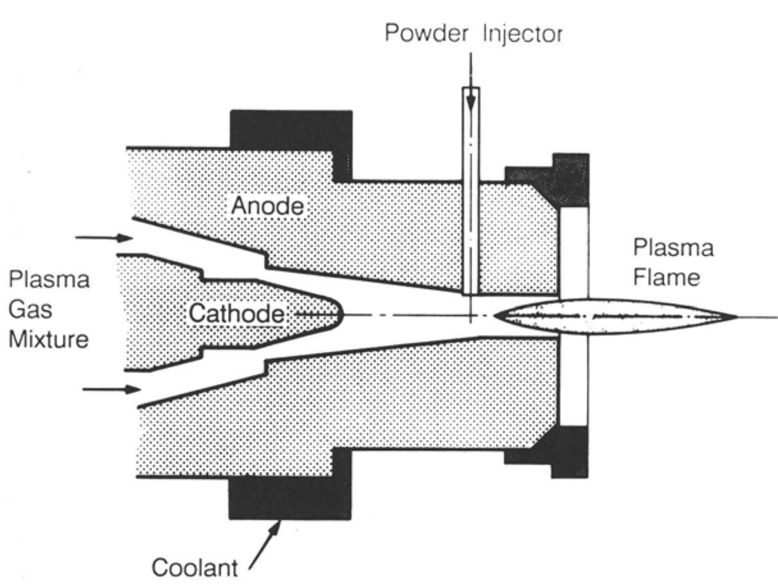

Figure 1. Schematic diagram of a plasma spray gun.

www.manaraa.com

This produces a small region of extremely high temperature into which, through a separate powder port, coating material particles can be injected. Local plasma temperatures in spraying torches are normally in the range 10,000-15,000°C but can reach 30,000°C in certain devices [2,4,5]. This implies that almost any material that can be melted without decomposition, including refractory metals or oxides, can be deposited by plasma spraying.

Water is circulated through passages in the anode and cathode to prevent them from being melted by the intense heat created in the plasma.

The arc core temperature depends not only on the current-voltage conditions, gas density and mass flow rate but strongly on the degree to which the arc can be constricted inside the torch. Arc constriction is achieved by reducing the anode bore diameter and by utilising phenomena known as thermal and magnet hydrodynamic punch [3].

In addition to the enthalpy reflected in its high temperature, the plasma contains enthalpy associated with the ionization of monatomic gases and the dissociation of molecules into their constituent atoms. Figure 2 shows the relationship between temperature and energy content of some gases commonly used in plasma spraying. It indicates that monoatomic gases (Ar, He) exhibit a linear relationship with respect to temperature until ionization takes place at very high temperatures. However, for di-atomic gases the heat content rapidly increases with temperature when dissociation occurs.

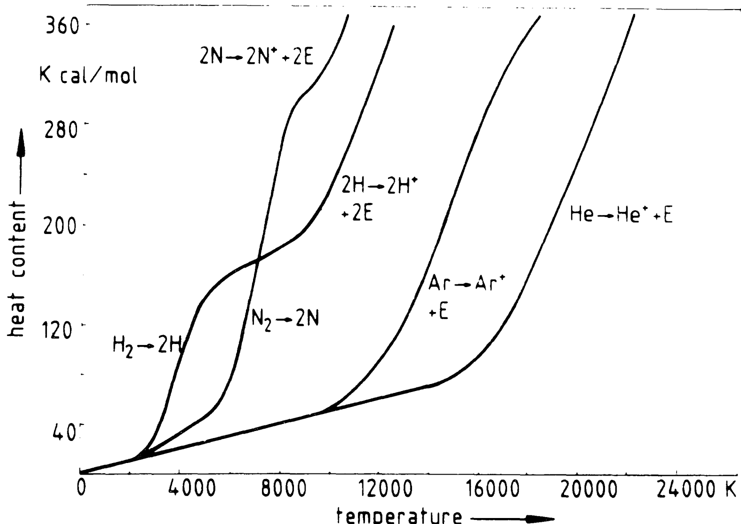

Figure 2. Relation between energy content and temperature of plasma gases (at atmospheric pressure) (Ref. 6).

www.manaraa.com

In practice, often pure argon or nitrogen is used as primary gas, together with additions of 5-25% of a secondary gas (hydrogen or helium) to increase enthalpy, but excessive flows of hydrogen or helium can cause rapid electrode erosion because of their high heat conductivity.

The high local temperature within the arc causes gas expansion whereby the gas velocity through the torch anode is controlled by its geometry and gas pressure. Most conventional plasma guns use subsonic gas flow conditions but by the incorporation of converging/diverging nozzle geometry in the anode supersonic gas flow rates can be achieved [7,8].

The velocity and temperature of the powder particles, injected with the aid of a carrier gas such as argon into the high energy plasma arc, are obviously directly related to the mass flow rate and temperature, and vary with time/distance from the entry point.

Although ideally the powder should be introduced uniformly upstream of the anode (to allow optimum distribution in the plasma stream and the longest dwell time), to avoid powder adhesion to the throat of the anode and resultant blockage, powder entry is normally arranged either where the nozzle diverges or just beyond the exit [2].

Typical powder velocities for conventional torches are in the range 120-350 m/s, while for certain high velocity torches values of 400-550 m/s are claimed [8].

For the production of dense high-strength coatings a number of delicately balanced criteria must be satisfied. The injected powder particles must absorb enough heat from the plasma jet to melt before they impinge on the substrate, or the previously deposited particles. In addition, the particles should gain, by the dragg effect, enough kinetic energy (velocity) to be able to flatten and spread out when they strike the target, flowing into crevices and tightly gripping the surface [3,9].

How effectively a given plasma flame heats and accelerates the powder particles depends on the kind of coating material, i.e. its composition, density, heat capacity, conductivity, size and shape of the particles [10]. For a given coating material and gun there is an optimum particle size. Particles much smaller than the ideal will overheat and vaporize, much larger particles will not melt and fall from the plasma jet or rebound from the target.

The way particles are fed into the flame also effects the melting and deposition, hence the quality of the produced coating. The pressure of the carrier gas must be adjusted to blow the particles into the flame but not through it. The angle of injection is critical as well; downwind injection minimizes the disruption of the plasma by the influx of particles and increases their velocity whereas injection in the upwind direction gives the powder more time to take heat from the plasma [3]. Figure 3 shows parameters involved in plasma spray processing and Figure 4 shows various positions of powder injection.

www.manaraa.com

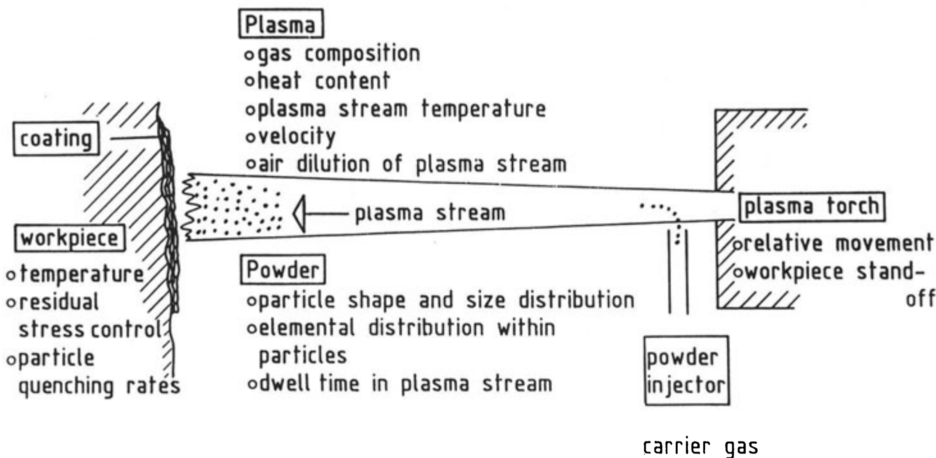

Figure 3. Parameters involved in plasma spray processing (Ref. 11).

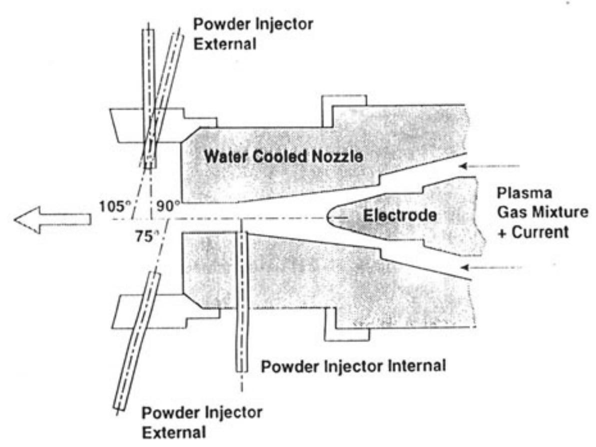

Figure 4. Plasma torch and powder injector positions (Ref. 10).

When plasma spraying is carried out in air (APS) the environment surrounding the plasma plays a significant role. Firstly the entrainment of environmental gases into the plasma jet will lower its temperature and slow down the particles as they collide with environmental gas molecules after leaving the plasma jet. Furthermore, if the entrained gas (e.g. O_2, N_2) are reactive towards certain powder elements (e.g. Al, Cr, Ti) then high temperature oxides or nitrides will be formed and included in the deposit [9] (See Figure 5).

www.manaraa.com

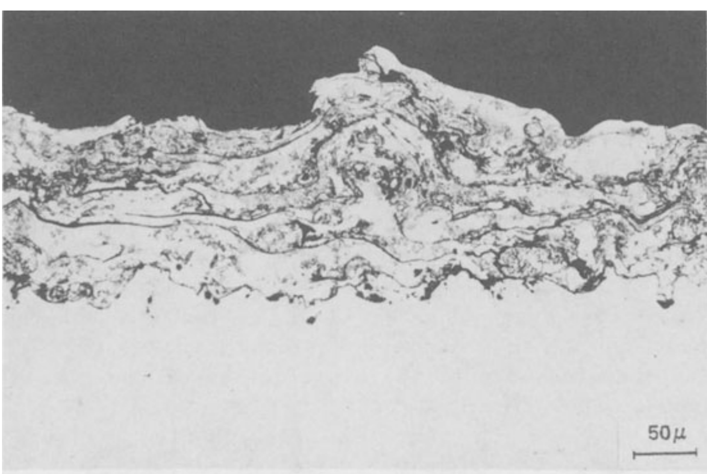

Figure 5. Optical micrograph of a representative cross-section of the aluminium coating APS deposited.

The in-situ oxidation of such elements can be reduced or totally eliminated by using an argon shroud around the plasma (ASPS) or by spraying in a chamber with inert atmosphere (IPS) or at low pressure (VPS), as will be described later. Figure 6 shows the vacuum plasma spray installation supplied by Plasma-Technik AG to the JRC Ispra Laboratory.

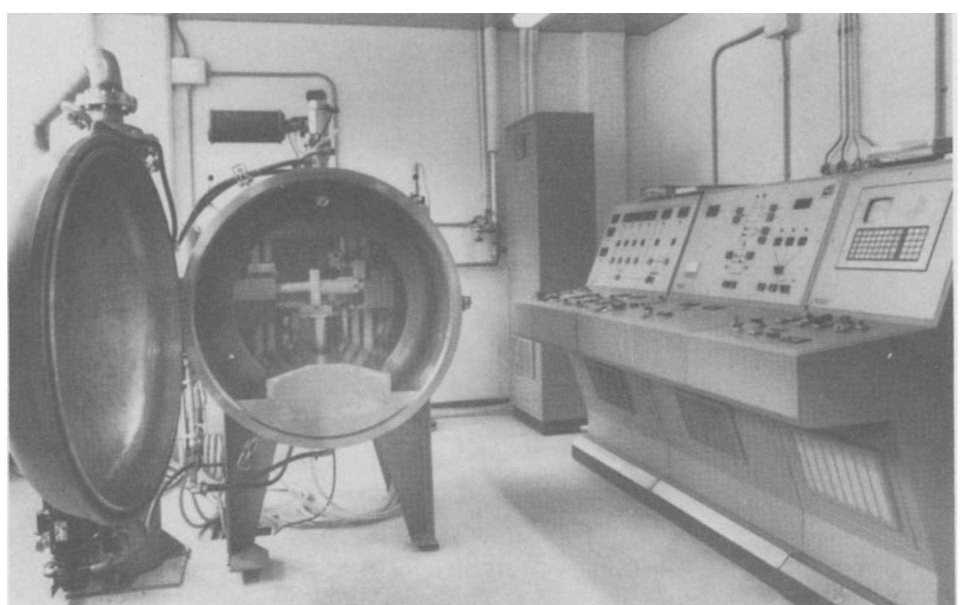

Figure 6. Computer controlled vacuum plasma spray facility.

المنارة للاستشارات
www.manaraa.com

From what has been outlined, it follows that due to the large number of parameters involved in the plasma spray process (see Figure 3) and the complex relationships that exist between some of the parameters, precise control and optimisation of the deposition process can be a very tedious and expensive operation [11]. It is for this reason that efforts are being made, at various laboratories, to develop a theoretical formulation for designing plasma spray systems by studying, in particular the interaction of particles and the plasma flame [12,13]. It has to be re-emphasized that the kinetic and thermal energy the particles gain in the plasma jet and retain until they impact on the target determine, in essence, the coating structure and thereby the coating properties. In the studies mentioned, for example, the axial and radial temperature and velocity distribution of the plasma jet have been determined as shown in Figure 7.

The spatial plasma temperature distribution (Figure 7a) was deduced from the measured volumetric emission coefficient of atomic or molecular lines for temperatures above 6000 K and by means of thermocouples. Laser doppler velocimetry on very fine Al_2O_3 particles (-3 μm) was used to determine the plasma velocity (Figure 7b).

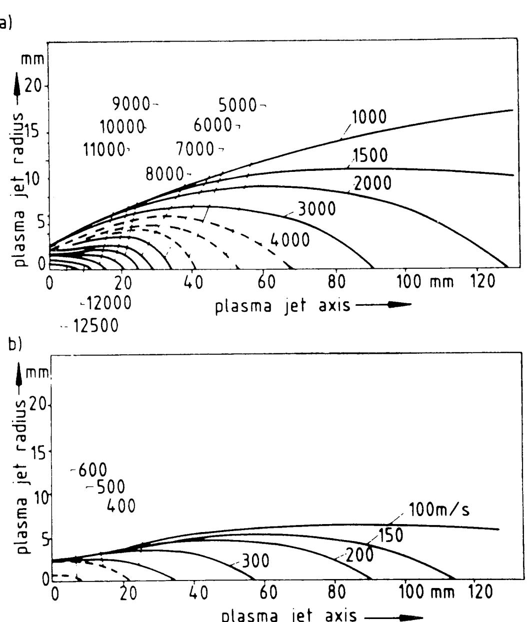

Figure 7. Axial and radial temperature (a) and velocity (b) isocontours of a N_2-H_2 DC plasma jet with P = 29 kW, N_2 = 37 NL/min, H_2 = 27 NL/min (Ref. 5).

www.manaraa.com

It is obvious that the radial temperature and velocity gradients across the plasma jet diameter cause the injected particles to arrive with different speeds and states of melting at the target, depending on their individual trajectory, which in turn is governed by their individual size and morphology.

Vardelle et al. [5] have experimentally determined the velocities of alumina particles of different size along a N_2-H_2 plasma jet axis. In the first part of the trajectory, the plasma gas velocity is very high (200-600 m/s) compared to the particle velocity (about 20 m/s). Therefore, the friction force of the plasma fluid on the particle, which is proportional to the relative velocity difference, is very high causing a considerable acceleration of the particles (up to 100,000 g). The 18 μm particles reach a maximum velocity of 275 m/s at 6 cm after the nozzle exit. The biggest particles achieve the smallest acceleration and the lowest velocity, however, they are also relatively less slowed down with increasing distance than smaller particles. By increasing the powder injection velocity (up to a certain level), the particles penetrate deeper into the high- velocity jet core resulting in higher mean particle velocities [5,9].

Also the distance from the gun to the substrate to be coated is a critical parameter, which for spraying in air typically varies between 5 and 10 cm.

3. DEPOSITION AND COATING MICROSTRUCTURE

The powder particles arrive, after having been sufficiently heated and accelerated by the plasma jet, as droplets at the target where, due to the impact, they flatten and spread out on the surface and rapidly solidify. Herman et al. [3] have extensively studied this process by scanning and transmission electron microscopy and concluded that as a splat solidifies, heat is lost to the substrate beginning at the centre which strikes the surface first. A solid core forms and remaining melt spills off it and hardens into a raised rim (see Figure 8).

At impact the particle can be solid (not molten), softened, semi-liquid or liquid and obviously the type of splat formed strongly determines the final coating structure and properties, see Figure 9. A typical 37 μm big powder particle after impact in the fully molten produces state a 1.5 μm thick disc of approximately 150 μm in diameter.

The coating is formed by the building-up of successive layers of liquid droplets flattened on impact.

The typical non-isotropic lamellar structure parallel to the substrate surface coatings is reported in Figure 9c. As Figure 10 shows, the formation of a plasma-sprayed coating is a "chaotic" process [3]. Molten particles spread out and interlock with one another. Voids resulting from shrinkage or from trapped air or gas are present, some

www.manaraa.com

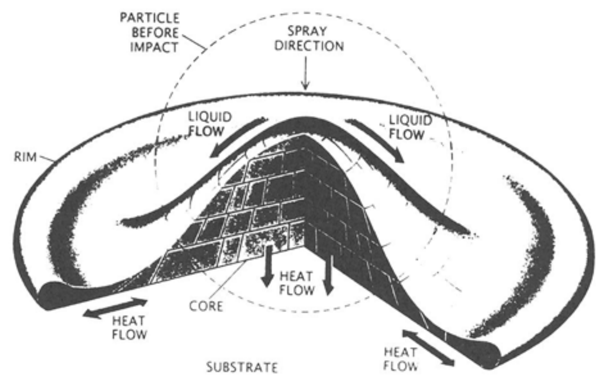

Figure 8. Splat resulting when a microscopic droplet of molten coating material strikes the surface, flattens out and solidified (Ref. 3).

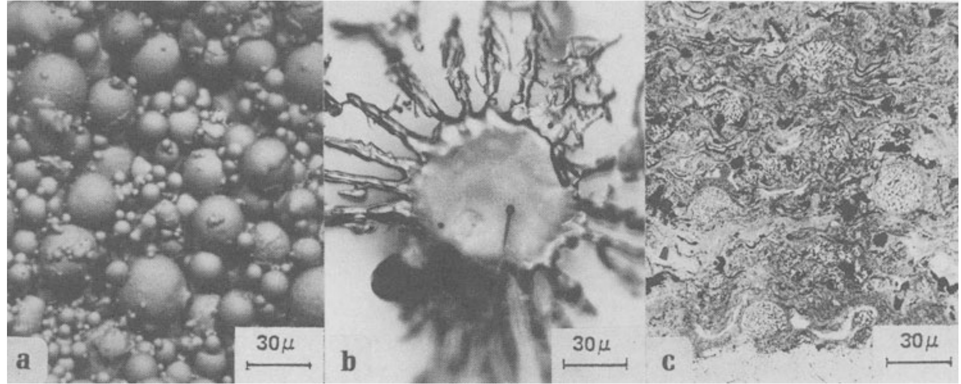

Figure 9. a) Powder of NiCoCrAlY alloy in spherical shape.
b) Molten and splashed particle.
c) Cross-section of composite NiCoCrAlY-25%Al_2O_3 coating containing molten and unmolten particles.

particles have become oxidized during their trajectory, while others may not have melted at all and simply get embedded in the deposit [14].

Cooling rates upon impact are estimated to be of the order of 10^6--10^8 Ks^{-1} [2] and the resulting rapid solidification rate produces generally a submicron grain size coating microstructure. In some cases this ultrafine cellular microstructure formed by plasma-spraying was found to have mechanical properties superior to cast or wrought materials of the same composition [15].

المنارة للاستشارات
www.manaraa.com

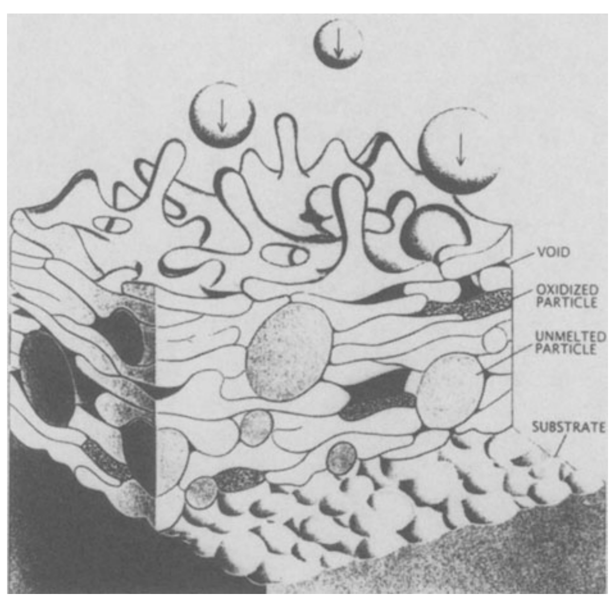

Figure 10. Schematic presentation of build-up of a plasma-sprayed coating.

Obviously the structure of a plasma-sprayed coating looks quite different from that obtained by PVD or CVD where the deposition occurs atom by atom while in spraying small, but macroscopic droplets, are striking the surface. Despite these differences in deposition mechanism and microstructure, surprisingly enough, protective coatings of the same material deposited by plasma-spraying and for example ion-plating show comparable service behaviour.

The thickness of plasma deposited layers can range from some ten microns to several mm or even cm.

4. ADHERENCE AND COHESION OF SPRAYED COATINGS

Coating-substrate adherence and inter- lamellae cohesion are of great concern since they ultimately govern the effectiveness of the sprayed deposit as a protective coating. Furthermore, the degree of contact between arriving droplets and substrate and between sequentially impinging particles affects the interface heat-transfer coefficient, hence the cooling rate experienced by the deposited splat.

To promote good coating-substrate adherence in spray deposition, it has become common practice to roughen the substrate surface by grit-blasting (with Al_2O_3, SiC or chilled steel grit) prior to spraying to a

المنارة للاستشارات
www.manaraa.com

roughness of some 4-5 μm or more. Prior to grit-blasing, of course, all oxide scales, other foreign matter, but also any oils and machinery lubricants must be eliminated. Components should therefore be degreased chemically.

The operative inter-particle and coating-substrate adhesion mechanisms have been classified by Nicoll et al. [9] into three major categories:

i) Mechanical bonding or interlocking:
A molten particle striking a roughened surface or an already solidified splat will assume the surface topography and the resulting mechanical interlocking between the existing protrusions of the surface and the deposit will lead to mechanical adherence.

ii) Metallurgical bonding:
Due to the high heat flux associated with the impinging molten droplets (and assisted by a high workpiece temperature) diffusion and microwelding between particles, and particles and substrate will occur leading to an interdiffusion zone or intermediate compound formation.

iii) Physical bonding:
The action of Van der Waal's forces may provide additional adhesion.

The bonding between coating and substrate and between individual splats is generally the result of two or more bonding mechanisms operating simultaneously. However, the degree to which a particular mechanism is operative strongly depends on the materials involved and the process variables employed. The adhesion strength of sprayed coatings may therefore vary between a few MPa and some 100 MPa.

5. ASPECTS CONCERNING POWDERS FOR PLASMA SPRAYING

Powders can be produced via various routes. For ceramics the standard method is to fuse the ceramic followed by crushing and classification (sieving). Newer methods can involve gas-atomization or the production of agglomerates starting from very fine particles (~ 1 μm) which can then be partially fused or sintered (Figure 11).

As can be seen from Figure 11 powders of a given material can have comparable grain size but quite different morphology, which has a significant influence on their spraying characteristics. Therefore, besides grain size the morphology of powder grains should also be specified.

Two powders can have the same average grain size and even the same grain size range ($\varnothing_{max}/\varnothing_{min}$) but still produce coatings of different properties using the same spray parameters if the grain size distribution is different.

www.manaraa.com

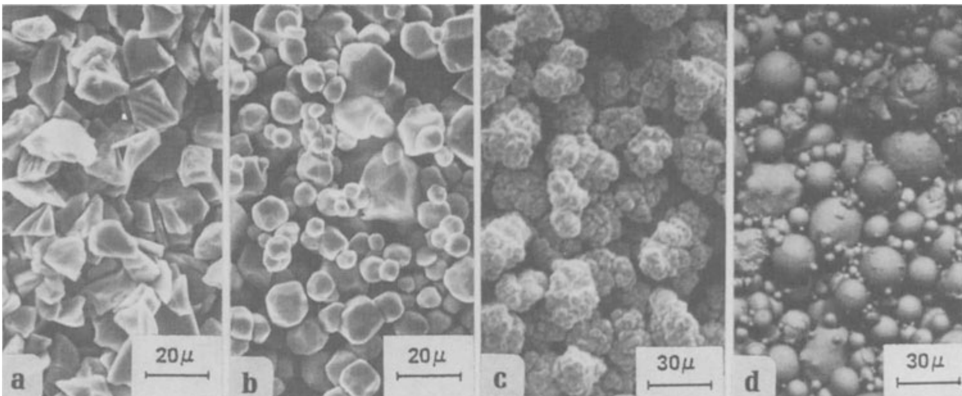

Figure 11. Morphology of plasma spray powders produced by different methods:
a) Fused and crushed (SiC).
b) Sintered (Cr_2O_3).
c) Agglomerated (Ni).
d) Argon atomized and spheroidized (NiCoCrAlY).

It has therefore to be stressed that not only the mean grain size is important but also the grain size distribution, in relation to this even the method by which the grain size distribution is being determined should be specified. Two machines for grain size distribution determination, both operating on the principle of sedimentation, have been standardised: the WAB (ASTM B 430-79) and US Sedimentometer (US ASB 7490-7967). Also Laser light scattering instruments are very successful in measuring grain size distribution of spray powders between 3 and 180 μm [9].

Most of the powder used for plasma spraying is between 5 and 80 μm in diameter. To achieve uniform heating and acceleration of a single component powder, a narrow size distribution (e.g. 5-45 μm, or 20-80 μm for ceramic thermal barrier coatings) is preferred, depending on the type of material, the required final surface quality and plasma system being used. Due to the shorter dwell time in the low pressure plasma jet, generally smaller grain sizes are used in VPS than in APS.

Small particles can not only evaporate in the flame but their trajectory may be so dominated by the momentum of the plasma gas that they follow the gas stream around the substrate rather than impacting on it. Large particles, on the other hand, may not melt or may fall from the flame or rebound from the target.

It is common practice to set for a powder screened to a particular mesh size range the spray parameters, including the spray distance. Particle temperatures are directly connected to the spray distance and with the pressure level as indicated in Figure 12 [17].

المنارة للاستشارات
www.manaraa.com

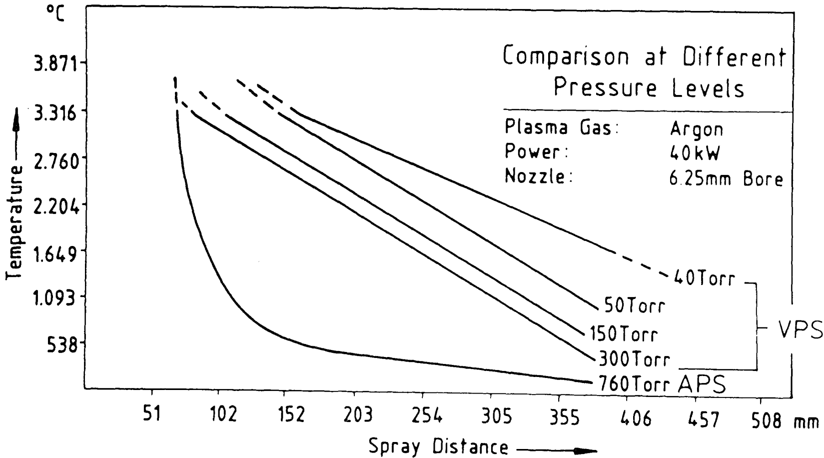

Figure 12. Centreline plasma temperature versus spray distance at different pressure levels (Ref. 17).

To allow constant powder feed rates, which is a prime condition to achieve a uniform coating thickness and quality, the powders to be injected into the plasma must possess good flow properties, which is again associated with their morphology and grain size. To avoid powder dispenser and/or torch blockage problems, i.e. to achieve smooth powder flow, the powders must be clean, carefully dried and vacuum-degassed (for VPS-application) before using them; often a heated powder hopper is also employed.

Powders are transported from the metering device to the injector via a carrier gas (argon or nitrogen) and the gas flow required to attain stable transport has been shown to be determined by

- diameter of the transport hose,
- powder density,
- size and shape of the powder,
- density and velocity of the carrier gas.

The location of the powder-injector varies with the nozzle design and/or the type of powder being sprayed and is either in the nozzle (anode) throat or downstream of the nozzle exit, in Figure 4 three possibilities are shown [9].

Composite coating structures can be obtained by using blended powders or by injecting two powders separately (possibly at different positions in the plasma) which are then simultaneously sprayed. Using two separate powder feed systems also allows production of graded coatings [18]. Coating of a MCrAlY + 20% alumina composite is shown in Figure 13.

www.manaraa.com

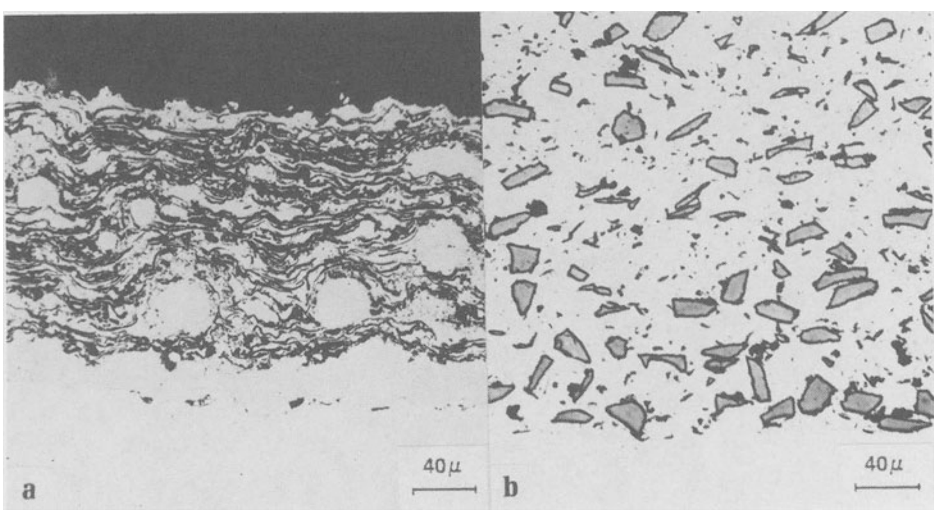

Figure 13. Composite coating structure VPS produced:
a) NiCoCrAlY + 35% Al_2O_3.
b) Al + 30% SiC.

6. THE EFFECT OF SUBSTRATE TEMPERATURE

The workpiece temperature during plasma spray is also an important process parameter highly affecting coating quality.

During the deposition the high influx of molten spray particles onto the substrate brings about a high energy input into the part due to the release of the melting enthalpy upon solidification, which will cause a continuous increase of the workpiece temperature.

An advantage of plasma spray processing is that by appropriate cooling (with e.g. compressed air or CO_2) the substrate temperature can be adjusted to higher or lower levels independent of the deposition process. If the substrate is kept at a high temperature (800-900°C) impinging particles do not solidify rapidly by quenching on impact but they stay molten longer, flowing and filling irregularities as they cool relatively slowly. This results in less porosity, better bonding and reduced residual stresses that otherwise could built up between substrate and coating [9].

In cases where a large mismatch in the thermal expansion exists between substrate and coating material, it is often preferred to keep the deposition temperature fairly low (200-300°C) to minimize the residual stresses between coating and substrate after cooling down to room temperature. The problem of the thermal, expansion mismatch could also be solved by an intermediate coating acting as a buffer between coating and base materials. See Figure 14.

المنارة للاستشارات
www.manaraa.com

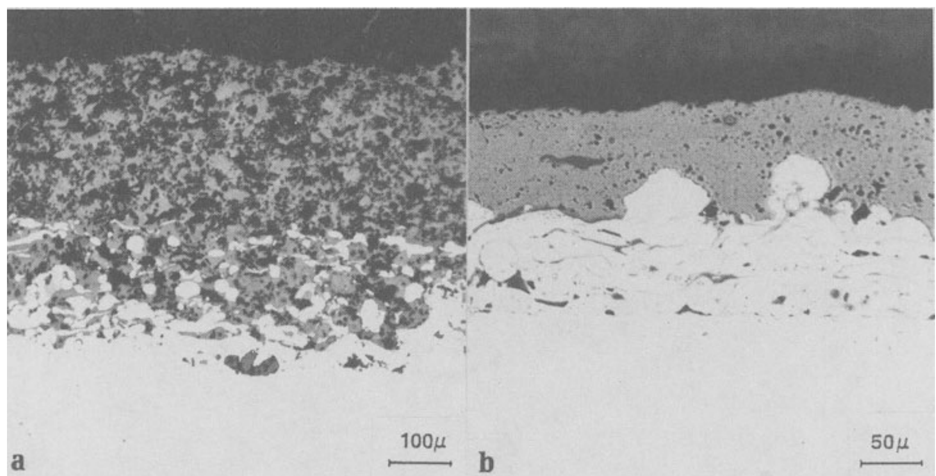

Figure 14. Intermediate layers acting as buffers for solving thermal expansion mismatch problems:
a) TBC coating joined to the Ni alloy by graded metal-ceramic bond. APS deposited.
b) Cr_2O_3 coating joined to the metallic substrate by NiAlCr interlayer.

7. EFFICIENCY

Although plasma spraying is technically a very powerful technique, it is not very attractive in terms of energy consumption. Arc current and voltage in a plasma torch vary with electrode design, gas flow, and composition while power consumption is normally in the range 5-80 kW. However, for ≈ 80 kW supplied to the AC/DC rectifier some 5-10% is lost. About 2/3 of the energy supplied to the torch is lost into the cooling water, while approximately another 30% are losses due to convection and radiation from the plasma to the environment. Hence only some 2.5-4% of the original electric energy is being supplied to the spray particles [19].

Another aspect concerns spray efficiency, i.e. how much of the injected powder is actually deposited as coating. Here losses start at the powder entry point: depending on where and under which inclination the particles are injected into the plasma, on the carrier gas flow and on their grain size and distribution varying amounts of powder may become rejected from or swept away by the expanding plasma jet. During flight, in particular, fine powder fractions may become overheated and evaporate. Depending on particle velocity and temperature at impact on the substrate, rebounding may occur or splashing may be associated with

المنارة للاستشارات
www.manaraa.com

the breaking up of the originally arriving droplets into finer particles which are reflected from the substrate (dust formation). Furthermore, when the target substrate surface is small compared with the size of the spray beam unavoidable overspray occurs. Although by careful selection of the plasma parameters in relation to the powder particles being sprayed, powder losses can be minimized to some extent, typical spray efficiencies only range between 60-85%.

8. VARIANTS OF PLASMA SPRAYING

Based upon the principles of the pressure and composition of the surrounding atmosphere, a number of process variants have been developped in recent years which concern either the way the plasma is being generated or the environment in which the spray process takes place with the general aim to further improve coating quality and/or the application range of the technique. Figure 15 gives the nomenclature of the spray processes as a function of pressure and composition of the surrounding atmosphere.

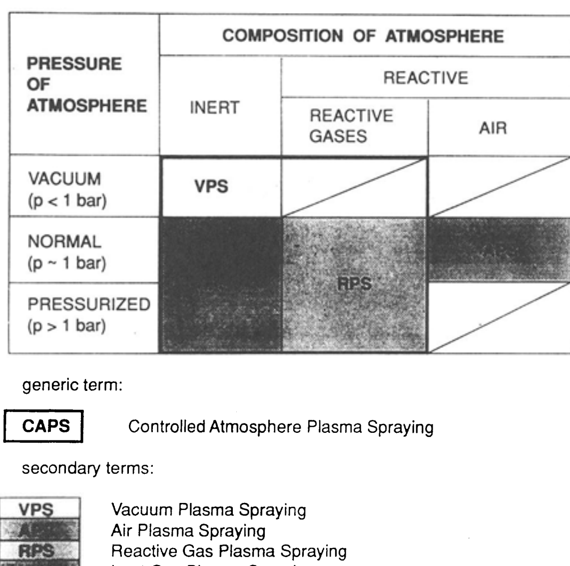

Figure 15. Nomenclature of spray processes as a function of pressure and composition of the surrounding atmosphere (Plasma-Technik AG).

المنارة للاستشارات
www.manaraa.com

8.1. Induction Plasma Spraying

Some workers are experimenting with a plasma gun in which a rapidly alternating electric field generated by a radio frequency coil replaces the DC arc as the plasma source [20]. These so-called RF plasma guns eliminate the electrodes of the arc plasma torches and thereby any contamination of the coating with material eroded from them. Although lower plasma temperatures than with the arc plasma are being obtained, the powder particles achieve due to the - here possible - axial injection longer dwell times in the plasma and a good melting degree. Other advantages of the inductive plasma are:

- uniform temperature distribution,
- high thermal efficiency,
- no pollution due to the electrodes.

Figure 16 is a sketch of both: a conventional HF plasma spray and a new Plasma-Technik inductive plasma.

8.2. High Power Plasma Spraying

This process variant, being presently still under development, achieves by a particular plasma gun configuration very high plasma power (up to 220 KW). Stabilization of the extended plasma jet, compared to conventional torches, occurs by a strong pinch of the plasma gases and additional injection of water into the HP torch [21]. This allows high deposition rates for high melting coating materials (e.g. ceramics).

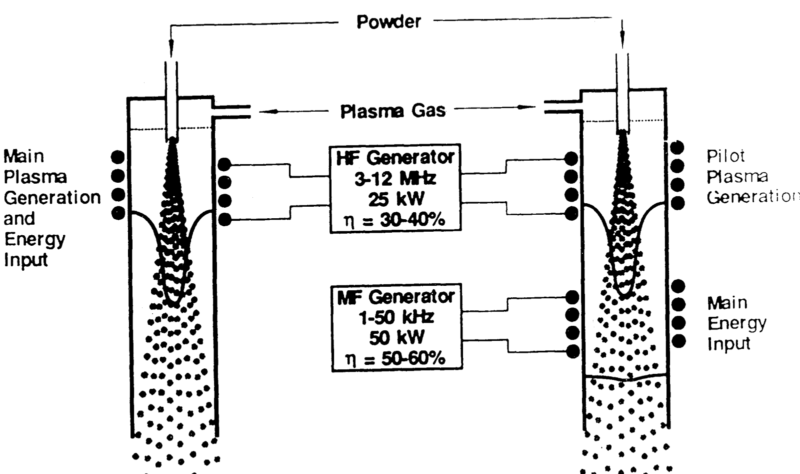

Figure 16. Conventional and new inductive plasma spray schematic (Plasma Technik AG).

www.manaraa.com

8.3. Under-Water Plasma Spraying

Another recently developed variant of plasma spraying is the underwater plasma spraying technique [22]. Although requiring very careful selection of spraying parameters, in particular of the spray distance, this technique reduces very much of the dust, sound and radiation problems as associated with APS and produces coatings of comparable quality as achievable with IPS or VPS, see below.

8.4. Gas-Tunnel Plasma Spraying

This process variant is based on a torch which utilizes a special negatively biased vortex nozzle creating a low pressure region called "gas-tunnel". Such a gas-tunnel plasma jet has a positive discharge characteristic (volt-ampere characteristic) and a high voltage. Therefore, a high power can easily be obtained. A gas-tunnel plasma jet is stable and has a high temperature and high energy density. To generate a plasma jet of the same power, a substantially smaller current is required than for a conventional plasma jet. As a result there is less damage to the electrodes. A gas- tunnel plasma-spraying apparatus feeds the spraying powder from the centre electrode of the spraying torch to the plasma. Powder supplied in this way is thoroughly melted as it travels through the long plasma jet and is then sprayed at a high speed. This type of plasma torch can be easily applied to the production of ceramic coatings [23].

8.5. Inert Gas Plasma Spraying

To reduce the possible chemical reactions of the spray particles occurring in air plasma spraying, a number of process variants have been developed.

Firstly, the Ar-shrouded plasma spray process (ASPS), developed in particular by Union Carbide, U.K., provides torch effluent protection by surrounding the powder stream with a local shield of argon gas, resulting in clean oxide-free deposits [2].

The same result can be achieved by carrying out the spray process in a chamber filled with inert gas (IPS). Such a chamber also allows processing under elevated pressure (up to 5 bar) to spray materials which may decompose at lower pressure or reactive spraying where the sprayed powder particles are deliberately reacted with a controlled atmosphere to produce new compound coatings [24]. For example, by spraying Ti-powder in an atmosphere containing methane or acetylene, partial carbide formation takes place leading to hard phase strengthened (Ti-TiC) compound coating.

The Figure 17 shows the variation in hardness values of the titanium coatings due to the increase of nitrogen content in the plasmogenic gases.

www.manaraa.com

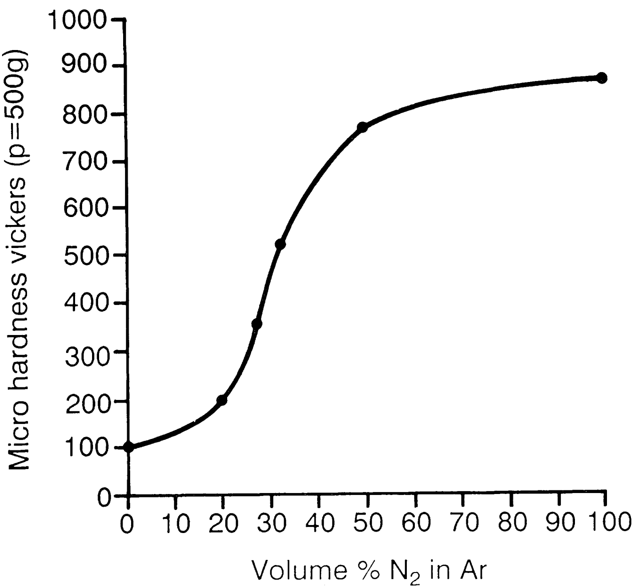

Figure 17. Variation of the hardness values of Ti VPS deposited as a function of the amount of N_2 in the plasmogenic gases.

By a particular variant of this Reactive Plasma Spraying (RPS) or Controlled Atmosphere Plasma Spraying (CAPS) process even diamond-like coatings have been deposited [25].

8.6. Vacuum Plasma Spraying

Vacuum Plasma Spraying (VPS) or Low Pressure Plasma Spraying (LPPS), as it is sometimes called, can be considered as a particular variant of IPS where spraying takes place in an inert atmosphere at reduced environmental pressure (typically at 50 mbar) see Figure 6.

The reduction in ambient pressure makes the plasma jet much longer, as a consequence the torch workpiece distance has to be increased compared to APS conditions to avoid substrate overheating. The increase in plasma stream length results in a greater particle dwell time in the plasma and more uniform particle heating, while due to the reduced environmental gas pressure (compared to APS) the braking force is removed, hence the plasma (and powder particle) velocity is much higher (up to Mach 3) whereby the droplets spread out more thoroughly when they strike the surface.

المنارة للاستشارات
www.manaraa.com

Under reduced pressure conditions, the plasma jet is not only much longer but also much greater in diameter than in APS leading to a reduction of the energy density and an increase in the simultaneously coated substrate area. The lower energy density of the LPPS-jet requires high power plasma torches (up to 120 kW) and/or the use of smaller grain size spray powder than for atmospheric plasma spraying.

Due to the longer plasma jet, slight variations in the spraying distance do not significantly affect the coating quality.

The partial pressure of the reactive residual gases, given by the final vacuum during chamber pump down, system leak rate and degassing of internal equipment surfaces, determines the remaining possible reaction of molten particles (and of the substrate) with oxygen, i.e. the oxide content of the VPS coating. Modern VPS installations are evacuated down to 10^{-3} bar and reduce the partial pressure of reactive gases to the same level as that of the plasma gases used.

Therefore, vacuum plasma spraying allows the deposition of coatings containing reactive elements, e.g. CoCrAlY or Ta, at a significantly higher quality level than is possible with APS or even the 1 bar argon shrouded process (ASPS or IPS) [26]. It can be seen from the typical micro-structure shown in Figure 18 that the VPS-route produces homogeneous, high density, almost pore-free coatings with excellent bonding and a relatively smooth surface.

While coatings produced by atmopspheric plasma spraying are typically about 75-85% dense and have an oxygen content of up to 2%, for VPS-sprayed coatings densities of up to 95% can be achieved with an oxygen content of 300-500 ppm.

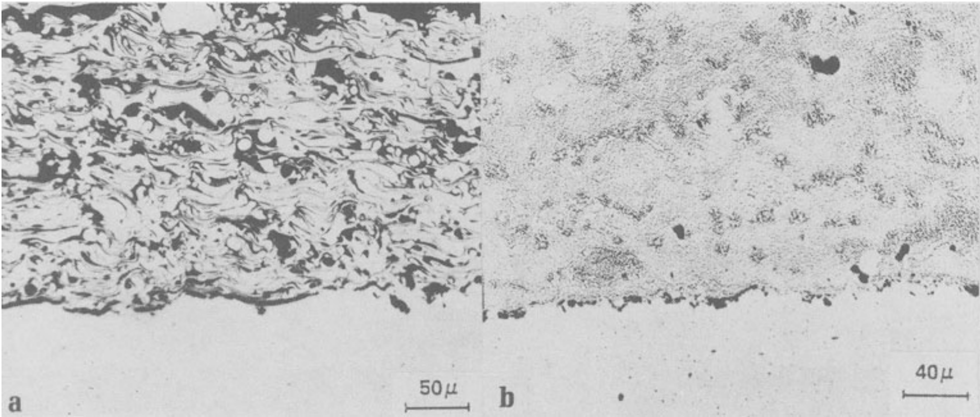

Figure 18. Cross-section of tribaloy T800 coating:
a) APS deposited.
b) VPS deposited.

www.manaraa.com

Although generally dense, pore-free coatings are the target of plasma-spraying, for certain applications (e.g. coatings for medical implants) coatings of controlled high porosity are desirable. This can be achieved by appropriate selection of the spray parameters and type of coating powder.

The VPS technique is mainly employed for the deposition of corrosion-protective MCrAlY-type (M = Fe, Ni or Co) coatings onto gas turbine components of high strength superalloys. Also wear-resistant Co-WC and nitride coatings, as well as reactive metals such as Zr, Ti, Nb, which would oxidize if they were sprayed in air, are being successfully deposited with this processing mode [27].

8.7. Transferred Arc

Operation of the plasma torch under reduced ambient pressure also allows to strike a second, so- called transferred arc between the torch and the (metallic) substrate [28]. By negatively biasing the work-piece to the gun anode, the substrate surface can be very effectively cleaned by sputtering prior to coating deposition which dramatically increases the coating/substrate bond strength. Some authors [16,29] even claim that sputter-cleaning by means of the transferred arc in VPS might substitute grit-blasting prior to deposition as a pre-treatment to obtain good coating adherence. The electrical set up of the transferred arc cleaning is shown in Figure 19.

Biasing the substrate positively to the torch anode prior to deposition leads to an intensive and rapid pre-heating of the workpiece, which gives rise to interdiffusion processes between coating and substrate resulting in good bonding. The positive substrate bias when

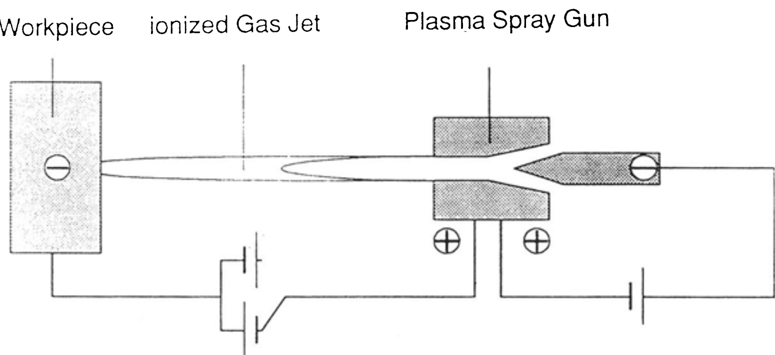

Figure 19. Basic transferred arc arrangement used for sputtered cleaning and heating substrate materials.

www.manaraa.com

applied during spraying supplies additional energy into the plasma jet, which is useful when depositing high melting materials. The advantages of this process are:

- reduction of the oxide layers,
- reduction of stesses between coating and base material and in coatings itself,
- improvement of adhesion interdiffusion between coating and base material.

9. POST-COATING TREATMENTS

Although as-deposited (metallic) coatings demonstrate good metallurgical bonding with the substrate, in particular when produced by the VPS-technique, it is advantageous to enhance the degree of coating/substrate interdiffusion by applying a post-coating heat treatment. This is normally accomplished under vacuum or inert environment using temperatures and times able to produce thin interdiffusion layers. Apart from providing enhanced bonding, this treatment also promotes recrystallization of the original lamellae structure leading to a homogenization of the coating composition and some reduction in residual porosity. See Figure 20.

Shankar et al. [26] have also shown that by a post-coating HIPing-stage porosity levels in plasma-sprayed coatings can effectively be reduced to 4%.

They have also indicated that shot peening can be a useful technique to densify certain types of plasma-sprayed coatings also reducing their surface roughness.

Laser and electron beam post-coating treatments have been (at least on laboratory scale) successfully employed to further improve

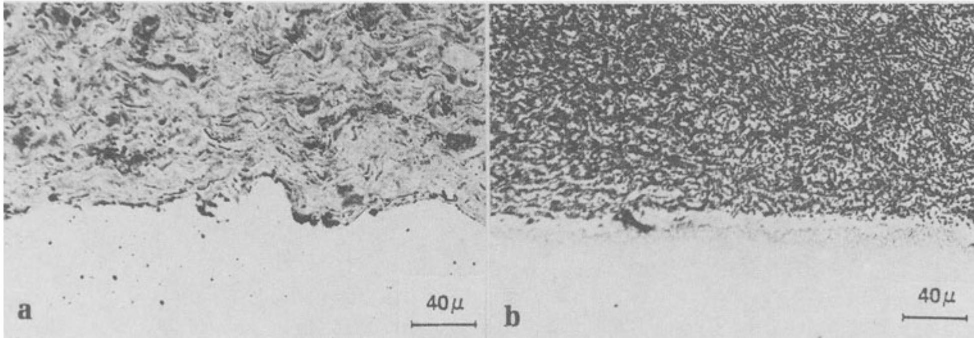

Figure 20. Coatings of the NiCoCrAlY alloy VPS produced:
a) As deposited.
b) After thermal treatment at 1080°C for 4 hours under vacuum.

www.manaraa.com

plasma-sprayed coatings [29]. Figure 21a shows a cross-section of a W-5Re coating VPS after electron beam surface remelting.

Other techniques referred to in the literature to close surface-linked porosity are post-coating chemical vapour infiltration [30], sealing with epoxy or phenolic resin [6,31,32,33] or liquid metal. See Figure 21b.

Coating surface roughness depends primarily on the powder grain size being used in the deposition and can be improved by using vibratory media finishing techniques or shot peening.

10. EQUIPMENT FOR PLASMA SPRAYING

Many authors [9,16,17,34,35] have already described in great detail modern fully automized systems for plasma spraying, at both ambient atmosphere and low pressure conditions, outlining the specific requirements for the various components of such sophisticated systems.

The basic structure of a VPS system is shown diagramatically in Figure 22.

Recently mini plasma torches have become available which will fit physically inside diameters > 45 mm and by which coatings at 90° spraying incidence can be applied to internal surfaces e.g. tubes. Mobile APS units have also been developed. This type of unit could have a wide range of applications in the field of in-situ repair and maintenance. Figure 23 shows the mobile plasma spray system produced by Plasma-Technik.

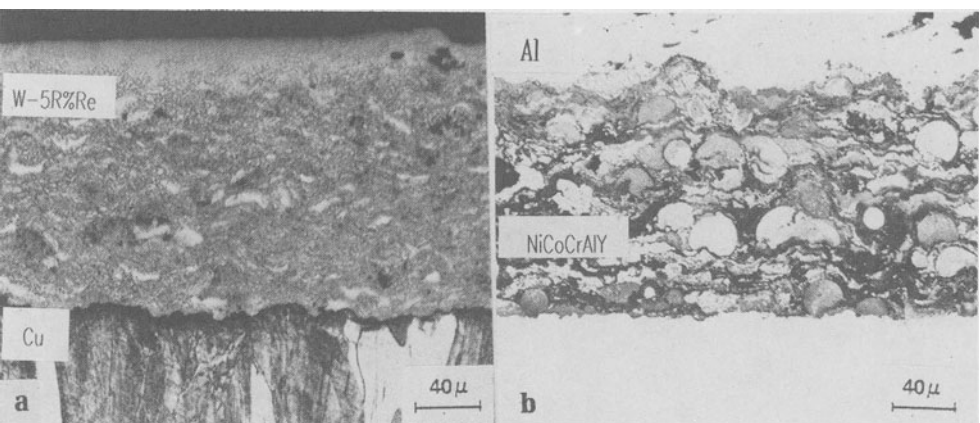

Figure 21. Cross-section micrograph of:
a) W-5% Re coating VPS after E.B. remelting.
b) NiCoCrAlY coating APS infiltrated by diffusion of liquid Al.

www.manaraa.com

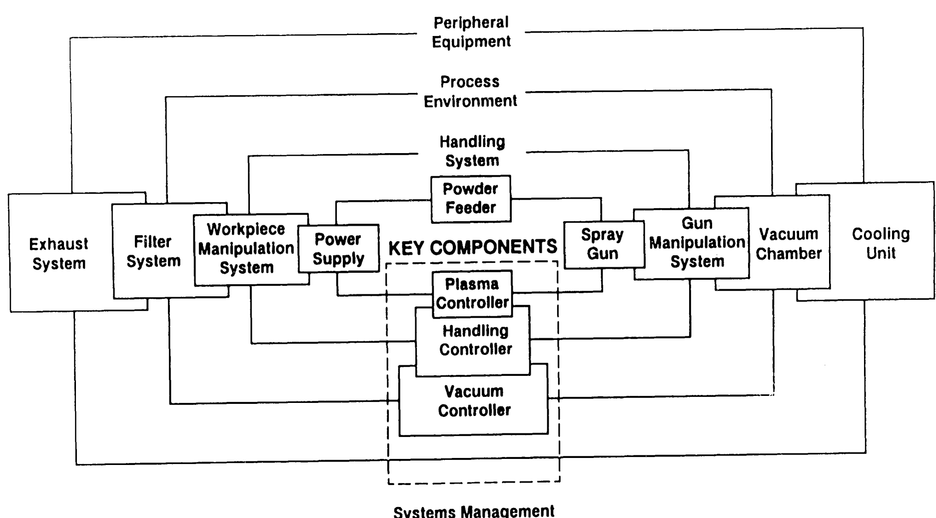

Figure 22. Schematic structure for a VPS/CAPS system.

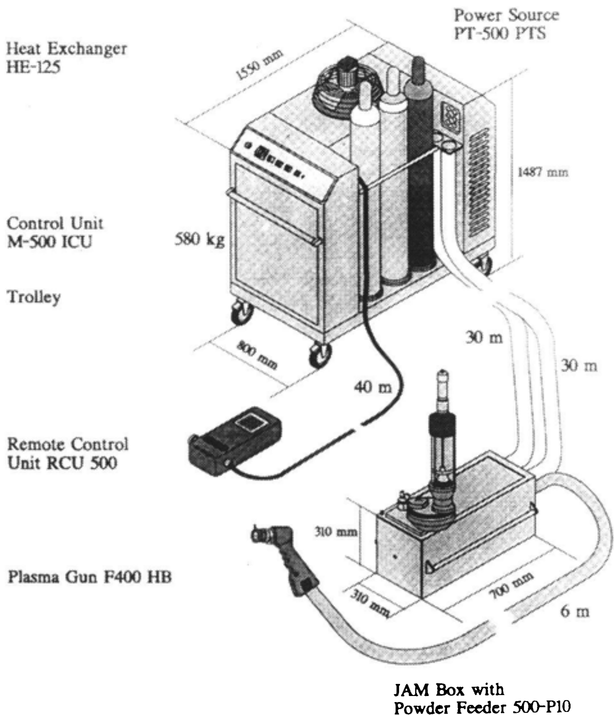

Figure 23. The mobile plasma spray system M-500T constructed by Plasma-Technik AG for in situ repair and maintenance.

المنارة للاستشارات
www.manaraa.com

10.1. Gun/Workpiece Handling

In a line-of-sight process such as plasma spraying the metallurgical structure of the coating varies with the angle of deposition. Coatings having the highest density and bond strength are achieved with 90° spraying incidence. The need to achieve a spray angle of as near to 90° as possible and to maintain torch-to-workpiece distance during spraying, which is essential to achieve uniform coating thickness, can cause problems in coating complex components (e.g. gas turbine airfoils).

This requirement and the need to eliminate, as much as possible, the human factor to achieve good, reproducible coating quality, has prompted the development of fully automated gun and workpiece manipulation systems. Mostly the gun is operated through a 5- or 6-axis robot, while the workpieces are correspondingly manipulated by a 3-axis CNC-controlled turntable or lathe. The relative movements of parts and torch are controlled by sophisticated computer programmes, which can also command the plasma spray parameters and the powder feed rates.

The disadvantage of high investment costs associated with a VPS-system is offset by the following advantages:
- considerably lower noise levels, radiation and dust problems,
- capability of spraying powders with high oxygen affinities,
- significant improvements in coating quality.

11. COATING MATERIALS

All materials which comply with the following requirements are suitable as spray materials for the production of high quality plasma-sprayed coatings:
- the spray material must melt without degradation, i.e. not thermally decompose, sublime or react with the plasma or environment gases,
- the spray material must be available as powder in a form suitable for spraying, e.g. appropriate grain size, distribution and grain shape.

At present, several hundred different materials are plasma sprayed. They can be classified as follows [1,36]:
- Pure metals: Al, Cr, Ni, Mo, Ta, Pb, Zn.
- Alloys: Ni-Al, Ni-Cr, Pb-Sn, Co-Mo-Cr, Ni-Cr-Al, Cu-Ni-In, MCrAlY (M = Co, Ni, Fe), Co-Cr-Ni-W, Co-Mo-Ni-Si, Ag-Cd-Sn-Cu, Co-Cr-W-Ni-V, NiCrSiBFe.
- Pseudo-alloys: Cu-W, Bronze-steel, Al-Mo.
- Ceramics:
  - borides: TiB_2, ZrB_2.
  - carbides: TiC, Cr_3C_2, NbC, TaC, WC, TiC-WC.
  - nitrides: TiN, ZrN, TaN.
  - oxides: Al_2O_3, TiO_2, Cr_2O_3, ZrO_2, Al_2O_3-Cr_2O_3, Al_2O_3-TiO_2, Cr_2O_3-TiO_2, ZrO_2-MgO, ZrO_2-SiO_2, ZrO_2-CaO, ZrO_2-Y_2O_3.

المنارة للاستشارات
www.manaraa.com

- Cermets:
  - carbide-metal Cr_3C_2-NiCr, WC-Co.
  - oxide-metal Al_2O_3-NiAl, Cr_2O_3-NiAl, CoCrTaAlYC-Al_2O_3, CoCrWNiVC-Cr_2O_3.
- Others: AlSi-polyester
  Ni-graphite
  NiCrFeAl-BN

An analysis of the technical literature on thermally sprayed ceramic materials over the last 20 years [37] revealed that 60% of the references were concerned with oxides and 21% with carbides. The scarcity of data on other materials does not reflect a lack of interest but rather the practical problems arising with materials that do not melt without decomposition (e.g. SiC, Si_3N_4) or react with oxygen (most borides, carbides and nitrides) as the hot particles traverse the ambient atmosphere between gun and workpiece (in APS).

Depending on the composition, combination and mixing ratios of the various spray material components, layers with unusual characteristics can be produced by plasma spraying. Such layers and properties cannot be obtained by other coating processes or with traditional homogeneous materials.

Of particular interest is the possibility of producing composite coating structures by combining two starting materials via one of the following routes:

- both materials melt in the plasma stream and impact as molten particles on the substrate, or
- only one material melts, while the other is built into the coating as solid particles. In this case, also materials with an unstable liquid phase can be incorporated in the coating.

Figure 24a shows Ni-graphite composite and Figure 24b a multilayer Al-Cu.

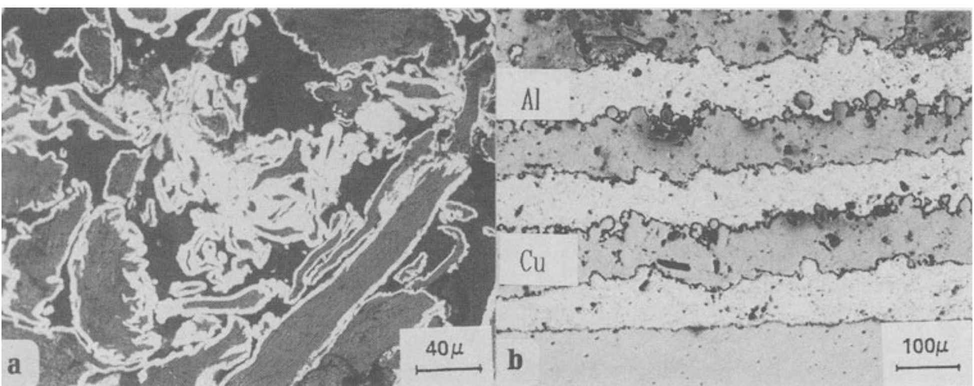

Figure 24. Cross-section of composite layers formed by VPS process:
a) Ni-graphite layer APS deposited.
b) Multilayer Al-Cu VPS deposited.

المنارة للاستشارات
www.manaraa.com

Gruner [18] has presented a detailed review of this interesting processing mode.

Another particular application of the plasma spraying technique is the deposition of materials in thick layers on a pre-formed mandrel. If the mandrel is removed afterwards, free standing bodies of complex shape and microstructure can be obtained.

By depositing on a Cu-mandrel a layer of hard Cr_3C_2+NiCr material and then a 2 mm thick layer of the superalloy René 80, Gruner [35] produced, after removal of the Cu-support, a small bore tube with a wear-resistant coating inside.

Ti capsule for dental prosthesis have also been produced at the J.R.C. using the same method [27].

12. QUALITY CONTROL

The coating evaluation can be made by destructive (DT) and non-destructive testing (NDT). The chemical composition of the deposited layers can be determined by chemical and/or Energy Dispersive X-ray Analysis (EDXA).

Metallographic techniques give information on the thickness, surface roughness, coating stratification, open and close porosity, cracks, oxide and inclusion concentrations, morphology and bonding flaw at the interface coating-substrate.

The bond strength of the plasma sprayed films is usually determined by bending and tensile adhesion tests. Destructive testing, applied on a laboratory scale, on random samples is then extrapolated to untested specimens prepared with the same coating parameters.

By extending industrial applications of plasma sprayed coatings into more sophisticated areas the NDT demand increases in view of more economic and a better qualified quality control.

Thus eddy current, thermographic and ultrasonic devices have been developed and applied to detect the coating thickness, cracks, pores, flaws and other defects in sprayed films.

Eddy-current measurement is the most used technique for determining the coating thickness of insulating coatings like TBCs even if other NDT are available such as thermo-electric touch or capacitance gauge.

Thermography employs an infrared (IR) detector which analyses a surface which has been heated by a laser beam. Porosity inclusion, coating detachments have an influence on the heat transfer and consequently on the relative IR image.

Bonding flaws, pore clusters and cracks can also be detected by ultrasonic testing (UT).

The automization of plasma spray processes increases the need for quality control throughout the deposition process and only NDT can satisfy this need.

www.manaraa.com

13. APPLICATIONS OF PLASMA-SPRAYED COATINGS

Up to now, plasma spray coatings have been successfully used for the following applications:

- wear protection against:
  - abrasion,
  - scuffing,
  - erosion,
  - fretting corrosion;
- corrosion protection against:
  - oxidation,
  - hot gas corrosion,
  - atmospheric corrosion,
  - immersion corrosion;
- thermal insulation (thermal barrier);
- repairing parts by adding material onto worn locations, or reconstituting a part which has been rejected due to faulty material or incorrect machining.
- surfaces with special properties:
  - electrically insulating or conducting,
  - self-lubricating coatings,
  - abradable coatings,
  - increase of surface area and structuring of surfaces
  - diffusion barriers
  - active or inert surface coatings,
  - surfaces with catalytic properties,
  - ion conducting conditions,
  - decorative coatings
  - coatings which are highly absorptive or reflective to light.

Table 1 gives an overview of the various materials which are being sprayed, the coating requirements and the corresponding application or function.

The principal applications for sprayed coatings lie in five areas: wear resistance, corrosion resistance and thermal barriers, electrical functions and special applications.

Particular commercial importance has been gained by MCrAlY-type coatings deposited by VPS-technique onto gas turbine components, both as oxidation corrosion protective layers and as bond layers for the so-called thermal barrier coatings (TBC), the thermally insulting layer, often partially-stabilized ZrO_2, is generally deposited by the APS mode.

Due to the capability of the plasma spraying technique to deposit a huge range of materials and its feasibility for mass production, plasma-sprayed coatings are finding steadily increasing use in nearly every sphere of industrial activity, e.g. aerospace [38,39,40], automotive [40,41], electronic [42,43], medical [44,45], nuclear [46,47,48], power generation [49,50], textile [51,52] etc.

المنارة للاستشارات
www.manaraa.com

TABLE 1. Coating materials, requirements and functions.

WEAR PROTECTION	CORROSION PROTECTION	THERMAL FUNCTION	ELECTRICAL FUNCTION	SPECIAL FUNCTION
- Abrasion	- Atmosph. corrosion	- Thermally insulation	- Insulating	- Bioactivity
- Adhesion	- Immersion corrosion	- Reflection	- Conductivity	- Repairing
- Erosion	- Oxidation	- Absorption	- HT-super-conduct.	- Free standing parts
- Pitting	- Sulfidation		- Shilding	- Sensors
- Fretting				- Catalytic
- Abradables				- Target
Coating requirem.	**Coating requirem.**	**Coating requirem.**	**Coating requirem.**	**Coating requirem.**
- Good wear charact.	- Corrosion resistance	- Oxidation resistance	- Electrical insulator	- Rough surface
- Good bond-ing	- Low poros-ity	- Low therm. conductiv.	- Electrical conductor	- Bonding
- Good cohesion	- Dense coating	- Comp. heat expansion coeff. with the sub-strate	- Low porosity	- Bone/tissue activity
- Homogenity	- Good bond-ing	- Thermal stability	- Insensitive to humidity	- Chemical stability
- Low poros-ity	- Comp. heat expansion coeff. with the sub-strate	- Mechanical properties	- No micro cracks	- Chemical reactivity
- High hardness		- Controlled porosity	- No oxide included	
Materials	**Materials**	**Materials**	**Materials**	**Materials**
- CuNiIn	- MCrAlY	- ZrO_2-Y_2O_3	- Al_2O_3	- HA
- WC-Co	- NiCr	- ZrO_2-MgO	- TiO_2	- Ti
- Al_2O_3+TiO_2	- Mo		- $Y_1Ba_2Cu_3O_7$	- Al_2O_3MgO
- Cr_2O_3	- Hastelloy			- NiAl
- AISI-Plastic	- Inconel			- TiN

المنارة للاستشارات
www.manaraa.com

The possibility of depositing composite coatings by plasma spraying has been indicated already, and Table 2 [18] gives an overview of various material combinations and their typical applications.

Special applications of plasma spraying techniques concern the production of moulds on dissolvable cores, i.e. fabrication of parts of complex shape from materials which are difficult to form or machine by traditional process routes (e.g. TiAl, Ti_3Al, Ta, etc.), refining and spherodizing of powders, production of sensors, etc.

The General Electric Company is using vacuum plasma spraying to make freestanding components, intricate aircraft-engine parts formed by plasma-spraying a superalloy on a removable substrate. Other workers spray ceramic particles or fibres and a metal powder simultaneously to produce a strong, stiff composite material with the ceramic particles dispersed in a metal matrix. In a joint program the U.S. Naval Research Laboratory and Metco have fabricated a thick film of high-temperature superconductor by plasma-spraying the compound in the form of a powder, a strategy that could play an important rôle in the manufacture of future superconducting devices [3].

TABLE 2. VPS - sprayed composite coatings and their applications (Ref. 18).

Material combination	Composite	Main property	Application
Metal/ Plastic	MCrAlY + Polyester	Controlled porosity	Abradable coating
Mixture of metals	Superalloy powder + Braze material	Controlled braze filler content	Wide gap brazing
Cermet	MCrAlY + Al_2O_3	Thermal conductivity	Oxidation + erosion protection
Metal/ refractory	Ti + TiB_2	Decrease sputter yield	Low-Z coating
Refractory/ metal	Cr_3C_2 + NiCr	Reduce carbon loss, increase ductility	Abrasion protection
Refractory/ refractory	non-stabilized and stabilized oxides	Increase thermal fatigue	T B C

www.manaraa.com

14. CONCLUSIONS

Plasma spraying technology, being essentially "materials engineering" as Villat [1] puts it, has a great potential in connection with:

- improvement of the performance of parts and machine components by the pairing of optimum base material and surface coating properties, so as to obtain a combination of characteristics which would not be possible with homogeneous materials;
- lowering of costs, since inexpensive base materials are improved by high grade coatings;
- decrease of economic dependency, i.e. where a vital or strategic material has to be obtained from another country and where supply bottlenecks have occurred;
- best use of resources, by sparing use of materials which are expensive, rare or otherwise difficult to obtain;
- innovation of technical products, by the provision of new fabrication possibilities and component properties, as well as new product characteristics.

Even though PS processes and in particular VPS are costly techniques, the market for the coatings produced will have more than doubled within the next ten years.

The superior properties of the films and their ability to provide solutions unattainable by other methods makes these processes most attractive. These coatings can also be prepared with a high deposition rate while maintaining excellent reproducibility.

By the use of complex composite powders and a more profound knowledge of the deposition parameters, the opportunity for new and challenging applications are offered which can greatly improve the coating performance.

The reproducibility of the coatings can only be increased by a better understanding of the processes, a stricter control on the materials and a thorough characterization of the coatings. Attempts are currently being made to increase the efficiency of the process by avoiding evaporation, non-melted particles, overspray and wearing of the electrodes and hence, a reduction in costs. Spheroidal powders are used which have a very small range of diameters. New types of torch guns are being studied in which the powder is introduced into the centre of the arc and then, heated over the maximum arc length.

Even higher yields can be obtained by the use of new equipment. The Plasma-Technik firm is now developing a new induction coupled (ICP) with two different radio frequency heating systems. With this new facility, the particle dwell time will be longer, the distribution of plasma will be more uniform and the heat exchange will be more efficient. There is also the possibility of carrying out the spheroidization of the powders and developing reactive plasma processes by mixing

www.manaraa.com

the plasmogenic gas with the reactive gases namely O_2, N_2, CH_4, silane, borane, etc.

New instruments with supersonic gun torches or high energy can provide coatings with reduced porosity and better corrosion resistance.

Presently, post-coating processing is being studied along with hot-isostatic pressing, sealing by liquid metal or polymers and surface alloying by means of laser and electron beam. The PS technique is extremely flexible and the number of potential future applications are numerous. The possibility of depositing metals and ceramics alone or mixed in thin or thick layers, or as a gradual coating on varying substrates offers a wide number of openings in the fields of transport (aircraft, automobile), energy production (gas turbine, power plants), chemistry, electronics and medicine.

It is foreseen that the thermal barrier coatings (TBC) will be the most sought after plasma spray activity industrially but, developments will also occur in the area of superconductors and the deposition of Ti and synthetic bone for prosthesis.

In order to automize the processes, a knowledge of NDT techniques coupled with sensors which are used for the characterization of the coatings during deposition are essential. For this, studies are required which highlight the correlation between the properties of the powders, the parameters of the process and the characteristics of the resultant coating.

15. LITERATURE

[1] M. Villat, "Functionally Effective Coatings Using Plasma Spraying", Sulzer Technical Review 3 (1986), p. 1.

[2] B.J. Gill and R.C. Tucker, "Plasma Spray Coating Processes", Jr., Mat. Sci. and Techn., 2(1986), p. 207.

[3] H. Herman, "Plasma-Sprayed Coatings", Scientific America, Sept. 1988, p. 78.

[4] A. Vardelle, J.M. Barnot, M. Vardelle and P. Fauchais, "Measurements of the Plasma and Condensed Particles Parameters in a DC Plasma-Jet", IEEE, Trans. on Plasma Science, Vol. PS-8 (1980), 4, p. 417.

[5] M. Vardelle, A. Vardelle and P. Fauchais, "Study of the Trajectories and Temperatures of Powders in a DC Plasma-Jet - Correlation with Alumina Sprayed Coatings", Proc. 10th Int. Thermal Spray Conf., Essen, DVS-Berichte, Vol. 80 (1983), p. 88.

[6] H.S. Ingham and A.P. Shepard, Flame Spray Handbook, Vol. III, 1965, Metco Inc., Westbury, N.Y.

[7] E. Muehlberger, US Patent 3914573.

[8] "Metco 77 Plasma Spray Process", Metco Bulletin 205, Metco, Westbury, N.Y.

www.manaraa.com

[9] A.R. Nicoll, H. Gruner, R. Prince and G. Wuest, "Thermal Spray Coatings for High Temperature Protection", Surface Eng. 1(1), (1985) p. 59.

[10] M. Vardelle, R. McPherson and P. Fauchais, "Study of the Influence of Particle Temperature and Velocity Distribution within a Plasma Jet Coating Formation", Proc. 9th Int. Conf. on "Thermal Spraying", The Hague, May 1980, Nederlands Instituut voor Lastechniek, p. 155.11]A.R. Nicoll, H. Gruner, G. Wuest and S. Keller Mat. Sci. and Techn., 2(1986), p. 214.

[11] A.R. Nicoll, H. Gruner, G. Wuest and S. Keller, "Future Developments in Plasma Spray Coating", Mat. Sci. Techn. 2(1986), p. 214.

[12] E. Pfender, "Heat and Momentum-Transfer to Particles in Thermal Plasma Flows", Pure and Appl. Chem. 57(9) (1985), p. 1179.

[13] P. Fauchais, A. Vardelle, M. Vardelle, J.F. Coudert and B. Pateyron, "Plasma Spraying and Extractive Metallurgy: Comparisons between Mathematical Modelling and Measurements and between Application and Development", Pure and Appl. Chem., Vol. 3, 57(9) (1985), p. 1171.

[14] F. Brossa and H. Gruner, "Thermal Conductivity and Shock Resistance of Vacuum Plasma Sprayed Cermet Coatings", High Tech. Ceramics, edited by P. Vincenzini, Amsterdam (1987), p. 2309.

[15] M. Jackson, J. Rairden and J. Smith, "Production of Metallurgical Structures by Rapid Solidification", J. Metals 33(11) (1981), p. 23.

[16] P. Wolf and F.N. Longo, "Vacuum Plasma Spray Process and Coatings", Proc. 9th Int. Conf. on "Thermal Spraying", May 1980, The Hague, Nederlands Instituut voor Lastechniek, p. 187.

[17] H. Gruner and E. Schwarz "Vakuum-Plasmaspritzen im Turbinenbau", DVS-Berichte, Vol. 98, DVS-Verlag, Düsseldorf, 1985, p. 116.

[18] H. Gruner Advances in Thermal Spraying, ITSC 1986, Montreal, Pergamon Press, p. 73.

[19] J.M. Houben Ph.D. Thesis, TU Eindhoven, 1988.

[20] M.I. Boulos, Advances in Induction Plasma Melting and Deposition of Materials, Proc. 2nd Plasma-Technik Symp., Luzern, 5-7 June 1991.

[21] D. Grasme Use of a 200 kW water-stabilized plasma torch for production of ceramic coatings. Proc. 1st Thermal Spray Conf., Essen, Aug. 29-31, 1990, p. 14.

[22] E. Lugscheider, E. Rass and A.R. Nicoll Underwater plasma spraying. Proc. 2nd Plasma-Technik Symposium, Luzern, 5-7 June 1991.

[23] Y. Arata, A. Kobayashi and Y. Habara, "Characteristics of Gas-Tunnel Plasma-Sprayed Coatings", High Temp. Technology 6(1) (1988), p. 9.

[24] S. Keller Controlled Atmosphere Plasma Spraying 1st Plasma-Technik Forum, Wohlen, Switzerland, Sept. 2-3, 1990.

www.manaraa.com

[25] E. Lugscheider, Th. Weber and W. Schlump General study associated with diamond synthesis by conventional vacuum plasma spraying 4th Nat. Thermal Spray Conf., Pittsburgh, May 2-7, 1991.
[26] S. Shankar, D.E. Koenig and L.E. Dardi J. Metals 33(10) (1981), p. 13.
[27] L. Paracchini, Thesis, "Plasma Spray Coatings for Improving Biocompatibility in Ti-Bioglass Dental Prosthesis".
[28] E. Muehlberger and R.D. Kremith U.S., "Electric Arc Plasma Spray Gun" and "Plasma Arc Coating Chamber and Pistol", Patent No. 4, 328.257, 1982.
[29] H.D. Steffens in "Coatings for high temperature applications" (ed. E. Lng) 1983, London, Applied Science, p. 121.
[30] T. Mantyla, P. Vuoristo and P. Kettunen Thin Solid Films, 118 (1984), p. 432.
[31] H.S. Ingham and A.P. Shepard Metco Flame Spray Handbook, Vol. I, Metal Spraying, Metco, Chobham, England, 1963.
[32] H.S. Ingham and A.P. Shepard Metco Flame Spray Handbook, Vol. II, The powder process, Metco, Chobham, England, 1963.
[33] B. Towler "Flame Deposition", Eng. Design Guides 25, Oxford, University Press, 1978.
[34] H.M. Höhle Advances in Thermal Spraying, ITSC 1986, Montreal, Pergamon Press, p. 209.
[35] H. Gruner "Möglichkeiten und Grenzen der Vakuum-Plasma-Spritztechnik", Lehrgang 6520/45.032, p. 2, Technische Akademie Esslingen (1983).
[36] H. Simon and M. Thoma Angewandte Oberflchentechnik für metallische Werkstoffe, Carl Hauser Verlag, 1985.
[37] P. Chagnon and P. Fauchais, "Thermal Spraying of Ceramics", Ceramics International 10(4) (1984), p. 119.
[38] R.H. Wedge and A.V. Eaves Coatings for the aero gas turbine, Proc. 9th Int. Thermal Spraying Conf., The Hague, 1980, p. 73.
[39] D.S. Duvall and D.L. Ruckie "Ceramic Thermal Barrier Coatings for Turbine Engine Components", ASME Paper 82-GT-322, New York 1982.
[40] J.P. Coad and K.T. Scott "Coatings for fuel economy or materials substitution", Materials Substitution and Recycling, AGARD Conf. Proc. No. 356 (1984), paper 12-1.
[41] I. Kvernes in "Coating of diesel engine components" in "Coatings for High Temperature Applications", (ed. E. Lang) 1983, London, Applied Science, p. 361.
[42] D. Downer and R.T. Smyth "Arc plasma sprayed electrical circuits and sputtering targets", Proc. 7th Int. Met. Spraying Conf., London (1973), p. 199.
[43] A. Gorecka-Drazazga, L. Goonka, L. Panlowski and P. Fauchais "Application of the plasma spray process ot the production of metal-ceramic substrates for hybrid microelectronics", Rev. Int. Hautes Temper. Refract. 21(1984), p. 153.

www.manaraa.com

[44] S.A. Bortz and E. Onesto "Flame-sprayed bioceramics", Am. Cer. Bull, 52(12) (1973), p. 898.

[45] C.M. Baldwin and J.D. Mackenzie "Flame-sprayed alumina on stainless steel for possible prosthetic application", J. Biomed. Mater. Res. 10(3) (1976), p. 445.

[46] E. Schwarz "Detonation gun coatings for nuclear and related industries", Proc. 9th Int. Therma. Spraying Conf., The Hague (1980), p. 21.

[47] K.T. Scott and J.P. Coad "Coatings for the use on the limiters of a fusion reactor", Thin Solid Films 80(1981), p. 279.

[48] M.F. Smith, J.B. Whitley and J.M. McDonald "Cermet coatings for a magnetic fusion reactor", Thin Solid Films 118(1984), p. 23.

[49] P.B. Chandler and M.B.C. Quigley "Plasma spraying developments in the Central Electricity Generating Board", Proc. 10th Int. Thermal Spraying Conf., Essen 1983, p. 75.

[50] G. Perugini "Anti-corrosive self-sealing coatings for metal protection in combustion technology", High Temps. - High Pressures 6(1974), p. 565.

[51] P.E. Gallant "Ceramic coatings for the synthetic fibre industry", Surfacing J. 12(1) (1981), p. 1.

[52] B.J. Gill "Designing and producing engineering surfaces", Mat. Eng., Inst. of Metal (1984), p. 191.

www.manaraa.com

LASER SURFACE TREATMENTS : MICROSTRUCTURAL ASPECTS

A. FRENK, W. KURZ
Department of materials
Swiss Federal Institute of Technology Lausanne
CH - 1015 Lausanne, Switzerland

ABSTRACT. Different laser surface treatments are briefly summarised. The principles which govern the formation of microstructures are presented. Macroscopic aspects of heat flux, which determine the local growth conditions, are discussed together with the formation of microstructures. Special emphasis is placed upon the effects associated with rapid solidification. Finally, the concept of microstructure selection maps, necessary for any rational alloy and process development, is introduced.

1. Introduction

High power lasers are being increasingly used in industry as heat sources for cutting, welding and, more recently, for surface treatments. Apart from the case of laser hardening, which will not be discussed here, all of these treatments involve melting and resolidification of the treated surface. As it is possible to focus the laser radiation to very high energy densities ($\approx 10^{10}$ Wm^{-2}), high processing speeds (≈ 1 ms^{-1}) can be employed during these treatments. The laser is used to generate a molten pool on the surface and by moving the specimen relative to the beam, a track is formed. The treatment of wider areas can be achieved by successive partially overlapping passes or by defocussing linearly. This leads to elevated solidification rates, which open new possibilities to advanced alloy design by considerable refinement of the microstructures, extension of the solubility limits and/or appearance of metastable phases.

During *laser surface remelting*, see Figure 1a, the surface of the material is melted and, due to the high thermal diffusivity of the substrate, rapidly resolidified. Both the pool geometry and the melt homogeneity (partial or complete dissolution of precipitates) can be controlled through the processing parameters. Higher hardnesses as well as better wear and/or corrosion properties are expected with the new microstructures formed.

W. Gissler and H. A. Jehn (eds.), Advanced Techniques for Surface Engineering, 235–252.
© 1992 *ECSC, EEC, EAEC, Brussels and Luxembourg.*

www.manaraa.com

Laser surface alloying is identical in principle, see Figure 1b, the only difference being that the chemical composition of the treated layer is altered by the addition of alloying elements.

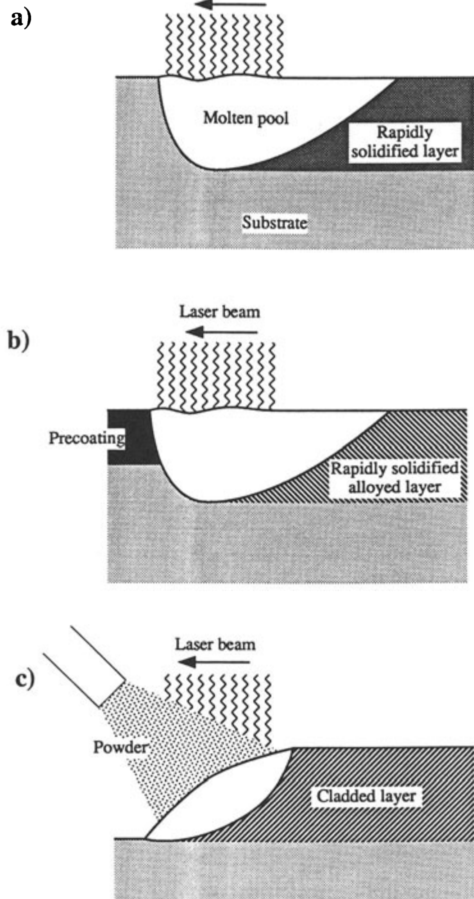

Figure 1 : Schematic of (a) laser surface remelting, (b) laser surface alloying, and (c) laser surface cladding

The aim of *laser cladding* is to deposit an alloy with different composition and properties on a workpiece surface, see Figure 1c. The process involves injecting powder, of the alloy to be clad, into a shallow molten pool generated by the laser on the substrate surface. Under correct processing conditions, it is possible to generate dense coatings, metallurgically bonded to the substrate, with low dilution.

المنارة للاستشارات
www.manaraa.com

In order to fully exploit the potential of these new surface treatments, it is necessary to control the structure that will be formed and thus the properties of the treated specimen. The principles which govern the formation of microstructures in laser treatments will be presented in this paper. We will start with the macroscopic aspects of heat flux, which determine the shape of the molten pool as well as the local solidification conditions (such as solidification speed, V_S, thermal gradient at the solid/liquid interface, G). Then we will discuss the formation of microstructures with special emphasis on the effects associated with rapid solidification. Finally, the concept of microstructural selection maps, necessary for any rational process and alloy development , will be presented.

2. Solidification conditions

During laser surface remelting, an approximately hemispherical pool is produced when the scanning velocity is lower than the rate of heat diffusion. The pool shape becomes elongated at high scanning velocities.

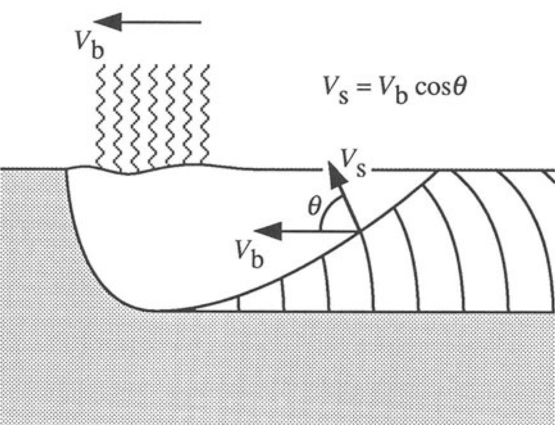

Figure 2 : Typical cut through the centerline of the molten pool during laser surface remelting. V_b is the scanning speed, V_s the solidification speed and θ the angle between V_s and V_b.

www.manaraa.com

As the liquid solidifies epitaxially from its own substrate, there is no nucleation barrier for crystallisation and growth will be columnar in the majority of cases. Local variations of the solidification speed can be determined from the orientation of the microstructure† or from the shape of the molten pool. For the case of laser surface remelting, the vectors of the scanning speed, V_b, and solidification speed are coplanar in a longitudinal plane through the centre of the pool, and therefore [1] :

$$V_s = V_b \cdot \cos\theta \qquad (1)$$

with θ the angle between V_s and V_b, see Figure 2. When the experimental determination of the microstructural orientation is not possible, the shape of the molten pool can be calculated by solving the heat flux equation using numerical techniques [2]. In the latter case however, there are always uncertainties about the boundary conditions, such as absorption of laser energy by the metallic surface. These problems do not arise if one measures the growth rate from the orientation of the microstructure, as explained above.

Figure 3 shows (for an Al-33wt%Cu alloy) the evolution, as a function of depth, of V_s, G, the cooling rate, $\dot{T}$ (= $G \cdot V_s$) and the ratio G/V_s, for two scanning speeds, obtained using the model presented in [2]. It is interesting to note that the solidification speed starts from zero, at the bottom of the trace, and rapidly increases to a value close to the scanning speed at the surface. Over the same distance the thermal gradient, which is strongly positive, decreases to a minimum value at the surface. The cooling rate increases very rapidly at the beginning and stays at a very high and approximately constant value throughout most of the laser trace, as is the case for V_s. The G/V_s ratio is very high at the bottom of the trace and therefore the formation of a planar interface is possible initially [3] (see also part 3.1 below). However, the very rapid increase of V_s often destabilises this interface before a stationary state is being reached.

---

† Strictly valid for microstructures growing parallel to the heat flux, as is usually the case for eutectic or high speed cellular-dendritic growth. In the case of well developed dendrites, see for example Rappaz *et al.*, Metall. Trans. 21A, 1990, 1767

www.manaraa.com

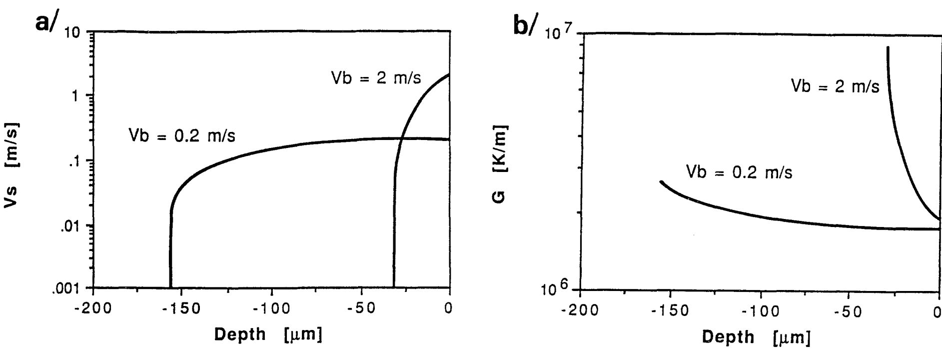

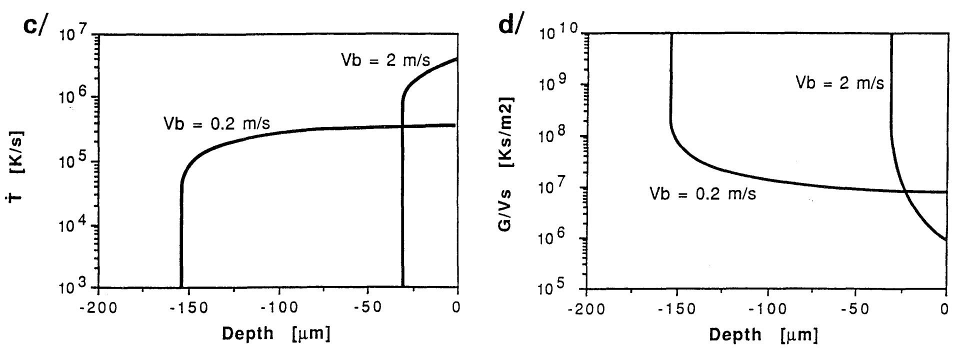

Figure 3 : Laser surface remelting of an Al-33wt%Cu alloy. Calculated results for two different scanning velocities showing the evolution as a function of depth of (a) the solidification speed, V_S, (b) the thermal gradient at the solid/liquid interface, G, (c) the cooling rate, $\dot{T}$ and (d) the ratio G/V_S.

During laser cladding a molten pool with a complex shape is formed. As before, liquid solidifies epitaxially from the substrate, there is no nucleation barrier, and growth is columnar. The highly alloyed materials usually used in laser cladding applications maintain a dendritic morphology with well developed secondary branches through the range of possible processing conditions. Therefore, the growth directions are essentially dictated by the cristallographic directions, and no simple relationship between the orientation of the microstructure and the solidification speed can be deduced. In order

www.manaraa.com

to have an idea of the solidification speeds occurring during the process, results from numerical calculations can be used.

Figure 4 shows (for Stellite 6 deposited on stainless steel) the molten pool shape calculated using a 2-D numerical model [4]. Two different isotherms were used to determine the limits of the liquid pool :

- The liquidus of the substrate material in front of the clad (ahead of the laser), as the substrate has to be melted in order to ensure a metallurgical bond.
- The liquidus of the clad material on the top of the clad (behind the laser).

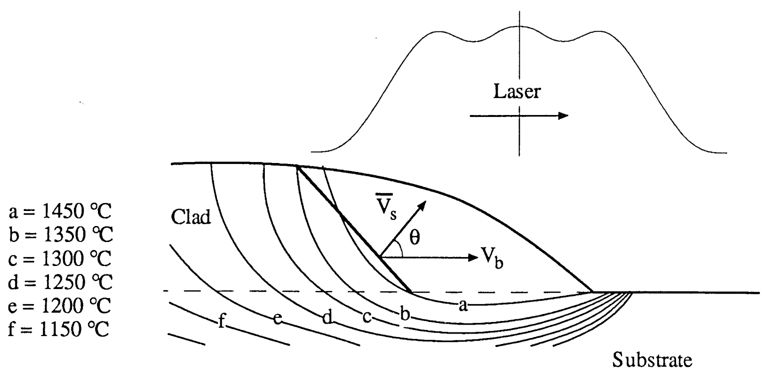

$$\overline{V}_s = V_b \cos\theta$$

Figure 4 : 2-D numerical simulation of the laser cladding process. Calculated quasi-stationnary temperature field in the specimen near to the laser beam during cladding of Stellite 6 onto stainless steel.

المنارة للاستشارات
www.manaraa.com

An average solidification speed can be determined for a given processing condition, as shown in Figure 4. The solidification speed occurring during the actual 3-D cladding process can be assumed to be situated between the average value from the 2-D model and the scanning speed, V_b. The calculations are assumed to give the correct order of magnitude for the thermal gradient. In the case of Stellite 6 cladded on stainless steel, Table 1 gives the calculated values for G and V_s for three conditions ranging from slow to high scanning velocities for the cladding process [5].

Table 1 : Calculated thermal gradients at the solid/liquid interface and estimated solidification speed for different laser cladding processing conditions

Process. condition	V_b [m/s]	G [K/m]	V_s [m/s]
Slow	$1.7 \cdot 10^{-3}$	$2 \cdot 10^{5}$	$1.4 \cdot 10^{-3}$
Intermediate	$1.33 \cdot 10^{-2}$	$6 \cdot 10^{5}$	$1.2 \cdot 10^{-2}$
Fast	$1.67 \cdot 10^{-1}$	$1 \cdot 10^{6}$	$1.1 \cdot 10^{-1}$

3. Solidification microstructures

During the solidification of an alloy, essentially two types of microstructures may be formed :

- A dendritic microstructure, implying the formation of essentially tree-like primary crystals, with growth directions following preferential crystallographic orientations. For metals with a cubic structure, these are the <001> axes.

- An eutectic structure, which implies the coupled growth of two or more phases. These microstructures can be characterised according to their morphology and growth type, see for example Ref [6]. The morphology can be lamellar or fibrous, depending on the volume fraction of the minor phase, and the growth type regular or irregular depending on the melting entropy of the minor phase.

Furthermore, under certain conditions the alloy can transform without the formation of a solidification microstructure, i.e. with a planar front. This can occur with both slow and fast solidification velocities. At high solidification rates, banded structures formed by the alternative growth of a planar front and dendritic or eutectic growth have also been observed [7, 8].

The models describing planar and dendritic growth will be presented below for constrained growth conditions (G>0). For the description of eutectic growth, see for example [6].

المنارة للاستشارات
www.manaraa.com

3.1 PLANAR FRONT GROWTH

Before considering planar front growth, it is necessary to know the conditions under which a planar front is stable. Mullins and Sekerka were the first to carry out a linear stability analysis of a planar solidification front and considered an alloy with composition C_o growing in a positive temperature gradient [9]. The main result of this study is illustrated in Figure 5.

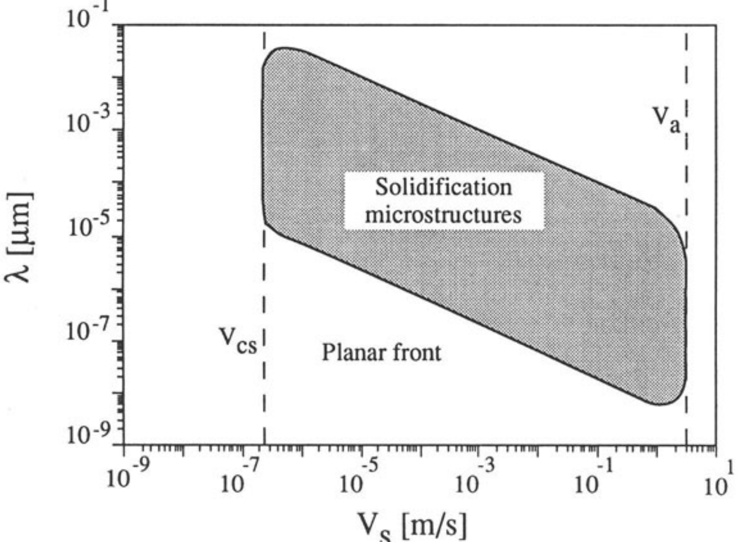

Figure 5 : Planar front stability domain calculated for the Ag-5wt%Cu, with G = 10^4 Km^{-1}. The constitutional surfusion limit, V_{cs}, and the absolute stability limit, V_a, are also indicated.

المنارة للاستشارات

www.manaraa.com

Between V_{cs} and V_a, there exists a range of wavelengths of morphological perturbations, λ, which destabilise the planar interface, and therefore the solidification microstructure will be cellular or dendritic. At low growth speed the limit of stability is of the same order as that given by the constitutional supercooling criterion [10] :

$$V_{cs} = \frac{G \cdot D_l \cdot k}{m \cdot C_o \cdot (k-1)} = \frac{G \cdot D_l}{\Delta T_o} \qquad (2)$$

where D_l is the solute diffusion coefficient in the liquid; k the partition coefficient obtained from the phase diagram, given as :

$$k = \frac{C_s}{C_l}$$

with C_s and C_l the equilibrium solute concentration in the liquid and solid phase respectively; m the liquidus slope; G the weighted thermal gradient at the interface, given by :

$$G = \frac{(G_s \cdot \kappa_s + G_l \cdot \kappa_l)}{(\kappa_s + \kappa_l)}$$

with κ_s and κ_l the thermal conductivities in the solid and liquid phase respectively; and ΔT_o is the liquidus-solidus temperature interval at C_o.

With increasing solidification speed, the characteristic solute diffusion distance ($\approx D_l/V_s$) diminishes faster than the size of the structure ($\approx 1/\sqrt{V_s}$). At high growth rates, the diffusion length is comparable to the size of the microstructure and the concentration gradients in front of the tips and troughs of a perturbed interface become similar. This effect restabilises the planar front at a critical velocity called the absolute stability limit, V_a, given by :

$$V_a = \frac{m \cdot C_o \cdot (k-1) \cdot D_l}{\Gamma \cdot k^2} = \frac{\Delta T_o \cdot D_l}{\Gamma \cdot k} \qquad (3)$$

where Γ is the Gibbs-Thomson coefficient.

Linear stability theory for constant partition coefficients predict that for growth rates below V_{cs} or above V_a the planar front is stable. Under stationary conditions, the growth temperature is that of the solidus and the concentration in the solid at the interface, C_s^*, equals C_o, i.e. the solidifying crystal has the composition of the melt. The concentration in the liquid at the interface, C_l^*, is given by C_o/k.

In the linear stability analysis carried out by Mullins and Sekerka [9] it was assumed that local equilibrium was always present at the interface. However, under high

المنارة للاستشارات

www.manaraa.com

solidification speeds, such as those associated with laser treatments, loss of local thermodynamic equilibrium at the growth front must be taken into account. When the displacement rate of the solid/liquid interface becomes high, the solid has insufficient time to reject the excess solute in order to equalise its chemical potential with that of the liquid. The concentration in the solid will therefore increase with respect to the equilibrium concentrations, leading to solute trapping. At very high solidification speeds, the solid and the liquid have the same chemical composition and the partition coefficient equals unity. This variation of the partition coefficient with the growth rate implies that the solidus and liquidus approach each other and converge about the T_o line of the phase diagram. Therefore, a modification of the equilibrium liquidus slope, m_e, with the solidification speed must be introduced. It is also necessary to account for the temperature dependence of some physical parameters, e.g. the diffusion coefficient. In addition, at very high growth rates (> 1 ms^{-1}) kinetic attachment effects must also be taken into account. The kinetic effects will not be taken into account here. The following equations give the velocity and temperature dependencies of k and m after Aziz [11] and Boettinger and Coriell [12] :

$$k(V_s,T) = \frac{k_e(T) + Pi}{1 + Pi} \tag{4}$$

with the interfacial Péclet number $Pi = \frac{a_o \cdot V_s}{D_l(T)}$

and the effective liquidus slope

$$m(V_s,T) = m_e \cdot \{1 + \frac{k_e - k \cdot (1 - \ln(k/k_e))}{1 - k_e}\} \tag{5}$$

where k_e and m_e are the equilibrium partition coefficient and liquidus slope respectively and a_o is a length characterising the thickness of the interface. A more complete description of the subject can be found in [6].

3.2 DENDRITIC GROWTH

The columnar growth characteristics of an alloy dendrite are essentially dictated by the solute field around the tip. In order to reject the solute efficiently, the crystal adopts the shape of a needle with a parabolic-like tip of radius R. For this morphology, Ivantsov [13] has obtained the following relationship between the supersaturation, Ω, and the Péclet number, Pe :

$$\Omega = Iv(Pe) = Pe \cdot \exp(Pe) \cdot \int_{Pe}^{\infty} \frac{\exp(-z)}{z} \cdot dz \tag{6}$$

المنارة للاستشارات
www.manaraa.com

with Ω and Pe given by :

$$\Omega = \frac{C_l^* - C_o}{C_l^* \cdot (1-k)} \qquad Pe = \frac{V_s \cdot R}{2D_l} \tag{7}$$

Equation (6) relates Ω to the product $R \cdot V_s$. In order to determine the undercooling for a given growth speed, the second equation needed can be obtained using a stability criterion [14] or the more recent and exact solvability criterion [15]. With

$$R = \{ \frac{\Gamma}{\sigma^* \cdot (m \cdot G_c \cdot \xi_c - G)} \}^{0.5} \tag{8}$$

where G_c is the solute concentration gradient in the liquid at the interface,

$$\sigma^* = \frac{1}{4\pi^2} \text{ and } \xi_c = 1 - 2k/\{[1 + (2\pi/Pe)^2]^{0.5} - 1 + 2k\},$$

the following quadratic equation is obtained for constrained growth conditions (G>0) [16] :

$$V_s^2 \cdot A + V_s \cdot B + G = 0 \tag{9}$$

$$\text{where } A = \frac{\Gamma}{\sigma^* \cdot (2Pe \cdot D_l)^2} \text{ and } B = \frac{m \cdot C_o \cdot (1-k) \cdot \xi_c}{D_l \cdot \{1 - (1-k) \cdot Iv(Pe)\}}$$

For normal growth speeds and negligible thermal gradients, it is possible to simplify (9) and one finally gets [6] :

$$R^2 V_s = \frac{4\pi^2 \cdot D_l \cdot \Gamma}{m \cdot C_o \cdot (1-k)} \tag{10}$$

Four terms in equation (9) are influenced by high solidification speeds :

- the term ξ_c, which comes from the Mullins-Sekerka stability analysis [17] and changes from 1 to zero at large velocities,
- the partition coefficient, k, and the liquidus slope, m, both reflecting the non-equilibrium condition at the interface,
- the diffusion coefficient, D_l, and its variation with interface temperature.

The dendrite tip temperature, T*, is given by :

www.manaraa.com

$$T^* = T_m + \frac{m \cdot C_o}{1 - (1-k) \cdot Iv(Pe)} - \frac{2\Gamma}{R} \qquad (11)$$

with T_m the melting temperature of the pure component.

Figure 6 shows for an Al-2wt%Fe alloy, the evolution of the characteristic size scales with solidification speed [18]. Primary and secondary dendrite spacings of around 50 nm have been measured. For comparative purposes, the calculated variation of the tip radius R is also shown. One can see that both the primary and secondary dendrite arm spacing follow relatively well a $\lambda^2 \cdot V_s$ = const. relationship, in a similar way to the calculated radius which diminishes with the speed (according to equation (10) at low and medium velocities) down to a minimum value. The absolute stability limit, as predicted by Mullins and Sekerka [9], is also shown and corresponds well to the maximum growth rate observed experimentally.

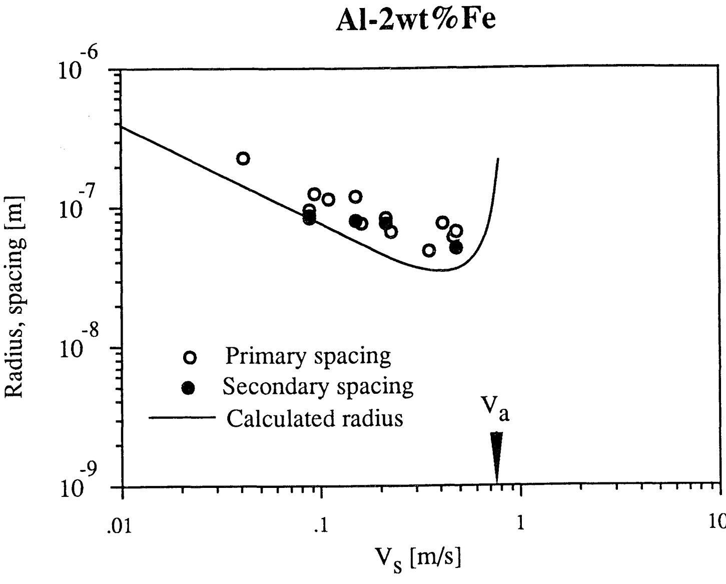

Figure 6 : Laser surface remelting of an Al-2wt%Fe alloy. Measured primary and secondary dendrite arm spacing, as well as calculated tip radius as a function of solidification speed. The arrow indicates the absolute stability limit predicted by Mullins and Sekerka.

www.manaraa.com

3.3 ABSOLUTE STABILITY AND BANDED STRUCTURE

In different studies on dendritic [18, 19, 20] and eutectic [19, 21] systems, the appearance of a banded structure at rates above absolute stability has been observed before complete planar front restabilisation occurred. Figure 7 [7] shows a TEM micrograph of such a structure. Studies have shown that the light bands consist of a supersaturated solid solution, interpreted as resulting from the high speed growth of a planar front, while the dark band structure was similar to that which occurred before the appearance of the bands (that is eutectic or dendritic). The growth speeds of the planar front and of the eutectic (or dendritic) front are very different, showing an oscillatory instability of the front of the type that has been discussed by Coriell and Sekerka [22] and Merchant and Davies [23]. The mean growth speed of the solidification front, imposed by the displacement rate of the thermal isotherms, is situated between these two extremes, i.e. maximum rate of eutectic (or dendritic) and minimum rate of stable plane front growth. A phenomenological model, based on these observations has been proposed to explain the origin of the bands [7, 8].

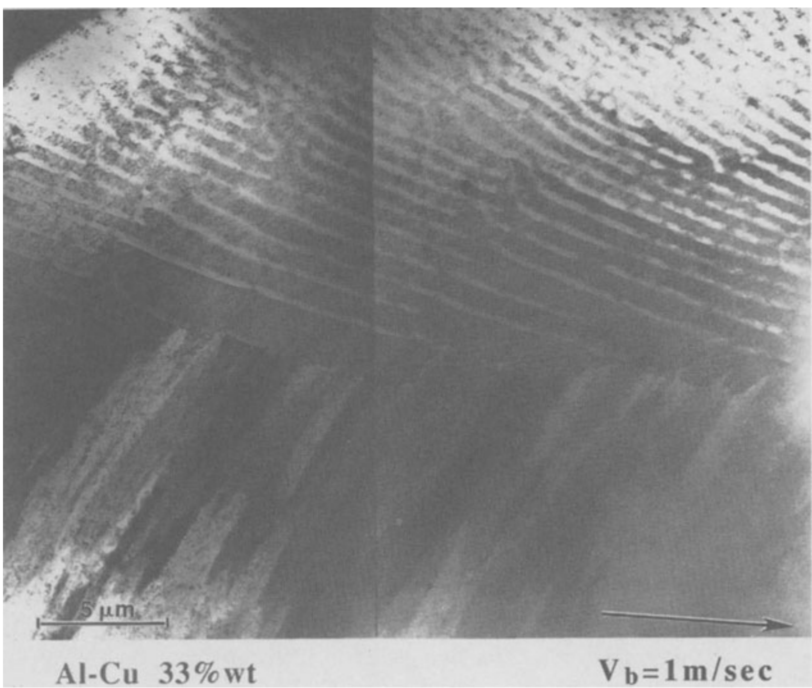

Figure 7 : Remelting of the Al-33wt%Cu eutectic alloy. Transition between the columnar eutectic grains and a banded structure. This transition occurs at a solidification speed of $V_s = 0.5\ ms^{-1}$.

المنارة للاستشارات
www.manaraa.com

4. Microstructure selection maps

The macroscopic heat flux conditions, in tandem with the microstructural models can be used to determine microstructure selection maps. The different microstructural domains for single phase growth can be indicated using a thermal gradient versus solidification speed diagram. Superposing the G and V_s values for different depths in the trace, calculated for a given laser treatment (see Figure 3), indicates the different microstructures that will appear in the laser trace. Figure 8 shows such an example, calculated for an Al-2wt%Fe alloy and for two scanning speeds [24]. In both cases planar front growth is predicted at the bottom of the trace, but most of the trace will exhibit a dendritic microstructure which becomes finer as the surface is approached. Using a scanning speed of 2 ms^{-1}, a banded structure will appear at the highest growth velocities, but no complete supersaturation of the solid.

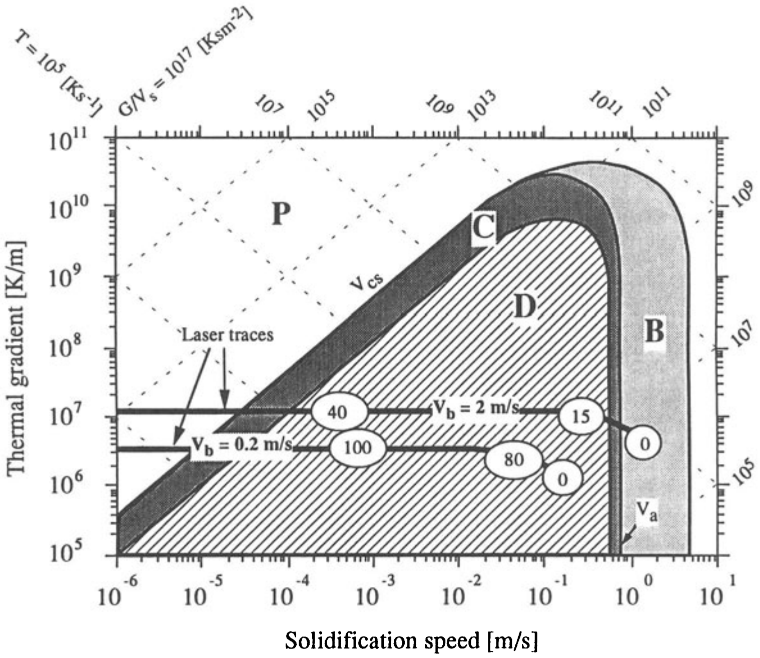

Figure 8 : Processing map relating the morphology of the solidification front and the thermal gradient for two different laser remelting traces (V_b = 0.2 and 2 ms^{-1}) numerically calculated in Al-2wt%Fe. (P) indicates planar, (C) cellular, (D) dendritic and (B) banded structure growth. The numbers on the processing traces indicate the depth from the surface (in [µm]) which is subject to the corresponding V_s-G pair.

www.manaraa.com

The thermal gradient affects the microstructure most strongly at low growth speeds. However, under laser processing conditions the solidification speed is usually high and thus it may be more useful to use the approach shown in Figure 9 [25]. When nucleation is easy (as is the case in most laser treatments where no nucleation barrier exists), the growth morphology that will appear under given solidification conditions is the one with the highest interfacial temperature (under constrained growth conditions), see for example [26]. Therefore, combining the different microstructural growth models, it is possible to predict the structure which will appear as a function of solidification speed and composition.

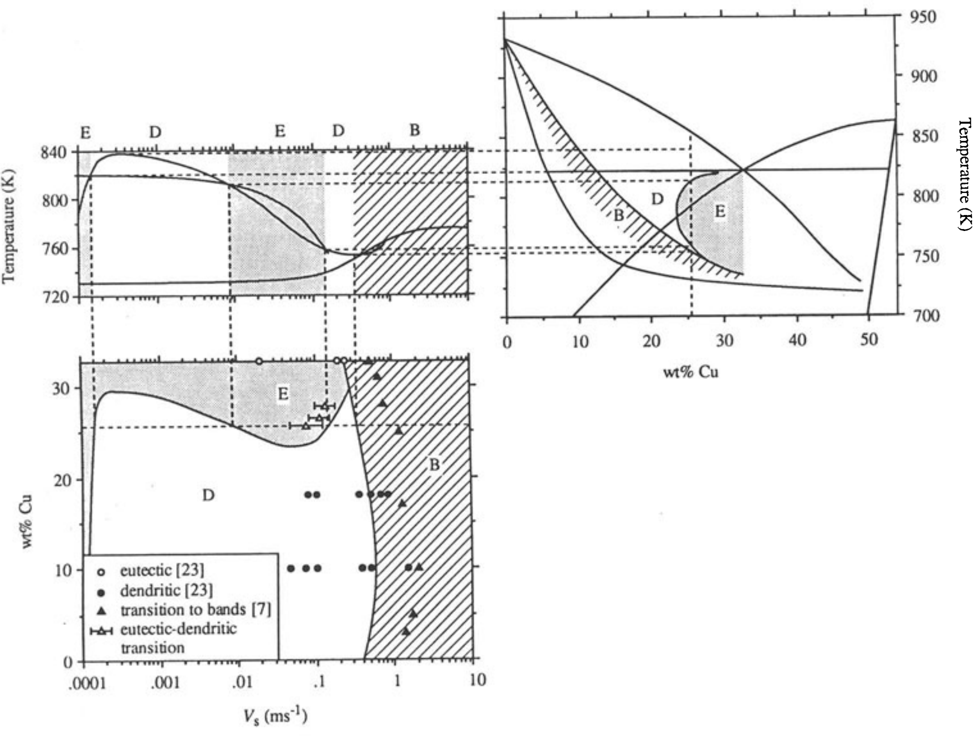

Figure 9 : (a) Predicted curves of T as a function of V_S for the 26wt%Cu alloy, divided in the velocity ranges for eutectic (E), dendritic (D) and banded or planar front growth (B). (b) The Al-Cu phase diagram, showing the predicted hypoeutectic side of the coupled growth zone and the regions of dendritic and banded or plane front growth. (c) Predicted microstructural map for alloy composition and V_S, for hypoeutectic alloy.

المنارة للاستشارات

www.manaraa.com

Figure 9 shows such a map, experimentaly determined and calculated for the binary Al-Cu system [25]. It can be seen that, for a broad range of compositions, a laser remelted hypoeutectic alloy will exhibit a eutectic structure.

Observed microstructural transitions

Solidification speed [cm/s]
100
10
1
Co-dendrites
Eutectic
Primary carbides
20
30
40
50
60
Carbide fraction [wt%]

Figure 10 : Experimental microstructure selection map of the pseudobinary (Co,Cr)-$Cr_{7-x}Co_xC_3$ system.

The other example concerns the quasi-binary system, Co-Cr_7C_3, which forms the basis of Stellite-type hardfacing alloys. Figure 10 shows the experimentally determined microstructure selection map [27]. For hypereutectic alloys close to the eutectic composition, the transition speed from a eutectic structure to a structure with primary Co-dendrites was determined. Furthermore, for highly hypereutectic alloys, transitions from a primary carbides plus eutectic structure towards an entirely eutectic structure were observed.

www.manaraa.com

5. Conclusions

Elevated solidification speeds can be achieved during laser materials processing. This unique aspect of these treatments opens new possibilities for the specific designing of new alloys. The processes leading to the formation of microstructure have been discussed. Different effects related to high solidification rates have been presented which affect the hardness (refinement of the size of the microstructure), as well as the properties such as the wear resistance (size and content of hard phases, morphological transitions). Models describing the microstructural growth at high solidification rates, combined with appropriate selection criteria, allow the development of maps for predicting the type of microstructure that will appear as a function of the process parameters. Processing conditions can then be determined in order to produce the optimum structure for a given application.

Acknowledgements

We would like to thank the "Commission pour l'Encouragement de la Recherche Scientifique", Berne, as well as Sulzer Innotec, SA, Winterthur, for financial support.

References

[1] M. Rappaz, M. Gremaud, R. Dekumbis, W. Kurz, *Proc. 1st Europ. Conf. Laser Treatment of Materials (1986)*, B.L. Mordike ed., DGM Verlag, Oberursel, 1987, 43

[2] A.F.A. Hoadley, M. Rappaz, M. Zimmermann, *Metall. Trans. B*, 22B, 1991, 101

[3] A. Munitz, *Metall. Trans. B*, 16B, 1985, 149

[4] A.F.A. Hoadley, M. Rappaz, to appear in *Metall. Trans.*

[5] A. Frenk, N. Henchoz, W. Kurz, unpublished research

[6] W. Kurz, D.J. Fisher, *Fundamentals of Solidification*, Trans Tech Publications, Aedermannsdorf, Switzerland, 3rd edition, 1989

[7] M. Zimmermann, M. Carrard, M. Gremaud, W. Kurz, *Materials Science and Eng.*, A134, 1991, 1278

[8] M. Carrard, M. Gremaud, M. Zimmermann, W. Kurz, *Acta Metall. Mater.*, 40, 5, 1992, 983

[9] W.W. Mullins, R.F. Sekerka, *J. Appl. Phys.*, 35, 1964, 444

www.manaraa.com

[10] W.A. Tiller, K.A. Jackson, J.W. Rutter, B. Chalmers, *Acta Metall.*, 1, 1953, 428

[11] M.A. Aziz, *J. Appl. Phys.*, 53, 1982, 1158

[12] W.J. Boettinger, S.R. Coriell, *Science and Technology of Undercooled Melts*, P. Sahm et al. ed., NATO ASI Series E - n°114, Martinus Nijhoff Publ., Utrecht, 1986, 81

[13] G.P. Ivantsov, *Dokl. Akad. Nauk. SSSR*, 58, 1947, 567

[14] J.S. Langer, H. Müller-Krumbhaar, *Acta Metall.*, 26, 1978, 1681

[15] W. Kurz, R. Trivedi, *Acta Metall. Mater.*, 38, 1990, 1

[16] W. Kurz, B. Giovanola, R. Trivedi, *Acta Metall.*, 34, 1986, 823

[17] R. Trivedi, W. Kurz, *Acta Metall.*, 34, 1986, 1663

[18] M. Gremaud, M. Carrard, W. Kurz, *Acta Metall. Mater.*, 38, 12, 1990, 2587

[19] W.J. Boettinger, D. Shechtman, R.J. Schaefer, F.S. Biancaniello, *Metall. Trans. A*, 15A, 1984, 55

[20] D.G. Beck, S.M. Copley, M. Bass, *Metall. Trans. A*, 12A, 1981, 1687

[21] M. Zimmermann, M. Carrard, W. Kurz, *Acta Metall.*, 37, 12, 1989, 3305

[22] S.R. Coriell, R.F. Sekerka, *J. Cryst. Growth*, 61, 1983, 499

[23] G.J. Merchant, S.H. Davis, *Acta Metall. Mater.*, 38, 12, 1990, 2683

[24] M. Gremaud, *Solidification rapide : étude microstructurale des alliages Al-Fe après fusion superficielle par laser*, Thèse EPFL n°885, Lausanne, Switzerland, 1990

[25] S. Gill, M. Zimmermann, W. Kurz, to appear in *Acta Metall. Mater.*, 1992

[26] W. Kurz, D.J. Fisher, *Int. Met. Reviews*, 5/6, 1979, 177

[27] Mao Xiemin, A. Frenk, unpublished research

www.manaraa.com

HYBRID PROCESSES

H. Freller, H. P. Lorenz
Siemens AG
ZPL 1 TW 54
P.O. Box 3220
W-8520 Erlangen
Deutschland

ABSTRACT. Especially for the deposition of hard materials hybrid processes are considered. The deposition of ternary layers composed of Ti and other metals and nitrogen and of Cr and other metals and nitrogen with a combination of reactive arc evaporation and magnetron sputtering is discussed in detail. For the plasma CVD process of TiN the influence of different plasma excitation methods is shown. The combination of PVD and plasma CVD is discussed for the deposition of metal-carbon coatings. The experimental difficulties of laser CVD for TiN deposition and its advantages in contrast to normal CVD are described.

1. Introduction

In the field of coatings against wear and friction a trend towards application-specific coatings can be observed. A prerequisite to develop and apply such coatings is the realisation and qualification of such coatings for different applications in a short time at low cost. This in turn needs a flexible and easily adaptable coating technique. Hybrid coating processes can be a way to achieve these flexibility. What does the terminus "hybrid deposition process" mean? Hybrid, from the Greek word for "outrage", in Latin means descent from dissimilar parents. So the expression "hybrid deposition process" will be used for deposition processes using different sources or using a combination of different processes simultaneously for one deposition or for one deposition run.

This paper will be limited to the description of the deposition of thin layers by vacuum coating processes, especially to hard coatings. Apart from this other hybrid deposition processes can be investigated, e.g. electrolytic deposition with laser beam activation etc..

2. Hybrid Deposition Processes

2.1. HYBRID PVD

Physical vapour deposition (PVD) is in principle a deposition of coatings from the vapour phase. Well known is the evaporation in high or in ultrahigh vacuum by heating the material by different means. The elevated temperatures for evaporation or sublimation are in most cases achieved by direct or indirect electrical current heating of wires and crucibles, or by bombardment of the material with a high voltage electron beam. Laser ablation is also a possibility. A very popular PVD method is the sputter process, high frequency sputtering

W. Gissler and H. A. Jehn (eds.), Advanced Techniques for Surface Engineering, 253–273.
© 1992 *ECSC, EEC, EAEC, Brussels and Luxembourg.*

www.manaraa.com

for insulating materials, and - now most important - magnetron sputtering of metals or reactive magnetron sputtering for different compounds. A new cathodic process with fast growing application is the arc evaporation where the material is evaporated from the cathode spot of an arc of low voltage and very high current density. A very interesting application of the hybrid PVD concept is the combination of such an arc evaporator and a magnetron sputter cathode.

2.1.1. *Combination of cathodic sputtering and arc deposition.* Recently the authors /1/ and others /2,3/ were able to show that processes using cathodic alloy sources, like the magnetron or the arc-evaporator, allow realisation of homogeneous ternary hard (Ti,Al)N-coatings as well as coatings with graded composition by changing the bias voltage in the course of the deposition run. In the development of application tailored ternary coatings, however, where the optimum composition is not yet known, the approach via alloy sources is expensive, difficult and time consuming and sometimes a separate developmental problem. For these reasons a different approach was investigated, using a hybrid source set-up with simultaneous deposition from a magnetron and arc-evaporators and elemental metals as starting materials.

2.1.1.1. *Experimental.* As a basis for the deposition set-up, an arc-ion-plating machine (type PVD 20, Interatom) was used, which allows installation of up to three random arc sources (Chamber size 130 l , rotary pump 65 m^3/h, diffusion pump 3000 l/s). For the magnetron source the mounting feed through in the top of the vacuum chamber was used , while the two horizontal mounting sites were used for the two arc sources. A schematic view of the deposition set-up is shown in Fig. 1. The magnetron was a specially designed 6"-source (Teer Coating Services Ltd., Hartlebury) with an unbalanced magnet system. The cathode design allows a relatively deep insertion of the target into the vacuum chamber. The set-up allows to change the distance between the rotatable substrate holder and the target between 200 and 300 mm. The following power supplies were used in the experiments: random arc cathodes (100 A, 25 V power source from Interatom), magnetron (10 A, 1000 V, from Advanced Energy), substrate bias (5 A, 1000 V, Interatom).

2.1.1.2. *System Ti - Al - N.* Because of the high droplet formation of the arc source with low melting materials like aluminium, aluminium was taken as sputtering cathode and titanium as the arc cathode. Different series of experiments were performed. First it was tried to work without argon in the vacuum atmosphere to investigate the influence of the sputtering effects arising from the metal ions originating from the arc sources which are accelerated towards the magnetron cathode. These experiments were performed in pure nitrogen in the pressure region of $(2\text{-}3) \cdot 10^{-3}$ mbar. In a second series of experiments, argon was added to the nitrogen to a total pressure of $2 \cdot 10^{-2}$ mbar. For the deposition of graded coatings, the power of the arc-sources was kept constant while the power of the magnetron was increased in steps. These experiments were also performed in an argon nitrogen atmosphere under the pressure conditions mentioned above.

Due to its high oxidation resistance, the ternary compound (Ti,Al)N is one of the most thoroughly investigated supplementary hard coatings to TiN /4/. So this compound was a good standard to start with this set-up and to compare the coatings achieved by the hybrid process with coatings achieved by use of alloy cathodes. After having shown the usefulness of this approach at this example by depositing homogeneous coatings as well as coatings with graded composition, however, numerous other ternary coatings were deposi-

www.manaraa.com

ted. The main emphasis was directed to systems consisting of TiN and the nitride of another metal [type(Ti, M2) N] and chromium nitride plus the nitride of another metal [type(Cr, M2)N].

The results of the initial experiments for depositing TiAlN-coatings without argon as a sputtering gas show that deposition rates above 3 μm/h and Al-concentrations in the coating above 12% were not achievable by this approach. So titanium ions from the arc source seem not to play an important role in sputtering of the aluminium cathode material. Deposition experiments with addition of argon to the sputter gas however allowed growth rates of up to 9 μm/h and Al concentrations of up to 50%, as shown in the diagrams in Fig. 2. The properties of these films are comparable with coatings deposited from alloy sources by use of the arc ion plating process. As shown in Fig. 3, increasing magnetron power not only increases Al concentration, parallel to this increase in Al concentration, a change in fracture morphology from columnar to glassy or nanocrystalline can be observed. Coatings with graded composition, either with increasing or decreasing Al concentration to the surface, were deposited by changing the magnetron power in the desired direction. In this case the same morphology changes were observed within the depth of the coating /5/. Following these encouraging initial results it was tried to synthesise other compound films.

2.1.1.3. *Coatings in the Systems (Ti, M2)N.* To realise coatings in the system (Ti,M2)N, combinations of titanium with a second metal (M2), such as Zr, V, Nb, Ta, Cr and W, were deposited in an argon-nitrogen atmosphere.

A first step to deposit two different compositions in every system, is using fixed power at every source and changing the distance between the magnetron target and the substrate in the experiments. The results of these experiments are summarised in table 1. In Fig. 4 fracture cross section micrographs of two different compositions of (Ti,Ta)N are displayed. While the composition with about 31 at.% tantalum still shows the columnar structure typical for TiN coatings, an increase of the tantalum concentration to 71 at.% in the second coating changes the morphology entirely to a nanocrystalline, glassy fracture morphology. XRD-analysis of such coatings shows very broadened reflexes of Ta_2N and TiN only.

In a second series of experiments for each system coatings with graded composition were deposited with a fixed target/substrate distance, either by changing magnetron power or arc-source power. In most cases, however, magnetron power was changed as this source allows variations over the whole useful power region without causing instabilities in the magnetron performance. As an example of such coatings the Auger-depth profile of a $Ti_xW_{1-x}N$ coating is shown in Fig. 5. The coating composition starts at the coating substrate interface with nearly pure titanium nitride and ends up with about 40% W at the surface.

2.1.1.4. *Coatings in the System (Cr,M2)N.* CrN hard coatings are on the way sharing a certain part of the market for coatings against wear, corrosion and friction, especially for coatings on tools used in the fabrication of components made from copper and copper alloys, where TiN has shown little success. Based on these facts, ternary hard coating systems with Cr as the base metal and addition of a second metal (M2), such as Al, V, Nb, Ti, Ta and W were realised by use of the hybrid process. In this group there are several combinations, where realisation of starting alloys in a quality which would allow evaporation by arc-sources, is itself a problem. The deposition parameters used, and typical properties like deposition rate, Knoop hardness and adhesion measured by the Rockwell indentation test, are shown in table 2. As chromium nitride itself is a material which tends

www.manaraa.com

to show glassy fracture it is not so surprising that in this group more coatings with glassy fracture were observed.

It is interesting to note that in most cases the coatings designated as layered did not show columnar growth in the fracture. These layered coatings are characterised by concentration changes of the sputtered material which may be originated by periodic argon partial pressure fluctuations caused by the pressureregulation system. As an example fracture cross sections of two compositions from the system (Cr,V)N with a relatively high Cr concentration are shown in Fig. 6.

Coatings with graded composition have also been realised for every combination in this group. As a typical example an Auger depth profile of (Cr,Ta)N is shown in Fig. 7.

2.2. PLASMA CVD PROCESS

In chemical vapour deposition (CVD) all starting materials are in the gaseous or vapour state, and they react by means of additional energy at surfaces to solid coatings. Plasma CVD can be taken as a hybrid process, because it combines pure plasma activated processes like the plasma polymerisation and the chemical vapour deposition. CVD normally is a high temperature deposition with gaseous precursor materials which gains its process energy from the substrate heating. In plasma CVD additionally a gas discharge is activated in the precursor gas mixture or in some of the gas mixture components. This can be done in addition to the substrate heating but normally it is used to lower the substrate temperature considerably. By this means the CVD coating process can be applied also to coat temperature sensitive substrate materials like hot work tool steels or semiconductor devices. All kinds of electrical sources and discharges are in use, DC, pulsed DC, radio frequency (RF), and microwave. The discharge can take place in the vicinity of the substrate or downstream plasma CVD can be used. In the latter case the activated species responsible for the deposition process are generated in some distance from the substrate. During their lifetimes, they travel to the substrate, and high energy particles from the gas discharge cannot damage the substrate.

2.2.1. *Deposition of TiN with plasma CVD* . A good example for showing the advantage of a hybrid deposition technique is the plasma CVD deposition of TiN. TiN coating of hard metals by high temperature CVD is a well known process for more than 20 years /6/. From thermodynamic calculations the overall reaction

$$2TiCl_4(g) + N_2(g) + 4H_2(g) \text{ ------> } 2TiN(s) + 8HCl(g)$$

gives a solid coating of TiN at temperatures higher than about 900 °C. So this coating process is only useful for hardmetal substrates like turning inserts. But also for hard metals the high coating temperature is a disadvantage because fracture toughness and transverse rupture strength are decreasing /7/, and tools coated in such a manner are thus not suitable for interrupted cutting. High temperature CVD TiN can be deposited with a rate of 2 μm/h. Its adherence to steel is very high, there is always a titanium carbide intermediate layer grown from the carbon contained in the steel. The surface is rather rough, shiny surfaces can only be achieved by polishing after deposition.

For the plasma CVD process the same overall formula is correct. But the deposition temperature can be below 500 °C, because the thermodynamically possible temperature limit is lowered by the activation delivered by the plasma /8/. With a typical set of parameters

www.manaraa.com

given in table 3 TiN can be deposited onto steel with sufficient adhesion.

Interesting is the influence of different methods to excite the plasma on the coating properties.

2.2.1.1. *Experimental.* For the deposition experiments a parallel plate reactor with symmetrical electrodes was used in a horizontal position. The electrodes were 15 cm in diameter and the distance between them 5 cm. The bottom electrode was the substrate electrode. It could be heated to 500 °C. The reactor was also symmetrical regarding gas flow. Process gas was introduced through a ring tube around the bottom electrode and 3 cm above it. The reactor was exhausted through holes around the bottom electrode. The mass flow was controlled at all gas inlets. The working pressure was set automatically by a throttle valve to a desired value.

The schematic drawings of the connection of electrical power supplies are shown in Fig. 8. The DC and the pulsed DC power sources were connected to the bottom electrode, while the top electrode is floating. The pulsed power source was used at a pulse amplitude of - 500 V, a pulse duration of 100 μs, and a variable pause time between 35 μs and 500 μs. The pulse/pause ratio can be used to control the substrate temperature. The radio frequency of 13.56 MHz was coupled capacitively to the top electrode. The bottom electrode was either floating, connected to ground, or to a negative bias voltage. The RF power levels were between 60 W and 100 W. Microwave excitation was used in a downstream configuration, so that in this case gas flow was asymmetric, i.e. from one side only. The gas was excited outside the reactor in a quartz tube of 1/2" diameter at a distance of 20 cm from the edge of the bottom electrode.

The deposition parameters were the same for the various deposition methods or were varied only within a narrow range (Table 3). The starting gases were always titanium tetrachloride, nitrogen, and hydrogen. The pressure range was 100 Pa to 600 Pa, with most of the experiments being done in the lower pressure range. The substrate temperature was always about 500 °C with small process dependent variations.

2.2.1.2. *Coating Experiments.* With the exception of the microwave downstream process it was possible to deposite TiN coatings with all of the plasma excitation methods. In the microwave process experiments with excitation of single gas components or mixtures led to various, unusable, results. Because of the poor layer features (colour and thickness), no further investigations, e.g. flow variations, and no analysis of the composition of the layers were made. The conclusion from the microwave experiments is that $TiCl_4$ has to be excited to deposit TiN from $TiCl_4$, N_2, and H_2 gas mixtures. When this is done however the reactions occur so rapidly that subsequent transport of excited components to the substrate position is not possible. Instead, deposition occurs in the quartz tube used for the excitation.

The general features of the TiN coatings obtained by DC plasma CVD, RF plasma CVD, and pulsed plasma CVD are quite comparable /9/.

2.2.1.3. *Chlorine Content.* TiN can be deposited even at 300 °C by plasma CVD, but the lower the substrate temperature is, the higher is also the chlorine content in the film, if $TiCl_4$ is used as a precursor gas. High temperature CVD TiN has no detectable chlorine incorporated, but for plasma CVD TiN the chlorine content can be very high, and this affects the corrosion resistance seriously. Fig. 9 shows the chlorine content varying with the substrate temperature and also with negative bias voltage.

www.manaraa.com

2.2.1.4. *Coating Uniformity onThree-Dimensional Parts*. One of the most interesting questions in the application of plasma CVD processes is how good is the throwing power in plasma CVD compared with that of HT CVD and with PVD processes. To answer this question test samples of high-speed tool steel (M2, DIN No. 1.3343) with dimensions 15 x 15 x 6 mm^3 and fine ground surfaces were coated via the different methods. They were arranged on the substrate electrode as shown in Fig. 10. In a first series of experiments RF plasma CVD's were performed. The substrate was floating, or biased with different negative voltages up to -500 V. Other coatings were made with negative DC voltages up to -800 V, but with a floating top electrode. The bars in Fig. 11 show the resulting thickness values at the various measurement points. The dotted line marks the mean value of all the thicknesses measured. The black bars show the values for a coating with RF plasma PVC and floating substrate, while the white bars show the thickness values for a DC plasma CVD coating experiment at -800 V glow discharge voltage. RF plasma CVD coatings with negative bias voltages at the substrate (e.g. -300 V) show intermediate values between these two sets of thicknesses.

The interpretation is as follows: In a pure RF plasma CVD all the activated species in front of the substrate react to the growing layer. So the layer thickness at a distinct location depends on the solid angle seen from this point. Inner edges form the smallest solid angle, and so the thickness decreases rapidly on the side walls towards the bottom electrode. The outer corners are preferred in deposition. In DC plasma CVD, we have a plasma chemical vapour deposition superimposed by a sputtering process. Sputtering occurs preferentially at outer corners, while inner edges gain additional thickness from the back-scattering effect which is pronounced at high pressures. Non-uniformity in the coating thickness of a pure RF plasma CVD layer can thus be compensated to some degree with an appropriate negative bias voltage.

This effect can also be emphasised by increasing the pressure. Fig. 12 shows the mean thickness values of the coatings of Fig. 10 (sample arrangement "B") for RF plasma CVD with floating potential, a DC plasma CVD, and of pulsed plasma CVD coating at 1.5mbar and at 6mbar working pressure for the top surface, the side surface, and for the bottom surface of the sample part jutting out. It is easy to see from the bars that especially pulsed plasma CVD at high pressure gives the best coating uniformity. In the case of normal DC plasma CVD an intensive hollow cathode discharge glowed below the part jutting out and seemed to suppress deposition on this part of the sample surface. Due to the switching frequency of about 5000 Hz hollow cathode discharge did not develop with pulsed plasma CVD and so a layer could be deposited.

As hard metals do not change fracture toughness and rupture strength at these temperatures, now special hardmetal inserts are coated commercially at about 600 °C substrate temperature with TiN by plasma CVD driven by a pulsed dc current /11/.

2.2.2. *Deposition of Diamond Layers*. An example for a low pressure and moderate temperature material synthesis that is only possible by combining different methods, is the deposition of diamond layers. These diamond layers have obtained great interest during the last years because diamond is a material with extremely outstanding features: diamond is the hardest material, its optical transmission gap in the wavelength scale is high, the heat conductivity is the highest of all materials at room temperature etc.. Diamond in thin layer can be produced using hydrogen/ hydrocarbon gas mixtures by deposition from acetylene flames, by the so-called hot-wire method, and with highest quality by microwave plasma CVD, Fig. 13. A typical set of deposition parameters for the last mentioned deposition

www.manaraa.com

method is given in table 4.

Trying to deposit from hydrocarbon gas with substrate temperature alone, that is trying pure CVD, results in the pyrolytic deposition of graphitic carbon layers. Plasma excitation of hydrocarbon gases and ambient temperature gives polymeric soft layers with high hydrogen content. Only by combining both processes diamond layers like that of Fig. 14 can be deposited.

According to the deposition parameters the layers contain more or less non diamond carbon,the best proof for diamond is the Raman spectroscopy /12/.

A very important treatment step is the substrate preparation. By this preparation growth sites must be made on the surface and the density of these sites influences the growth velocity of continuous layers. An example for the different effects of ultrasonic treatment with diamond suspension are given in Fig. 15. It can be seen that low growth site density results in the growth of rather big single crystallites. Fig. 16 shows such single crystallites.

2.3. COMBINATION OF PVD AND PLASMA CVD

The very low friction coefficient against itself and against steel and the low wear of layer and counterpart make the diamond like carbon coatings (DLC) very interesting for tribological applications. The tribological features of DLC depend mostly on the low interference and the high chemical inertness of the carbon. DLC made by plasma CVD from hydrocarbon gases like methane contains about 30 at.% hydrogen and has a considerable part of diamond like bonds depending on the deposition conditions. It can be made very hard but hardness is difficult to measure because of the large part of elastic recovery after the hardness indentation. Usually DLC shows high compressive stress. The chemical inertness - useful in tribological applications - simultaneously hinders a good adhesion to steel substrates. Together with compressive stress this results in low coating adherence. It has be shown /13/ that small amounts of metals with concentration below 10 at.% lower the stress of DLC and make it possible to coat steel with sufficient adherence. These Me:C coatings composed of DLC with metal carbides dispersed in it /14/ show the same tribological features as pure diamond like carbon.

In practice a Me:C coating should be a layered coating with smooth transition from pure metal to Me:C with very low metal content. The deposition process, table 5, starts with magnetron sputtering in an argon discharge /15/. This is a pure PVD process which deposits the first metallic interface layer giving the high adherence to the substrate. In a second step an increasing hydrocarbon gas flow is mixed to the argon. This starts two mechanisms. First the hydrocarbon is cracked in the sputter discharge and carbon is incorporated in the deposited metal layer. Second carbon is also deposited onto the sputter target thus poisoning this target more and more. As a result the sputter rate of metal decreases drastically and the deposited layer becomes carbon rich. At least the process is dominated by plasma CVD from the hydrocarbon/argon discharge, because the sputter rate of carbon from the poisoned target is too low to be alone responsible for the growth rate of the Me:C layer.

The adherence to various steels and hardmetals was tested by depositing Zr:C of 3.5 μm under identical conditions. The bias voltage was only -50V so that layers with a low hardness of HK0.05 = 500 but also with low stress were deposited. This should result in a relatively high adherence to the steel. In the diagram Fig. 17 the critical loads are plotted

www.manaraa.com

for the different steels and hardmetals. Both acoustic critical loads and optically measured critical loads are shown. As usual for the acoustic critical load the onset of a high and continuous acoustic emission was taken; for the optical value the beginning of a continuous damage of the coating aside the scratch line was measured by microscope.

There are three groups of materials. The Zr:C coatings adhere quite well to the steels from the first group, that are cold work tool steels; the mean critical load F_c of this group is 50 N. Nearly no adherence - the critical load is below 5 N - exists to the hardmetals tested here. Hot work tool steels behave quite different. No adherence can be achieved to the steel 1.3207, and there is no difference whether the steel is made by powder metallurgy (index "p") or by a melting process (index "s"). But the adherence to the steel M3 (1.3344) is 40 N and that is comparable to the adherence values of the steels of the first group.

When looking at the components of the steels and hardmetals, there is one component common to all materials to which Zr:C does not adhere, that is cobalt. All other components do not seem to influence the adherence behaviour so drastically.

2.4. LASER CVD

Similar to plasma CVD which delivers additional excitation energy to the CVD process by the plasma, in laser CVD the excitation is given by the laser light. In contrast to the other CVD methods laser CVD enables the very localised deposition of layers without need of any masking techniques or etching after deposition. A second important advantage is the low temperature of the bulk of the substrate because heating occurs also localised to the surface region involved in the coating process.

Two mechanisms can be distinguished in principle. In pyrolytic laser CVD the laser beam is directed perpendicular to the surface to be coated. It heats the top of the surface to such a temperature that the conventional high temperature CVD process can start at this localised surface region. In photolytic laser CVD the laser beam is directed parallel to the surface to be coated. It excites the gas mixture in front of the substrate, so that excited species can diffuse to the surface and react there in building the coating. Of course both processes can also be combined.

To get useful coatings a lot of parameters must be taken into account. The lasers can be used in the continuous wave mode or in the pulsed mode and pulse frequencies can be varied. These parameters influence especially the surface temperature, but also the growth rates e.g. when diffusion limited steps are involved. The laser wave length rules the absorbance in the gas mixtures but also in the substrate surfaces. In addition a growing layer changes the absorption of the laser light and changes in the growth velocity and very high temperature changes can be the result. Further experimental difficulties can arise from dark reactions and unwanted depositions on entrance windows.

An experimental set-up is shown in Fig.17 /16/. It is assembled for the deposition of TiN in the pyrolytic way. As precursor gases $TiCl_4$ or Tetrakis (Tetrakisdimethylaminotitanium), N_2 or NH_4 are used. The Fig.18 shows a deposited layer. The Ar^+laser beam was scanned over the steel substrate. The ripple formation seen in the high magnification picture is probably due to interference effects /16/.

www.manaraa.com

3. Other Hybrid Processes

A new approach is a source configuration constructed to allow operation in the magnetron discharge regime or in the arc discharge mode /17/. Among other possibilities one can think about as hybrid processes the laser induced galvanic deposition is in the experimental state /18/. Laser triggering of a cathodic arc could also be seen under this item /19/. Surely other methods can be combined for special purposes when the combination gives an advance for the coating process.

4. Summary

The combination of different sources or processes to form a hybrid deposition process always then is meaningful when special conditions are necessary which cannot be achieved by one of the processes or sources alone. This was shown for the hybrid PVD deposition. Combination of arc with high ion density and droplet-free magnetron sputter source easy to be regulated for low rates , is a simple and inexpensive possibility to develop ternary compounds of varying composition. With plasma CVD the coating temperature can be lowered to such a degree that temperature sensitive substrate materials are not changed in their properties during coating. New processes like diamond deposition at low pressure and moderate temperatures can be used with reasonable deposition rates. Combining PVD and plasma CVD in consecutive steps enables the deposition of complex coatings like Me:C with metallic interface layer for enhanced adherence to steel substrates. By use of laser beams in a CVD environment localised and, for the bulk of the substrate, low temperature depositions are possible without the need of masking.

Acknowledgements

This work was partly supported by funds of the European Communities under the Brite Contract Number P-1053-1-85, the Brite/Euram Contract Numbers BREU-0098-C and BREU-3327, and funds of the Bundesministerium für Forschung und Technologie under the contract number 13 N 5605 2.

Literature

/1/ H. Freller, H. Häßler, Thin Solid Films, **153** (1987) 67 - 74

/2/ O. Knotek, M. Atzor, F. Jungblut, H.-G. Prengel, Surf. and Coat. Technol., **39/40** (1989) 445-453

/3/ B. F. Coll, R. Fontana, A. Gates and B. Sathrum, Mat. Sci. Eng., **A140** (1991) 816 - 24

/4/ H. Jehn, S. Hofmann, W. D. Münz, Metall **42** (1988) 658

/5/ H. Freller, in Jahrbuch Oberflächentechnik (1991) Bd. 47, Metall-Verlag GmbH Berlin/Heidelberg, 238-252

/6/ H. Freller, K. G. Günther, H. Häßler, Annals of the CIRP, **37** (1988) 165 - 169

www.manaraa.com

/7/ U. König, H. van den Berg, R. Tabersky, V. Sottke, 12th International Plansee Seminar '89, Proc. Vol. 3, p. 13 - 25
/8/ S. Verprek, Thin Solid Films, **130** (1985) 135
/9/ H. Freller, H. P. Lorenz, Mat. Sci. Eng., **A140** (1991) 534 - 538
/10/ F. Sanders, Philips CFT, Eindhoven, private communication
/11/ Krupp Widia, Essen, FRG
/12/ P. V. Huong, Diamond and Related Materials, **1** (1991) 33 - 41
/13/ H. Dimigen, H, Hübsch, Reaktiv und nichtreaktiv aufgestäubte Hartschichten zur Minderung von Reibung und Verschleiß, Proceedings Verschleiß- und Korrosionsschutz durch ionen- und plasmagestützte Vakuumbeschichtungstechnologien, Internationale Tagung an der THD, 15./16.3.1983, THD Schriftreihe Wissenschaft und Technik 20, Technische Hochschule Darmstadt, Darmstadt 1983, p. 257
/14/ W. van Duyn, B. van Lochem, Thin Solid Films, **181** (1989) 497 - 503
/15/ H. Freller, A. Hempel, J. Lilge, H. P. Lorenz, Diamond and Related Materials, **1** (1992) 563 - 569
/16/ G. Reiße, R. Ebert, U. Illmann, Ingenieurhochschule Mittweida, private communication
/17/ P. Robinson, A. Matthews, Surf. Coat. Technol., 43/44 (1990) 288 - 298
/18/ R. E. Acosta, L. T. Romankiw, R. J. von Gutfeld, Thin Solid Films, **95** (1982) 131 - 132
/19/ H. J. Scheibe, P. Siemroth, W. Pompe, B. Bücken, in "Wer macht was in den physikalischen Technologien", Band I Poster (1990) S. 266 -268, Hrsg. VDI Technologiezentrum, VDI-Verlag, Düsseldorf

المنارة للاستشارات
www.manaraa.com

Table 1 Deposition conditions and properties of coatings in the system (Ti,M2)N

Coating	I_{ARC} A	I_{MAG} A	Rate µm/h	Metal 1 at.%	Metal 2 at.%	fracture morphology	Hardness (HKN 0.05)	Rockwelltest
Ti-Al-N	60	7,5	7,1	70,9	28,7	dense, column.	2747	-1
	60	9,5	9	42,3	57,3	microcryst.	1760	-1
Ti-V-N	60	8	12,8	50	50	dense, column.	2350	2
Ti-Cr-N	60	5	11	40	60	dense, column.	2300	1
	90	5	10,3	70	30	microcryst.	2700	1
Ti-Ta-N	60	8	10,6	28	72	glassy	3472	1
	60	4	7	68	32	layered	2611	2
Ti-W-N	60	4	7,9	36,5	63,5	layered	3324	0
	60	2	4,9	66	34	layered	2514	1

(Bias voltage 50 V, distance from magnetron target 200 mm, Argon pressure $2 \cdot 10^{-2}$ mbar, Nitrogen flow 60 ml/min)

Table 2 Deposition conditions and properties of coatings in the system (Cr,M2)N

Coating	I_{ARC} A	I_{MAG} A	Rate µm/h	Metal 1 at.%	Metal 2 at.%	fracture morphology	Hardness (HKN 0.05)	Rockwelltest
Cr-Al-N	60	10	10,6	70,4	29,4	glassy	2778	1
Cr-Nb-N	60	10	13,2	34	65,8	dense, column.	2737	0
Cr-V-N	60	8	8,4	58	42	glassy	2254	0,5
	90	8	9,6	62	38	glassy	2260	0,5
Cr-Ta-N	60	7	11,7	33	67	dense, column.	2728	1
	60	3,5	8,4	73	27	layered	2450	1
Cr-W-N	60	4	6,9	40	60	dense, column.	2693	0,5
	60	2	4,9	67	33	layered	2406	1

(Bias voltage 50 V, distance from magnetron target 200 mm, Argon pressure $2 \cdot 10^{-2}$ mbar, Nitrogen flow 60 ml/min)

www.manaraa.com

Table 3 Process Parameters for Plasma CVD of TiN

hydrogen flow	1000 cm^3/min (standard conditions)
nitrogen flow	200 cm^3/min (standard conditions)
$TiCl_4$ flow	5 cm^3/min (standard conditions)
total pressure	2 mbar
rf power density	0.7 W/cm^2 (13.56 MHz)
substrate temperature	460 °C
growth rate	2.5 μm/h

Table 4 Diamond Deposition by Microwave Plasma CVD

methane flow	2.5 cm^3/min (standard conditions)
hydrogen flow	497.5 cm^3/min (standard conditions)
total pressure	30 mbar
microwave frequency	2.45 GHz
microwave power	1 kW
substrate	silicon wafer, scratched with diamond polish paste (1 μm and 0.25 μm)
substrate table temperature	800 °C
growth rate	0.3 μm/h

Table 5 Hybrid PVD - plasma CVD Zr:C coating process

process step	**target power**	**time** min	**substrate temperature**	**pressure** **($Ar+CH_4$)** mbar	**sustrate bias** V	**ethine flow** ml/min	**layer thickness** μm
sputter cleaning	-	15	RT -> 180°C	$6 \cdot 10^{-2}$	-2000	0	-
Zr interface layer	high	1		$6 \cdot 10^{-3}$	-100	0	0.1
intermediate layer	low	10		$6 \cdot 10^{-3}$	-100 -> -250	0 -> 80	1
Zr:C layer	low	25	130°C	$6 \cdot 10^{-3}$	-250	80	3

المنارة للاستشارات
www.manaraa.com

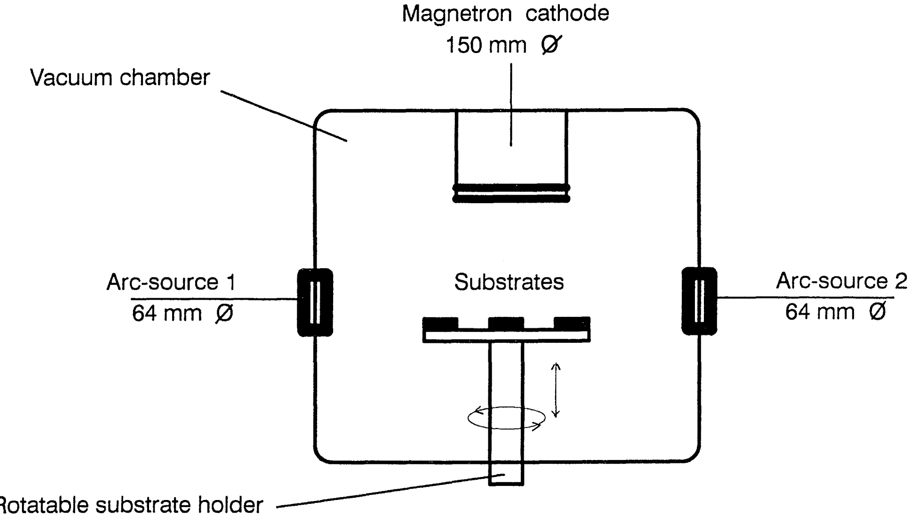

Fig. 1 Schematic view of the PVD hybrid set-up

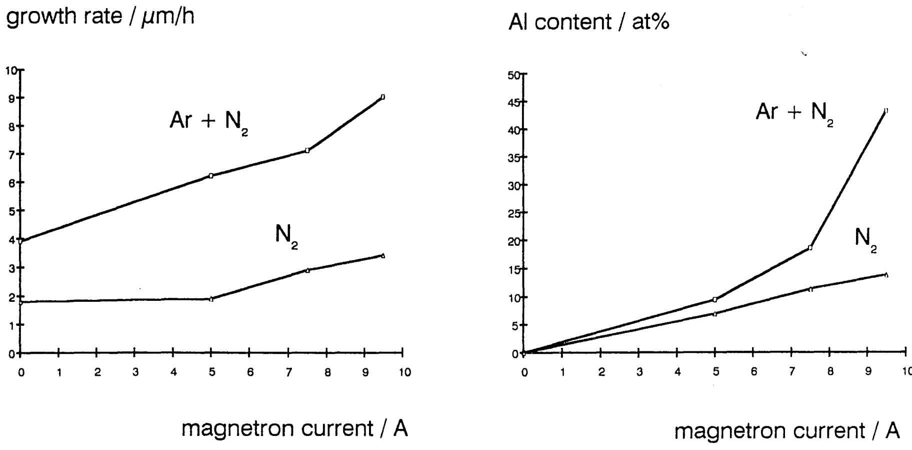

Fig. 2 Deposition rate and Al-concentration in (Ti,Al)N-coatings in dependence of magnetron current
arc current 60 A bias voltage 50 V $p_{N2} = 2 \cdot 10^{-3}$ mbar $p_{Ar} = 2 \cdot 10^{-2}$ mbar

www.manaraa.com

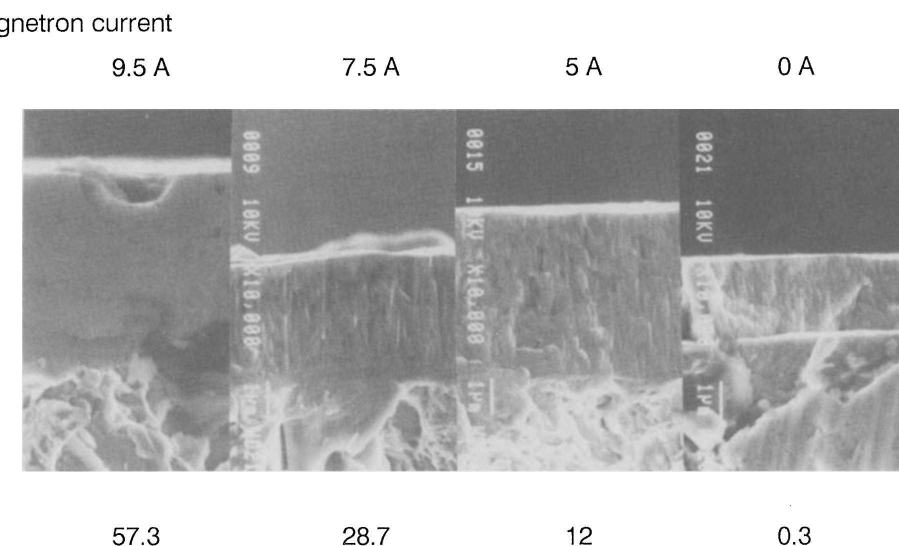

Fig. 3 Fracture cross section of (Ti,Al)N-coating with different Al concentra tion

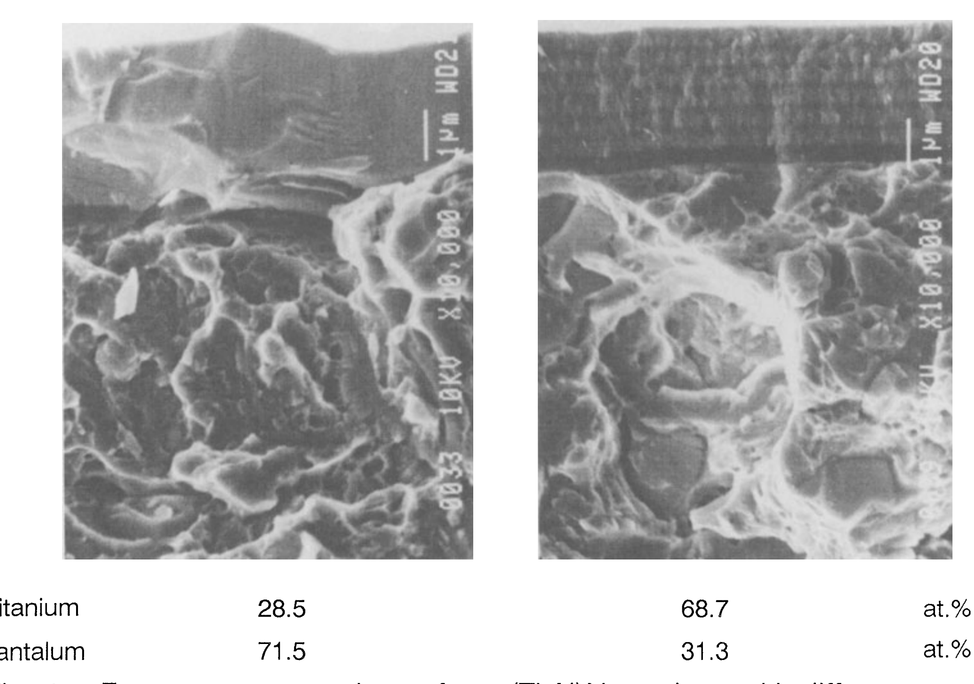

Fig. 4 Fracture cross sections of two (Ti,Al)N-coatings with different composition

المنارة للاستشارات
www.manaraa.com

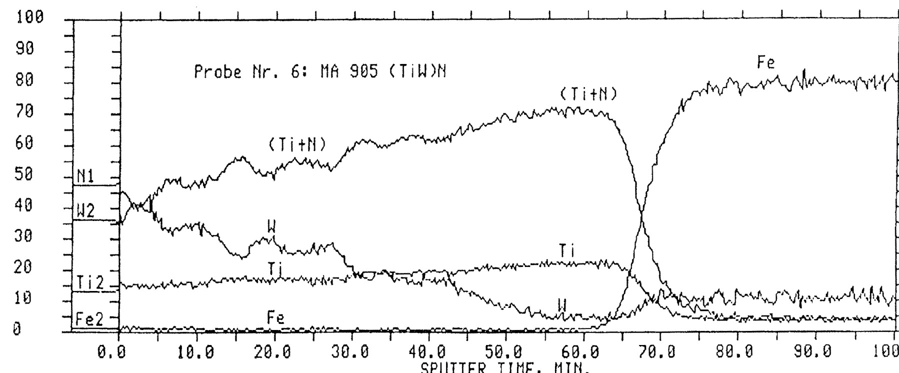

Fig. 5 Auger depth profile of a (Ti,W)N-coating with graded composition

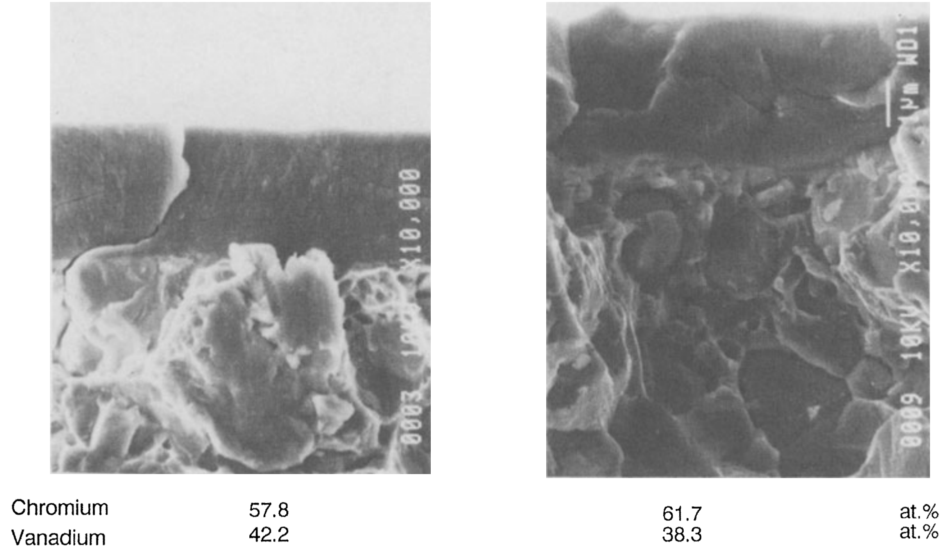

Chromium	57.8	61.7	at.%
Vanadium	42.2	38.3	at.%

Fig. 6 Fracture cross sections of two (Cr,V)N-coatings with different composition

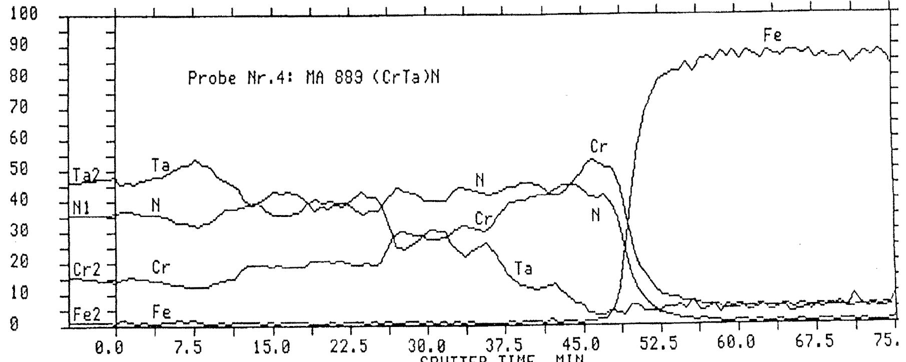

Fig. 7 Auger depth profile of a (Cr,Ta)N-coating with graded composition

المنارة للاستشارات
www.manaraa.com

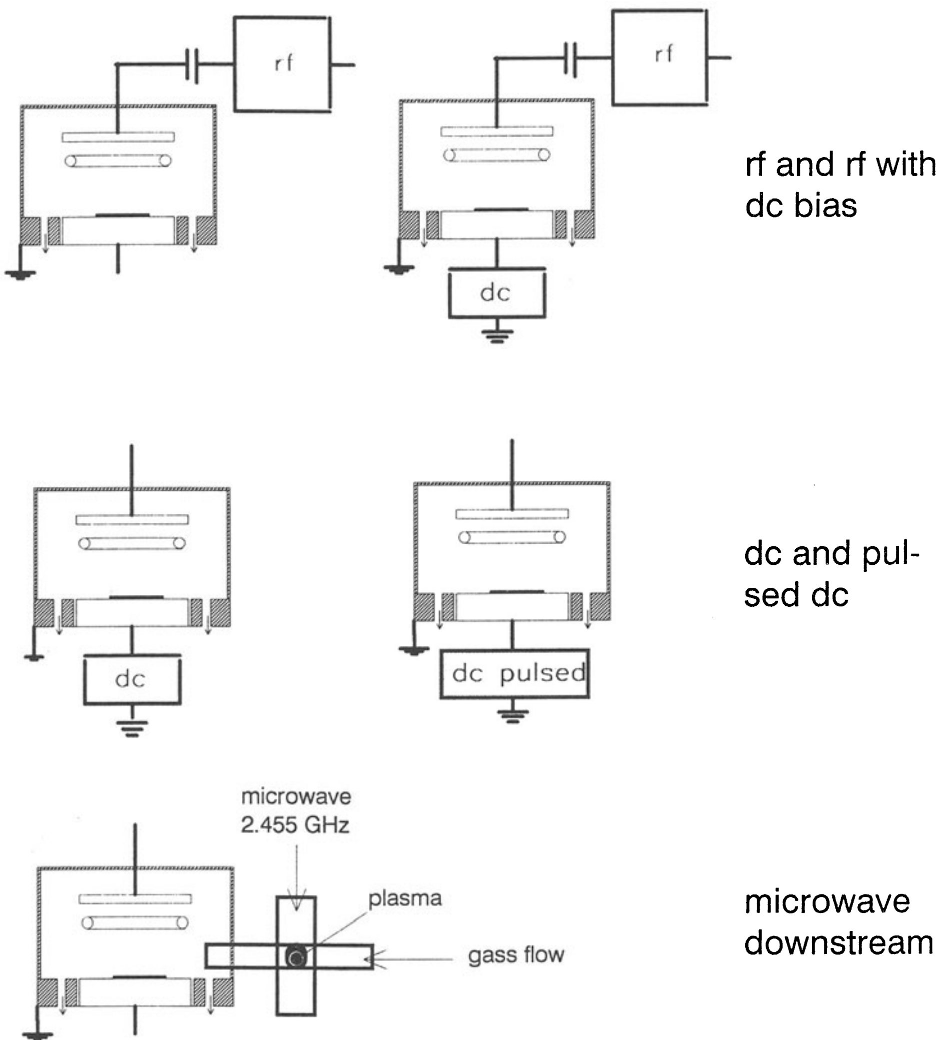

Fig. 8 Plasma CVD of TiN with different power supplies for the plasma discharge

www.manaraa.com

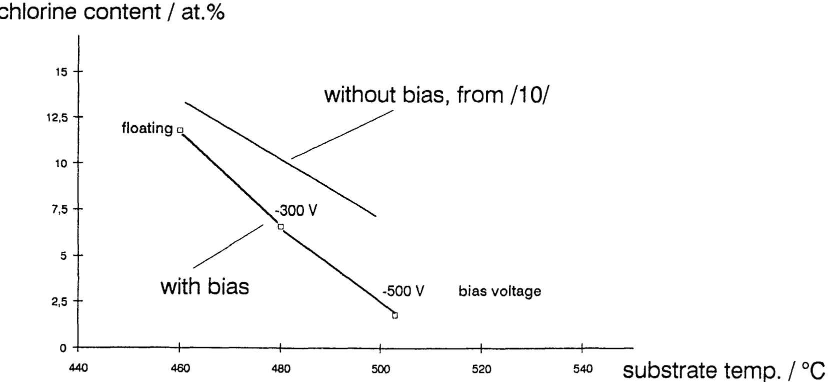

Fig. 9 Chlorine content in plasma CVD TiN
Influence of substrate temperature and substrate bias voltage

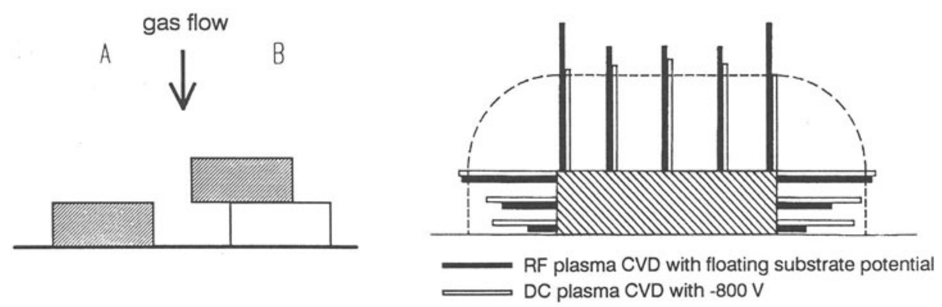

Fig. 10 Substrate arrangements for 3-D coating experiments
Samples of steel 1.3343, 15 x 15 x 6 mm³

Fig. 11 Thickness distribution
Comparison between RF deposition at floating potential and DC deposition at -800 V

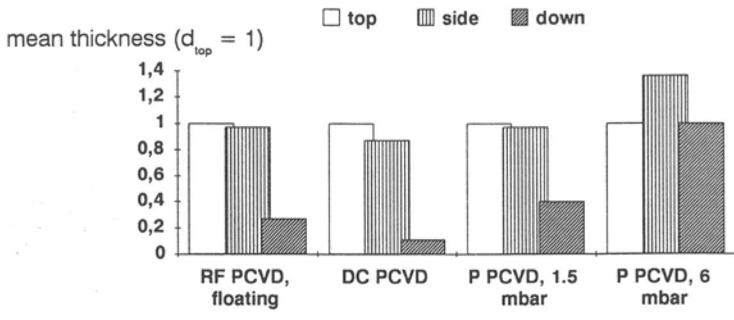

Fig. 12 Mean thickness of coatings obtained by different plasma conditions

www.manaraa.com

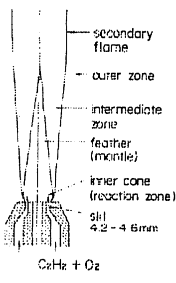

Oxygen-Acethylene flame deposition 1) 2)

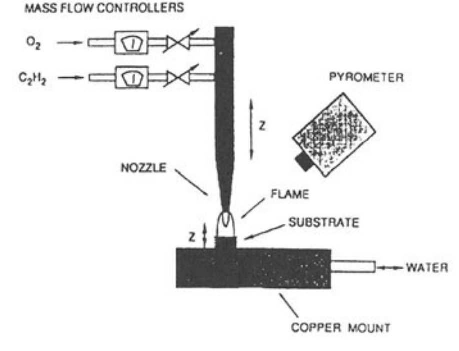

Filament

0.8 mm

8 mm

50 mm

Hot filament deposition 3)

gas inlet

filament

electrode

substrate

quartz tube

substrate holder

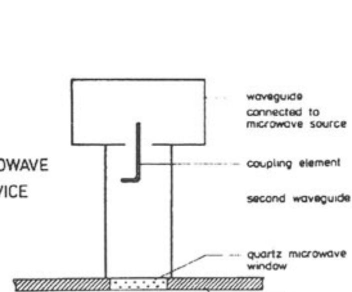

Microwave plasma deposition 4)

quartz microwave window

metallic vessel wall

plasma

REACTION VESSEL

substrate

substrate holder

thermocouple

Fig. 13 Diamond deposition methods

Drawings (partly modified) from: 1)Y. Matsui et al., Diamond and Related Materials, 1(1991) 19-24 2) L. Hansen et al., Thin Solid Films, 196 (1991) 271
3) S. Okoli et al., Surface and Coating Technol., 47 (1991) 585-599 4) A. Ohl, et al. Surface and Coating Technol., 47 (1991) 29-38

www.manaraa.com

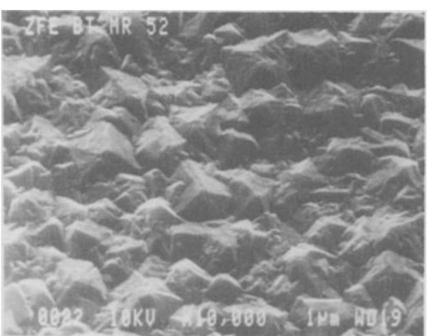

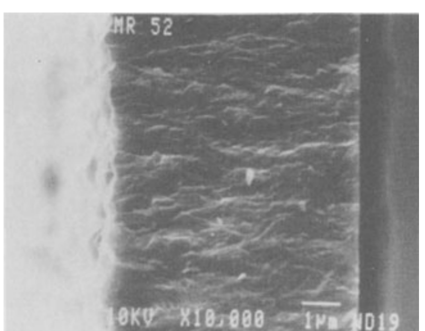

Fig. 14 Plasma CVD diamond layer, surface and fracture cross section

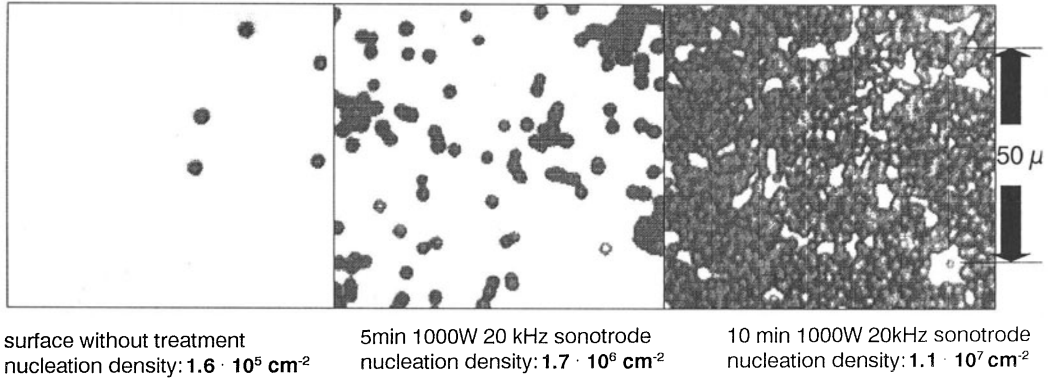

surface without treatment
nucleation density: **1.6 · 10^5 cm^{-2}**

5min 1000W 20 kHz sonotrode
nucleation density: **1.7 · 10^6 cm^{-2}**

10 min 1000W 20kHz sonotrode
nucleation density: **1.1 · 10^7 cm^{-2}**

Fig. 15 Nucleation density effect of ultrasonic treatment of the silicon surface with 1μm diamond polish suspension

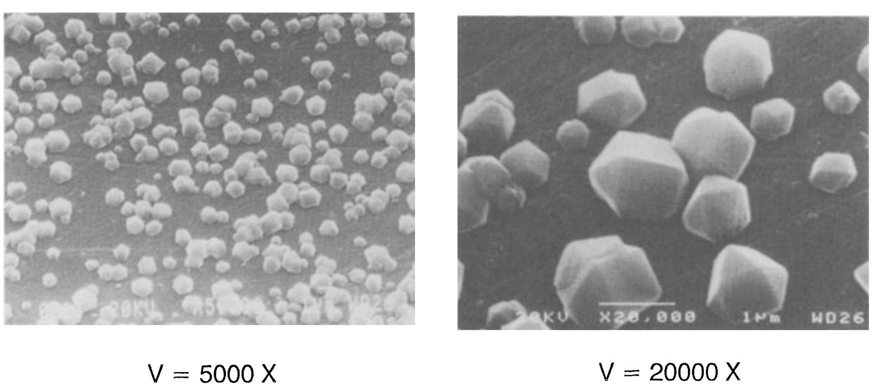

V = 5000 X

V = 20000 X

Fig. 16 Plasma CVD diamond single cristallites

المنارة للاستشارات
www.manaraa.com

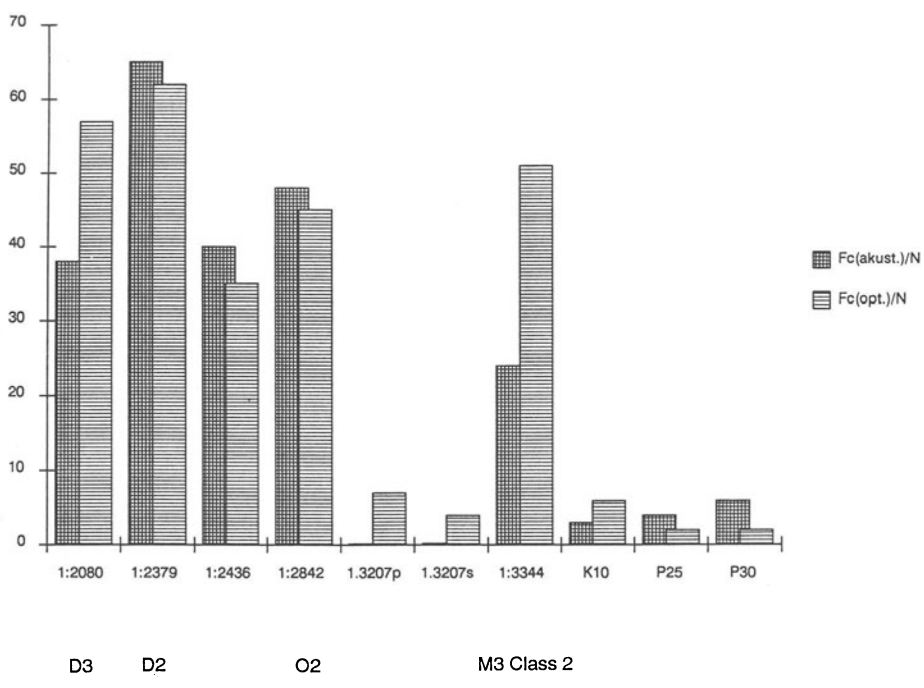

Fig. 17 Adherence of Zr:C (scratch test)
HK(25gf) = 500 d = 4.5 μm 0.5 μm Zr / 1 μm transition layer / 3μm Zr:C
[Zr] < 10 at%

المنارة للاستشارات
www.manaraa.com

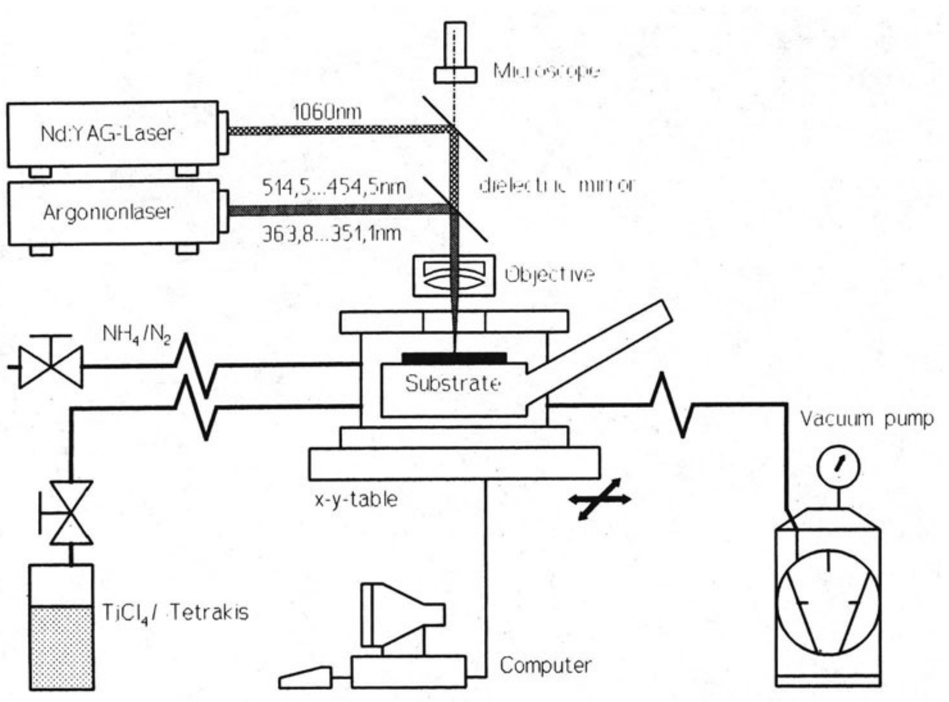

Fig. 18 Laser CVD set-up

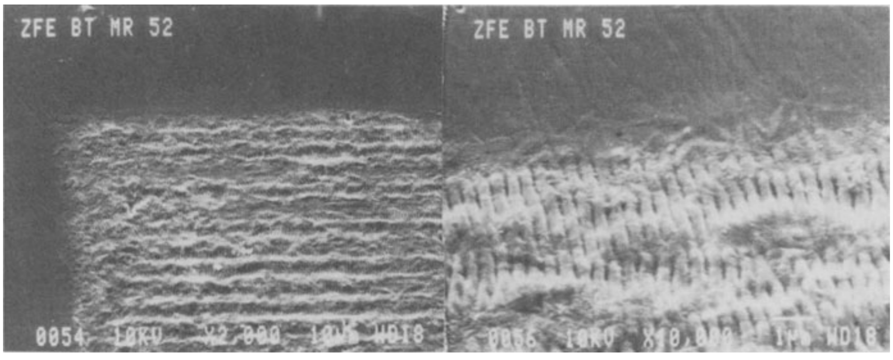

A: magnification 2000 B: magnification 10000

Fig. 19 cw-mode deposition with Ar^+Laser , (precursor Tetrakis, $V_s = 50\ \mu m/s$, $P = 0.8$ W)

www.manaraa.com

MEASUREMENT OF MECHANICAL PROPERTIES OF THIN SOLID FILMS I: HARDNESS, ELASTICITY AND STRESS

Klaus H. Taube
Fraunhofer-Institute for Thin Film and Surface Engineering
Vogt-Kölln-Straße 30
W-2000 Hamburg 54
Federal Republic of Germany

ABSTRACT. This article gives an overview of current techniques to determine hardness, Young's modulus and stress state of a thin solid film on a substrate. The former two are measured with an instrument sometimes referred to as a nanometer indenter. It is capable of detecting continuously the indentation depth of a diamond tip in dependence of load on the indenter with nanometer precision. From loading-unloading cycles the mechanical parameters hardness and Young's modulus are calculated. The stress state of thin films can be obtained by measuring the curvature of a bent substrate with the stressed film fixed to it or by x-ray techniques to determine the spacing between strained crystal planes. The mathematical theory, assumptions and limitations of these techniques are discussed and two examples of the information obtained from these measurements are presented.

1. INTRODUCTION

For an optimisation of the performance of thin wear resistant films, but also just to make sure that films will stand their expected service life in other applications, a precise determination of their mechanical properties is necessary. The hardness and Young's modulus, though not the only parameter, strongly influence the wear behaviour by determining the degree of strain around abrasive particles ploughing through the film. The stress in the film on the one hand increases or decreases the strain the film can bear before fracture occurs. On the other hand it also determines, together with the adhesive force between film and substrate, whether the film keeps attached to the substrate during tangential loading or whether it buckles, cracks or spalls off at intolerable low loads.

In the last years great progress has been made in determining the "simple" mechanical properties hardness, Young's modulus and stress by theoretically describing, at least approximately, the stress fields in loaded films on substrates. Parallel to these developments - and often before them - instruments with the required precision have been developed being capable of precisely positioning a sample with sub micron and millirad accuracy and measuring displacements with Ångstrom resolution. Only from these developments it is understandable that today mechanical properties of films with thickness of less than 1 µm can be determined without troubling influence of the substrate material.

W. Gissler and H. A. Jehn (eds.), Advanced Techniques for Surface Engineering, 275–294.
© 1992 *ECSC, EEC, EAEC, Brussels and Luxembourg.*

www.manaraa.com

2. THEORY

2.1. Hardness and Young's modulus

In conventional hardness measurements the contact area between indenter and specimen is measured in an optical microscope after removal of the load. Due to the extremely small dimensions of the imprints used in thin films testing, this method can not be applied because of the finite resolution capabilities of optical microscopes. Curves of displacement vs. load and time data are used instead. They give much more information about elasticity, plasticity and time dependent behaviour of the sample than conventional hardness measurements. Furthermore the measurement systems can be used to obtain load-displacement data for specially machined samples like beams and thin film membranes from which Young's moduli, yield and residual stresses of the layers can be determined.

2.1.1. Indentation of thin films on substrates

2.1.1.1. Determination of contact area

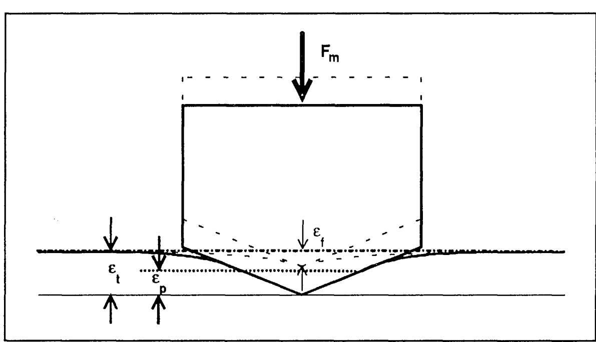

Figure 1. Definition of geometric parameters of indenter-sample contact. Under maximum load F_m (thick lines) the contact is described by the total depth ε_t and plastic depth ε_p, after load removal (broken lines) by the final depth ε_f.

The major drawback of nanoindentation is that the exact contact area between indenter and sample is unknown. The contact area, however, is the value which is essential in determination of hardness and Young's modulus as is shown in this chapter. Unfortunately no closed analytical solutions for the elasto-plastic contact problem of indentation exist. Plastic theory can give only an estimate for a material that yields at a certain stress and exhibits no work hardening [1, 2, 3]. On the other hand elastic theory [4, 5, 6] of course neglects all effects of plasticity which play a crucial role in indentation deformation. Older conventional hardness measurements [7] and recent theoretical considerations [8] and experiments [9] show, however, that it can also give an approximate, but satisfying description of the elastic displacements around the plastically deformed zone immediate to the indenter.

For any axisymmetric indenter penetrating an elastic half space, the relationship between the contact stiffness S, contact area A and the reduced Young's modulus E_r of half

www.manaraa.com

space (E_0, ν_0) and indenter (E_i, ν_i) is given by ($\beta = 2/\sqrt{\pi}$ for conical and spherical indenters) [8]

$$S = \frac{dF}{d\varepsilon} = \beta E_r \sqrt{A} \tag{1}$$

with
$$\frac{1}{E_r} = \frac{1 - \nu_0^2}{E_0} + \frac{1 - \nu_i^2}{E_i} \tag{2}$$

The hardness of the sample is defined as the ratio of maximum load F_m to the contact area A under load.

$$H = \frac{F_m}{A} \tag{3}$$

The difficulty lies in properly determining the plastic indentation depth ε_p that is a measure of the contact area. Several experimental studies show [9, 10, 11, 12] that the observed unloading curves on a variety of materials ranging from soft metals and polymers to hard ceramics and single crystals like sapphire can be described by the elastic unloading of a smooth rotational symmetric punch, whose shape function is given by

$$y = p^* |x|^m \tag{4}$$

Equation (4) with $m = 1$ describes a conical punch, with $m = 2$ a parabolic one and with $m \to \infty$ a flat ended cylindrical punch. The resulting unloading curves are given by (ε_f: final depth at zero load)

$$\varepsilon - \varepsilon_f = \alpha^* F^{1 - \frac{1}{1+m}} = \alpha^* F^n \tag{5}$$

that is for

the cone: $$\varepsilon - \varepsilon_f = \alpha^* F^{1/2} \tag{6}$$

the parabolic punch: $$\varepsilon - \varepsilon_f = \alpha^* F^{2/3} \tag{7}$$

the flat ended punch: $$\varepsilon - \varepsilon_f = \alpha^* F^{1} \tag{8}$$

That means the unloading curves vary between linear and parabolic behaviour. Loubet [10] and Doerner and Nix [11] pointed out, that with a large range of materials the linear approximation gives a satisfying description. Recently Oliver and Pharr [9] found even better consistency of measured Young's moduli with literature values when using the parabolic punch approximation ($m = 2$) especially with materials of a high hardness to modulus ratio.

In any case the plastic depth is calculated from a model of elastic reloading the plastically deformed sample (situation after load removal) to the total indentation depth ε_t.

$$\varepsilon_p = \varepsilon_t - c^* \frac{F_m}{S} \tag{9}$$

المنارة للاستشارات
www.manaraa.com

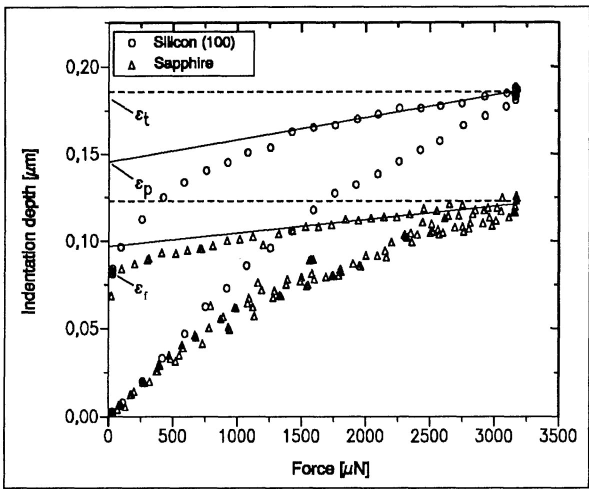

Figure 2. Loading-unloading curves from measurements on silicon (100) and sapphire (1000). Shown are the definitions for the symbols used in the text. ε_t: total indentation depth, ε_p: plastic indentation depth, ε_f: final indentation depth, F_m: maximum load.

The values of c are $^2/_\pi*(\pi-2)$ for the conical, 0.75 for the parabolic and 1 for the flat ended cylindrical punch (the Loubet-Doerner-Nix approximation). The contact area is calculated from $A = k * \varepsilon_p^2$ and the hardness from

$$H = \frac{F_m}{k\,\varepsilon_p^2}, \tag{10}$$

where k is a proportionality constant describing the bluntness of the indenter ($k = 24.5$ for the Berkovich-type indenter usually used in thin film testing and also for the Vickers-type indenter), which can be calculated from simple pyramidal geometry. So hardness and Young's modulus of the sample can be determined in principle from the unloading curve with the help of equations (1) and (11).

The procedure is the following:

a.) Following Loubet, Doerner and Nix set $c = 1$, do a least-squares-fit to the first linear part of the unloading curve and calculate the plastic depth and contact stiffness.

b) Following Pharr and Oliver, do a least-squares-fit of equation (5) to the experimental data, determining α, ε_f and n. Differentiate analytically equation (5) at maximum load F_m to obtain the unloading stiffness S. If $n \approx 1.5$ use the parabolic punch approximation (with $c = 0.75$) to determine the plastic depth, hardness and Young's modulus.

2.1.1.2. Indentor geometry

Due to the very small size of the indentations allowable in thin film testing (see chapter 2.1.1.3.) the perfection of the indenter tip plays a crucial role. The three-sided

المنارة للاستشارات
www.manaraa.com

Berkovich-type indenter (Apex-angle 115°) is preferred to the conventional four-sided Vickers-type indenter as it can be ground to a better tip normally. Careful examinations [11, 13, 14], however, have shown, that the inevitably rounded tip geometry has to be accounted for. Fortunately this can be done with a correction function depending on indentation depth.

Doerner and Nix [11] calculated an 'area function' describing the depth dependence of the true sectional area of the pyramid. They obtained it by comparing the sizes of indents in a soft metal (determined by TEM replication methods) and the experimental load-displacement data. This is a rather complicated and time consuming method. A simpler one is making a series of impressions at various loads in a reference material (single crystal silicon in [13], single crystal aluminum and fused silica in [9]). Then it is assumed that the material properties (hardness of silicon in [13], Young's modulus of aluminum and fused silica in [9]) are independent of indentation depth, so that any deviation measured is due to

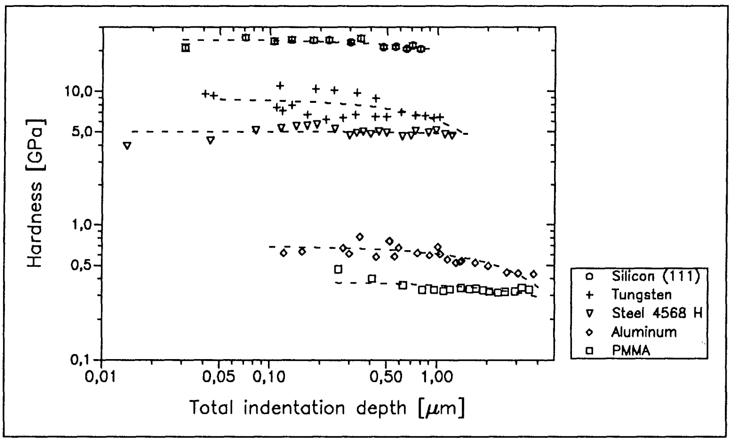

Figure 3. Measurements on various bulk materials including geometric correction (three-sided pyramid, $k = 3{,}854$). Shown is the depth dependence of the measured hardnesses for (see legend) silicon (111), tungsten, steel 4568 H, aluminum and PMMA. Metal samples were mechanically polished, silicon and PMMA were measured as delivered.

the tip rounding. The area function can then be determined from the deviation of measured hardnesses or Young's moduli resp. from a constant value.

Fryda and Taube [13] used the following correction function for the plastic depth ε_p to determine a corrected contact area $A = k\, \varepsilon_{p\ corr.}{}^2$

$$\varepsilon_{p\ corr.} = \varepsilon_{p\ uncorr.} + \varepsilon_t * \left(\frac{a}{\varepsilon_t{}^b} - c + 1\right) \quad (11)$$

whereas Oliver and Pharr [9] propose

المنارة للاستشارات
www.manaraa.com

$$A_{corr.} = k^*\varepsilon_{p\ uncorr.}{}^2 + C_1{}^*\varepsilon_{p\ uncorr.} C_2{}^*\varepsilon_{p\ uncorr.}{}^{1/2} + C_3{}^*\varepsilon_{p\ uncorr.}{}^{1/4} + \ldots + C_8{}^*\varepsilon_{p\ uncorr.}{}^{1/128} \qquad (12)$$

Results from measurements on various bulk materials show that with the use of equation (12) nearly depth independent value of hardnesses and Young's moduli are obtained (figures 3 and 4). Variations can be attributed to the mechanical polishing of the metallic samples.

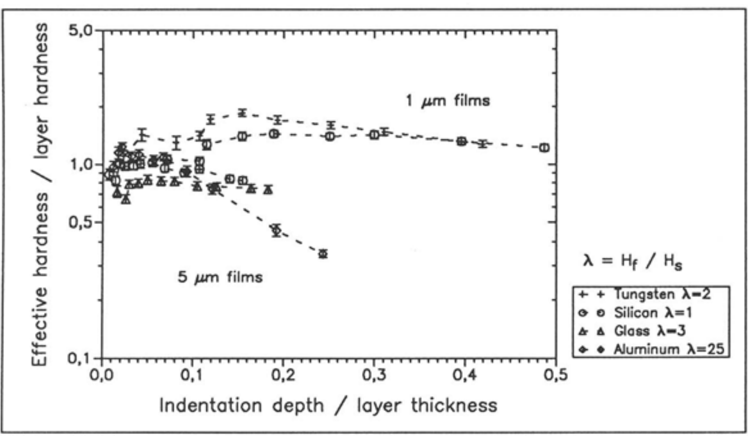

Figure 4. Results from the same measurements as in figure 3. Broken lines indicate literature values of Young's moduli of the samples. Shown is the depth dependence of the measured Young's moduli for (see legend) tungsten, silicon (111), steel 4568 H, aluminum and PMMA.

2.1.1.3. Substrate influence

A reason of major concern in thin film hardness testing has to be the substrate influence on the measured hardness. As long as no analytical indentation theory for thin films on substrates exist, limits to the allowed indentation depths have to be found. An older conservative rule established by Bückle [15] for hardness testing is that the indentation depth should not exceed 10% of the film thickness. This result was also found in a work describing purely plastic behaviour of the material [3], but larger indentation depths should be allowed if layer and substrate are similar. The 10% rule of thumb was confirmed by experiment [13] (see figure 5) and in several numerical studies by finite element methods (FEM) [16, 17, 18]. A FEM study of the indentation of thin films by conical indenters by Bhattacharya and Nix [16] indicates that two separate equations for the cases soft film on hard substrate (case 1) and hard film on soft substrate (case 2) can describe the numerical results for the composite hardness. How well these equations work in practice has yet to be demonstrated. Bhattacharya and Nix found for the hardness of the film substrate composite (t_f: film thickness, ε: indentation depth, σ_S, σ_f: yield stress of the substrate and film resp.)

المنارة للاستشارات
www.manaraa.com

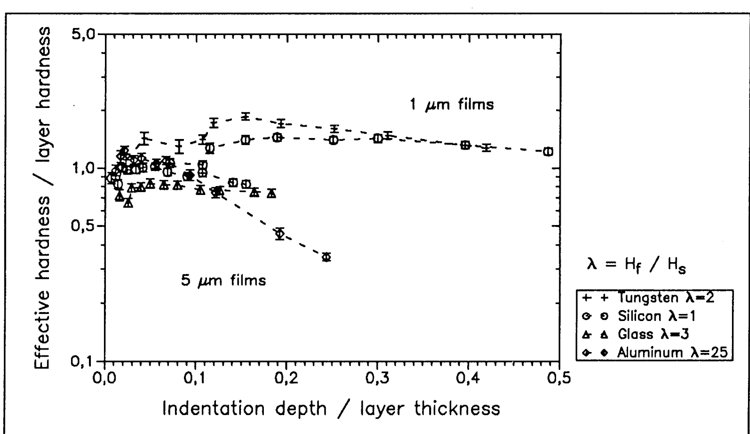

Figure 5. Substrate influence on the measured hardness of sputtered tungsten films on (legend from top downwards) bulk tungsten, silicon, glass and aluminum. Shown is the ratio of measured hardness to reference hardness vs. the ratio of indentation depth to film thickness. Reference value is the hardness of thick films at large indentation depths of 15 GPa. λ: ratio of film hardness to substrate hardness.

Case 1:
$$H = H_S + (H_f - H_S)\exp\left(-\frac{\sigma_f/\sigma_S}{E_f/E_S}\left(\frac{\varepsilon}{t_f}\right)^2\right) \tag{13}$$

Case 2:
$$H = H_S + (H_f - H_S)\exp\left(-\frac{H_f/H_S}{\sigma_f/\sigma_S\sqrt{E_f/E_S}}\frac{\varepsilon}{t_f}\right) \tag{14}$$

Elastic theory for the substrate influence on the measured Young's modulus predicts a lower limit of less than 5% [19, 20], which was also found experimentally [13] (figure 6). A probably useful expression for relating the measured elastic contact stiffness with the film and substrate geometrical and mechanical properties was given by King [21].

$$S = \beta E_r \sqrt{A}\,\frac{E_{r0}}{\frac{1-\nu_f^2}{E_f}\left(1-e^{-\alpha t_f/\sqrt{A}}\right)+\frac{1-\nu_S^2}{E_S}e^{-\alpha t_f/\sqrt{A}}+\frac{1-\nu_0^2}{E_0}}, \tag{15}$$

where t_f is the layer thickness, E_{r0} the reduced modulus of substrate and indenter and E_0 and ν_0 the elastic constants of the indenter. The parameter α also depends on the geometry and the ratio $t_f/\sqrt{A}$. α was calculated numerically and can be obtained from King's article where it is presented graphically.

King found that the right side of equation (1) has to be multiplied with a factor in order to account for the exact geometry of the indenter ($\beta = 2/\sqrt{\pi} = 1.129$ for a conical indenter, $\beta = 1.142$ for a quadrangular indenter, $\beta = 1.167$ for a triangular indenter). Here, too, the practical usefulness of King's equations has not been demonstrated yet.

www.manaraa.com

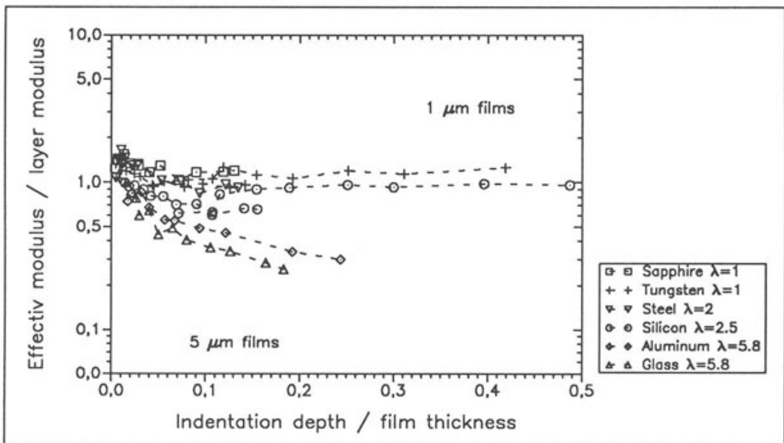

Figure 6. Substrate influence on the measured Young's moduli of sputtered tungsten films on (legend from top downwards) sapphire, bulk tungsten, steel, silicon, aluminum and glass. Shown is the ratio of measured modulus to the Young's modulus of bulk tungsten (406 GPa) vs. the ratio of indentation depth to film thickness. λ: ratio of layer modulus to substrate modulus.

2.1.1.4. Limits

Besides the errors resulting from the imperfect indenter tip geometry and the substrates influence, there are some restrictions for the morphology of the layers to be tested. Due to the extremely small imprint sizes, effects of surface roughness, crystallite size, film inhomogeneity and surface contamination can have a significant influence on measurement results. The determination of the contact area with the method described above relies on the assumption of a smooth plane contact between surface and indenter. Therefore, in order to get reliable results with an acceptable variance, the sample has to be homogeneous and flat at least on the length scale of the imprints. Comparison with literature values of the Young's moduli of bulk materials show, that at least with polished samples hardnesses and Young's moduli can be determined with an agreement within 10% from the load-indentation depth data.

On the other hand one can test the lateral distribution of mechanical properties of the sample with very high resolution. 0.5 μm are possible with conventional X-Y-tables and even better with piezo drives. Some people even speak of their nanometer-indentation system as a mechanical properties microprobe. The ability of probing locally the mechanical response is the most interesting feature of this measurement method and perhaps can give a better understanding of processes happening at the asperities of contacting bodies in friction and wear.

www.manaraa.com

2.1.2. Other methods for determination of Young's modulus

2.1.2.1. Cantilever and beam bending

Another method for determining Young's modulus and yield stress is offered by the microbeam technique [22]. By microelectronic fabrication methods free-standing cantilevered microbeams of the substrate with the film on it are prepared. The load-deflection data from measurements in a nanometer-indentation system can be used to determine both the in-plane elastic modulus and the yield strength of film material. From the slope of the initial linear portion of the load-displacement curve Young's modulus is calculated from

$$w = \frac{4\,F\,l^3}{b\,E_f\,t^3}\,(1 - \nu_f^2)\,, \tag{16}$$

where w is the deflection, l the effective length, b the width and t the thickness of the beam. The yield is calculated from the load, at which yielding occurs, i. e. when the load-deflection data become irreversible, through

$$\sigma_y = \frac{6\,F\,l}{b\,t^2}\,. \tag{17}$$

An advantage of this technique is, that it evaluates the in-plane Young's modulus, which can be different from that measured by indentation, and that the yield stress of the film can be measured directly provided that the substrate does not yield earlier. The disadvantages include complicated sample preparation and the necessity of determination of certain geometrical sample parameters with great precision.

2.1.2.2. Membrane method

Still another method which uses the superior load and displacement resolution of nanoindentation-systems is the deflection of a free standing circular section of the film, where the substrate has been removed, e. g. by chemical etching, so that the film forms a drumhead like membrane [23]. When deflected by a point load in its centre, the displacement of the centre w is given by

$$w = \frac{F\,a^2}{16\,\pi\,D_f}\,g(k)\,, \tag{18}$$

with a being the radius of the membrane, D_f the flexural rigidity of the film given by

$$D = \frac{E_f\,t^3}{12\,(1 - \nu_f^2)}\,, \tag{19}$$

and the function $g(k)$ depending on the tension in the membrane and its geometry.

2.2. Stresses

Stresses in thin films can result from various sources. Usually they are composed of thermal stresses, resulting from the differing thermal expansion coefficients of film and substrate, and internal stresses, whose sources are often not quite clear. In polycrystalline films tensile stresses can arise through recrystallization, so that crystal boundaries vanish

المنارة للاستشارات
www.manaraa.com

and the volume of the film shrinks. In amorphous films like a-C:H the carbon network normally exhibits high compressive stresses due to bending and compressing of C-C bonds. In either case the stress of the film is a factor critically influencing its adhesive properties, but also properties like hardness and fracture strength. For promoting good adhesion a film without any stresses is wanted, whereas compressive stresses lead to a higher fracture strength by hindering crack nucleation and growth.

Methods to measure stresses using continuum mechanics (determination of substrate curvature) normally are applicable only to simple biaxial stress states parallel to the substrates surface, but have the advantage of inexpensive and quick determination. The x-ray methods are much more time (and money) consuming, but are able to give the complete three dimensional stress state of the sample (at least in principle) if the elastic constants are known. Of course they are not applicable to materials without sharp diffraction peaks like amorphous layers.

2.2.1. Curvature methods

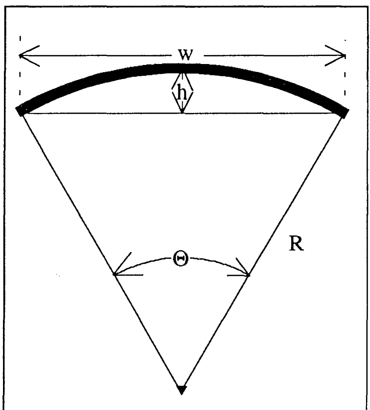

Figure 7. Geometry used in beam and plate bending (after [24]).

One method is to measure the bending of a free standing beam or plate of a relatively thin substrate by the stresses of the film deposited on it. Elastic theory for the deflection of a beam gives [25]

$$\sigma = \frac{4}{3} \frac{E_S}{1 - \nu_S} \frac{t_S^2}{l_S^2} \frac{h}{t_f} \tag{20}$$

with t_S and t_f the thicknesses of substrate and film resp., l_S its length and h the height of the middle of the beam over the foundation.

In the case of a plate bent by a film (biaxial in-plane stress) elastic theory gives [26]

$$\sigma = \frac{E_S}{1 - \nu_S} \frac{t_S^2}{6 R t_f} \tag{21}$$

www.manaraa.com

where R is the radius of curvature of the free standing sample. Ways to determine the deflection or curvature resp. are given in the experimental section.

2.2.2. X-ray methods

Methods requiring a higher experimental effort are the x-ray diffraction techniques. By determining the lattice spacing of certain crystalline orientations, at least the biaxial stress state of the sample and with more experimental effort the complete three-axial stress in the film can be determined in principle, if the elastic compliances are known.

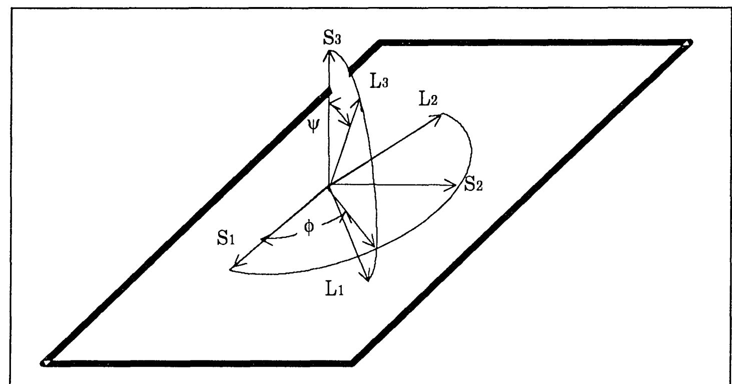

Figure 8. Co-ordinate systems (L: laboratory, S: sample) and geometry used for polycrystalline x-ray residual stress determination (after [27])

A quite common method known as the '$\sin^2\psi$ method' is described e. g. by Shute et al. [27]. This method is applicable to elastically isotropic materials. The laboratory and sample co-ordinate systems are defined in figure 8. The x-ray beam impinges on the sample surface in the L_1L_3 plane with L_3 being the direction of the half angle between incident and reflected beam having an angle ψ with the samples surface. It measures the distance between diffracting crystal planes $d_{\phi\psi}$ in the direction given by the normal L_3. The strain in this direction ε_{33} is then given by

$$(\varepsilon_{33})_{\phi\psi} = \frac{d_{\phi\psi} - d_0}{d_0} \quad (22)$$

Six independent strain measurements must be performed in order to completely determine the samples stress tensor. The strain found in the laboratory system can then be transformed to strains in the sample co-ordinate system by standard tensor transformations, and by use of Hooke's law the following equation for an elastically isotropic material results (σ_{ij}: elements of the engineering 6x6 stress array).

المنارة للاستشارات
www.manaraa.com

$$\frac{d_{\phi\psi} - d_0}{d_0} = \frac{1+\nu}{E}(\sigma_{11}\cos^2\phi + \sigma_{12}\sin 2\phi + \sigma_{22}\sin^2\phi - \sigma_{33})\sin^2\psi$$
$$+ \frac{1+\nu}{E}\sigma_{33} - \frac{\nu}{E}(\sigma_{11} + \sigma_{11} + \sigma_{33})$$
$$+ \frac{1+\nu}{E}(\sigma_{13}\cos\phi + \sigma_{23}\sin\phi)\sin 2\psi \qquad (23)$$

In the case of a biaxial stress state, i. e. for a film under stress parallel to the substrate surface ($\sigma_{33} = \sigma_{13} = \sigma_{23} = 0$), this reduces to

$$\frac{d_{\phi\psi} - d_0}{d_0} = \frac{1+\nu}{E}\sigma_\phi \sin^2\psi - \frac{\nu}{E}(\sigma_{11} + \sigma_{11})$$

with
$$\sigma_\phi = (\sigma_{11}\cos^2\phi + \sigma_{12}\sin 2\phi + \sigma_{22}\sin^2\phi) \qquad (24)$$

For a homogeneous stress distribution, σ_ϕ is independent of ψ and can be determined from the slope of the *'d'* vs. $sin^2\psi$ plot. Deviations from this expected linear behaviour can be attributed to inhomogeneous stress distributions in the sample [27]. Stresses in the sample can be measured with an accuracy of better than 5 MPa.

Methods for determining stresses in elastically anisotropic and textured films have also been developed (for an overview see e. g. [28]). The experimental procedure is the same, i. e. lattice plane spacings have to be determined in various ϕ and ψ directions and from this together with the knowledge of the elastic constants of the material the stress state can be determined. If the films exhibit texture, e. g. (111) typical for FCC metals, no knowledge of the lattice parameters of the unstrained crystals is required as the equations simplify to

$$\varepsilon_\phi^{\text{ñll}[111]} = \frac{d_\psi - d_0}{d_0}$$
$$= \sigma\left(\frac{2 s_{11} + 4 s_{12} - s_{44}}{3} + \frac{s_{44}}{2}\sin^2\psi\right) \qquad (25)$$

where d_ψ is a set of particular planes with normals at an angle ψ with respect to the sample surface, and s_{ij} is a component of the engineering 6x6 compliances array .

By measuring two peaks with different ψ this equation can be solved for the unknown stress σ and unstrained lattice spacing d_0. This analysis is valid for both epitaxial and fibre-textured films and corresponds to the $sin^2\psi$-method described above.

3. EXPERIMENTAL

3.1. Nanoindentation

In the literature several nanometer-indentation systems are described [29, 30, 31, 32, 33, 34, 35] of whom at least one is commercially available. They differ in their depth and force resolution capabilities (resolutions better than 0.1 nm and 0.01 µN resp. are achieved in the better systems), the way the penetration depth is measured (inductive or capacitive transducers) and the overall construction of the apparatus. Load is typically applied either through a coil and magnet assembly (and is calculated from the current through the coil) or by the use of a piezoelectric drive for which a load cell is needed in the load train.

www.manaraa.com

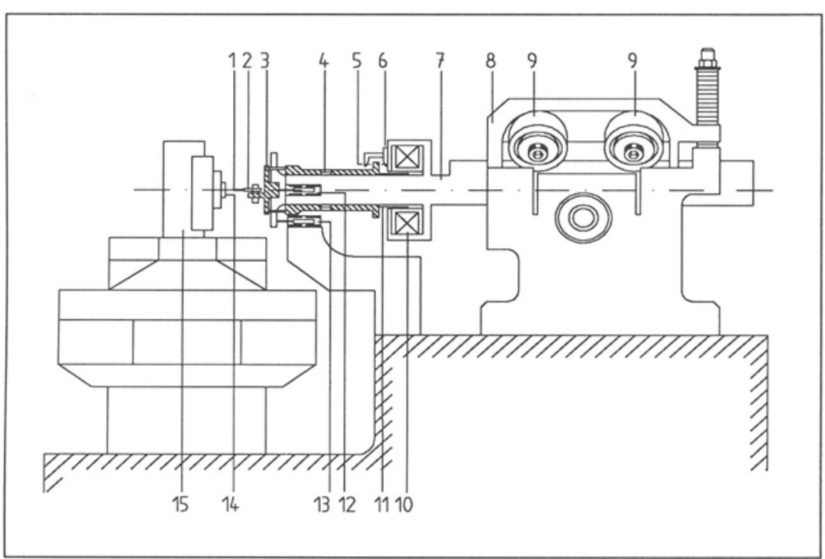

Figure 9. Sketch of the nanometer-indentation system used by the author. (1, 14, 15) sample on X-Y-stage, (2) indenter tip, (3) indenter tip holder (shaded), (4) air bearing, (5, 6) stops for holder movement, (7) central shaft, (8, 9) friction drive system with linear motor, (10, 11) electromagnet and coil (force), (12) inner and (13) outer inductive displacement transducer.

Figure 9 shows a sketch of the indentation system used by the author which was originally constructed in the PHILIPS Research Laboratories in Eindhoven in the Netherlands by Wierenga and Franken [33] . The central shaft (7) is used for placing the indenter and holder assembly (2, 3) on the sample. The automatic move control stops the shaft when the indenter holder is somewhere in the middle between the stops (5, 6). Transducer (12) measures the indenter movement relative to the shaft (7), transducer (13) the shaft movement. Both work with a resolution of better than 2 nm at depths up to 5 µm. Forces between 10 µN and 50 mN can be applied with a resolution of 5 µN. Due to the horizontal construction measurements are started with the indenter tip touching the sample with a force of about 10 to 30 µN. This preload gives an uncertainty in the zero of indentation depth which can be neglected at least with hard films.

3.2. Substrate Curvature

The curvature of substrates with stressed films on them can be measured in various ways. Flinn [24] gives estimates of the measurement accuracy necessary to determine the stress with a resolution of a few MPa.

The displacement of the middle of the bent sample h and the angle Θ is given by (figure 7)

$$h = R\left(1 - \sqrt{1 - \frac{w^2}{4\,R^2}}\right) \approx \frac{w^2}{8} * \frac{1}{R} \tag{26}$$

المنارة للاستشارات
www.manaraa.com

$$\Theta = 2 \arcsin\left(\frac{w}{2R}\right) \approx w * \frac{1}{R} \tag{27}$$

A typical a-C:H film prepared at the FhG-IST has a thickness of 2 μm on a silicon wafer ($E_S = 167\ GPa$, $\nu_S = 0.25$, $t_S = 350\ \mu m$). At a stress of, say, 500 MPa this leads (equation 22) to a radius of curvature of 4.55 m. Using a 3" wafer, a height of 159.5 μm must be measured with an accuracy of 1% to obtain a precision of 5 MPa. For the same precision an angle Θ of 16.7 mrad must be measured with an accuracy of 1%.

A simple method is to prepare samples on cover glass stripes (e. g. 70 mm long, 10 mm wide and 150 μm thick, $E_S = 70\ GPa$). The height of the sample's surface over a reference plane with the sample lying on it can be detected by scanning the surface with an optical displacement sensor. Sensors with an accuracy of 0.1 μm are readily available.

Another way is to use two parallel laser beams and measure the angle between the deflected beams [36]. If this is done by measuring the position of the reflected beams at a distance L the distance between the two beams is given by

$$D = w\left(1 + \frac{2L}{R}\right). \tag{28}$$

To obtain the precision of 1% at a distance $L = 2\ m$ with the data above, D must be measured with a resolution of 0.1432 mm which is no problem for position sensitive photo diodes [24].

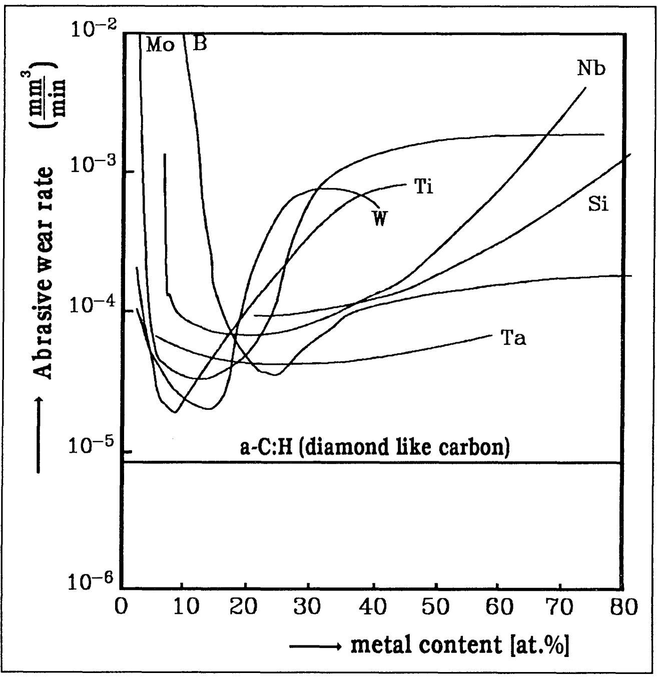

Figure 10. Dependence of abrasive wear rates of various Me-C:H films on metal content.

المنارة للاستشارات
www.manaraa.com

4. CASE STUDIES

4.1. Metal-containing hydrogenated carbon films (Me-C:H)

Me-C:H films represent a very promising layer material as they exhibit excellent abrasive and adhesive wear properties, combined with a low friction against e. g. steel and good adhesion on metallic substrates [37, 38, 39, 40]. At the FhG-IST they are prepared in a DC-Magnetron or RF sputtering process where additionally a hydrocarbon gas (typically ethine) is decomposed. They exhibit a significant minimum in abrasive wear at metal contents of about 10 at.%. Figure 10 shows the typical dependence of the abrasive wear rates of various Me-C:H films (Me = Mo, B, W, Ti, Nb, Si, Ta) on metal content compared to that of a pure a-C:H layer ('diamond-like carbon' deposited in a rf plasma CVD process on the cathode).

Fundamental investigations were performed in the last years to correlate the wear behaviour of the films with structural and mechanical properties of the films at the example of Nb-C:H films [41]. The structure of the film can be explained by a simple model of nanocrystalline NbC particles embedded in an amorphous hydrocarbon matrix. The size of the carbide particles increases from around 20 to 50 Å with increasing metal content, their number density remaining almost constant [40]. From IR spectroscopy a decreasing H content of the films with increasing metal content can be concluded. The strong increase of absorption in the NIR which is more than expected from the increasing metal content can perhaps be attributed to formation of graphite clusters. Probably the degree of cross linking is strongly influenced by the degree of bombardment with Ar ions and neutrals reflected from the metal target [41].

Nanometer indentation experiments were performed to see whether the minimum in abrasive wear could be correlated with a maximum of hardness and/or Young's modulus or their ratio. The latter is considered as a measure of the degree of elastic strain around the impression [42, 43].

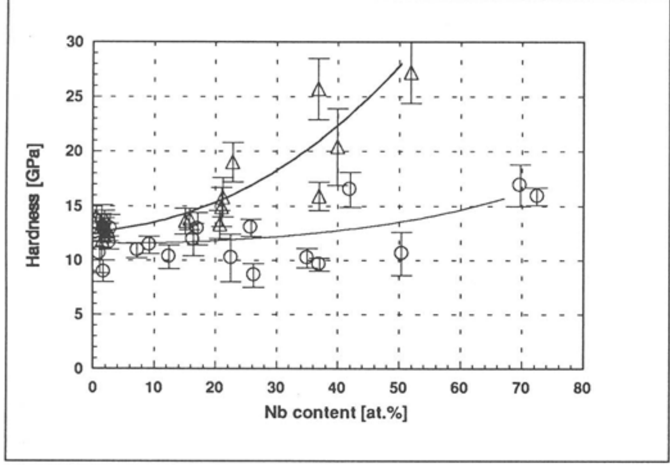

Figure 11. Influence of metal content and Argon pressure during deposition on the hardness of Nb-C:H films (Δ: 1.3 Pa Ar, **O**: 2.3 Pa Ar).

www.manaraa.com

Figure 11 and 12 show the dependence of hardness and Young's modulus of Nb-C:H films on metal content and Argon pressure during deposition. As can be seen from the figures the minimum in abrasive wear can not be explained by a maximum of hardness and Young's modulus alone. Also the friction and fracture properties of the films have to be taken into account [40] leading to a quite simple model of their wear properties [41].

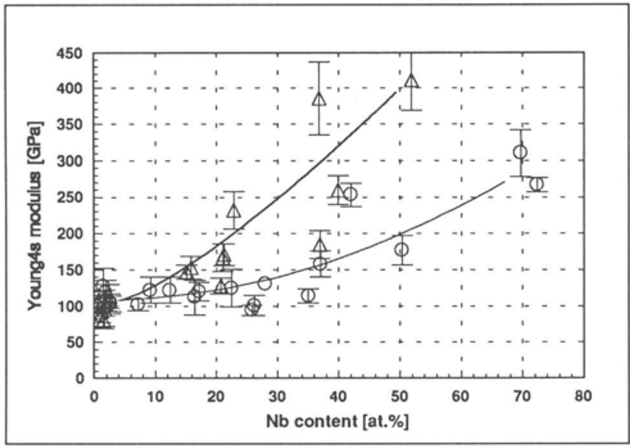

Figure 12. Influence of metal content and Argon pressure during deposition on the Young's modulus of Nb-C:H films (Δ: 1.3 Pa Ar, **O**: 2.3 Pa Ar).

The variation of hardness and Young's modulus with carbide content can be understood from simple rules of mixtures of a carbide and an a-C:H phase [14, 41]. With Nb-C:H films a lower dependence of mechanical properties on Ar pressure was found than with other metal containing films [39]. The main trend, however, is found that films deposited at lower pressure exhibit higher hardnesses and Young's moduli and better wear resistance. From this a significant influence of Ar bombardment on the mechanical properties of the a-C:H matrix is concluded. This has consequences especially for film deposition on three dimensional substrates in a parallel plate deposition chamber as here the bombardment varies with orientation of the substrate surfaces relative to the electrode plates.

4.2. Polycrystalline diamond films

As the adhesion of diamond films to the substrate is a major problem in the application of the films to cutting tools, it is necessary to control the intrinsic stresses of the films. Films with low residual stresses should exhibit at least less adhesion losses during service. For the application of diamond films as a carrier membrane for x-ray absorber masks in x-ray lithography it is of utmost importance that the films do not buckle due to compressive stresses in the films.

In our laboratory diamond film stresses were monitored during layer deposition by the wafer curvature technique described above [36]. Two parallel laser beams were reflected by the sample surface in a distance of 2 cm and their position was monitored on a screen 2 m away from the deposition chamber. Because of the non-vanishing substrate

المنارة للاستشارات
www.manaraa.com

curvature developing during deposition the angle between the two beams changed. From the angle the substrate curvature could be calculated and is shown in figure 13. The film thickness during deposition was calculated from the average growth rate, i. e. film thickness divided by deposition time.

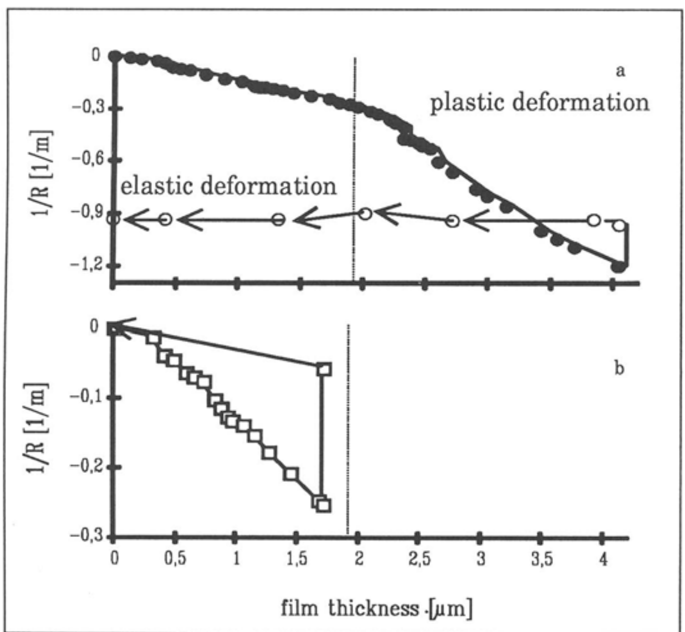

Figure 13. Development of the reciprocal radii of curvature 1/R during deposition of diamond films at 950 °C (a) and at 850 °C (b). The increase of 1/R at the end of each curve is caused by deformation due to compressive stress induced by cooling to room temperature. The arrows point at values of 1/R after etching away of the diamond film. Plastic deformation of sample (a) is confirmed by the non-vanishing radius of curvature after complete removal of the diamond film by reactive ion etching.

Sample (a) from figure 13 was deposited at 950°C on a silicon wafer. Due to the growing film having intrinsic tensile stresses the substrate bends more and more. At a thickness of 2.3 μm deposition was stopped for 1.5 h, but the temperature was kept at 950°C. As can be seen from the step in the curve, the substrate continues bending though no film is growing. Then deposition continued and was stopped at a film thickness of 4.1 μm. On cooling to room temperature compressive stresses are induced due to different thermal expansion coefficients of diamond and silicon (shown by the decrease of |1/R|). Then the diamond film was etched away in an Ar/O_2 plasma. The residual bending of the substrate at the end of etching is a clear indication of plastic deformation of the silicon (111) wafer.

Sample (b) was deposited at only 850°C and grown to a thickness of only 1.7 μm. With this sample nearly all stresses are released upon cooling and a nearly stress free film is left. Upon etching away of the diamond film the rest of the substrate stresses are released

المنارة للاستشارات
www.manaraa.com

showing that at this lower deposition temperature and smaller deposition time no creeping of silicon took place.

The consequence of these and other experiments was the finding that by choosing a proper deposition temperature and a certain substrate pretreatment (leading to films with the right grain size), tensile growth stresses can be controlled and compensated by the compressive thermal stresses due to thermal contraction of film and substrate, thus leading to a nearly stress free film at room temperature.

5. CONCLUSION

Due to recent instrumental developments more fundamental mechanical properties like hardness, Young's modulus and residual stress of thin films of only a few microns down to sub micron thickness can be determined. This yields a better understanding of processes occurring in wear and friction during service of coated substrates. With the knowledge of these parameters models of more complicated mechanical properties can be validated and a systematic optimisation of the layer-substrate composite is possible thus avoiding the usual trial and error approach to given wear situations.

ACKNOWLEDGEMENT

Fruitful discussions with my colleagues Dr. L. Schäfer and M. Fryda and especially Dr. C.-P. Klages, who also kindly reviewed the manuscript, are thankfully acknowledged.

LITERATURE

1. D. Lebouvier, P. Gilormini, E. Felder - A kinematic solution for plane-strain indentation of a bilayer - J. Phys. D: Appl. Phys., 18 (1985) 199
2. D. Lebouvier, P. Gilormini, E. Felder - A kinematic model for plastic indentation of a bilayer - Thin Solid Films, 172 (1989) 227
3. J. C. Pivin, D. Lebouvier, H. M. Pollock, E. Felder - Fields of plastic deformation in indented bilayers: comparison between kinematic calculations and experimental data obtained at scales ranging from one centimetre to ten nanometres - J. Phys. D: Appl. Phys., 22 (1989) 1443
4. J. Boussinesq - Applications des potentiels à l´étude de l´equilibre et du ´mouvement des solides élastiques - Gauthiers-Villars (Paris, 1885)
5. H. Hertz - Über die Berührung fester elastischer Körper - J. Reine und angewandte Mathematik, 92 (1881) 156
6. I. N. Sneddon - The relation between Load and Penetration in the Axisymmetric Boussinesq Problem for a Punch of Arbitrary Profile - Int. J. Eng. Sci., 3 (1965) 47
   N. Sneddon - Boussinesq's problem for a rigid cone - Proc. Cambridge Phil. Soc., 44 (1948) 492
7. N. A. Stilwell, D. Tabor - Elastic recovery of conical indentations - Phys. Proc. Soc., 78 (2) (1961) 169
8. G. M. Pharr, W. C. Oliver, F. R. Brotzen - On the generality of the relationship among contact stiffness, contact area and elastic modulus during indentation - J. Mater. Res., 7 (3) (1992) 613 - 617
9. W. C. Oliver, G. M. Pharr - An improved technique for determining hardness and elastic modulus using load and displacement sensing indentation experiments - J. Mater. Res., 7 (6) (1992) 1564

www.manaraa.com

10. J. L. Loubet, J. M. Georges, G. Meille - Vickers indentation curves of elastoplastic materials - in "Microindentation Techniques in Materials Science and Engineering", P. J. Blau, B. R. Lawn, Edts., ASTM Special Technical Publication 889 (1985) 72
11. M. F. Doerner, W. D. Nix - A method for interpreting the data from depth-sensing indentation instruments - J. Mater. Res. 1 (4) (1986) 601
12. K. Taube - unpublished results
13. M. Fryda, K. Taube, C.-P. Klages - Nanometer-indentation measurements on metal-containing amorphous hydrogenated carbon films (Me-C:H) - VACUUM, 41, Proc. IVC-11, 25.-28.9.1989, Köln, (Pergamon, 1990) 1291
14. K. Taube - Untersuchung der mechanischen Eigenschaften von dünnen Schichten mit einer Ultramikro-Eindruckmethode - PhD Thesis, University of Hamburg 1991 and Fortschritt-Berichte BDI, Reihe 18, Nr. 102 (Düsseldorf, VDI-Verlag 1991)
15. H. Bückle - Metallurgical Reviews (London, Institute of Metals) 4 (1959) 49
    H. Bückle - L'essai de microdureté et ses application - Publications scientifiques et techniques du ministère de l'air, N.T.90 (Paris, 1960)
16. A. K. Bhattacharya, W. D. Nix - Analysis of elastic and plastic deformation associated with indentation testing of thin films on substrates - Int. J. Solids. Structures, 24 (12) (1988) 1287
17. T. A. Laursen, J. C. Simo - A study of the mechanics of microindentation using finite elements - J. Mater. Res. 7 (3) (1992) 618
18. J. M. Olaf - Ein Verfahren zur Bewertung des mechanischen Verhaltens von Randschichten - PhD Thesis, University of Freiburg (1992)
19. W. T. Chen - Computation of stresses and displacements in a layered elastic medium - Int. J. Eng. Sci., 9 (1971) 775
20. W. T. Chen, P. A. Engel - Impact and contact stress analysis in multilayer media - Int. J. Solids Struct., 8 (1972) 1257
21. R. B. King - Elastic analysis of some punch problems for a layered medium - Int. J. Solids Structures, 23 (12) (1987) 1657
22. T. P. Weihs, S. Hong, J. C. Bravman, W. D. Nix - Mechanical deflection of cantilever microbeams: a new technique for testing the mechanical properties of thin films - J. Mater. Res., 3 (5) (1988) 931
23. T. P. Weihs, S. Hong, J. C. Bravman, W. D. Nix - J. Elec. Mater. 19 (1990) 903
25. G.G. Stoney - Proc. R. Soc., London , A82 (1909) 172
24. P. A. Flinn - Principles and applications of wafer curvature techniques for stress measurements in thin films - Mat. Res. Soc. Symp. Proc. 130 (1989) 41
26. S. Timoshenko, S. Woinowsky-Krieger - Theory of Plates and Shells - McGraw-Hill, New York (1959)
27. C. J. Shute, J. B. Cohen, D. A. Jeannotte - Residual stress analysis of Al alloy thin films by X-ray diffraction as a function of film thickness - Mat. Res. Soc. Symp. Proc. 130 (1989) 29
28. B. M. Clemens, J. A. Bain - Stress determination in textured thin films using x-ray diffraction - Mat. Res. Bull. 17 (7) (1992) 4628
29. F. Fröhlich, P. Grau, W. Grellmann - Physica Status Solidi, A42 (1977) 79
    F. Fröhlich, P. Grau, W. Grellmann - Untersuchung mechanischer Eigenschaften von Glas mit Hilfe moderner Härtemeßverfahren - Wiss. Ztschr. Friedrich-Schiller-Univ. Jena, Math.-Nat. R., Jg. (1979) H. 2/3, 449
30. M. Nishibori, K. Kinosita - Ultra-microhardness of vacuum-deposited films I: Ultra-microhardness tester - Thin Solid Films, 48 (1978) 325
31. D. Newey, M. A. Wilkins, H. M. Pollock -An ultra-low-load penetration hardness tester - J. Phys. E: Scientific Instruments, 15 (1982) 119
32. J. B. Pethica, R. Hutchings, W. C. Oliver - Hardness measurements at penetration depths as small as 20 nm - Phil. Mag. A, 48 (1983) 593

المنارة للاستشارات
www.manaraa.com

33. P. E. Wierenga, A. J. J. Franken - Ultramicroindentation apparatus for the mechanical characterisation of thin films - J. Appl. Phys, 55 (12) (1984) 4244
    P. E. Wierenga, A. J. J. Franken - Indentation measurements on thin films - Philips Technical Review, 42 (3) (1985) 85
34. T. W. Wu, C. Hwang, J.Lo, P. Alexopoulos - Microhardness and microstructure of ion-beam-sputtered, nitrogen-doped NiFe-films - Thin Solid Films, 166 (1988) 299
35. Nano Instruments, Inc., P.O. Box 14211, Knoxville, TN 37914, USA
36. L. Schäfer, X. Jiang, C.-P. Klages - In-situ measuring of stress development of diamond thin films - Applications of diamond films and related materials, Y. Tzeng, M. Yoshikawa, M. Murakawa, A. Feldman (Edts.), (Elsevier 1991) 121
37. H. Dimigen, H. Hübsch - Applying low-friction wear-resistant thin solid films by physical vapour deposition - Philips Tech. Rev., 41, (1983) 186
38. H. Dimigen, H. Hübsch, R. Memming - Tribological and electrical properties of metal-containing hydrogenated carbon films - Appl. Phys. Lett., 50 (1987) 1056
39. C.-P. Klages, R. Memming - Microstructure and properties of metal-containing amorphous hydrogenated carbon films - in "Properties and Characterisation of Amorphous Carbon Films", J.J. Pouch, S. A. Alterovitz, Edts., Materials Science Forum 52&53, (1990) 609
40. M. Fryda, C. Benndorf, C.-P. Klages, K. Taube - Structural and mechanical properties of niobium-containing amorphous hydrogenated carbon films (Nb-C:H) - Diamond and related materials, 1 (1992) 558
41. M. Fryda - PhD Thesis, University of Hamburg (1992)
42. B. R. Lawn, V. R. Howes - Elastic recovery at hardness indentations - J. Mat. Sci., 16 (1981) 2745
43. D. L. Joslin, W. C. Oliver - A new method for analysing data from continuous depth-sensing microindentation tests - J. Mater. Res., 5 (1990) 123

www.manaraa.com

MEASUREMENT OF MECHANICAL PROPERTIES OF THIN SOLID FILMS II: FRICTION AND WEAR

A MATTHEWS
Research Centre in Surface Engineering
University of Hull
Hull
HU6 7RX
UK

K HOLMBERG
Laboratory of Production Engineering
VTT Technical Research
Centre of Finland
SF-02151 Espoo
Finland

ABSTRACT

The friction and wear performance of surfaces is critical to the functionality of industrial mechanisms, engines transmissions and all manner of process plants, especially with regard to their efficiency of operation and life cycle costs. Whilst typically dominated by mechanical properties, it is increasingly realised that surface chemistry also plays a mojor role in determining the friction and wear behaviour. Thus in recent years there have been many attempts to formulate a basic understanding of friction and wear, and to develop equipments and test procedures which allow the study and standardised testing of couples for different applications. The theoretical and practical background to this subject is covered in this chapter.

1. Introduction

When one considers the range of uses to which surface engineered components are put, it is evident that no single test method can ever fully characterise a surface for every possible use. In different applications, temperatures involved may be very low (eg cryogenic) or very high (eg molten metal) the contact pressure may vary considerably and the nature of the contact (eg sliding or impact) can differ. Similarly the environment may be inert or even vacuum. In fact the range of possible operating conditions is so wide that many researchers have voiced the view that the only effective way to evaluate the tribological properties of a surface or mechanism is to run it in its normal operating mode. The problems with this are that it gives limited scope for accelerated testing, it can be expensive and does not provide a standardised procedure, which can be adopted at different laboratories and which can form the basis of standard specifications for coatings. Thus, in spite of their drawbacks, standardised friction and wear test methods are being developed, and these will be discussed in this chapter.

2. Friction and Wear Basics

2.1 FRICTION

Friction is the tangential resistance to motion which is experienced whenever one solid body moves on another. The coefficient of friction, u, is given by the frictional force F divided by the normal load W on the contact:

$$\mu = F/W.$$

The mechanism of friction in sliding contacts has been explained by the adhesional effect between surface asperities. This concept was developed by Bowden & Tabor (Ref 1), who explained that when two asperities are forced into contact they may weld together. When one of the solids moves relative to the other their shear strength causes a resistance to motion. During sliding, new microwelded junctions can be expected to be formed and broken continuously.

W. Gissler and H. A. Jehn (eds.), Advanced Techniques for Surface Engineering, 295–312.
© 1992 *ECSC, EEC, EAEC, Brussels and Luxembourg.*

www.manaraa.com

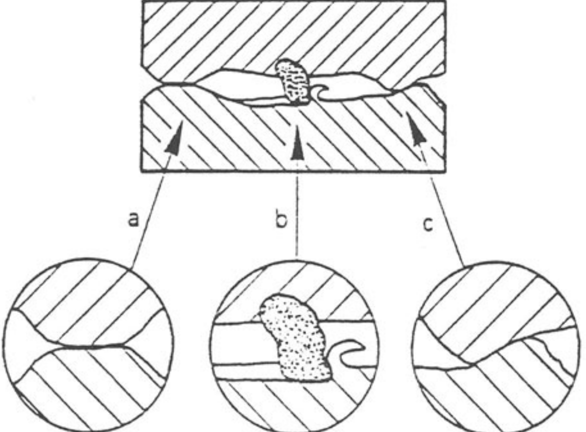

Fig 1 The three components of sliding friction are
a) adhesion, b) ploughing and c) asperity deformation.

The adhesion model of friction has, however, been criticised, since:

i) the agreement between the theoretical and experimental values of the coefficient of friction is not particularly good,
ii) the model does not take into account the surface roughness effect on friction,
iii) there is a lack of evidence that the junctions will be produced or be of the necessary strength,
iv) when the normal force pressing the surfaces together is removed an adhesive force cannot be detected.

Bowden and Tabor have also included the ploughing effect in their concept of friction in Ref 1. When a hard asperity or a hard particle penetrates into a softer materials, and "ploughs" out a groove by plastic flow in the softer material this action creates a resistance to motion as shown in figure 1 (b).

Some workers (reviewed by Rigney and Hirth (Ref 2)) have concentrated even more on the effect of plastic deformation losses in friction. The influence of plastic deformation of asperities was considered by Green (Ref 3) and extended by Edwards and Halling (Ref 4). They showed that resistance to motion arises from the work done when asperities are plastically deformed as they slide over each other, as shown in figure 1 (c). On the basis of studies concentrating on plastic deformation losses in the materials, Heilmann and Rigney (Ref 5) suggest an energy-based friction model where metallurgical effects are included.

A new concept of friction, called the genesis of friction, has been presented by Suh and Sin (Ref 6). They show that the mechanical properties affect the frictional behaviour to a greater extent than chemical properties when sliding occurs without a significant interfacial temperature rise. They divide the effect of friction into three basic mechanisms, one due to asperity deformation, one due to adhesion and one due to ploughing. the adhesional mechanism in many practical cases may not be the most dominant of the three. They also stress the influence of the history of sliding on the frictional force. On the basis of experiments carried out with specimens made of engineering materials they give the following typical values for the three components of the coefficient of friction (with maximum values in brackets where appropriate):

www.manaraa.com

i) Friction due to asperity deformation, μ_d = 0 - 0.43 (0.75). It appears that asperity deformation is largely responsible for the static coefficient of friction.
ii) Friction due to adhesion, μ_a = 0 - 0.4. The low value is for a well lubricated surface, the high value for identical metals sliding against each other without any surface contamination or oxide layers.
iii) Friction due to ploughing, μ_p = 0 - 0.4 (1.0). The low value is obtained when either wear particles are totally absent from the interface or a soft surface is slid against a hard surface with a mirror finish.

In a study of the microscopic mechanisms of friction Kim and Suh (Ref 7) found that the component of ploughing of the surfaces by wear particles is the most important in most sliding situations. They show that friction at the microscopic scale is a result of bond breaking of individual atoms, instigated by strong adhesion or by mircroasperity interlocking, and slip along the crystal planes in the presence of defects. Breakage of cohesive bonds will occur during microsplastic deformation or fracture. Depending on the relative strength of the interfacial bond and the cohesive bonds of the solids, breakage of the bonds will occur at locations that offer the least resistance to sliding. In another review on adhesion, friction and wear Landheer and de Gee (Ref 8) point out that a boundary lubricant film only a few molecules thick, in the nanometer range, can effectively reduce friction, eg from u = 1.0 to 0.1, without affecting asperity interaction and thus, the ploughing effect. Based on knowledge available the mechanisms of friction in sliding contacts it seems that the particle ploughing effect and the adhesion effect are important and either of them may dominate the frictional behaviour depending on the tribological contact conditions. The existence of interfacial films, as contaminants, oxides or coatings can crucially affect the behaviour.

So far we have considered friction mechanisms only in relation to the sliding of one surface over another. In the case of rolling, the coefficient of friction is normally much smaller. The general considerations in relation to contact mechanisms are also valid for rolling contacts, but because of the difference in contact kinematics other contact effects may dominate the frictional behaviour.

The main contributions to friction in rolling contacts are:

i) micro-slip effects within the contact area,
ii) elastic hysteresis of the contacting materials,
iii) plastic deformation of the materials and
iv) adhesion effects in the contact.

The contact mechanics for rolling are certainly complex but fairly well understood on a macroscopic level (eg Refs 9, 10, 11). The study of influence of surface coatings in rolling is less well developed.

2.2 WEAR

Wear typically involves the removal of material from solid surfaces as a result of one contacting surface moving over another. Thus both friction and wear are the results of the same tribological contact process that take place between two moving surfaces. However, their interrelationship is not well understood. It is common that low friction corresponds to low wear and high friction to high wear as shown in Ref 12 by Saka. However, this is not a general rule and there are several examples (eg Franklin Ref 13) of contradictory behaviour. Furthermore, the changes in the wear value may well change by several orders of magnitude as opposed to the coefficient of friction, which very rarely changes by more than one order of magnitude.

www.manaraa.com

Typical wear mechanisms are adhesion, abrasion, fatigue and chemical wear. It is very common that in a real contact more than one wear mechanism is acting at the same time. (Ref 14). Indeed one may instigate another (Ref 15), as shown in Fig 2.

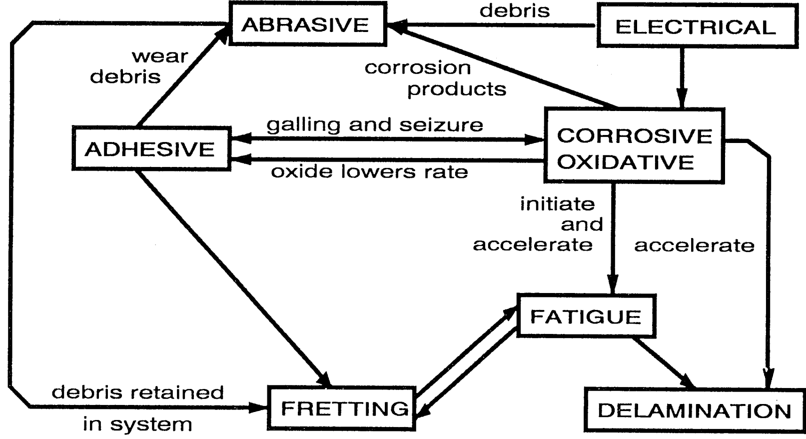

Fig 2 Interacting Wear Mechanisms

The combination of wear mechanisms operating depends on the contact conditions and will result in a specific type of wear or wear modes. Examples of wear modes are scuffing, fretting, scoring, mild wear, severe wear, impact wear, erosion, cavitation, diffusion wear, solution wear, melt wear and oxidational wear. The wear mode is typically defined based on how the surface appears after the contact. The wear mode defines a certain set of conditions where the interrelationship between the influencing parameters is similar and thus the different effects can be physically described and mathematically formulated. One example of this is the suite of wear-rate equations used in the wear maps devised by Lim and Ashby (Ref 16).

The basic mechanisms of wear are shown in figure 3

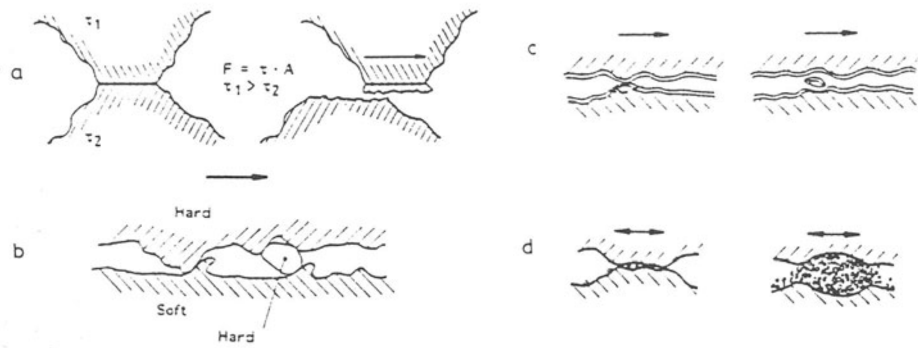

Fig. 3 The basic mechanisms of wear are a) adhesion, b) abrasion, c) fatigue and d) chemical wear.

المنارة للاستشارات
www.manaraa.com

ADHESIVE WEAR.

When asperities of one surface come into contact with asperities of the counterface they adhere strongly to each other and form asperity junctions. Relative tangential motion of the surfaces causes separation in the bulk of the softer asperities and material is removed. In adhesive wear the surface material properties as well as protecting surface films or contaminants, play important roles.

The adhesive wear mechanism was described by Bowden and Tabor (Ref 1) and it has been the dominant wear theory for sliding contacts since the. The adhesion wear theory has however, been criticised (eg Ref 17) by the following arguments:

i) it seems unlikely that the interface is stronger than either of the bulk materials,
ii) it cannot explain the wear of the harder surface which frequently is observed
iii) it cannot explain observed effects of surface roughness,
iv) the maximum work required to generate wear particles is two to three orders of magnitude smaller than the external work done,
v) it cannot explain the relation between friction and wear, and
vi) it does not take into account mirostructure and metallurgical parameters.

There is, however, enough experimental evidence to prove that adhesion may occur in many sliding situations. In failure modes like scuffing and seizure the effect of adhesive wear is particularly important.

ABRASIVE WEAR AND ASPERITY DEFORMATION

Wear by plastic deformation takes place both in abrasive wear and during asperity deformation.

Abrasive wear occurs in contacts where one of the surfaces is considerably harder than the other or where hard particles are introduced into the contact. The harder surface asperities are pressed into the softer surface which results in plastic flow of the softer material around the hard surface. When the hard surface moves tangentially, ploughing and removal of softer material takes place with grooves or scratches in the surface resulting. Depending on the geometry of the harder surface and the degree of penetration, the removal of material can take different forms, such as ploughing, wedge formation or cutting.

A distinction is often made between two-body and three-body abrasive wear, where the latter refers to situations when hard particles are introduced between the moving surfaces. The mechanism of abrasive wear has been studied extensively and has been described by several authors (eg Refs 18, 19, 20).

FATIGUE AND DELAMINATION WEAR

Loading and unloading of surface, that results in a stress level in the material that it can sustain once but not if it is repeated many times, results in a fatigue crack. Fatigue can form the origin for large scale cracking and liberation of surface material to form wear debris.

Classic surface fatigue wear is a lifetime limiting failure in ball and roller bearings and in gear contacts. In these concentrated contacts the Herzian pressure at the surface creates a stress field beneath the contact zone. The maximum shear stress occurs about one third of the contact length beneath the surface in the case of pure rolling and moves to the surface with increasing traction. For coefficients of friction exceeding 0.32 the maximum shear stress will be found on the surface (Ref 21).

www.manaraa.com

CHEMICAL WEAR

In chemical wear the wear process is dominated by chemical reactions in the contact, initiated by the influence of the environment, in combination with mechanical contact mechanisms. Rubbing in combination with the chemical reactions in the contact results in wear product formation and removal of material. The rubbing action can result in increased temperatures at the surface and creates surface cracks more chemical reactions taking place. On the other hand the chemical reactions at the surfaces will make them softer and weaker and thus decrease their resistance to new crack formations and liberation of surface material to produce wear products. The mechanisms of chemical wear have been discussed by Czichos (Ref 10) and Buckley (Ref 20).

Oxidational wear is the most common chemical wear process. A thin layer of oxides will almost always be formed on the top of metal surfaces. This is in fact an important protecting layer because without it both the friction and wear in metal contacts would be extremely high. If this layer is continuosly removed by a rubbing action, and the formation of new layers is speeded up by a high humidity environment that can reach the contact the result is a typical form of oxidational wear.

In certain cases wear can be due to chemical instability of the materials. Examples of this are found in the metal cutting process where the chip moves rapidly along the tool surface. Temperatures at the interface are often up to over 700° C and the surface of the chip that slides against the tool is virgin and may be partly molten. This process can result in two kinds of wear due to chemical instability, as shown by Suh (Ref 22). One is the solution wear due to dissolution of the tool material in the chip. The other is the diffusion of elements from the tool material into the chip, leading to weakening and ultimate failure of the cutting tool.

VELOCITY ACCOMODATION CONCEPT

A different approach to the question of how wear mechanisms should be classified is the velocity accomodation approach developed by Berthier et al (Refs 23 and 24) and Godet (Ref 25). They identify four basic mechanisms with which the velocity difference between two surfaces in relative motion can be accomodated. They are by elastic deformation, fracture, shear and rolling. These basic mechanisms may occur in either of the two surfaces (first bodies) or in the lubricant between them (third body). The advantage with this approach is that the fundamental tribological mechanisms are simplified to well known mechanisms of material behaviour that can be characterized by properties such as the Youngs modulus, fracture toughness and shear strength. It is, however, clear that much has to be done before these basic properties can be combined to form a model that represents friction and wear behaviour in real contacts. However this does seem to be a promising direction.

WEAR EQUATIONS

Because of the complexity of the wear process, which cover many materials, contact conditions and environmental parameters in a number of different combinations, it has not been possible to formulate a universal equation of wear. Numerous authors (reviewed in Ref 26) have developed wear equations for the different wear modes but all of them are quite limited in their range of validity.

A more general approach is taken by Lim and Ashby (Ref 16) when they show the validity ranges of six different wear modes in a wear map with normalised contact pressure and normalised velocity as coordinates and also give wear equations for each wear mode. The identified wear modes are ultramild wear, delaminatin wear, mild oxidational wear, severe oxidational wear, melt wear and seizure. The presentation is, however, limited to a steel sliding pair in a pin-on disc machine.

www.manaraa.com

It is possible to observe some common features when studying the proposed wear equations for the different wear modes. Often the worn volume is directly proportional to the normal load and the distance of movement and inversely proportional to the hardness of the material. This relationship was earlier observed by Holm (Ref 27) and Archard (Ref 28) and it can be formulated as:

$$V = K \frac{W.s}{H}$$

where V is the worn volume, W is the normal load, s is the distance of movement, H is the hardness and K is a constant. This should not be considered as a universal wear equaton because there are several examples of tribological contacts where it is absolutely invalid.

WEAR RATE

For design and material development purposes it is necessary to have some universal quantitative parameter for wear. To use only the volume of material removed is not sufficient because of the very different test conditions in use. The Holm wear relationship is often used for formulating the wear rate, this gives a practical and more general value for the amount of wear. We will use for the wear rate, K', the value of the constant K' divided by the hardness H in accordance with common practice today. Thus the wear rate is:

$$K' = \frac{V}{W.s}$$

which is often given with the dimensions ($10^{-15}m^3/Nm$). Even though this is still not the ideal way of expressing wear, it has widespread support. There is also a clear physical argument for using the wear rate as defined above because it is the worn volume divided by the mechanical energy input into the contact. The contact energy input can be described as the product of the normal load, the velocity and the applied time which again is the same as the product of load and distance which is in the equation. It is strongly recommended that this way of expressing wear should be taken into use as widely as possible to make is possible to compare and utilize wear data produced in different contact conditions.

The above overview of the basics of wear emphasises contacts between solid surfaces in relative motion. No mention has been made of wear mechanisms involving erosion, for example by the imprringement of fluids or solid particles. The response of a surface to such impact will depend on a number of factors, such as the impact angle and the velocity. In many studies it has been shown that a brittle material will erode more when the impact is at normal incidence, whilst a tougher or more elastic material will erode more at grazing incidence.

3. Friction and Wear of Coated Surfaces

It is considered to be outside the scope of the Chapter to go into detail on the various contact stress distribution models which have been developed for coated surfaces. An excellent review of the case of the stress-strain relationship for elastic layers on elastic substrates loaded by rigid spheres is given by Tangena (Ref 31). For other aspects, such as the effects of thermal stresses, intrinsic stresses and cracks, the reader is referred to Ref 32.

The macromechanical tribological mechanisms describing the friction and wear phenomena involve the stress and strain distribution in the whole contact, the total elastic and plastic deformations they result in and the total wear particle formation process and its dynamics. In contacts with one or two coated surfaces four main parameters can be defined which control the tribological contact process. They are

المنارة للاستشارات

www.manaraa.com

i) the coating to substrate hardness relationship,
ii) the thickness of the coating,
iii) the surface roughness and
iv) the size and hardness of the debris in the contact

The relationship between these four parameters will result in a number of different contact conditions characterized by specific tribological cntact mechanisms. Ref 32 discusses typical tribological contacts when a hard spherical slider moves on the coated flat surface, in relation to the above parameters.

One effect, noted by Bowden and Tabor, is the mechanism by which a soft film can reduce the friction coefficient (see Fig 4). This gives rise to the concept of an optimum film thickness to reduce the friction coefficient.

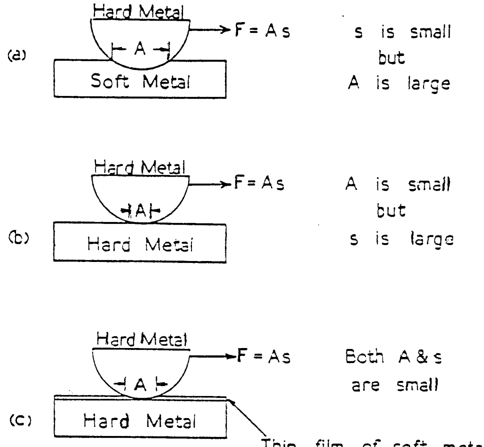

Fig 4 Reduction in friction by depositing a soft film.

In terms of the basic mechanisms coated surfaces follow most of the behaviours referred to in section 2, although modern coating techniques now provide the possibility to optimise for given requirements (eg resistance to chemical diffusion or abrasion). A model for the identification of optimal ceramic coatings is presented by Kramer (Ref 33).

4. Friction and Wear Tests

4.1 BACKGROUND

Given the variety of possible mechanisms operating during a tribological contact, it is not surprising that there are very many different configurations available to test the friction and wear behaviour of coated surfaces. There is an ASTM book devoted to this subject (Ref 29), and Bhushan and Gupta (Ref 30) cite 8 typical contact geometries, just for sliding tests. There are many more than this, to simulate different wear mechanisms. Some of these are reviewed below.

4.2 SLIDING TESTS

Considering the tests listed in Table 1, taken from Ref 30; the pin on disk is by far the most widely cited standard test amongst tribologists. Indeed it is the subject of an international interlaboratory excercise aimed at standardisation under the auspices of VAMAS (Versailles Project on Advanced

www.manaraa.com

Materials and Standards). The lessons learned from this excercise have been used for an ASTM wear testing standard (G-99) and a draft DIN standard (DIN 50324)

TABLE 1. Details of Typical Geometries for Friction and Wear Testing (After Ref. 30)

Geometry	Type of contact	Type of loading	Type of motion
1. Pin-on-disc (face loaded)	Point/ conformal	Static, dynamic	Unidirectional sliding,osciallating
2. Pin-on-flat (reciprocating)	Point/ conformal	Static, dynamic	Reciprocating sliding
3. Pin-on-cylinder (edge loaded)	Point/ conformal	Static, dynamic	Unidirectional sliding osciallating
4. Thrust washers (face loaded)	Conformal	Static, dynamic	Unidirectional sliding, oscillating
5. Pin-into-bushing	Conformal	Static, dynamic	Unidirectional sliding, oscillating
6. Flat-on-cylinder (edge loaded)	Line	Static, dynamic	Unidirectional sliding, oscillating
7. Crossed cylinders	Elliptical	Static, dynamic	Unidirectional sliding, oscillating
8. Four balls	Point	Static, dynamic	Unidrectional sliding.

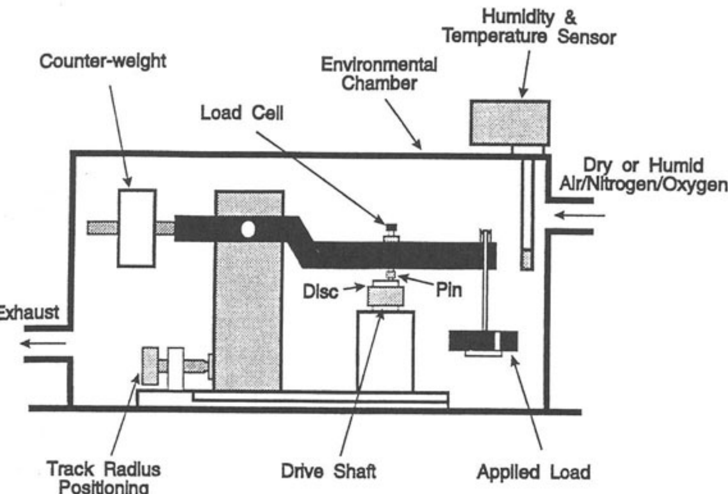

Fig 5 Schematic of a Pin on Disc Tester

Fig 5 showns a typical pin on disc layout. Control of humidity and temperature is critical to repeatability in pin on disc (and indeed all) tribological tests. In the authors' laboratories a spherically-ended pin geometry has been adopted (most conveniently a ball of 10mm diameter), run with a 10N normal force at a 0.1 m/sec sliding speed. A test distance of 100 to 1000 m is typical, at a relative humidity of 50%. Some typical results are given later. Measurement of wear should ideally be achieved by profilometry.

www.manaraa.com

4.3 ABRASION TESTS

The best known tests in this category are the Taber test (shown in Fig 6), and the rubber wheel test (shown in Fig 7).

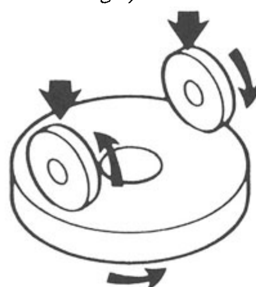

Fig 6 The Taber test

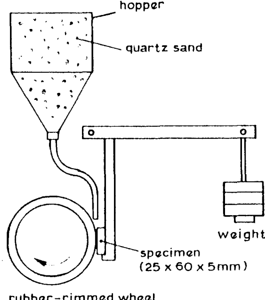

Fig 7 The Rubber Wheel Test

The first of these relies on the abrasiveness of the wheel to create wear, whilst the second utilises a "third body" particulate abrasive (either dry or in a slurry). A typical medium is sand, and the specification for the dry sand test is ASTM G65, whilst the wet test is known as the SAE wet sand rubber-wheel test. Further details are in Ref 29, with practical results later in this Chapter.

4.4 ROLLING CONTACT TESTS

Many tribological contacts involve a rolling action, which may be combined with sliding. The most common test to sumulate this is the "twin disc" machine (Fig 8), which can be used as varying slid-roll ratios. This is used, for example, to investigate the performance of carburised surfaces for gears, which are subjected to Hertzian-type contacts.

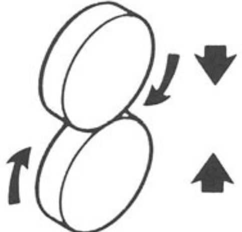

Fig 8 The twin disc configuration

Other rolling contact tests, such as the rotating four ball test or the rolling element on flat test are useful for evaluating lubricants and high-cycle fatigue behaviour of ball bearings.

www.manaraa.com

5. PRACTICAL TEST RESULTS

5.1 PIN ON DISC TESTS

5.1.1 Interlaboratory Comparison

The authors have conducted a pin on disc test on a number of ceramic coatings, in particular as part of a round robin study (Ref 34). This investigation was carried out in order to identify the variability in tests carried out in 3 different laboratories, under nominally identical conditions. Three coating combinations were used, as summarised below:

Coating Source Material	Laboratory Designation	Coating Method
TiB_2 + BN (A)	UH	DC ionisation assisted EBPVD
TiB_2 + N (B)	THD	RF magnetron sputtering
TiAlN (C)	VTT	DC ionisation assisted EBPVD.

Several coating thicknesses were included, in the range 2 to 8 µm, representing typical values for PVD deposits. The substrate material in each case was polished ASP 23 tool steel hardened to 64 RC, with a surface finish of 0.4µm Ra. The tests were carried out using a fixed 10mm diameter polished ball as the pin (M50 steel), hardened to 62 RC. The tests were performed unlubricated at a sliding speed of 0.1m/sec and a normal force of 10N, for 250m sliding distance. The relative humidity during testing was 50 ± 2% at VTT and UH, and 68 ± 4% at THS. The temperature for the VTT and UH tests was 21 ± 2°C, whilst for THD it was 23 ± 1°C.

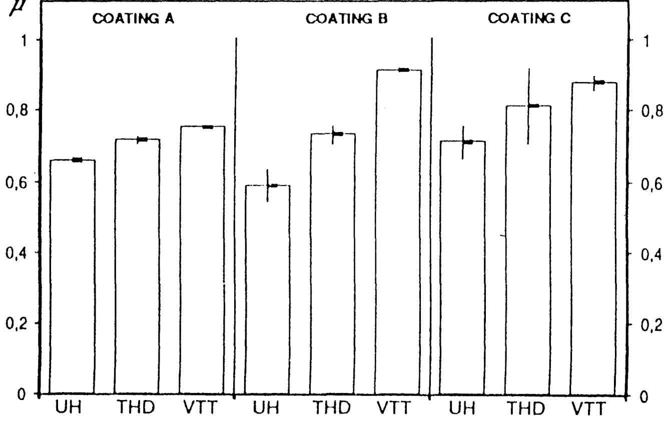

Fig 9 Steady state coefficient of friction in pin on disc tests. Error bars show standard deviations.

The tests were carried out twice in each laboratory for each coating. Figure 9 shows the values of the steady state friction coefficients. For coatings, A and C the correlation is good, whereas for coating B the variation in the coefficient of friction is from 0.59 to 0.91. The lowest values were measured at UH and the highest at VTT. This may be an indication of differences in the measuring equipment or

www.manaraa.com

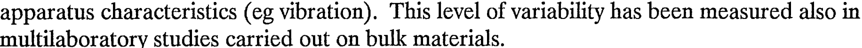

apparatus characteristics (eg vibration). This level of variability has been measured also in multilaboratory studies carried out on bulk materials.

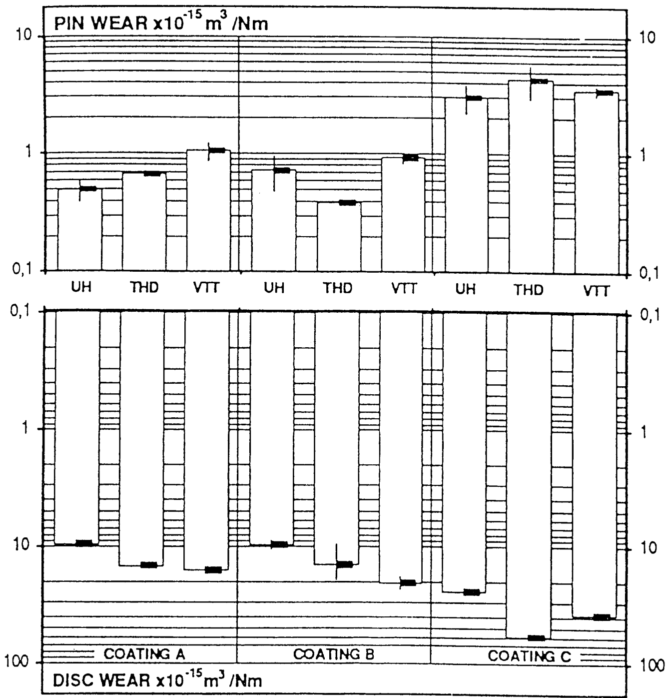

Fig 10 The mean values of the wear rates

The wear rate values and standard deviations are summarised in Figure 10. The wear rates of the coated discs follow the same order as the steady state coefficient of friction. Even though the standard deviations are quite large, the wear rates in the tests carried out in different laboratories are of a similar order of magnitude. The wear rates for steel pins and coated discs for coatings A and B are in agreement, whereas the tests carried out in THD on coating C gave higher values compared to the others, which is probably due to the influence of a higher relative humidity at THD, but could also be related to the fact that the disc orientation was vertical at THD and horizontal at the other laboratories (meaning that debris retention would be less in the former case). During the tests a white powdery debris was observed, and examination of the wear surface showed the formation of transfer layers on the pins. The worn surfaces of the discs were smooth with some scratches. The dominant wear mechanisms were thus regarded as similar in each test. It should be pointed out that different wear track diameters were used to ensure similar sliding speeds. This meant that the number of wear passes differed; UH being the greatest, followed by THD and then VTT. There was, however, no systematic increase in wear rate related to the number of passes. This confirms the importance of tribological processes, compared to ones based on fatigue alone in this kind of contact.

The above interlaboratory study demonstrated the variations which can occur in pin on disc tests, even when identical coatings are being tested and when similar wear mechanisms occur. Other work has shown that if parameters such as the relative humidity or operating environment change then the differences in friction and wear performance can be dramatic. Thus there is a need in this test (as in all tribological tests) to try to ensure identical conditions, and to perform repeat testing to assertain the level of reliability. Total repeatability should not, however, be expected since friction and wear are due

www.manaraa.com

to contact phenomena, usually on surfaces with properties which must exhibit some variability (eg in terms of crack formations and composition), thus tribological phenomena will exhibit statistical variability and this must be borne in mind when interpreting data.

5.1.2 Other Results

In addition to the study outlind in 5.1.1, there have been very many results of pin on disc tests on coatings reported in the literature. Hintermann and co-workers have been most prolific in this regard (eg Ref 35). In particular, Hintermann has highlighted the possibility to engineer specific friction and wear properties by appropriate selection of surfaces. He identifies four modes:

I High friction - high wear
II Low friction - high wear
III Low friction - low wear
IV High friction - low wear

Specific application requirements may require different modes. For example, a clutch system may need to operate in mode IV, whilst a bearing may require to operate in mode III. In most applications it will be necessary to define which of the contacting surfaces is required to exhibit the greater wear.

Ref 36 reports test carried out on a range of PVD coatings and bulk materials, which gave the following conclusions with regard to pin on disc wear and friction:

Requirement	Solution
i) Low friction and low pin on disc wear	TiN or TiC coated pin against TiN coated disc
ii) Intermediate friction and low pin and disc wear	TiC or TiO_2coated pin against uncoated steel disc
iii) High friction, high disc wear	TiN or uncoated steel pin against uncoated steel disc

For rubbing contacts against copper, molybdenum nitride was found to be preferable to the titanium-based coatings.

The couple of TiN or TiC against TiN or TiC is an example of a situation where "like on like" does not necessarily produce high adhesive wear. Clearly contact chemistry is an important consideration here, and there have been reports that beneficial oxides may form to prevent adhesion. The situation is aided by the relatively inert nature of most ceramics.

A class of materials which is attracting considerable interest presently are the "diamond-like" carbon (DLC) coatings, produced typically by plasma assisted CVD methods. These films are usually amorphous and contain hydrogen. They can be very hard, though they may lack temperature and environmental stability. In Ref 37 a series of pin on disc tests are reported on various hard carbon coatings, doped with various additional elements, rubbing against SAE 52100 steel balls (10mm in diameter) at normal forces of 10, 20 and 30N, unlubricated, for 100m. Two different deposition

www.manaraa.com

techniques were used, one not involving plasma assistance (Set One) and the other with plasma assistance during deposition (Set Two). The substrate (disc) was polished ASP 23 steel (nominal 64 Rc). Figures 11 and 12 summarise some results. The coating source materials were as follows:

a) Graphite
b) Graphite + Boron Nitride
c) Graphite + Titanium Diboride/Boron Nitride
d) Grapite + Tungsten

The mean Vickers micro-hardnesses of the coatings were:

	Set One	Set Two
a)	2005 (15g)	4790 (25g)
b)	1760 (15g)	3460 (25g)
c)	1370 (15g)	3750 (25g)
d)	1190 (15g)	3940 (25g)
Substrate	1055 (15g)	950 (25g)

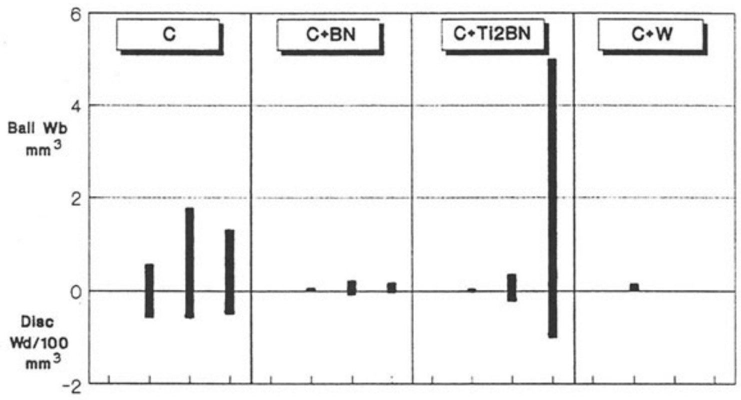

Fig 11 Volumetric Pin on Disc Wear, Set Two

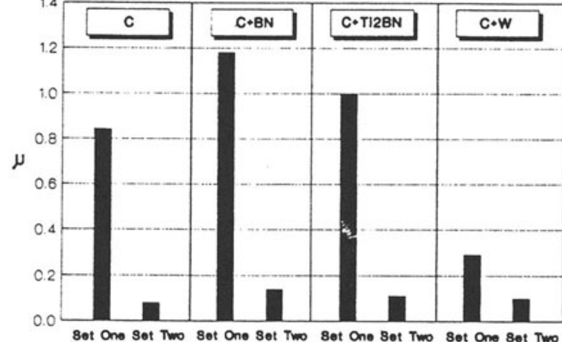

Fig 12 Steady state friction coefficients

www.manaraa.com

This study highlighted the importance of both tribochemistry and mechanical properties. Firstly, note that the carbon plus tungsten film was relatively brittle, and gave good wear resistance at 10N, but broke-up and could not be tested at loads above this. Secondly, note that the best wear performance was exhibited by the C + BN film, even though this was not the hardest. Thus the message from this work is that the optimum coating for one tribological contact, may not be the best for another, indeed a "horses for courses" approach must be adopted when selecting, and testing , coatings. By way of confirmation of this observation, note that if low friction was the main objective, rather than low wear, in this test the carbon film proved best.

5.2 ROLLING CONTACT TEST

Until a few years ago, conventional theories would have predicted that in rolling (Hertzian) contact situations the required depth of surface hardening would have to be much greater than the thickness levels normally associated with PVD coatings. This was based on consideration of the depth of the maximum shear stress. Recently considerable evidence has been accumulated to prove that this is not the case, and indeed that thinner PVD coatings than standard may be desirable in contact fatigue situations. Refs 28-42 deal with aspects of work in this field.

In Ref 37 both soft (copper) and hard (TiN) films (thicknesses 2000A to 2µm) were tried in rolling contact fatigue tests which involved balls rolling round a vertical rod. Tests were carried out at two contact stress levels 5.42GPa and 4.04GPa. Various other variables were included including changes in the ball materials and roughening of the balls. Both coatings provided improvements, but it was felt that the mechanisms operating were different in each case. The copper acted as a solid lubricant, and, due to its deformation, provided an increased contact area and a reduced Hertzian stress. The mechanism of improvement by the TiN was not fully explained but was believed to be related to its high hardness and low friction coefficient. Significantly the thinner TiN coatings deformed with the load, but the thicker ones cracked or delaminated. A similar result was observed by Chang et al in Ref 40. Using a twin-disc arrangement they showed that 1um thick TiN coated surfaces underwent principally elastic deformation without coating debonding, even at Herzian contact stress levels of 2.3GPa, whereas for uncoated rollers cross-sectional micrographs revealed many near-surface microcracks parallel to the surface. These authors of Ref 40 believe that the hard coating suppresses the initiation of microcracks. Even after 33 million cycles no spalling or cracking occured, even though the uncoated surfaces were heavily deformed even after 10 million cycles. They present the graph shown in Fig 13 giving the dependence of life on thickness.

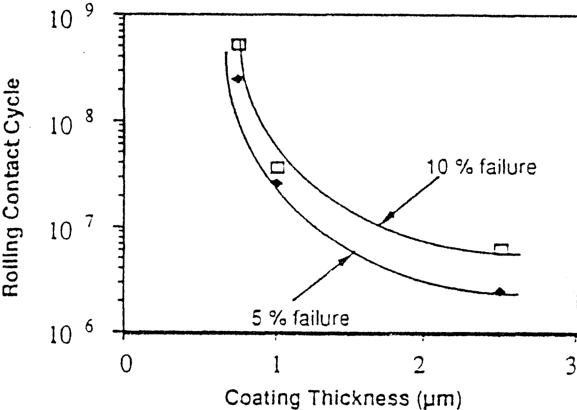

Fig 13 Rolling Contact Life Cycles versus TiN Coating Thickness

www.manaraa.com

5.3 OTHER TESTS

In Ref 43 results were reported of dry sand abrasive wheel tests on titanium nitride coatings deposited over plasma nitrided steel substrates. This work confirmed the importance of a good surface finish in such contact conditions, where asperity removal can lead to accelerated wear. The test has also been useful in evaluating wet slurry abrasion resistance, for example of carburised steel surfaces, as in Ref 44. The test is quick to, taking only a few minutes to produce measurable wear; assessment is easily carried out by profilometry of worn regions, or by weight loss.

For purely erosive wear a very effective test method is to use to particle air-blast test, as described in Ref 45. This has the benefit of providing controlled erodent supply (including speed and direction). The method can even be used as a single- particle test, whereby the damage due to one impact can be carefully assessed (Ref 46). Another erosion test is described in Ref 47; it is based on a centrifuge principle, with particles fed into the centre of a rapidly rotating disc. The authors of that paper also cite this method as providing a useful means of adhesion asssessment. Conversely it is interesting that the scratch test (the most common test of adhesion for thin PVD films) is increasingly used as a friction and multi-pass wear test (Ref 48).

There are other tests which have been designed to simulate specific industrial contact conditions. An example is the bending under tension test (Ref 49), which replicates a press-forming operation and permits the evaluation of coatings for press tools. The test involves pulling strip metal over a coated die, and is a severe test of the anti-galling (heavy adhesive wear) resistance of the coating.

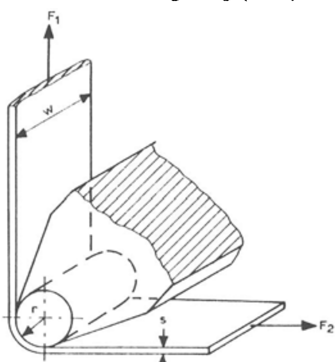

Fig 14 The bending under tension test.

Such tests are vital prior to a coating's use on expensive industrial machine tools, since failure in service can be very costly in down-time. For this reason many tests are also being developed to simulate metal cutting conditions, to permit evaluation of coatings for cutting tools (eg Refs 50,51).

6.0 Conclusions

In surface engineering ther is a clear need for standardised friction and wear tests for coatings and treatments. Such standards would enable new coatings to be evaluated against existing ones and would encourage design engineers and others who specify coatings to do so more widely. However it must be borne in mind that no single test can ever fully simulate all real operating conditions, and a coating performing best in one test or application may not be the most suitable for another application. The is thus a need to develop tests which simulate as near as possible the specific application for which a coating is intended. Only then will users be able to have full confidence in the functionality and durability of an engineered surface.

www.manaraa.com

REFERENCES

1. Bowden, F.P. & Tabor, D., Friction and lubrication of solids. Part I, Clarendon Press, Oxford, 1950. 374p.
2. Rigney, D.A. & Hirth, J.P., Plastic deformation and sliding friction of metals. Wear, 53 (1979) 2, 345-370
3. Green, A.P., Friction between unlubricated metals, a theoretical analysis of the junction model. Proc. R. Soc., 228A (1955) 191.
4. Edwards, C.M. & Halling, J., An analysis of the plastic interaction of surface asperities and its relevance to the value of the coefficient of friction. J. Mech. Engng. Sci., 10 (1968) 2, 101-110.
5. Heilmann, P. & Rigney, D.A., An energy based-model of friction and its application to coated systems. Wear, 72 (1981) 195-217.
6. Suh, N.P., The genesis of friction. Wear, 69 (1981) 91-114.
7. Kim, D.E. & Suh, N.P., On microscopic mechanisms of friction and wear. Wear, 149 (1991) 199-208.
8. Landheer, D. & De Gee, A.W.J., Adhesion, friction and wear. MRS Bulletin, Oct. (1991) 36-40.
9. Halling, J. (ed.), Principles of tribology. MacMillan Press, London, 1975. 401p.
10. Czichos, H., Tribology - a systems approach to the science and technology of friction, lubrication and wear. Tribology series, 1. Elsevier, Amsterdam, 1978. 400p.
11. Johnson, K.L., Contact mechanics. Cambridge University Press, Cambridge, 1985, 452p.
12. Saka, N., Effect of microstructure on friction and wear of metals. In: Fundamentals of Tribology, Suh, N.P. & Saka, N. (eds), The MIT Press, London, 1980, 135-170.
13. Franklin, S., The frictoin and wear characteristics of several wear-resistant surface coatings. Philips CFT technology, CTR 545.91.0043 (1991) 24p.
14. Holmberg, K., Tribological bases for accelerated testing. In: Operational reliability and systematic maintenance, Holmberg, K. & Folkeson, A. (eds.). Elsevier, London 1991, 31-50.
15. Farrow, M. & Gleave, C., Wear resistant coatings, Trans. Inst. Met. Fin. 62 (1984) 2.
16. Lim, S.C. & Ashby, M.F., Wear-mechanism maps. Acta Metall., 35 (1987) 1, 1-24.
17. Jahanmir, S., On the wear mechanisms and the wear equations. In: Fundamentals of Tribology, Suh, N.P. & Saka, N. (eds), The MIT Press, London, 1980, 455-467.
18. Khruschow, M.M., Principles of abrasive wear. Wear, 28 (1974) 69-88.
19. Moore, M.A., A review of two-body abrasive wear. Wear, 27 (1974) 1-17.
20. Buckley, D., Surface effects in adhesion, friction, wear, and lubrication. Elsevier, Amsterdam, 1981.
21. Schouten, M.J.W., Einfluss elastohydrodynamischer schmierung auf reibung, verschleiss und lebendsdauer von Getrieben. Doctoral thesis, Eindhoven Technical University, 1973a. 388p.
22. Suh, N.P., Tribophysics. Prentice-Hall, Englewood Cliffs, New Jersey, U.S.A., 1986, 489p.
23. Berthier, Y., Vincent, L. and Godet, M, Velocity accomodation in fretting. Wear, 125 (1988) 25-38.
24. Berthier, Y., Godet, M. and Brendle, M., Velocity accomodation in friction. Tribology Trans. 32 (1984) 490-496
25. Godet, M., Third bodies in Tribology. Proc. 5th Int. Congr. on Tribology. Vol 1, Holmberg, K. and Nieminen, I. (Eds). Helsinki 12-15 June 1989, 1-15.
26. Bahadur, S., Wear research and development. J. of Lubrication Technology, Trans. ASME, 100 (1978) 449-454.
27. Holm, R., Electric Contacts, Hugo Gebers Forlay, Stockholm, 1946.
28. Archard, J.F., Contact and rubbing of flat surfaces. J. Appl. Phys. 24 (1953) 981-988.
29. Bayer, R.G. (ed.), Selection and use of wear tests for Coatings, ASTM Publication 769, ASTM Philadelphia 1982.
30. Bhushan, B. & Gupta, B.K., Handbook of Tribology: materials, coatings and surface treatments, McGraw-Hill, New York, 1991.

www.manaraa.com

31 Tangena, A.G., Tribology of thin film systems, Doctoral thesis, Eidhoven Technical University, 1987, 130p.

32. Holmberg, K. and Matthews, A., Tribological coatings: properties, techniques and applications in surface engineering. In press, Elsevier Sequoia

33. Kramer, B.M., J. Vac. Sci. Technol., A4 (1986) 2870.

34. Ronkainen, H., Varjus, S., Holmberg, K., Fancey, K.S., Pace, A.R., Matthews, A., Matthes, B., & Brosceit, E., Coating evaluation methods, Proceedings of the 16th Leeds-Lyon symposium on Tribology, Lyon, 1989, Dowson, D., Taylor, C.M., Godet, M. (eds.), Elsevier Sequoia, Amsterdam, 1990.

35. Hintermann, H.E., CVD/PVD and tribological coatings. Proc. Int. Ion Engineering Congress, Kyoto, IEEE (Japan), 1983

36 Matthews, A., Valli, J.and Stainsby, J.A., Tribological characterisation of some second generation ceramic coatings deposited by ionisation - assisted physical vapour deposition. Institution of Mechanical Engineers Paper No C163/87, IMechE, London, 1987.

37 Matthews, A., Tither, D. and Holiday, P., Diamond carbon-based coatings, Proc. 5th Int. Cong. on Tribology, Helsinki, 1989. The Finnish Society for Tribology 1989.

38. Dill, J.F., Gardos, M.N., Hintermann, H.E. and Boving, H.J., Rolling contact fatigue evaluation of hardcoated bearing steels. Proc. 3rd ASlE Conf. on Solid Lubr., August 1984, ASLE, 1984.

39. Hochmann, R.F., Erdemir, A., Dolan, F.J. and Thorn, R.L., Rolling contact fatigue behaviour of Cu and TiN coatings on bearing steel substrates. J. Vac. Sci. Technol., A3(6) (1985) 2348.

40. Chang, T.P., Cheng, H.S., Chiou, W.A. and Sproul, W.D., A comparison of fatigue failure morphology between TiN coated and uncoated lubricated rollers. Proc. ASME/STLE Tribology Conf., Toronto, 1990, STLE, 1990.

41. Chang, T-S P, Cheng, H.S., Sproul, W.D. The influence of coating thickness on lubricated rolling contact fatigue life. Proc. 8th Int. Conf. on Thin Films and 17th Int. Conf. on Metallurgical Coatings, San Diego, 1990.

42. Douglas, A., Doyle, E.D. and Jenkins, B.M., Surface modifications for gear wear. Proc. Int. Tribology Conf. Melbourne, 1987.

43. Sirvio, E.H., Sulonen, M. and Sundquist, H., Abrasive wear of ion-plated titanium nitride coatings on plasma-nitrided steel surfaces. Thin Solid Films, 96 (1987) 93.

44. Stevenson, P., Leyland, A., Parkin, M. and Matthews, A., The effect of process parameters on plasma carbon diffusion of stainless steels at low pressure. Proc. Int. Conf. on Metallurgical Coatings and Thin Films, San Diego, 1992. To be published in Surf. Coat. Technol.

45. Bayer, R.G., Selection and use of wear tests for metals, STP-615, ASTM, Philadelphia, 1976.

46. Stephenson, D.J., Nicholls J.R., and Hancock, P., Wear, 111 (1986) 31.

47. Jonsson, B., Akre, L., Johansson, S. and Hogmark, S., Evaluation of hard coatings on steel by particle erosion. Thin Solid Films, 137 (1986) 65.

48. Matthews, A., Bennett, S., Perry, A.J., Sproul, W.D. and Bull, S., Multi-pass scratch testing at sub-critical loads. Proc. Int. Conf. on Metallurgical Coatings and Thin Films, San Diego, 1992. To be published in Surf. Coat. Technol.

49. Sundquist, H.A., Sirvio, E.H. and Kurkinen, M.T., Wear of metal-working tools ion plated with titanium nitride. Metals Technology, 10 (1983) 130.

50. Hedenquist, P. and Olsson, M., Sliding wear testing of coated cutting tool materials, Tribology International 24 (1991) 143.

51. Hedenquist, P., Olsson, M., Wallen, P., Kassman, A., Hogmark, S. and Jacobson, S., How TiN coatings improve the performance of high speed steel cutting tools. Surf. Coat. Technol., 41 (1990) 243.

www.manaraa.com

MICROSTRUCTURAL CHARACTERIZATION OF FILMS AND SURFACE LAYERS

W. GISSLER AND J. HAUPT
Institute for Advanced Material
Joint Research Centre of the CEC
C.P. 1, I-21020 Ispra (Va), Italy

ABSTRACT. The chapter is subdivided in two parts: structural and morphological characterization. The first part contains a short summary of the basic principles of diffraction: Bragg's law and intensity determination of diffraction lines. Evaluation methods of powder diffraction patterns and the influence of grain size and strain on the diffraction line widths are then described. X-ray diffractometer techniques, in particular Bragg-Brentano and Seemann-Bohlin types, and also the glancing angle x-ray diffractometer, are discussed. Finally the unique features of neutron diffraction techniques are shortly mentioned. The second part contains a description of the principles of scanning (SEM) and transmission electron microscopy (TEM). Several application examples are given. Special consideration is made of the various modes of TEM microscopy: Bright and dark field imaging, out of focus imaging and selected area diffraction.

Introductory Remarks

It is well known that the microstructure of a material strongly influences its macroscopic properties. The importance of such a relationship also for coatings and surface layers was established in the last decade. Most film deposition techniques dispose of special means (see the foregoing chapters on deposition methods) to influence the film microstructure. Actually the investigation of the interrelationship between microstructure and macroscopic properties became subject of intensive research. The term 'microstructure' is usually associated with several structural properties such as the crystallographic structure and the orientational distribution of the crystal grains. However, the morphology of coatings (grain size, void distribution and second phase appearance) and the film growth mode as described in the various structure zone models (see e.g. [1]) are also comprised within the term microstructure. The main structural characterization methods are based on x-ray diffraction and are described in part I of this chapter. Characterization of the film and surface morphology are performed mainly by scanning and transmission electron microscopy. These techniques are discussed in part II.

W. Gissler and H. A. Jehn (eds.), Advanced Techniques for Surface Engineering, 313–333.
© 1992 *ECSC, EEC, EAEC, Brussels and Luxembourg.*

www.manaraa.com

I. Structural Characterization of Thin Films and Surface Layers

1. Introduction

The crystallographic structure of a film or surface layer is of crucial importance for its properties and performance. One of the best known examples is given by the various structural modifications of carbon: if carbon atoms are arranged in the diamond lattice we are confronted with the hardest and best insulating material in existence, whereas if arranged in the graphite lattice the material is soft and electrically conducting.

The classical method for structure determination is based on diffraction techniques of x-rays, electrons and neutrons. However, there are many other methods based on structure sensitive properties of the film material. For example Raman spectroscopy can be used to reveal the existence of diamond domains in carbon films; this method is much more sensitive than x-ray diffraction. Another example is infrared absorption spectroscopy which is the standard method to distinguish between hexagonal and cubic boron nitride films. In a similar way many other properties such as index of refraction, electrical and thermal conductivity, hardness and elasticity may be used to quickly identify the possible phases of a film. However, it is evident that to correlate these properties with a certain structure an 'a priori' structure determination must be performed, and this is only possible by diffraction spectroscopy.

In the following section the most common x-ray diffraction (XRD) techniques, their advantages and disadvantages, structure determination methods and evaluation procedures will be discussed. For more detailed information the reader is referred to standard books on x-ray [2-4], electron [5] and neutron [6] diffraction.

2. Basic principles of crystal diffraction

2.1. BRAGG'S LAW

Fig. 1 shows a schematic view of the geometric arrangement of a diffraction experiment. A monochromatic beam of wavelength λ hits the film/substrate from which it is diffracted in several directions. The diffracted intensity is recorded as a function of the diffraction angle ϑ. As is well known from standard physics textbooks the intensity of the diffracted beam is non-zero only at those diffraction angles where the Bragg condition

$$2d_{hkl} \cdot \sin\vartheta = \lambda \qquad (1)$$

is satisfied. d_{hkl} is the spacing of the lattice planes with the Miller indices h k l . The Bragg condition is the result of a coherent superposition of elementary waves from the origin of each cell of the lattice. It reflects the translational symmetry of the Bravais lattices, but does not contain information on the basis of the unit cell, i.e. on the atomic arrangement of atoms in the unit cell if it contains more than one atom.

www.manaraa.com

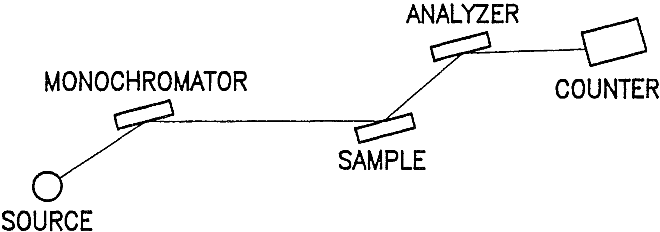

Fig. 1: Schematic layout of the beam geometry in a diffractometer

If the film material is polycrystalline consisting of randomly oriented grains, the diffraction intensity is directed into cones. If these are projected on a flat surface which is normal to the incident beam concentric rings are formed (Debye-Scherrer rings). With monocrystalline film material (epitaxial layers) a pattern consisting of single points (Laue pattern if the incident beam is polychromatic) is formed. If the crystal grains of the film material have a preferred orientation (texture) then a pattern is obtained which consists of rings of non-uniform intensity. Crystal structure determination is based on an analysis of the angular position and intensity of the diffraction lines and spots, respectively. The principles are the same for x-ray, electron and neutron diffraction.

2.2. THE INTENSITY OF DIFFRACTION LINES

The intensity $I(\vartheta)$ of the diffracted beam depends on several factors. Besides the structure of the film it depends also on the experimental method employed, the volume of the irradiated film/substrate combination, the geometry of the diffractometer and many other factors. In general it is sufficient to determine only relative intensities. The most important factors are given in the following.

The atomic form factor, f: The dependence of f on $4\pi\sin\vartheta/\lambda$ is shown in Fig. 2 for several atoms and ions. The rapid decrease of f with $\sin\vartheta/\lambda$ is due to destructive interference in the electron cloud

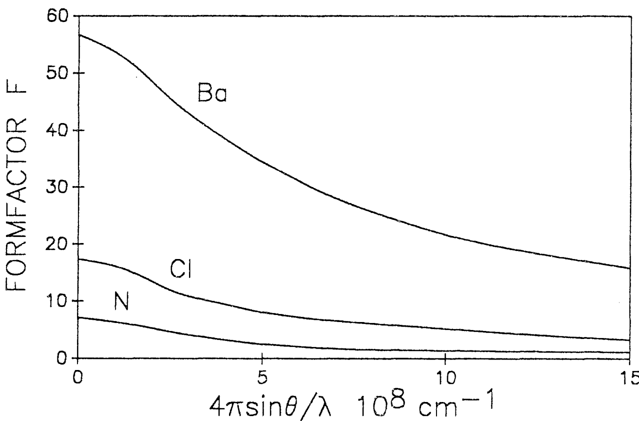

Fig. 2: The atomic form factor F for Ba, Cl and N vs. $4\pi\sin\vartheta/\lambda$

www.manaraa.com

of the atom which is comparable in size with the wavelengths of x-rays used for diffraction experiments (1 - 2 Å). This means that the signal to noise ratio of a diffraction pattern worsens with increasing $\sin\vartheta/\lambda$. Furthermore, the maximum value f(0) is proportional to the number of electrons in the electronic cloud. If the film material under investigation is composed of light and heavy elements and their form factors differ considerably it will be very difficult to observe diffraction peaks caused by light atoms in the presence of heavy ones, particulary since the form factor enters quadratically in the expression for the intensity I.

The temperature factor or Debye-Waller factor, T: It is caused by the thermally induced oscillations of an atom and is given by the expression $\exp(-K^2u^2)$ where u is the mean oscillation amplitude of the atom and $K = 4\pi\sin\vartheta/\lambda$. This factor also decreases with the diffraction angle, but to a smaller amount than the atomic form factor f.

The absorption factor, A: Both the incident and the diffracted beams in passing through the film are partially absorbed leading to an absorption factor A(K). Its dependence on ϑ is just opposite to that of the temperature factor T. It has been shown in many cases that these factors cancel each other and that better results are obtained by ignoring both factors than by attempting to allow for them.

The structure factor, F: This factor is the most important one, because it contains the information on the position of atoms in the unit cell of the lattice. It is given by the expression

$$F(hkl) = \sum_j f_j \exp[-i2\pi(u_j h + v_j k + w_j l)] \qquad (2)$$

The summation has to be performed over all atoms j in the unit cell. The position of the jth atom in the unit cell is given by the coordinates $a \cdot u_j$, $b \cdot v_j$ and $c \cdot w_j$, where a, b and c are the dimensions of the unit cell in the three main axis directions and f_j is the atomic form factor of the jth atom. F(hkl) is complex, but the intensity is given by the real quantity $/F/^2$. Simple expressions are obtained for cubic lattices. For a bcc structure $/F/^2 = 0$ when h+k+l is an odd integer and $/F/^2 = 4 \cdot f^2$ when h+k+l is an even integer. For a fcc lattice $/F/^2 = 16 \cdot f^2$ if all Miller indices are even or odd integers; if they are partly even and partly odd $/F/^2 = 0$. For example TiN crystallizes in a fcc structure, therefore the diffraction peak sequence of hkl is 111, 200, 220, etc.

The multiplicity factor M: In general more than one plane hkl in a crystal can have the same spacing. In the powder diffraction technique which is most widely used in film structure analysis all planes with the same spacing contribute to the same diffraction ring. By the multiplicity factor this circumstance is considered, and M is equal to the number of lattice planes of all different hkl combinations giving rise to the same spacing.

Other factors: primary and secondary extinction due to reduced intensity of the incident beam as a consequence of the multiple diffraction process has to be considered in monocrystals and polycrystalline materials of grain size > 10 µm, but do not play an important role in film structure determination.

The two most important factors contributing to the intensity of the diffracted beam are therefore the stucture factor and the multiplicity. The intensity of the diffracted beam is therefore given by:

$$I_{hkl} = |F|^2 \cdot M \qquad (3)$$

Equ. (3) gives the intensity for all combinations of planes hkl having the same lattice spacing. To calculate the diffraction angle for a diffraction line hkl the spacing of the corresponding lattice planes has to be calculated and then the Bragg equation (1) has to be applied.

www.manaraa.com

3. Evaluation of powder diffraction patterns

3.1. COMPARISON WITH POWDER DIFFRACTION STANDARD FILES

Diffraction analysis serves in the practice of thin film and coating laboratories to identify the structure of a deposited film rather than to elaborate the structure of new unknown substances. The latter would better be performed with bulk material and in particular with monocrystals. Therefore diffraction analysis as discussed here is essentially limited to a comparison of the experimentally obtained diffraction pattern with patterns of substances the structure of which is already known. This procedure is facilitated by the fact that in general the composition of the material in question is known and that therefore the number of possible structures which might have been formed is limited. For such comparisons in principle, the intensity of the diffraction peaks has to be calculated with the help of equ. (4). An easier way, however, is to rely on the Powder Diffraction Standards. These are a collection of experimentally determined relative intensity values for a huge number of substances (Joint Committee on Powder Diffraction Standards, JCPDS [7]). They are available as books, microfilms and cards, and can also be retrieved from disks and data banks. The data are divided in an organic and inorganic part and have several subdivisions as e.g., minerals, metals and alloys. Fig. 3 shows, as an example, such a card for TiN. It contains in the top part the diffraction lines with the highest intensity and their corresponding d values; this type of information is detailed in the table on the right of the card and complemented by the corresponding hkl indices. Furthermore the cards contain information on the crystal system and space group, the lattice constant, on physical properties such as density, melting point, colour and hardness and also on the experimental conditions and their origin. Corresponding cards are available also for several non-stoichiometric TiN_X compounds.

6 - 0642 MAJOR CORRECTION

d	2.12	2.44	1.50	2.44	(TiN)8E
I/I_1	100	75	55	75	TITANIUM NITRIDE (OSBORNITE)

Rad. Cu λ 1.5405 Filter Ni
Dia. Cut off Coll.
I/I_1 DIFFRACTOMETER d corr. abs.?
Ref. BEATTLE AND VERSNYDER, TRANS. ASM 45, 397 (1953)

Sys. CUBIC S.G. FM3M (225)
a_0 4.240 b_0 c_0 A C
α β γ Z 4
Ref. IBID.

ε α n ω β ε γ Sign
2V Dx 5.40 mp Color YELLOW
Ref. IBID.

CONTAINS TRACE OF ZR

d Å	I/I_1	hkl	d Å	I/I_1	hkl
2.44	75	111			
2.12	100	200			
1.496	55	220			
1.277	25	311			
1.223	16	222			
1.059	8	400			
0.972	12	331			
.948	20	420			
.865	20	422			
.816	---	333,511			

Fig. 3: Example of a JCPDS powder diffraction file of stoichiometric titanium nitride.

المنارة للاستشارات
www.manaraa.com

For demonstration in Fig. 4 a comparison is shown between a diffraction spectrum which was obtained with a glancing angle x-ray spectrometer (see below) from an ion beam sputtered TiN film on a glass substrate at 77° K [8] and the line spectrum as obtained from the d_{hkl} values and their corresponding relative intensities as shown on the JCPDS card of Fig. 3. It is evident that the experimental line positions agree relatively well (besides a small shift to lower diffraction angles caused by strain), but the line intensities differ considerably. This is due to the fact that TiN films grow with a preferred orientation of the (111) plane parallel to the substrate surface. Furthermore it is interesting to note that the width of the lines are quite large which is due to small crystallite size and /or strain in the film (see below).

Besides the JCPDS files a considerable number of other data banks exist from which crystallographic information can be obtained. The most important in Europe are the Cambridge Crystallographic Data File [9] and the Inorganic Crystal Structure Database [10]. Furthermore several additional helps are available such as the Hanawalt index [11] in which substances are ordered according to the d_{hkl} values of their strongest lines.

Modern diffractrometers are computer controlled and have several routines for data collection, data display and data evaluation. Peak search routines facilitate the measurement of peak positions and intensities, and deconvolution routines allow the separation of overlapping peaks. In many cases it is possible to immediately compare the measured diffraction pattern with peak positions and intensities of a great variety of standard materials with powder standard files.

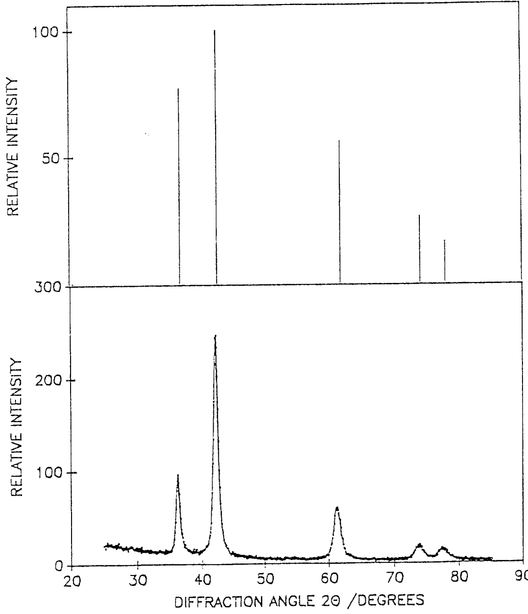

Fig. 4: Comparison of a diffraction pattern as obtained by glancing angle x-ray diffractometry from an ion beam sputtered (at 77° K) TiN film [8] with the line spectrum as obtained from d_{hkl} values and their relative intensities from the JCPDS card shown in Fig. 3

3.2 COMPARISON WITH COMPUTER GENERATED DIFFRACTION PATTERNS

Modern film deposition methods make it possible to deposit polycrystalline films with ultrafine grains in the nanometer size range. Diffraction peaks reach in such cases line widths of the order of

www.manaraa.com

10° (see below) with the consequence that several peaks overlap and a structure determination by a simple comparison with diffraction line positions and their relative intensities as obtained from standard powder diffraction data is not anymore possible. In such cases it might be convenient to model diffraction spectra by computer calculations and to try to find out the grain structure by comparison with the experimentally obtained diffraction pattern.

An example of such a procedure is shown in Fig. 5 where a XRD spectrum obtained from a 15 μm thick boron nitride film which was sputter-deposited on a glass substrate (a) is compared with computer generated diffraction spectra (b). Like carbon , boron nitride occurs in several modifications among them a graphite-like (hexagonal) and two diamond-like (zincblende and wurtzite) crystal structures. For the calculation of the diffracted intensity I(K), where $K = 4\pi \sin\vartheta/\lambda$, the Wierl formula [12] was used which is valid for randomly oriented crystallites

$$I(K) = \sum f_i f_j \{\sin(Kr_{ij}) / Kr_{ij}\} \qquad (4)$$

r_{ij} is the distance between the ith and j^{th} atom and the other variables have the same meaning as in formula (1). The average number n of BN molecules contained in a crystallite was choosen in such a way that the widths of the calculated diffraction peaks were nearly equal to the experimentally observed ones. From a comparison of such computed diffraction patterns with the experimental one it becomes evident that the film consists of a mixture of grains with hexagonal and cubic BN. It turned out that the hexagonal grains are much smaller than the cubic ones. Interestingly this result could also be confirmed by TEM investigations (see below).

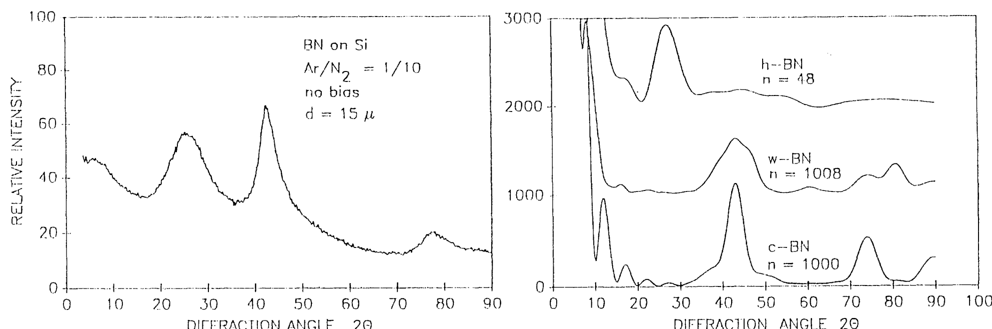

Fig. 5: X-ray diffraction pattern of a BN film which was sputter deposited on a Si wafer (a). Results of a computer generated diffraction pattern for the three different BN modifications (b).

3. Grain Size and Strain

The width of a diffraction line is determined by the number of elementary waves which are added coherently to build-up the interference pattern and hence by the average size of crystal grains of which the material is composed. Taking into account an experimental angular resolution of the diffractometer of $\Delta\vartheta = 0.01°$ then a line broadening effect is observable if the grain size D is lower

www.manaraa.com

then approximately 1μm. With film deposition techniques such as bias sputtering, ion plating or ion beam assisted PVD dense films consisting of grains in the submicron and even in the nanometer region are obtained. Therefore their grain size determination is usually possible by a line width analysis.

If β_{gs} is the full width at half maximum intensity of the diffraction peak, then D can be determined according to the Scherrer formula (see e.g., [2]):

$$\beta_{gs} = \frac{K \cdot \lambda}{D \cdot \cos\vartheta} \tag{5}$$

K is a constant which depends on the shape of the crystal grain and assumes in extreme cases values of 0.7 and 1.4, respectively. For most cases, however, it can be assumed K = 1 in good approximation.

Another important factor contributing to a diffraction line broadening is the formation of strain in the film or surface. It is well known that good wear resistant films are very often subject to compressive stress of the order of several GPa [13]. This has the consequence that the crystal grains of which the material is made up are non-uniformly distorted resulting in the formation of slightly different lattice spacings. These effect a distribution of the diffracted beam over a small range of angles around the line position of the undistorted crystal. The line broadening β_{st} due to strain is given by the expression [2-4]:

$$\beta_{st} = 4 \cdot \varepsilon \cdot \tan\vartheta \tag{6}$$

In general line brodening might be caused both by a limited grain size and by strain in the material. In order to separate both contributions it is very often assumed that the total width β_{tot} is given approximately by $\beta_{gs} + \beta_{st}$. Then we obtain after some rearrangment the relation

$$\beta_{tot} \cdot \frac{\cos\vartheta}{\lambda} = \frac{1}{D} + 4 \cdot \varepsilon \cdot \frac{\sin\vartheta}{\lambda} \tag{7}$$

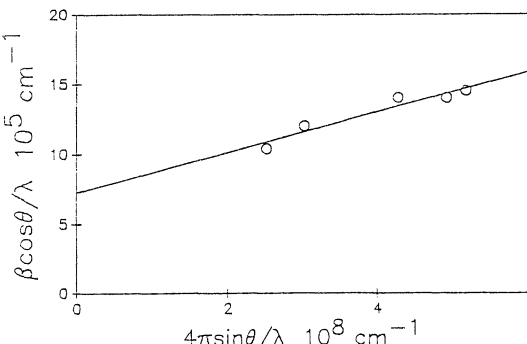

Fig. 6: Williamson-Hall plot of the TiN diffraction pattern shown in Fig. 4. For the grain size and strain values of D = 130 Å and ε = 0.6 % were obtained, respectively [8].

المنارة للاستشارات
www.manaraa.com

By plotting the expression $\beta\cos\vartheta/\lambda$ versus $\sin\vartheta/\lambda$ for different diffraction lines, D and ε can separately be determined. Such a plot is called Williamson-Hall plot and is often applied for films and coatings. Fig.6 shows an example, which was obtained from an evaluation of the diffraction pattern shown in Fig. 4. β_{tot} was taken from the widths of the 111, 200, 220, 311 and 222 peaks. For D and ε values of 130 Å and 0.6 % were obtained [8].

5. X-Ray Diffractometers

X-ray diffraction is a relatively low-cost technique that is non-destructive, and often complementary to other techniques, giving results that cannot be obtained as easily or with the same degree of precision by other methods. Most x-ray characterization of thin film material is done via powder diffraction methods. In general satisfactory results are obtained if the films under investigation are composed of atoms of high atomic number and thickness is in the order of several micrometers.

A large number of x-ray diffraction methods were developed in the past. However, in recent times diffractometers equipped with high-power x-ray sources and counters to measure diffracted intensities are most commonly used for thin film and coating investigations. There are essentially three different methods; their principles, advantages and disadvantages will be discussed in the following.

5.1. BRAGG-BRENTANO AND SEEMANN-BOHLIN GEOMETRY

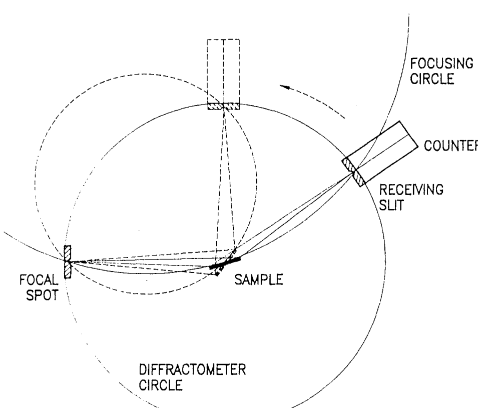

Fig. 7: X-ray diffractometer in the Bragg-Brentano geometry.

The arrangement of a diffractometer in the standard Bragg-Brentano (BB) geometry is shown schematically in Fig.7 [14, 15]. Focal spot, sample and receiving slit are positioned on the focussing circle. The sample is placed tangentially to the focussing circle, enabling the use of a large sample area. The radius of the focussing circle depends on the Bragg angle. The incident beam is monochromatized either by a single crystal or by x-ray filters and then directed through a collimator onto the sample. The diffracted beam is analyzed as a function of the scattering angle ϑ. In the BB geometry, the angle that the sample surface makes with the incident beam, increases directly with

المنارة للاستشارات
www.manaraa.com

2ϑ, thus reducing the sample volume in proportion to $1/\sin\vartheta$ for films of thickness d « 1/μ (μ is the linear absorption coefficient). Together with the general reduction in scattering cross section with increasing scattering angle, this causes an extreme diminuition of the intensity of the higher 2ϑ Bragg reflections. Because the only atomic planes which contribute to diffraction in a Bragg-Brentano powder pattern are parallel to the sample surface, any sample texture affects diffracted intensities, and strong texture renders most reflections inaccessible. A consequence of this is strong substrate diffraction if any substrate atomic planes are within a degree or so parallel with the substrate surface. Diffraction from these planes may mask the presence of weak thin film peaks.

In the Seemann-Bohlin (SB) geometry (Fig. 8*)* the focal spot, sample and receiving slit are also mounted on a focussing circle [14, 15]. However, the sample is kept at a fixed angle to the incident x-ray beam, and the receiving slit of the detector is moved along the focussing circle. The incident angle can be as small as ~ 5° and may now be different from the Bragg angle. The sample volume remains thereby fixed resulting in larger diffracted intensities in particular at large Bragg angles. However, the major advantage for thin film applications is that small incidents angles can be used. This is important also in cases where strong texture effects might reduce the signal/background ratio.

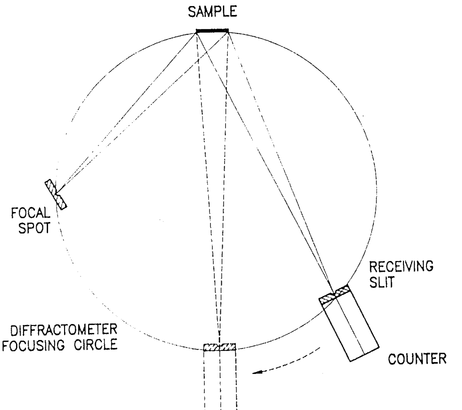

Fig. 8: X-ray diffractometer in the Seeman-Bohlin geometry

5.2. GLANCING ANGLE X-RAY DIFFRACTOMETRY

If the thickness of the films under investigations is in the sub-micrometer range the diffracted intensity may be strongly masked by substrate contributions. To improve the signal/background ratio a control of the penetration depth of the x-ray beam is necessary. This can be done by a relatively new surface-sensitive technique, glancing angle x-ray diffraction (GAXRD)[8, 14, 17, 18]. This technique is based on the fact that with decreasing angle of incidence the penetration depth of x-rays is diminished. In *Table I* the penetration depths for several materials are compared for the cases of normal BB, SB and glancing angle incidence GA at 1° [16]. From this comparison it becomes evident that for most films having a thickness in the submicrometer range the angle of incidence should be considerable smaller than 5° in order to avoid a penetration into the substrate material.

www.manaraa.com

Table 1. Penetration depth of Cu K_a radiation in various materials

Material	Norm. to Surface	BB at Φ=60°	SB at Φ=5°	GA at Φ=1°
Au	2.5	1.25	.2	440 Å
stell (AISI 304)	4.6	2.3	.4	800 Å
TiN	11.4	5.7	1	2000 Å
Al	76	38	6.6	1.3
BN (hexagonal)	862	431	75	15.0
C (diamond)	620	310	54	10.8
SiO_2	115	57	10	2

penetration depts in μm if not otherwise indicated; BB = Bragg-Brentano geometry, SB = Seemann-Bohlin geometry, GA = glancing angle geometry, Φ = incident angle

In order to reduce the angle of incidence to values $\phi < 5°$ it is necessary to abandon focussing arrangements and use a parallel beam geometry. Instead of a diverging incident beam, a high precision slit has been added to allow accurate control of the angle of incidence on the sample. Diffraction from the entire illuminated section of the sample surface is collected via a Soller slit for angular resolution. A monochromator may be placed after the exit Soller slit to discriminate in favor of the characteristic K_α lines of the source. Alternatively, a solid state semiconductor detector may be employed (these have a typical energy resolution of 2 %). Fig. 9 shows a schematic view of a GAXRD instrument being a modification of the SB focusing geometry. This arrangement is known as the glancing incidence asymmetric Bragg (GIAB) geometry. The resultant loss of intensity in this

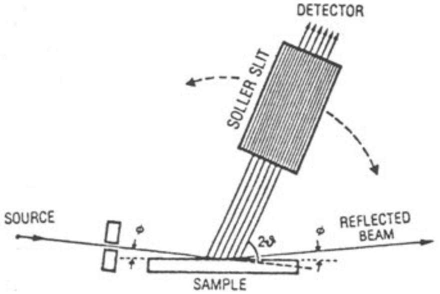

Fig. 9: Glancing angle x-ray diffractometer in the assymetric Bragg geometry

geometry is high with repect to the focussing geometry, but is compensated by a considerable increase in the signal/background ratio. Fig. 10 shows as an example the diffraction pattern of a 0.3 μm thick TiN film deposited on a glass substrate at three different graze angles of 4°, 1.5° and 0.5° [8]. The broad diffraction peak near $2\vartheta = 25°$ typical for an amorphous material disappears at the graze angle of 0.5° because the x-ray beam is almost completely confined to the TiN film.

المنارة للاستشارات
www.manaraa.com

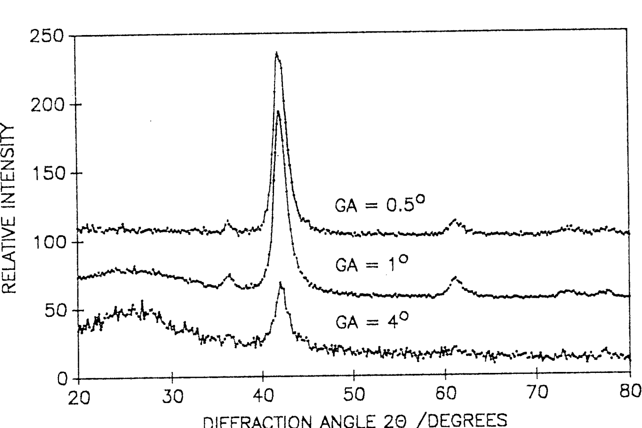

Fig. 10: Diffraction pattern of a 0.3 μm thick TiN film deposited on a glass substrate at three different graze angles of 4°, 1.5° and 0.5° [8]

6. Neutron Diffraction

Up to now few experiments on thin films and coatings structure investigations have been performed with neutron diffraction. The main reasons for this are: i) powder diffraction studies with neutrons require a sample volume in the order of cm^3; ii) neutron scattering experiments are expensive with respect to x-ray and electron diffraction and iii) access to neutron spectrometers is difficult and requires a relatively long procedure. However, with the availablility of high flux neutron reactors in recent years this situation might change.

This technique is mentioned here because it has some unique features which are not available in x-ray and electron diffraction. In contrast to x-rays, neutrons have the great advantage that the (coherent) scattering amplitude a_c (corresponding to f(K) for x-rays) shows no regular dependence on the atomic number. For example deuterium has a relatively large value for a_c and allows therefore the determination of the position also of hydrogen atoms if substituted by the deuterium isotope even in presence of heavier atoms. Furthermore, due to the fact that neutrons interact with the atomic nucleus and not with the electron cloud (as for x-rays and electrons) a_c is constant and independent of the momentum transfer and does not display an angular dependence. This makes the accessible range of K values much larger. Another important characteristic of neutrons is their unique capability to interact with magnetic moments. Actually all essential magnetic structure investigation have been performed with neutron diffraction. Recently the first neutron diffraction experiments on TiN coatings were reported [19].

www.manaraa.com

II. Morphology of Thin Films

1. Introduction

In this chapter we will distinguish between film surface morphology and the structure of crystal grains, grain boundaries and small voids in the bulk of the film. These two domains are usually investigated by two different techniques: scanning electron microscopy (SEM) and transmission electron microscopy (TEM). Due to the central role of SEM and TEM in this field we will not deal in this article with other techniques like optical, tunneling and atomic force microscopy.
By 'surface morphology' we mean not only the film surface but also fracture surfaces, which show the type of growth morphology.

2. Surface Morphology by SEM

2.1. DESCRIPTION OF THE SCANNING ELECTRON MICROSCOPE

A typical setup of a scanning electron microscope is given in Fig. 11: An electron beam from a tungsten or LaB_6 tip is accelerated by the anode (range 5 to 50 kV) and focussed via two magnetic lenses (magnification about 1/1000) in order to get a fine spot on the sample. At the same time the beam is scanned in x and y direction by two coil pairs. The emitted electrons from the sample are either collected by a detector for reflected electrons (RE) or a detector for secondary electrons (SE). After amplification this signal modulates the intensity of a cathode ray tube which is deflected synchronously with the microscope electron beam. The magnification of the image is adjusted by the amplitude of deflection in the two coil pairs. The elastically reflected electrons have the same energy (disregarding a small energy loss due to electron phonon interaction) as the incident beam and show a strong directional effect. Their backscattering coefficient depends strongly on the type of material: the heavier the element, the higher the backscattering coefficient. Secondary electrons leave the sample with energies smaller than 50 eV, independent of the primary beam energy (the energy range between 50 eV and the primary beam energy can be disregarded for SEM due to the weak intensity of these electrons). About one to two secondary electrons are generated per incident primary electron. Secondary electrons show almost no directional effect and can be collected from positions of the sample which are not directly seen by the detector, if a slight positive bias is applied to the specimen. Their emission intensity does not depend much on the material. Therefore the strong shadowing effect seen with reflected electrons is not observed; instead they display a more uniform illumination of the sample independent of the local elemental composition of the specimen. Fig. 12 shows the fracture surfaces of boron nitride films deposited by magnetron sputtering with a bias of -20 V (left) and -100 V bias (right) [20]. The specimen deposited with low bias exhibits a more granular structure, whereas the high bias film shows a distinctly fibrous fracture with an irregular dome-like surface morphology. The reason for this exceptional behaviour is due to a mixed phase deposition: cubic BN crystallites are embedded in a very fine grained hexagonal matrix, as will be discussed later. The images of Fig. 12 could be obtained without adverse charging effects (BN is an insulator) at an accelerating voltage of 4.5 kV. At this voltage a charge balance of primary beam electrons (falling on the specimen) with scattered and secondary electrons (which leave the

www.manaraa.com

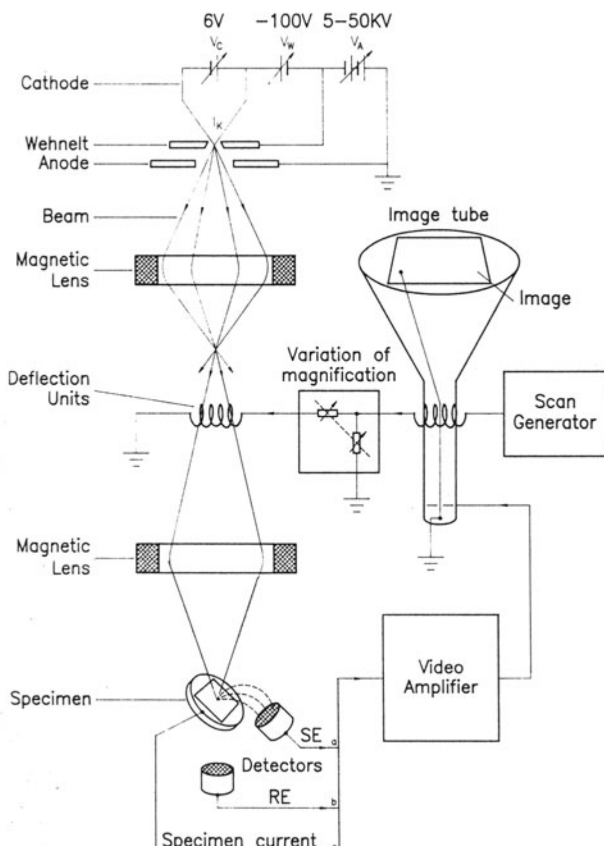

Fig 11: Schematic diagram of a scanning electron microscope

specimen) reduces the charging effects. Charging can also be avoided by depositing a thin metallic film on the specimen surface. This, however, modifies the surface properties. Modern scanning electron microscopes have a beam resolution of better than 1 nm. However limitations in image quality due to specimen charging and specimen preparation are often encountered.

3. Bulk Structure of Films Studied by TEM

For TEM investigations thin foils of thickness 5 to 500 nm (depending on the material and type of investigation) have to be prepared from the "bulk" of the films. The foil preparation procedure will be described in a later chapter. With these foils it is possible to visualize structures in the nm range. It should be mentioned that in the case of single crystals it is even possible in the so called lattice imaging mode to see the projection of single atom columns and to locate dislocation lines in the

www.manaraa.com

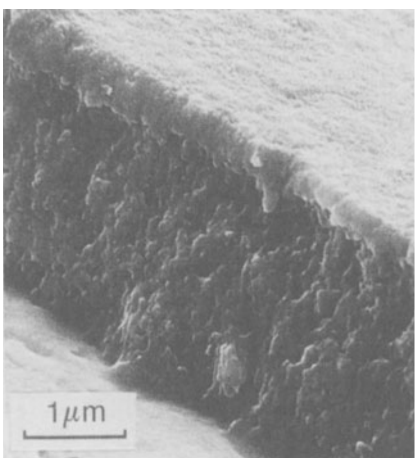

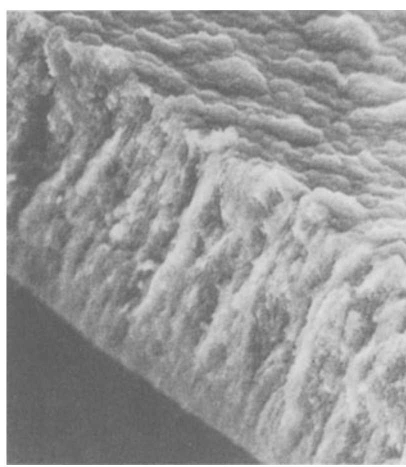

Fig. 12: Fracture surfaces of two magnetron sputtered BN films as studied by a JEOL 840F scanning electron microscope: the film on the left was sputtered with -20 V and that one on the right with -100 V [20]. The low bias film exhibits a more granular structure and the high bias film a distinctly fibrous structure

crystal [21]. Also boundaries between specially prepared monocrystals of different materials can be studied by this technique [22]. Here we are more interested in films with crystallite sizes in the µm to nm range. TEM can be used not only for imaging but also for diffraction studies.
It has, however, one great advantage with respect to the technique mentioned in the diffraction chapter: the area of diffraction can be reduced to 1 µm in diameter (with a special option, the so called STEM lens, a further reduction to only 3 nm is possible). This type of diffraction is called SAD (small area diffraction). It allows us to study only a few crystallites, in special cases only one.

The combination of diffraction with imaging offers new imaging modes. If the image is constructed by the light of the 0th order diffraction it is called bright field (BF) imaging and in the case of higher orders it is called dark field (DF) imaging. In the BF case all electrons pass through the microscope except the scattered electrons, in the DF case only the scattered electrons pass through the microscope, we see bright object details (i.e. crystallites in Bragg orientation) on a black background.

3.1.DESCRIPTION OF THE TRANSMISSION ELECTRON MICROSCOPE

A scheme of a three lens transmission electron microscope is given in Fig. 13. As with an optical microscope lenses are used to create a magnified picture of the object. However the lenses are magnetic and the image is formed from the intensity distribution of the electrons leaving the bottom surface of the specimen.The most important part concerning the resolution is the objective lens. The resolution (Scherzer resolution) depends mainly on the beam voltage: for a 100, 200 and 400 kV microscope it reaches 0.33, 0.25 and 0.19 nm, respectively. In Fig. 13a the beam pathway for bright field imaging is shown and in Fig. 13b the pathway for selected area diffraction (SAD) is illustrated.

www.manaraa.com

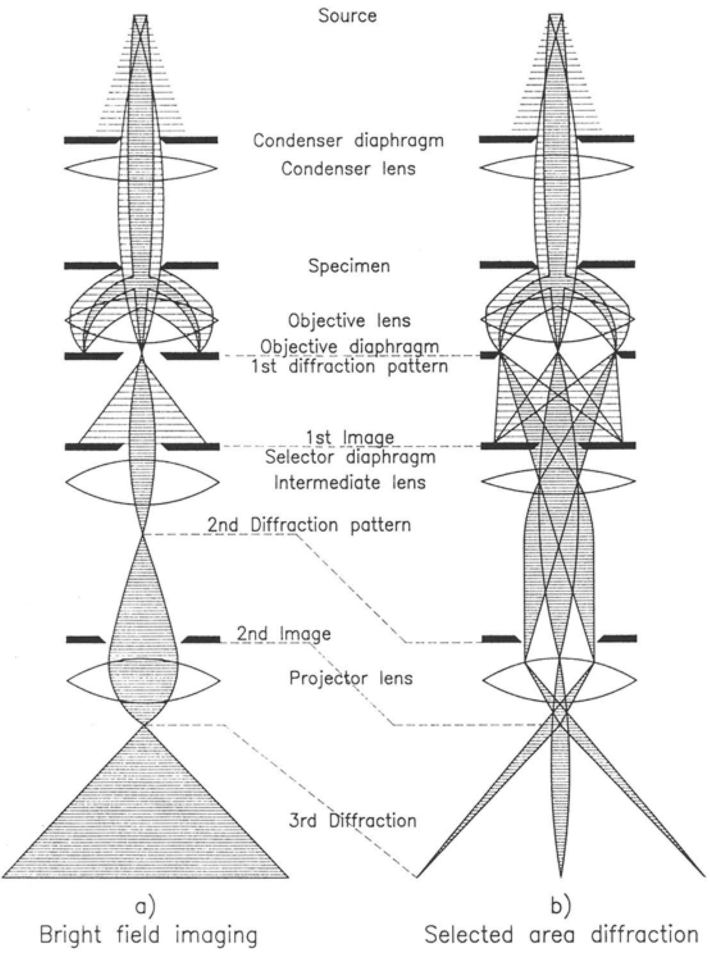

Fig. 13: Schematic diagram of the beam pathway of a transmission electron microscope a) for bright field imaging and b) for selected area diffraction. The working principle of the objective diaphragm and the selector diaphragm are indicated

For BF and DF imaging the objective diaphragm, placed in the back focal plane of the objective lens, selects the order of diffraction of the image light. In SAD the specimen area used for diffraction is selected by the selector diaphragm which is located in the plane of the first image (see Fig. 13). With a magnification M of the first lens and a diameter d of the diaphragm, the selected area for diffraction has the diameter d/M. For phase imaging applications the objective diaphragm in fig. 13a has to be wide enough that also higher order diffractions are allowed to pass.

www.manaraa.com

Contrast of the images is generated in two different ways: a) by phase contrast: in this case the direct and diffracted beams are allowed to interfere with one another. Local phase shifts of an electron wave are created e.g., by voids or the coulomb potential of heavier atoms. Phase contrast imaging gives the highest resolution in transmission electron microscopy, as used for example in lattice imaging. Also out of focus imaging, which will be discussed later, uses the phase contrast mode. b) by amplitude contrast as in BF and DF imaging. In this case the diffracted light of other diffractions than the selected one is eliminated by a small aperture of the objective diaphragm. A first example for BF and DF imaging is given in Fig. 14 for a BN film [20]. This material is of special interest due to the appearance of mixed cubic and hexagonal phases, as mentioned earlier. The first broad diffraction ring (see Fig. 14d) is due to the hexagonal phase and the second narrower ring to the cubic phase. This favourable circumstance allows to see the grains of both crystal

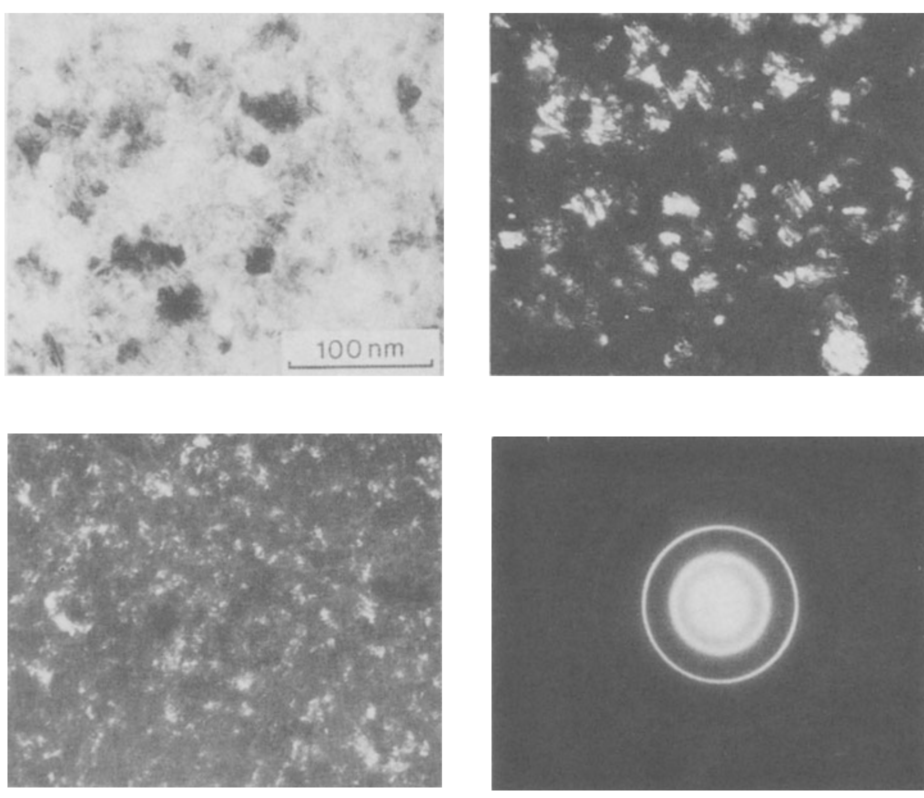

Fig. 14: Transmission electron micrographs of a magnetron sputtered BN film: a) bright field; b) dark field using (111) cubic reflection; c) dark field using (00.2) hexagonal reflection; d) electron diffraction pattern [20]. The studies were performed with a JEOL 200CX transmission electron microscope.

www.manaraa.com

structures independently by using DF imaging with the electrons of the (111) cubic reflection or the (00.2) hexagonal reflection ring. The BF image (Fig. 14a) shows both the cubic and hexagonal grains as dark spots. Some larger cubic grains exhibit evidence of internal faulting, presumably due to twinning (cubic BN twins on {111}). Details especially of the small hexagonal grains are lost in the BF image but can be seen in the DF images (Fig. 14b and c).

3.2. OUT OFF FOCUS IMAGING

Films deposited with PVD techniques at low deposition temperatures often include many voids, in some cases even a network of microchannels. For film applications such as anticorrosive, wear resistant, sensor coatings, etc., it is important to know more about the morphology of microcavities in the nm domain. This is done by "out of focus" imaging technique which allows the identification of microcavities in the range from 1 to 5 nm diameter. These cavities are weak phase objects that are invisible in focus (objective lens focused on bottom surface of the specimen). However, when imaged under appropriate out-of-focus conditions (a few μm), they produce in underfocussed condition bright spots surrounded by dark Fresnel fringes and in overfocused conditions dark spots surrounded by bright Fresnel fringes. The outer diameter of the central spot corresponds fairly well to the diameter of the cavity. More details on this contrast effect are given in the paper of Rühle and Wilkens [22] who analysed this effect for small strain free cavities. Fig.15 shows an example of an under focus image of a (V,Ti)C film deposited by activated reactive evaporation (ARE) at a relatively high acetylene pressure of 10^{-3} torr and 700 °C [23].

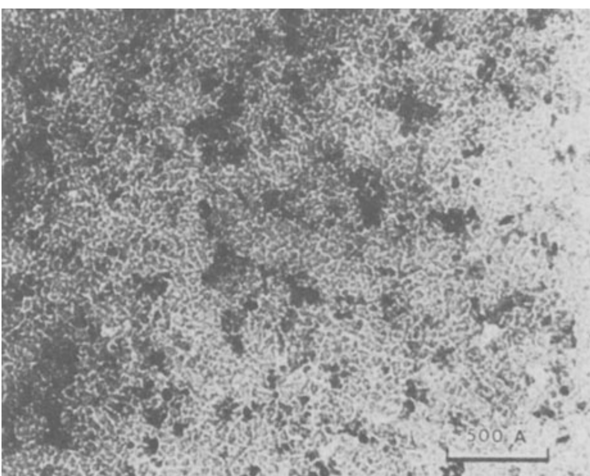

Fig. 15: Out off focus image of a (V,Ti)C film deposited by activated reactive evaporation at an acetylene gas pressure of 10^{-3} Torr and 700°C. The underfocus condition reveals the faint network of cavities present [23]

The relatively high acetylene pressure in combination with a relatively low deposition temperature causes a high deposition rate, a very fine-grained structure and a faint network of fine cavities. Higher temperature deposits with a smaller deposition rate show large grains and no cavities. The Knoop hardness increases from 1385 for the cavity rich structure to 2900 for the cavity poor structure. The usual trend that the smaller the grain size the harder the material is overcompensated by the presence of the cavity structure.

www.manaraa.com

3.3. SELECTED AREA DIFFRACTION AND IMAGING

The possibility of combining diffraction with imaging makes TEM such a powerful tool. By inspection of the specimen image before a SAD experiment a direct comparision of microstructure and electron diffraction of a region as small as 1 μm is possible. This allows us to study single large crystal grains of the film. However, even for fine grained specimens SAD and imaging are complementary. It is possible with diffracted Debye-Scherrer rings to use DF imaging modes. The grain size can be determined by both methods: directly by DF imaging and indirectly from the width of broad diffraction lines. In recent years it has become common practise to add to each TEM image as insert the diffraction pattern. Fig. 16 shows as an example the BF images with the corresponding diffraction inserts for WSi_x coatings on a Si(100) substrate during an annealing process [24]. The average grain size (GS) increases from 2.5 nm for the as deposited sample to 265 nm for the sample tempered at 1100°C. The SAD spectrum shows the typical Debye-Scherrer rings of rather large

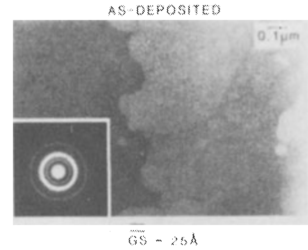

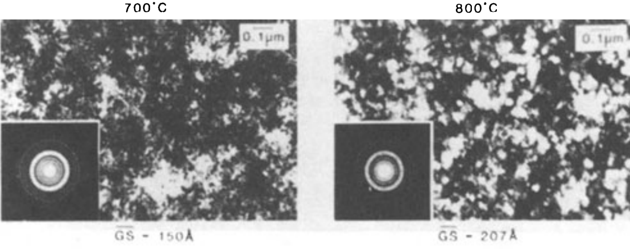

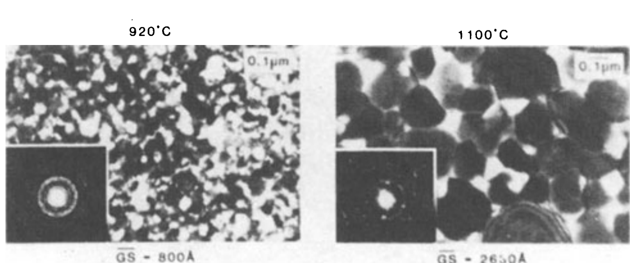

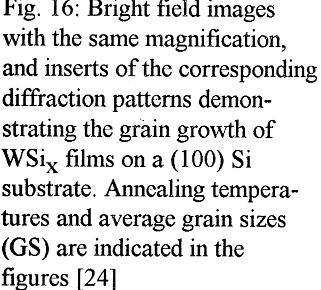
Fig. 16: Bright field images with the same magnification, and inserts of the corresponding diffraction patterns demonstrating the grain growth of WSi_x films on a (100) Si substrate. Annealing temperatures and average grain sizes (GS) are indicated in the figures [24]

width for the films of small grain size and only a few diffraction spots for the films with large grain size. Recently instruments for analytical electron microscopy can focus the beam (with the STEM lens) to a spot of only a few nm in diameter. This micro diffraction is called convergent beam

المنارة للاستشارات
www.manaraa.com

electron diffraction (CBED). Several other modes of using a transmission electron microscope are not discussed here. One of them is surface chemical analysis which can be performed in high resolution.

Limitations for TEM are on the low magnification end: due to the limited area, that can be made transparent for electrons, morphological variations on a coarser scale are difficult to observe. X-ray diffraction reveals more accurate lattice spacings for phase characterization than electron diffraction because it uses larger areas and volumes of the specimen. Texture studies are also better performed with x-rays.

3.4. SPECIMEN PREPARATION FOR TEM

Besides the great advantages which TEM bulk investigations offer in thin film research it has also a disadvantage: the preparation of an appropriate thin foil. A well prepared foil is the prerequisite for a successful TEM analysis. It involves, however, a tedious process that requires patience and some experience. The foil thickness is usually less than 1 µm; for high resolution TEM it may even be less than 10 nm. Specimen thinning is made in two steps: two sample slices of about 1x1x2 mm are fixed with the coatings face to face in the inner rectangular hole of a Ti disc with the coating surfaces perpendicular to the disk. The whole disc including the sample slices is then mechanically polished to 0.1 to 0.2 mm. In the second step the center region of the disk is further thinned either by electropolishing with a fine jet of etching liquid which is pumped against the mechanically polished sample (jet-polishing) or by ion beam milling with an Ar^+ beam of about 5 keV which is directed under an angle of 5 to 20 degrees against the sample surface [25] until perforation occurs. The smooth edges of this center hole are used for TEM investigations. For metals and semiconductors jet polishing is used preferentially whereas for insulators and ceramic materials ion beam milling is applied because jet polishing is not suitable in this case.

Another method to produce foils is the deposition of a sufficiently thin film on a soluble substrate (e.g. Al on NaCl). After dissolution of the substrate the film is transfered on a Cu grid which acts as specimen holder. Direct deposition of the film on a thin amorphous carbon layer, which is deposited on a copper grid, is also possible; the thin amorphous carbon film is almost transparent to the electron beam.

7. References

[1] Thornton, J. A. (1982) 'Coating Deposition By Sputtering', in Bunshaw, R.F. (ed.), Deposition Technologies for Films and Coatings, Noyes Publications, New Jersey

[2] Taylor, A. (1961) X-ray Metallography, John Wiley & Sons, Inc. , New York

[3] Klug ,H.P.and Alexander (1959), L. E. X-ray Diffraction Procedures, John Wiley &Sons, Inc. London

[4] Krischner, H. (1987) Einführung in die Röntgenstrukturanalyse, F. Vieweg & Sohn, Braunschweig

[5] Hren, J. J. , Goldstein, J. I. and Joy D. C. (1979) (eds.), 'Introduction to Ananlytical Electron Microscopy', Plenum Press, New York

[6] Gurevich, I. I. and Tarasov, L. V.(1968) 'Low Energy Neutron Physics', North Holland Publ. Comp., Amsterdam (N.H.)

www.manaraa.com

[7] Powder Diffraction File, Joint Committee on Powder Diffraction Standards, International Center for Diffraction Data, Swarthmore. PA. 1972 - present
[8] Buschert, R.C., Gibson, P.N., Gissler, W., Haupt, J. and Crabb, T. A. (1989), Colloque De Physique, Colloque C7, suppl. au Nr 10, Tome 50, 169-173
[9] Cambridge Crystallographic Data File, Crystallographic Data Centre, University Chemical Laboratory, Lensfield Road, Cambridge, CB2 1EW, U.K.
[10] Inorganic Crystal Structure Database, Fachinformationszentrum , D-7514 Eggenstein-Leopoldshafen 2, Germany
[11] Hanawalt, J. D, Rinn, H. and Frevel, L. K. (1938), Ind. Eng. Chem. Anal. 10, 457
[12] see e.g., Barrow, G. M. (1979) Physikalische Chemie, Bohmann/Vieweg & Sohn, Braunschweig, Germany
[13] Moll, E., Buhl R. , Pulker, K. and Bergmann, E. (1989), 'Industrial PVD Processes for Hard Coatings', in H. Czichos and L. G. E. Vollrath (eds.), Oberflächentechnik, C. Hanser Verlag, München
[14] Segmüller A. a. Murakami, M. (1985), 'Characterization of Thin Films by X-Ray Diffraction', in K. J. Klabunde (ed.), Thin Films from Free Atoms and Particles, Academic Press, NewYork
[15] Finn, P.A. and Waychunas, G.A. (1988), J. Vac.Sci. Technol. B, 6, 1749
[16] Gibson, P. N. (1992), priv. communication
[17] Marra, W.C., Eisenberger, P. and Cho, A. Y. (1987), Appl. Phys. Lett., 50, 6927
[18] Gibson, P.N. (1991), 'Tin Films: X-Ray Characterization', in R. W. Cahn and M. B. Bever Encyclopedia of Materials Science and Engineering, Suppl. Vol. 2,1328-1332
[19] Reichel, D. G. and Yelon, W. B. (1988), Surface and Coatings Technol. 36, 617 - 629
[20] Rickerby,D.G., Gibson, P.N., Gissler, W. and Haupt, J. (1992) Thin Solid Films, 209, 155
[21] Bourret, A., Desseaux, J. and Renault,A. (1982) Phil. Mag. A 45, 1
[22] Rühle, M. and Wilkens, M. (1972) Proc. 5th Eur. Conf. Electron Microscopy, Manchester, The Inst. of Physics (eds.), London, p. 416
[23] Jacobson, B.E., Bunshah, R.F. and Nimmagada, R. (1979) Thin Solid Films, 63, 357 Jacobson, B. E. (1982) "Microstructures of PVD-Deposited Films Characterized by Transmission Electron Microscopy", in Bunshaw, R. F. (ed.), Deposition Technologies for Films and Coatings, Noyes Publications, New Jersey
[24] Magee, T.J., Woolhouse, G.M., Kawayoshi, H.A., Niemeyer, I.C., Rodrigues, B., Ormond, R.D. and Bhandia, A.S. (1984) J. Vac. Sci. Technol. B2, 756
[25] Barna, A. (1992), Proc. Fall Meeting MRS, 1991, 2 - 6 Dec., Boston, Proceedings published as Volume 254 of MRS Symposium Proceedings Series, 287 - 307

www.manaraa.com

SURFACE ENGINEERING FOR HIGH TEMPERATURE CORROSION RESISTANCE

M.F. STROOSNIJDER[(1)], M.J. BENNETT[(2)] and R. MEVREL[(3)]

(1) *Commission of the European Communities - Joint Research Centre, Institute for Advanced Materials - Ispra Site, 21020 Ispra (VA), Italy*
(2) *AEA Technology, Surface Science and Technology Department, Harwell laboratory, Didcot, Oxfordshire OX11 ORA, UK*
(3) *ONERA, Materials Science Department, B.P. 72, 92322 Chatillon, France*

ABSTRACT. This review considers surface engineering techniques for high temperature corrosion resistance. A brief description of high temperature corrosion is given and criteria for surface engineering are outlined. The most important classes of surface treatments for high temperature corrosive applications are discussed, notably surface alloying, diffusion coatings and metallic and ceramic overlay coatings. Also, the important role of surface modification techniques, in particular ion implantation, as a research tool for corrosion science is highlighted.

1. Introduction

Processes involving high temperatures (i.e. typically between 600 and 1200°C) form an important part of modern industrial activity. Fundamental thermodynamics predict that an increase in temperature leads to a higher overall efficiency, e.g. in the conversion of thermal to mechanical energy and subsequently to other forms of power. For example, if the inlet temperature of a gas turbine is increased from 900°C to 1250°C (for the same energy consumption) the resultant power output increases by about 30%. Other industrial processes, which become more efficient as the temperature is increased, are those in which the limiting factors involve microstructural or molecular kinetic processes; in such cases higher efficiency corresponds to a shorter reaction time and therefore higher productivity for the installed equipment. Applications of high temperature processes are widely spread and include propulsion units (turbine and rocket), energy production (including nuclear energy), coal conversion, automotive and chemical industry, waste incineration and metals processing (Fig. 1). The achievement of enhanced process efficiency and economics is dependant crucially upon the development and application of improved structural materials.

Several aspects influence the selection of a metallic or ceramic material for high temperature applications, including corrosion resistance, mechanical properties, resistance to erosion, materials conservation and cost effectiveness. Increasingly greater demands imposed on materials make it more difficult or, at the current

W. Gissler and H. A. Jehn (eds.), Advanced Techniques for Surface Engineering, 335–358.
© 1992 *ECSC, EEC, EAEC, Brussels and Luxembourg.*

www.manaraa.com

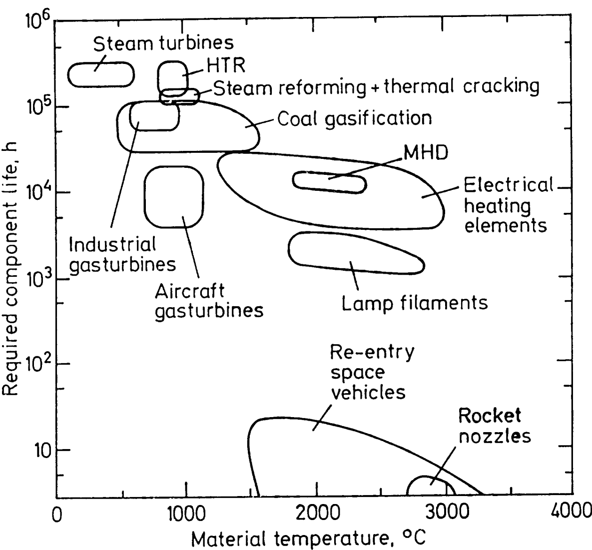

Fig. 1. Required component life and material temperature of various high temperature processes. HTR: high temperature gas cooled reactor; MHD: magneto- hydrodynamic energy conversion.

stage of development, even impossible to combine the different properties required in one single material. Therefore, a composite system of a base material, for example providing the necessary mechanical strength, with a corrosion protective surface layer, different in structure and/or chemical composition, supplied by a surface treatment can be an optimum choice in combining materials properties. In the following text the term surface treatments will be used to indicate both surface modifications and coatings.

Although protective surface treatments are widely applied at low temperatures, the use of these at elevated temperatures is more recent. Current high temperature applications are limited largely to the aerospace industry. An enormous challenge exists now to develop and apply these techniques to other high temperature applications, such as in process industries and diesel engines.

The purpose of this paper is to review the surface treatments available for high temperature applications, with emphasis on applications in corrosive conditions. This will concentrate on metallic materials, excluding refractory metals. However, it should be noted that the number of studies dealing with surface treatments for non-oxide ceramic materials is rapidly increasing. For example, in the case of ceramic composite materials, coatings are essential for their satisfactory operation [1-3]. By its very breadth of scope and wealth of detail it is difficult to review the subject in a comprehensive manner. The objective of this paper, therefore, will be to provide a balanced overview with firstly, a brief outline of the main parameters determining high temperature corrosion. This is followed by a discussion of the requirements for and the main classes of surface treatments for high temperature applications. A division is made between surface alloying and diffusion coatings and overlay coatings.

www.manaraa.com

2. High Temperature Corrosion

Alloys, which are used for structural components at high temperature are generally austenitic and ferritic stainless steels and superalloys based on iron, nickel or cobalt. They serve in a wide variety of environments depending on the type of process and process parameters. Oxygen, sulphur, carbon and nitrogen are the aggressive reactive species most frequently encountered, however, halogens, sodium and vanadium may also play an important role. The elements or their compounds may be present in either a gaseous or liquid form or in deposits. Various types of corrosion can be anticipated within different industrial processes, which will be surveyed. More detailed analysis is outside the scope of this paper and the interested reader is referred to the various textbooks on this subject [4,5].

Since in most of the high temperature environments oxygen is present, oxidation is the most important form of high temperature corrosion. Most materials are subject to oxidation if exposed, at a high temperature, to air or to oxygen rich environments. Oxidation resistance depends mainly on the potential of the alloys to form and maintain a protective oxide scale of Cr_2O_3 , Al_2O_3 or SiO_2 with low rates of growth. The role of this scale is to isolate the bare alloy from the environment and thereby to limit the corrosive attack. Oxides of other high temperature alloy constituents, like Fe, Ni and Co, or mixed oxides are generally less protective. Silicon has the drawback that at concentrations necessary for selective oxidation it can form low melting point and/or brittle phases with the other alloy constituents. For this reason protection by silica formation is used primarily via coatings. Up to about 950°C alloys relying upon a Cr_2O_3 oxide scale can be utilised, whereas, at higher temperatures, where Cr_2O_3 tends to convert to volatile CrO_3 , alloys or coatings capable of forming the more stable Al_2O_3 are preferred.

In a large number of applications other reactive species, in addition to oxygen, are present and attack by other gaseous species must be taken into account. These species are mostly incapable of forming protective scales and may even form low melting or volatile compounds with the alloy. Sulphur is the most common contaminant, usually introduced from fuels, such as coal and oil. Sulphidation can reduce significantly the service life of metallic components and it is a matter of considerable concern, not only in processing plants in the petrochemical industries, but also in various energy conversion processes. The fact that oxide layers generally form a barrier against other reactive gaseous species means that the resistance of alloys to mixed gaseous attack depends on their ability, also under these conditions, to form a protective oxide scale either of Cr_2O_3 or Al_2O_3. This will be more difficult in environments of low oxygen and high sulphur activities, like for example encountered in coal gasification processes. Under these conditions, corrosion kinetics will determine whether a protective oxide scale will be established rapidly to protect the alloy from degradation by sulphur [6].

The corrosive action of a salt deposit and a gas may be greater than that of a gas alone. This form of attack is called "hot corrosion", an example of which occurs in gas turbines. Sulphur from the fuel and NaCl from the ingested air may react at high temperature to form salt vapours, such as Na_2SO_4. At lower temperatures these vapours condense on component surfaces. Corrosion proceeds essentially in two stages. In the incubation period a protective oxide scale is formed, whereas in the propagation stage protection is lost due to its mechanical rupture or to its dissolution by the molten salt ("fluxing"). Hot corrosion appears only at intermediate temperatures determined by the melting point and the dew point of the salt. In general two different types of hot corrosion are distinguished, one appearing at higher temperatures (Type I: 800-950 °C) and one at lower temperatures (Type II: 600-750 °C). The

www.manaraa.com

degradation modes depend on various factors including temperature range, nature of contaminants, gas composition and alloy composition [7]. Alumina forming materials with a low Cr-content are very prone to these types of attack. Si additions improve the corrosion protection, but have the drawbacks mentioned previously. For these reasons most alumina forming materials rely on the addition of Cr for resistance against hot corrosion.

Even if a protective scale has formed, superimposed erosive, thermal and/or mechanical loading, as generally encountered under operating conditions, may undermine the scale stability causing it to crack and spall, thereby leading to accelerated corrosive attack of the underlying alloy. Successively less protective oxides, e.g. those of Fe and Ni, will form a larger part of the oxide scale and in the presence of other reactive species different corrosion products than oxides might be formed. In the case of corrosion protection arising from an artificially applied layer, spallation of this layer might be disastrous. Additionally the spalled fragments may cause severe erosion or blocking of gas flows. Cracking and spallation of protective oxide scales under practical conditions, therefore, is a subject of increasing concern. In this context during the last decade the beneficial role of reactive elements, such as yttrium, cerium and other rare earths, has received considerable attention [8-10]. These elements added in small amounts (less than 0.1%) to the bulk alloy or to the surface dramatically improve the resistance of scales against spallation. The exact underlying mechanism of the reactive element effect is still subject of discussion.

3. Requirements for Surface Treatments for High Temperature Applications.

The purpose of a surface treatment is to provide enhanced protection over that afforded by the oxide scale formed naturally in the particular corrosive environment. Several factors influence the selection of a surface treatment, both in terms of composition of the layer and technique of application. These are related to the system of application, substrate material, surface material (including processing) and costs (Fig. 2).

Concerning the application, the main question is whether the surface treatment can supply an adequate improvement in lifetime taking into account the service conditions of corrosion, erosion, mechanical strains, temperature and thermal changes. Also with regard to component geometry requirement it might be necessary that the surface treatment is applicable to complex shaped objects and into small holes (aerofoil cooling technology). In several applications any change of shape or dimensions due to the treatment can be critical. It should be noted that the operating conditions of what seems to be a similar application, might differ largely. In the 1970s Al-rich coatings, which were used successfully for aircraft turbine applications, were found to fail when they were first used for the protection of industrial gas turbines. Later it was recognized that the general corrosion degradation mechanisms were different in these applications. For example gas turbines for marine propulsion are susceptible to both Type I and II hot corrosion, whereas in general those for aircrafts, operating at higher temperatures (Fig. 1) and using cleaner fuels, are more subject to oxidation. However, Type I hot corrosion is becoming an important degradation mechanism also for aircraft gas turbines operating under coastal or marine conditions. The requirements upon gas turbine materials for military and commercial aircrafts also differ. A military aircraft gas turbine for example needs to provide rapid acceleration, thus leading to severe temperature cycles with subsequent risks

www.manaraa.com

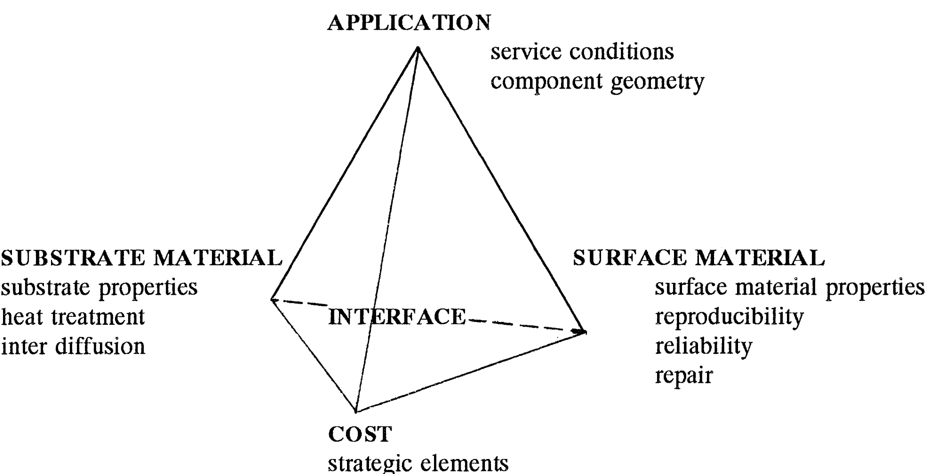

Fig. 2. Requirement pyramid of surface treatments.

for cracking and spalling of protective surface layers. However, for military applications more frequent inspection and shorter time between overhauls is acceptable, sometimes being as short as 100 hours compared to several thousand hours for commercial aircraft. This clearly illustrates the requirement to treat every application of a surface treatment individually.

Choice of the surface material is governed both by the properties of the material, as well as by the mode of application of the surface treatment. A necessary prerequisite is that the surface layer has sufficient metallurgical stability throughout the required service life. Very often the coating and base alloy will have widely different compositions. The activity gradients of the various elements across the coating/base alloy interface could cause diffusion, which can be rapid at elevated temperatures. Additionally, reaction between elements from the surface layer and base alloy may form detrimental phases. Elements from the base alloy might also diffuse to the coating/gas interface and impede the formation of a protective oxide scale. On the other side diffusion of elements from the surface layer into the alloy, occurring during application of the coating or in service, might seriously affect, for example, the mechanical properties of the base material. It should be kept in mind that during service at high temperature, the composition and structure of a surface layer could change continuously and therefore their properties are susceptible to modification accordingly. A point related to this is the self healing capability, under the operating conditions, in the event of local failure. Another important fact to consider is whether the surface treatment will reduce the thermal conductivity of the system significantly. This can be detrimental in the case of heat exchanger applications, whereas on the other hand this can be advantageous and is the major reason for the application of thermal barrier coatings. Concerning the technique side, the main requirements are whether the surface material can be produced in a reproducible and reliable way and whether the technique is applicable in the field. This raises an important point of the possibility of repair. Depending on the application in situ coating repair might be of great advantage, although this imposes considerable extra problems in the choice of surface treatments.

Turning to the substrate, the influence of the treatment on its properties by e.g. heat treatment or interdiffusion, has to be considered. Taking into account the complex and

المنارة للاستشارات
www.manaraa.com

carefully controlled heat treatment cycles required to optimize mechanical properties of several advanced high temperature alloys it can be recognized that the temperature cycles of the surface treatment must be carefully tailored in the overall fabrication procedure. This especially applies to CVD-techniques, which are mostly characterised by high process temperatures (up to 1150°C). Post-coating corrective heat treatments are sometimes required to optimize the composite properties.

From the above discussion it becomes clear that the role of the interface between the substrate and the coating is critical in providing good adhesion, a low chemical interdiffusion rate and good adaption of properties. In some instances an additional layer between the coating and substrate material might be necessary to achieve optimum performance.

Finally, the cost factor must be taken into account. The costs involved need to be compared with those for other possible solutions, like the use of another (more expensive) material or replacing the component more frequently. Also, the use of any strategic element in the protective surface treatment must be considered.

4. Surface Treatments

Most surface layers for high temperature corrosion protection rely again on the formation, by interaction with the environment, of an oxide scale. The role of this scale is to isolate the base material from the environment and thereby to limit the corrosive attack. A major requirement is its ability to reform in case of spallation. However, inert corrosion resistant ceramic barrier coatings can also be supplied to the surface, mainly oxides like silica. It should be emphasized, however, that their use implies that coating failure due to cracking or spallation is not detrimental to the foreseen component life, since the protection cannot be restored in these systems.

Several schemes have been proposed for the classification of the surface treatments. None of these are entirely satisfactory since several processes have characteristics that would fall into different categories and several procedures, e.g. laser surface alloying, are a combination of different techniques. In general surface treatments can be divided into four categories:

- diffusion coatings and surface alloying,
- overlay coatings,
- mechanical working,
- thermal surface treatments.

A detailed description of all these techniques and their potential applications falls outside the scope of this paper. Discussion will be limited specifically to those techniques which are in use or are showing promise in high temperature corrosive applications. As a consequence it will concentrate on surface alloying and diffusion coatings and on metallic and ceramic overlay coatings.

4.1. SURFACE ALLOYING AND DIFFUSION COATINGS

The surface layers considered under surface alloying and diffusion coatings are formed by the interaction of the substrate with elements applied to its surface. The formation of the surface layer involves intermixing phenomena and its final composition is strongly dependant on the

www.manaraa.com

substrate composition. The main surface alloying techniques used are ion implantation and laser surface treatments involving surface alloying, remelting and cladding. Although up to now these techniques have only found limited high temperature application, they are showing potential for use in the future. In contrast, diffusion coatings are widely used to provide high temperature corrosion protection. Three global classes will be discussed: simple metallic, modified metallic and oxide diffusion coatings.

4.1.1. *Ion Implantation* In ion implantation high energy ions are generated in an ion accelerator and implanted into the alloy surface. Penetration depths are typically of the order of 0.01-1 μm, while the concentration distribution has a maximum with values up to several tens of percent. Ion implantation offers several advantages, such as: thin layers are produced, a wide range of elements can be implanted, low process temperatures and a good reproducibility of the process. The absence of a definite interface solves the problem of adhesion. The radiation damage, which is also generated during implantation and which might have an important additional effect at low temperatures is rapidly annealed at moderate to high temperatures. The major drawbacks of ion implantation are the necessity of working under vacuum and the need for ion sources capable of supplying high ion doses, which make the process expensive. Because of this, there is no real industrial application yet and possible applications can only be expected for small components in which quality and durability is essential and as a means of conservation of extremely expensive and rare alloying elements. However, far more important for corrosion science is the role of ion implantation as a research tool.

Ion implantation has been used extensivly and successfully for studying the mechanisms underlying the crucial and dominating role of specific elements upon the corrosion behaviour of metals and alloys. Paramount among these is the understanding of the so-called reactive element effect. In general it is found that the influence of these elements are similar whether the reactive element is implanted, applied as a coating or present as an alloy or oxide dispersoid addition. The effects are on the initial nucleation, growth and adherence of the corrosion scale. As an example. the reduction in the attack (expressed as weight gain per unit area) of a chromia forming austenitic stainless steel in an oxidizing

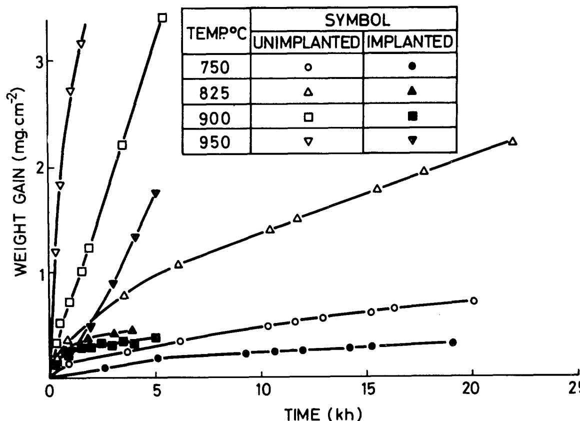

Fig. 3. Effect of implantation of 10^{17} Ce ions/cm^2 on the extent of the oxidation of 20Cr-25Ni-Nb stainless steel in CO_2 at 750-950°C [11].

www.manaraa.com

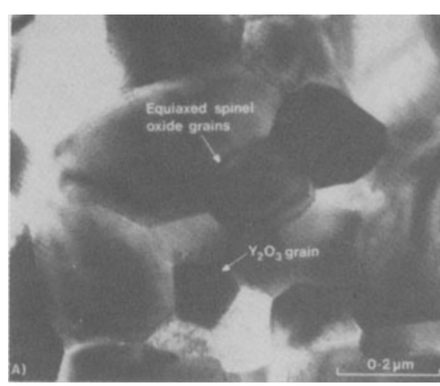

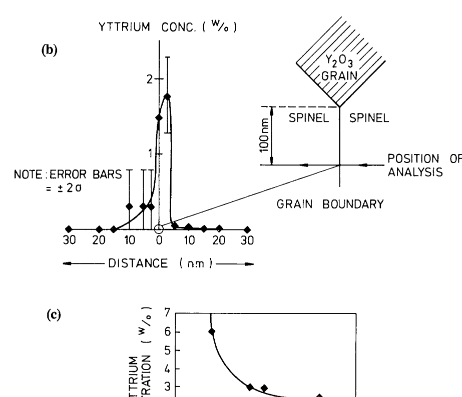

Fig. 4. (a) Microstructure of the spinel oxide layer formed on yttrium implanted 20Cr-25Ni-Nb steel after 775 h oxidation in CO_2 at 825°C . (b) Energy dispersive analysis using a field emission scanning transmission electron microscope of the yttrium concentration profile across a spinel-spinel grain boundary at 100 nm from a Y_2O_3 grain. (c) Variation of the yttrium concentration along a spinel-spinel grain boundary with distance from a Y_2O_3 grain [11].

environment by the implantation of cerium is shown in Fig. 3. Despite the shallow implantation depth (less than about 0.1 μm), the benefits of ion implantation were maintained during extended exposures. The main leap forward in understanding undoubtedly has been to demonstrate how reactive elements, by segregating along oxide grain boundaries (Fig. 4), inhibit the growth of scales by cation diffusion. It could well be significant that the breakthrough in scale growth understanding followed the emergence of advanced surface analytical techniques, which enabled the precise location of the reactive elements within the scale to be established.

For practical applications of far more importance are the effects of reactive elements upon scale adherence. In general above a threshold scale thickness spallation will occur. For example, in an extensive study [11], both yttrium and cerium ion implantations were shown to reduce the extent of chromia scale spallation from a 20Cr-25Ni-Nb stabilized stainless steel by a combination of inhibiting the scale growth rate and increasing the threshold scale thickness for spall initiation. Fig. 5 compares the time to initiate spallation during isothermal exposure as a function of temperature for the unimplanted material and for the cerium and yttrium implanted steel. This demonstrates that a dramatic four orders of magnitude improvement is afforded by cerium and yttrium ion implantation. Although the ion implantation studies have thrown into question several proposed theories for the improvement in spallation resistance, there has been only limited positive progress in understanding.

It should be noted that most ion implantation studies have concerned oxidation. There is a considerable scope also for using the technique to address mechanistic questions concerned with more complex corrosion conditions, for example mixed oxidizing/sulphidizing conditions, which to date, with a few notable exceptions [12,13], have received little attention.

المنارة للاستشارات
www.manaraa.com

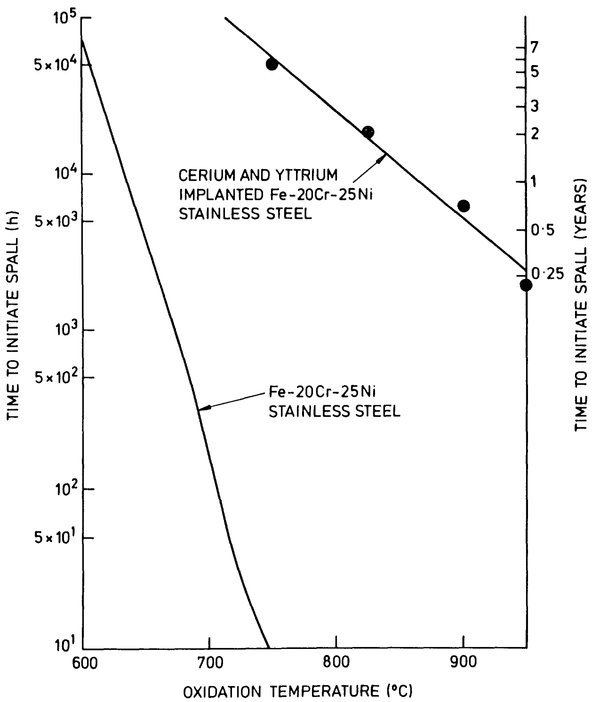

Fig. 5. Increase by Ce and Y ion implantation of the time for initiation of spallation upon cooling to room temperature of the scale formed on the 20Cr-25Ni-Nb steel [11].

4.1.2. *Laser Surface Treatments* Although this discussion will be concentrated on laser processes, it should be mentioned that electron beams can be used similarly. However, lasers offer the considerable advantage over electron beams that vacuum systems are not required. On the other hand the process of electron beam interaction is better understood theoretically. Electron beams can also be screened electronically, thus avoiding the necessity of workpiece movement. In both these processes, the surface is bombarded with energetic particles. Part of the energy is converted into heat which can melt the surface. The underlying substrate material removes the heat rapidly (up to 10^{10} K/s). Interaction depths can be varied up to several mm. This allows the application of rapidly quenched materials in forms other than thin ribbons or sheets. Among the possible effects of electron beam and laser surface melting are increased solid solubility, formation of non-equilibrium microstructures, epitaxial growth and homogeneous fine grained microstructures. These beams can also be applied as a post-coating treatment to decrease coating porosity and increase adherence. A major problem is the development of surface stresses, which can also alter the bulk mechanical properties to a significant extent and might be detrimental. Other problems are related to surface crack formation induced by these stresses and the fact that treatment of irregular surfaces might be difficult. High temperature applications for these techniques are still limited, however, research is increasing rapidly. Although the range of laser processes is extensive, for the high temperature corrosion protection of metallic materials, three approaches are possible: surface remelting, laser surface alloying and laser surface cladding.

www.manaraa.com

By laser remelting essentially only the micro structure of a surface layer is modified, although additionally the distribution of elements in the melted zone might change. Due to a new surface structure the nucleation and growth of corrosion products are affected, in some instances leading to improved oxide adherence [14]. Laser remelting has been applied successfully also to plasma sprayed coated surfaces to reduce coating porosity, long range chemical inhomogeneities and coating/substrate adherence.

During laser surface alloying specific elements are added, for example in the form of a powder, to the melt pool, leading to changes in both microstructure and chemical composition. Laser alloying of high temperature alloys with powders containing reactive elements has been studied [15]. The rapid cooling rates during the laser treatment allow an extended solid solution of these elements in the surface, which is essentially controlled by the depth of the laser penetration. Another interesting research area is the production of thick, amorphous, oxide coatings. Amorphous ceramic coatings, because of the absence of grain boundaries, provide a better diffusion barrier than the naturally formed oxide scales. The effectiveness of this approach is well known for thin (<20 μm) amorphous silica coatings, applied by vapour deposition techniques [16]. Coatings, which were essentially amorphous and significantly thicker, can be deposited on metallic substrates by laser melting crystalline silica or alumina powders applied directly onto the surface. These coatings, by acting as a diffusion barrier, provided outstanding corrosion protection to the base alloy in both oxidizing and sulphidizing environments [17].

Laser cladding, in which a preplaced layer is fused onto the substrate, has been used successfully in a number of systems, especially as a possible way to fuse MCrAlY type coatings, in which M can be Ni, Fe or Co, on another substrate material. A complete and sound interface can be established with this technique.

4.1.3. *Simple Metallic Diffusion Coatings* Diffusion coatings are among the most widely applied surface treatments [18]. They are used mostly to increase the surface content of aluminium ("aluminizing"). A few processes apply chromium or silicon, i.e. "chromizing" and "siliconizing" respectively, however, they are employed primarily for moderate temperature applications. Aluminizing processes are used to form a layer of aluminides (for example β-NiAl and β-CoAl respectively on Ni- and Co-based high temperature alloys) . In the case of chromizing, since Cr has a large solubility in Fe, Ni and Co based alloys, in general only an enrichment, up to about 30%, is sought.

The coating elements are usually supplied by pack cementation, a conventional reactive CVD process. The components are immersed in a powder mixture in a retort placed inside a furnace and heated at high temperatures (700-1150°C) under an inert or reducing atmosphere to prevent oxidation. The pack normally contains the coating element source, an activator and an inert filler. In the aluminizing process, the source can be either the pure element or an aluminium alloy, depending on the aluminium activity required in the pack. The activator, usually an halide salt, e.g. NH_4Cl or NaF, dissociates at the process temperature, reacts with the coating element to form metal halides, which are transported to and subsequently disproportionate on the surface of the components. The inert filler, usually alumina, prevents the pack from sintering at high temperatures.

A variation of this process uses a pulse pressure step which is based on cycled variations of the vapour phase pressure. In a gas phase (PWA 275 and SNECMA APVS) process, the parts to be protected are isolated from the pack. With such a configuration, the components can be cooled rapidly at the end of the coating cycle and in this way the time-temperature programme can coincide with the heat treatment of the substrate material.

www.manaraa.com

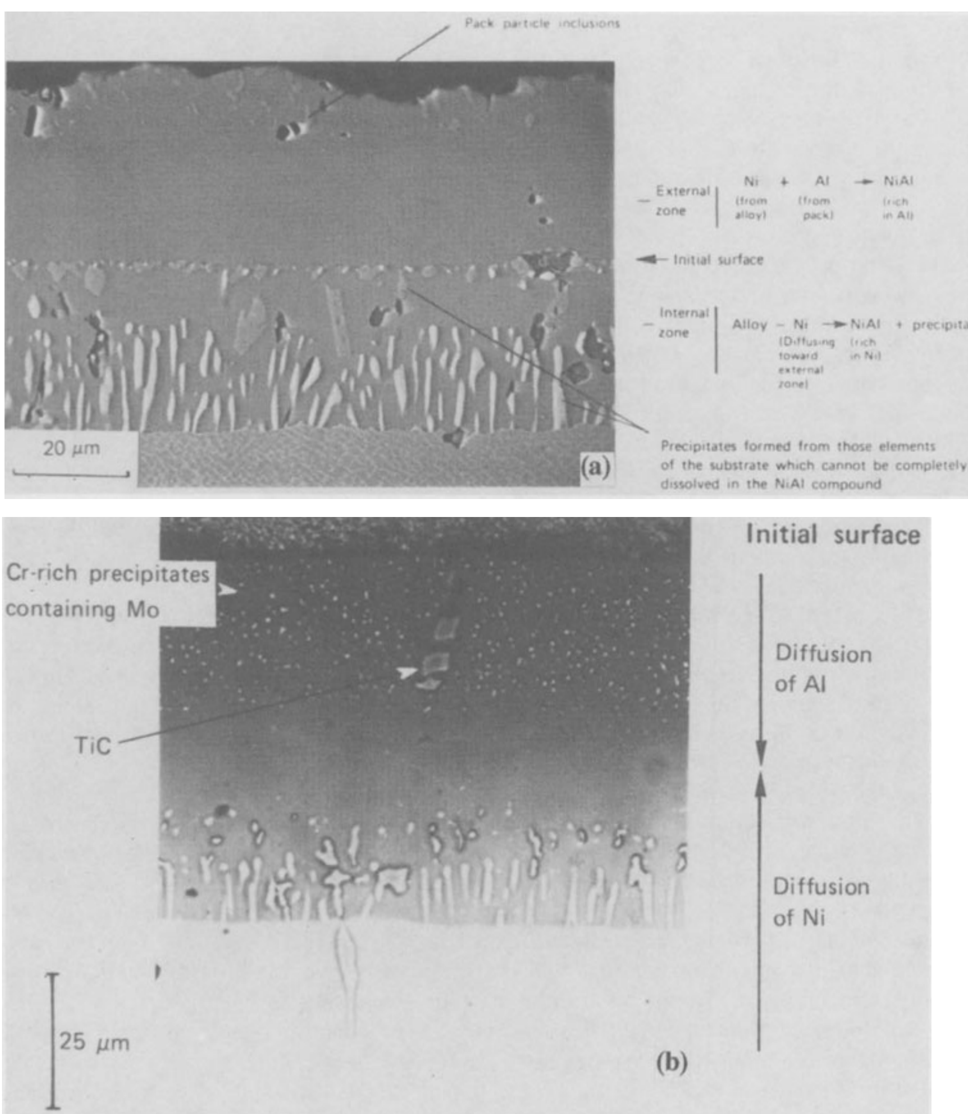

Fig. 6. Comparison of the structures of aluminide coatings on nickel base superalloys: (a) low activity; (b) high activity process [18].

Moreover, the troublesome handling of fine powders can be avoided. Both types of process can be envisaged for protecting internal cooling passages inside airfoils.

Depending upon the Al activity of the pack, low activity and high activity aluminizing can be distinguished. In the low activity process (Fig. 6a), for a Ni-based alloy, outward diffusion of Ni leads to an outer NiAl layer and an inner zone with transformation products, due to interaction of substrate and NiAl layer. In the low activity process particles from the

المنارة للاستشارات

www.manaraa.com

pack can often be entrapped in the outer layer. In the high activity process, Ni_2Al_3 is formed by inward Al diffusion. A post heat treatment is necessary to convert this brittle layer to NiAl. The morphology of high activity coatings is characterised by a three layered structure (Fig 6b). The two inner ones are similar to those for the low activity coatings. Additionally an outer zone contains several of the elements from the substrate alloy, either in solution or in the form of second phase particles, such as carbides. Breakdown of these aluminide coatings generally results from a partial transformation of the outer NiAl layer in γ'-Ni_3Al, which has inferior corrosion resistance.

With pack cementation techniques both a large number of components and large sized components can be treated, the actual limit is the size of the furnace. The capital investment cost for the coating equipment is relatively low and the unit cost is one of the lowest among coating techniques. Coating adherence to the substrate in general is very good. Additionally the entire surface of a complex shaped component can be coated uniformly. These advantages explain the wide use of these coating processes for protecting high temperature alloys, but due to its mode of formation its suffers from several limitations.

The achievable coating thicknesses are constrained by the process duration used industrially. The thickness of diffusion coatings increases roughly as the square root of the process time. In practice this means that a thickness only in the order of 50-100 μm is attainable for durations less than 20 hours. In contrast much thicker coatings can be applied by overlay techniques. Another disadvantage of these diffusion coatings is that the component must be heated to fairly high temperatures (700-1150°C). These high process temperatures do not allow all alloys to be coated by these techniques, due to alterations in microstructure of the substrate alloy and degradation of the mechanical properties. This is a particular drawback for the low activity aluminizing process, which is conducted at the higher temperatures. The formation of a diffusion coating affects a substantial subsurface zone of the substrate material. This zone can have reduced mechanical properties and its presence must be taken into account, especially when designing thin-walled components.

The most severe limitation with simple diffusion coatings is the lack of flexibility in controlling the composition of the coatings formed. Generally only a single element is transferred to the surface during the process. Moreover, the composition, and thus the properties, of the coating strongly depends on the substrate composition. The corrosion protection afforded by the coating is influenced strongly by the composition of the substrate, not in the least by minor elements. This is particularly true for inward growing diffusion coatings, as for instance in the case of high activity aluminizing.

4.1.4. *Modified Metallic Diffusion Coatings* To counteract the limitations mentioned above, advanced aluminide coatings have been developed. The idea is to incorporate a "modifier" element in the coating in order to improve its oxidation or hot corrosion resistance. The incorporation is carried out by either a pretreatment or a codeposition. Three modifier elements are commonly introduced in aluminide coatings namely chromium, platinum and palladium and all of them are known to improve hot corrosion resistance.

In the case of chromium-modified aluminide coatings the goal is to establish a surface Cr-content of about 20%. Three routes have been developed to enrich aluminide coatings in chromium. The first one consists in successively chromizing and aluminizing the components. Industrially available Cr-modified aluminide coatings include, for instance, C1A and PWA32. It has been shown also that the external zone of low activity aluminide coatings can be enriched in chromium through the incorporation of Cr-Al particles during a pack process [19]. Finally, several studies have demonstrated that codepositing Cr and Al in a single step

www.manaraa.com

cementation treatment, with conditions determined through thermodynamic calculations, is feasible [20,21].

One of the most significant improvements of high-temperature protective diffusion coatings has been the incorporation of noble metals in aluminide coatings, which significantly enhances their resistance against Type I hot corrosion. The main reason seems to be the increased stability of the β-NiAl phase. The first commercial system, designated LDC-2 [22], was produced by initially electroplating a thin platinum layer (<10 μm thick) onto a substrate and then aluminizing it for several hours at 1050°C. The final coating, with a thickness of about 80 μm, presents a continuous nickel-containing $PtAl_2$ outer layer on top of a NiAl zone. A slightly different process (RT22) results in a somewhat less brittle duplex structure comprised of a mixture of Ni(Al,Pt) and $PtAl_2$ phases.

Early attempts to replace platinum in the coatings by palladium, in the hope of reducing production costs, did not meet with overwhelming success due to the excessive brittleness of these coatings. A critical analysis of coating formation [23] resulted in a processing route avoiding hydrogen incorporation. In one process, palladium is first electrodeposited as a Ni-Pd alloy layer and is followed by an aluminizing process. In hot corrosion laboratory tests, the performance of these palladium-modified aluminide coatings compare well with those of MCrAlY and Pt-modified coatings (Fig. 7). The resulting coatings exhibit hot corrosion and high temperature oxidation resistance, determined in burner rig tests, equivalent to commercial platinum-modified coatings [25].

These examples demonstrate the possibility of incorporating a second element in coatings obtained by pack cementation. It must be reckoned though that the range of accessible compositions remain limited, and in spite of extensive effort, the incorporation of reactive elements is still the object of laboratory studies. The main problem is related to the low solubility of these elements in high temperature alloys.

4.1.5. *Ceramic Diffusion Coatings* Two types of processes have been developed to produce corrosion resistant ceramic layers on alloys. The first group are techniques that

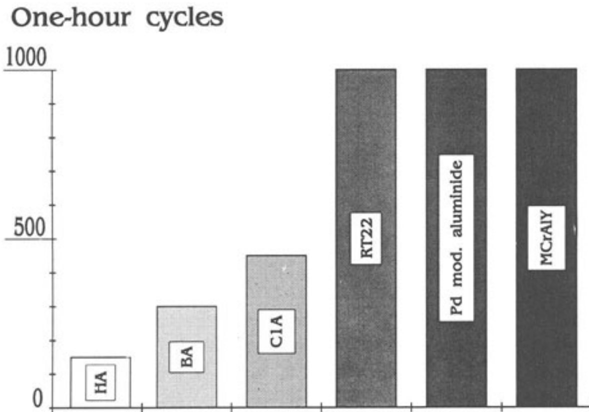

Fig. 7. Hot corrosion resistance of various protective coatings on IN-100 (Ni-15Co-10Cr-5Al-5Ti). Number of cycles till propagation stage of hot corrosion at 850°C, one-hour cycles, 0.5 mg/cm^2 Na_2SO_4 every 50 cycles. HA: high activity simple aluminide; BA: low activity simple aluminide; C1A: Cr modified aluminide; RT 22: Pt modified aluminide; MCrAlY: overlay coating [24].

المنارة للاستشارات
www.manaraa.com

modify the oxide scales which grows naturally on substrate alloys or metallic coatings. The increase in corrosion resistance can result from a diffusion barrier effect or from an improvement in the oxide scale adherence. The second group comprises the techniques which cover the alloy with an inert, thermodynamically stable, ceramic coating. Thermal barrier coatings fall in the second class and will be considered under overlay coatings. Some of these processes have characteristics that overlap into the two categories of diffusion and overlay coatings.

Concerning the modification of the natural oxide, two ways are open. The first is the relatively easy and inexpensive approach of pre-oxidation under well controlled environmental conditions. The second approach is to chemically modify the surface of the alloy, possibly followed by a pre-oxidation treatment, before exposure to the corrosive environment. Among the process parameters for the pre-oxidation treatment the most important one is environment. Generally a pure oxidizing gas with a low oxygen activity is preferred in order to promote selective formation of the most stable oxides, however, air is practically more relevant. Additionally the maximum temperature of pre-oxidation can be higher than that of application in order to rapidly form an oxide scale with a reasonable thickness. The rates of heating and cooling during the whole cycle is another point of control, especially related to stressing and related cracking and spalling of the oxide scale. Pre-oxidation has been shown to give some level of protection in oxidizing, carburizing and sulphidizing environments, however, in general this is maintained only for a relatively short times of several thousand hours or less [26], i.e. less than that required for industrial service.

The approach by which the surface composition is changed most significantly utilizes the reactive element effect. This might be achieved, for example, through ion implantation or sol/gel coating techniques [16]. Subsequently, the treated material can be either pre-oxidized or directly exposed to the aggressive environment. Especially due to improvement in the spallation resistance of the oxide layer, the corrosion resistance in oxidizing, carburizing and sulphidizing conditions can be increased markedly and be effective also for longer times [see e.g. 11,12,16,26,27].

Using various vapour deposition techniques, including plasma assisted CVD (PACVD) [16,28,29], metal organic CVD (MOCVD) [30,31] and laser CVD (LCVD) [32], thin (< 20 μm) amorphous silica and alumina coatings have been produced on various alloys. Due to the amorphous nature of these oxides the fast transport of reactive species along grain boundaries is absent and these layers are thus more protective than naturally formed oxides scales. These coatings led to remarkable protection under oxidizing, carburizing and sulphidizing conditions. Protection against oxidation in CO_2 at 825°C has been maintained throughout test durations in excess of 40.000 h [16]. A critical factor for the protectiveness of these coatings is the interlayer between substrate and the coating, formed by a prior pre-oxidation or CVD treatment [29]. Without such an interlayer no adherent uniform coating can be deposited and coating integrity cannot be expected to be maintained during erosive, thermal and/or mechanical loading. The performance of these coatings can be undermined, by an extent increasing with both temperature and time, by two mechanisms (Fig. 8). Crystallisation introduces grain boundaries, providing fast diffusion paths through the oxide coating. Additionally, alloy constituents, by forming more thermodynamically stable oxides, such as titanium and aluminium, can degrade the silica layer by reaction at the coating/substrate interface.

المنارة للاستشارات
www.manaraa.com

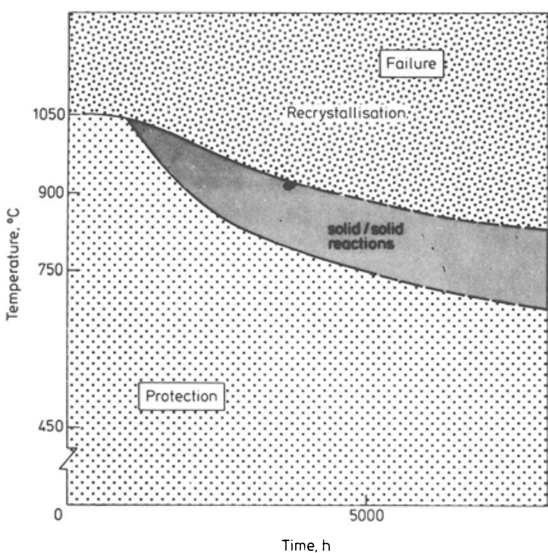

Fig. 8. Schematic time temperature interaction diagram for oxidation protection provided by amorphous silica coatings produced by PACVD [29].

4.2. OVERLAY COATINGS

Although they present definite advantages, the range of compositions and structures attainable with diffusion coatings remains narrow. In order to overcome these limitations overlay coatings have been introduced. Their development has been linked directly to that of the deposition techniques, such as electron beam PVD (EBPVD) and plasma spraying. This class also includes thermal barrier coatings, whose primary task is not resistance against corrosion but whose development takes this into account, since they are employed in aggressive conditions.

4.2.1. *Metallic Overlay Coatings* Although metallic overlay coatings can be deposited by several techniques, plasma spraying and physical vapour deposition are the most important, while coextrusion is also used. The first technique employed, was EBPVD. Increasingly plasma spraying of powders at atmospheric pressure and more recently under argon or at low pressure (LPPS) have been used. The latter lead to better quality coatings due to reduced porosity and amount of entrained oxides. Processing often includes an additional heating step to reduce coating porosity and improve adhesion. The major advantages over diffusion coatings are increased thickness, generally about 100 μm, and flexibility in the composition of the coating. This is nearly independent of contamination from the substrate, but constrained by limitations of the deposition technique, especially by vapour pressure considerations. In general overlay coatings are more expensive than diffusion coatings. At high temperatures interdiffusion might become a matter of concern. The majority of the metallic overlay coatings belong to the MCrAlY family. A wide range of compositions is commercially available, as shown in Table 1.

المنارة للاستشارات
www.manaraa.com

Table 1. Examples of commercially available MCrAlY coatings (nominal composition, weight %).

Designation[a]	Ni	Co	Fe	Cr	Al	Y	Other
LCO 29		Bal.		18	8	0.5	
ATD 5		Bal.		18	11	0.3	
LCO 5		Bal.		19	10	0.5	
ATD 2		Bal.		23	12	0.3	
LCO 7		Bal.		23	13	0.6	
ATD 14		Bal.		30	5	0.5	
Amdry 961	Bal.			17	6	0.5	
Amdry 962	Bal.			22	10	1	
ATD 16	Bal.			25	12	0.3	
Amdry 963	Bal.			25	5	0.4	
ATD 1	Bal.			38	11	0.3	
ATD 7	Bal.	22		18	12	0.3	
ATD 9	Bal.	20		42	5	0.3	
LN 21	Bal.	22		21	7.5	0.5	
Amdry 997	Bal.	23		20	8.5	0.6	4 Ta
LN 34	Bal.	0.5		20	11	0.5	0.5 Mo
LCO 22	32	Bal.		21	7.5	0.5	
Amdry 995	32	Bal.		21	8	0.5	
LCO 37	23	Bal.		30	3	0.5	
Amdry 996	10	Bal.		25	7	0.6	5 Ta
Amdry 970			Bal.	24	8	0.4	
ATD 8			Bal.	24	11	0.6	

[a] ATD : coatings produced by EBPVD (Airco Temescal) ; LN and LCO : coatings produced by argon shield plasma spraying (Union Carbide); Amdry : powders available for low pressure plasma spraying (Alloy Metals).

The selection of an MCrAlY composition for a particular problem must be based on considerations of the structure and the properties of these alloys. MCrAlY alloys are generally multiphase materials. If the aluminium content is not too high, Ni- and Co-base alloys consist basically of a ductile γ-solid solution containing a dispersion of β-NiAl or β-CoAl phases. The actual microstructure can be more complex [33] and include γ'-Ni_3Al, sigma, M'_5Y and Y_2O_3 phases, in addition to γ and β in NiCoCrAlYTa alloys. Moreover it has to be borne in mind that the microstructure of MCrAlY alloys may depend on their thermal history (heat treatments and cooling rates). If the aluminium content is too high, the brittle β phase percolates and contains a dispersion of γ-Ni particles. Such a structure is certainly less favourable in terms of ductility. In a field of the Ni-Cr-Al ternary system, a phase transformation occurs at about 1000°C whereby γ + β, stable at high temperature, transform into γ'-Ni_3Al + α-Cr. This reaction is accompanied by a significant volume variation, which may be deleterious for the mechanical integrity of a coating/substrate system. It is recommended therefore that an alloy composition outside this field is selected whether by limiting the Al content, or by adding cobalt to destabilize γ' formation.

المنارة للاستشارات
www.manaraa.com

The corrosion behaviour of MCrAlY alloys depends on a variety of factors, including alloy composition, temperature, oxygen partial pressure, duration and thermal cycling. A typical oxidation sequence for an MCrAlY alloy starts with the formation of transient oxides (NiO, spinels,etc.), growing rapidly until a continuous stable oxide layer of either chromia or alumina has formed underneath. As the diffusion of oxygen and metallic species is slow in chromia and even slower in alumina, this layer provides oxidation resistance to the alloy. The presence of chromium in these alloys reduces the minimum level of Al required to form a protective alumina scale. The presence of as little as 5 - 10% Cr reduces the amount of Al necessary from 40 at.% to about 10 at.%.

To improve the corrosion resistance of Al_2O_3 forming alloys under hot corrosion conditions Cr has to be added. About 25 to 40% Cr is required for Type II hot corrosion protection, whereas 15 to 25%Cr is recommended for Type I resistance. It is to be noted though that too high a chromium content may have deleterious effects on the structural stability of the substrate alloy as a consequence of inward chromium diffusion.

Alumina scales formed on MCrAl are not adherent in thermal cycling conditions, presumably as a result of both growth and thermal stresses. In order to improve the adherence of the alumina scale, reactive elements are incorporated in these alloys in small amounts (less than 1%). A uniform distribution of these elements is essential and the simultaneous addition of several reactive elements, e.g. Y and Hf [34], can be beneficial.

Other additional elements may play a beneficial role: tantalum for example, although not particularly good for oxidation resistance, prevents the outward diffusion of elements such as titanium, which are particularly deleterious for oxidation resistance, by tying them up, with carbon, in stable MC carbides. All these considerations explain the wide use of standard NiCoCrAlY (+Ta)-base compositions with about 20% Co, 20% Cr, 8-12 % Al and <1% Y (wt.%).

Despite the flexibility they permit, the techniques commercially available to deposit MCrAlY coatings, namely EBPVD and plasma spraying under inert atmosphere, remain line-of-sight processes and this, in addition to their relatively high cost, can be a real drawback for coating components having complex shapes. Alternative processes have been developed, among which are electrolytic codeposition, electrophoresis and cladding, including coextrusion.

MCrAlY coatings have been obtained by co-electrodeposition of a dispersion of fine CrAlY powder particles within a Co or Ni matrix [35]. This operation can be carried out in a barrel plating unit. The barrel containing the specimens and the powder particles (10 μm diameter) is immersed into a Co and/or Ni bath and rotated. The coated components are subsequently heat treated for alloying and diffusion bonding the coating to the substrate. This process presents obvious economical advantages, especially low capital costs (claimed to be an order of magnitude less than existing commercial systems, unit production costs about half those of competing systems). Reliability performances of coatings produced by this route have not been published, while the technique has not yet been scaled up.

The electrophoresis process is based on the migration of fine powder particles suspended in a polar solution under a dc voltage. In the process developed at SNECMA [36], MCrAlY powders, with sizes less than 40 μm, are deposited by electrophoresis on the components to be coated with deposition rates up to 100 μm/min. In order to densify the deposit and adjust the composition, the components are then aluminized by a vapour phase process. With adequate electrode geometry, components with complex shapes can be uniformly coated. The facilities required are relatively simple, so capital investments, as well as running costs, are much less than for either the EBPVD or LPPS processes.

www.manaraa.com

In various energy conversion and chemical processes, the limited thickness of the coatings discussed so far are often not sufficient for long term utilization, preferably up to the full plant life of 30-40 years. Cladding is used in these cases to apply layers up to several millimetres thick. Weld deposit and plasma transfer arc processes are used, but they are general too slow. Coextrusion [37], is a process route which can be used to produce bimetallic tubes. With this process it is even possible to fabricate three layer tubes having (different) corrosion resistant layers on the outside and inside of the base material, which is supplying the mechanical strength. Several material combinations have been successfully produced, an example is Fecralloy 'A' steel (Fe-20Cr-5Al-0.3Y) on various substrate materials [38]. It was shown that corrosion resistance after 10.000 h exposure to air at temperatures up to 1000°C, was up to a factor of 10 better than that of the base material alone. Moreover, after 10.000 hours, even at the highest temperature, over 80% of the original overlayer thickness was still available to provide continuing protection to the substrate material. In the United Kingdom during the past 15 years over 150 km of coextruded tube has been installed in coal fired boilers [37]. It is important in these applications that welding of the coextruded tubing is possible without any major loss in properties.

4.2.2. *Thermal Barrier Coatings* The application of ceramic overlay coatings, also known as thermal barrier coatings (TBC), has gained major impetus during the last decade. Beside corrosion resistance, those coatings have a thermal conductivity an order of magnitude lower than that of normal alloys. As a consequence, by acting as a thermal barrier, these coatings provide a temperature gradient from the gas to the substrate alloy. The temperature difference across the coating can be as high as 150°C. This allows an increase of the inlet temperature and/or a decrease in cooling. The latter is very interesting, not only for aerospace applications but also for example in diesel engines for trucks and ships. In this application, not only efficiency will be improved, but also the cooling system might be eliminated, leading to a decrease in overall weight and a more simplified design. The cooling system of a diesel engine often contains more than 300 parts and is responsible for half of the engine failures. The main coating technique used for producing thermal barrier coatings is plasma spraying. Typical coating thicknesses range from about 300 μm in combustion chamber and gas turbine applications up to about 3 mm in diesel engines.

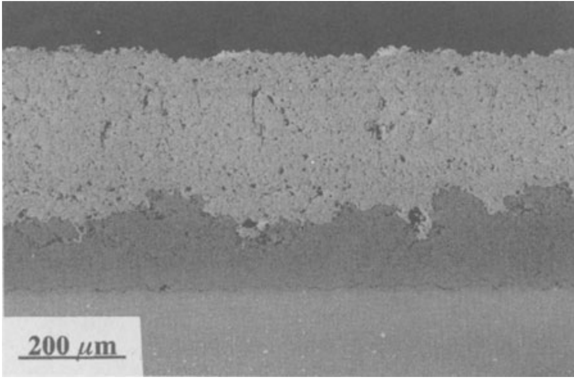

Fig. 9. Cross-section of a thermal barrier coating, showing (from top to bottom) partially stabilized zirconia, MCrAlY bond coat and superalloy substrate.

www.manaraa.com

Thermal barrier coatings have been used since the 1950s for rocket propulsion and space applications and have been plasma-sprayed onto sheet metal combustor components for nearly 20 years. Only recently [39] have they been used in the more highly stressed turbine section of commercial gas turbine engines. Thermal barrier coatings over the entire airfoil of PW4000 turbine vanes were certified in the U.S.A for production use in 1986. This progress was achieved by a proper control of porosity, microcrack distribution, and residual stresses in the coating.

Fig. 9 illustrates the cross section of a typical thermal barrier coating. Although various ceramic coatings could be deployed, the most important ones in current use, are zirconia-based, partially or fully, stabilized with appropriate additions of Y_2O_3, MgO or CaO. Zirconia offers a good compromise with a low thermal conductivity (about 2 W/mK) and high a thermal expansion coefficient (10.10^{-6} K^{-1}). Zirconia is monoclinic at room temperature and tetragonal above approximately 1050°C. This change in structure is associated with a large volume change of about 7%. Above 2370°C zirconia is cubic. The additions stabilize the cubic structure over the entire temperature range. Yttria partially stabilized zirconia, containing 6 to 8 wt % Y_2O_3, has been found empirically to be most resistant in thermal cycling conditions [40]. This composition corresponds to the formation of a metastable tetragonal t' phase when the cooling rate during fabrication is sufficiently high, as in plasma spraying. With proper parameter adjustment, plasma spraying gives a microcracked structure particularly tolerant in compression.

Recent studies [41-43] have demonstrated that thermal barrier coatings obtained by EBPVD have superior properties to those produced by plasma-spraying. This might be attributed to the anisotropic microcrack network and also to the crystallographic texture of the EBPVD zirconia deposits.

The major problem with ceramic overlay coatings is spallation sensitivity, mainly caused by the thermal expansion mismatch between the coating and the substrate. To

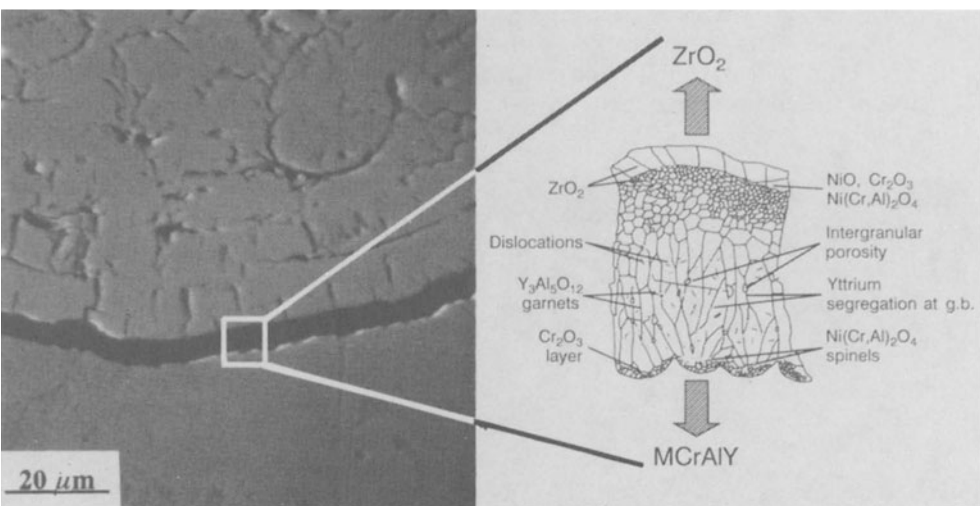

Fig. 10. Typical example of the aluminide layer formed at the zirconia/MCrAlY interface and schematic representation [after 44] of the various phases formed, as determined from TEM investigations.

المنارة للاستشارات
www.manaraa.com

overcome this problem a metallic bond layer is applied. The bond layer is generally about 100 μm thick MCrAlY (typically 30-40%Co, 30-50%Ni, 20%Cr, 10% Al, 0.5% Y), which in addition to better spallation resistance, also hinders the fast oxygen transport through the porous ZrO_2 to the substrate. Mechanical adaptation of this interlayer is more complex than just a simple matching of the respective thermal expansion coefficients. In fact, the expansion coefficients of MCrAlY alloys are generally higher than those of superalloys. In these systems, strain accommodation does not occur via a purely elastic deformation but it is thought to occur, in a large part, by plastic deformation of the MCrAlY bondcoat, as MCrAlY alloys have a low flow stress above about 400°C.

Thermal barrier coatings are dynamic systems in the sense that the zirconia topcoat, the MCrAlY bondcoat and the substrate superalloy interact at high temperature. Fig. 10 shows a representative alumina layer, which has formed at the zirconia/MCrAlY interface during high temperature exposure. The schematic representation of the phases present in this alumina layer, as determined with TEM, show how complicated is the system. Microstructural and microanalytical investigations have indicated [34] that the formation of this oxide layer results from the MCrAlY oxidation, as well as from the interaction between alumina and zirconia. It is important to remark that the interfaces in this multilayer system are sound and in practice, spallation rarely occurs at interfaces. Instead, failure of thermal barrier coatings happens generally (Fig. 11a) by propagation of a macrocrack inside the zirconia layer, near the alumina/zirconia interface. The crack propagation results from compressive stresses arising in the top coat on cooling because of the thermal expansion mismatch. More extended internal oxidation of the bondcoat can destroy the barrier, as shown on Fig. 11b, as the transformation of the MCrAlY alloy into oxide is accompanied by a volume expansion, which generates additional stresses inside the zirconia topcoat.

Although good performance has been obtained in applications using clean fuels, premature coating failure may result from hot corrosion (Fig. 12). Under cyclic oxidation conditions a regular increase in mass is observed, mainly due to oxidation of the MCrAlY bond coat. However, with the simultaneous addition of a salt, a dramatic degradation occurs after short testing times. Several mechanisms have been proposed to explain the degradation modes of TBC in hot corrosion conditions, namely: zirconia destabilization, bondcoat sulphidation, solidification of sulphate in cracks and crack propagation assisted by sulphate vapours [45].

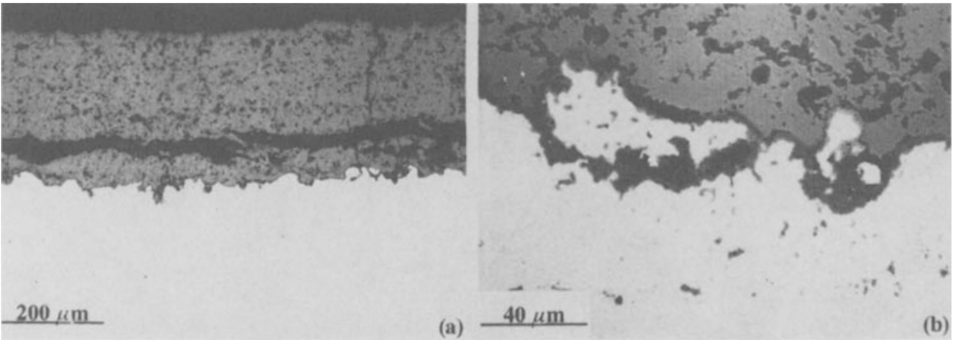

Fig. 11. Typical degradation modes of thermal barrier coating : (a) propagation of a main crack parallel to the ceramic/bond coat interface and (b) internal oxidation of bond coat.

المنارة للاستشارات
www.manaraa.com

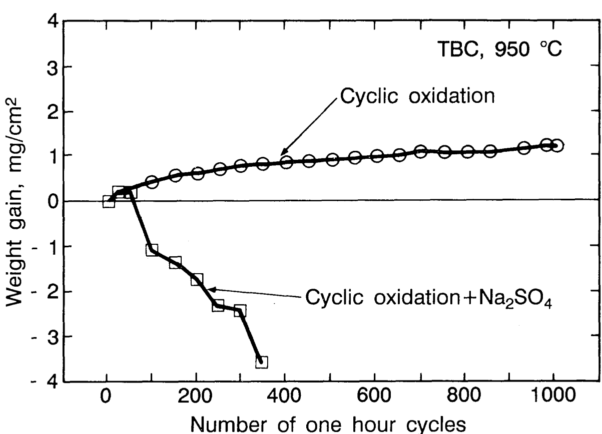

Fig. 12. Weight variations of a thermal barrier coating tested at 950°C in cyclic oxidation with and without the addition of a salt [45].

Despite present problems with some types of high temperature corrosion, the spallation resistance and reliability of thermal barrier ceramic overlay coatings are very promising. Further improvements can be expected in both processing and composition, both of the oxide coating and bond coat. Modelling of the mechanical behaviour and life of thermal barrier coatings, which is being carried out, currently especially in the U.S.A. [46], could be particularly beneficial. The existing models have been developed from a predominantly phenomenological approach and involve a number of empirical parameters. It must be emphasized that, up to now, several aspects are poorly understood, especially the creep and inelasticity of ceramic and bond coatings, geometry effect (roughness of metal/ceramic interface), oxidation-induced damages and evolution in service of properties of the different layers.

5. Concluding remarks

The applications of surface treatments to metallic components operating at elevated temperatures under corrosive conditions, can improve to a considerable extent the efficiency with which they operate, may increase component life in an economically significant manner and may even be essential to their effective performance. For the various surface treatments, improvements both in composition and techniques, are available and significantly better properties might be anticipated. It must be kept in mind that the surface layer must be developed as an integrated system, related to the selection pyramid of application, substrate material, surface material and economics.

Surface engineering for high temperature corrosion resistance is an extremely active field of research in which constructive interactions between industrial needs, process development and materials science are crucial. A variety of treatments is presently available, giving the designer the possibility, in principle, to tailor surface treatments in response to specific needs. It must be recognised though that in order to exploit the full potential of the

www.manaraa.com

latest developments, additional effort is required to go beyond the empirical (and successful) approach often used up to now. More specifically, in order to meet the most challenging applications (such as the design of thermal barrier coatings on highly stressed components and the formulation of coatings for use in extreme conditions) extensive work has to be undertaken in particular on acquiring detailed knowledge of basic phenomena (interfacial reactions, interdiffusion, scale adhesion) and on modelling the behaviour of coated systems. This should be accompanied by developing equipment for testing surface treated materials in conditions simulating, as closely as possible, the practical applications. This needs to include testing under mechanical loading, i.e. creep and fatigue (thermal and mechanical fatigue), combined with corrosion and erosion, possibly with in situ diagnostics. This not only raises the need for advanced testing techniques, but also that of standards for testing mechanical, physical and chemical properties and for inspection techniques.

It should be remarked that the main current use of advanced surface treatments for high temperature components are largely in the field of aero gas turbines. Other industrial processes can benefit from the knowledge obtained from this application, as well as from coatings used in non high temperature applications, like the micro-electronic industry. This diversification could provide substantial economic and environmental benefits.

Additionally, surface engineering techniques, in particular ion implantation, can be used as research tools to study corrosion mechanisms. The significance and potential of this indirect contribution to corrosion science should not be underestimated. More extensive exploitation of these possibilities can be expected to provide firm scientific guidance necessary for innovative material engineering, including surface engineering.

References

1. D.C. Cranmer, 'Fiber coating and characterization', Ceramic Bull. 68 (1989) 415-419.
2. H.E. Fisher, D.J. Larkin and L.V. Interrante, 'Fiber coatings derived from molecular precursors', MRS Bull. 16 (1991) 59-65.
3. J.R. Strife and J.E. Sheehan, 'Ceramic coatings for carbon-carbon composites', Ceramic Bull. 67 (1988) 369-374.
4. N. Birks and G.H. Meier (1983) Introduction to High Temperature Oxidation of Metals, Edward Arnold Publishers, London.
5. P. Kofstad (1988) High Temperature Corrosion, Elsevier, Essex.
6. M.F. Stroosnijder and W.J. Quadakkers, 'Review of high temperature corrosion of metals and alloys in sulphidizing/oxidizing environments', High Temperature Technology 4 (1986) 83-96 and 141-151.
7. R.A. Rapp, 'Chemistry and electrochemistry of hot corrosion of metals', Mater. Sci. Eng. 87 (1987) 319-327.
8. W.E. King (Ed.) (1989) The Reactive Element Effect on High Temperature Oxidation - After Fifty Years, Trans Tech Publications, Switzerland.
9. E. Lang (Ed.) (1989) The Role Of Active Elements in the Oxidation Behaviour of High Temperature Metals and Alloys, Elsevier, Amsterdam.
10. D.P. Whittle and J. Stringer, 'Improvements in high temperature oxidation resistance by additions of reactive elements or oxide dispersions', Phil. Trans. R. Soc. Lond. A295 (1980) 309-329.
11. M.J. Bennett and A.T. Tuson, 'Improved high temperature oxidation behaviour of alloys by ion implantation', Mater. Sci. Eng. A116 (1989) 79-87.

www.manaraa.com

12. M.F. Stroosnijder, J.F. Norton, V. Guttmann, M.J. Bennett and J.H.W. de Wit, 'Effect of ion implantation on the corrosion of Alloy 800H in an S-O-C environment', Mater. Sci. Eng. A116 (1989) 103-110.
13. V. Srinivasan, D.E. Goodman and A.R. Kraus, 'Effects of ion implantation on the mixed gas corrosion of a chromia former', Mater. Sci. Eng. A121 (1989) 525-530.
14. F.H. Stott, P.K.N. Bartlett and G.C. Wood, 'Laser surface treatment and its influence on the development of healing of Cr_2O_3 scales on nickel-chromium alloys', Oxid. Met. 27 (1987) 37-55.
15. W. Wu, R. Streiff and M. Wang, 'Effect of laser surface modification on high temperature oxidation and corrosion behaviour of alloys and coatings', Mater. Sci. Eng. A121 (1989) 499-507.
16. M.J. Bennett, 'New coatings for high temperature materials protection', J. Vac. Sci. Technol. B2 (1984) 800-805.
17. S.R.J. Saunders, A.A. Ansari, M.J. Bennett, A.T. Tuson, F. Fellowes and W.M. Steen, 'New corrosion resistant ceramic coatings by laser processing', SPIE 952 (1988) 705-712.
18. R. Mévrel, C. Duret and R. Pichoir, 'Pack cementation processes', Mater. Sci. Technol. 2 (1986)201-206.
19. C. Duret, R. Mévrel and R. Pichoir, 'Aluminide coatings on superalloys', in Surface Engineering (eds. R. Kossowsky and S. Singhal), Martinus Nijhoff Pub.(1984) 452-458.
20. G.H. Marijnissen, 'Codeposition of chromium and aluminium during a pack process', in High Temperature Protective Coatings (Ed. S.C. Singhal), The Metall. Soc. of AIME (1983) 27-35.
21. R.A. Rapp, D. Wang and T. Weisert, 'Simultaneous chromizing-aluminizing of iron and iron base alloys by pack cementation', Proc. of TMS-AIME Symposium on Metallurgical Coatings (Orlando, 1986).
22. G. Lehnert and H.W. Meinhardt, 'Electrodeposition', Surface Treatments 1 (1972) 189.
23. S. Alpérine, P. Steinmetz, A. Friant-Costantini and P. Josso, 'Structure and high performance of various paladium-modified aluminide coatings', Surf. Coat. Technol. 43/44 (1990) 347-358.
24. S. Alpérine and P. Josso, unpublished results.
25. P. Monge-Cadet, P. Walter, P. Lamesle and P. Steinmetz, unpublished results.
26. M.F. Stroosnijder, V. Guttmann, T. Fransen and J.H.W. de Wit, 'Corrosion of Alloy 800H and the effect of surface applied CeO_2 in a sulphidizing/oxidizing/carburizing environment at 700°C', Oxid. Met. 33 (1990) 371-397.
27. P.Y. Hou and J. Stringer, 'Effect of surface applied reactive element oxide on the oxidation of binary alloys containing Cr', J. Elec. Soc. 134 (1987) 1836-1849.
28. M.J. Bennett, A.T. Tuson, C.F. Knights and C.F. Ayres, 'Oxidation protection of alloy IN 738 LC by plasma assisted vapour deposited silica coating', Mater. Sci. Technol. 5(1989) 841-852.
29. M.J. Bennett, C.F. Knights, C.F. Ayres, A.T. Tuson, J.A. Desport, D.S. Rickerby, S.R.J. Saunders and K.S. Coley, 'Corrosion-resistant silica coatings obtained by plasma-assisted chemical vapour deposition', Mater. Sci. Eng. A139 (1991) 91-102.
30. R.W.J. Morssinkhof, T. Fransen, M.D. Heusinkveld and P.J. Gellings, 'The protective properties of thin alumina films deposited by metal organic chemical vapour deposition against high temperature corrosion of stainless steels', Mater. Sci. Eng. A121 (1989) 449-455.
31. R. Hofman, J.G.F. Westheim, T.Fransen and P.J. Gellings, 'The protection of alloys against high temperature sulphidation by SiO_2-coatings deposited by MOCVD', Materials and Manufacturing Processes 7 (1992) 227-238.
32. J. Pou, S.J. Spencer, D. Fernandez, P. Gonzalez, E. Garcia, B. Leon, S.R.J. Saunders and M. Perez-Amor, 'The effect of coating density on the strain tolerance of corrosion resistant amorphous silica', Thin Solid Films, in press.
33. M. Frances, P. Steinmetz, J. Steinmetz, C. Duret and R. Mévrel, 'Hot corrosion behaviour of low-pressure plasma-sprayed NiCoCrAlY + Ta coatings on Ni-base superalloys', J. Vac. Sci. Technol. 3 (1985) 2537-2544.

www.manaraa.com

34. D.K. Gupta and D.S. Duvall, 'A silicon and hafnium modified plasma sprayed MCrAlY coating for single crystal superalloy', in Superalloy 1984 (Eds. M. Gell et al.), The Metall. Soc. of AIME (1984) 713-720.
35. F.J. Honey, E.C. Kedward and V. Wride, 'The development of electrodeposits for high temperature oxidation/corrosion resistance', J. Vac. Sci. Technol. A4 (1986) 2593-2597.
36. R. Morbioli, 'Revêtements d'aluminiures complexes obtenus par dépôts électrophorétique consolidé par aluminisation', Mater. Sci. Eng. A121 (1989) 373-378.
37. E.P. Latham, D.B. Meadowcroft and L. Pinder, 'Coextrusion cladding for oxidation protection', Mater. Sci. Technol. 6 (1989) 913-915.
38. A.T. Tuson and M.J. Bennett, 'The oxidation of Fecralloy steel co-extruded on to strong steel substrate', Int. J. Pres. Ves. Piping 30 (1987) 391-403.
39. J.W. Fairbanks and R.J. Hecht, 'The durability and performance of coatings in gas turbine and diesel engines', Mat. Sci. Eng. 88 (1987) 321-330.
40. R.A. Miller, 'Current status of thermal barrier coatings', Surf. Coat. Technol. 30 (1987) 1 - 11.
41. K.D. Sheffler and D.K. Gupta, 'Current status and future trends in turbine application of thermal barrier coatings', Trans. of the ASME J. of Engineering for Gas Turbines and Power 110 (1988) 605-609.
42. F.C. Toriz, A.B. Thakker and S.K. Gupta, 'Flight service evaluation of thermal barrier coatings by physical vapor deposition at 5200h', Surf. Coat. Technol. 39/40 (1989) 161 - 172
43. L. Lelait, S. Alpérine and C. Diot, 'Microstructural investigations of EBPVD thermal barrier coatings', to be published (1992).
44. S. Alpérine and L. Lelait, 'Microstructural investigations of plasma sprayed yttria partially stabilized zirconia TBC', ASME 92-GT-317 (1992).
45. S. Alpérine, 'Molten salt induced high temperature degradation of thermal barrier coatings', in High Temperature Surface Interactions AGARD CP N°461 (1989) 6.1-6.18.
46. R.A. Miller, 'Life modelling of thermal barrier coatings for aircraft gas turbine engines', NASA TM 100283 (1988).

www.manaraa.com

DECORATIVE COATINGS

H.A. JEHN
Research Institute for Precious Metals
and Metals Chemistry
Katharinenstr. 17
D-7070 Schwaebisch Gmuend
Germany

ABSTRACT. Vapour-deposited hard coating like TiN, ZrN and a great number of ternary or multicomponent compounds of the transition show a variety of colours out of which the golden TiN is the most well-known tint. The use of such coatings for decorative purposes combines their decorative properties with their excellent wear resistance and good corrosion resistance. In the present paper first the colours and their dependence on composition and process parameters are discussed followed by information on the corrosion behaviour of coating/substrate systems and their testing methods. Finally, examples are given for the application of decorative hard coatings and specific coating sequences for improvement of the corrosion resistance if less noble substrate materials have to be coated.

1. Introduction

Since the beginning of technological development men tried to modify surfaces by coating or other treatments. And also since the very beginning decorative coatings were in the focus of interest besides functional purposes. The parts to be coated were first in the area of subjects of religion as well as political might and power. Later jewelry and things of daily use were decoratively coated and nowadays the applications are numerous ranging from architectural purposes and household parts to custom jewelry. Regarding the processes, the technical possibilities changed from massive coatings like leaf gold via pastes as used in fire gilding, enamels, paints and lacqueurs to the variety of electroplating processes (elctrochemical deposition - ECD - with atom by atom deposition) and other elctrochemical reactions like anodical oxidation. Most recently the physical vapour deposition (PVD) processes were successfully applied. Besides the intrinsic colours of metals and alloys also coloured compounds like nitrides or carbides can be deposited by PVD. The latter coatings combine decorative aspects (even if limited in their colour variation) with high wear resistance and good corrosion resistance. Starting from the golden colour of TiN (and also ZrN and HfN), changes in the N content or additions of C or O and of other metal components yield variation in the colour towards light gold, metallic silver, greenish gold, reddish gold, brownish yellow or dark blue. Other transition metal compounds exhibit metallic, grey or black colours.

As PVD coatings normally are not defect-free but show pores and pinholes, corrosion attack of the coated parts can occur if corroding substrate materials are used. The actual research activities

W. Gissler and H. A. Jehn (eds.), Advanced Techniques for Surface Engineering, 359–370.
© 1992 *ECSC, EEC, EAEC, Brussels and Luxembourg.*

www.manaraa.com

are therefore directed to develop denser film structures and corrosion resistant interlayers deposited by ECD or PVD. Furthermore, new colours are searched.

In the present paper the colours of hard coatings and their variation will be discussed as well as the corrosion behaviour of decorative coating systems. Finally, examples of presently applied decorative coating systems will be given. The emphasis is laid on decorative PVD hard coatings even if other techniques still play a very important role and also show new developments.

2. COLOURS OF HARD COATINGS

Colour is the most important property of decorative coatings. It, however, needs solid state physics to understand the physical processes. Without any further discussion, it is mentioned that colour is due to the selective reflectance of certain wavelengths in the visible range of electromagnetic waves (380 - 780 nm). It is correlated to the band structure and the density of states. The colour of conductive solids is due to interband transitions whose threshold lies in an energy range corresponding to the visible region of the electromagnetic waves. The impression of colour in the human eye is the result of the reception of the spectral composition of the radiation entering the eye, which is done by three different kinds of photoreceptors in the retina. The individual sensitivity govern the colour impression of men.

Colours can be characterized by several standards. According to DIN 5033 they are given by tristimulus values. Another wiedly used system is CIEL*a*b*. For a well-defined characterization also the illumination has to be standardized (angle of incidence and angle of viewing, e.g. 45/0 geometry, or diffuse illumination and normal viewing, d/0; or vice versa 0/45 or 0/d). These geometries were successfully applied in colorimetry and the appearance of gloss and mat, or structured and non-structured surfaces. The colour appearance of decorative coatings can also depend on the direction of illumination and viewing. The CIEL*a*b* values are especially suitable for the measurement of colour differences. The a* value reflects red and green colours when positive an negative, respectively, and b* gives yellow (positive) and blue (negative) colours. The brilliance is given by the L* value [1].

2.1.COLOUR OF BINARY COMPOUNDS

The best known decorative hard coating is TiN. Figure 1 shows the reflectance of TiN in comparison that of two gold alloys [2,3]. It can be seen that the spectral dependency is relatively similar but the absolute values are noticeable lower for TiN. The colour of TiN (and also all the other nitrides) depend strongly on the N content. It changes from bright golden to a light gold and metallic silver with decreasing N content and to brownish yellow for overstoichiometric compositions. This means that the colour depends strongly on the deposition parameters, especially the N_2 flow [2-11] as is illustrated in Fig. 2 [2,3]. Other process parameters influencing the colour via chemical composition or film structure are the deposition process (sputtering, arc evaporation, ion plating), substrate temperature, substrate bias, deposition rate, geometrical arrangement of target and substrate (distance and direction of metal atom incidence), and surface roughness. Thermal posttreatments (aging} may influence the colours of the IVa metal nitrides. Such changes are accompanied by changes in the lattice parameters [12-14]. Also the other IVa metal nitrides ZrN and HfN show golden colours, but shifted to greenish and brownish, respectively. The first one matching the brass colour [15]. The colours of some other binary and multicomponent hard coatings together with

www.manaraa.com

some Vickers hardness numbers are given in Table 1. The bold-typed compounds are of major technical application up to now.

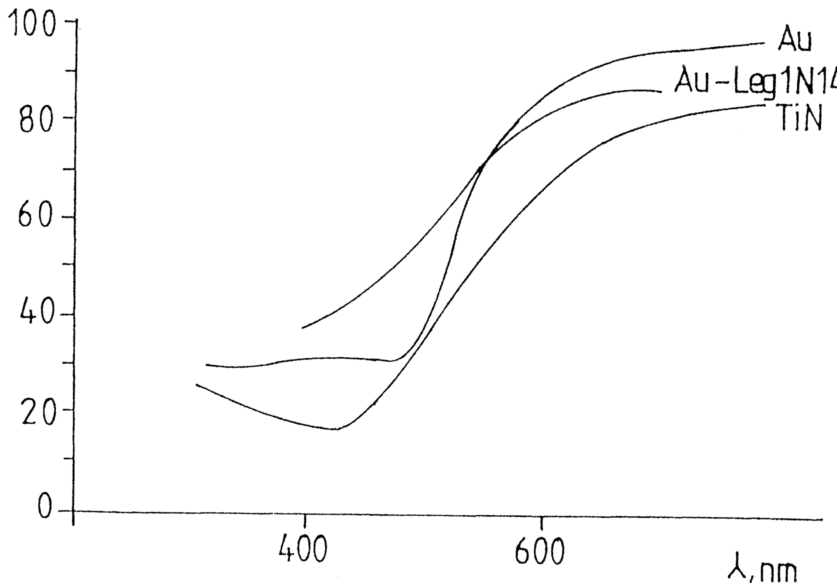

Figure 1. Reflectance of TiN, Au and a gold alloy as a function of wavelength [2,3]

2.2. COLOURS OF "TERNARY" COMPOUNDS

Additions of O_2 or hydrocarbons to the reactive atmosphere for the reactive PVD process yields some O and C contents in the film, i.e. oxy- or carbonitrides are obtained which are characterized by more or less pronounced colour changes when compared to the pure binary hard coating. On the other hand, additions of a second metallic component may result in drastic colour changes, of course depending again on the nitrogen content. It has to be mentioned that high amounts of a second metal (up to 60 %) do not alter the f.c.c. lattice structure of the TiN, even if the second nitride, like AlN (hex) exhibits a different lattice structure [29].

Within the search for new colours, a great number of "ternary" compounds based on the IVa metal nitrides have been studied, e.g. (Zr,Al)N, (Zr,Cr)N, (V,Al)N [17], (Ti,Cr)N [17,18], (Ti,V)N, (Zr,V)N [19] (see also Table 1). Examples of the colour change are illustrated in Fig. 3 and 4, showing the L^*, a^* and b^* values as a function of N_2 flow rates. In the latter the variation for different base materials with the same addition is demonstrated. The curves start at the center of the axis (metallic grey) and turn with increasing N content (from increasing N_2 flow) towards yellow and mostly some reddish touch. In part, some slightly greenish golden colours are also obtained.

Other colorimetric studies were made e.g. with Zr-B [20]and Zr-B-N [21] films.

www.manaraa.com

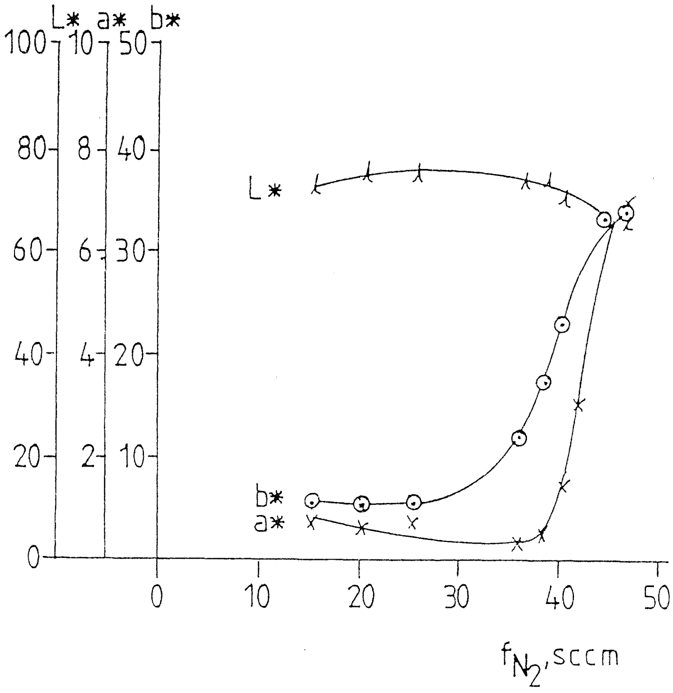

Figure 2. Colour of sputter-deposited TiN_x films as a fuction of N_2 flow

TABLE 1. Colour and hardness of some hard coatings

Coating	Colour	Hardness
Mg_3N_2	yellow - green	
TiN	yellow golden	2400
ZrN	greenish yellow	2600
HfN	yellow - brown	2750
Cr_2N, CrN	grey	2500
TaN	greyish blue	2700
Be_2N	red	
CeC_2	yellow - red	
TiC	light grey	1500 - 2900
TiC/WC	dark grey	1400
NbC	light brown	
TaC	pale yellow - brown	1800
SiC	black	3500

المنارة للاستشارات
www.manaraa.com

TABLE 1. cont.

Ti(C,N)	red - yellow - violett	2700
Zr(C,N)	silver - golden yellow	
V(C,N)	pale yellow	
(Ti,Al)N	yellow - dark blue	2400 - 2900
(Ti,Al)(O,N)	black	
(Ti,Zr)N	golden colours	

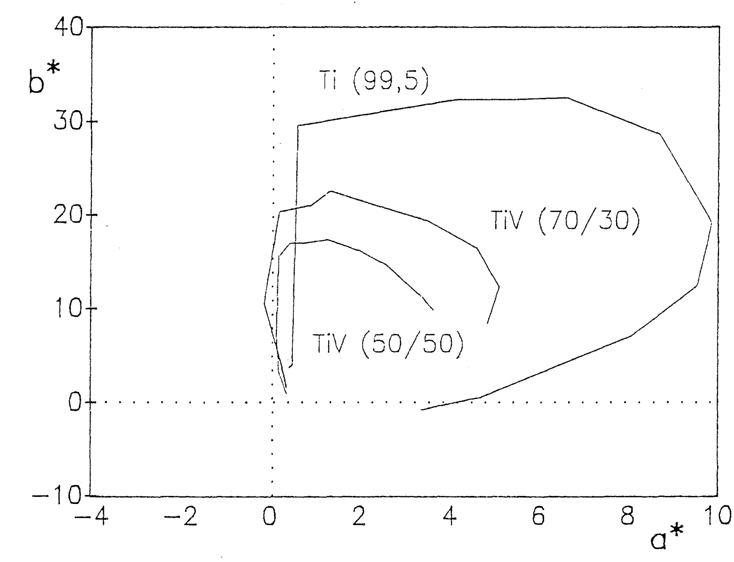

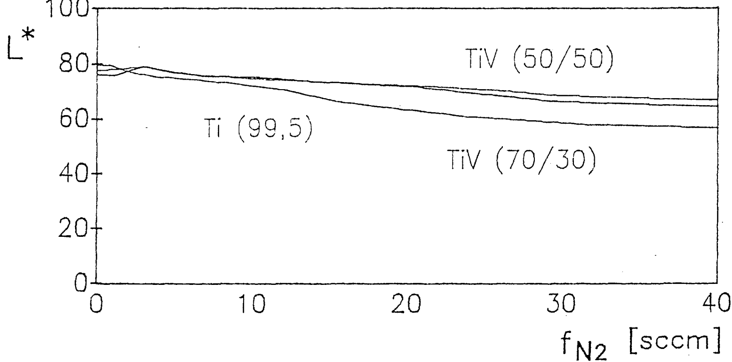

Figure 3. Colour variation of TiN_x and $(Ti,V)N_x$ films as a function of N_2 flow [17]

www.manaraa.com

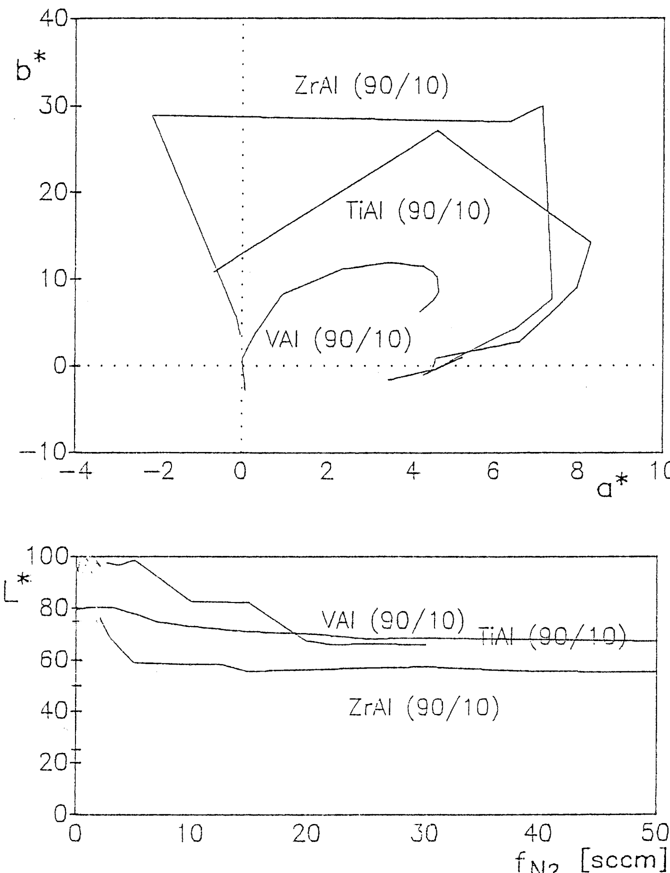

Figure 4. Colour variation of Al-containing IVa metal nitrides as a function of N_2 flow [17]

3. Corrosion of Coating/Substrate Systems

Decoratively coated parts are often exposed to environmental attack resulting in a more or less severe corrosion. The hard coating material itself show a relatively noble behaviour when studied from the electrochemical point of view. When deposited on a less noble substrate material, e.g. like steel or brass, the so-called galvanic corrosion may take place where the substrate material is severely corroded at places of film defects like pores or pinholes. Thus, decorative coatings have not only to be studied for their colour but also with respect to the corrosion behaviour of the coating/substrate system [22].

The corrosion test can be divided into the two classes of technical short-time tests and electrochemical measurements. In the first, actual environmental attack is simulated by certain spraying or immersion tests to accelerated corrosion. The latter allow to draw detailed information on the corrosion mechanism. Tables 2 and 3 summarize the major corrosion tests.

www.manaraa.com

TABLE 2. Short-time test for corrosion studies

Test	Conditions	Information
a Condensed water-contg. climate	Saturated water vapour 40 ^{o}C, 24 h cycles	Behaviour in humid environm.
b Condensed water alternating atmosphere	Water vapour + 0.07 vol.% SO_2, 18-28 ^{o}C/40% hum. and 75-300 ^{o}C/40% hum, cycles, 24 h each	As (a) with polluted gas
c Salt spray test	NaCl, 50 g/l, 35 °C, pH 7	Ocean climate
d Salt spray test ctg. acetic acid	As (c) + CH_3COOH, 35 °C, pH 3.2	Salted roads
e CASS	As (d) + 0.26 g'l $CuCl_2.H_2O$, 50 °C, pH 3.2	
f Artificial sweat	40 °C, 24 h cycles	Wearing of decorative parts
g Immersion test	solutions of HCl, HNO_3, etc.	Corrosion in aqueous media

As an example, Fig. 5 shows the potential-current density curves of PACVD-TiN coatings on stainless steel SS41 as a function of film thickness. As can be seen, the corrosion current decreases strongly with increasing thickness. But even at 14 um the behaviour of pure TiN (on glass) is not yet reached completely [23].

www.manaraa.com

TABLE 3. Electrochemical measurements in corrosion studies

Test	Condition	Information
Potentiostatic	U = const.	Time dependence of corrosion current
Potentiodynamic	U variable	Corrosion mechanism
Galvanostatic	I = const.	Time dependence of corrosion potential
Galvanodynamic	I variable	Corrosion mechanism
Potential	I = 0	Behaviour in galvanic corrosion
Polarization resistance	U variable around corros. potential	Absolute corrosion rate
Impedance	RF voltage	Changes in surface states

Bold-typed: Most used methods.

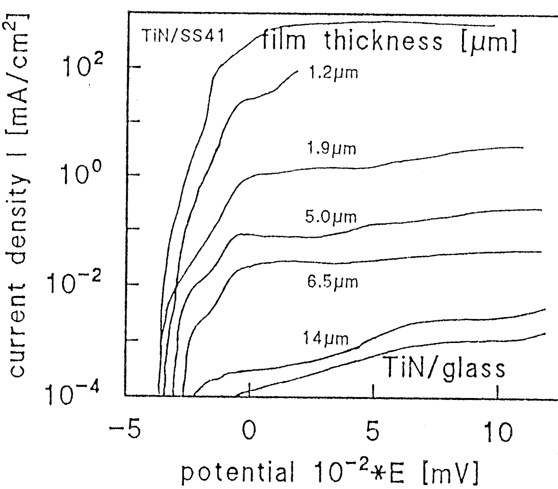

Figure 5. Current-potential curves for PACVD-TiN on SS41 as a function of film thickness tested in 1 M HCl. For comparison TiN on glass [23]

www.manaraa.com

The evidence of corrosion studies can be summarized as follows [22]:
(i) Short-time test with accelerated attack can only partly simulate actual corrosion; they give qualitative and reproducible results in laboratory tests or quality assurance.Simulation of corrosion in practical use is improved by ation of different short-time tests.
(ii) Electrochemical measurements reflect the fundamental behaviour of the coating/substrate system; only the corrosion rate is influenced but not the mechanism. The information obtained always reflect the total system medium-coating-substrate. A low corrosion current density does not necessarily mean a better coating material but only a better coating/substraet behaviour.
(iii) Little, if any, correlation exists between technical and electrochemical results.
The corrosion behaviour of PVD hard coating/substrate systems can be improved by the following measures:
(i) Dense coating structures have to be produced by suitable selection of deposition parameters (temperatue, bias, etc.)
(ii) More noble substrate material and improved surface quality of the substrate reduce the corrosion tendency.
(iii) Dense and noble interlayers deposited by ECD or PVD decrease the corrosion attack.

4. **Decorative Coating Systems**

4.1. DEPOSITION OF DECORATIVE COATINGS

The decoratively coated parts comprise a great number of parts of the daily use like watch cases, watch bands, eyeglass frames, writing utensils, custom jewelry, household parts, door knobs, metal fittings, sanitary parts, and even cutlery.

Decorative hard coatings are deposited by reactive PVD processes like magnetron sputtering [5], cathodic arc evaporation [24] and ion plating [9,10,25]. In all processes the N content can easily be controlled (and changed if desired) by controlling the N_2 pressure or flow. For a homogeneous coating of complex parts, they have to be rotated or siimultaneously coated by different sources like, e.g., the double cathode sputtering device [2,3,5].

The decorative coating procedure can be performed in batch equipment; the different process steps all are done within on system having total charging times of 70 - 90 min. In contrast, in-line coating systems show a number of advantages: e.g. several processes can be performed simultaneously by transportation of the parts via locks, better vacuum conditions, lower risk of contamination, simple realization of sandwich layers. Disadvantages can be seen if different reactive gases have to be applied, if no intermediate locks exist. Furthermore, the break of one module stops the complete process [26,27].

The following list gives an example for the various process steps to be performed after the substrate cleaning and ECD interlayer deposition [27]:

Visual control of incoming parts
Placement on transport racks
Ultrasonic wet cleaning and solvent drying
Heating and outgassing
Ion etching
PVD plating (e.g. sputter ion plating), 0.3 - 1 µm
Cooling

www.manaraa.com

Deloading
End control (visual inpection and others)

4.2. INTERLAYERS

While noble or passivating substrate materials (titanium, stainless steel, etc.) can directly be coated, other materials need a corrosion resistant interlayer deposited by ECD or PVD techniques (see Fig. 6).

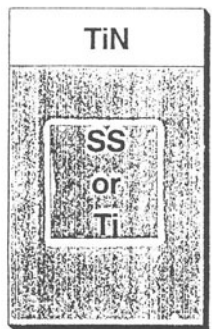

Substitution of substrate material

corrosion protection by electroplated interlayer

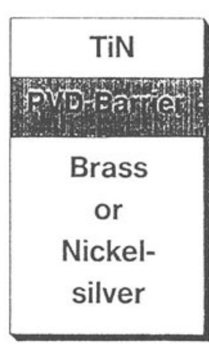

Corrosion protection by PVD barrier

FIGURE 6. Possible solutions for corrosion resistant barrier layers [28]

Such interlayers might be electroplated Ni which also allows the selection of certain surface effects (bright, semibright, pearl, etc.) according to the bath applied. Electroplatings also show a leveling effect resulting in smooth substrate surfaces. The presently best coating sequence for decorative coatings on brass or German silver substrate consists of a Ni and a Pd-Ni interlayer (see Fig. 7). The reasons are levelling effect of Ni, dense and pinhole-free structure of Pd-Ni and the electrochemical properties of Pd-Ni. There, however, is a need to replace Ni-containing interlayers because of the increasingly observed nickel allergy, even if - compared to electroplated gold coatings - practically no wear of the decorative hard coatings is observed.

The use of PVD interlayers would simplify the overall coating process because "only" another PVD step has to be included in the in-line procedure and no other "wet" coating has to be applied. Requirements for PVD coatings are: dense pore-free structure, diffusion barriers (for Zn, Pb of the substrate material), corrosion resistance, matching the electrochemical potentials, sufficient ductility, non-toxic and physiologically non precarious, and finall competitive cost of material and target processing.

The disadvantages of PVD coatings, i.e. pores and pinholes. can, in part, be overcome by intermediate etching processes as was proved by electrochemical measurements of coating systems (e.g. Ti). Among a large number of PVD barrier layers studied the following turmed out to best up to now: TiNiMo 56/24/20, TiMo 70/30, CrAl 75/25 and Ti [28]. Like in decorative PVD films, the process parameters (bias power, cathode power, total pressure, magnetic field, intermediate etching) exhibit a strong influence on the efficiency of the PVD barrier layers

المنارة للاستشارات
www.manaraa.com

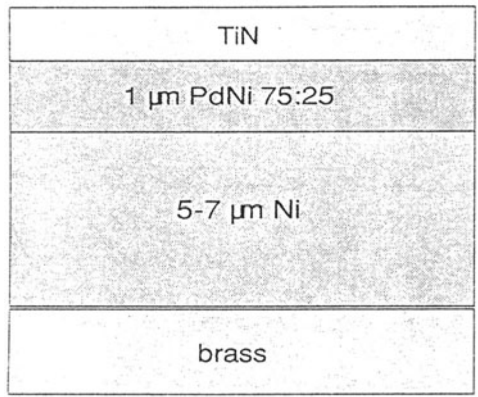

Figure 7. Presently best results of corrosion protection in decorative coating [28]

Finally, it should be noted that, in part, a final gold flash is vapour deposited in order to get the lustre of true gold or to match completely the colour values of the gold standards. This top coating has additionally the advantage that it will not be completely worn due to the microroughness of the PVD hard coatings (see Fig. 8.)

For technical papers see also [30 - 35].

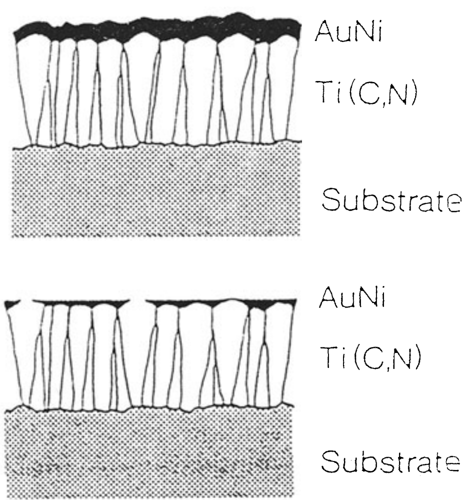

Figure 8. Wear of thin precious metal overlayers on hard coatings

www.manaraa.com

References

[1] IS O 7724/1,2,3 (1984) (E)
[2] Hofmann, D., Leybold-Heraeus Report 11-SO20.01
[3] Hofmann, D. (1986) in H. Fischmeister and H. Jehn (eds), Hartstoffschichten zur Verschleissminderung, DGM, Oberursel pp.337-352
[4] Hashimoto, M., Miyajima, S., Ito, W., Ito, S., Murata, T., Komori, T., Ito, L., and Onoyama, M.(1988) Surf. Coat. Technol. 36, 8370845
[5] Muenz, W.-D., and Hofmann, D. (1983) Metalloberflaeche 37, 279-285
[6] Perry, A.J. (1986) Thin Solid Films 148, 73-85
[7] Huang, Y.C., and Takei, H. (1978) Thin Solid Films 54, 61-65
[8] Stanislav, J., Sikac, J., and Cermak, M. (1990) Thin Solid Films 191, 255-273
[9] Matsumura, Y., and Huang, Y.C. (1984) J. Met. Finish. Jap. 35, 39
[10] Matsumura, Y., and Huang, Y.C. (1984) J. Met. Finish. Jap. 34, 289
[11] Perry, A.J., Georgson, M., and Ribbing, G.C. (1986) J. Vac. Sci. technol. A4, 2674
[12] Perry, A.J. (1987) Thin Solid Films 146, 165-174
[13] Perry, A.J. (1986) J. Vac. Sci. Techniol. A4, 381
[14] Perry, A.J., Georgson, M., and Sproul, W.D. (1988) Thin Solid Films 157, 255-265
[15] Deco Coatings, Part IV, Leybold Report 11-S.42.02
[16] Rack, A. (1991), Proc. Leybold Deco Symposium, Buedingen 1991, Leybold Report 11-S39.02
[18] Jehn, H.A., Thiergarten, F, Fabian, D., and Ebersbach, G. (1991), Surf. Coat. Technol. (Proc. Intern. Conf Metallurgical Coatings, San Diego, CA 1991)
[19] Reiners, G., Hantsche, H., Jehn, H.A., Kopacz, U., and Rack, A. (1992) Surf. Coat. Technol. (Proc. Intern. Conf. Metallurgical Coatings, San Diego, CA 1992)
[20] Mitterer, C., Losbichler, P., Werner, W. S. M., Störi, H., and Baroung, J. (1992) Surf. Coat. Technol.(Proc. Intern. Conf. Metallurgical Coatings, San Diego, CA 1992)
[21] Mitterer, C., Übleis, A., and Ebner, R. (1991) Mater. Sci. Eng. A 140, 670 - 675
[22] Jehn, H. A., and Baumgärtner, M. E.,(1992) Surf. Coat. Technol.(Proc. Intern. Conf. Metallurgical Coatings, San Diego, CA 1992)
[23] Makabe, R. (1988) Welding 2, 733
[24] Randhawa, H., and Johnson, P. C. (1988) Met. Finish. No. 9, 19 - 22
[25] Pulker, H. K. (1989) Oberfläche Surface 21, 32- 37
[26] Riedl, R. (1989) Galvanotech. 80, 3391 - 3397
[27] Riedl, R. (1990) Proc. Leybold Deco Symposium, Aschaffenburg 1990, Leybold Report 11 - S 38.02
[28] Bennecker, H.Proc. Leybold Deco Symp., Buedingen 1991, Leybold Report 11-S39.02
[29] Holleck, H. (1989) Metall 43, 614
[30] Bastian, S. (1990) Galvanotechnik 81, 2706-2709
[31] Erhart, H. (1990) Metalloberfl. 44, 59-62
[32] Erhart, H. (199) Galvanotechn. 81, 1216-1218
[33] Kopacz, U., and Schulz, S. (1992) Galvanotechn. 83, 844-848
[34] Schulz, S. (1990) Proc. Leybold Smposium Decorative Hard Coatings, Aschaffenburg 1990, Leybold Report 11-S38.02
[35] Sezerko, P., Kopacz, U., and Schulz, S. (1989) Galvanotech. 80, 4274 - 4277

www.manaraa.com

DIAMOND AND DIAMOND-LIKE CARBON FILMS

François ROSSI
Commission of the European Communities
Joint Research Centre
P.O. Box 2
1755 ZG Petten
The Netherlands

ABSTRACT : Diamond and diamond-like layers present outstanding possibilities of development, and in many cases like in optics or microelectronics, decisive technological jumps are expected. This is due to the exceptional combination of properties of these materials. The properties of diamond and diamond-like layers, the expected markets and applications of diamond and diamond-like films are presented. The techniques available for diamond films production by thermal and plasma activated methods are reviewed. A description of the principal mechanisms of diamond deposition as well as the problems related to it are discussed. In the case of diamond-like carbon, the mechanisms of densification under ion bombardment are presented.

1. Introduction

Diamond and hard carbon materials have been the object of intense research programmes in the past 40 years. The work has primarily concentrated on synthesis of diamond by high pressures and temperatures with a solvent catalyst : under these conditions, diamond is the stable phase of carbon. This research has been successful, and production of stones by this technique is now a common practice in industry. The work on production of diamond films at low pressures, where it is metastable, has started over 3 decades ago, but only reached a level of significant activity in the last five years. This long incubation period is due to the skepticism of the scientific community concerning the very low deposition rates obtained at the beginning : For this reason, the work on production of diamond films at low pressures, although started in the US in the 50 by Eversole [1], was then progressively abandoned. At the same time, in USSR, Derjaguin and Fedoseev [2] have pursued intensively their work on the subject for more than 20 years. When the deposition rates reached the order of 1µm/h, a large impulse was given by the Japanese teams in the 80's [3,4,5,6], soon followed by US researchers and an US DoD Diamond programme in the mid to late 80's, as well as a large effort in Europe. Today, the low pressure methods are studied worldwide, the growth rates reach typically a few tens of µm per hour, and industrial companies like De Beers, Norton, Diamonex or Crystallume are able to produce stand alone layers of diamond of 0.5 to 500 µm thickness on areas of several square centimeters. In addition, the properties of hard diamond like or hydrogenated carbon coatings, discovered during the same period, are particularly interesting for applications in

W. Gissler and H. A. Jehn (eds.), Advanced Techniques for Surface Engineering, 371–397.
© 1992 *ECSC, EEC, EAEC, Brussels and Luxembourg.*

www.manaraa.com

wear resistance technology. The use of diamond films will grow considerably in the next ten years, and the world market for diamond films is expected to be several billions $ in year 2000.

2. Diamond films

2.1. STRUCTURE AND PROPERTIES OF DIAMOND

The diamond cubic lattice consists in two interpenetrating fcc lattices displaced by one quarter of the cube diagonal. Each carbon atom is placed at the center of a tetrahedron (see Fig.1), and linked to its neighbours by covalent σ bonds arranged as hybrid sp^3 atomic orbitals : the high strength and the symmetry of the bonds are responsible for the hardness of diamond. The lattice can also be visualized as planes of saturated carbon cycles of 6 C atoms stacked in an ABC ABC sequence along <111> direction . Each cycle is in a "chair" configuration and all C-C bonds are staggered. This cubic structure is the most abundant form of diamond. However, another lattice with an hexagonal symmetry can be constructed with the same tetrahedral nearest neighbor configuration. In this hexagonal diamond (or lonsdaleite), the planes of the chairs are stacked in a ABABAB sequence [7]. In simple organic molecules, this configuration is usually less stable because of steric interactions. This is why hexagonal diamond is usually not obtained, although it could be formed by homogeneous precipitation from an activated vapor phase [7,8].

In graphite, the carbon atoms are linked by sp^2 orbitals in a planar structure (Fig 2), with a weak binding between planes, allowing easy sliding and giving lubricating properties to graphite.

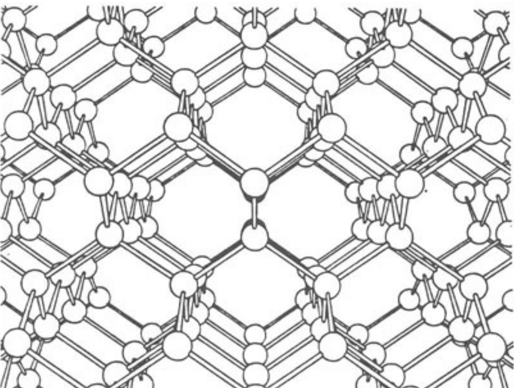

Figure 1 : Carbon configuration in the diamond structure

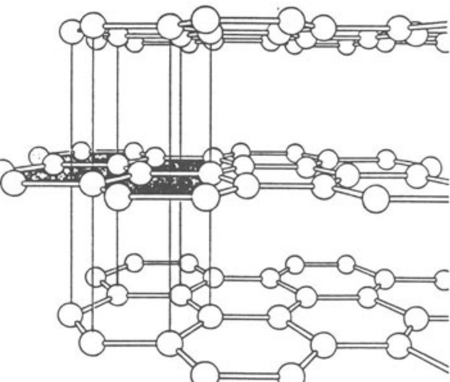

Figure 2: Carbon configuration in the graphite structure [7]

The interest in diamond comes from its exceptional combination of properties as compared with other materials (Table 1). For instance, the combination of high thermal conductivity and low thermal expansion makes diamond a very good choice for heat dissipation for advanced electronic systems.

المنارة للاستشارات
www.manaraa.com

Material	Thermal expansion (10^{-6} /°C)	Thermal Conductivity (W cm^{-1} K^{-1})
Bulk Diamond	2.6	20
CVD Diamond		10
Cu	4.5	4.0
BeO	5.9	2.6
AlN		1.7
Al_2O_3	5.4	0.2

Table 1 : Comparison of thermal properties of Diamond to other materials

The mechanical properties of diamond are outstanding (see Table 2): its hardness and Young's modulus are the highest known. It is resistant to corrosion and has an excellent thermal conductivity. It could be used as a coating for tools but problems of poor adhesion of the films to the substrates still limit its applications [9].

Material	**E (GPa)**	**H (GPa)**	**Y (GPa)**
Diamond	1050	103	59
Si	130	10.4	112
a-C:H	50-150	5-15	3-10
WC	534	35	
Steel	212		
Al	71		

Table 2 : Comparison of mechanical properties of materials with diamond: Elastic modulus (E), Hardness (H) and Young's modulus (Y) [9].

The electronic properties of diamond make it a very attractive in device applications: its band gap is 5.45eV, and its conduction band is similar to that of Si. This means that diamond is very resistant to radiation (factor of 100 compared to Si) and makes it a very good candidate for applications in high power electronic systems (microwave generators) or aggressive environments (space, nuclear reactors). It has moreover a very high breakdown value (10^7V/cm). It has also a very high resistivity (10^{13} to 10^{16} Ωcm), a high carrier mobility (2200 cm^2/Vs for electrons and 1600 for holes) : this high mobility is insensitive to magnetic fields, which is interesting for High Frequency systems [9].
Diamond has also a very high sound velocity (18200m/s), is transparent to radiations in a large domain of wavelength between IR to UV, and has a good transmission coefficient for X rays and UHF.

2.2 PRESENT APPLICATIONS OF POLYCRYSTALLINE DIAMOND FILMS :

The many applications where diamond is already routinely in use, take advantage of its exceptional bulk properties, listed above, where the inclusion of large number of defects in the layer have little or no detrimental effect on the layer performance. Such applications already are or soon will be economical and viable industrial applications, for instance [10] :

- Superhard wear resistant protective coatings for cutting tools and wear parts [11,12].
- Abrasive powders

المنارة للاستشارات
www.manaraa.com

Applications	Properties utilized	Material
Bearings	A,B,C,D,E,F	2,3,4,5,6
Barrier coatings	B,C,F	3,4,5,6
Heat sinks	F	1,2,3,4,5,6
Cutting tools	A,B,D,E,F	1,2,3,4,5,6
Surgical blades	A,D	1,3,4,5,6
Knives	A,B,D,E	1,3,4,5,6
Abrasives	A,F	2,3,5,6
Medical implants	A,B,C,E	3,4
Wire drawing dies	A,B,D,E,F	1,2,3,5

Table 3 : Mechanical applications of superhard materials (see legend next page)

Applications	Properties utilized	Material
Transistors		
High performance	F,M	1,5,6
High temperature	B,C,F,L,M,N	1,5,6
Radiation hard	F,J,L,M,N	1,5,6
High power	F,L,M,N	1,5,6
Electrical insulator	B,J,K,M	1,3,4,5,6
Substrates, heat sink	F,K,M	1,3
X ray masks	A,B,C,D,G	1,3,4
Direct write microelect.	A,B	4
Magnetic disks, heads	A,B,E	1,4
High voltage switches	F,K,M	1,5,6
Thermistors	F,J	1,3,5,6
Packaging	A,C,F,K,M	1,3,4

Table 4 : Electronic applications of superhard materials (see legend next page)

المنارة للاستشارات
www.manaraa.com

Applications	Properties utilized	Material
Windows, lenses, mirrors	A,B,C,D,F,H,I,J	1
XRays windows	A,B,C,D,F,G	1,3,5,6
Mirror substrates	A,B,C,F	1
Heats sinks	F,K,M	1,3,5,6
Optical emitters, lasers	F,J,L	1,5,6
Opt. activated switches	F,J,L,M,N	1,5,6
UV detectors	J,L	1,6
Optical waveguides	C,H,I,O	1,3

Table 5 : Optical applications of superhard materials (see legend below)

Properties	Material
A - Hardness	1 - Diamond single crystal
B - Chemical stability	2 - Diamond, polycrystalline composite
C - Low permeability	3 - Diamond, polycrystalline film
D - Young's modulus	4 - Diamond-like material
E - Friction coefficient	5 - SiC
F - Thermal conductivity	6- c-BN
G - X Ray transmission	
H - Infrared Transmission	
I - Visible transmission	
J - Large band gap	
K - Electrical insulating	
L - Semiconducivity	
M - Dielectric strength	
N - Carrier mobility	
O - Refractive index	

Legend for Tables 3, 4 and 5.

المنارة للاستشارات

www.manaraa.com

- Decorative, scratch or corrosion-resistant surfaces to be used for medical, optical, chemical and other applications.
- Heatsinks for chips, taking advantage of diamond high thermal conductivity.
- Components for tweeters and acoustic equipment, taking advantage of diamond sound transmission capabilities.
- Mechanical supports for crucibles where chemical inertness, rigidity and high melting point are necessary. A summary of the properties used and their related applications is proposed in Table 3, 4 and 5 [13].

2.3. DEPOSITION TECHNIQUES

Most of the techniques of deposition of diamond films are based on gas phase decomposition of hydrocarbon compounds in the presence of an excess of atomic hydrogen. The processes can be all classified as Chemical Vapour Deposition (CVD) techniques and the different mechanisms of diamond production are explained in the next section. These CVD reactions can be performed at low pressure (10 to 200 mbar) or atmospheric pressure: The low pressure type lead to films of high purity, good uniformity, which are produced at deposition rates of 0.5 to 10 µm/h. For the high pressure technique, deposition rates can reach 10 to 100µm/h and more, but uniformity is generally lower [10]. One of the most important aspects of diamond deposition is the presence of atomic hydrogen. Sufficient quantities of H can be obtained by two basic activation methods : Activation by high temperatures, and activation by electric of electromagnetic gas discharges:

2.3.1. Thermally Activated Chemical Vapour Deposition (TACVD) : In TACVD, the chemical reaction leading to the formation of diamond is activated by a heat source. The main techniques are the following :

- Laser Enhanced Chemical Vapour Deposition [24] (Fig 3): an ArF excimer laser (193nm) is used to locally induce the chemical reaction of C_2H_2 and H_2 at the laser spot impact at the surface. Low deposition rates are obtained, and the applications of this type of technique will probably be limited by the fact that it is a discontinuous process, i.e. the laser spot has to be displaced on the surface in order to get a film of large dimensions.

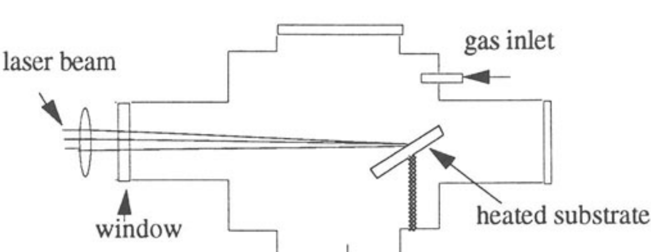

Figure 3 : Laser enhanced chemical vapour deposition.

المنارة للاستشارات
www.manaraa.com

- Hot Filament Chemical Vapour Deposition (HFCVD) [14,15]: A tungsten filament or foil is heated to 2000 to 2800K to dissociate gas mixtures containing from 0.2 to 2% CH_4 in H_2, at a pressure between 6000 Pa and atmospheric pressure (Fig.4). At these temperatures, the dissociation products are mainly radicals such as CH_2, CH_3, C_2H and CH, acetylene and atomic hydrogen as well as unreacted CH_4 and H_2 [16,17,18,19]. The filament is typically placed at a distance of 1cm from the surface to minimize thermalization and radical recombination. Filament of W, Ta, Mo and Re have been used successfully to produce diamond[20].

- Combustion Flame Technique [21,22,23]: based on the combustion of an acetylene oxygen mixture (ca. 1:1) at atmospheric pressure (Fig.5), this simple procedure leads to very high deposition rates. The combustion reaction produces reactive species which lead to diamond deposition on a water cooled substrate, placed between 1 and 5 mm away form the flame. Still some work has to be performed to assess the economic viability of the process.

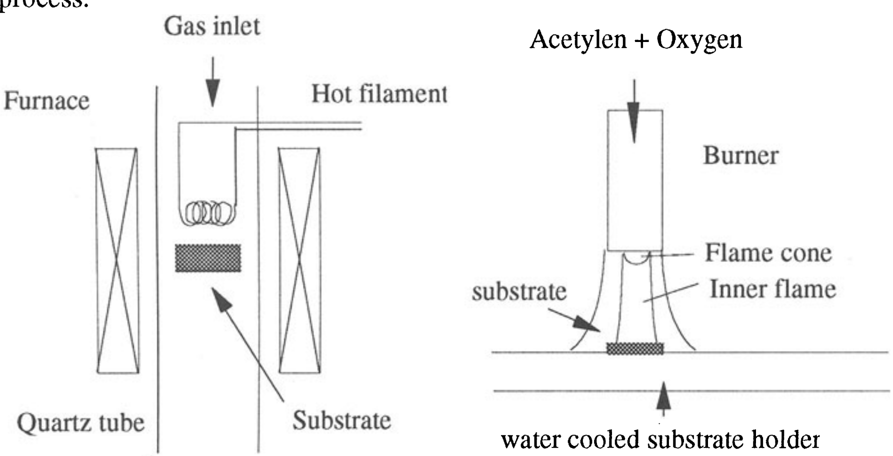

Figure 4 : Hot Filament CVD

Figure 5 : Hot flame technique

2.3.2. *Plasma Activated Chemical Vapour Deposition :* Instead of thermal energy, a plasma discharge in the gas mixture can be used to create the reactive species necessary to produce diamond. The systems the most used is Microwave Plasma Chemical Vapour Deposition (MPCVD) [25,26]. It generally consists in a tubular reactor into which the reactive gases (mainly carbon compounds and H_2) are introduced (Fig.6). In the microwave cavity, energetic electrons are produced, which lead to dissociation and excitation of the gases. The substrates are placed in the gas discharge itself, parallel or perpendicular to the gas flow. The microwave power is generally of the order of 100 to 800 W, and the pressures used can vary between 10 and 200 mbar. However, lower working pressures can be reached by working in the Electron Cyclotron Resonance (ECR) mode [27]. The advantage of working with MPCVD is that plasmas of high densities can be produced, which lead to a high concentration of reactive products, and hence relatively higher deposition rates.

Radio Frequency discharge (Fig. 7) can also be used for diamond deposition [28]. The experimental conditions are similar to the ones described above. However, due to the lower efficiency of the discharge for H_2 dissociation, this system is less adapted to the production of diamond films of good quality and deposition rates are lower than MPCVD.

المنارة للاستشارات
www.manaraa.com

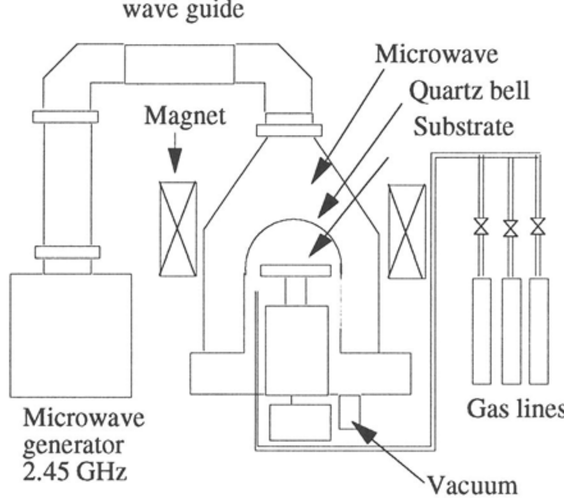

Figure 6: Microwave Plasma CVD and magnetic confinement

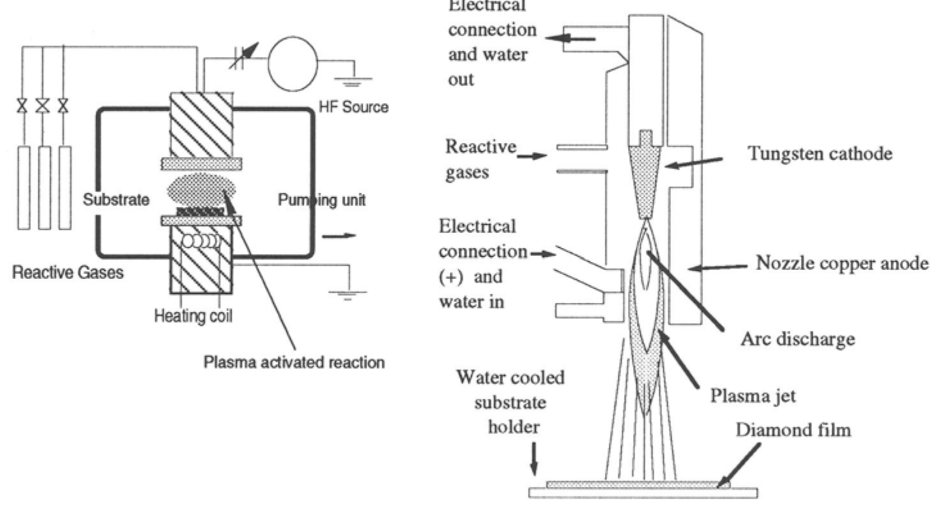

Figure 7 : Radio Frequency Plasma Assisted CVD

Figure 8 : DC plasma arc system

www.manaraa.com

DC, RF or MW plasma discharges working at atmospheric pressures have also been used [14,29]. These systems produce high deposition rates, between 20μm/h and 80μm/h [30]. However, because of the hydrodynamics of the gas phase in the reactor and on the substrate surface, the film thickness uniformity is difficult to control. A modification of the technique consists in creating the plasma at atmospheric pressure and expanding it in a chamber at low pressure[29,56]. The deposition uniformity is thus improved and the deposition rates are still several tens of μm per hour.

Hybrid techniques, combining one or several of the above mentioned, have been also reported, for instance Filament Assisted MPCVD [27], or Hot Filament and bias voltage, referred to as Electron Assisted CVD (EACVD) [31].

2.4. MECHANISMS OF DIAMOND DEPOSITION

The formation of diamond under metastable conditions is possible because of the small difference of free energies of formation of diamond and graphite (at 298K, the difference is only 0.03 eV per atom, only slightly greater than the thermal energy kT) and a finite probability of growth thus exists for the two allotropes in the kinetic controlled regime. Diamond CVD processes can be considered as a combination of gas phase chemical reactions with surface controlled kinetics.

2.4.1. *Different chemical reactions :* The atomic attachment mechanisms at the diamond gas interface are not clear in all details, and several possible models have been proposed recently for instance by Frenklach and Spear [34] and Tsuda et al [35]: Typically, one can consider several deposition reaction, leading to diamond (d-C), graphite (g-C), and different amorphous carbon and hydrogenated amorphous carbon (a-C, a-C:H), competing against each other as well as against etching reactions of these same compounds by the gas phase. They can be summarized in the following way [26,36]:

• Deposition of carbon compounds : Most of the reactions studied up to now are related to the atomic hydrogen- carbon radical reaction, which can be expressed as :

$$(C_xH_y, C) + (d\text{-}S) \xrightarrow{H} \text{a-C, g-C, a-C:H}$$

$$(C_xH_y, C) + (d\text{-}S) \xrightarrow{H} \text{d-C}$$

where (C_xH_y) indicates the mixture of hydrocarbon compounds in the gas phase and d-S a diamond formation site at the surface.

• Etching of the deposits in presence of atomic hydrogen :

$$\text{d-C} \xrightarrow{H} (d\text{-}S) + CH_4$$

$$\text{a-C, a-C:H, g-C} \xrightarrow{H} (d\text{-}S) + CH_4$$

For all these reactions, the role of atomic hydrogen is of primary importance, as will be explained in section 2.4.3.The proportions of the different components in the gas phase (H: 90-99%, CH_4: 0.5 to 5% and O_2 : 0 to 2%) play also an important role on the crystalline quality of the deposit, its microstructure and the deposition rate. In particular, the nature of the carbon source (CH_4, CO, ethanol, acetone...) has a direct influence on the concentration of precursors in the gas phase, which in turn determines the efficiency of the reaction. It seems however that diamond production based on H-O-C_xH_y components always proceeds through the same types of reactions: for instance, Cerio et al [32] showed that starting with CO for the carbon feed material, the chemistry involved in the gas phase

المنارة للاستشارات
www.manaraa.com

was similar to that which occurs when diamond is grown using hydrocarbons as carbon source gas, although deposition rates were lower.

Other types of reactions based on carbon-hydrogen-halogen reactions have also been reported[33], and it seems that low T (250°C-750°C) deposition is possible through different mechanisms which still have to be identified.

The difficulty of growing diamond comes from selecting the process parameters leading to the highest differences between deposition reactions of diamond and the corresponding etching reactions. The different mechanisms are detailed in the next sections but it must be kept in mind that the effects of all the parameters are coupled.

2.4.2. *Type of precursor :* The nature of the precursors determines the thermodynamic driving force of the reaction, which produces a modification in the nucleation density and thus on the film microstructure. Tsuda et al.[35] and Harris [38] have proposed growth mechanisms based on CH_3 radicals. Tsuda's model required the participation of CH_3^+, which is very unlikely in the case of HFCVD. On the other hand, Harris [38] correctly predicted the growth rates obtained in HFCVD (0.5 to 5µm/h) by proposing a CH_3 surface reaction and adjusting gas phase reaction rates. The principles of the reaction is the following : CH_3 is produced at the surface by a reaction of the type $CH_4 + H \rightarrow CH_3 + H_2$, where CH_3 and H are adsorbed on the surface. The surface diffusion of the species is impossible, because of the high adsorption energy and the high coverage of the sites, and CH_3 is adsorbed on a step at the surface, which creates a displacement of the interface. Free surface and step sites are created by a H abstraction mechanism which can be described in the following way :

$$H_g + H_{step} \rightarrow {}_{step} + H_2.$$

These reaction mechanisms were used by Goodwin [37] who successfully modelled and predicted the high deposition rates (20 to 200µm/h) of DC plasma and oxygen-acetylen torches processes.

Another mechanism based of the ethyl radical has also been proposed by Frenklach and Spear [34] and is still the object of discussions.

It seems however that both methyl and ethyl radicals can act as precursors for the different types of deposition techniques, but with different efficiencies : for instance, in the case of MPCVD, Harris and Martin[38], Harris and Weiner [39], or Martin and Hill [40,41] could grow diamond from acetylene and methane. From the deposition rates, they found that methane seemed the most probable species for diamond formation, and that the quality of the films obtained was better in that case. Martin and Hill [40,41] modelled the kinetics of the flow tube experiments and found that the reaction efficiencies for CH_3 and C_2H_2 were 10^{-3} and less than 10^{-5} respectively. Chu et al.[42], using carbon 13, could show that in presence of both reactants, diamond seemed to form more readily from methane than acetylene, without being able to rule out completely the latter hypothesis. Muranaka et al. [43] showed that by suppressing C_2H_2 in the gas phase, diamond growth rate was increased. In a DC plasma system, Plano et al.[44] showed that both the CH_3 radical concentration and the diamond deposition showed the same power law dependance on the initial CH_4 concentration.

As a conclusion, it can be said that different reactants can be used for diamond formation, depending in particular on the CVD reaction type and the atmosphere composition. What emerges is that diamond production has to be made preferably in such conditions that a large amount of CH_3 is formed, and that CH_3 is the most efficient species in the case of pure hydrocarbon-hydrogen atmosphere both for MPCVD and HFCVD. More work has to be performed to identify the surface mechanisms through which diamond crystals nucleate in order to get a better control on diamond nucleation.

www.manaraa.com

Furthermore, the use of halogens in the gas phase to promote new deposition mechanisms seems to be very promising.

2.4.3. *Role of H :* A lot of work has been devoted to the analysis of the role of atomic hydrogen. It was found that its presence in supersaturation was an absolute requisite for the formation of diamond, because of its high reactivity: for instance, the enthalpy of formation of CH_4 from graphite and H_2 is 50 to 80kcal/mole, and only 7 to 9 kcal/mole when the reaction is made with atomic hydrogen [45]. Its action is multiple and is related to sp^3 bond stabilization, to selective etching of g-C, a-C and a-C:H, and gas phase reactions which can be in certain cases promoted. This can be summarized as follows :

- H being very reactive, it adsorbs readily on the growing surface and terminates dangling bonds of the C atoms, preventing the formation of sp^2 bonds with the neighbouring atoms adsorbed at the surface.[46,47] Celii and Butler [17] have shown that this action was even more important than the promotion of reaction in the gas phase in the case of HFCVD between 1100 to 1300K.

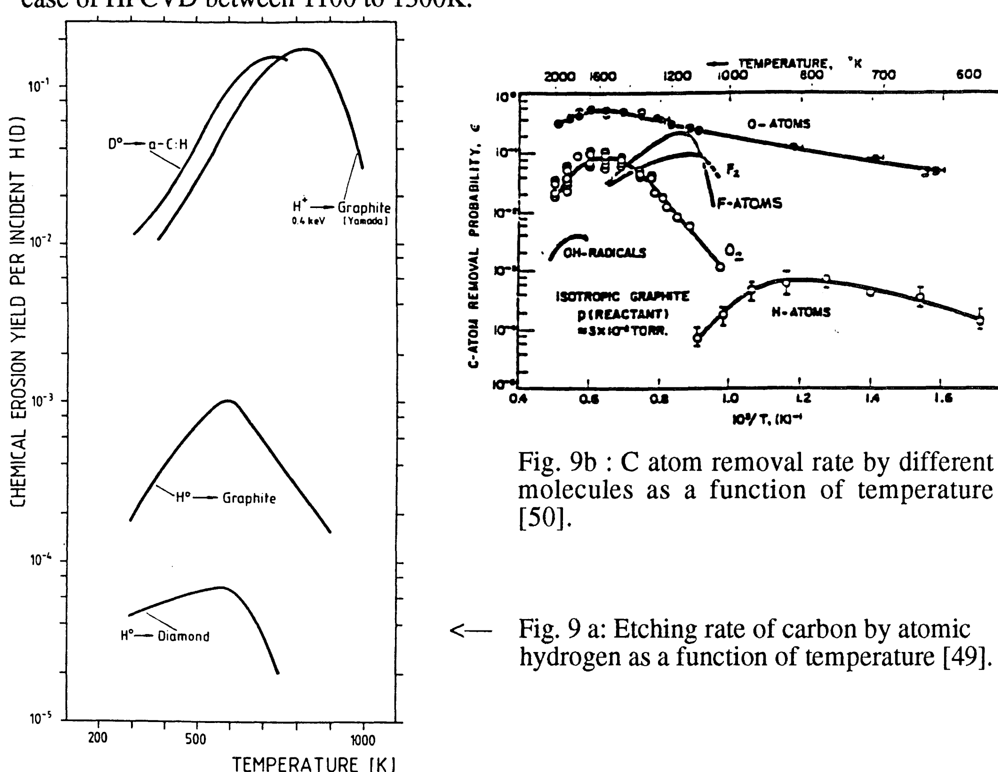

Fig. 9b : C atom removal rate by different molecules as a function of temperature [50].

<— Fig. 9 a: Etching rate of carbon by atomic hydrogen as a function of temperature [49].

- Based on thermodynamic calculations and on comparison with the results of the early work of the Russian teams, Frenklach and Spear [34] proposed that the role of H could be twofold : reaction with hydrocarbon molecules to form C_2H_2 (supposed to be the most important precursor of growth), and activation of the surface by H abstraction, following the reaction :

$$C_S\text{–}H + H \xrightarrow{H} C_S^* + H_2$$

المنارة للاستشارات
www.manaraa.com

the activated species on surface acting as a preferential site for precursor adsorption.

- In a very interesting paper on MPCVD with a $CO/H_2/He$ atmosphere, Muranaka et al.[48] showed that without the presence of H atoms, C and C_2 radicals were formed in the gas phase, and only sootlike carbon was deposited. H addition to the gas phase was found to enhance diamond growth by suppressing the formation of these C and C_2 radicals, which inhibited diamond growth by blocking the nucleation sites. Moreover, it was found that atomic hydrogen in the ground state enhanced diamond growth by removing the amorphous carbon deposits (selective etching), while electronically excited hydrogen was found to combine to a-C to form a-C:H for which the etching reaction was slower. However, it is not certain that these results can be extended to other atmosphere compositions and other techniques.

- The role of H as an etching agent has been studied by Vietzke et al.[49] and Rosner [50] (see Fig. 9a and b). It is found that the etching rate of diamond is 1 order of magnitude smaller than graphite, and 3 orders of magnitude smaller than a-C:H. Mucha et al. [26] also showed the role of selective etchant of a-C and a-C:H by atomic hydrogen . The ratio H/Hydrocarbon concentration in the reactants has also a strong effect on the microstructure of the film, as shown on Fig. 10 [23].

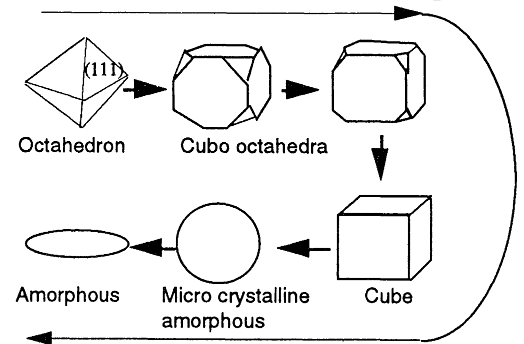

Figure 10 : Effect of H/Hydrocarbon on diamond microstructure.

2.4.4. *Role of Oxygen :* It has been shown very early that small additions of oxygen to the gas discharge had a beneficial effect on the deposition of diamond [51,52]: the deposition rates obtained were higher, the quality of diamond films measured by Raman spectroscopy was improved, and oxygen generally increases the parameter domain in which good diamond crystals can be obtained (see Fig.11 a and b). However, oxygen also increases the etching reaction rates and a large quantity of O (larger than 1 to 5% approximately depending on the process) suppresses completely the diamond deposition.

The role of oxygen can be attributed to :

- an increase in the H concentration, which selectively etches a-C or g-C and decreases the C_2H_2 concentration leading to the effects explained above [36,40] . However, using thermodynamic calculations, Mucha et al. [26] showed this effect can explain only a factor of 2 in improvement, and not for the factor of about 10 or more as generally obtained experimentally.

- an acceleration of the etching reactions of a-C and g-C by H, or selective etching by O of non diamond carbon [26].

www.manaraa.com

- saturation of the reactor walls by O adsorption, thus preventing the wall recombination of H and increasing its concentration in the gas phase [26,40].

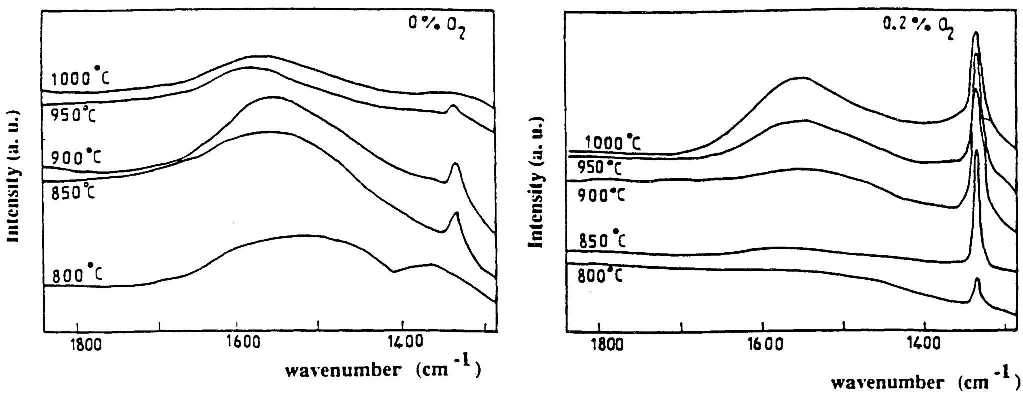

Figure 11 a: Evolution of the Raman spectra vs temperature with and without oxygen in an HFCVD system (30mbar, 1.5%CH4, 120W) [57].

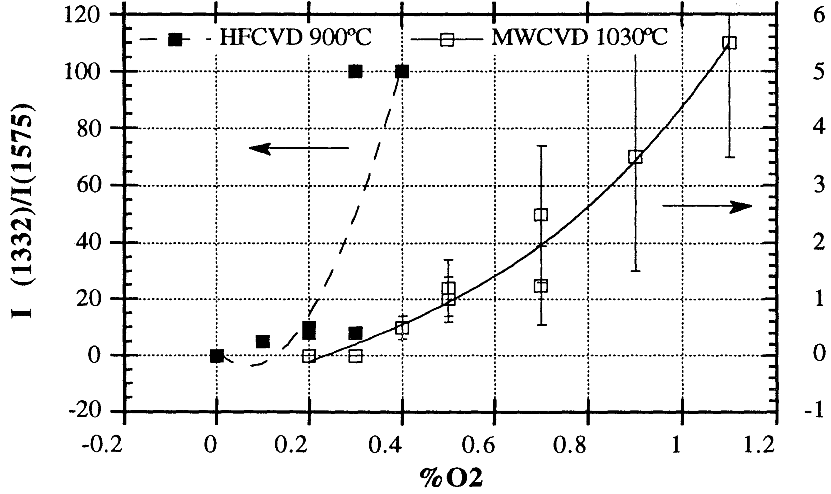

Figure 11b : Ratio of the Raman diamond peak to the graphite band height as a function of O_2 concentration for MPCVD (400W, 30mbar, 100sccmn^{-1}) and HFCVD (120W, 30mbar, 100scc mn^{-1}) [57].

المنارة للاستشارات
www.manaraa.com

- formation of CO bonds on the diamond surface, which react with H_2 to give H, increasing the H concentration [26].

It is probable that several of these mechanisms are active simultaneously, with relative importances depending on the deposition technique used.

2.4.5. *Kinetics of diamond growth :* Kinetics of diamond growth depends strongly on the process used, as well as the gas composition: several orders of magnitude of difference between the deposition rates for different processes (e.g HFCVD and Oxygen Acetylen torch) have already been mentioned above.

The process temperature has a multiple and complex effect on the reaction rates of the different chemical reactions in the gas phase, as well as on the transport kinetics to the surface; the combination of these different effects changes in a very complex way the deposition and etching reaction rates described above, and thus the diamond deposition kinetics. For instance, Kweon et al.[53] studied the kinetics of diamond deposition with HFCVD form a mixture of CH_4 and H_2. They showed the variation of growth rate with temperature shows a distinct maximum around 900 to 950°C, this maximum being shifted to somewhat higher temperatures when the methane concentration is increased. Similar results were obtained with different oxygen composition, as shown on Fig. 12 [56,57]. This behaviour can be attributed to the decrease of H supersaturation with increasing temperatures resulting in changes in the competition between growth and etching processes. Kweon et al. also showed that in their operating conditions, the growth rate of diamond could be described by the rate constant of a first order reaction, and that the deposition is controlled by surface reaction for T lower than 1100K, with an activation energy of 11 kcal/mole. They suggested that the controlling step for this reaction was H abstraction, in agreement with Frenklach and Spear[34] . At higher temperatures, they found that the reaction was controlled by transport in the gas phase with an activation energy of 3.8 kcal/mol, confirmed by the results of Rau and Pitch [54].

Muranaka et al.[36,45] studied the kinetics of diamond deposition in the case of MPCVD from CO/H_2 and $CO/O_2/H_2$ mixture between 600 and 1000K. Their deposition rates were much larger (up to one order of magnitude) than CH_4/O_2 and $CH_4/O_2/H_2$ systems. The deposition rates followed an Arrhenius behaviour, with activation energies of 5.2 and 7.0kcal/mol for CO/H_2 and $CO/O_2/H_2$ respectively, lower than the value reported above. At lower temperatures (403K), the Arrhenius law was not followed in the two systems, indicating a probable change of mechanism in the deposition conditions, as the deposition of a mixture of diamond and graphitic phase. The difference of the activation energies can be attributed to the very different conditions (MPCVD and HFCVD, as well as gas compositions) between the two sets of experiments.

Temperature has also an effect on the preferential growth of crystalline orientations : for instance, Muranaka [36] reported the preferential diamond growth of (001) direction at high temperature and (111) at low temperature (400-750°C) in MPCVD of $CO/H_2/O_2$ gas mixtures.

2.4.6 *Nucleation density :* The microstructure of the films depends on the nucleation density and the deposition rate. The nucleation density depends on the type of substrate, on its preparation, on the temperature and on the gas composition. Generally, for given experimental conditions, the nucleation density increases strongly when temperature decreases [55,56,57], as shown on Fig.13.

For instance, Muranaka et al.[36,48] studied the nucleation densities in MPCVD. The nucleation densities observed between 690 and 995K followed also an Arrhenius law, with an activation energy of 8.8kcal/mol, close to the value for diamond growth obtained before suggesting the intervention of mechanisms similar of those of deposition.

www.manaraa.com

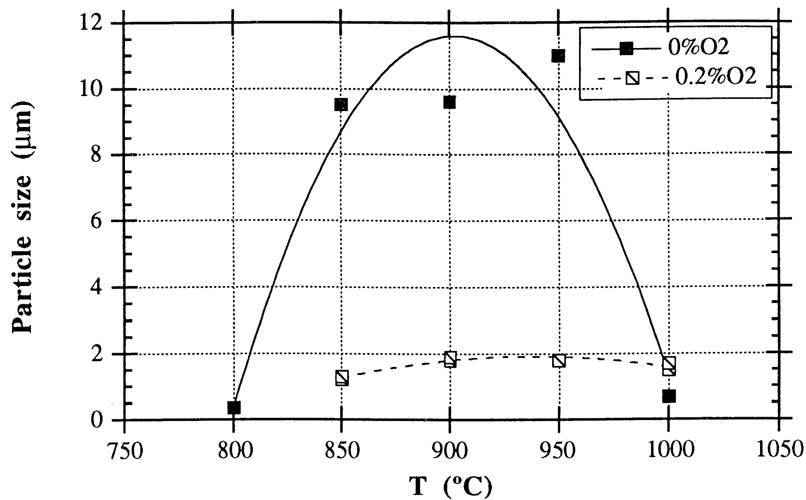

Figure 12 : Average size of diamond particles vs T for 2 oxygen concentrations in HFCVD (120W, 30mbar, 100sccm, 1.5%CH_4) [57].

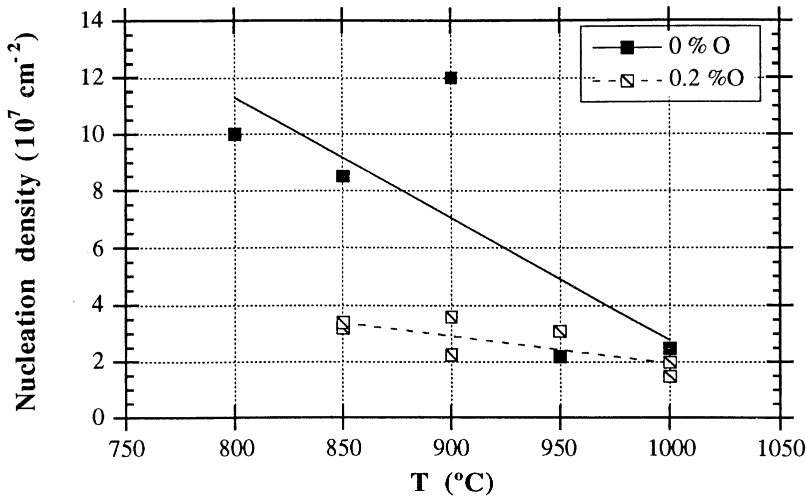

Figure 13 : Nucleation density as a function of T for 2 oxygen concentration with HFCVD (120W, 30mbar, 100sccm, 1.5%CH_4) [57].

المنارة للاستشارات
www.manaraa.com

Chang et al.[52] also studied the effect of pressure on nucleation density in Filament Assisted MPCVD with $CH_4/H_2/O_2$ mixtures between 850 and 950K. They showed that the nucleation density decreases when increasing the pressure up to 10 Torr. Beyond this value, the tendency was reversed.

2.4.7. *Effect of the discharge and presence of charged particles (e- and ions) :* The efficiency of the discharge, and particularly the efficiency of creation of atomic hydrogen determines the maximum hydrocarbon source concentration for which crystalline diamond is obtained. However, it has been demonstrated that energetic ions have a detrimental effect on diamond formation, the bombardment destroying the local order of crystal [3,62]. On the other hand, Sawabe and Inuzuka [31] have shown the effect of electron bombardment during diamond growth by HFCVD. They reported that the growth rate of diamond was accelerated by concomitant electron bombardment of the surface. It was also found that when a negative voltage was applied to the substrate holder in MPCVD, diamond and SiC were grown. On the other hand, if a positive voltage was applied, the growth rate of diamond was accelerated and no SiC was deposited. It was suggested from these results that electrons promote the formation of atomic hydrogen, or hinder its recombination on the substrate surface [45]. Threshold energies to produce atomic hydrogen and its ions by $e^- \rightarrow H_2$ collision is 8.5eV for $H_2 \rightarrow 2H$, 13.5 eV for $H \rightarrow H^+$, and 15.4eV for $H_2 \rightarrow H_2^+$. It was then suggested that the optimum energy for electrons in EACVD would be between 8.5 and 13.5eV [45].

2.5 EFFECT OF SUBSTRATE AND SURFACE PREPARATION

The strong influence of surface preparation on diamond deposition has been demonstrated. Generally, the substrates are scratched or abraded with a diamond paste or treated in an ultrasonic bath with diamond particles suspension in alcohol [58]. This preparation method increases the nucleation rate, and can decrease the deposit quality [58] although no satisfactory explanation was found. Recently, Dennig and Stevenson [59] have investigated the effect of surface topography on the nucleation behaviour of diamond films. The Si surfaces were submitted to a controlled etching, without any polishing. It was found that the initial presence of diamond crystallite was not necessary for nucleation and that diamond growth occurred preferentially on locations that protrude from the surface, such as edges or apices, as opposed to sharp valleys or flat regions [60]. Scanning tunneling microscopy results seem to support this observation [61]. Several explanations were proposed, namely the minimizing of interfacial energy by forming diamond nuclei on sharp convex surfaces, the presence of more dangling bonds at sharp corners which promotes the chemisorption of nucleating species, and larger reactant fluxes on these sites. However, the nucleation and growth rates were not reported, and quantitative comparison with the conventional scratching technique was not possible.

More recently, B.R. Stoner et al.[62] showed that nucleation of diamond on silicon was greatly enhanced by substrate biasing at the beginning of growth. Moreover, they could show that the deposited carbon at the early stage of growth was converted to amorphous silicon carbide by reaction with the substrate under bombardment. For a critical thickness of a-SiC, carbon clusters were formed on which dismond nuclei could grow.

The influence of the nature of substrate has been studied by Singh et al.[63]. It was found that deposition rate depends on the ability of the substrates to form carbides, and on the diffusion rate of carbon in the material. For instance, for high carbon solubility and

www.manaraa.com

high temperature, the diffusion of carbon in the material consumes all the reactive species on the surface and prevents diamond growth.

2.6 REMARKS :

An interesting observation is that the techniques used for diamond deposition are very different. In the Thermally Assisted methods, such as HFCVD, thermal plasmas, and DC plasma jet, the temperature of the neutral species and the electrons are the same, and much higher than the substrate temperature. In Microwave CVD and DC glow discharges, the electron temperature is much greater than the neutral species and substrate temperature (typically 10000 to 20000K against about 1000K). However, both techniques produce diamond although the thermal methods can achieve the highest rates.

Another interesting observation of the same nature was made by Bachmann et al. [64] who showed that low pressure diamond synthesis was observed only within a well defined composition field of the C-H-O phase diagram. This observation was made from several publications describing work performed with different temperatures and processes, and starting from different precursor materials (CH_4-H_2, C_2H_2-H_2, CO-H_2, CH_3COCH_3-O_2....). Surprisingly, all these experiments show this common feature, although all of the experimental parameters (T, p, flow rates, plasma density, and so on) which we have shown have a strong influence on diamond production and growth, are not taken into account in this simple phase diagram. However, this work could allow prediction of gas phase composition and starting materials suitable for diamond production.

3. Diamond-like carbon (DLC)

3.1. INTRODUCTION

A large research work has been carried out recently to produce carbon films with good mechanical and optical properties and high resistivity with PVD or CVD techniques. These films have unusual and interesting properties : they are typically harder, more dense and resistant to chemical reactions than polymers. Owing to the large variety of production methods of these films, leading to large spectrum of properties, Angus [14] has proposed to classify them following their density in gram-atom of carbon per cm^3 and H content, which defines thus 2 domains of existence of diamond-like carbon corresponding to a-C and a-C:H, as shown on Fig.14 [14].

3.2. DEPOSITION TECHNIQUES

The deposition techniques for producing diamond-like carbon are divided into Ion Beam Techniques, Plasma Deposition Techniques and Laser ablation. In all the deposition techniques, carbon is condensed on a surface from a carbon source, under ion beam assistance. The carbon source can be either a gas or a solid target, each one leading to a different type of composition of the film and impurity content, as mentioned in Table 8.

www.manaraa.com

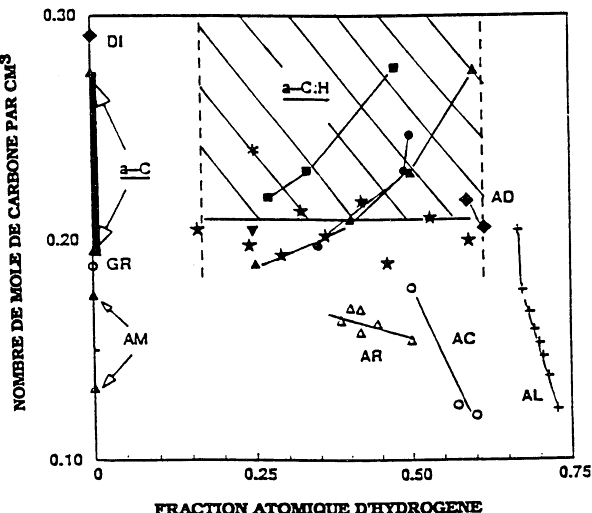

Figure 14 : Classification of carbon compounds with H content (abcissa) and carbon atom density[14]. DI=Diamond, GR=graphite, AD = adamantanes, AL=alcanes, AR = polynuclear aromatics, AC=oligomers of acetylene, AM = low density amorphous carbon.

The common characteristics of all these processes and the main difference with diamond deposition is the presence of energetic species (10 to 500eV) which collide with the surface atoms of the film during the growth: this bombardment has a strong effect on the properties of the film [56], such as hardness, stress and density [65,66] as will be detailed below. For most of the techniques presented above like CVD or bias sputtering, the bombardment conditions are not independently controlled during the process, and it is hard to determine what was the effect of bombardment alone.

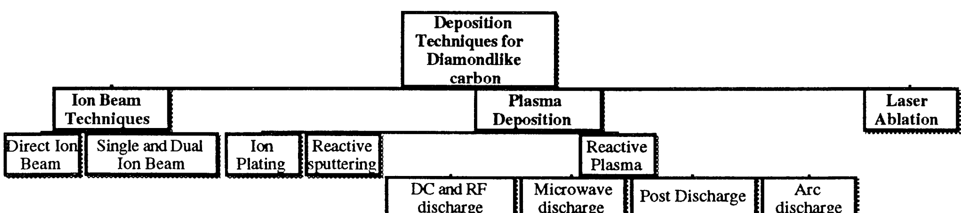

Figure 15 : Methods of diamond-like carbon deposition

www.manaraa.com

	Processes from hydrocarbon gases				Processes from solid C		
	PACVD (DC or RF)	Hydrocarb. Ion Beam	Ion Plating	Arc Discharge	DC or RF Sputtering	Ion Beam Sputtering	Laser Ablation
Pressure (Torr)	0.01-0.5	10^{-7} to 10^{-5}	0.1	0.75	< 5 10^{-3}	< 10^{-3}	< 10^{-6}
Gases	CH_4, C_2H_2 C_6H_6 C_4H_{10}	CH_4, C_2H_2 C_4H_{10}/Ar CO, CO_2	C_6H_6		Ar, Ar + H_2 Ar + CH_4	Ar Ar + H_2	-
Solid target	-	-	-	-	Graphite	Graphite	Graphite
Impurity source	Gas React. walls	Filament React. walls Gas	Grid React. walls Gas	Gas React. walls	Gas React. walls Target	Gas React. walls Target	powder React. walls

Table 6: Different DLC deposition techniques and their characteristics[56].

On the other hand, in DIBS and IBAM techniques (Fig. 16 and 17) the bombardment source is completely independent from the deposition process and a very fine control of the effect of bombardment can be analyzed as explained in the next section. In the following, we will restrict the discussion to non hydrogenated diamond like carbon (a-C), although most of the results are similar for a-C:H. For more information of other types of DLC, references like for instance Angus et al. [3,14,67] and Robertson [9] could be consulted.

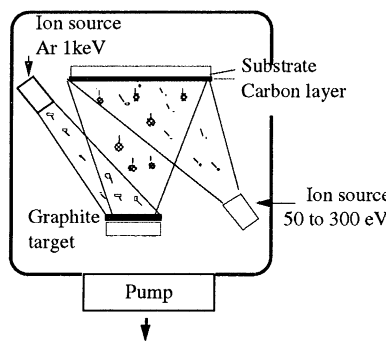

Figure 16 : Dual Ion Beam Sputtering: one beam is used for sputtering the C target, and the other for assistance.

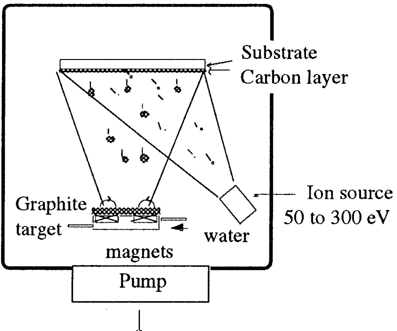

Figure 17 : Ion Beam Assisted Deposition. The ion beam is used for deposition assistance.

المنارة للاستشارات
www.manaraa.com

3.4. MECHANISM OF a-C DEPOSITION

It is well established that low energy ion bombardment of a growing film leads to dramatic changes in the properties of the PVD and CVD coatings [68,69]. In the case of carbon deposition, the bombardment under controlled conditions of the film can promote the diamond-like character of the deposited layer [69,70]. Different models have been proposed to explain this phenomenon[72,73]. For instance, Weissmantel [75] has proposed a model in which a pressure front due to the local heating by the cascade is assumed to favour the higher density sp^3 structure. The preferential sputtering of sp^2 sites has also been proposed[73]. Another idea suggested by Lifshitz et al.[72] was the preferential displacement of atoms depending on their bond type: the energy of the bonds between diamond atoms being greater than in graphite, it was suggested that a preferential displacement of sp^2 atoms occurred in a layer under bombardment, leading to an increased sp^3 concentration. The preferential displacement model was confirmed by Rossi and André [65] by comparison of Monte Carlo calculations and density measurements on carbon films made by IBAM and DIBS. For instance Fig. 18 shows the evolution of density of diamond like films made by DIBS (at 200eV and 10μA/cm^2) which clearly shows the changes in density of the carbon film with the ion mass. These results are directly related to ballistic effects since the densification is proportional to the energy transfer during collisions as shown in Fig.19. A maximum of density is also found for a given ion with energy, the position and the value of which depend on ion/atom fluxes ratio and ion mass (Fig. 20).

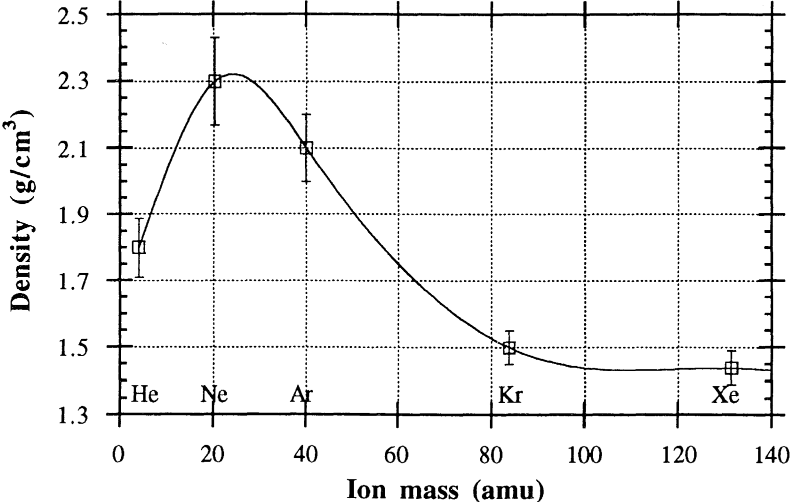

Figure 18 : Evolution of density of a C film made by DIBS vs the ion mass (200 eV and 10μA/cm^2)[65].

المنارة للاستشارات
www.manaraa.com

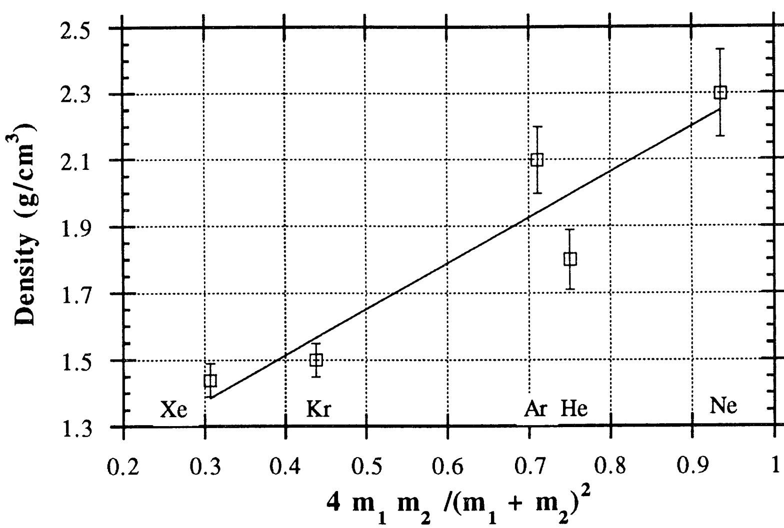

Figure 19 : Evolution of the density of DIBS film as a function of ballistic factor $K=4m_1m_2/(m_1+m_2)^2$, where m_1 and m_2 are the ion and atom mass.(for a constant energy 200eV and current)[65].

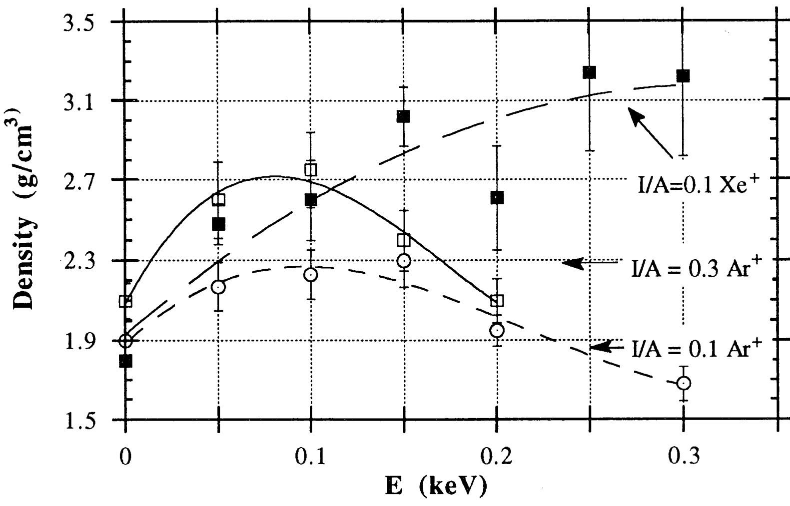

Figure 20: Evolution of the C density vs ion energy and ion flux for Ar and Xe.[65]

المنارة للاستشارات
www.manaraa.com

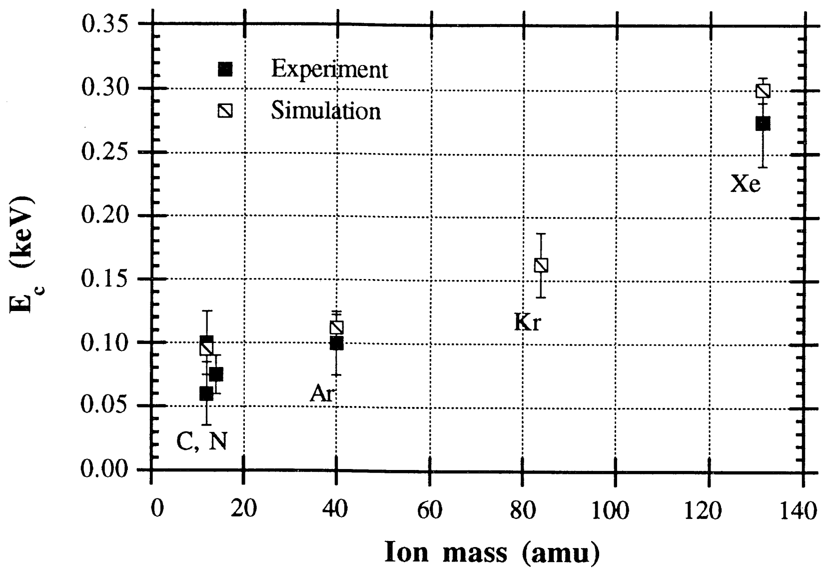

Figure 21: Optimum densification energy for DLC as a function of ion mass [65].

This result can be interpreted by the fact that below a given ion energy, only the carbon atoms linked with sp^2 bonds are displaced. The displacements produce rearrangements of the carbon atoms which can be linked in sp^3, thus increasing the film density. Beyond a critical collision energy, sp^3 atoms are displaced and the bonding changed to sp^2, thus decreasing the density. The critical collision energy depends on the ion mass, as shown in Fig.21[65] and is correctly predicted by the Monte Carlo simulation of preferential displacement. However, other calculations made by Möller [74] have shown that preferential displacement alone could not explain the observed changes in density. This result still has to be confirmed, but a possible explanation could be linked to the changes in defect size distribution due to bombardment.

Fig.22 shows the stress build up in the diamond-like films as a function of ion energy and flux [76] for Ar ions. It can be seen that stress increases rapidly with ion bombardment but that the decrease in density at higher energies is not followed by a decrease in residual stress. In the case where mechanical applications of a-C are considered, a trade-off between density and stress has to be found.

3.3. STRUCTURE OF a-C AND A-C:H

The physical properties of DLC films depend on the method of preparation. For a given method, the ratio sp^3/sp^2 can be affected by the presence of H in the films. Several models of structures for diamond-like carbon have been proposed: Robertson [77] proposed a model based on graphite inclusions in a sp^3 hybridized atoms network. The network

www.manaraa.com

would be responsible for the mechanical properties of the layer, as the size of sp^2 aggregates would be responsible for optical and electrical properties. Conversely, Collins et al. [78] explains the high densities of a-C obtained in laser ablation with a structural model consisting of sp^3 hybridized atoms aggregates (75% in volume) linked to each other by sp^2 and sp^3 atoms. Galli et al. [79] using molecular dynamics calculations showed that the a-C structure was made up of 85% sp^2 atoms and sp^3 clusters. Finally, using Raman spectrometry and HRTEM, André [71] found that a-C made by Ion Beam Assisted methods consisted of graphite microcrystals linked by sp^3 atoms: the increase of density observed with bombardment was correlated with decrease in graphite aggregates sizes.

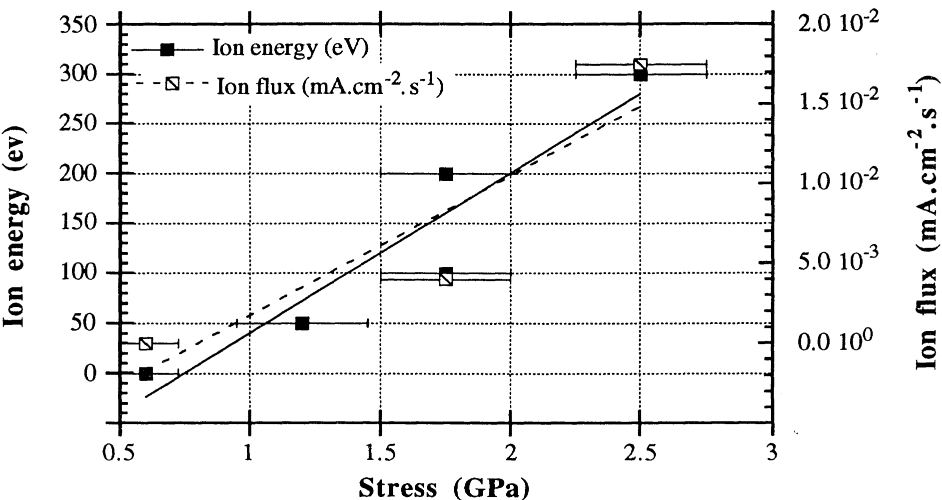

Figure 22 : Compressive stress in the film as a function of Ar ion energy (constant flux of 0.01 $mA.cm^{-2}s^{-1}$) and ion flux (energy =100eV) [66].

DLC films can be very hard, and values of the order of 30 to 40 GPa have been reported[70,71], see Fig. 23. The diamond-like coatings have a low friction coefficient (0.02 to 0.2), increasing with humidity, and their wear resistance is quite good [71,80]. The DLC films generally absorb in the visible but have good transmission in the IR region and can be used as IR antireflection coatings on germanium optics and Si solar cells. DLC has a high electrical resistivity, and is chemically stable.

3.4 Applications of Diamond-like Carbon

We have seen in the first sections that there is a considerable interest in growing pure diamond films for mechanical or optical applications [80]. However, many of the coatings requirements can already be met using DLC with even some advantages that diamond films do not have yet (low surface roughness for instance). This leads to many potential applications as friction and wear resistant coatings, antireflection coatings on Ge [81,82],

المنارة للاستشارات
www.manaraa.com

protective coatings on ZnS windows, on aluminium mirrors or for photothermal conversion of solar energy[81]. Biomedical applications should be a domain of application of DLC films for several reasons : good compatibility with living tissues, low friction coefficient and low wear rate : applications like anti clogging for veins or parts of artificial hearts, or anti wear coatings for protheses. Currently, the main market for DLC films is related to IR windows, but the new markets mentioned above should develop rapidly in the near future.

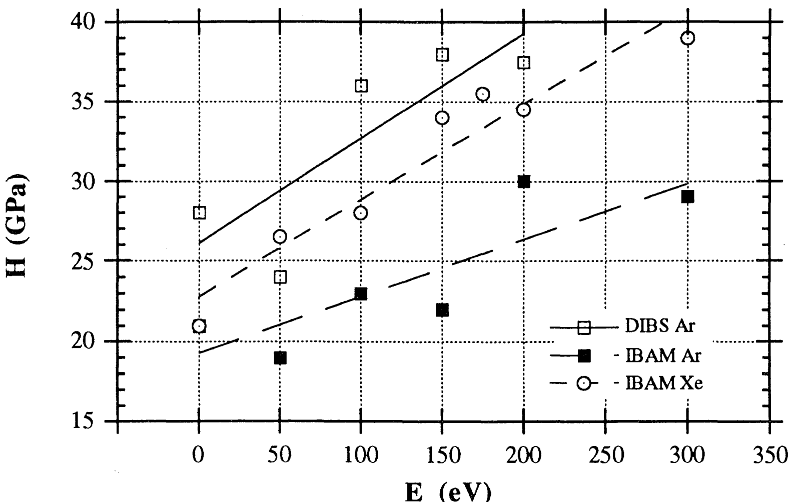

Fig.23 : Hardness of DLC films as a function of ion energy for DIBS and IBAM films under Xe and Ar ion assistance [71].

4 Conclusions

Although CVD diamond devices are already industrially produced today, the important role of these films for a large number of applications in mechanics, optics and electronics still remain a challenge.The nucleation density, the growth rate, the adhesion to the substrate and the surface roughness must be improved. The quality, the microstructure and the properties of the diamond films depend on the substrate, its preparation, the first stage of deposition and the plasma characteristics. Further research still has to be performed to optimize the deposition conditions in order to make diamond coatings industrially more attractive.

Applications of diamond-like carbon, although not as important as those of diamond, are already on the market, for instance for IR windows. The technological problems to be solved are related to improvement of adhesion and internal stress control. It is expected that DLC layers will be used intensively for applications where optical properties combined

المنارة للاستشارات
www.manaraa.com

with a low friction coefficient, smoothness and wear resistance make them the material of choice in some industrial applications already mentioned.

Acknowledgements : Scientific discussions with A. Gicquel are gratefully acknowledged.

References :

[1] Eversole W.G. , US Patents 3030187 et 3030188 (1962)
[2] Derjaguin B.V. and Fedoseev D.V. , Russ. Chem. Rev. **39**, 783 (1970); Derjaguin B.V. et al. J. Cryst. Growth **2**, 380 (1968); Derjaguin B.V. and Fedoseev D.V. , Russ. Chem. Rev. **39**, 783 (1970); Derjaguin B.V. and Fedoseev D.V. , Scientific America, 102,233, (1975).
[3] Matsumoto S. , Sato Y. , Tsutsumi M. and Setaka N., J. Mater. Sci. **17**, (1982), 3106
[4] Kobayashi K. et al. J. Appl. Phys. **59**, 3 (1986) 910
[5] Kikuchi N. et al. Mater. Sci. Eng. A105, (1988), 525
[6] Hirose Y. , Terasawa Y. ; Jap. J. Appl. Phys. 25 (1986) 519
[7] Spear K.E. , Phelps A.W. and White W.B. J. Mater. Res. 5 (1990) 2277
[8] Howard W. , Huang D. , Yuan J. , Frenklach M., Spear K.E. , Koba R. and Phelps A.W. , J. Appl. Phys. **68** (1990) 1247
[9] Robertson J. Surf. Coat. Technol. 50 (1992) 185
[10] Lux B. and Haubner R. , 12th Int. Plansee Seminar, Reute, Austria May 1989
[11] Yoshikawa M. , Diamond Films and Technology, 1 (1991) 1
[12] Narutaki N. , Ususki H. , Itoh T. and Yamane Y. , Surf. Eng. 7 (1991) 305
[13] Angus J.C Int. Conf. on Diamond films '90. Crans Montana (1990)
[14] Angus J.C. and Hayman C.C., Science 241 (1988) 913
[15] Kawato T. and Kondo K. Jpn. J. Appl. Phys. **26** (1987) 1429
[16] Celii F.G. and Butler J.E. Appl. Phys. Lett. **54** (1989) 1031
[17] Celii F.G. and Butler J.E. , J. Appl. Phys. **71** (1992) 2877
[18] Harris S.J. , Weiner A.M. and Perry T.A , Appl. Phys. Lett. **53** (1988) 1605
[19] Celii F.G. , Pehrsson P.E. , Wang H.-t and Butler J.E. , Appl. Phys. Lett. **52** (1988) 2043
[20] Sommer M. and Smith F.W., J. Mater. Res. 5 (1990) 2433
[21] Matsui Y. , Yabe H. and Hirose Y. Jap. J. Appl. Phys. **29**,8 (1990) 1552
[22] Morrison P. W. , Cosgrove J.E. and Solomon P.R. , Appl. Phys. Lett. **60** (1992) 565
[23] Ravi K.V. , Koch C.A. , Hu H.S. and Joshi, A. J. Mater. Res. **5**, 11 (1990) 2356
[24] K. Kitaham, K. Kirata, H. Nakamatsu, S. Kawai, Appl. Phys. Lett. **49** (1986) 634
[25] Chang C.P. , Flamm D.L. , Ibotson D.E., Mucha J.A. J. Appl. Phys. **63**, 5, (1998)
[26] Mucha J.A. , Flamm D.L. and Ibbotson D.E. J. Appl. Phys. **65**, 9, (1989) 3448
[27] Chang J.J. , Mantei T.D. , Vuppuladhadium R. and Jackson H.E. , Appl. Phys. Lett. **59**, 10 (1991) 1170
[28] Rudder R.A. , Hudson G.C. , Posthill J.B. , Thomas R.E. , Hendry R.C. , D.P.Malta and Markunas R. J. , Appl. Phys. Lett. **60**, 3 (1992) 329
[29] Mitsuda Y. , Yoshida T. and Akashi K, Rev. Sci. Instrum. 60(1989) 249. See also Smith D.K., Sevillano E., Besen M., Berkman V., and Bourget L. Diamond and Related Materials 1 91992) 814

المنارة للاستشارات
www.manaraa.com

[30] Suzuki H. , Sawabe A. , Yasuda H. and Inuzuka T. , Appl. Phys. Lett. **50** (1987) 728
[31] Sawabe A. and Inuzuka T. I, Appl. Phys. Lett. **46** (1985) 146
[32] Cerio F.M. , Weimer W.A. and Johnson C.E. J. Mater. Res. 7 (1992) 1195
[33] Patterson D.E. , Chu C.J. , Bai B.J., Xiao Z.L. , Komplin N.J. , Hauge R.H. and Magrave J.L., Diamond and Related Materials 1 (1992) 768
[34] Frenklach M. and Spear K.E , J. Mater. Res. **3** (1988) 133
[35] Tsuda M. , Naajima M. and Okinawa S. s, J. Am. Chem. Soc. **108**(1986) 5780
[36] Muranaka Y. , Yamashita H. and Miyadera H. , J. Appl. Phys. **69** (1989) 8145
[37] Goodwin D.G. , Appl. Phys. Lett. **59**, (1991), 277
[38] Harris S.J. and Martin L. R. , J. Mater. Res. **5** (1990) 2313
[39] Harris S.J. and Weiner A. , J. Appl. Phys. **67** (1990) 6520
[40] Martin L.R. and Hill M.W. , Appl. Phys. Lett.**55**, (1989) 2248
[41] Martin L.R. and Hill M.W. , J. Mater. Sci. Lett. **9**, (1990) 621
[42] Chu C.J. , M. P. D'Evelyn, R. H. Hauge and J.L. Margrave, J. Mater. Res. **5** (1990) 2405
[43] Muranaka Y. , Yamashita H. and Miyadera H. , Surf. Coat. Techno. **47** (1991) 1
[44] Plano L.S. , Stevenson D.A , and Carruthers J.R. , in Proceedings of the Second International Conference on New Diamond Science and Technology, ed. R. Messier and J. Glass (Materials Research Society, Pittsburg, PA, 1991) p257.
[45] Setaka N. , J. Mater. Res. **4**, (1989) 664
[46] Lander J.J. and Morrison J. , Surf. Sci.**4**, (1966) 241
[47] Machlin E.S. , J. Mater. Res.**3** (1988) 958
[48] Muranaka Y. , Yamashita H. , Sato V, and Miyadera H. , J. Appl. Phys. **67** (1990) 6247
[49] Vietzke E. , Philipps V. , Flaskamp K. , Koidl P. and Wild W. , Surf. Coat. Technol. 47 (1991) 156
[50] Rosner D.E. , Annual Review of Materials Science, 2, (1972) 573
[51] Liou Y. , Inspektor A. , Weimer R. , Knight D. and Messier R. , J. Mater. Res. **5** (1990) 2305
[52] Chang J.J. , Mantei T.D. , Vuppuladhadium R. and Jackson H.E. , J. Appl. Phys. **71** (1992) 2918
[53] Kweon D.W. , Lee J.Y. and Kim D. J. Appl. Phys.**69** (1991) 8329
[54] Rau H. and Picht F. , J. Mater. Res. **7** (1992) 934
[55] Harker A. B. and DeNatale J.F., J. Mater. Res. **5** (1990) 818
[56] Gicquel A. , "Plasma and Thin Films Growth", Course 3rd Int. Symp. on Trends and New Applications in Thin Films, part 2, ed. Société Française du Vide, Strasbourg (1991).
[57] Gicquel. A., Heau C. , Fabre D. and Perriere J., Diamond and Related Materials 1 (1992) 776
[58] Gicquel A., Anger E., Fabre D., Le Vide Les Couches Minces, Suppl. n°261 (1992) 289
[59] Dennig P.A. and Stevenson D.A. J. Appl. Phys. Lett. **59** (1991) 1562
[60] Ramesham R. and Ellis C., J. Mater. Res. 7, (1992) 1189
[61] Turner K.F. , Stoner B.R. , Bergman L. , Glass J.T. and Nemanich R.J. , J. Appl. Phys. **69** (1991) 6400
[62] Stoner, B.R., Ma G.-H. M., Wolter S.D. and Glass J.T., Phys. Rev. B 45 (1992) 11067
[63] Singh B., Mesker O.R. , Levine A.W. and Arie Y., Appl. Phys. Lett. **52** (1988) 1658

المنارة للاستشارات
www.manaraa.com

[64] Bachmann P.K. , Leers D. and Lydtin H., Diamond and Related Materials, 1 (1991),1
[65] Rossi F. and André B. Jpn. J. Appl. Phys. Part 1,Vol 31 (1992) 15.
[66] André B., Rossi F. and H. Dunlop, Diamond and Related Materials 1 (1992) 307
[67] Angus J.C. , Koidl P. and Domitz S. in J. Mort and F. Jansen (eds) Plasma Deposited Thin Films, CRC Press, Boca Raton FL 1986
[68] Martin P.J. J. Mat. Sci 21 (1986) 1
[69] Harper J.M.E. , Cuomo J.J. , Gambino R.J. and Kauffman H.R. in Ion Bombardment Modification of Surfaces. Ion Beam Modification of Materials. O. Aucellio and R. Kelly Ed. Elsevier 1984, 127
[70] Savvides N. , Thin Solid Films 163 (1988) 13
[71] André B. , PhD thesis Grenoble (1991)
[72] Lifshitz Y. , Kasi S.R. , Rabalais J.W. Phys. Rev. Lett. 62, 11, (1989) 1290
[73] Spencer E.G. , Schmidt P.H. , Joy D.C. and Sausalone F.J. . Appl. Phys. Lett. 29 (2) (1976) 118
[74] Möller, W. Appl. Phys. Lett. **59** (1991) 2391
[75] Weissmantel C. , Bewilogua K. , Dietrich D. , Erler H.J. , Hinneberg H.J. , S. Klose, W. Nowick and G. Reisse. Thin Solid Films 72 (1980) 19
[76] André B., Rossi F. and Dunlop H. Diamond and Related Materials 1 (1992) 307
[77] Robertson J. , Phys. Rev. Lett. 68 (1992) 220
[78] Collins C.B. , Davanloo B. , Jander D.R. , Lee T.J. , Park H. and You J.H. , J. Appl. Phys. 69 (1991) 7862
[79] Galli G. Martin R.M. Car R. and Parinello M. , Phys. Rev. Lett. 62 (1989)555
[80] Hirvonen J-P. , Lappalainen R. , Koskinen J. , Anttila A. , Jervis T.R. and Trkula M., J. Mater. Res. 5 (1990) 2524
[81] Wu, R.L.C, Surf. Coat. Techn., 51 (1992) 258
[82] Lettington A.H., Smith C., Diamond and Related Materials 1 (1992) 805
[83] Vedovotto N. , Mackowski J.M., and P. Collardelle, Proc. Optical Society of America, Optical Interference Coatings, Tucson (1988)
[84] Kurihara K. , Sasaki K. , Kawaradi M. and Koshino N. , Appl. Phys. Lett. **52** (1988) 437

المنارة للاستشارات
www.manaraa.com

Subject Index

absorption factor 315
activated reactive evaporation 146
adhesion 31,32
adhesion test 46
 indentation methods 53
 pull-off method 48
 scratch test method 59
 shockwave methods 57
 tensile and bending testing 49
 applications 224
 coating materials 221, 225, 226
 post-coating treatment 118
 quality control 223
arc depostion 181
 cathodic 189
 thermionic 186
atomic form factor 315

boriding of steels 75
 industrial applications 76
 process principle 76
 techniques 76
Bragg's law 314
Bragg-Brentano geometry 321

cantilever and beam bending method 283
carburizing of steels 69
 atmosphere 71
 mechanical applications 72
 process principle 70
 procedure 70
cathodic arc deposition 189
ceramic diffusion coatings 347
 chemical reaction 36
 mixing by ion bombarding 36
coatings, decorative 358
 combination with PVD 252
 graded deposition 255
 optical 193
 wear resistant 186
condensation rate 141
contamination, evaporated films 139
 sputtered films 176
corosion tests 364
corrosion at high temperatures 335
crack propagation 77
CuK_a - penetration depths 323

CVD reactors 108
 electrodeless 108
 magnetron type 114
 with external electrodes 110
 with internal electrodes 111

Debye-Waller factor 315
decorative coatings 359
deposition
 of stoichiometric compounds 181
 metal containing polymer films 123
 multicomponent films 254
deposition rate 141, 150
 monitoring 150
 sputtering 165
diamond 371
 cubic 372
 deposition mechanism 379
 deposition techniques 376
 effect of substrate preparation 386
 electronic properties 373
 hexagonal 372
 kinetics 384
 mechanical properties 373
 nucleation density 384
 polycrystalline films373, 358, 287
 thermal properties 373
diamond-like carbon 371
 deposition techniques 388
 deposition mechanism 396
 structure 372
diode sputtering 153
 effecting factors 39

elasticity of thin solid films 275
 cantlever and beam bending method 283
 membrane method 283
electroplating
 in combination with PVD 367
evaporation
 activated reactive 145
 alloys 144
 compounds 135
 reactive processes 145
evaporation rate 137
evaporation sources 149

failure initiation 39
failure modes 37

www.manaraa.com

film growth 20
  modeling 21
films prepared by plasma CVD
  from Si containing monomers 128
  of fluoropolymers 114
friction and wear tests 302
  abrasion test 304
  pin-on-disk test 303, 305
  rolling contact test 304, 309
  sliding test 302
friction coefficient, steady state 308
friction 295

glancing angle x-ray diffractometry 322
glow discharge deposition processes 106
  etching-deposition competition 106
  gas phase-surface competition 107
grain size 319
graphite 372
growth of films 20
  of nuclei 6
  of sputter-deposited films 176

hardness 275
hard coatings
  corrosion 364
  decorative 360
  wear 186
hot corrosion 337, 354
hybrid processes 253

image storage in PLZ ceramics 95
indentation of thin films 276
indentor geometry 279
interdiffusion 35
interfaces 31, 340
interfacial engineering 1
interfacial structures 32
  effective contact area 34
interlayers
  electroplated 368
  PVD 368
ion beam assisted deposition 192
ion beam deposition 181
ion beam mixing 32
ion impact during deposition 184
ion implantation 83, 341
  metallurgy 86
  microelectronics 92
  optical properties of glasses 100
  insulators 100
  tribology 87
  technology 91
  of glasses 95
  mechanical properties modifications 99
ion plating 181
  reactive low voltage 194
  thermionic arc 186

laser cladding 236, 344
laser CVD 260
laser surface, remelting 235, 344
  alloying 236, 344
laser surface treatment 235, 343
  solidification conditions 237
life improvements 1
lonsdaleite 372

magnetic bubbles memory devices 94
magnetron sputtering 172
MCrAlY coatings 349
Me-C:H films 287
mechanical keying 34
mechanical properties of thin solid films 275
membrane method 283
Messier, structure zones 25
Movchan-Demchisin
  structure-zones 23
metallic diffusion coatings 344
microstructure 313
microstructurural charcterization 313
multicomponent coatings 135, 144, 254
  hybrid processes 255
multiplicity factor 316

nanoindentation 287
neutron diffraction 324
nucleation 5
nucleation density 34

optical coatings 193
overlay coatings 349
oxidation 337

pack cementation 344

www.manaraa.com

physical vapor depostion 135, 181
  combination with electroplating 357
  combination with plasma CVD 259
plasma nitriding of steels 72
  equipment 74
  industrial applications 74
  metallurgical aspects 73
  principle 73
plasma spraying (PS) variants 212
  gas-tunnel PS 213
  high power PS 213
  induction PS 213
  inert gas PS 214
  transferred arc PS 217
  under-water PS 213
  vacuum PS 215
plasma spraying 199
  adherence and cohesion 209
  coating microstructure 207
plasma-enhanced chemical vapor deposition 105, 256
  coating uniformity 258
  laser assisted 260
  plasma assisted 256
polymer films 123
porosity, of coatings 343
powder diffraction patterns 316
powder diffraction standard files 316
  properties and applications 127

reactive elements 338, 348
reactive evaporation 145
  activated 146
reactive ion plating 194

scale adherence 342
scanning electron microscope 325
Scherrer formula 319
scratch test method 59
  Weibull statistical ananlysis 63
Seemann-Bohlin geometry 321
SEM 325
sliding friction, components 296
  adhesion 296
  asperity deformation 296
  ploughing 296
  solidification speed 240
solidification microstructures 241
  absolute stability 247
  banded structure 247
  dendritic 241, 244
  eutectic 241
  planar front growth 242
spallation 338, 342
  sputter deposited films 176
sputter deposition 164
  growth of films 176
  hybrid processes 253
  improving techniques 40
  reactive 175
  sputter etching 44
  substrate temperature 166
sputtered species 162
sputtering 152
  diode 153
  low pressure 170
  magnetron 172
  mechanism 155
  threshold energy 160
  yield 156
strain 319
stress determination 283
  curvature methods 284
  x-ray methods 285
structure factor 315
structure zone models 23
substrate curvature method 286
sulphidation 337
surface engineering
  components 1
  equipment market 4
  market situation 3
surface morphology 313

teflon-like films
  chemical structure 121
  deposition mechanism 117
  effect of substrate temperature 120
  feed composition 118
TEM 326
temperature factor 315
ternary coatings
  colour 360
  hybrid processes 254
thermal barrier coatings 352
thermionic arc ion plating 186
thin layer activation 84
Thornton, structure zones 176, 136

www.manaraa.com

transmission electron microscope 326
amplitude contrast 329
bright field 327
dark field 327
convergent beam e-diffraction 332
out of focus imaging 330
phase contrast 329
selected area diffraction 331
small area diffraction 327, 331
specimen preparation 332

wear, 295, 297
abrasive 299
adhesive 299
asperity deformation 299
chemical 300
delamination 299
equations 300
fatique 299
mechanism 298
rate 301, 306
velocity accomodation concept 300
wear resistant coatings 186
Wierl formula 318
Williamson - Hall plot 320

x-ray diffraction 313

Young's modulus 276

www.manaraa.com